Mechanistic Studies into the Catalytic Activity of Half-Sandwich Ruthenium Complexes

Neetisha Shantilal Mistry

PhD

University of York

Chemistry

September 2013

Abstract

A mechanistic investigation into the catalytic activity of half-sandwich ruthenium complexes, $[Ru(\eta^5\text{-}C_5H_5)(L)_3]^+$ (where L = phosphorus- or nitrogen- donating ligands) for the alkenylation of pyridine is reported. Mechanistic studies have demonstrated that $[Ru(\eta^5\text{-}C_5H_5)(PPh_3)(NC_5H_5)_2][PF_6]$ is an important intermediate in the formation of *E*-2-styrylpyridine derivatives. Collaboration between the reported experimental and additional theoretical studies (conducted by David Johnson) has allowed for a catalytic cycle for the alkenylation of pyridine to be proposed, highlighting the role of vinylidene and pyridylidene ligands.

A general synthetic procedure for a range of $[Ru(\eta^5\text{-}C_5H_5)(PR_3)(L)_2][PF_6]$ complexes from $[Ru(\eta^5\text{-}C_5H_5)(NCMe)_3][PF_6]$ was performed, where R = Ph, Me, ^{i}Pr, OPh; and L = pyridine, 3-methylpyridine, 4-methylpyridine, 4-dimethylaminopyridine, 1-methylimidazole, t-butylimidazole. The properties of these complexes have been investigated.

The reactivity of $[Ru(\eta^5\text{-}C_5H_5)(PPh_3)(NC_5H_5)_2][PF_6]$ with terminal alkynes was investigated in two different reaction media (dichloromethane and pyridine). The stoichiometric reaction of $[Ru(\eta^5\text{-}C_5H_5)(PPh_3)(NC_5H_5)_2][PF_6]$ with phenylacetylene in a dichloromethane solution generated a vinylidene-containing intermediate $[Ru(\eta^5\text{-}C_5H_5)(PPh_3)(NC_5H_5)(=C=CHPh)][PF_6]$. This reacts further to produce a pyridylidene-containing complex $[Ru(\eta^5\text{-}C_5H_5)(PPh_3)(\kappa^3\text{-}C_3\text{-}C_5H_4NCH=CHPh)][PF_6]$. Upon the addition of excess pyridine a 1-ruthanaindolizine species is generated. Similar observations have been made with alkynes HC≡CR (where R = 4-F-C_6H_4, 4-CF3-C_6H_4) and $[Ru(\eta^5\text{-}C_5H_5)(PPh_3)(L)_2][PF_6]$ (where L = 3-methylpyridine, 4-methylpyridine, 4-dimethylaminopyridine) and the substituent effects and properties of the pyridylidene-containing complexes are compared to the literature.

The addition of phenylacetylene or 4-ethynyl-α,α,α-trifluorotoluene to $[Ru(\eta^5\text{-}C_5H_5)(PPh_3)(NC_5H_5)_2][PF_6]$ in a pyridine solution at 50 °C produces 2-substituted *E*-styrylpyridine derivatives in a 100 % atom efficient manner. The formation of the 1-ruthanaindolizine complex results in catalyst deactivation. A range of reaction conditions have been investigated to identify the optimum catalyst performance.

Table of Contents

List of Schemes

List of Figures

List of Tables

List of Equations

List of Accompanying Material

CD of cif Files for X-ray Crystallography Data

Bookmark of Diagrams

Acknowledgements

I have thoroughly enjoyed my time in York and it is thanks to all the people I have met and spent time with that have made this experience very memorable. I would like to express a very big thank you to Jason for the extensive advice, assistance and supervision during the past few years. It has been a great experience and I have been really lucky. Also, to John whose supervision and optimistic outlook has been a great motivation. Additionally, thank you to Ian for the advice and guidance during the TAP meetings. I am very grateful for the assistance in learning more about the techniques and the services provided by Heather and Dave for NMR spectroscopy, Adrian, Rob and Natalie for X-ray crystallography, Karl and Ed for mass spectrometry and Graeme for the elemental analysis. I wouldn't have been able to do my work without them.

To DFT Dave, thanks for the theoretical calculations and it has been fun working with you and throwing the stress-balls around the office and all the research students Rosanne, Lucy and Sally who have also worked on this project. A big thank you to Christine for the high-quality training and always answering a simple question, meant I found my feet easily and allowed me to get through all the lab-work. Over the past few years Sharifa has always had time for a chat and has offered a lot of support, so I would like to express a special thank you. Thank you to Richard for all the evenings at his (even when it was unexpected) and always putting in the extra effort. Also, to Lizzie who has always provided a helping hand in the lab. For all the great food and company thanks to Rifa, Rich, Barby, Christine and Becci, it was a great fun. I have enjoyed being part of the SLUGS group and department it has been a very entertaining few years and I am glad to have met Abeda, Andy, Becci, Barby, Dan, Dan, David, Flip Flop John, Lee, Lucy, Luisa, Ollie, Rosanne and Steve. Outside of the 'chemistry bubble' it has been great getting to know Adam, Lena, Sean, Zac, Ringo and Shulan. Thanks to them for always listening, being patient and helping out.

Most importantly, I would like to thank my family for all their support and always being there. Dad thank you for the hard-work and all the 'read and writes' and to my Nalu as Aj would say 'don't worry be happy'. Pranay (Puday) remember to keep smiling. Vilas (a.k.a. Poppet/ Little Weirdo) no one knows me like you do and if one of us says it, the other one was always thinking it!

Author's Declaration

I hereby declare that the work described in this thesis was carried out in the Department of Chemistry, University of York between October 2009 and March 2013 under the supervision of Dr Jason Lynam and Dr John Slattery. The research presented here is, to the best of my knowledge, original except where due to reference has been made to other authors or co-workers.

For my family

Chapter 1. Introduction

1.1 Metal complexes in catalysis

The requirement for greener chemical processes entails that any potential waste by-products should be avoided, with the ability of reactions to be performed with 100 % atom efficiency.[1-3] Catalysis by transition metal centres allows for these goals to be acheived. From understanding how stoichiometric reactions proceed, a shift from stoichiometric to catalytic reactions *via* transition metal complexes provides a route to synthesising new carbon-carbon or carbon-heteroatom bonds in a selective manner. A higher atom efficiency from the removal of pre-functionalised carbon-halogen bonds and methods to selectively functionalise C-H bonds has become more appealing for the synthesis of new carbon-carbon, -oxygen or -nitrogen bonds.[4-8]

Nobel prizes have been awarded in the areas of 'development of the metathesis method in organic synthesis' in 2005 to Chauvin, Grubbs and Schrock[9-12] and more recently in 2010 for the 'palladium-catalysed cross couplings in organic synthesis' to Heck, Negishi and Suzuki.[13, 14] The mechanism-driven approach for the development of ruthenium catalysts in olefin metathesis lead to the formation of highly active, more efficient catalysts for organic and polymer chemistry.[10-12] The usefulness of palladium cross coupling reactions arises from the processes being able to be performed in a highly selective manner, with a low catalyst loading. Additionally, there is a high functional group tolerance therefore reducing the number steps required to reach the final compound.[13-15]

This introduction will discuss the literature surrounding the significance of transition metal complexes in the formation of vinylidene and pyridylidene ligands (in particular ruthenium complexes) as they provide a route to more atom economical reactions. Several aspects of vinylidene- and pyridylidene-containing complexes will be covered, including the mechanism through which these ligands are generated, their bonding and properties and lastly their roles as reactive intermediates for potential applications in the catalytic transformation of organic molecules is highlighted. Finally, the ruthenium-catalysed alkenylation reaction of pyridine is mentioned to lay a foundation for the research described in this thesis.

1.2 Ligands and substituent effects

The coordination of ligands to transition metal centres can change the reactivity the metal complex exhibits. The ligands and their substituents will affect the level of electron density present at the metal centre, the number of coordination sites available and will impact the environment around the metal centre.[16] An initial discussion of phosphorus and nitrogen ligands with reference to their substituents will be made.

1.2.1 Phosphorus-containing ligands

The bonding mode of phosphorus (III) ligands to transition metals centres involves coordination *via* the lone pair of the phosphorus atom, which acts as a σ donor.[17, 18] Additionally, a π-acceptor interaction from the metal centre to the empty orbitals of the phosphorus atom can occur (Figure 1.1). The empty orbitals at the phosphorus centre are considered to be a σ* orbital.[19] The strength of the interactions are determined by the substituents of the phosphorus ligand and the nature of the transition metal centre. For example, PCy_3 is considered to be a better σ donor than PF_3, however the latter is considered to be a better π-acceptor.

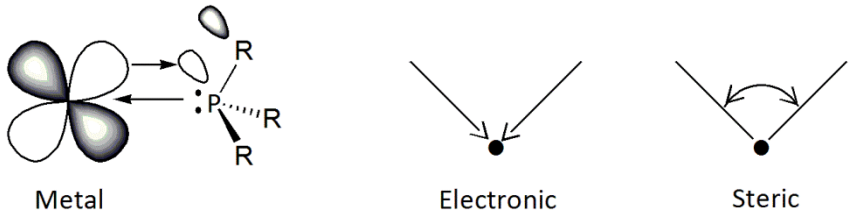

Figure 1.1: Bonding diagram of a phosphorus (III) ligand to a transition metal centre and schematics of electronic and steric effects at the phosphorus atom.

The changes in both the steric (θ) and electronic (ν) factors of the substituents of a phosphorus ligand, can account for the differences observed in the reactivity of transition metal complexes (Figure 1.1).[20-22] A wide library of substituents at a phosphorus centre have been screened with respect to the electronic and steric parameters using $[Ni(CO)_4]$. Substitution of the carbonyl ligand to give $[Ni(CO)_3L]$ (where L = phosphorus-containing ligand) was used to measure the electronic effect of different phosphine ligands on transition metal complexes, by observing changes in ν_{CO} of the A_1 stretching frequency. The general trend demonstrated that more electron donating substituents at the phosphorus centre, the lower the ν_{CO} A_1 stretching frequency was for the $[Ni(CO)_3L]$. The phosphorus ligands that will be mentioned in this thesis are PPh_3, PMe_3, P^iPr_3 and $P(OPh)_3$ where the reported ν (cm^{-1}) values

observed were 2068.9, 2064.1, 2059.2 and 2086.1 respectively. On going from a triphenylphosphine ligand to triisopropylphosphine the $[Ni(CO)_3L]$ complex has a lower ν_{CO} than the triphenylphosphine ν_{CO} and free ν_{CO} at 2143 cm^{-1}, which indicates triisopropylphosphine has a larger net donation (accounts for two factors the σ donation and π acceptor properties) and that the CO bond order decreases. Changing the ligand from triphenylphosphine to triphenylphosphite also dramatically changes the steric and electronic properties. Triphenylphosphite exhibits a lower net donation the metal centre, due to the oxygen atoms being more electronegative than carbon. The net donation exhibited the trend $P^iPr_3 > PMe_3 > PPh_3 > P(OPh)_3$.

The steric impact at the metal centre created by different phosphine ligands plays a significant role, as experimental observations could not always be explained purely by considering the electronic parameters.[20-22] This was investigated by measuring the exchange equilibrium between NiL_4 and L' (where L = coordinated phosphorus ligand and L' = attacking phosphorus ligand) where steric factors play a more dominant role. These data were then compared to the phosphorus ligand cone angles, where the cone angles were predicted assuming a tetrahedral bonding mode and where the metal to phosphorus bond was assumed to be 2.28 Å. A semi-quantitative study between the strength of coordination of the phosphorus ligands and ligand cone angles revealed that cone angles closer to the tetrahedral bonding orientation displayed a stronger ligand coordination, however when this cone angle is exceeded the stability of these species decreases. For the cone angles mentioned in thesis, there is a trend of P^iPr_3 (160 °) > PPh_3 (145 °) > $P(OPh)_3$ (130 °) > PMe_3 (118 °). The cone angle of triphenylphosphite is smaller than triphenylphosphine due to the oxygen atoms providing further flexibility, therefore rendering it is much less sterically demanding when bound to a metal centre.

It should be noted that the Tolman cone angles mentioned above act as a guideline. Further investigations in to the steric influence of phosphorus ligands have been summarised in a review by Brown and Lee where additional factors such as conformation of the substituents and the effects of other ligands present at the metal centre have an impact on the cone angles observed at the metal centre.[23] More recently, Gusev conducted theoretical calculations on a 18 electron $[Ir(\eta^5\text{-}C_5H_5)(CO)L]$ system (where L = two electron donor ligand) to analyse net donor ligand effects. This system posed several advantages from avoiding ligand repulsion, eliminating vibrational effects from a second CO ligand and removing the *trans* effect. The calculations exhibited very

similar trends to those reported by Tolman and in some cases the numerical differences were smaller than those originally reported.[24]

1.2.2 Nitrogen-containing ligands

The literature does not seem to cover the steric and electronic effects of nitrogen donor ligands in as much detail as phosphorus-containing ligands. However, there are a wide variety of chelating nitrogen coordinating ligands commonly employed in transition metal complexes. The types of nitrogen-containing ligands employed in this thesis are sp^2-hybridised. The mono-substituted sp^2-hybridised nitrogen ligands are used extensively in coordination chemistry *via* donation of the nitrogen lone pair.[16] In terms of the σ donating and π-accepting qualities the nitrogen ligands exhibit one of the weakest *trans* effects with respect to phosphorus-containing ligand or carbon monoxide.[25] The coordination of pyridine and nitrile ligands at an iron (II) species to generate $[Fe(\eta^5\text{-}C_5H_5)(CO)_2(L)][BF_4]$, where L = mono-substituted nitrogen ligand was investigated. In comparison, the nitrile ligands were found to coordinate more weakly to the metal centre with respect to the pyridine ligands, which were considered stronger σ-donors.[26]

The substituent effects of sp^2-hybridised N-containing heterocycles of pyridines were established by the pK_{HB} (hydrogen-bonding basicity) to give information on the Lewis base strength.[27] A set of 65 different compounds were analysed by this method, where pyridine was found to have a medium base strength regarding the hydrogen bonding (pK_{HB} = 1.86). Strong bases were found to be 4-methylpyridine (pK_{HB} = 2.07) and 4-dimethylaminopyridine (pK_{HB} = 2.80). On the other hand pentafluoropyridine (pK_{HB} = ~-0.49) was described as a weak base. The steric influence of a substituent at the 2-position of the pyridine ring generally displayed a weak base quality, however the electronic influence of the substituents also had an effect causing deviations from the expected steric trends. In addition, theoretical calculations to determine substituent effects of pyridine derivatives on halogen bonding have been conducted, where similar finding have been reported.[28]

1.3 Vinylidenes

1.3.1 Organic vinylidenes

The tautomerisation of an alkyne to its carbene form gives a vinylidene species (Figure 1.2). Free vinylidenes ($R_2C=C:$) are extremely reactive species. Their reactivity is due to the presence of only six valence electrons at the terminal carbon atom.[29, 30] The lone pair on the terminal carbon atom is very unstable, and hence in its free form it is in equilibrium with its alkyne form; where the free vinylidene has a lifetime of 10^{-10} seconds.[30, 31]

Figure 1.2: Acetylene to vinylidene tautomerisation.

Several experimental and theoretical studies for the transformation of unsubstituted acetylenes to vinylidenes have found that the process is endothermic by approximately 184-197 kJ mol^{-1}.[30, 31] An experimental study by Ervin *et al.* determined the bond dissociation energies for acetylene, HC≡CH to HC≡C + H (549.3 ± 17.6 kJ mol^{-1}) and vinylidene, $H_2C=C:$ to HC≡C + H (351.0 ± 2.9 kJ mol^{-1}) using negative ion photoelectron spectroscopy and gas phase proton transfer kinetics. The isomerisation for acetylene to vinylidene was then calculated to be 198.3 ± 17.0 kJ mol^{-1}.[32] Another approach reported by Colussi *et al.* involved the thermolysis of acetylene which yielded benzene, however intermediates detected *via* mass spectrometry suggested the initial formation of the vinylidene species before reacting further.[33] Parallel to these experimental investigations were theoretical studies. Gallo *et al.* have determined using theoretical methods that the energy difference between acetylene and vinylidene is approximately 180 kJ mol^{-1} which corroborates with experimental findings.[34]

Silvestre and Hoffman studied the isomerisation of acetylene to vinylidene *via* a 1,2 – hydrogen shift using Walsh diagrams to understand the interactions of the molecular orbitals.[35] Cleavage of the C-H bond results in an increase in energy of the two σ_{C-H} and σ_{C-C} orbitals, namely the σ_{C-C} bond which displays the highest energy and is now partly located in the HOMO. Additionally, the cleavage of the C-H bond has resulted in the LUMO being lower in energy due to fewer repulsions.

The interest in vinylidene species arises as they appear to be reactive intermediates in the formation of new molecules and therefore understanding the nature of these species may shed further light into reaction mechanisms.[36, 37] Synthetically, free vinylidenes only exist under extremely harsh reaction conditions. In the total synthesis of the compounds ±-isoptychanolide and ±-clovene the construction of the backbone of the molecules were hypothesised to go *via* vinylidene intermediates. For the synthesis of ±-isoptychanolide (***a***, Scheme 1.1) the formation of the vinylidene (***b***, Scheme 1.1) was achieved by heating the alkyne (***c***, Scheme 1.1) at 620 K in the gas phase.[38, 39] These conditions are not efficient and do not provide control over the reactivity, therefore a more accessible route may be achieved by introducing a transition metal centre, which can stabilise the vinylidene intermediate.[40]

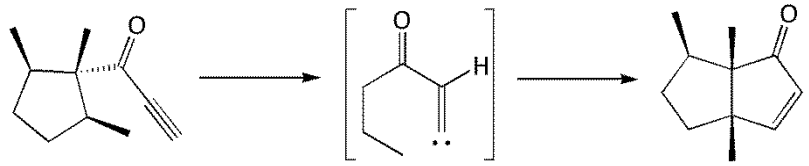

a ***b*** ***c***

Scheme 1.1: Vinylidene intermediate for the synthesis of the backbone of ± - isoptychanolide.

1.3.2 Metal vinylidenes

1.3.2.1 Introduction

The stabilisation of an organic vinylidene can be achieved through coordination to a transition metal centre, where the metal centre is essentially acting as protecting group to enhance the lifetime of the organic species (Figure 1.3).[31, 35, 41, 42] The ability to isolate metal vinylidene complexes has allowed for a thorough investigation of the properties and reactivity of these species which therefore has allowed potential applications to be exploited.[1, 30, 31, 40, 43-47] For example, metal vinylidene complexes have become a useful tool in providing a method of synthesising new carbon-carbon bonds or carbon-heteroatom bonds, under more atom-economical conditions. Section 1.3.2.2 provides an insight into the molecular orbital diagram of vinylidene complexes, the synthesis of vinylidene ligands and reaction mechanism for the formation of these species in the presence of transition metal centres.

Figure 1.3: Alkyne to vinylidene tautomerisation at a metal centre.

1.3.2.2 Molecular orbital diagram of Fischer vinylidene complexes

The properties of the vinylidene ligand can tuned depending on the metal fragment it is coordinated too.[30, 31] These can be categorised into two forms, Schrock- and Fischer-type vinylidene ligands.[48, 49] Schrock-type vinylidene complexes involve the earlier transition metal centres and contain a nucleophilic α-carbon atom. Alternatively, the later transition metal centres (Groups 6-10, e.g. ruthenium (II), manganese (I)) in a low oxidation state, generate Fischer-type vinylidene complexes.

The Fischer-type vinylidene complexes involve an electron rich transition metal centre where there is an electrophilic α-carbon atom and nucleophilic β-carbon atom.[30, 50, 51] A general molecular orbital diagram of the Fischer vinylidenes complexes shows the π electron distribution between the M=C bond, this interaction is between the metal d_{xy} and d_{xz} orbitals and the vinylidene π, p, and π* orbitals (Figure 1.4). The HOMO involves π anti-bonding interactions between the metal d orbital and the C=C bonding orbital. The HOMO makes the β-carbon atom or metal centre prone to electrophilic attack. The LUMO orbital has a significant contribution from the empty p orbital on the vinylidene component and hence makes the α-carbon atom electron deficient and therefore prone to attack by nucleophiles.

A detailed study conducted by Kostic and Fenske calculated the molecular orbital diagram of several $[Fe(\eta^5\text{-}C_5H_5)]^+$ complexes which were coordinated to vinylidene ligands.[52] One of the key findings was that the metal to carbon π interaction was strong suggesting a bond order between 2 and 3. The vinylidene ligand was modelled to coordinate to the metal centre in both a horizontal and vertical position, and in both of these cases metal to ligand π back bonding was present, where the horizontal interaction is preferred. Additionally, the overall charge distribution at these complexes was investigated. Generally, for $[Fe(\eta^5\text{-}C_5H_5)(CO)_2(CCH_2)]^+$, the species is electrophilic in nature and therefore electrophilic attack is not very likely. However, attack by nucleophiles has been noted to occur regioselectively at the α-carbon atom of the vinylidene ligand. This is due to approximately 60 % of the LUMO being localised at

the α-carbon atom, which accounts for the bond polarity for Fischer vinylidene transition metal complexes.

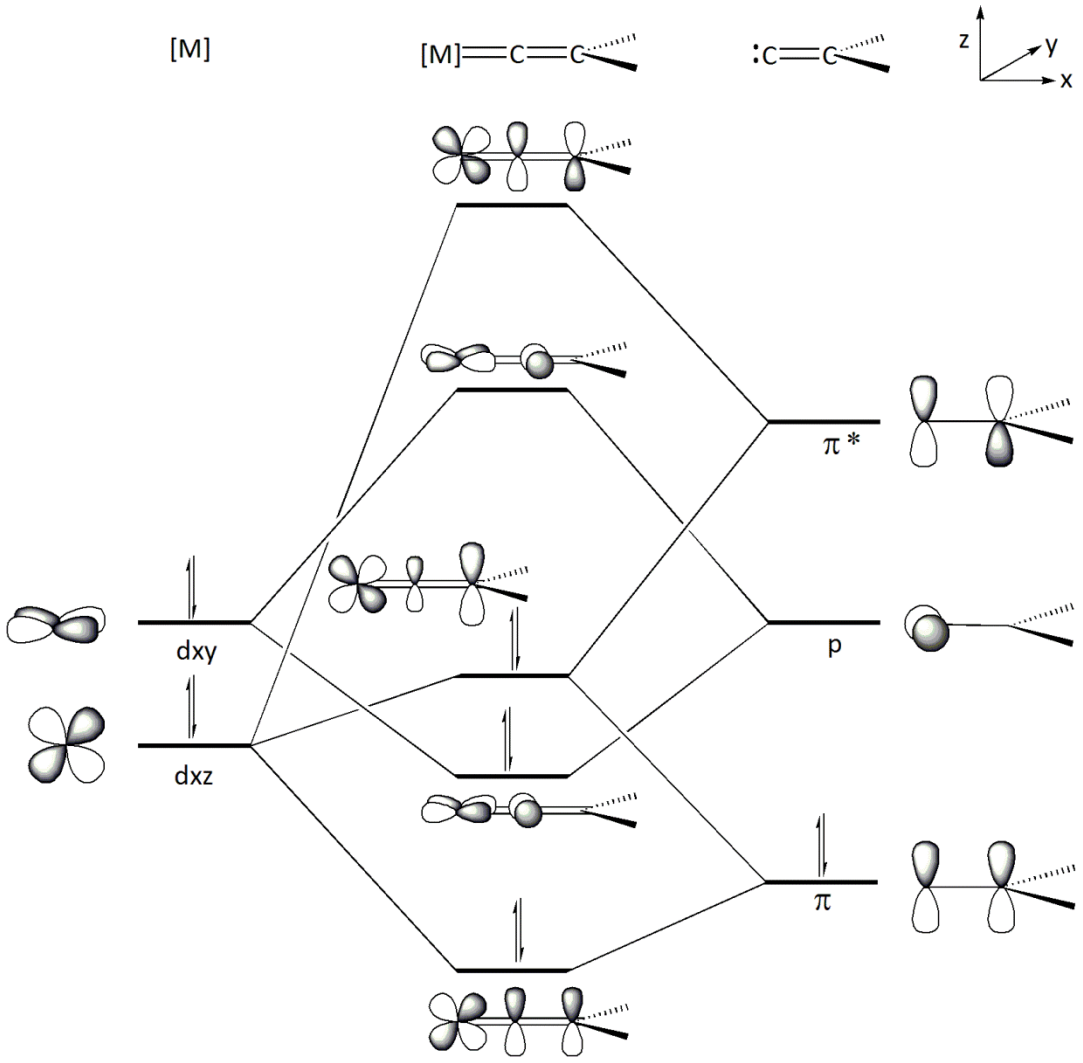

Figure 1.4: Simplified molecular orbital diagram of the π orbital interaction for Fischer type transition metal vinylidene complexes.

1.3.2.3 Synthesis of ruthenium vinylidene complexes

Several reviews have highlighted potential synthetic pathways for the formation of mononuclear vinylidene transition metal complexes which includes a 1,2-hydrogen migration pathway of 1-alkynes at a metal centre, electrophilic attack at metal acetylide complexes and deprotonation of carbyne ligands.[31, 47, 53] Generally, the formation of metal vinylidene complexes occur under milder reaction conditions than the metal free route and the properties of these ligands can be tuned by changing the metal fragment.[30]

One of the most popular methods to achieve metal vinylidenes utilises 1-alkynes, where a d^6 metal centre is required for the coordination of the alkyne. This requires a ligand at the metal centre to dissociate or a vacant coordination site.[30] In 1979, Bruce and Wallis

published a popular method to independently synthesise cationic ruthenium vinylidene complexes.[54] The complex $[Ru(\eta^5\text{-}C_5H_5)Cl(PPh_3)_2]$ (***a***, Scheme 1.2) could be transformed into a cationic ruthenium vinylidene complex by the addition of a terminal alkyne (HC≡CR) and a halide scavenger with a suitable counter-ion, and heating in methanol for a brief period of time. Prolonged heating under these nucleophilic conditions allows for the methanol to act as a nucleophile towards the resulting vinylidene species. The resulting vinylidene species $[Ru(\eta^5\text{-}C_5H_5)(PPh_3)_2(=C=CHR)][PF_6]$ (***b***, Scheme 1.2) had 18 valence electrons and a full coordination sphere.[44] The NMR spectra of the vinylidene ligand exhibits extremely characteristic features for the complexes $[Ru(\eta^5\text{-}C_5H_5)(PPh_3)_2(=C=CHR)][PF_6]$ (***b***, Scheme 1.2). The ^1H NMR spectrum exhibits a coupling from the hydrogen atom on the β-carbon atom to the phosphorus-containing ligands. Additionally, the $^{13}C\{^1H\}$ NMR spectrum displays a downfield resonance for the α-carbon atom of the vinylidene ligand as it is generally detected around 360 ppm and the β-carbon atom exhibits a resonance at approximately 120 ppm.[55]

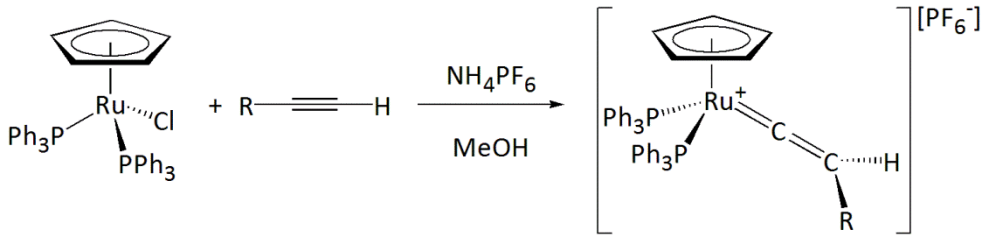

a ***b***

Scheme 1.2: Synthetic preparation of metal vinylidene complexes from Bruce and Wallis.

Alternatively, metal vinylidene complexes can be synthesised through an electrophilic attack at the β-carbon atom of an acetylide ligand in the presence of a counter-ion to yield the cationic metal species.[54] An example by Bruce has demonstrated that the addition of either HBF_4 or HPF_6 to $[Ru(\eta^5\text{-}C_5H_5)(PPh_3)_2(C\equiv CR)]$ yields the respective vinylidene complexes. The β-carbon atom is electron rich and therefore addition of the electrophile at this position has been justified to be controlled by charge distribution.[30, 31] This process can be reversed in the presence of a nucleophile to return to the acetylide complex. The protonation and deprotonation steps can be repeated and quantitative conversion is observed for during each of these steps.[54, 56, 57]

In the literature there are extensive examples where this type of chemistry has been exploited.[58, 59] Cadierno *et al.* have synthesised a range of functionalised alkynes and enynes where the cationic ruthenium fragment $[Ru(\eta^5\text{-}C_9H_7)(PPh_3)_2]^+$ can be recycled

therefore being able to repeat this procedure.[60-63] The chemistry entailed the addition of propargylic alcohols to the ruthenium complex yielding an allenylidene species, followed by nucleophilic attack at the electron deficient γ carbon atom. The subsequent acetylide complex is protonated at the β-carbon atom with $HBF_4.OEt_2$ to give the corresponding vinylidene species. When heated at reflux in an acetonitrile solution the cationic ruthenium species $[Ru(\eta^5\text{-}C_9H_7)(PPh_3)_2]^+$ is regenerated and the functionalised alkyne released.

1.3.2.4 Mechanistic aspects

There is extensive literature on the formation of metal vinylidene complexes. Mechanistically, there are many potential reaction pathways that could occur, some of the most common mechanisms include a 1,2-hydrogen migration or an oxidative addition followed by an 1,3-hydride shift or a route involving a metal alkenyl species (Scheme 1.3).

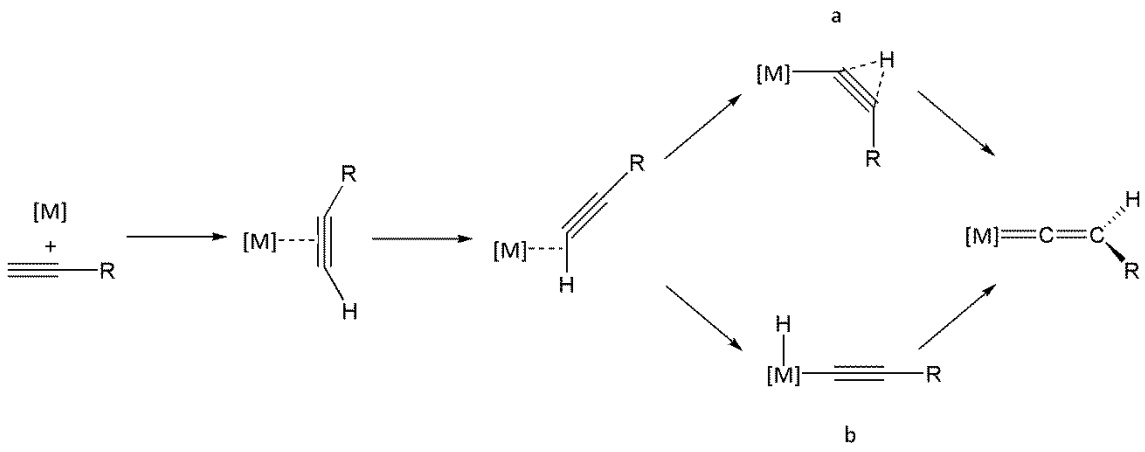

Scheme 1.3: Mechanisms on the formation of a vinylidene complex, a) 1,2-hydrogen migration, b) oxidative addition followed by 1,3-hydride shift.

A very detailed investigation into the 1,2-hydrogen migration mechanism in acetylene to vinylidene interconversion in the presence of the species $[Mn(\eta^5\text{-}C_5H_5)(CO)_2]$ was conducted by Silvestre and Hoffman.[35] The $[Mn(\eta^5\text{-}C_5H_5)(CO)_2]$ species is isolobal to $[Ru(\eta^5\text{-}C_5H_5)(PR_3)_2]^+$ which has been studied in this thesis. The mechanism entailed initial coordination of the acetylene molecule to the metal fragment. A 1,2-hydrogen migration concerted mechanism from the η^2-coordinated alkyne to the metal vinylidene species exhibited a high barrier of 230 kJ mol^{-1} and therefore this mechanism was disregarded. The alternative non-concerted pathway was found to have a lower activation barrier of approximately 121 kJ mol^{-1} for the formation of the vinylidene

species. The non-concerted pathway required the η^2-alkyne species to slip to an η^1 coordinated alkyne through the alkyne C-H bond. This can then undergo a 1,2-hydrogen migration where the hydrogen atom migrates over the C≡C bond to the β-carbon atom and yields the vinylidene species. Additionally, the MO diagrams of the η^2-coordinated alkyne and the metal vinylidene species were compared. It was found that the HOMO for the η^2-coordinated alkyne complex was high in energy as it was an anti-bonding orbital, however for the metal vinylidene complex the HOMO displayed a degree of non-bonding character which is therefore lower in energy. From these calculations it is apparent that the more stable species is the metal vinylidene complex with respect to the metal η^2-coordinated alkyne complex. Wakatsuki *et al.* determined that the $RuX_2(PPh_3)_3$ complex (where X = Cl, Br) in the presence of *tert*-butylacetylene undergoes a 1,2-hydrogen migration pathway to give $RuX_2(PPh_3)_2(=C=CH^tBu)$. The key factors included i) initial σ C-H interaction at the metal centre and ii) the empty metal d orbitals accepting electron density from lone pair of the vinylidene ligand.[64]

An alternative route involves the oxidative addition of the C-H bond of the acetylene molecule from the η^1-coordinated species to yield a metal hydrido-acetylide. A further 1,3-hydride shift from the metal centre to β-carbon atom results in the formation of the metal vinylidene complex. Silvestre and Hoffmann's calculations revealed that the 1,3-hydride shift possessed a higher activation barrier than the 1,2-hydrogen migration pathway and therefore described this route as 'prohibitive'.[35] Theoretical studies by De Angelis *et al.* have found that the oxidative addition followed by the 1,3-hydride shift is generally not favourable at d^6 metal centres (e.g. manganese (I), ruthenium (II)) with respect to the 1,2-hydrogen migration pathway *via* the η^2-coordinated C-H intermediate.[65, 66] Wakatsuki *et al.* reported that it is thermodynamically unfavourable for the metal centre to access a d^4 configuration.[64] The oxidative addition has a higher barrier, but has been found to be more accessible when the d^6 metal centre is more electron rich.[67] A range of hydrido-acetylide complexes were synthesised by Valerga *et al.*, from the electron-rich ruthenium complex, $[Ru(\eta^5\text{-}C_5Me_5)Cl(dippe)]$ and terminal alkynes in the presence of $NaBPh_4$ in MeOH.[68-70] These complexes were observed to give the vinylidene complexes *via* a proposed deprotonation of the hydride ligand to give an acetylide complex and a proton, followed by a reprotonation at the β-carbon atom. This has been extended to the complexes $[Ru(\eta^5\text{-}C_5Me_5)(PMe^iPr_2)_2][B\{3,5\text{-}C_6H_3\text{-}(CF_3)_2\}_4]$[71] and $[Ru(\eta^5\text{-}C_5Me_5)Cl(PEt_3)_2]$[72] where similar reactivity patterns have been observed. When the ruthenium centres possess less electron density due to different

ligands (e.g. η^5-C_5H_5, η^6-C_6H_6 or CO) the η^2-coordinated alkyne species was observed.[69, 73]

Another potential pathway has been reported by Oliván *et al.*, where [RuHX(H_2)L_2] and terminal alkynes yield the hydrido-vinylidene complex [RuHX(=C=CHR)L_2] (Scheme 1.4).[60, 74] The mechanistic and theoretical studies have found that the alkyne inserts into the Ru-H bond giving a 14 electron ruthenium-alkenyl complex (***b***, Scheme 1.4). The hydrogen atom at the α-carbon atom then migrates to the ruthenium centre yielding the final vinylidene product (***c***, Scheme 1.4). Theoretically this was the energetically preferred pathway relative to a 1,2-hydrogen migration or a 1,3-hydride shift. This concept has now been applied to the synthesis of enamides and enimides which have a strong structural link to biological molecules[75] and in the hydration of terminal alkynes to give aldehydes.[76]

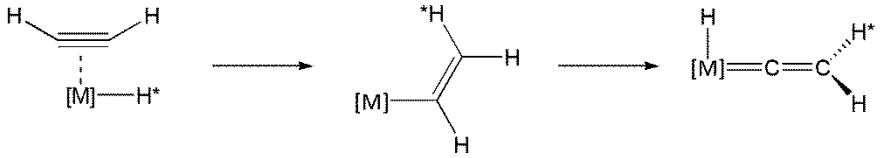

a ***b*** ***c***

Scheme 1.4: Formation of vinylidene complex from a ruthenium hydride complex.

1.3.2.5 Terminal alkyne substituent effects on the rate of formation of vinylidene complexes

The kinetic and thermodynamic effects in a reaction mixture will change the course of a reaction and since an equilibrium is always present between the metal vinylidene and the η^2-coodinated alkyne this will impact the formation of vinylidene intermediates.[44, 60] The substituent effects from changing the R group in terminal alkynes for the formation of vinylidene complexes was investigated using [$RuCl_2$(NCMe)(dcpmp)] where dcpmp = 2,6-bis((dicyclohexylphosphino)methyl)pyridine (***a***, Scheme 1.5).[77] The effects of the R substituents at the terminal alkynes that were investigated included 4-$MeOC_6H_4$, 4-MeC_6H_4, Ph, 4-BrC_6H_4, 4-$MeO_2CC_6H_4$ and ^{t}Bu, where the first five substituents differed in their electron donating abilities and the latter was sterically bulkier. The kinetic studies revealed that the formation of the vinylidene species required three major processes 1) dissociation of the acetonitrile ligand (slowest step) to give a five-coordinate ruthenium species (***b***, Scheme 1.5), 2) coordination of the terminal alkyne

and 3) tautomerisation to give the vinylidene complex (***c***, Scheme 1.5). The more electron-donating substituents at the terminal alkynes increased the rate of formation of the vinylidene species. Additionally, the ^{t}Bu substituent decreased the rate of formation of the vinylidene species which is probably due to the larger steric impact.

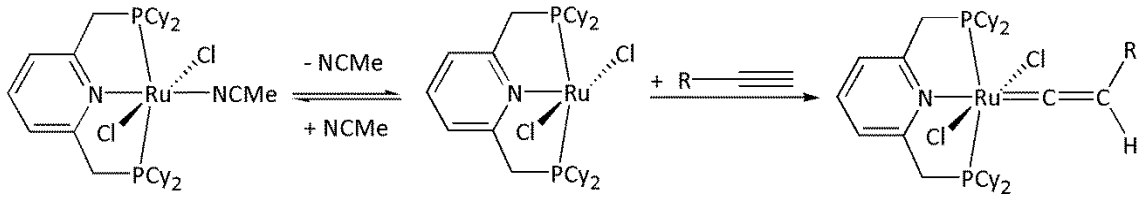

a ***b*** ***c***

Scheme 1.5: Formation of vinylidene complexes [$RuCl_2$(=C=CHR)(dcpmp)] with different R substituents (where R = 4-$MeOC_6H_4$, 4-MeC_6H_4, Ph, 4-BrC_6H_4, 4-$MeO_2CC_6H_4$ and ^{t}Bu).

1.3.2.6 Stabilisation of the vinylidene fragments by different d^6 metal centre.

The effect of varying the electron density present at ruthenium (II) centres with respect to the η^2-coordinated alkyne and the metal vinylidene tautomerisation was investigated by De Angelis *et al*. An increase in the electron density at the metal centre favoured the formation of the more stable vinylidene complex. This was attributed to two major factors i) the π-acceptor properties of the vinylidene ligand and ii) avoiding the repulsive interaction between the filled metal d orbital and the filled π orbital of the η^2-coordinated alkyne.[67]

The [Ru(η^5-C_5Me_5)(^{i}Pr_2PXPy)]$^+$ (Cp*Ru) and [RuTp(^{i}Pr_2PXPy)]$^+$ (TpRu) fragments (where X = CH_2, S and Py = NC_5H_5) were reacted with internal alkynes to give the corresponding vinylidene complexes through a 1,2-carbon shift. Interestingly, the TpRu species yielded the vinylidene complexes whereas Cp*Ru only generated the η^2-coordinated alkyne. This was attributed to i) a weaker interaction between the η^2-coordinated alkyne and TpRu; ii) a steric repulsion in the 1,2-shift of the Cp*Ru complex. Theoretical calculations exhibited a lower transition state to the vinylidene complex for TpRu of approximately 21 kJ mol^{-1} relative to Cp*Ru.[78, 79]

1.4 Reactivity of vinylidene-containing complexes

The reactivity of ruthenium vinylidene-containing complexes has been exploited for applications in catalysis where these complexes are involved in either nucleophilic addition at the α-carbon atom, migration of the alkyl/ alkenyl group from the metal centre to the α-carbon atom or [2+2] cycloaddition of a metal-carbon bond with a carbon-carbon bond.[80-82] This section covers the examples of ruthenium vinylidene chemistry and their proposed reaction mechanisms to demonstrate how these intermediates play a crucial role in determining the selectivity of the observed products.

1.4.1 Dimerisation of terminal alkynes

The catalytic coupling of terminal alkynes to give either 1,4- or 2,4-disubstituted enynes or butatrienes with ruthenium centres is well established in the literature (Figure 1.5).[43, 80, 83] The *E* and *Z* selective 1,4-enyne products are most commonly observed when ruthenium catalysts are employed.[84-87] This atom efficient process has great potential, as if the enyne molecules are produced in a regio- and stereoselective manner the products have potential applications as a monomer unit for polymerisation[88] or in natural product synthesis.[2]

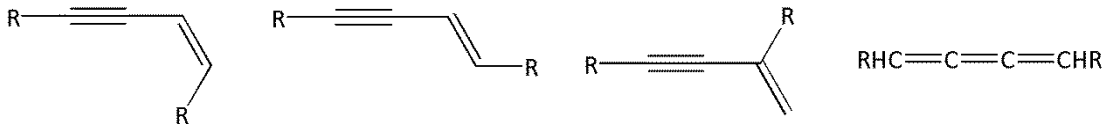

Figure 1.5: Dimerisation products from terminal alkynes: *Z*-, *E*- 1,4- and 2,4-disubstituted enynes and butatrienes.

Effective ruthenium catalysts for this transformation contain electron-donating, bulky ligands, for example PP_3 type ligands e.g. $P(CH_2CH_2PPh_2)_3$; NP_3 type ligands e.g. $N(CH_2CH_2PPh_2)_3$; Tp or C_5Me_5.[84, 85, 89, 90] A few reported successful ruthenium catalysts include [RuTp(L)(L')Cl] (where L and L' = N, P, O donor ligands)[90], $[Ru(PP_3)H(H_2)][BPh_4]$[84] and $[Ru(NCMe)(NP_3)][OTf]$.[91] General features for a successful catalyst include the metal complex containing labile ligands to allow for substitution by terminal alkynes; the coordinated ligands should be sterically bulky in order to stabilise a 16 electron intermediate; and avoidance of π-acceptor ligands as they do not promote dissociation of the ligands.[90] Various studies have exhibited that changes in either the ligand environments, reaction conditions or alkyne substituents can impact the *E*:*Z* ratios of 1,4-disubstituted enynes,[85-87] access competitive C-O formation reactions[92] or cyclotrimerisation[93] reactions. Additionally, the reaction

conditions have been developed further to allow for selective dimerisation reactions to occur in aqueous media[87] or alternatively, if applicable, in neat alkyne.[91] Interestingly, hydration products from the reaction of the ruthenium complexes with water were not observed (Section 1.4.2).

A general mechanism for the dimerisation of terminal alkynes is mentioned below.[80] The addition of two equivalents of terminal alkyne to a ruthenium catalyst (***a***, Scheme 1.6) yields a ruthenium alkynyl-vinylidene intermediate (***b***, Scheme 1.6), where it is possible that the alkyne undergoes a 1,2-hydrogen migration to give the vinylidene ligand.[84] Complex ***b*** can then undergo a carbon-carbon coupling reaction *via* a migratory insertion of the alkynyl ligand to the vinylidene. The resulting ruthenium enynyl complex (***c***, Scheme 1.6) undergoes protonation to give the final dimerisation products.

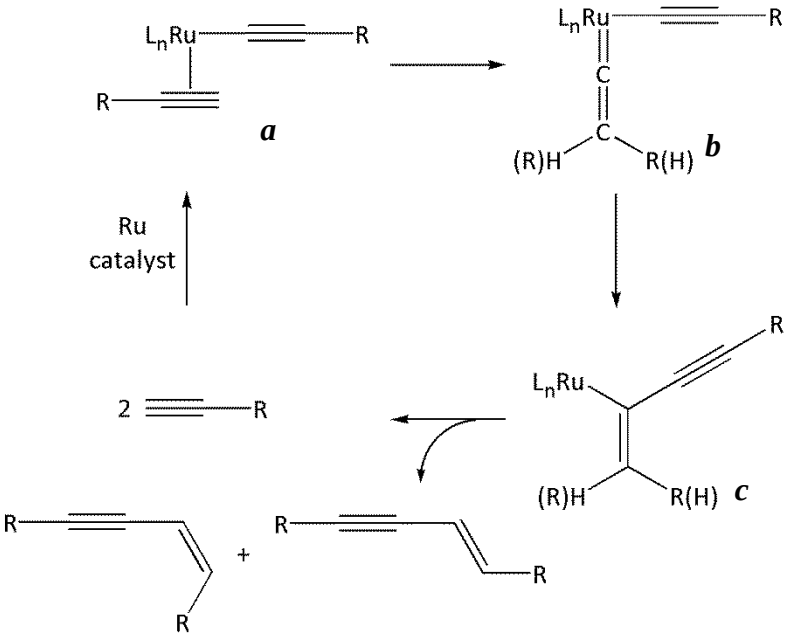

Scheme 1.6: General mechanism for the dimerisation of terminal to give 1,4-disubstituted enynes.

Isolation and characterisation of various ruthenium intermediates has provided insight into the reaction mechanism. The role of vinylidene ligands was confirmed *via* NMR spectroscopy and the distinct characteristic α-carbon resonance (top left, Figure 1.6).[89] Bianchini *et al.* observed the alkynyl-hydride, $[Ru(PP_3)H(C{\equiv}CPh)]$ and *bis*-alkynyl, $[Ru(PP_3)(C{\equiv}CPh)_2]$ ruthenium complexes, where the former complex was observed to convert to the *bis*-alkynyl complex. The *bis*-alkynyl complex was the final ruthenium complex observed before the formation of the *Z*-1,4-disubstituted enyne (middle reaction scheme, Figure 1.6).[94] Additionally, several ruthenium η^3-coordinated

butenynyl complexes have been isolated and characterised by X-ray crystallography, where the bond lengths suggest a degree of electronic delocalisation (top right, Figure 1.6).[84, 89, 95, 96]

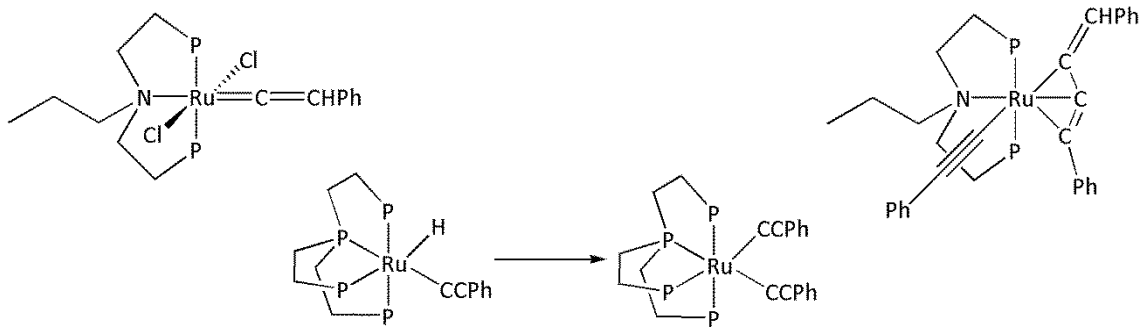

Figure 1.6: Significant ruthenium intermediates in the dimerisation of terminal alkynes.

The reaction of complexes, *cis*-[$RuCl_2$(P-P)$_2$] (where P-P = dppm, dppe), with $NaPF_6$ and an excess phenylacetylene afforded a vinylidene species (***a***, Scheme 1.7). Subsequent deprotonation of ***a*** by another molecule of phenylacetylene, a weak nucleophile, yielded the alkynyl complex (***b***, Scheme 1.7). Coordination of a further alkyne molecule in the form of a vinylidene ligand yielded an alkynyl-vinylidene complex (***c***, Scheme 1.7). Mechanistic studies demonstrated that the quantity of the vinylidene species ***c*** reduced as the coupled butenynyl products (***d*** and **e**, Scheme 1.7) increased. The butenynyl complex was found to be an active catalyst for the dimerisation of phenylacetylene.[96]

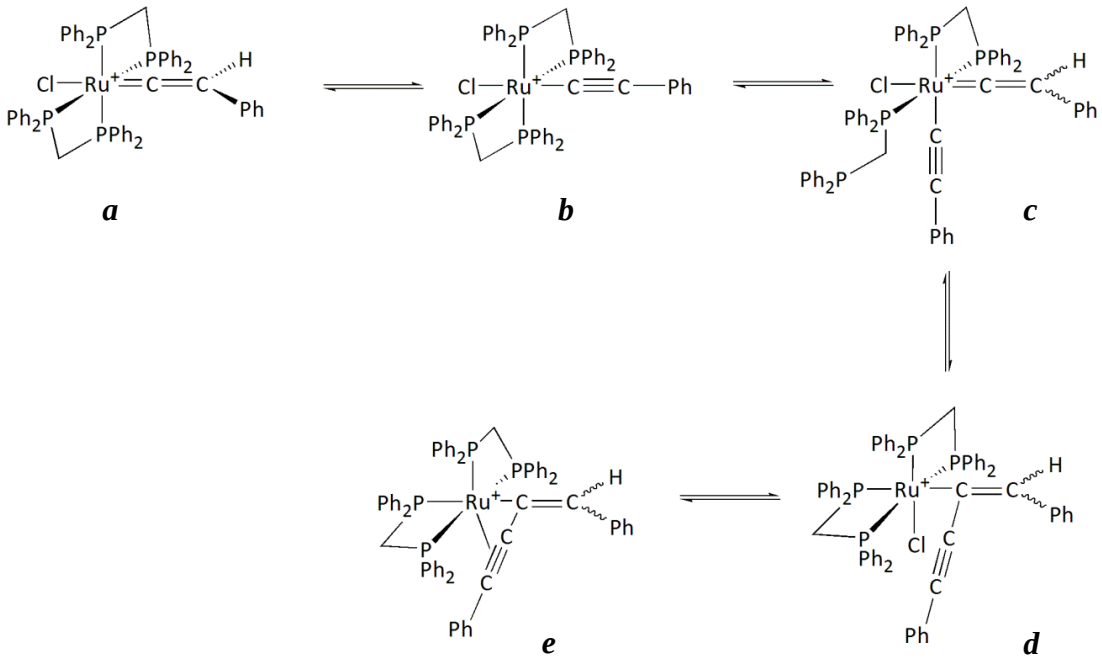

Scheme 1.7: Proposed mechanism for the dimerisation of phenylacetylene with *cis*-[$RuCl_2$(dppm)$_2$].

1.4.2 Cyclotrimerisation of alkynes

The cyclotrimerisation of alkynes provides an atom economical route for the synthesis of substituted aromatic compounds.[97-99] There is no evidence of ruthenium vinylidene intermediate complexes, but this highlights key changes in reactivity when different ligands are present at the metal centre. Complexes commonly employed for these transformations include $[Ru(\eta^5\text{-}C_5Me_5)Cl(COD)]$, $[Ru(\eta^5\text{-}C_5Me_5)Cl(PPh_3)_2]$, $[Ru(\eta^5\text{-}C_5Me_5)Cl]_4$, where these complexes lose ligand(s) or cleave the μ-Cl bonds to give an electronically unsaturated active fragment. The proposed catalytically active fragment, $[Ru(\eta^5\text{-}C_5Me_5)Cl]$ has been studied extensively as it is believed to be responsible for the [2+2+2] cyclotrimerisation of alkynes, where the presence of the chloride atom is necessary to observe any reactivity.[100, 101]

There is some experimental evidence for ruthenium intermediates in the cyclotrimerisation mechanism (Figure 1.7). Additionally, computational studies have provided further insight to the reaction pathway. Mechanistic investigations into the role of the ruthenium complex for the cyclotrimerisation reactions have been conducted.[100] In order to stabilise the ruthenium centre and potential 16 electron intermediates, the more sterically demanding η^5-1-methoxy-2,4-*tert*-butyl-3-neopentyl-cyclopentadienyl ($Cp^{\wedge}$) ligand was used. Isolation and characterisation of ruthenium η^2-coordinated alkyne complexes (left, Figure 1.7) and a ruthenacyclopentatriene complex (right, Figure 1.7) were detected by X-ray crystallography, suggesting the reaction pathway proceeded in a step-wise manner. Increased regioselectivity for the arene products was observed with $Cp^{\wedge}$ with respect to Cp* which was attributed to the higher steric demands of the $Cp^{\wedge}$ ligand.[100]

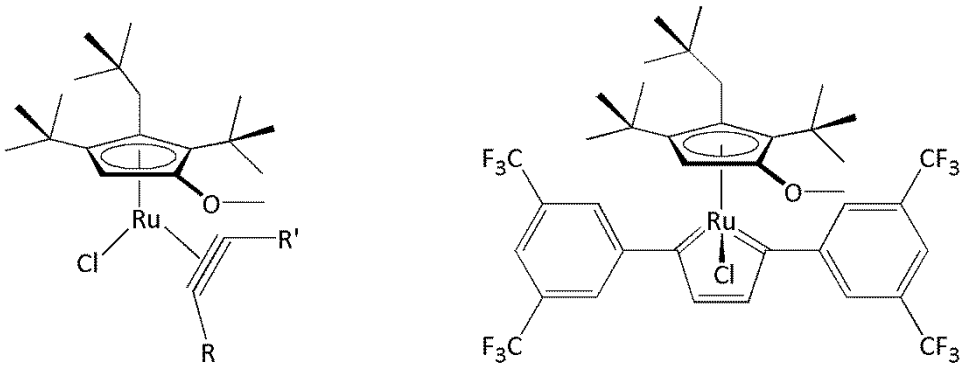

Figure 1.7: Isolated ruthenium complexes for the cyclotrimerisation of alkynes.

Computational studies have allowed for a general mechanism for cyclotrimerisation to be proposed (Scheme 1.8). The initial coordination of the alkyne (***a***, Scheme 1.8) gives

an η^2-alkyne complex, (***b***, Scheme 1.8). The coordination of an additional alkyne molecule at a free coordination site, gives a disubstituted alkene species (***c***, Scheme 1.8). The two coordinated alkyne molecules undergo an oxidative carbon-carbon coupling reaction to produce a ruthenacyclopentatriene species (***d***, Scheme 1.8). The metallacyclic complex ***d*** reacts with a final alkyne molecule in a few possible stages. The insertion of another alkyne molecule in a stepwise manner gives a ruthenabicyclo[3.2.0]heptatriene complex (***e***, Scheme 1.8), which undergoes a ruthenium-carbon bond cleavage reaction. This leads to either the formation of a seven membered metallacyclic species (***f***, Scheme 1.8) or a metallanorbornadiene complex (***g***, Scheme 1.8). Finally, a reductive elimination yields an arene molecule (***h***, Scheme 1.8) and regenerates the original [Ru(η^5-C_5Me_5)Cl] complex (***a***, Scheme 1.8). The Cp* ligands in these systems have also been noted to undergo a change in hapticity to allow for the formation of the arene molecule. [97, 100, 102-104]

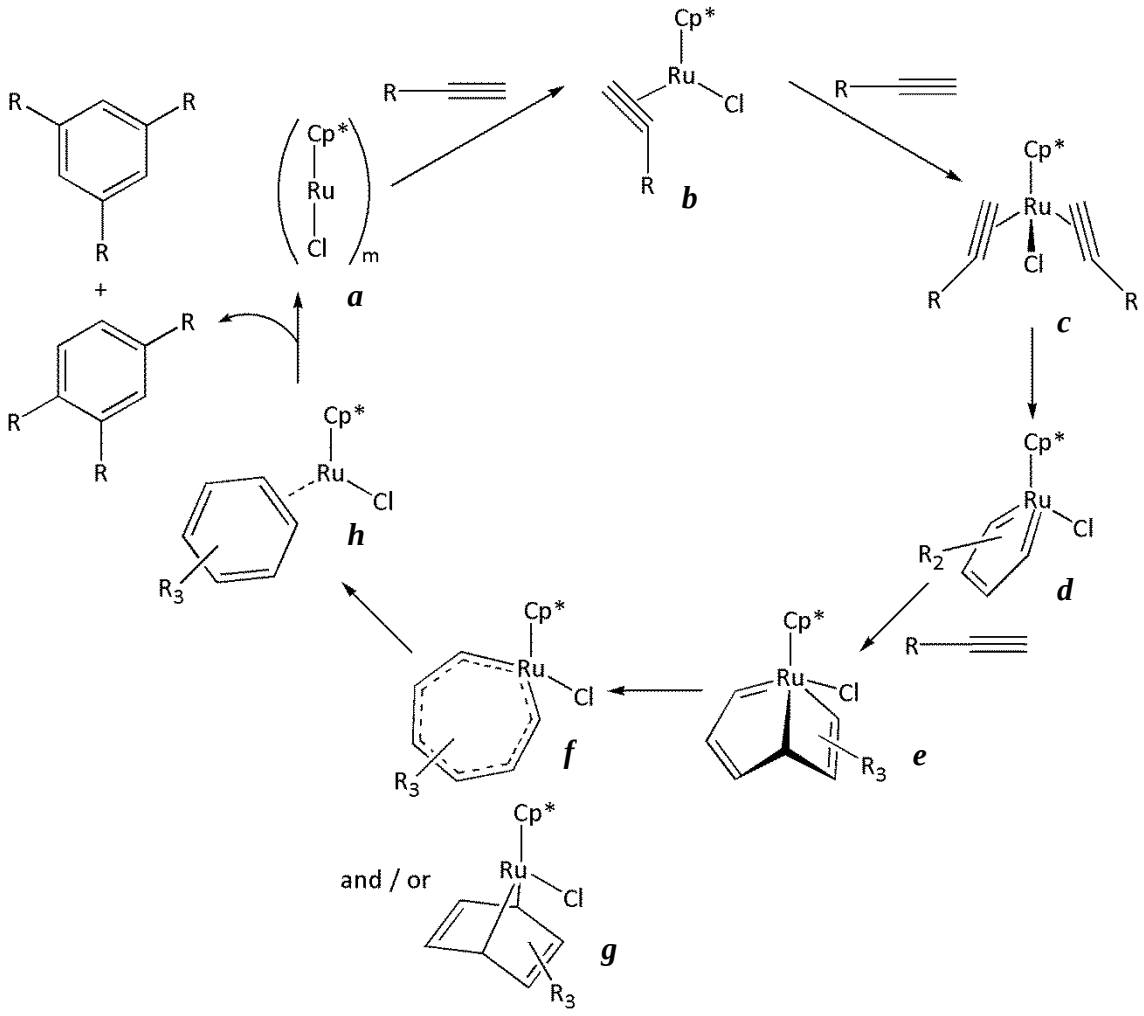

Scheme 1.8: General cyclotrimerisation mechanism of terminal alkynes, where Cp* = η^5-C_5Me_5.

1.4.3 Reactivity of ruthenium vinylidenes in the presences of water

The hydration of terminal alkynes in the presence of certain ruthenium catalysts generates an aldehyde. The reaction proceeds *via* a vinylidene intermediate which means the less common anti-Markovnikov selectivity is observed. This has challenged other metal catalysts (mercury and gold) in the field, as usually a methyl ketone is produced from a Markovnikov reaction (Scheme 1.9).[105, 106] The production of primary alcohols from the reduction of the aldehyde products highlights a key potential industrial application.[107]

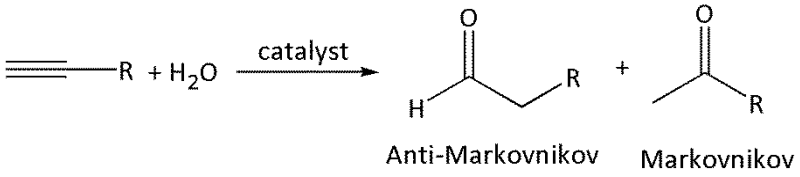

Scheme 1.9: Reaction of water and terminal alkynes in the presence of different catalysts.

Major contributions in the area regarding catalyst development and determination of the reaction mechanism are from the groups of Wakatsuki and Tokunaga, Grotjahn, and Bianchini *et al*.[30, 108, 109] The ruthenium (II) complexes $[RuCl_2(C_6H_6)]_2$ in the presence of a phosphine ligand, P (where P = $PPh_2(C_6F_5)$ or $P(3\text{-}C_6H_4SO_3Na)_3$),[108] $[Ru(\eta^5\text{-}C_5H_5)Cl(dppm)]$ (where dppm = bis(diphenylphosphino)methane)[109] and $[Ru(\eta^5\text{-}C_5H_5)Cl(PPh_3)_2]$[76] were found to perform the transformation. In addition, bifunctional catalysts have successfully been applied in the synthesis of aldehydes where the rate of reaction is accelerated between 1000 to 10000 times.[110-112] The air-stable, cheaper ruthenium pre-catalyst $[Ru(\eta^5\text{-}C_5H_5)(\eta^6\text{-naphtalene})][PF_6]$ has been employed to generate an *in situ* catalyst in the presence of the required ligands and avoid the independent synthesis from the more expensive complex $[Ru(\eta^5\text{-}C_5H_5)(NCMe)_3][PF_6]$.[113, 114]

Grotjahn *et al*. studied the role of bifunctional catalysts for the production of aldehydes, where the significance of a pendant N-containing heterocyclic group (either pyridyl or imidazolyl derivatives) at a phosphorus ligand was investigated.[111, 115] Evidence was established for the presence of a ruthenium vinylidene complex (***b***, Scheme 1.10) which arises from a π-coordinated alkyne, and for an acyl intermediate (***c***, Scheme 1.10).[116] The close proximity of the nitrogen atom allows for facile formation of the vinylidene ligand and the addition of water to the α-carbon atom of the vinylidene ligand *via* the movement of protons and a hydrogen bonding stabilisation.[110, 117, 118] The

pyridylphosphine ligands were found to require a bulky substituent (such as *tert*-butyl) close to the nitrogen atom to prevent coordination to either the ruthenium centre or the α-carbon atom of the vinylidene ligand.[110] A complete mechanism has not yet been fully identified, however it already differs to a reaction mechanism that has been proposed by Wakasuki *et al.* which involves a ruthenium (IV)-vinyl intermediate.[76]

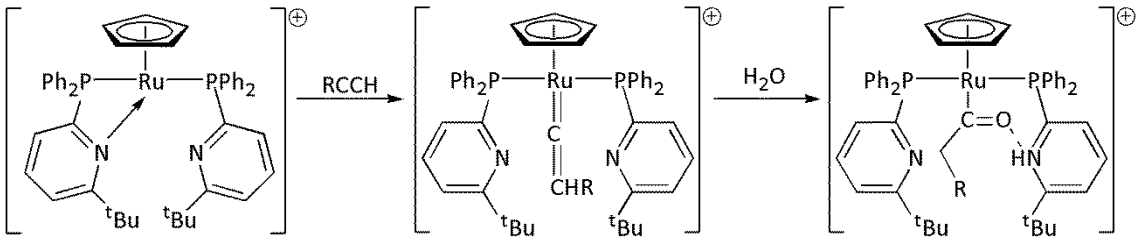

a ***b*** ***c***

Scheme 1.10: Key intermediates identified in the bifunctional catalysis for the hydration of terminal alkynes.

1.4.3.1 Involvement of a ruthenium carbonyl complex

Ractions between metal vinylidene complexes and water have been found to produce a metal carbonyl complexes, indirectly suggesting the mechanism for the hydration of terminal alkynes goes *via* a vinylidene intermediate.[93, 119, 120] Bianchini *et al.* conducted a detailed mechanistic investigation of the ruthenium complex *mer, trans*-[$RuCl_2$(PNP)(PPh_3)] (where PNP = $CH_3CH_2CH_2N(CH_2CH_2PPh_2)_2$) (***a***, Scheme 1.11), phenylacetylene and water. Upon conducting this experiment the carbonyl complex *fac, cis*-[$RuCl_2$(PNP)(CO)] (***b***, Scheme 1.11) and toluene were detected. A reaction in the absence of water produces the ruthenium vinylidene complex exclusively and the subsequent addition of water sees the formation of the carbonyl complex (***b***, Scheme 1.11).

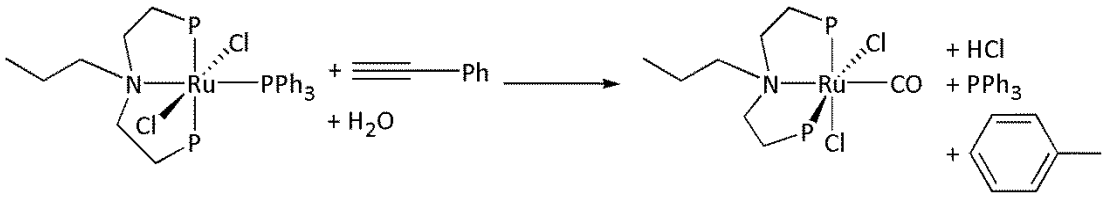

a ***b***

Scheme 1.11: Reaction of *mer, trans*-[$RuCl_2$(PNP)(PPh_3)] (where PNP = $CH_3CH_2CH_2N(CH_2CH_2PPh_2)_2$) with phenylacetylene and water.

A proposed reaction mechanism involved attack of water at the cationic ruthenium vinylidene complex (***a***, Scheme 1.12) to produce a hydroxyl-carbene intermediate (***b***, Scheme 1.12).[119, 120] Elimination of HCl generates an unsaturated metal complex which contains an σ-acyl group (***c***, Scheme 1.12). A CO de-insertion process gives the ruthenium carbonyl complex (***d***, Scheme 1.12). The loss of toluene from the reaction with HCl produces the carbonyl complex (***e***, Scheme 1.12).

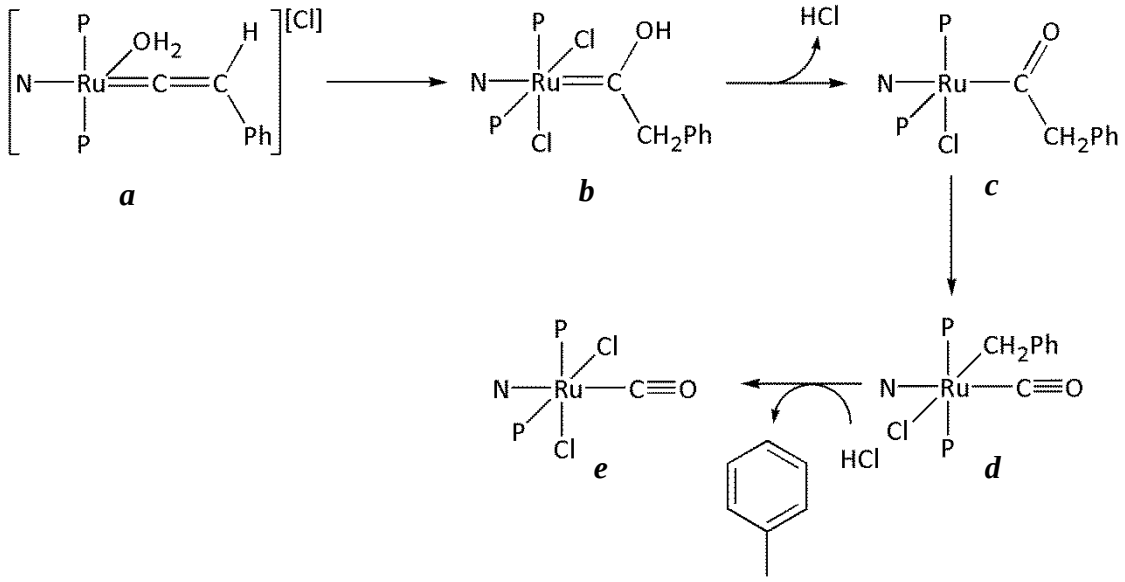

Scheme 1.12: Proposed mechanism for the formation of the ruthenium carbonyl complex.

1.4.4 Attack at vinylidene ligands by nitrogen donor groups

Catalytic reactions involving the addition of a nitrogen centre to an alkyne molecule with a ruthenium catalyst have been reported. When ruthenium transition metal complexes are employed, some of these reactions again are proposed to go *via* a ruthenium vinylidene species; where a nucleophilic attack of the nitrogen atom at the α-carbon atom of the vinylidene ligand occurs to generate a new carbon-nitrogen bond to synthesise nitriles,[121] enamides[122, 123] and substituted indoles.[30, 80, 124] In comparison to the formation of carbon-carbon and carbon-oxygen bonds from vinylidene complexes, there are fewer examples with nitrogen nucleophiles.

The enamide structure is found in natural products which are used in pharmaceutical drugs. Additionally, they are being used increasingly in organic synthesis. Goosen *et al.* reported the successful catalytic reaction to selectively synthesise *E*-enamides, where the ruthenium catalyst [Ru(methylallyl)(COD)] (2 mol %) was used to achieve high yields of above 94 % (Scheme 1.13).[123, 125]

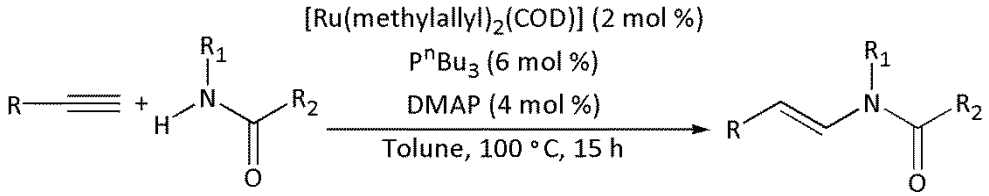

Scheme 1.13: Catalytic reaction for the formation of *E*-enamides.

Recently, an investigation into the ruthenium-catalysed hydroamination reaction demonstrated strong evidence for the mechanism by which enamide compounds are synthesised.[75] An initial N-H oxidative addition at a ruthenium (0) species (***a***, Scheme 1.14) produces a ruthenium (II) hydride complex (***b,*** Scheme 1.14). An alkyne molecule inserts in to the ruthenium-hydride bond (***c***, Scheme 1.14) to yield a ruthenium-vinyl species (***d***, Scheme 1.14), which rearranges to generate a vinylidene-containing complex (***e***, Scheme 1.14). The nitrogen donor atom attacks the α-carbon atom of the vinylidene ligand (***f***, Scheme 1.14) and a final reductive elimination step produces the *E*-enamide product with an anti-Markovnikov selectivity.

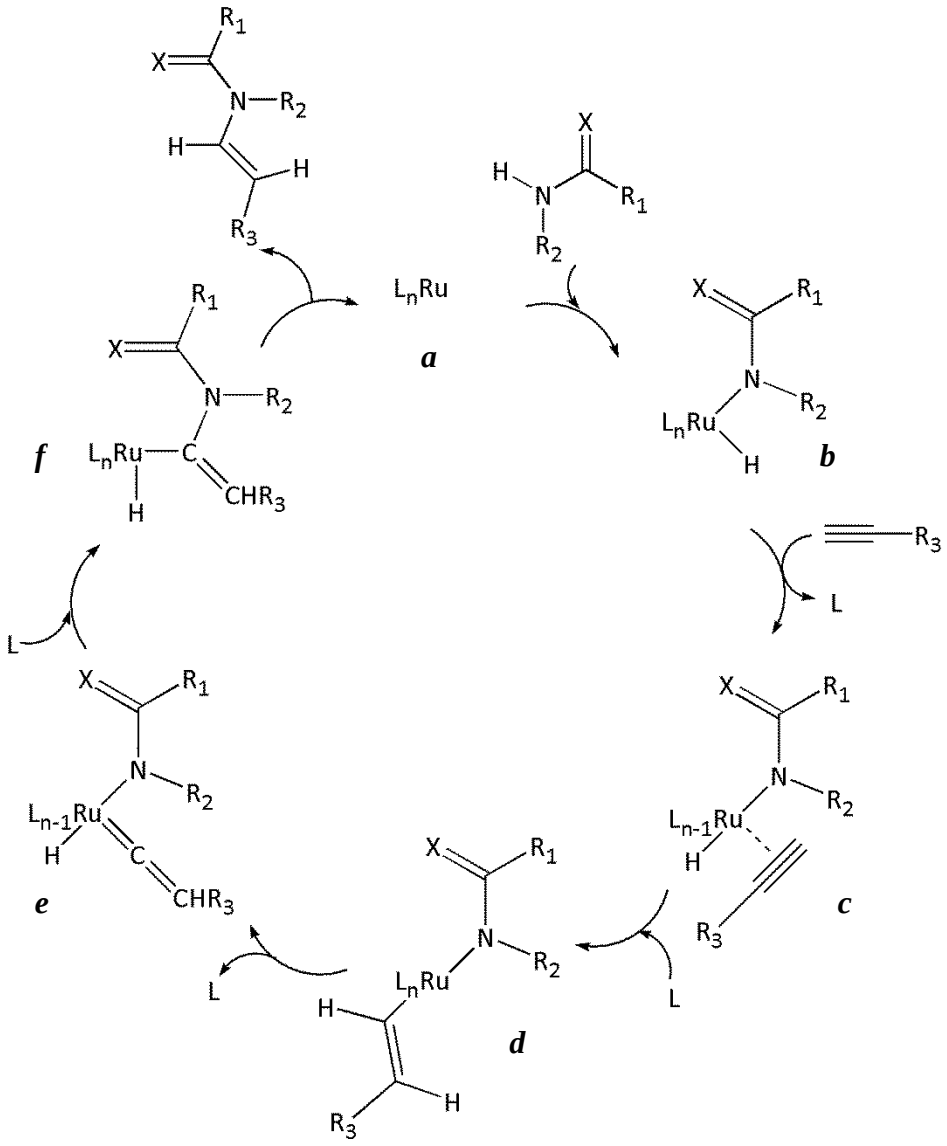

Scheme 1.14: Proposed mechanism for the formation of *E*-enamides, where L = DMAP, R_1 and R_2 = 2-pyrrolinidone, R_3 = ^{n}Bu and X = O.

1.5 Synthesis and reactivity of $[(\eta^5\text{-}C_5H_5)Ru(PR_3)]^+$ fragment

Reactive 14-electron ruthenium intermediates have applications in catalysis, where the vacant coordination sites at the metal centre make it is possible to carry out cyclotrimerisation of terminal alkynes (Section 1.4.2). This process allows for the formation of new carbon-carbon bonds, which is highly desirable in synthetic applications. Kirchner *et al.* have carried out an extensive investigation on the reactivity of the $[Ru(\eta^5\text{-}C_5H_5)(PR_3)]^+$ fragment, where R = Me, Ph, Cy). The $[Ru(\eta^5\text{-}C_5H_5)(PR_3)(NCMe)_2][PF_6]$ species was regarded as a pseudo 14 electron species, with two vacant coordination sites due to the labile nature of the acetonitrile ligands and therefore creating a reactive intermediate.[126] The synthesis of these types of complexes were reported from $[Ru(\eta^5\text{-}C_5H_5)(NCMe_3)_3][PF_6]$ and this method has been used widely in the literature due to lability of the acetonitrile ligands.[127-130] The reactivity towards alkynes has also been studied.[131, 132]

1.5.1 Synthesis and properties of pseudo 14 electron species, $[Ru(\eta^5\text{-}C_5H_5)(PR_3)]^+$

The synthesis of the $[Ru(\eta^5\text{-}C_5H_5)(PR_3)(NCMe)_2][PF_6]$ (where R = Me, Ph, Cy) complexes (***b***, Scheme 1.15) were achieved from the stoichiometric addition of the phosphine ligand to $[Ru(\eta^5\text{-}C_5H_5)(NCMe)_3][PF_6]$ (***a***, Scheme 1.15).[131] This synthetic procedure has been extended to other monodentate ligands such as $AsPh_3$, $SbPh_3$.[133] Merbach and Ludi have demonstrated the labile nature of the acetonitrile ligands of various ruthenium (II) acetonitrile complexes.[134, 135] The complexes $[Ru(NCMe)_6]^{2+}$, $[Ru(\eta^6\text{-}C_6H_6)(NCMe)_3]^{2+}$ and $[Ru(\eta^5\text{-}C_5H_5)(NCMe)_3]^+$ exhibited exchange rates of 8.9 x 10^{-11}, 4.07 x 10^{-5} and 5.6 s^{-1} respectively, increasing by five orders of magnitude.

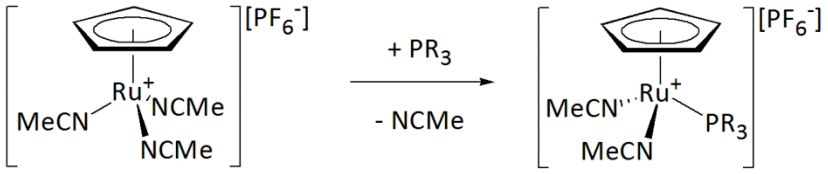

a ***b***

Scheme 1.15: Synthesis of the complexes, $[Ru(\eta^5\text{-}C_5H_5)(PR_3)(NCMe)_2][PF_6]$.

The rate constants for the exchange of acetonitrile of all the phosphine complexes decreased from $[Ru(\eta^5\text{-}C_5H_5)(NCMe)_3][PF_6]$, due to higher enthalpies of activation. The lability of the two acetonitrile groups remaining on the ruthenium metal centre for PPh_3 and PMe_3 were a lot lower than $[Ru(\eta^5\text{-}C_5H_5)(NCMe)_3][PF_6]$.[131] However, in the case of

PCy_3, the rate of acetonitrile exchange increased, probably due to ligand repulsion (Table 1.1). The reaction kinetics suggested a dissociative mechanism. The two factors which were potentially responsible for the acetonitrile exchange rates included the electron donating ability (electronic) or cone angles (steric) of the phosphine ligands. The steric influence was reported to influence more predominantly the exchange rates, where the cone angles were PMe_3 (118°) <PPh_3 (145°) < PCy_3 (180°).[20-22]

	$[Ru(\eta^5\text{-}C_5H_5)(NCMe)_3][PF_6]$[135]	$[Ru(\eta^5\text{-}C_5H_5)(PR_3)(NCMe)_2][PF_6]$[131]		
		PPh_3	PMe_3	PCy_3
k^{298}/ s^{-1}	5.6	2.9 x10^{-3}	2.7 x10^{-3}	0.38

Table 1.1: Rate of exchange of acetonitrile ligands in ruthenium(II) complexes.

If the stoichiometric addition is exceeded it is possible to substitute further acetonitrile ligands to give $[Ru(\eta^5\text{-}C_5H_5)(PR_3)_2(NCMe)][PF_6]$. Alternatively, the stoichiometric addition of a different ligand to $[Ru(\eta^5\text{-}C_5H_5)(PR_3)(NCMe)_2][PF_6]$ will yield a chiral ruthenium complex. The reactivity of $[Ru(\eta^5\text{-}C_5H_5)(PR_3)(NCMe)_2][PF_6]$ (***a***, Scheme 1.16) was probed further by the addition of chelating ligands, COD and butadiene [131, 134] An η^2,η^2-COD coordinated complex (***b***, Scheme 1.16).was observed with PPh_3 and PMe_3; however the coordinated butadiene species was only observed with the PMe_3 ligand. These results demonstrated that substitution of the acetonitrile ligands is highly dependent on the steric crowding present around the ruthenium centre.

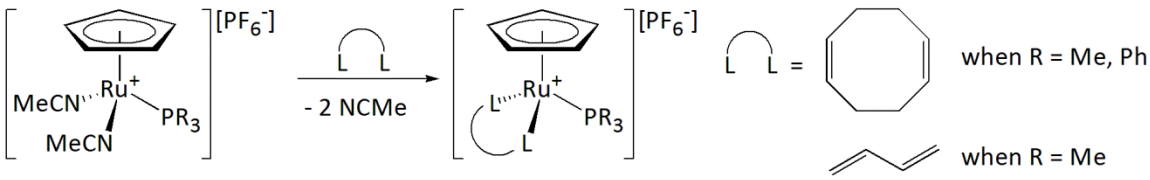

a ***b***

Scheme 1.16: Reaction of of $[(\eta^5\text{-}C_5H_5)Ru(PR_3)(NCCH_3)_2]^+PF_6^-$ with chelating ligands, where L'L' = COD R = Ph, Me and where L'L'= butadiene R= Me.

1.5.2 Reactivity of pseudo 14 electron species, $[Ru(\eta^5\text{-}C_5H_5)(PR_3)]^+$

The reactivity of the $[Ru(\eta^5\text{-}C_5H_5)(PR_3)(NCMe)_2][PF_6]$ (where R = Me, Ph, Cy) complexes was probed due to the selective substitution of the acetonitrile ligands, in comparison to the complexes $[Ru(\eta^5\text{-}C_5H_5)Cl(PPh_3)_2]$ or $[Ru(\eta^5\text{-}C_5H_5)Cl(CO)_2]$ where selectively replacing one of the PPh_3 or CO ligands is difficult.[131, 136, 137] The addition of terminal alkynes, HC≡CR' (where R' = Ph, C_6H_9, ^{n}Bu, H, $SiMe_3$, C_6H_4-4-OMe) or 1,6-heptadiyne to $[Ru(\eta^5\text{-}C_5H_5)(PR_3)(NCMe)_2][PF_6]$ at room temperature was investigated (Scheme 1.17). The stoichiometric addition of 1,6-heptadiyne or alternatively two equivalents of HC≡CR' yielded a range of ruthenium η^3-allyl carbene complexes (***c***, Scheme 1.17). The reaction was complete within a few minutes and thought to proceed *via* a ruthenacyclopentatriene intermediate (***b***, Scheme 1.17). The alkynes were always found to couple selectively in a head-to-tail manner. The coupling of two alkyne molecules at the metal centre gives a metallacyclopentatriene complex, which are thought to be intermediates in cyclotrimerisation reactions (Section 1.4.2), however this has not been observed due to the strongly electrophilic nature of the complex and therefore an alternative type of reactivity has been observed where the phosphine ligand migrates to one of the electrophilic carbon atoms. Experimental and theoretical calculations support this hypothesis.[132, 138]

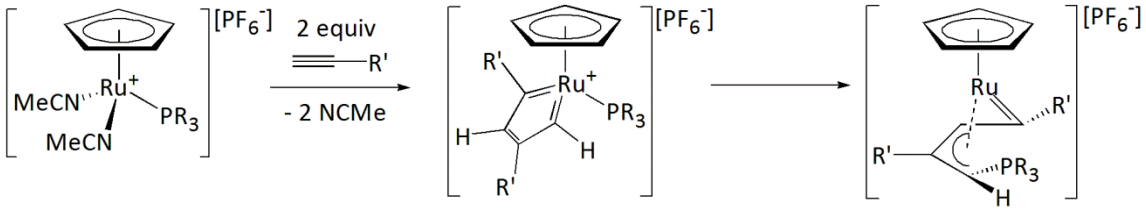

a ***b*** ***c***

Scheme 1.17: Reaction between $[Ru(\eta^5\text{-}C_5H_5)(PR_3)(NCCH_3)_2][PF_6]$ and HC≡CR' (where R = Me, R' = Ph, C_6H_9, ^{n}Bu, H, $SiMe_3$, C_6H_4-4-OMe).

Interestingly, when a combination of PMe_3 and two equivalents HC≡CR' (where R' = Ph, C_6H_9, ^{n}Bu, H, $SiMe_3$, C_6H_4-4-OMe, C_6H_4-4-NO_2) were employed, this generated the ruthenium η^3-allyl carbene complexes, that could be isolated. The characterisation of the η^3-allyl carbene complexes was carried out mainly by NMR spectroscopy, where the $^{13}C\{^1H\}$ NMR spectra exhibited characteristic resonances for the carbene and terminal allyl carbon atoms were observed between 279-236 and 41-26 ppm respectively and exhibited carbon-phosphorus couplings. The high field resonance of the terminal allyl carbon atom was attributed to it having an sp^3-hybridised character.[136, 139] However, in

the presence of bulky PR_3 substituents (e.g. Ph, Cy) the η^3-allyl carbene complexes (***a***, Scheme 1.18) were unstable and a further C-H activation occurred at one of the R groups of the phosphorus ligand to give an orthometallated group on a η^4-butadiene ligand (***b***, Scheme 1.18).[139]

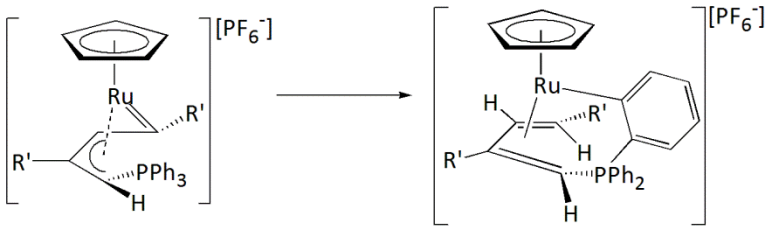

a ***b***

Scheme 1.18: Intramolecular C-H activation of the R group of PPh_3 from the η^3-allyl carbene complex.

Additionally, a further type of reactivity was exhibited by the η^3-allyl carbene complexes (***a***, Scheme 1.19) in the presence of a donor ligand (e.g. PPh_3). A nucleophilic addition at the ruthenium centre by a triphenylphosphine ligand resulted in a η^3-butadienyl complex which had undergone a stereo-chemical change in the carbon chain (***b***, Scheme 1.19).

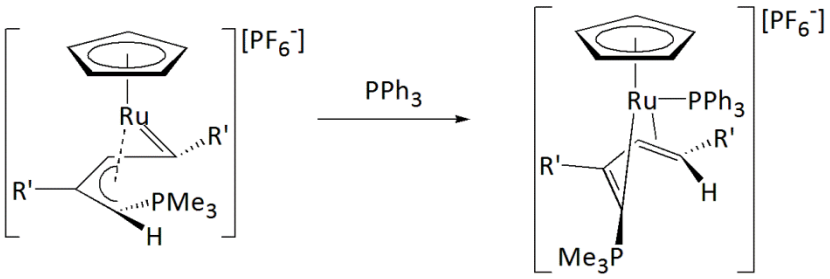

a ***b***

Scheme 1.19: Nucleophilic addition by PPh_3 at the η^3-allyl carbene complex.

1.6 Synthesis and properties of metallacyclic complexes

This part of the introduction will describe metallacyclic complexes in the literature, since later in this thesis novel ruthenium-containing metallacycles will be described. Metallacyclic complexes containing a heteroatom have been investigated due to their structural properties and their involvement in the formation of carbon-carbon or carbon-heteroatom bonds.[140, 141] The synthesis and properties of these complexes is described and will provide useful information for the complexes described later.

1.6.1 Osmium-containing metallacycles

The formation of 3-osmaindolizine complexes and a 3-ruthenaindolizine species was reported by Esteruelas *et al.*[142, 143] The reaction of $[MTp(\kappa^1\text{-}OCMe_2)_2(P^iPr_3)][BF_4]$ (where M = Os, Ru and Tp = hydrido*tris*(pyrazolyl)borate) and $[Os(\eta^5\text{-}C_5H_5)(NCMe)_2(P^iPr_3)][PF_6]$ with 2-vinylpyridine in the presence of base produces metal indolizine complexes (Figure 1.8). The aromatic 10-π indolizine rings were found have an almost planar geometry, where an average deviation of 0.08 Å at the nitrogen atom was found. X-ray crystallography revealed that the metal-carbon bond lengths of 2.000(6) (***a***, Figure 1.8) and 1.983(2) (***c***, Figure 1.8) Å were between that which is expected for the respective metal- alkenyl and alkylidene complexes, therefore demonstrating a metal-carbon bond with partial double bond character. Additionally, the metal-nitrogen bond lengths were reported to be significantly shorter than in the respective metal-nitrogen bond to a pyridine ligand. The $^{13}C\{^1H\}$ NMR spectra exhibited resonances for the carbon bound directly to the metal of the 3-osmaindolizine complexes at 203.8 ppm (***a***, Figure 1.8) and 197.8 ppm (***b***, Figure 1.8), and for the 3-ruthenaindolizine[143] at 226.3 ppm (***c***, Figure 1.8).

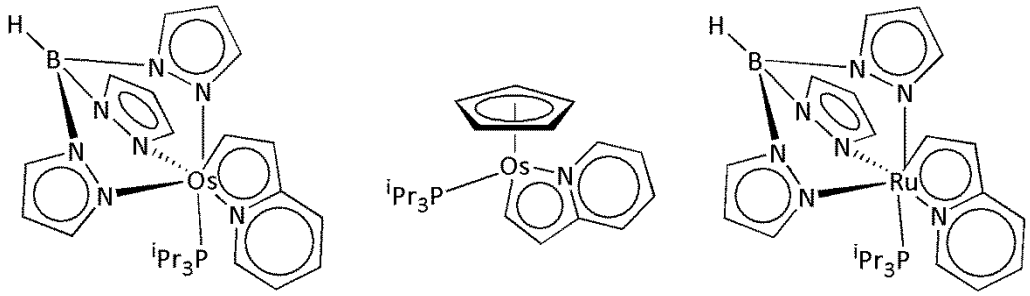

a ***b*** ***c***

Figure 1.8: Osmium and ruthenium indolizine complexes.

A set of metallopyrrole complexes (***b***, Scheme 1.20) were also synthesised by Esteruelas *et al*. from the addition of $NaBH_4$ and methanol to the imino-phosphine complexes (***a***, Scheme 1.20).[144] The chemical shifts of the carbon atoms in the metallocycle suggested that the electron density was delocalised around the ring. The $^{13}C\{^1H\}$ NMR spectra displayed the chemical shifts for the carbon atoms at the osmium-carbon were between 222-224 ppm, the carbon-hydrogen were between 126-129 ppm and the nitrogen-carbon were between 178-180 ppm.

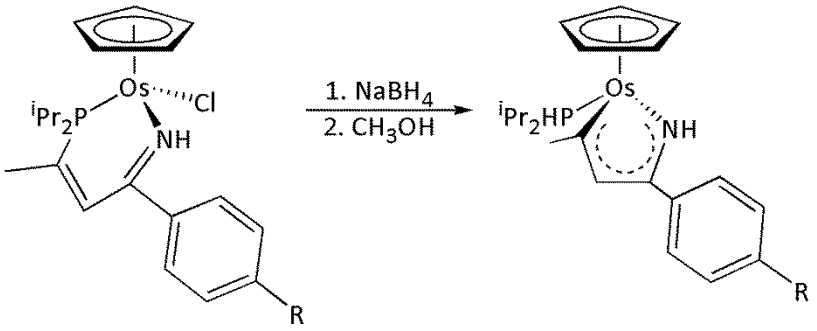

a ***b***

Scheme 1.20: Formation of metallopyrrole complexes from an imino-phosphine derivative, (where R = CH_3, H, Cl).

When the alkenyl-allenylidene complexes (where R = Ph, Cy) (a, Scheme 1.21) were heated at reflux in an acetonitrile solution, the 1-osma-4-hydroyclopenta[*c*]pyrrole complexes were generated (***f***, Scheme 1.21).[145] The mechanism of formation for the osmacyclopentapyrrole complex involved an initial migratory insertion of the allenylidene ligand into the osmium-alkenyl bond to generate an allenyl complex (***b***, Scheme 1.21) The resulting allenyl complex (***b***, Scheme 1.21) in the presence of acetonitrile resulted in the coordination of another acetonitrile molecule (***c***, Scheme 1.21). Electrophilic addition of the acetonitrile molecule produces the metallopyrrole complex (***d***, Scheme 1.21) and a final ring closure (***e***, Scheme 1.21) and protonation generates the product.

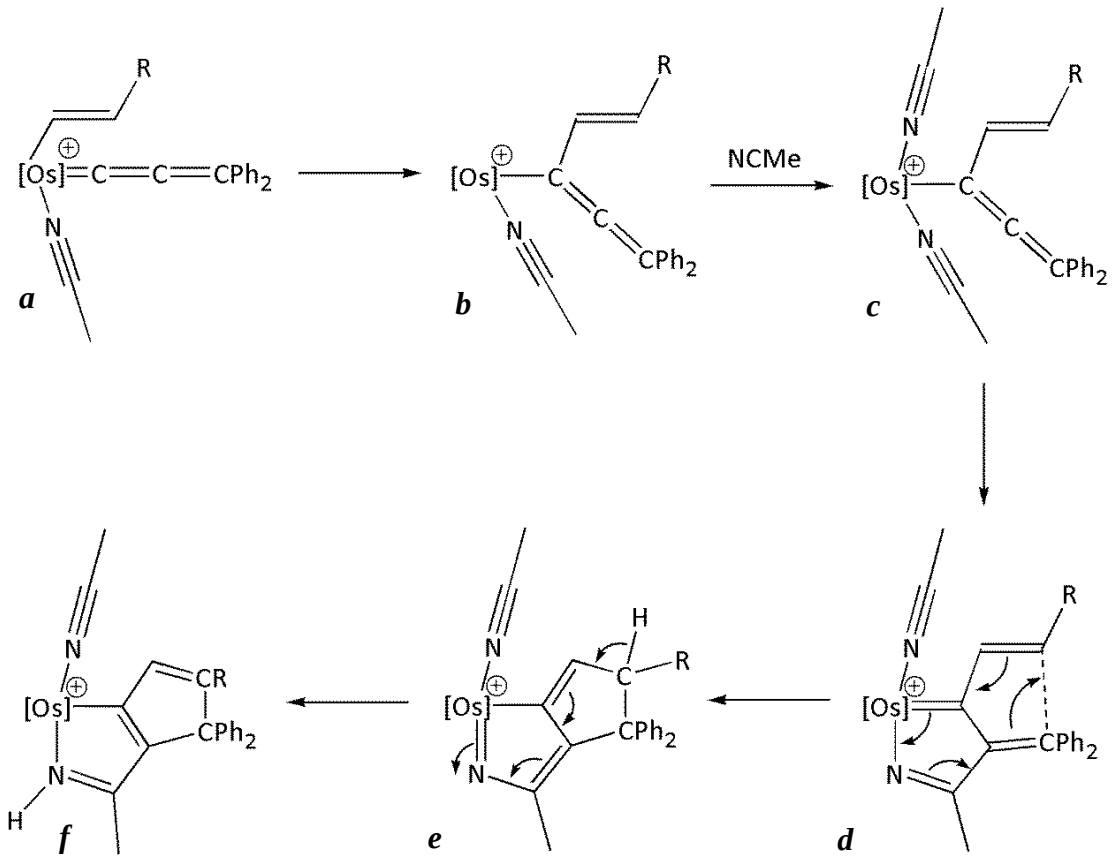

Scheme 1.21: Reaction mechanism proposed for the formation of the osmacyclopyrole derivatives, where [Os] = $[Os(P^iPr_3)_2(NCMe)]$ and R = Ph or Cy.

Significant data on the nature of complexes (***f***, Scheme 1.21) were obtained from the IR spectra, $^{13}C\{^1H\}$ NMR spectra and an X-ray structure of the phenyl analogue.[145] The geometry was described as a distorted octahedron, where the osmacyclopentapyrrole fragment has been described to contain a low level of aromaticity (opposite to Figure 1.8). This was demonstrated in the distinct carbon-carbon bond lengths. The $^{13}C\{^1H\}$ NMR spectra exhibits the carbon atom coordinated to the osmium centre between 204 – 210 ppm, which is approximately 20 ppm higher field than the previously mentioned metallapyrrole complex (***b***, Scheme 1.20).

1.6.2 Iridium-containing metallacycles

Carmona *et al.* published the synthesis of an iridapyrrole complex (***b***, Scheme 1.22) from the $Tp^{Me2}Ir(C_2H_4)_2$ complex, where Tp^{Me2} = hydro*tris*(3,5-dimethylpyrazolyl) borate (***a***, Scheme 1.22).[146-148] The reaction mechanism was proposed to involve a intramolecular [3+2] cycloaddition reaction of the iridium-vinyl and acetonitrile fragments. The formation of the iridapyrrole complex was catalysed by the presence of water and therefore suggested that the iridapyrrole species (which is not usually detected) may act as a reactive intermediate. The characteristic qualities of the IrNCCC ring was determined by NMR spectroscopy and X-ray crystallography. The $^{13}C\{^1H\}$ NMR spectra demonstrated that the carbon atom bound directly to the iridium centre resonated at 191.3 ppm, and was characteristic of the carbon atom being in between the resonances expected for those belonging to a metal carbene and vinyl complex. In addition, the short bond lengths around the iridapyrrole ring suggested the electron density was delocalised.

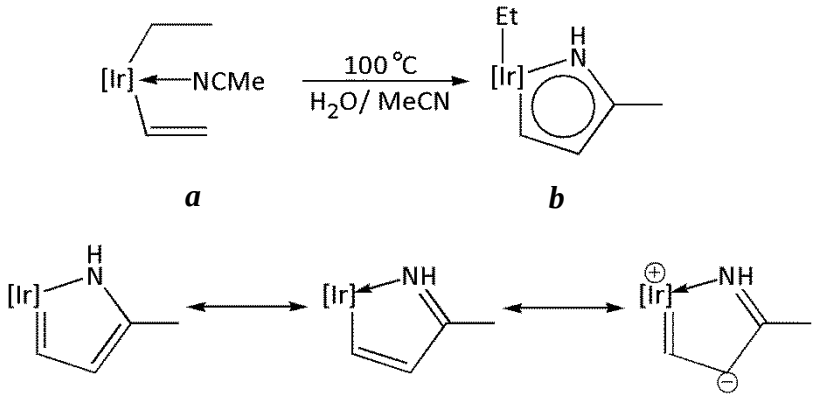

Scheme 1.22: Synthesis of an iridapyrrole complex, where [Ir] = where $Tp^{Me2}Ir$.

The iridium metallapyrrole complexes differ to those mentioned for the osmium system where a low degree of electron delocalisation was mentioned. However, in both of these systems the carbon atoms bonded directly to the metal centres display partial double bond character.

1.6.3 Ruthenium-containing metallacycles

Several ruthenium metallacycles which incorporate a nitrogen heteroatom have been reported in the literature. The preparation and properties of a ruthenapyrrolinone and a ruthenapyrrole complex will be described.

The reaction of allenylidene ligand (***a***, Scheme 1.23) with diallylamine results in the formation of a new carbon-nitrogen bond (***b***, Scheme 1.23).[149] This process presumably occurring by nucleophilic attack at the electrophilic α-carbon atom. Nucleophilic attack of a nitrogen donor at an electron deficient α-carbon atom of ruthenium vinylidene ligands have been reported in the literature (Section 1.4.4). The addition of base NaOMe, generates a ruthenapyrrolinone species (***c***, Scheme 1.23). The ruthenapyrrolinone ring exhibits a delocalisation of electron density around the Ru-C-N bond, where the resonance form on the right hand side displays a more accurate description of the bonding (Scheme 1.23). The $^{13}C\{^{1}H\}$ NMR chemical shifts of the carbon atoms Ru-*C*-N and Ru-*C*-O were 262.2 and 259.8 ppm respectively, where the structure has been described to have an amino-carbene nature.

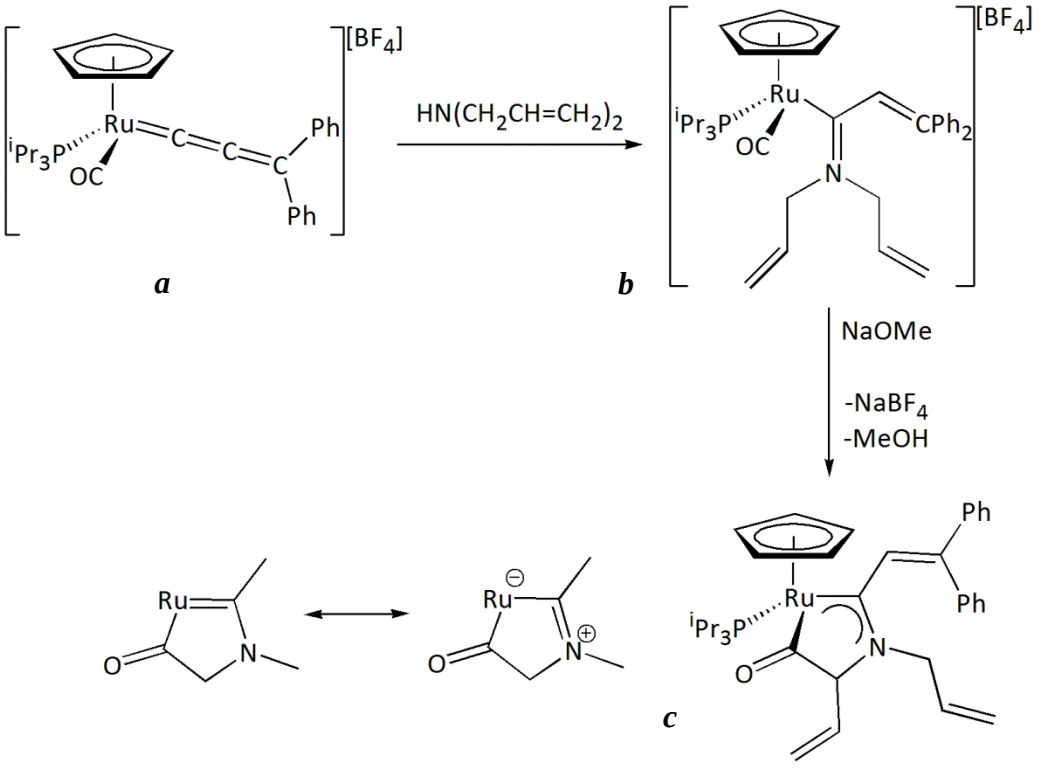

Scheme 1.23: Synthesis of the ruthenapyrrolinone complex ***c***.

The 1,3-ruthenapyrrole complex in Figure 1.9 was prepared from by a dinuclear ruthenium complex $[Ru_2(\mu\text{-}CN(Me)CH_2Ph)(\mu\text{-}CO)(CO)_2(\eta^5\text{-}C_5H_5)][SO_3CF_3]$.[150] The $^{13}C\{^1H\}$ NMR spectrum of the RuCNCC ring displayed characteristic resonances at 217.3 (Ru*C*N), 152.6 (N-*C*-C) and 98.0 (Ru-*C*-C) ppm. The respective iron (II) complex similar to the structure in Figure 1.9 was also synthesised, where the $^{13}C\{^1H\}$ NMR spectrum exhibited similar peaks. The X-ray structure of the iron (II) complex, suggested the Fe-*C*-N atom possesses a diaminocarbene character (bond lengths of iron-carbon and carbon-nitrogen were 1.937(5) and 1.356(6) Å respectively), where as the Fe-*C*-C atom was described as an enamide anion (bond lengths of iron-carbon and carbon-carbon were 1.967(5) and 1.309(7) Å respectively).

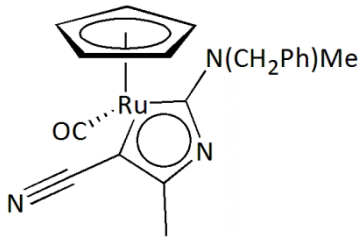

Figure 1.9: Diagram of the ruthenapyrrole species.

The spectroscopic data of the ruthenium metallapyrrole complexes described here have demonstrated that the Ru-*C*-N carbon atom exhibits an amino-carbene characteristic. However, the data for the remaining carbon atoms in the metallapyrrole is dependent on the substituents present.

1.7 *N*-Heterocyclic Carbenes (NHCs)

1.7.1 Conventional *N*-heterocyclic carbene ligands

Transition metal complexes containing NHC ligands have made a considerable contribution to the development of catalytic systems,[151] such as the ruthenium-mediated olefin metathesis[10, 12, 152-155] and palladium-catalysed cross-coupling reactions.[13, 14] The most commonly employed *N*-heterocyclic carbenes (NHCs) employed in transition metal chemistry are the imidazol-2-ylidene class of ligands.[156] There are three common methods to prepare these ligands, which include: i) deprotonation of the azolium salt; ii) reductive sulphurisation and iii) thermal α-elimination (Scheme 1.24).[157] The strong σ donor properties and adaptability of the steric influence at transitions metal centres has made them ideal ligands.[151]

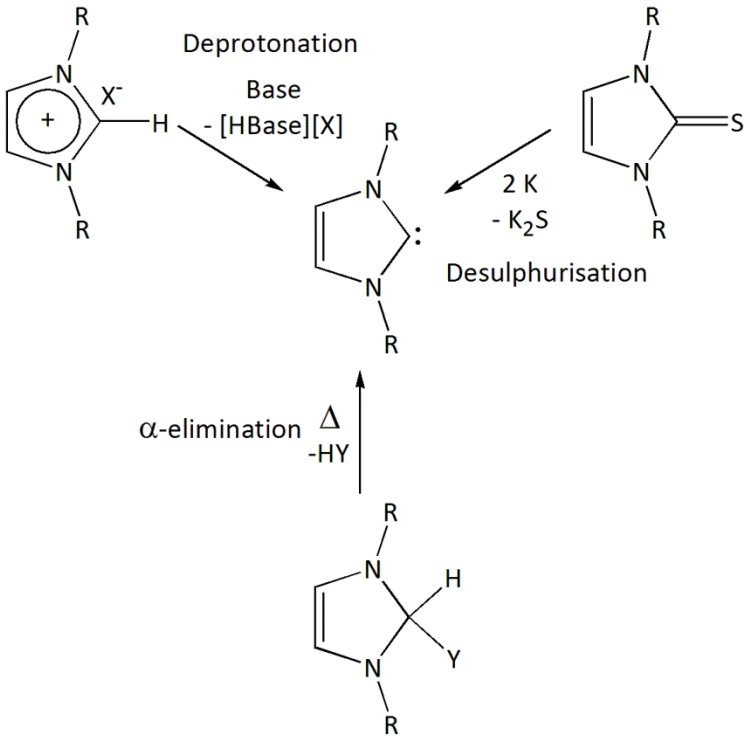

Scheme 1.24: Potential methods to synthesise imidazol-2-ylidene ligands.

The electronic configuration in NHCs determines the reactivity that will be observed. The carbene carbon atom in $:CR_2$ can orientate itself in several geometries (linear, bent) which affects the relative energies of its orbitals (Figure 1.10). A linear carbene is an extreme case which is sp-hybridised and contains two non-bonding, degenerate p_x and p_y orbitals. However, a bent carbene geometry is sp^2-hybridised, where the p_y orbital remains as a non-bonding orbital (also referred to as a p_π orbital). The remaining sp^2-hybridised orbital is stabilised, where it contains s-character and is referred to as a σ

orbital. For the sp^2-hybridised system the electron distribution could yield either a triplet or singlet carbene. The triplet carbene has been described to have a diradical character where two electrons of a parallel spin fill the σ and p_π orbitals ($\sigma^1 p\pi^1$). Alternatively, a singlet carbene involves the electrons filling the σ orbital in an anti-parallel orientation. Whether the singlet or triplet carbene state is present, is dependent on the size of the energy gap between the σ and p_π orbitals (an energy difference of 2 eV or higher results in the preference of the singlet carbene). Factors which control the size of this energy gap include the steric and electronic properties of the α substituents to the carbene carbon atom.[157, 158]

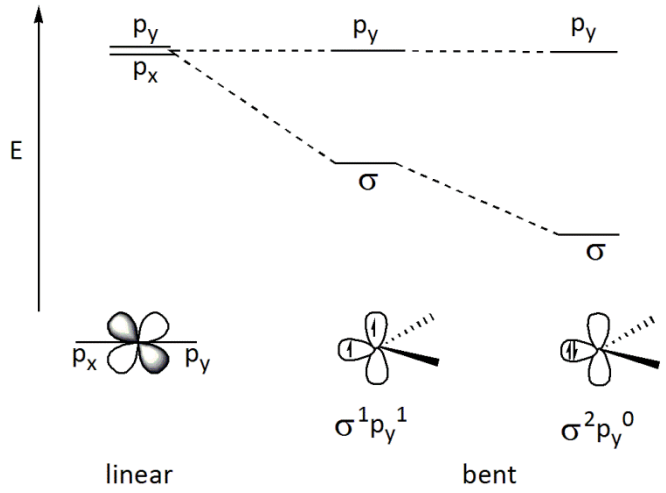

Figure 1.10: Electron configuration of the carbene atoms in the linear and bent geometries.

The two adjacent nitrogen atoms in an NHC ligand stabilise the carbene tautomer though a mesomeric effect, where the π electrons at the nitrogen atoms interact with the p_y orbital raising the energy of this orbital (Figure 1.11).[159, 160] The consequence is the energy gap between the σ and p_y orbital increases and therefore the singlet state is stabilised. When considering the bonding in NHC ligands, they are acknowledged as being stronger σ-donors but weaker π-acceptor ligands relative to phosphine ligands.[154, 161-163] Additionally, a small contribution from the electron density in the π C-N bond has been shown to interact with transition metal centres.[164, 165]

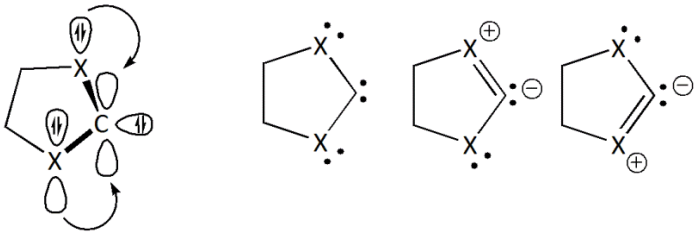

Figure 1.11: Schematic representing stabilisation provided by adjacent nitrogen atoms to the carbene atom.

1.7.2 Rhodium-catalysed transformations *via* C-H activation

Catalytic C-H activation by transition metal centres and functionalisation of these organic molecules to synthesise new carbon-carbon or carbon-heteroatom bonds holds many advantages, for example reducing the number of reaction steps to obtain an organic molecule by avoiding the need to synthesise pre-functionalised reagents allows for cheaper production of compounds and more readily accessible starting materials.[166] In addition, unwanted potentially toxic by-products are avoided.[167] Bergman *et al.* have reported extensive literature on the functionalisation of rhodium *N*-heterocyclic carbene complexes.[167, 168] These complexes have been used in coupling reactions for the alkylation of pyridine[169] and other N-containing heterocycles,[170] arylation of azoles,[171] synthesis of functionalised pyridines[168, 171-174] and piperidines[175] which play key roles in biological systems. In addition to rhodium (I) complexes their reactions have also included the less commonly used rhodium (III) complexes.[176, 177]

Bergman *et al.* have also stated that it is crucial to understand the mechanism through which these reactions occur in order to develop more active catalytic systems.[168, 178] Therefore, a mechanistic study for the synthesis of *N*-heterocyclic carbene rhodium complex (***b***, Scheme 1.25) was reported by Bergman *et al*. This provided significant information on the C-H activation pathway and therefore the formation of the NHC ligands which are known to undergo coupling reactions. A mechanism-driven approach employing experimental techniques such as isotopic labelling and rate studies and theoretical computational studies were employed to identify potential intermediates. The reaction between $[RhCl(PCy_3)_2]$ (***a***, Scheme 1.25) and 3-methyl-3,4-dihydroquinazoline yielded an NHC complex where a C-H activation occurred and the proton was transferred to the nitrogen atom.

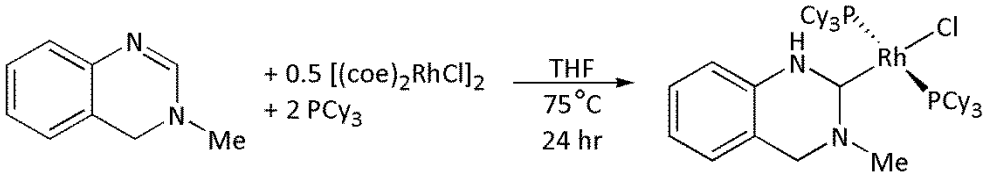

a ***b***

Scheme 1.25: Reaction of $[RhCl(PCy_3)_2]$ and 3-methyl-3,4-dihydroquinazoline.

A potential intermediate was identified at a lower reaction temperature as the N-coordinated complex (***b***, Scheme 1.26), which was confirmed through the use of ^{15}N and ^{13}C isotope labelling experiments. To determine the role of the N-coordinated complex two reactions were designed; one which looked at the reaction of $[(PCy_3)_2RhCl]$ (***a***, Scheme 1.26), with the N-heterocycle; and one which began with the N-coordinated heterocycle. They noted the former reaction established a rapid equilibrium with the N-coordinated species; and that both reactions yielded the C-H activated species (***c***, Scheme 1.26). Kinetic rate studies determined that the N-coordinated species was an intermediate in the C-H activation mechanism. A double-labelling crossover experiment determined that the C-H activation step occurred in an intramolecular fashion.[178]

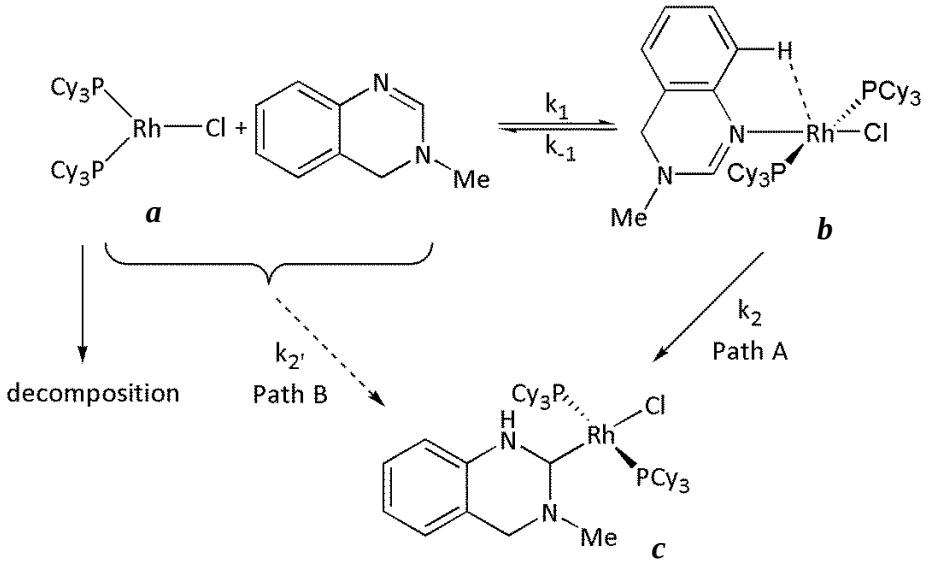

Scheme 1.26: Potential mechanisms for the formation of the rhodium-NHC complex.

1.7.3 Non-conventional *N*-heterocyclic carbenes: Pyridylidenes

There has been an increase in attention focussed on the preparation of non-conventional NHC ligands in the literature, due to the success of traditional NHCs. This has led to investigations being conducted on a variety of non-conventional NHC ligands. This section will discuss the properties of pyridylidene ligands, which are the carbene forms of six-membered N-containing heterocycles which contain only one nitrogen atom (Figure 1.12).[179-181] This section will become more relevant later in this thesis, as novel ruthenium pyridylidene-containing complexes have been synthesised.

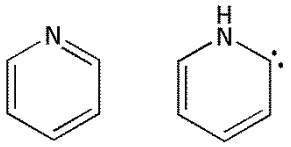

Figure 1.12: Pyridine and pyridylidene.

Accessing the tautomeric forms of pyridines were first mentioned in the 1930's by Hammick *et al*. where it was proposed that a radical intermediate played a role in the decarboxylation of the carboxylic acids of pyridine, quinoline and isoquinoline.[182, 183] Since then a wide range of potential routes to access pyridylidenes have been described.[180] Some of these methods include the N-functionalisation of pyridyl ligands,[184] oxidative addition of halide-substituted pyridine molecules,[185, 186] deprotonation of a C-H bond of pyridinium salts[187-190] and the tautomerisation of pyridine by transition metal complexes (Section 1.8).

Schwarz *et al.* later identified that a one electron reduction of pyridine produced the 2-carbene tautomer of pyridine in the gas phase and provided experimental and theoretical evidence (Figure 1.13).[191, 192] The theoretical studies demonstrated that the 2-carbene tautomer of pyridine is approximately 188 - 209 kJ mol^{-1} higher in energy than pyridine. The gas-phase intramolecular isomerisation between pyridine and its 2-carbene tautomer was calculated to have a transition state of approximately 356 kJ mol^{-1} relative to pyridine. This high barrier suggested an isomerisation between the two forms under these conditions was not likely to occur, however in the condensed phase intermolecular processes are more likely to intervene.[193] The 3- and 4- carbene isomers of pyridine have also been investigated, where these tautomers are even higher in energy than the 2-carbene form at approximately 251 kJ mol^{-1}.

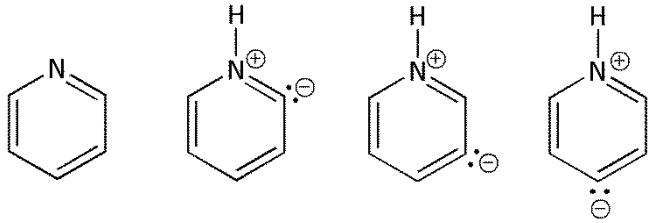

Figure 1.13: The tautomeric forms of pyridine.

Recently, pyridylidenes have been coupled to imidazolidene or triazolylidene ligands at transition metal centres in order to study the potential coordination modes and achieve ligands with strong σ-donor properties.[194] Some examples of these complexes describe these ligands as being robust and easily handled in the presence of air- and moisture.[195,

[196] Applications of these ligands include them being potential hydride carriers[195, 196] or for water oxidation.[197]

1.7.4 The nature of the metal-carbon bond in pyridylidene complexes

The bonding of pyridylidene ligands to transition metal centres has been analysed by a range of spectroscopic techniques including IR, $^{31}P\{^{1}H\}$, $^{13}C\{^{1}H\}$ NMR spectroscopy and X-ray crystallography.[198-200] Additionally, computational studies are also a useful tool in determining the metal ligand interactions.[181]

The bonding of pyridylidene ligands to transition metal centres has been studied by Frenking *et al*. The reported experimental and theoretical investigations are based around the Group 10 transition metal centre complexes, $[M(PPh_3)_2Cl(C_5H_4NMe)]$ (where M = Ni, Pd and Pt).[200-202] The $^{13}C\{^{1}H\}$ NMR data demonstrated that upon metallation the carbon bound to the metal centre (Ni, Pd) undergoes a deshielding effect. In the 2-pyridylidene complexes, the carbon atom at the 2-position exhibited δ_c resonances at approximately 190 ppm, where as for 2-choloropyridine the respective carbon atom is observed at 151.5 ppm.[200] Similar observations were reported by Bercaw *et al.* with a range of $[Pt(CH_3)L(N\text{-}(2\text{-pyridyl})\text{-R-pyridine-2-ylidene})]$ complexes (where R = 4-H, 4-NMe_2, 4-^{t}Bu and L = CO, DMSO), where downfield $^{13}C\{^{1}H\}$ NMR resonances were observed between 160-175 ppm.[188]

An investigation into an X-ray structure of $Ni(PPh_3)_2Cl(C_5H_4NMe)$ (left, Figure 1.14) demonstrated that the N(1)-C(6) and C(2)-C(3) bond lengths were longer with respect to pyridine and therefore suggested a diene type structure.[200] The bond lengths were found to follow a similar pattern to 2-pyridone (right, Figure 1.14). Interestingly, the M-C bond lengths to the carbon atom of the NHC ligand did not necessarily always correlate to the calculated bond energies.[202, 203]

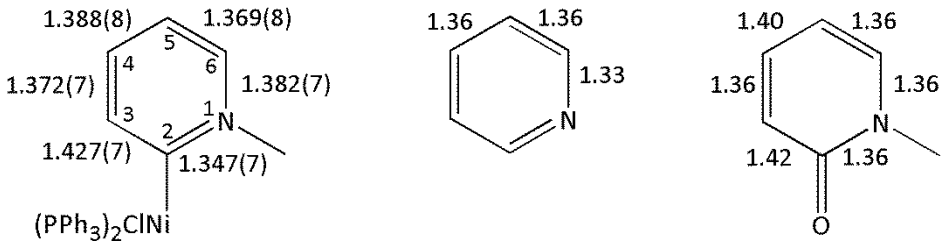

Figure 1.14: X-ray structure comparison of the pyridylidene ligand in $Ni(PPh_3)_2Cl(C_5H_4NMe)$, pyridine and 2-pyridone.

DFT studies by Frenking *et al.* on the [MCl(PH_3)L] complexes, (where M = Ni, Pd, Pt and L = *N*-heterocyclic carbene ligand) were conducted (Figure 1.15). It was established that there was a significant σ bonding interaction in the pyridylidene complexes, which resulted in an electrostatic interaction. In addition, there was also a smaller π back-bonding interaction present in these complexes. The HOMO of the ligands was considered to be the σ lone pair on the carbon atom of the pyridylidene ligands. Overall, these studies highlighted there was a 'non-negligible M=C bond' present in these systems.[200, 202]

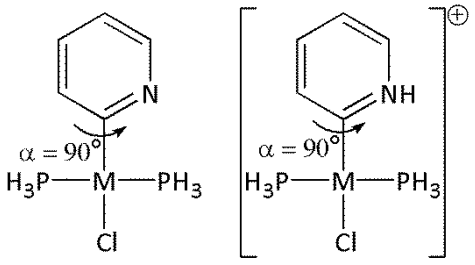

Figure 1.15: Square planar metal complexes used for DFT calculations to determine the nature of the metal-carbene bond, where M = Ni, Pd, Pt.

Raubenheiner *et al.* compared the bonding of different NHC ligands, a six-membered 4-pyridylidene (left, Figure 1.16) and a five-membered imidazolin-2-ylidene (right, Figure 1.16) at a palladium (II) transition metal centre using DFT calculations. It was determined that the σ orbital (HOMO) of the carbene atoms was higher in energy (1.28 eV) for the 4-pyridylidene complex and therefore a better σ donor. Additionally, the π back-bonding ability in the imidazolin-2-ylidene system was more limited with respect to the 4-pyridylidene ligand.[204]

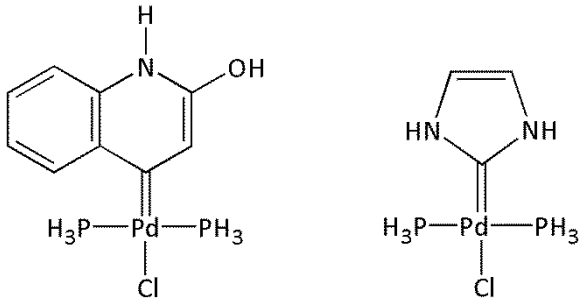

Figure 1.16: Comparisons between a six-membered NHC and five-membered NHC ligand at a palladium (II) centre.

1.8 Tautomerisation of pyridine by transition metal centres

Literature on the tautomerisation of pyridine and substituted pyridines by transition metal centres is not extremely common. Major contributions regarding the 2-carbene tautomers of pyridine from 2-substituted pyridines have been made from the research groups of Carmona and Esteruelas *et al*. The most commonly employed transition metal centres are iridium and osmium, however some ruthenium examples have been reported to successfully yield the respective 2-carbene tautomer of pyridine.[205] In a similar fashion to the alkyne-vinylidene tautomerisation, transition metal centres may be employed to reduce the activation barrier to access the tautomers of pyridine and their reactivity observed. The formation of pyridylidene ligands through this method is proposed later in this thesis.

1.8.1 Synthesis and reactivity of iridium pyridylidene complexes

Carmona *et al*. have reported a library of iridium (III) N-heterocyclic carbene (NHC) complexes. The synthesis of the NHC ligands from pyridine and substituted pyridines was achieved by heating the N-containing heterocycles in the presence of an unsaturated 16-electron iridium (III) complex.[206-208] The commonly employed starting materials included $[Tp^{Me2}Ir(C_6H_5)_2(N_2)]$ and $[Tp^{Ms"}Ir(N_2)]$ (where Tp^{Me2} = hydrotris(3,5-dimethylpyrazolyl)borate and $Tp^{Ms"}$ = a dimetallated hydrotris(3-mesitylpyrazol-1-yl) borate), where substitution of the N_2 ligand by the incoming N-containing heterocycles occurs (Figure 1.17).

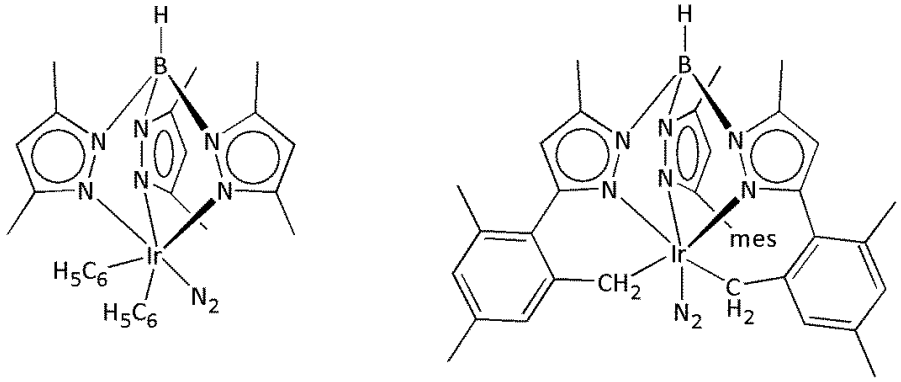

Figure 1.17: Iridium(III) precursors $[Tp^{Me2}Ir(C_6H_5)_2(N_2)]$ (left) and $[Tp^{Ms"}Ir(N_2)]$ (right).

1.8.1.1 Reactivity observed with 2-substituted pyridines

The reaction of various 2-substituted pyridines with $[Tp^{Me2}Ir(C_6H_5)_2(N_2)]$ (***a***, Scheme 1.27) yielded iridium NHC complexes where the C-H bond at the 2-position of the aromatic molecules was activated and the hydrogen atom is transferred to the nitrogen atom (***b***, Scheme 1.27). High yields of the iridium-NHC complexes were obtained with the bulkier R substituents ^{t}Bu, NMe_2, $SiMe_3$ under milder conditions (60 °C). However, when R = Me, Ph and C(O)Me, higher reaction temperatures of 90 °C were required to access the 2-carbene tautomer, as lower reaction temperatures generated the kinetic product, the N-bound complex.[206-208] Additionally, the 2,3-substituted pyridine, quinoline reacted in a similar method to 2-methylpyridine and has also been extended to polypyridine ligands to form the corresponding pyridylidene complexes.[209-211]

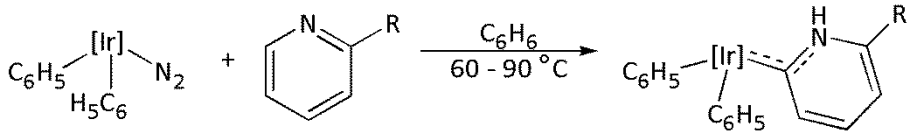

a ***b***

Scheme 1.27: Reaction of 2-substituted pyridines with $[Tp^{Me2}Ir(C_6H_5)_2(N_2)]$, where [Ir] = $Tp^{Me2}Ir$ and R = Me, Ph, ^{t}Bu, NMe_2, C(O)Me, $SiMe_3$.

A potential rationalisation given for the formation of these N-heterocyclic carbene complexes from the 2-substituted pyridine molecules was due to decreased activity of the Lewis base due to an increase in steric demand at the 'front' of the Lewis base (otherwise known as 'F-strain').[212] The steric strain destabilises the N-bound isomer, therefore generating the iridium (III) NHC complexes. The iridium (III) NHC complexes ***b*** (Scheme 1.27) display characteristic spectroscopic data. The $^{13}C\{^1H\}$ NMR spectrum displays resonances for the carbene atom between 170 - 180 ppm. Additionally, the X-ray crystallography data for the iridium-carbon bonds of the NHC complexes are between 1.98 - 1.99 Å (e.g. R =Me 1.982(2) Å, R = Ph 1.978(3) Å), which is significantly shorter than an iridium-carbon bond for a phenyl complex, where an expected bond length is approximately 2.05 Å.[213]

Additionally, Esteruelas *et al.* have studied the behaviour of the iridium complexes $IrHCl_2(P^iPr_3)_2$ (***a***, Scheme 1.28) and $IrCl(\eta^2\text{-}C_8H_{14})(P^iPr_3)_2$ with several N-containing heterocycles (quinoline, 8-methylquinoline, 2-methylpyridine, benzo[*h*]quinoline).[214] The hydride containing complex $IrHCl_2(P^iPr_3)_2$ (***a***, Scheme 1.28) reacts with the N-containing heterocycles to produce the respective iridium (III) NHC complexes, which are stabilised by a N-H--Cl hydrogen bond (***b***, Scheme 1.28). The spectroscopic data

exhibited a characteristic iridium-carbon bond length of approximately 1.99 Å and in the $^{13}C\{^{1}H\}$ NMR spectrum the carbene carbon atoms were observed between 165 – 175 ppm. Interestingly, it was found that the lack of a hydride atom at the metal centre in $IrCl(\eta^2\text{-}C_8H_{14})(P^iPr_3)_2$ rendered the complex unable to generate the NH tautomer. A proposed mechanism involved an initial hydrogen migration from the iridium centre to the nitrogen, followed by a C-H bond activation at the 2-position of the N-containing heterocycle to give the final metal NHC product. The presence of a hydride atom at the iridium centre displayed significant changes in reactivity between the N-bound and C-bound tautomers.

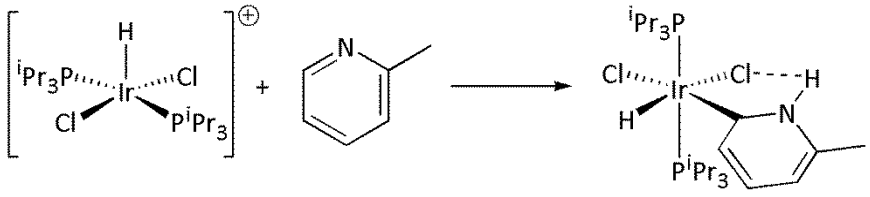

a ***b***

Scheme 1.28: Reactivity observed between $IrHCl_2(P^iPr_3)_2$ and 2-methylpyridine.

1.8.1.2 Synthesis of unsubstituted iridium pyridylidene complexes

Carmona *et al.* have studied the reaction of unsubstituted pyridine with $[Tp^{Me2}Ir(C_6H_5)_2(N_2)]$ which produced only the N-bound isomer (even when heated to 150 °C). Similar observations were also found when either an NMe_2 or CF_3 substituent was present at the 4-position. However, when the reaction was conducted in an excess of pyridine or 4-substituted pyridines at elevated temperatures and for long periods of time the N-bound complex is the only product, suggesting it is the thermodynamic product of this reaction.[208]

The reaction between $[Tp^{Ms}Ir(N_2)]$ (***a***, Scheme 1.29) and pyridine, results in a mixture of products of the N-coordinated adduct (***b***, Scheme 1.29), and the NHC complex (***c***, Scheme 1.29) The two species did not convert between each other, hence it could be concluded that there are two competitive reactive pathways occurring and that the N-coordinating adduct was not an intermediate species. The C-H activation step was studied in more detail in an attempt to better understand the mechanism. The kinetic isotope effect was studied by comparing the rates of reaction with NC_5H_5, and NC_5D_5, and found a k_H/k_D of 2.0 (±0.2) for the C-H activation route, making this the rate-limiting step. The N-coordinated adduct did not lose any of its deuterium atoms,

indicating this is not involved in the mechanism for the formation of the NHC isomer.[207, 208]

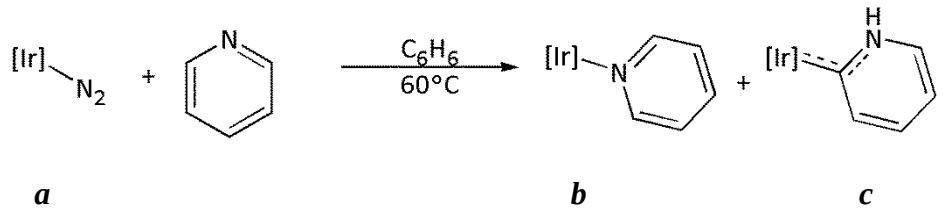

a ***b*** ***c***

Scheme 1.29: Reaction of [Tp^{Ms}Ir(N_2)] and pyridine.

An alternative route to the iridium (III) NHC complex of pyridine was achieved through further reactivity of the complex where R = $SiMe_3$ (***a***, Scheme 1.30). The addition of NaOH removes the $SiMe_3$ group to generate the pyridylidene complex (***b***, Scheme 1.30).

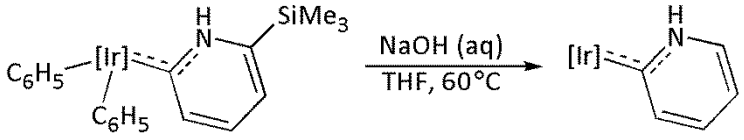

a ***b***

Scheme 1.30: Alkaline hydrolysis to produce an unsubstituted iridium pyridylidene complex, where [Ir] = Tp^{Me2}Ir.

1.8.1.3 Determining the mechanism for the formation of the iridium pyridylidene complexes

Theoretical calculations on the experimental findings for the tautomerisation of 2-substituted pyridines were conducted by Carmona *et al.* The stability of the unsubstituted pyridine complex with its carbene tautomer (***c***, Scheme 1.29) revealed that the N-bound isomer (***b***, Scheme 1.29) was 17.1 kJ mol^{-1} more stable. However, for 2-methylpyridine the opposite stability was observed, where the pyridylidene complex was more stable by 15.1 kJ mol^{-1} (and therefore is considered the thermodynamic product).[208]

The tautomerisation mechanism to the pyridylidene complex was determined to proceed *via* a σ-complex assisted metathesis mechanism (σ-CAM) (Scheme 1.31). From the σ-C-H coordination of 2-methylpyridine species (***b***, Scheme 1.31), the tautomerisation involves a hydrogen migration of the C-H bond of the 2-methylpyridine molecule to the neighbouring coordinated C_6H_5 group, to produce a σ-bound C-H benzene intermediate

(***c***, Scheme 1.31). A subsequent hydrogen migration to the pyridylic nitrogen atom then generates the iridium (III) NHC complex (***d***, Scheme 1.31). [208]

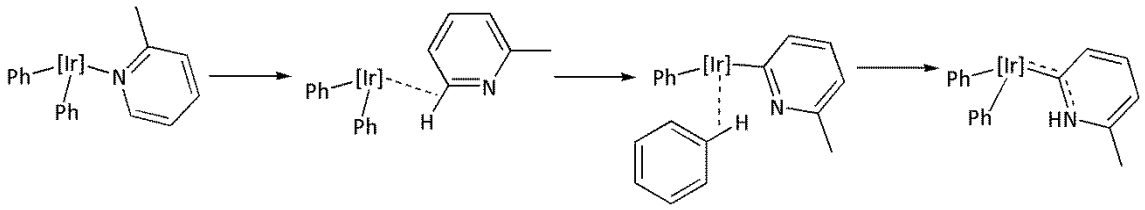

a ***b*** ***c*** ***d***

Scheme 1.31: Proposed σ-CAM mechanism for the formation of the iridium pyridylidene complex of 2-methylpyridine, where [Ir] = $Tp^{Me2}Ir$.

Li *et al.* reported that the iridium (I) pyridylidene complexes (Figure 1.18) originating from 2,3-bipyridyl ligands, a δ_C for the carbene carbon atoms were in the range of 175 - 180 ppm (consistent with those reported by Carmona *et al.*). These complexes were found to be stabilised by two factors, a chelation effect and a hydrogen bond between the N-H group and the oxygen atom of the tethered amide group on the basis of DFT calculations. Li *et al.* proposed a mechanism in which the formation of the complexes (left, Figure 1.18) was assisted by the presence of water in the reaction mixture. The water molecules catalyse the reaction by allowing protons to be transferred from the C-H bond to a hydrate intermediate (right, Figure 1.18), where a subsequent proton transfer yields the pyridylidene complex (left, Figure 1.18).[215, 216]

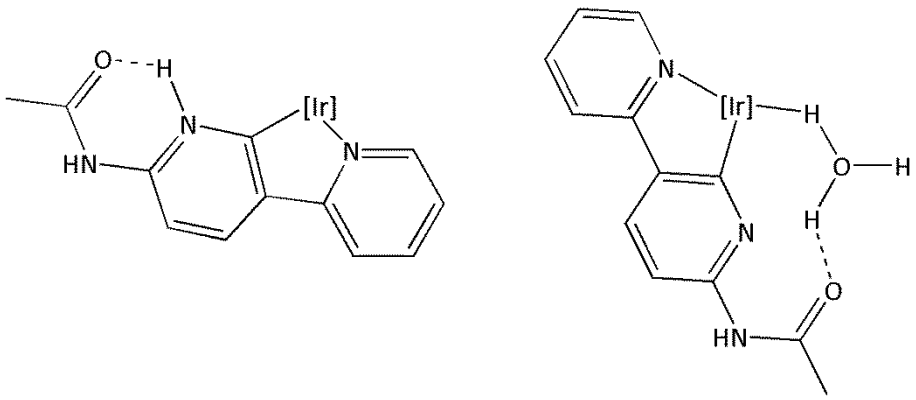

Figure 1.18:Left: Iridium (I) pyridylidene complex stabilised by a hydrogen bonding, where [Ir] = Ir(COD); Right: Hydrate intermediate proposed by DFT mechanism, where [Ir] = Ir(COD).

1.8.1.4 Reactivity of the iridium pyridylidene complexes

Carmona *et al.* also studied the reactivity of complex [Tp^{Me2}Ir(Ph)$_2$(pyridylidene)] with ethene, propene and acetylene, to give respective iridacyclic pyridylidene complexes (Scheme 1.32). The reaction of [Tp^{Me2}Ir(Ph)$_2$(pyridylidene)] with ethene results in an irreversible, clean conversion to a five membered iridacycle complex (***b***, Scheme 1.32). However, the reaction of propene is reversible and the carbon-nitrogen bond formation proceeds in a regioselective manner (***c***, Scheme 1.32). The reversibility of these reactions is thought to be dependent on the strength of the carbon-nitrogen bond, where the C(H_2)-N bond is stronger relative to the C(HMe)-N bond. This was consistent with the inability to observe the respective iridacyclic complex when *tert*-butylethylene was used.[213, 217, 218]

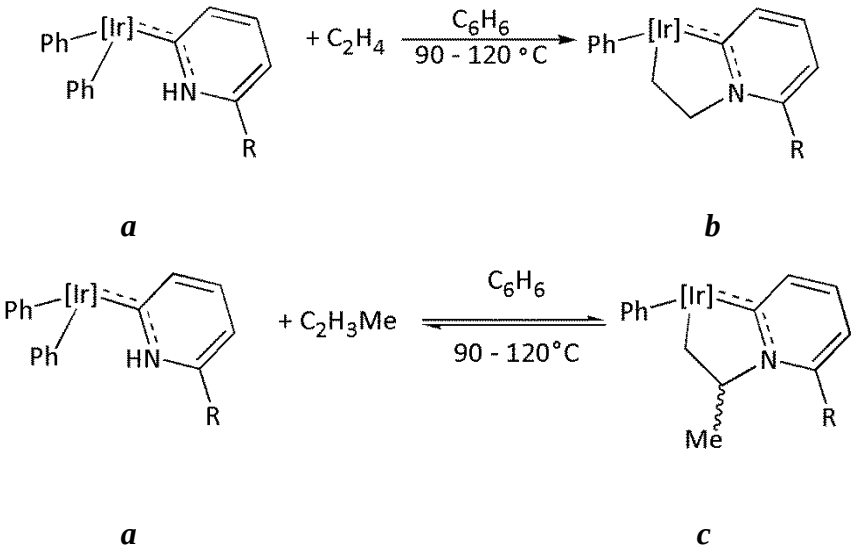

Scheme 1.32: Reactivity observed between [Tp^{Me2}Ir(Ph)$_2$(pyridylidene)] with ethylene (top) and propene (bottom), where R = Me or Ph and [Ir] = [Tp^{Me2}Ir].

The reaction from the addition of acetylene to complex [Tp^{Me2}Ir(Ph)$_2$(pyridylidene)] at 90 °C under anaerobic conditions produces a 4-membered iridacycle complex (***d***, Scheme 1.33). If an additional acetylene molecule is introduced a carbon-carbon coupling occurs between one of the phenyl rings and the acetylene molecule (***e***, Scheme 1.33).[213] A mechanism has been proposed by Carmona *et al.*, which proceeds *via* a vinylidene intermediate in a pyridylidene-assisted intramolecular fashion (based on work published by Grotjahn *et al.*, Section 1.4.3) and is corroborated with DFT studies quoting the free energies of the complexes.[217] An initial η^2-coordinated alkyne species (***b***, Scheme 1.33) undergoes a hydrogen atom migration to give an acetylide-pyridylidene complex, where the hydrogen atom is abstracted by the nitrogen atom of the pyridyl ligand (overcomes a transition state of 12.8 kJ mol^{-1}). The N-H hydrogen

atom then migrates to the β-carbon atom to give a vinylidene intermediate (***c***, Scheme 1.33) (where transition state is 18.1 kJ mol^{-1}). It is not unusual for ligands to assist in the formation of a metal vinylidene complex.[219, 220] The subsequent carbon-nitrogen bond formation was described as 'almost barrierless'.

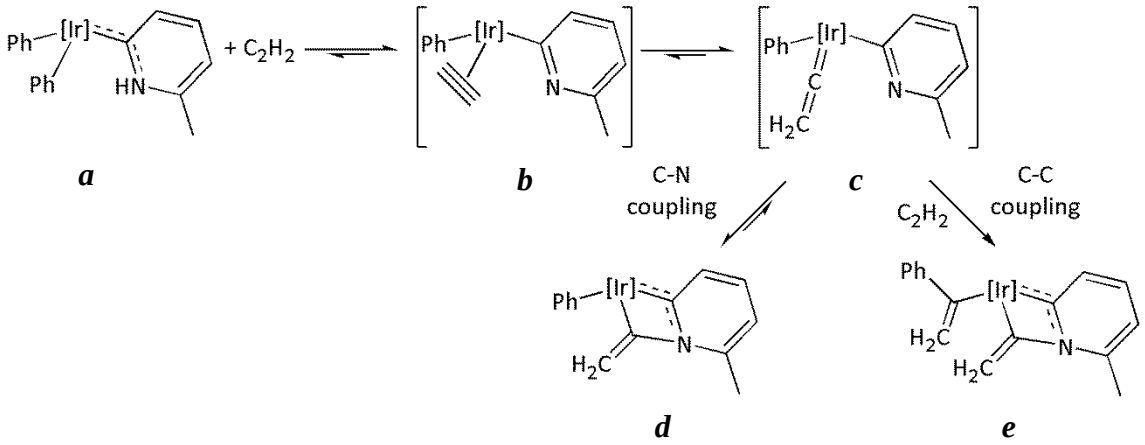

Scheme 1.33: Reaction of $[Tp^{Me2}Ir(Ph)_2(pyridylidene)]$ and acetylene, where [Ir] = $[Tp^{Me2}Ir]$.

1.8.2 Synthesis and reactivity of osmium pyridylidene complexes

An extensive set of osmium pyridylidene complexes have been reported by Esteruelas *et al*. The reaction of osmium (IV) and (VI) complexes $OsH_2Cl_2(P^iPr_3)_2$ and $OsH_6(P^iPr_3)_2$ with various N-containing heterocycles is now described.

1.8.2.1 Reactivity of 2-substituted pyridines

The dihydride Os(IV) complex $OsH_2Cl_2(P^iPr_3)_2$ generates the NH tautomers when reacted with 2,3-substituted pyridines (quinoline, 8-methylquinoline, benzo[*h*]quinoline)[221, 222] and 2-methylpyridine[223] (Scheme 1.34). The properties of the osmium pyridylidene complexes have been determined, where the δ_c of the carbon atom bound to the metal centre is observed between 182-200 ppm. X-ray structures of the NH tautomers exhibit a range of osmium-carbon bond lengths between 2.005(6) – 2.137(5) Å.[221] A key feature of these complexes is that the N-H bond forms an intramolecular hydrogen bond with a chloride or oxygen atom which stabilises the N-H tautomer.

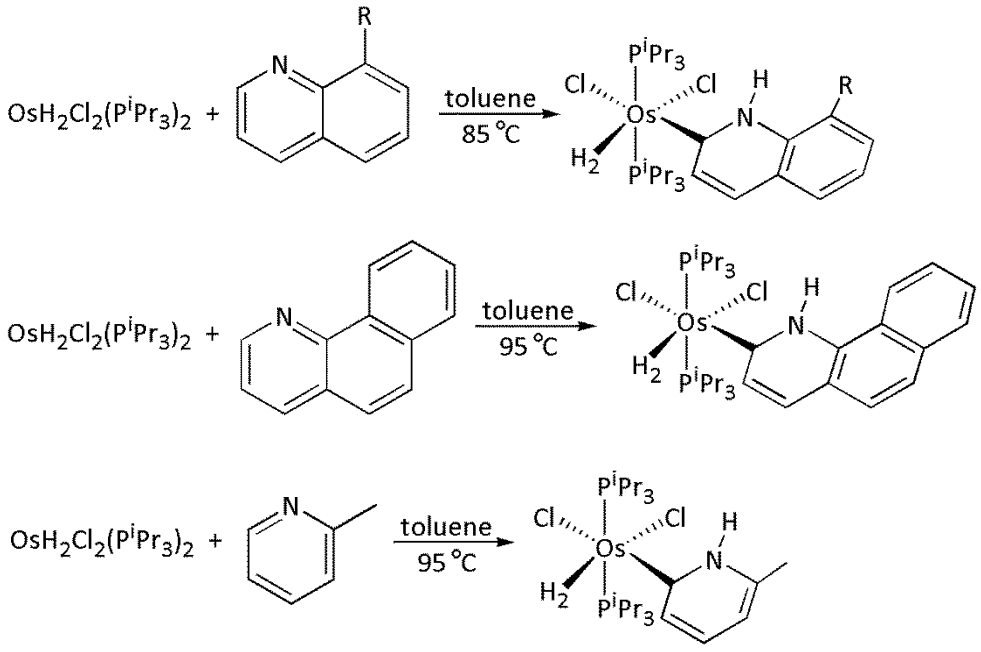

Scheme 1.34: Synthesis of osmium pyridylidene complexes from $OsH_2Cl_2(P^iPr_3)_2$ with top reaction: quinoline (R = H) and 8-methylquinoline (R = Me); middle reaction: benzo[*h*]quinoline and bottom reaction: 2-methylpyridine.

An alternative route from $OsH_6(P^iPr_3)_2$ and 2-vinylpyridine produces the osmium NHC complex of 2-ethylpyridine in the presence of benzophenone (***b***, Scheme 1.35).[224] In a similar manner to the previously reported complexes, the pyridylidene fragment is stabilised by an N-H- -O hydrogen bond to the orthometallated ketone ligand. The stability of this ligand was tested, and it was found that the 'retrotautomerisation' to 2-vinylpyridine is disfavoured with respect to the loss of the C-H activated ketone ligand (Scheme 1.35).

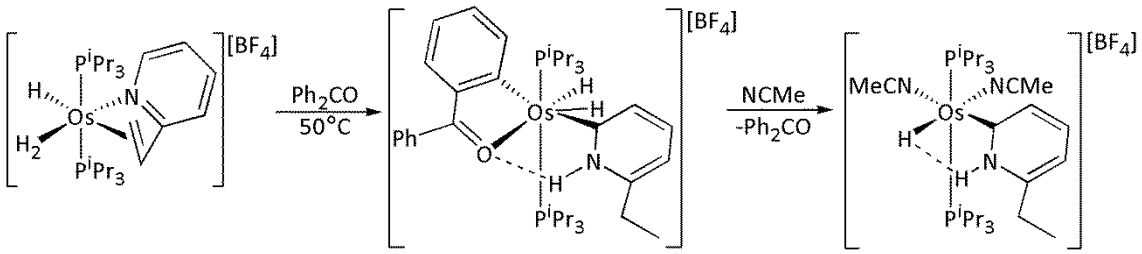

a ***b*** ***c***

Scheme 1.35: Osmium NH tautomer of 2-ethylpyridine.

Differences in reactivity towards the N-containing heterocycles have been reported. The reaction of the osmium (IV) complex, $OsH_2Cl_2(P^iPr_3)_2$ with 2-vinylpyridine does not produce the NH tautomer.[224, 225] Additionally, the reaction of the osmium (VI) complex, $OsH_6(P^iPr_3)_2$ with 2-methylpyridine does not yield expected the pyridylidene complex, instead a C-H activation at the position generates a η^2-(C,N) pyridyl complex (Figure 1.19).[224]

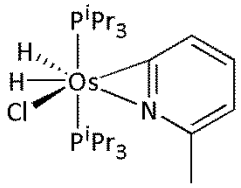

Figure 1.19: Formation of an η^2-(C,N) pyridyl complex.

1.8.2.2 Reactivity with unsubstituted pyridine

The reactions of pyridine with $OsH_2Cl_2(P^iPr_3)_2$ (***a***, Scheme 1.36) and $OsH_6(P^iPr_3)_2$ generates the N-bound complexes $OsCl_2(NC_5H_5)_3(P^iPr_3)$ (***b***, Scheme 1.36) [223] and $OsH_4(NC_5H_5)(P^iPr_3)_2$[226] respectively. These studies highlighted the importance of the substituent at the 2-position of the N-containing heterocycle, where a steric hindrance must be experienced between the 2-substituted pyridine and the metal complex to allow for the pyridylidene complex to be produced, consistent with results presented by Carmona *et al*.

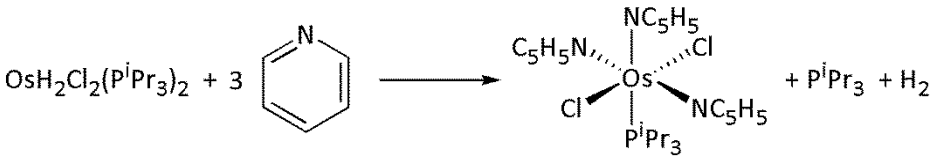

a ***b***

Scheme 1.36: Synthesis of $OsCl_2(NC_5H_5)_3(P^iPr_3)$.

1.8.2.3 Determining the mechanism for the formation of the osmium pyridylidene complexes

DFT calculations for the tautomerisation mechanism of the substituted pyridines (2-methylpyridine and quinoline) at the osmium centre $OsH_2Cl_2(PMe_3)_2$ were investigated by Esteruelas e*t al.*, where they quoted the changes in the free energy (ΔG). A general three step mechanism was reported involving an initial intermolecular hydrogen migration from the metal centre to the nitrogen atom of the heterocycle. A subsequent C-H activation at the 6-position of the protonated N-containing heterocycle, followed by a dihydride to dihydrogen tautomerisation. The systems with 2-methylpyridine and quinoline were both found to have different rate determining steps. The C-H activation at the 2-position in the case of 2-methylpyridine was the rate determining step, with a transition state of 30.2 kJ mol^{-1}. However, the respective step with quinoline was lower (22.1 kJ mol^{-1}), therefore making the intermolecular hydrogen migration the rate determining step. The differences in the two potential energy surfaces was attributed to the ability of quinoline to delocalise electron density within the ring and therefore results in a stabilisation effect.[214, 221, 223, 224, 226]

1.8.2.4 Reactivity of the osmium pyridylidene complexes

Esteruelas *et al.* recently reported the stoichiometric reaction of an $[OsTp(\kappa^1\text{-}OCMe_2)_2(P^iPr_3)][BF_4]$ complex (***a***, Scheme 1.37) with 2-methylpyridine in the presence of fluorobenzene to generate the osmium pyridylidene complex (***b***, Scheme 1.37).[227] This is consistent with the previously mentioned findings where the substituent in the 2-position promoted the tautomerisation to the NHC complex. The reaction of the pyridylidene complex (***b***, Scheme 1.37) with phenylacetylene produces the alkenylation product (***f***, Scheme 1.37). A reaction mechanism was proposed which involved the formation of an osmium pyridylidene-vinylidene complex (***c***, Scheme 1.37), which in the presence of a base deprotonates the vinylidene ligand to generate an alkynyl-pyridylidene species (***d***, Scheme 1.37). Upon heating complex (***d***, Scheme 1.37) the hydrogen atom on the nitrogen atom of the pyridylidene ligand is transferred to β-carbon of the alkynyl ligand to generate a pyridyl-vinylidene ligand (***e***, Scheme 1.37). Finally, the vinylidene ligand is proposed to undergo a 1,2-migratory insertion into the osmium-carbon bond to the pyridyl ligand to yield the alkenylation product (***f***, Scheme 1.37). The role of transition metal pyridylidene and vinylidene complexes as reactive intermediates in this reaction highlights their applications in the formation of new carbon-carbon bonds.

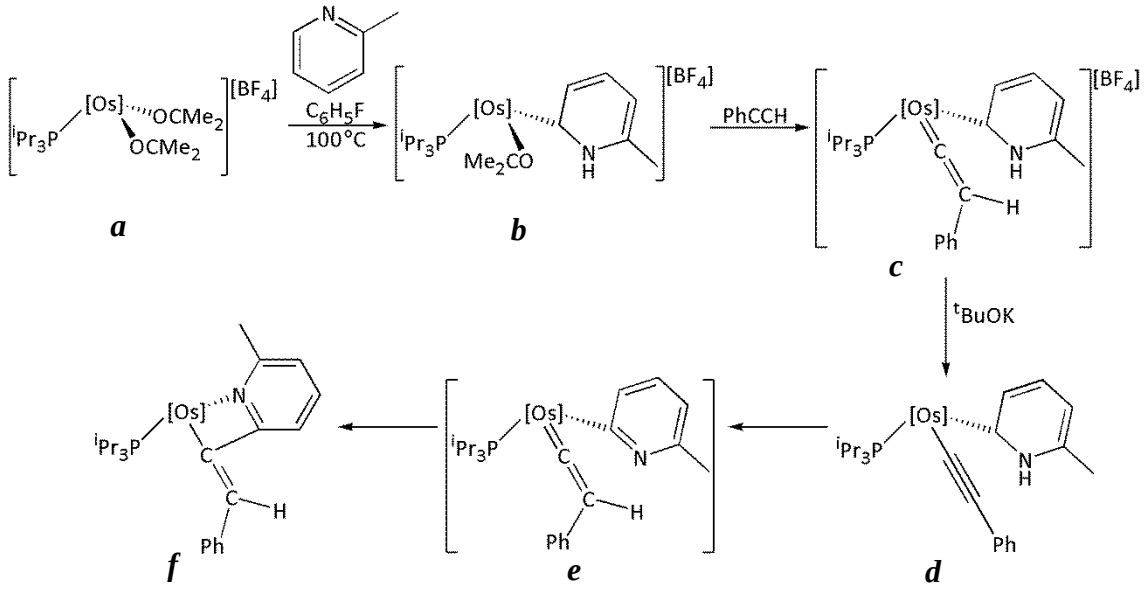

Scheme 1.37: Alkenylation reaction involving an osmium pyridylidene-vinylidene complex, where [Os] = [OsTp].

1.8.3 Synthesis of ruthenium pyridylidene complexes

Esteruelas *et al.* reported that the ruthenium dihydride species, $RuH_2Cl_2(P^iPr_3)_2$ generated the respective 2-carbene tautomers of quinoline (***a***, Figure 1.20), 8-methylquinoline (***b***, Figure 1.20), benzo[*h*]quinoline (***c***, Figure 1.20)[221, 222] and 2-methylpyridine (***d***, Figure 1.20).[223] Similar complexes were observed to those mentioned previously (Scheme 1.34). Stabilisation of the ruthenium NHC complex was achieved through a hydrogen bond between the N-H group and the adjacent Cl ligand. However, upon the formation of a NHC ligand at the ruthenium centre, the loss of dihydrogen was reported therefore creating the five coordinate complexes (Figure 1.20). Differences in reactivity were observed between the dihydride osmium complex $OsH_2Cl_2(P^iPr_3)_2$. The loss of dihydrogen from the ruthenium complexes was attributed to the poorer overlap between the ruthenium orbitals and the coordinated ligands with respect to osmium. This resulted in a weaker π back-bonding interaction to the H_2 ligand and therefore created a weaker bond.[223]

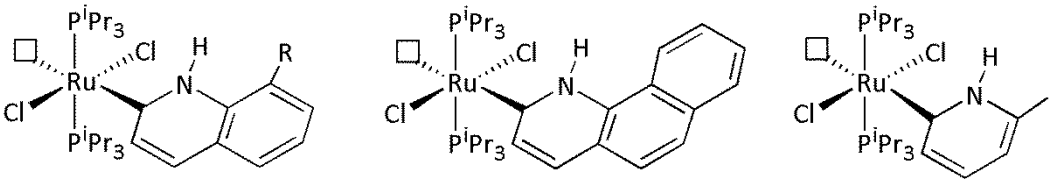

a, b ***c*** ***d***

Figure 1.20: Ruthenium pyridylidene complexes with ***a***: quinoline (R = H), ***b***: 8-methylquinoline (R = Me), ***c***: benzo[*h*]quinoline, ***d***: 2-methylpyridine.

The ruthenium pyridylidene complexes exhibited characteristic NMR resonances for the pyridylidene ligand. In the $^{13}C\{^{1}H\}$NMR spectra, the chemical shifts for the carbon directly coordinated to the ruthenium centre were exhibited between 205 – 220 ppm, which had shifted further downfield in comparison to the Ir and Os pyridylidene complexes. Additionally, an X-ray structure obtained of the ruthenium pyridylidene complex of 8-methylquinoline (***b***, Figure 1.20) found a ruthenium-carbon bond length of 1.925(3) Å. [221-223]

Additionally, the reaction of $RuH_2Cl_2(P^iPr_3)_2$ (***a***, Scheme 1.38) with pyridine only produced the N-bound complex (***b***, Scheme 1.38) (in a similar fashion to the osmium reaction, Section 1.8.2.2). The species was collected in a high yield (70 %) and considered stable (Scheme 1.38).[223]

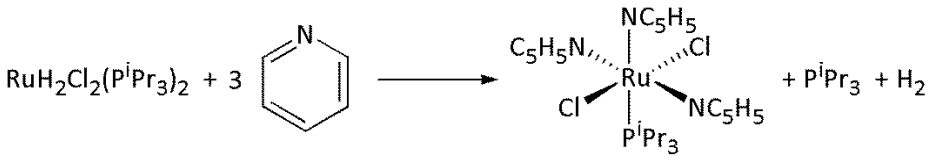

a ***b***

Scheme 1.38: Reaction of $RuH_2Cl_2(P^iPr_3)_2$ with pyridine.

1.9 Alkenylation of pyridine

The research in this thesis will include the functionalisation of pyridine molecules and therefore an introduction into the relevance has been given. Pyridine plays a crucial role in biologically-relevant structures, therefore the selective functionalisation of this molecule is highly desired.[228, 229] A 2006 report stated that the pyridine backbone presented itself in 26 out of the 128 potential drug molecules, thereby signifying its importance for functionalisation in synthetic preparations.[230, 231] Some key biologically-relevant molecules are shown below. For example, the pharmaceutical molecules pioglitazone is used as an anti-diabetic drug (***a***, Figure 1.21) or epibatidine has pain-relieving features (***b***, Figure 1.21) or singulair has anti-inflammatory properties against allergies (***c***, Figure 1.21).[232, 233] On the other hand, in nature it is possible to find the pyridine sub-structure in nicotinic acid (vitamin B_3) (***d***, Figure 1.21) or the oxidising agent nicotinamide adenine dinucleotides (NAD^+, where the reactive part of the molecules is the nictotinamide) (***e***, Figure 1.21).[29]

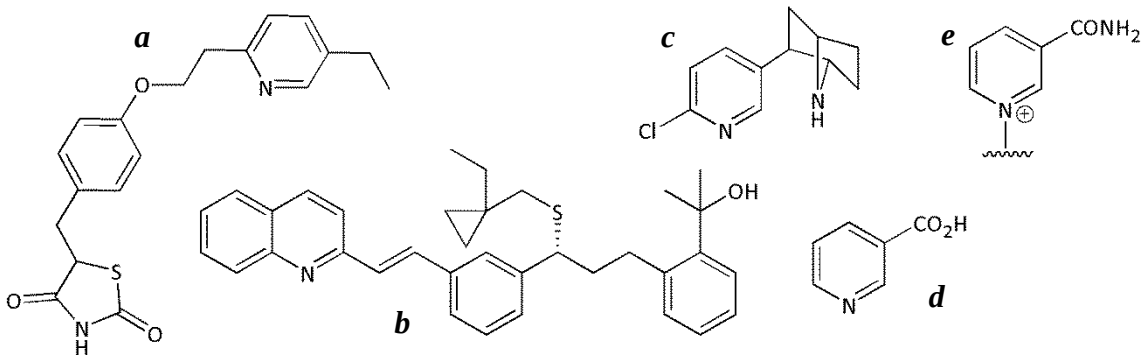

Figure 1.21: Important biologically relevant molecules from left to right: pioglitazone (***a***), singulair (***b***), epibatidine (***c***), nicotinic acid (***d***) and fragment of NAD^+ (***e***).

Unfortunately, due to the high stability of the pyridine π-system relative to benzene the aromatic system can be regarded as electron deficient and therefore difficult to functionalise *via* electrophilic aromatic substitution which presents significant challenges for synthetic chemists.[29, 228, 232] This is represented by the pK_a values of the C-H bonds around the pyridine ring, where the theoretically calculated values are 43.6, 41.9 and 40.3 at the 2-, 3- and 4- positions respectively.[234] In order to achieve electrophilic aromatic substitution at the more difficult 2- and 4- positions of pyridine, the most common methods include condensation and cycloaddition reactions or the use of activated pyridines.[235] Alternatively, nucleophilic addition *via* a carbon-halogen bond could be achieved using the widely acknowledged cross-coupling methods.[236]

Pyridine N-oxides exhibit higher reactivity than pyridine at the 2- and 4- positions of the ring as a lone pair of electron on the oxygen atom can delocalise around the pyridine ring. Nakao *et al.*, reported that the alkenylation of activated pyridine molecules with internal alkynes occurred in a regio- and stereoselective manner at the 2-position of the pyridine ring. The use of either N-oxides or Lewis acids in the presence of the catalyst $Ni(COD)_2$ (COD = cyclooctadiene) and a phosphorus ligand exhibited cooperative effects which allowed for milder reaction conditions. This was later extended to functionalisation reactions at the 4-position of the pyridine ring where the phosphorus ligand was substituted with a bulky NHC ligand, 1,3-(2,6-diisopropylphenyl)imidazol-2-ylidene. The differences observed in the regioselectivity were stated to be due to the highly sensitive steric and electronic factors of the initial η^2-interaction of the pyridine ring to the nickel centre.[237-239]

1.9.1 Literature methods for the preparation of 2-styrylpyridine

The thesis will focus on the synthesis of 2-styrylpyridine derivatives and therefore some background literature on the formation of these compounds is included. The preparation of *E*-2-styrylpyridine has been mentioned in the literature 78 times.[240] Common preparation methods include the use of transition metal catalysts. The palladium cross-coupling Mizoroki-Heck[241-246] (coupling of an aryl halide with an alkene) or Suzuki-Miyaura[247, 248] (coupling of an aryl halide with an organoboronic acid) reactions are the most common methods. Despite low catalyst loadings these reactions usually require a pre-functionalised group on the pyridine ring and additional equivalents of base coupled with high reaction temperatures. The Suzuki-Miyaura methods require the additional group, however these reactions are more selective when additional functional groups are present on the N-containing heterocycle. A more atom economical palladium catalysed reaction employing pyridine has recently been reported, although reaction temperatures of 140 °C were required.[249] An example of the palladium cross-coupling reaction which employed milder reaction conditions (60 °C) between aryl trimethoxysilanes and vinyl groups was demonstrated by Ye *et al.* (Scheme 1.39).[245] However, the expensive silver fluoride salt was required in three equivalents relative to the reagents, where the fluoride source was thought to be responsible for activating the aryl trimethoxysilane and to regenerate the palladium catalyst.

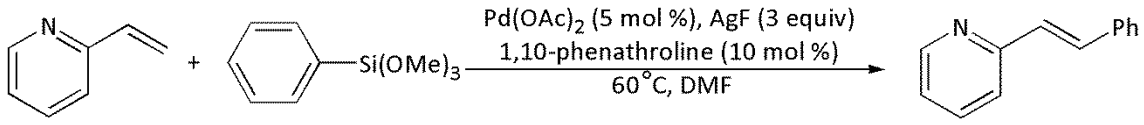

Scheme 1.39: Palladium-catalysed route to (*E*)-2-styrylpyridine *via* an aryl trimethoxysilane and vinylic substrates.

Other transition metal catalysed reactions employing rhodium,[250] iron[251] and copper[233] have also been reported to afford *E*-2-styrylpyridine. The iron and copper catalysed systems presented advantages of using cheaper more accessible metal complexes, however are not necessarily more atom efficient. Interestingly, a few metal free routes have also recently been mentioned, but reagents are pre-functionalised in order to obtain regioselective products.[243, 252]

1.9.2 Alkenylation of Pyridine: Murakami and Hori

In 2003, Murakami and Hori reported the ruthenium-catalysed alkenylation of pyridine and TMS-substituted alkynes.[253] The synthesis of the new carbon-carbon bond was extremely promising considering the reaction was regio- and stereoselective, especially when taking into account that a direct functionalisation of the C-H bond at the 2-position of the pyridine molecule had occurred. The catalytic reaction utilised the convenient precursor $[Ru(\eta^5\text{-}C_5H_5)Cl(PPh_3)_2]$ (20 mol %) in the presence of a halide scavenger $NaPF_6$ (22 mol %) with respect to the TMS-substituted alkyne in a pyridine solutions (20 equivalents) (Scheme 1.40). The reaction mixture was heated at 150 °C for 7 hours, where the final 2-styrylpyridine derivatives were isolated by preparative TLC.

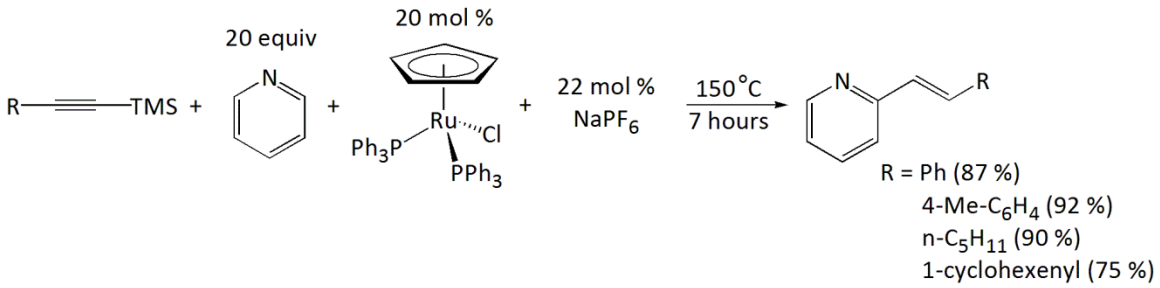

Scheme 1.40: The alkenylation reaction of pyridine and TMS-substituted alkynes with $[Ru(\eta^5\text{-}C_5H_5)Cl(PPh_3)_2]$.

The addition of a range of cationic ruthenium vinylidene-containing complexes $[Ru(\eta^5\text{-}C_5H_5)(PPh_3)_2(=C=CHR)][PF_6]$ (where R = Ph, 4-F-C_6H_4, 4-Me-C_6H_4, 4-OMe-C_6H_4, n-C_5H_{11}, t-C_4H_9) to a pyridine solution (20 equivalents) was investigated. The reported yields of the alkenylation products for these reactions ranged between 54-82

%, apart from when the sterically bulky t-C_4H_9 was employed, where a 0 % yield was obtained. The reactivity and regioselectivity of methyl substituted pyridine molecules was investigated in the 4-, 3- and 2- positions. Both of the 4- and 3- methyl substituted group produced the alkenylation products, where 3-methylpyridine regioselectively formed a new carbon-carbon bond at the position of the N-containing heterocycle. The 2-methylpyridine molecule did not give any of the 2-styrylpyridine derivative presumably due to a steric interactions between the ruthenium centre and the methyl substituent.

A proposed reaction mechanism for the alkenylation of pyridine suggested the cationic ruthenium vinylidene-containing complex (***a***, Scheme 1.41) was the active catalyst in the alkenylation reaction. The subsequent substitution of a phosphine ligand by pyridine results in the formation of (***b***, Scheme 1.41), which after a [2+2] cycloaddition reaction generates (***c***, Scheme 1.41). Another pyridine molecule is involved in the deprotonation of the of the β-hydrogen atom to give a neutral π-azaallyl complex (***d***, Scheme 1.41). This complex is then protonated at the carbon atom to yield the product (Scheme 1.41).

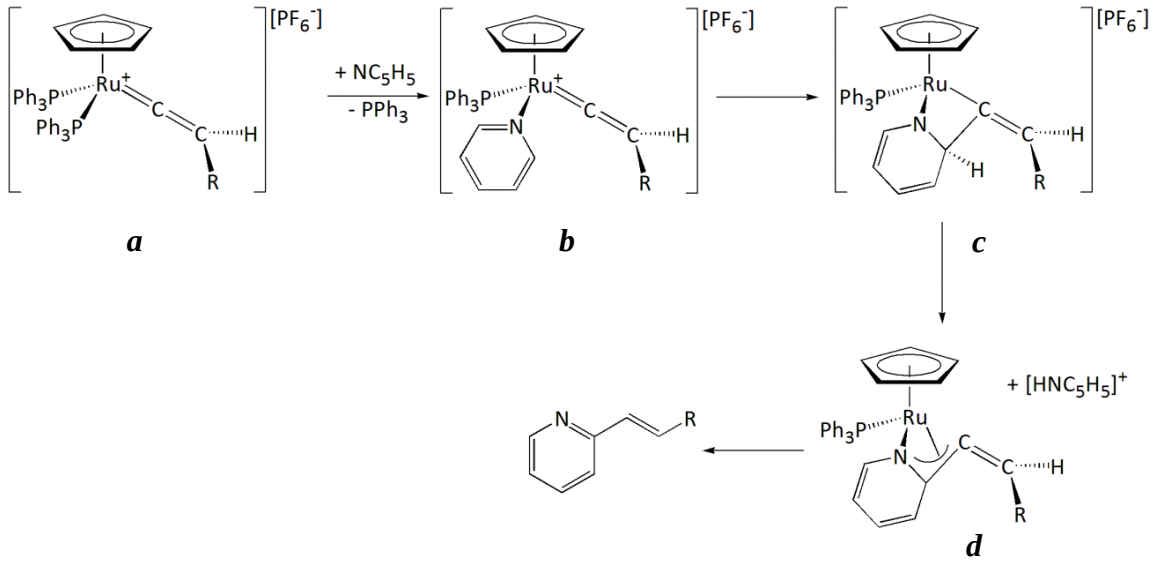

Scheme 1.41: Proposed mechanism for alkenylation of pyridine *via* a vinylidene complex.

The reported reaction conditions required high catalyst loadings (20 mol %) and temperatures (150 °C). When a lower catalyst loading was employed (10 mol %) the isolated yield dramatically reduced to 24 %. Additionally, the TMS-substituted alkyne was required in order to prevent the dimerisation of the alkynes, which was mainly observed with terminal alkynes under their reported reaction conditions (Section 1.4.1). Several potential factors could be changed regarding the catalyst loading, reaction temperatures and atom efficiency in this reaction.

1.10 Aims and objectives

The main objective for this project was to study the behaviour of the half-sandwich ruthenium complexes for the alkenylation of pyridine previously published by Murakami and Hori.[253] Using the knowledge gained from understanding how the reaction mechanism proceeds, will allow for well-educated changes to be applied to the catalytic system and which should eventually lead to the preparation of a novel catalytic system. The mechanism-led approach entailing both an experimental and theoretical perspective would provide significant information on the role of the ruthenium centre. The experimental results will be discussed in this thesis, where the major methods of characterisation include multinuclear NMR spectroscopy, isotopic labelling studies (^{13}C and ^{2}H), ESI and EI mass spectrometry and X-ray crystallography. The theoretical DFT calculations were conducted by David Johnson and will be mentioned in the last chapter.

Our initial aims began with observing the roles of the proposed ruthenium pre-catalyst $[Ru(\eta^5\text{-}C_5H_5)Cl(PPh_3)_2]$ with alkynes in a pyridine solution and the behaviour of the proposed active catalyst $[Ru(\eta^5\text{-}C_5H_5)(PPh_3)_2(=C=CHPh)][PF_6]$ in a pyridine solution. Once, the role of the ruthenium catalysts has been established further mechanistic investigations will be conducted. The mechanistic studies were conducted in a d_2-dichloromethane solution in order to potentially observe and isolate any relevant ruthenium intermediates and monitor their behaviour in solution. Further investigations into the substituent effects at the N-containing heterocycle and alkynes, the phosphorus ligand and the cyclopentadienyl ligand will be conducted to develop the ruthenium catalysed system and establish the scope of potential reagents. Alongside the experimental findings DFT calculations (from David Johnson) will be combined which will use a high level of theory to model the ruthenium-catalysed alkenylation of pyridine to gain insight into the entire catalytic cycle and the substituent effects. These findings will be used to develop the catalyst and allow for improvements (in terms of atom and energy efficiency) to be made for the alkenylation of N-containing heterocycles.

Chapter 2. Initial Mechanistic Studies

2.1 Introduction

Catalysts aim to perform organic transformations under more efficient reaction conditions and increase atom efficiency (maximise the number of atoms of the raw materials that end up in the product by reducing the number of side products).[2, 7, 254] The simplest and most atom efficient method to synthesise C-C bonds would be to utilise reagents with C-H bonds.[4, 6] This would create a truly 100 % atom efficient system, as there would be no need to remove any wasteful side products which are usually formed in C-C coupling reactions, since one of the most common methods in catalysis involves using a pre-functionalised C-X bond (where X = halogen or triflate).[7]

An alkene functional group can be incorporated into an organic structure by the palladium catalysed Mizoroki-Heck reaction, between an organic halide and an olefin group.[7, 246, 255-258] A salt of the type HX or $[HNR_3X]$ (where X = halide, R = alkyl group) is a typical by-product of such a reaction.[259-261] Alternatively, a more atom efficient method has been reported by Fujiwara *et al.* who investigated alkenylation reactions between acetylenes and arenes in the presence of trifluoroacetic acid using $Pd(OAc)_2$ as a catalyst. This utilises C-H bond activation in a selective manner to create alkene/aryl products.[254, 257, 262-264]

In 2003, Murakami and Hori published the alkenylation reaction of pyridine with TMS substituted alkynes.[253] The reaction utilises a half-sandwich ruthenium complex, $[Ru(\eta^5\text{-}C_5H_5)(PPh_3)_2Cl]$ which performs the catalytic transformation, in the presence of the halide scavenger $NaPF_6$. The proposed active catalyst in the alkenylation reaction was the vinylidene complex $[Ru(\eta^5\text{-}C_5H_5)(PPh_3)_2(=C=CHPh)][PF_6]$.[253]

This work began by firstly examining the synthesis of $[Ru(\eta^5\text{-}C_5H_5)Cl(PPh_3)_2]$ **1** and the vinylidene-containing complex $[Ru(\eta^5\text{-}C_5H_5)(PPh_3)_2(=C=CHPh)][PF_6]$ $\mathbf{2^R}$. Preliminary mechanistic studies were based on investigating the properties of the vinylidene-containing complexes $\mathbf{2^R}$ in d_5-pyridine to determine how the reaction proceeded. This resulted in the formation of several ruthenium complexes which have been identified and their roles within the catalytic reaction determined.

2.2 Pre-Catalysts and Proposed Active Catalysts

2.2.1 Synthesis of $[Ru(\eta^5\text{-}C_5H_5)(PPh_3)_2Cl]$

The synthetic preparation of the ruthenium complexes $[Ru(\eta^5\text{-}C_5H_5)Cl(PPh_3)_2]$ **1**,[265] and $[Ru(\eta^5\text{-}C_5H_5)(PPh_3)_2(=C=CHPh)][PF_6]$ $\mathbf{2^{Ph}}$,[54] are well established in the literature by Bruce *et al*. The complex **1** was implemented as a pre-catalyst in the alkenylation reaction, as it provided a source of a cationic ruthenium species.[253]

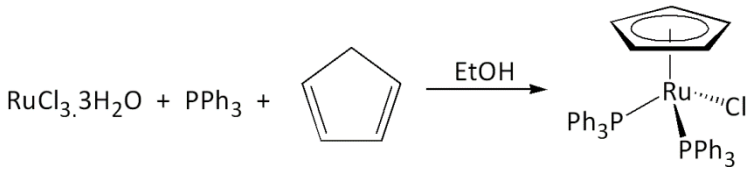

1

Scheme 2.1: Synthesis of complex **1**.

The ruthenium complex $[Ru(\eta^5\text{-}C_5H_5)Cl(PPh_3)_2]$ **1** was synthesised following the literature preparation method.[265] The synthetic procedure to prepare the pre-catalyst **1** was achieved using freshly distilled dicyclopentadiene, triphenylphosphine and $RuCl_3.3H_2O$ and heating at reflux for one hour (Scheme 2.1). The product was shown to be pure by NMR spectroscopy and collected as either red crystals or as an orange precipitate in a high yield (72 %). The characteristic signals in the ^1H NMR spectrum were observed for the cyclopentadienyl protons in d_2-dichloromethane at 4.09 ppm, and the phosphorus atom of the triphenylphosphine ligands observed in the $^{31}P\{^1H\}$ NMR spectrum at 39.5 ppm.

2.2.2 Synthesis of cationic vinylidene complexes of the type $[Ru(\eta^5\text{-}C_5H_5)(PPh_3)_2(=C=CHR)][PF_6]$

The synthesis of the vinylidene complexes, $[Ru(\eta^5\text{-}C_5H_5)(PPh_3)_2(=C=CHR)][PF_6]$, $\mathbf{2^R}$ were carried out as described by Bruce and Wallis.[54] The complex $[Ru(\eta^5\text{-}C_5H_5)Cl(PPh_3)_2]$ **1** was heated at reflux in the presence of a terminal alkyne and an appropriate halide ion scavenger, in a methanol solution. The reaction mixture was heated for a brief period of time (10-20 minutes) to yield the vinylidene complexes $\mathbf{2^R}$ (Scheme 2.2). Extensive heating may result in the α-carbon atom of the vinylidene ligand being susceptible to attack by nucleophiles due to its electrophilic nature; hence the methanol may react with the cationic vinylidene species at the α-carbon atom to give a methoxy carbene complex (Section 1.4.3).[266] The products were purified by recrystallisation.

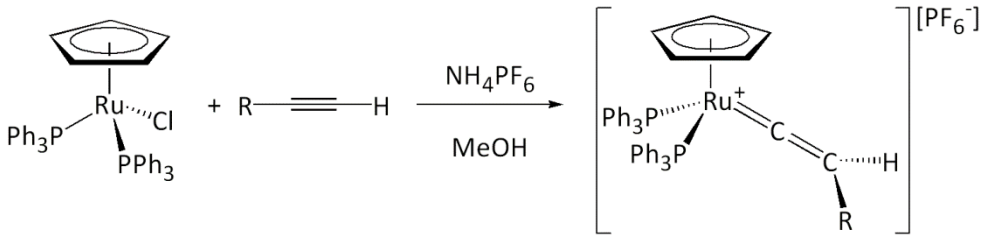

1 $\mathbf{2^R}$

Scheme 2.2: General synthesis of cationic vinylidene complexes $\mathbf{2^R}$ (R = Ph, C_6H_4-*p*Me, ^{t}Bu).

The red products $\mathbf{2^R}$ exhibited very characteristic resonances in their NMR spectra in d_2-dichloromethane solution. For complex $\mathbf{2^{Ph}}$, the proton bonded to the β-carbon atom of the vinylidene ligand displayed a triplet resonance at 5.43 ($^4J_{HP}$ = 2.4 Hz) in the ^{1}H NMR spectrum. Additionally, in the $^{13}C\{^1H\}$ NMR spectrum the α-carbon atom exhibited a triplet signal at 354.4 ppm ($^2J_{CP}$ = 15.5 Hz). The $^{31}P\{^1H\}$ NMR spectrum exhibits two signals; one of these is a septet peak for the $[PF_6]^-$ at -143.5 ppm ($^1J_{PF}$ = 710 Hz); and the other for the triphenylphosphine ligands at 43.4 ppm (singlet).

A range of cationic vinylidene species were also synthesised for use in the mechanistic studies in d_5-pyridine: a methyl group in the 4-position on the phenyl ring of the vinylidene ligand $\mathbf{2^{C6H4\text{-}4\text{-}Me}}$, and a ^{13}C label introduced at the α-carbon position of the vinylidene ligand $\mathbf{2^{Ph}\text{-}^{13}C}$ (this reaction was carried out using PhC≡^{13}CH) were used to provide additional NMR data on how the reaction proceeded.

2.3 Initial Mechanistic Studies

2.3.1 Reactivity of the vinylidene species [Ru(η^5-C_5H_5)(PPh_3)$_2$(=C=CHR)][PF_6]

The alkenylation reaction published by Murakami and Hori[253] proposed the cationic vinylidene complex [Ru(η^5-C_5H_5)(PPh_3)$_2$(=C=CHPh)][PF_6] **2^{Ph}** as the active catalyst in the formation of 2-styrylpyridine compounds. Upon taking complex **2^{Ph}** in pyridine and heating at 125 °C for 24 hours 2-styrylpyridine was generated.

Our initial mechanistic studies were based on the addition of d_5-pyridine to the vinylidene complexes **2^{R}**, and the reaction monitored *via* ^{1}H, ^{31}P{^{1}H}, and ^{13}C{^{1}H} NMR spectroscopy.

A mechanistic study involved the addition of **2^{Ph}-^{13}C** to d_5-pyridine, followed by heating the reaction mixture at 85 °C within the NMR spectrometer was carried out in the presence of air, where no attempt was made to dry the solvent in order to recreate the reported reaction conditions by Murakami and Hori (Scheme 2.3: Top reaction).[253] A further mechanistic study involved the addition of degassed d_5-pyridine to **2^{Ph}-^{13}C** in order to prevent oxidation of the reaction mixture, and heating to 125 °C in a graphite bath to recreate the reaction temperatures reported by Murakami and Hori (Scheme 2.3: Bottom reaction).[253]

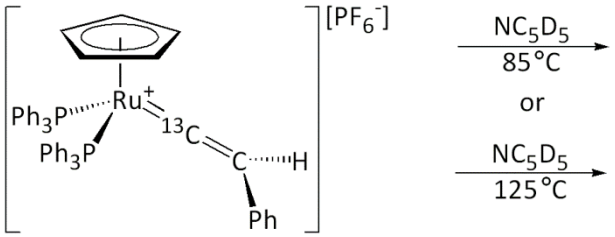

2^{Ph}-^{13}C

Scheme 2.3: General scheme of the reactions carried out with complex **2^{Ph}-^{13}C** in d_5-pyridine.

2.3.2 Initial addition of complexes 2^R to d_5-pyridine

On immediate addition of d_5-pyridine to the complexes $\mathbf{2^R}$ a colour change from the characteristic red colour of the vinylidene-containing complexes $\mathbf{2^R}$ to bright yellow solution indicated a reaction had occurred. The characteristic peaks of the cationic vinylidene-containing complex $\mathbf{2^{Ph}}$ were no longer present in the ^{1}H and ^{31}P{^{1}H} NMR spectra (Scheme 2.4). The ^{1}H NMR spectrum (d_5-pyridine) did not exhibit the vinylidene proton at 5.43 ppm (CD_2Cl_2), and a major change in the chemical shift of the cyclopentadienyl protons from 5.27 ppm (CD_2Cl_2) to 4.58 ppm (d_5-pyridine) was observed. In addition, in the reaction of ^{13}C-labelled vinylidene $\mathbf{2^{Ph}}$-^{13}**C** to d_5-pyridine in the ^{13}C{^{1}H} NMR spectrum displayed no evidence for the α-carbon atom at 354.4 ppm (CD_2Cl_2).

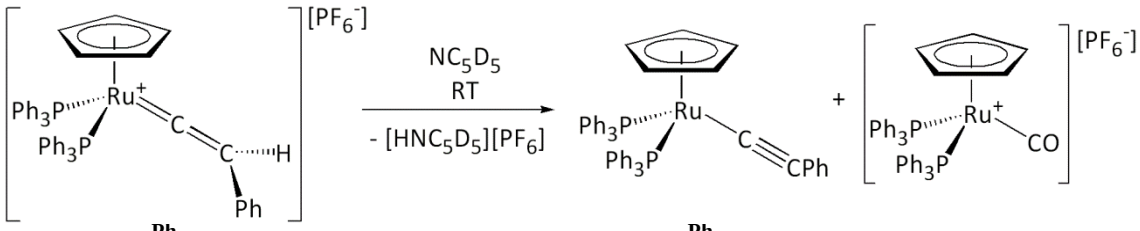

$\mathbf{2^{Ph}}$ $\mathbf{3^{Ph}}$ **4**

Scheme 2.4: Observations made on initial addition of d_5-pyridine to complex $\mathbf{2^{Ph}}$.

From the NMR spectra of the reaction mixture of $\mathbf{2^{Ph}}$ in d_5-pyridine there appeared to be two products in the reaction mixture in different quantities: one major and one minor which could be identified. This was most notably observed in the cyclopentadienyl region of the ^{1}H NMR spectrum as there were two new singlet resonances at 4.58 and 5.30 ppm. This was also confirmed by the ^{31}P{^{1}H} NMR spectrum where two resonances at 50.3 and 42.1 ppm were observed for two PPh_3 environments. The ratio of the two species varied in different reaction mixtures.

For the unlabelled vinylidene species $\mathbf{2^{Ph}}$ in d_5-pyridine the major species in the ^{1}H NMR spectrum exhibited a singlet resonance for the cyclopentadienyl protons at 4.58 ppm. For the major species in the ^{31}P{^{1}H} NMR spectrum a singlet was observed at 50.2 ppm. However, in the ^{13}C-labelled study a doublet peak at 50.3 ppm ($^2J_{PC}$ = 24.8 Hz) was observed. From this it was clear that the ^{13}C labelled atom was coupling to the equivalent PPh_3 groups, and hence the ruthenium centre must contain a ^{13}C labelled organic ligand from the PhC≡^{13}CH molecule. Additionally, the ^{13}C{^{1}H} NMR spectrum displayed a resonance for the ^{13}C-labelled atom at 117.7 ppm (broad). The NMR data gathered from comparing the labelled and non-labelled studies suggested an acetylide

complex [Ru(η^5-C_5H_5)(C≡CPh)(PPh_3)$_2$] **3^{Ph}** was formed upon the addition of d_5-pyridine to **2^{Ph}**. This was confirmed by comparison of the NMR spectra of the reaction mixture with an independent synthesis of **3^{Ph}** following a literature preparation by Bruce *et al*.[54]

The minor species in the reaction mixture in the ^{1}H NMR spectrum had a singlet cyclopentadienyl resonance at 5.30 ppm, which correlated to a singlet peak at 42.1 ppm in the ^{31}P{^{1}H} NMR spectrum (determined through relative integrations). The minor product present in the reaction mixture was confirmed to be the carbonyl-containing complex **4**, which was independently synthesised by a method reported by Conroy-Lewis and Simpson.[267] The reaction of oxygen or water with vinylidene complexes is reported extensively in literature and results in the formation of a metal carbonyl compound (Section 1.4.3). The relative amounts of the carbonyl species **4** would therefore differ depending on the aerobic quality of the d_5-pyridine. This would therefore account for the observation in reactions where the degassed d_5-pyridine has been used, as less **4** was observed in the reaction mixture.

At room temperature upon addition of d_5-pyridine to complexes **2^{R}**, the major species was assigned as [Ru(η^5-C_5H_5)(C≡CR)(PPh_3)$_2$] **3^{R}**, and the minor product as [Ru(η^5-C_5H_5)(PPh_3)$_2$(CO)][PF_6] **4**.

2.3.3 Observations made upon heating the reaction mixture of 2^{R} in d_5-pyridine

In order to recreate the reaction conditions[253] reported by Murakami and Hori the reaction mixture containing $\mathbf{2^{Ph}}$ in d_5-pyridine (Scheme 2.4) was heated to observe the reaction as it proceeded, to determine any potential ruthenium intermediates. Upon heating the sample to 85 °C for 30 minutes within the NMR spectrometer, resonances for a new compound emerged in the NMR spectra. By comparison of the non-labelled and labelled studies the structure of the new complex was determined.

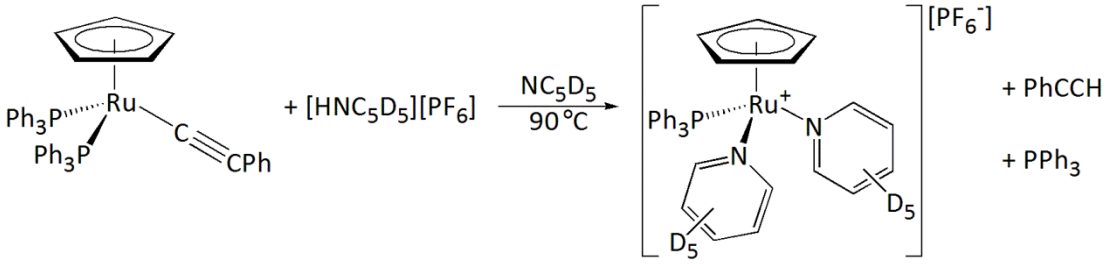

$\mathbf{3^{Ph}}$ **5**

Scheme 2.5: Formation of a new ruthenium complex **5** upon heating the initial reaction mixture of $\mathbf{2^{Ph}}$ in d_5-pyridine.

In the non-labelled study the ^{1}H NMR spectrum at 85 °C displayed a new cyclopentadienyl proton environment at 4.54 ppm, and a resonance assigned to the terminal proton of uncoordinated phenylacetylene at 3.69 ppm. In the $^{31}P\{^{1}H\}$ NMR spectrum at 85 °C two new singlet signals were observed in a 1:1 ratio at 48.7 and -3.9 ppm. The resonance at 48.7 ppm is in the region for a new coordinated triphenylphosphine resonance of a novel ruthenium complex, and the resonance at -3.9 ppm is characteristic of uncoordinated triphenylphosphine. In addition, conversion of triphenylphosphine to triphenylphosphine oxide was also observed in the $^{31}P\{^{1}H\}$ NMR spectrum.

From the ^{13}C-labelled study more information was gathered about the nature of the ruthenium complexes formed. In the ^{1}H NMR spectrum a doublet at 3.69 ppm ($^{1}J_{HC}$ = 252 Hz) was observed, for uncoordinated ^{13}C-phenylacetylene. The signal at 3.69 ppm integrated in a 1:5 manner to the new cyclopentadienyl proton peak at 4.55 ppm. In addition, the resonance for the new ruthenium complex in the $^{31}P\{^{1}H\}$ NMR spectrum at 48.7 ppm remained as a singlet, therefore indicating there was no coupling between the phosphorus atom and the ^{13}C-labelled atom. A resonance for the ^{13}C-labelled atom of uncoordinated ^{13}C-phenylacetylene was observed at 79.3 ppm in the $^{13}C\{H\}$ NMR spectrum.

The resonances observed by NMR spectroscopy indicated that the new complex had lost phenylacetylene and one triphenylphosphine ligand. The loss of these ligands from the metal centre created two vacant coordination sites and the product was therefore proposed to be $[Ru(\eta^5\text{-}C_5H_5)(PPh_3)(NC_5D_5)_2][PF_6]$ **5**, due to the excess d_5-pyridine in the reaction mixture. The full identification of **5** was determined by comparison of NMR spectra of the reaction mixture and an authentic sample (Section 3.4.1.2).

A similar reaction was repeated using $\mathbf{2^{Ph}\text{-}^{13}C}$ and degassed pyridine; the reaction was heated at a higher reaction temperature of 125 °C in a graphite bath and for longer time periods (1, 6, 23, and 47 hours). The reaction mixture was allowed to cool to room temperature and then monitored by NMR spectroscopy in order to observe the reactivity seen by Murakami and Hori (Figure 2.1).[253] After 1 hour at 125 °C, the ratio of the acetylide complex $\mathbf{3^{Ph}\text{-}^{13}C}$ and complex **5** was approximately 1:1, as the $^{31}P\{^1H\}$ NMR spectrum revealed two resonances at 50.3 and 49.2 ppm for the triphenylphosphine ligands respectively. After 47 hours the ratio of complexes $\mathbf{3^{Ph}\text{-}^{13}C}$:**5** was approximately 1:17, indicating the majority of the acetylide complex has been converted to **5**. The $^{13}C\{^1H\}$ NMR spectra allowed the fate of the ^{13}C label to be monitored through the reaction. After heating for 1 hour at 125 °C, the ^{13}C label was observed mainly at 117.8 and 79.9 ppm, which are peaks characteristic of the acetylide complex $\mathbf{3^{Ph}\text{-}^{13}C}$ and uncoordinated $PhC{\equiv}{}^{13}CH$ respectively. Heating the reaction mixture for a further 6 hours, resulted in the majority of the ^{13}C label being observed at a chemical shift of 129.2 ppm; and upon further heating, this peak increased in intensity. From comparison of an authentic sample of 2-styrylpyridine the peak at 129.2 ppm can be assigned as one of the alkene carbon atoms of the desired organic product. These observations therefore indicate the importance of **5** as a catalyst in the formation of 2-styrylpyridine.

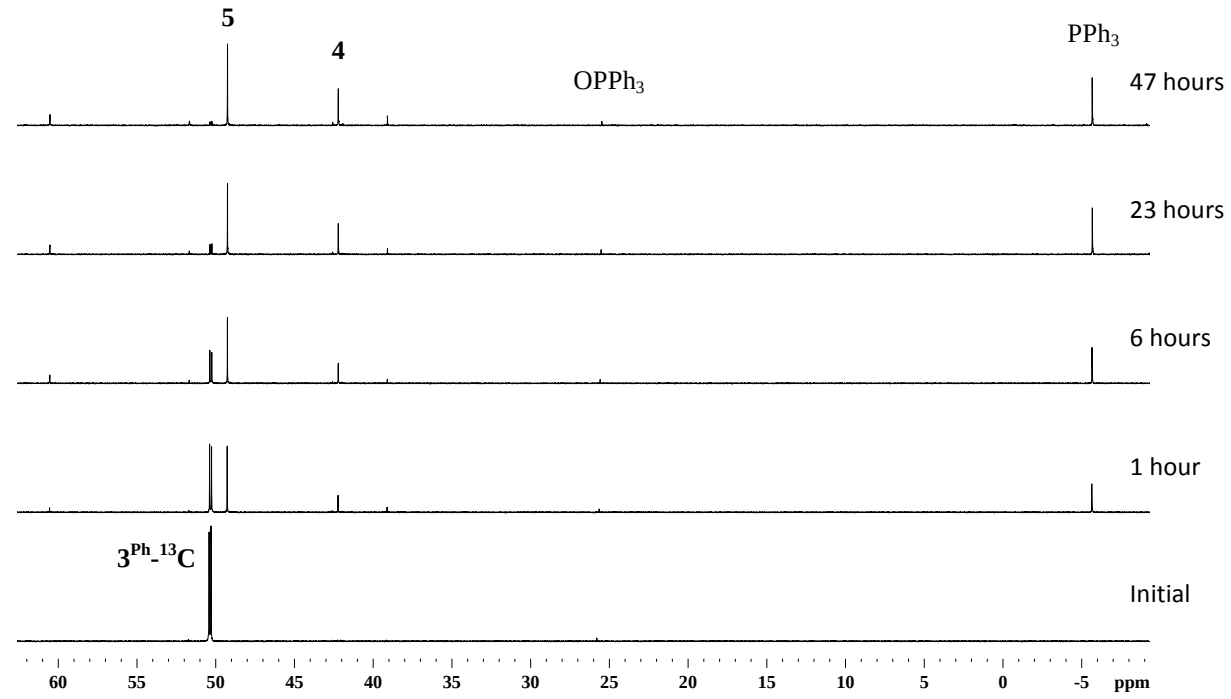

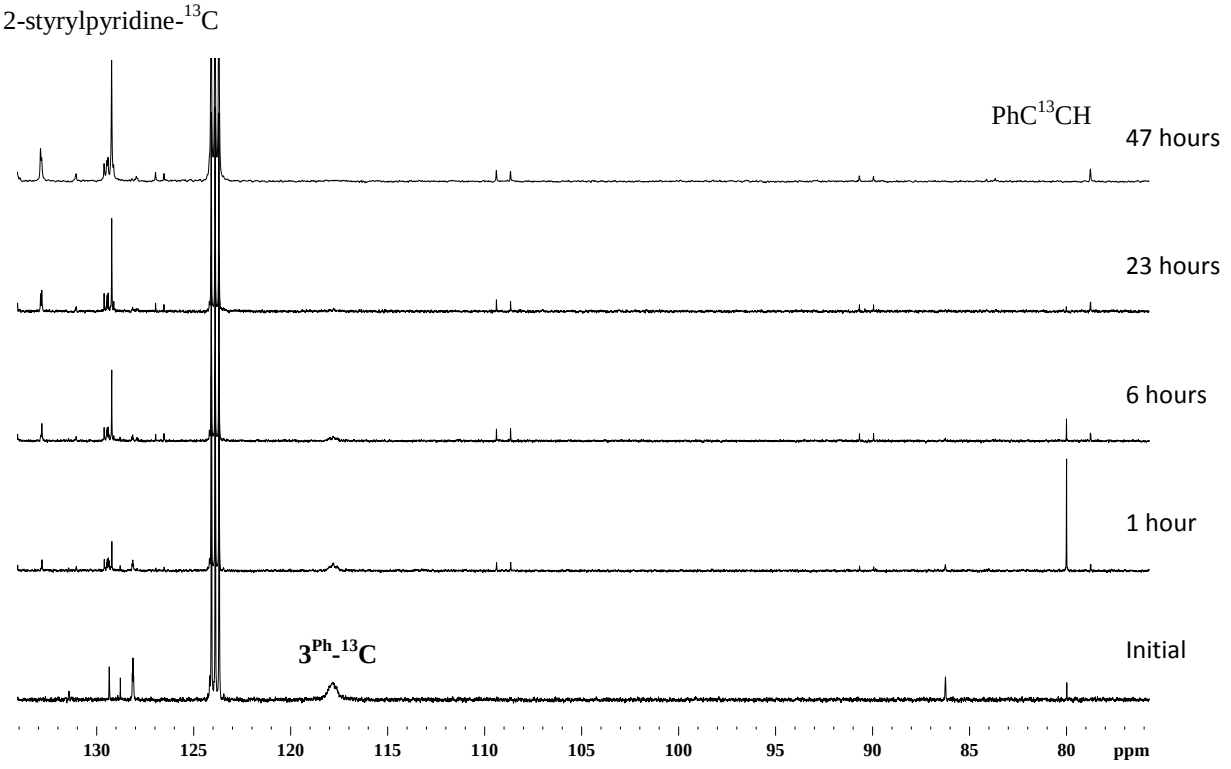

Figure 2.1: $^{31}P\{^{1}H\}$ and $^{13}C\{^{1}H\}$ NMR spectra of the reaction of **2^{Ph}-^{13}C** in degassed d_5-pyridine heated at 125 °C after a) initial addition, b) 1 hour, c) 6 hours, d) 23 hours, e) 47 hours.

2.3.4 Conclusions

In the reaction between the vinylidene-containing complexes **2**$^{\mathbf{R}}$ and d_5-pyridine, the immediate major ruthenium-containing species was found to be the acetylide complex **3**$^{\mathbf{R}}$. From this reaction it appears that the d_5-pyridine is acting as a base and deprotonating the acidic proton on the vinylidene ligand. Upon heating the same reaction mixture for 6 hours (and a total duration of 47 hours) the major ruthenium-containing complex was identified as $[Ru(\eta^5\text{-}C_5H_5)(PPh_3)(NC_5D_5)_2][PF_6]$, **5**. This has been determined to form concurrently with equivalent amounts of uncoordinated phenylacetylene and triphenylphosphine. The presence of complex **5** strongly suggests its role in the catalytic cycle must be significant in the formation of 2-styrylpyridine. Further investigations into the synthesis and reactivity of **5** would help in understanding its role in the catalytic system reported by Murakami and Hori.[253]

Chapter 3. Synthesis of Half-Sandwich Ruthenium Complexes

3.1 Introduction

The most common precursors to ruthenium cyclopentadienyl complexes are the species $[Ru(\eta^5\text{-}C_5H_5)(PPh_3)_2Cl]$, **1** or $[Ru(\eta^5\text{-}C_5H_5)(CO)_2Cl]$.[137] However, for a transition metal to perform catalytic reactions the metal centre must be coordinatively unsaturated.[134] The two ruthenium precursors mentioned above contain ligands (PPh_3 and CO) and therefore may hinder a number of synthetic transformations taking place.[137] An alternative approach utilises the half-sandwich ruthenium complex $[Ru(\eta^5\text{-}C_5H_5)(NCMe)_3][PF_6]$ **8** which provides labile acetonitrile ligands which can be easily substituted[135] and therefore opens a gateway to a range of half-sandwich ruthenium complexes[127, 128, 131-134, 136, 139, 268] and potential catalytic transformations.[40, 129, 269-272]

The catalytic redox isomerisation of allylic alcohols to their corresponding aldehydes and ketones significantly improved when $[Ru(\eta^5\text{-}C_5H_5)(PPh_3)_2Cl]$, **1** and NH_4PF_6 were substituted with $[Ru(\eta^5\text{-}C_5H_5)(PPh_3)(NCMe)_2][PF_6]$, $\mathbf{9^{Ph}}$. The original research conducted by Trost *et al.* reported reaction conditions where **1** (5 mol %), NH_4PF_6 (10 mol %) and the allyl alcohol were heated at 100 °C in dioxane.[2, 40, 273] The reaction was developed by Kirchner *et al.* using a significantly lower catalyst loading of $\mathbf{9^{Ph}}$ (0.03 mol %) and at a milder temperature of 80 °C, where the reaction was complete within 10 minutes.[274] The higher reactivity was attributed to the pseudo 14-electron $[Ru(\eta^5\text{-}C_5H_5)(PR_3)]^+$ which allows coordination of the allylic alcohol at the ruthenium centre, and therefore loss of a PPh_3 at the ruthenium centre was not required.

Previously $[Ru(\eta^5\text{-}C_5H_5)(PPh_3)(NC_5D_5)_2][PF_6]$, **5** was determined to be the major ruthenium-containing species from the addition of $\mathbf{2^R}$ to d_5-pyridine (Chapter 2). A general synthesis for the $[Ru(\eta^5\text{-}C_5H_5)(PR_3)(L)_2][PF_6]$ complexes (where R = Ph, OPh, ^{i}Pr, Me, and L = nitrogen-containing ligand) was required. This chapter focuses on the synthesis and properties of half-sandwich ruthenium complexes of the type $[Ru(\eta^5\text{-}C_5H_5)(PR_3)(L)_2][PF_6]$ from the starting cationic *tris*-acetonitrile ruthenium complex $[Ru(\eta^5\text{-}C_5H_5)(NCMe)_3][PF_6]$, **8**.

3.2 Preparation of $[Ru(\eta^5\text{-}C_5H_5)(NCMe)_3][PF_6]$, 8

The role of the cationic fragment $[Ru(\eta^5\text{-}C_5H_5)]^+$ in catalysis has been well documented (Section 1.5). The complex $[Ru(\eta^5\text{-}C_5H_5)(NCMe)_3][PF_6]$, **8** is therefore an useful starting material for the synthesis of various half-sandwich ruthenium complexes, especially due to the labile nature of the acetonitrile ligands. However, the synthesis of **8** has not always been simple and even purchasing it from chemical suppliers can be costly (Sigma-Aldrich 1g, £275.50).[275] The synthetic preparation of **8** has been developed through the years and will be discussed here.

The complex $[Ru(\eta^5\text{-}C_5H_5)(NCMe)_3][PF_6]$, **8** can be prepared from several different literature methods. Gill and Mann first reported the synthesis of **8** from the irradiation of the species $[Ru(\eta^5\text{-}C_5H_5)(\eta^6\text{-}C_6H_6)][PF_6]$ in acetonitrile (Scheme 3.1).[276] However, the formation of the complex $[Ru(\eta^5\text{-}C_5H_5)(\eta^6\text{-}C_6H_6)][PF_6]$ requires a two step process from $RuCl_3.nH_2O$, 1,3-cyclohexadiene in ethanol to yield $[Ru(\eta^6\text{-}C_6H_6)Cl_2]_2$; this dimer is then reacted with a stoichiometric equivalent of TlCp in acetonitrile before the addition of NH_4PF_6 to precipitate the cationic product $[Ru(\eta^5\text{-}C_5H_5)(\eta^6\text{-}C_6H_6)][PF_6]$.[277, 278] Unfortunately the thallium salts and the waste products are toxic in nature and are difficult to remove hence this procedure would not be an ideal method to synthesise large batches of complex $[Ru(\eta^5\text{-}C_5H_5)(NCMe)_3][PF_6]$, **8**.

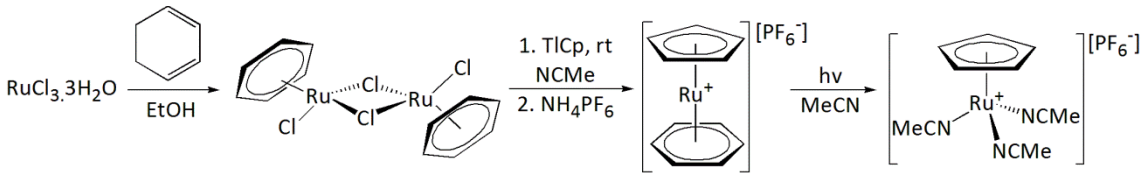

8

Scheme 3.1: Preparation of complex **8** by Gill and Mann.[276]

An alternative method by Bennett reported the synthesis of $[Ru(\eta^5\text{-}C_5H_5)(\eta^6\text{-}C_6H_6)][PF_6]$ (precursor for the formation of complex **8**), using $[Ru(\eta^6\text{-}C_6H_6)Cl_2]_2$ in the presence of excess cyclopentadiene with Na_2CO_3 in ethanol at reflux.[137] This was developed from earlier research by Bennett *et al.* involving the substitution of Cl ligands from the precursor $[Ru(\eta^6\text{-}C_6H_6)Cl_2]_2$ in the presence of the diene ligands 1,5-cyclooctadiene or 1,3-cyclohexadiene.[279, 280] This method avoided the use of the toxic thalium salts, however the reported yields were low due to a side reaction producing ruthenocene.[137] In 2002, Trost and Older reported another method to prepare $[Ru(\eta^5\text{-}C_5H_5)(\eta^6\text{-}C_6H_6)][PF_6]$ from $[Ru(\eta^6\text{-}C_6H_6)Cl_2]_2$ and found that the choice of base

and solvent were important in obtaining a high yield. Optimal reaction conditions were discovered to be the reaction between $[Ru(\eta^6\text{-}C_6H_6)Cl_2]_2$, cyclopentadiene and K_2CO_3 in ethanol at a lower temperature of 60 °C, followed by precipitation with NH_4PF_6 (Scheme 3.2). In this case only 2-3 % of ruthenocene was formed as a side product. The complex $[Ru(\eta^5\text{-}C_5H_5)(\eta^6\text{-}C_6H_6)][PF_6]$, was obtained in a high yield of 80 %, and an adapted procedure from Gill and Mann was used to obtain **8**.[137]

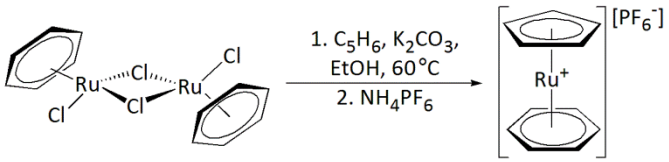

Scheme 3.2: Revised synthesis of precursor to complex **8** by Trost and Older.[137]

The method used for the synthesis of complex $[Ru(\eta^5\text{-}C_5H_5)(NCMe)_3][PF_6]$, **8** in this thesis has been reported by Kündig *et al.* (Scheme 3.3).[281, 282] A three step process from the starting material $RuCl_3.3H_2O$ was employed to synthesise ruthenocene **6**; one of the cyclopentadienyl ligands was then substituted by a more labile naphthalene ligand to give the complex $[Ru(\eta^5\text{-}C_5H_5)(naphthalene)][PF_6]$ **7**; followed by the substitution of the naphthalene ring by three acetonitrile ligands to yield **8**.[281] The advantages of this preparation method of **8** are that it avoids the use of toxic thallium salts and there is no requirement for specialised photolytic quartz apparatus[137] or continuous flow reactors (for alternative preparation methods for the synthesis of **8**).

Kündig *et al.* investigated the substitution of one of the cyclopentadienyl ligands of ruthenocene with an arene group. This proved to be challenge as the reaction conditions required for ferrocene cyclopentadienyl/arene exchange (80-100 °C, $AlCl_3$, Al, methylcyclohexane) did not work for ruthenocene, **6**.[282-284] This is probably due to stronger π interactions between the p_z orbitals of the cyclopentadienyl ligand and the d_{xz} and d_{yz} orbitals of the ruthenium centre, which results in a larger heterolytic dissociation energy of ruthenocene.[285, 286] DFT studies revealed that at the B-PW91 level of theory, ruthenocene had a dissociation energy of 2862 kJ mol^{-1}, whereas ferrocene had a lower dissociation energy of 2774 kJ mol^{-1} (which is within a +4 % error of experimental findings of 2657 kJ mol^{-1}).[285] Kündig *et al.* noted a patent report where $TiCl_4$ had been employed to 'trap the cyclopentadienyl ligands to form titanocene dichloride', and upon the addition of this reagent to the reaction mixture and under optimised reaction condition **7** was synthesised in a high yield.[281, 282]

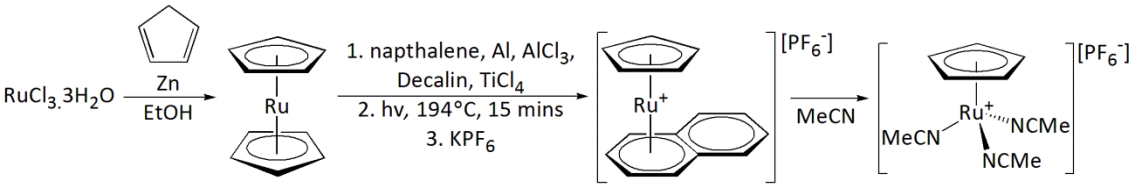

6 **7** **8**

Scheme 3.3: Preparation of complex **8** from ruthenocene.[281]

Preparation of ruthenocene, **6** was achieved by the addition of zinc to a cooled reaction mixture of freshly distilled dicyclopentadiene and $RuCl_3.3H_2O$ in ethanol (Scheme 3.3). The zinc reduced the ruthenium to an oxidation state of +2, and a pale yellow complex was collected in a high yield (79 %). Identification of the neutral complex was extremely straightforward using NMR spectroscopy, as in the ^{1}H NMR and $^{13}C\{^{1}H\}$ NMR spectra, only one resonance was observed due to equivalent proton and carbon environments at 4.55 ppm and 70.2 ppm respectively. This was consistent with the literature reported data.[281, 287, 288]

The preparation of $[Ru(\eta^5\text{-}C_5H_5)(naphthalene)][PF_6]$ **7**, required microwave irradiation of the sample at 194 °C for 15 minutes (Scheme 3.3). However, purification of **7** was not always very effective and hence the purity of the end product was compromised due to unidentified impurities. The ESI-MS had a peak at *m/z* of 295, which was indicative of the cationic fragment $[Ru(\eta^5\text{-}C_5H_5)(naphthalene)]^+$, and the isotope pattern matched that of a ruthenium containing complex. NMR spectroscopy revealed that the collected complex **7** was slightly impure, yet the signals observed matched those reported by Kundig *et al.*,[281] where in the ^{1}H NMR spectrum the cyclopentadienyl protons displayed a resonance at 5.00 ppm, and the four naphthalene resonances were seen as multiplets with an integration of 2H each between 6.30 – 7.73 ppm.

The final stage of the procedure was to stir **7** in acetonitrile, in order to substitute the naphthalene with three acetonitrile ligands, to produce $[Ru(\eta^5\text{-}C_5H_5)(NCMe)_3][PF_6]$, **8** (Scheme 3.3). The reaction mixture was stirred under a nitrogen atmosphere for 48 hours and several pentane washes were performed to remove uncoordinated naphthalene. The end product matched the NMR data reported.[281] The ^{1}H NMR spectrum had a singlet resonance at 2.37 ppm for the acetonitrile protons which integrated to 12H with respect to the cyclopentadienyl protons at 4.25 ppm, which had an integration of 5H. The ESI-MS of complex **8** contained *m/z* peaks with ruthenium isotope patterns of 248.9 and 207.9 which was interpreted as the fragments $[Ru(\eta^5\text{-}$

$C_5H_5)(NCMe)_2]^+$ and $[Ru(\eta^5\text{-}C_5H_5)(NCMe)]^+$ respectively. The cationic fragment of **8** $[Ru(\eta^5\text{-}C_5H_5)(NCMe)_3]^+$ could not be detected, however the expected fragmentation products were observed. In addition, in the ESI-MS the starting complex $[Ru(\eta^5\text{-}C_5H_5)$ (naphthalene)$]^+$ fragment was not detected either. However, other ruthenium-containing products were present; unfortunately these have not been identified.

The initial experiments to synthesise $[Ru(\eta^5\text{-}C_5H_5)(NCMe)_3][PF_6]$, **8** resulted in a product that was approximately 70 % pure and this affected the ability to perform accurate stoichiometric additions at later stages. The purity was based upon the later stoichiometric studies from the addition of triphenylphosphine to **8**. The microwave reaction to synthesise **7** created many impurities and hence the purification stages involving extraction with dichloromethane, filtering with Celite and recrystallisation from diethyl ether stages needed to be repeated in order to obtain a pure product.

A crystal suitable for X-ray diffraction of **7** was obtained from a reaction mixture containing **7**, furan and CD_2Cl_2, which had been left over several weeks under a nitrogen atmosphere in a Youngs NMR tube, to obtain pale yellow crystals (Figure 3.1). The preparation of this complex had previously been reported by Kündig *et al.*,[281, 282] however a crystal structure of this specific complex has not been reported previously. The unit cell contained two cationic $[Ru(\eta^5\text{-}C_5H_5)(naphthalene)]^+$ units and two $[PF_6]^-$ anions. Bond lengths of the two cationic units of **7** appeared to be mostly identical and followed the same trend stated below. The η^6-bonding mode of ruthenium to the naphthalene ligand was not identical for all carbon atoms. The C-H carbon atoms had shorter Ru-C bond lengths between 2.2051(18) - 2.2279(19) Å, when compared to the quaternary carbon atoms which had Ru-C bond lengths of 2.2623(17) and 2.2653(17) Å. The η^5-bonding mode between ruthenium and the cyclopentadienyl ring was shorter than the η^6-bonding of ruthenium to naphthalene, as the Ru-C bond lengths were between 2.156(2) - 2.178(2) Å. The bond angles of the six membered ring coordinated to the ruthenium are not equal, and for C(19)-C(20)-C(21) and C(16)-C(21)-C(20) are 119.37(16) ° and 118.81(16) ° respectively, which are the smallest bond angles. Similar observations have been noted by Hintermann *et al.*, where the cationic unit $[Ru(\eta^5\text{-}C_5H_5)(naphthalene)]^+$ has been crystallised with a different anion, Δ-TRISPHAT.[289] A range of cationic $[Ru(\eta^5\text{-}C_5H_5)(arene)]^+$ complexes have been studied by Perekalin *et al.*,[290] and several X-ray structures have been reported for $[Ru(\eta^5\text{-}C_5H_5)(1,4\text{-}C_6H_4Me_2)]^+$, $[Ru(\eta^5\text{-}C_5H_5)(C_6H_5COOH)]^+$, $[Ru(\eta^5\text{-}C_5H_5)(p\text{-cymene})]^+$ and $[Ru(\eta^5\text{-}C_5H_5)(2,2\text{-paracyclophene})]^+$.[291] From studying the ruthenium to arene interactions, the

first three complexes are mentioned have Ru-C bonds which are either similar or shorter to the cationic unit $[Ru(\eta^5\text{-}C_5H_5)(naphthalene)]^+$ (approx. average 2.21 Å). However, the latter ruthenium cation $[Ru(\eta^5\text{-}C_5H_5)(2,2\text{-paracyclophene})]^+$ has longer Ru-C bond lengths (where longest bond is 2.3400(9) Å) than those observed for the cation of **7**.[291]

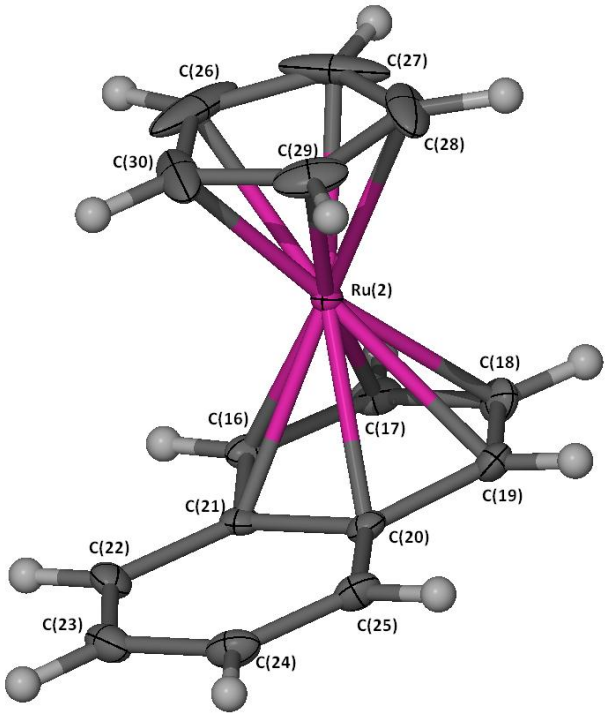

Figure 3.1: X-Seed diagram of one of the ruthenium-containing cation $[Ru(\eta^5\text{-}C_5H_5)(naphthalene)]^+$ in complex **7**. The $[PF_6]^-$ anion has been omitted for clarity, and where shown the thermal ellipsoids are at a 50 % probability level. There was evidence of slight disorder over both cyclopentadienyl rings and $[PF_6]^-$ anions, however a suitable model could not be fitted to the data.

	Bond lengths (Å)		Bond angles (°)
Ru(2)-C(16)	2.2150(18)	C(16)-C(17)-C(18)	120.03(17)
Ru(2)-C(17)	2.2279(19)	C(19)-C(18)-C(17)	120.22(18)
Ru(2)-C(18)	2.2182(19)	C(18)-C(19)-C(20)	120.67(18)
Ru(2)-C(19)	2.2051(18)	C(19)-C(20)-C(21)	119.37(16)
Ru(2)-C(20)	2.2623(17)	C(16)-C(21)-C(20)	118.81(16)
Ru(2)-(C21)	2.2653(17)	C(17)-C(16)-C(21)	120.73(17)
Ru(2)-C(26)	2.178(2)		
Ru(2)-C(27)	2.156(2)		
Ru(2)-C(28)	2.163(2)		
Ru(2)-C(29)	2.170(2)		
Ru(2)-C(30)	2.172(2)		

Table 3.1: Selected bond lengths (Å) and angles (°) for complex **7**.

3.3 Mono-Substituted Half-Sandwich Ruthenium Complexes, $[Ru(\eta^5\text{-}C_5H_5)(PR_3)(NCMe)_2][PF_6]$, $\mathbf{9^R}$

The complex $[Ru(\eta^5\text{-}C_5H_5)(NCMe)_3][PF_6]$, **8** contains labile acetonitrile ligands, which can be substituted with various phosphorus- or nitrogen-containing ligands.[135, 274] Since the acetonitrile ligands are extremely labile the addition of phosphorus ligands may form mono-, *bis*-, or even *tris*-substituted complexes.[131, 134, 274] In this thesis, complexes $\mathbf{9^R}$ therefore act as intermediates, through to the desired $[Ru(\eta^5\text{-}C_5H_5)(PR_3)(L)_2][PF_6]$ complexes (where L= N-containing heterocycle). In this section, the general synthesis and characterisation of complexes $\mathbf{9^R}$ are described. Kirchner *et al.*, reported a general preparation method for complexes $\mathbf{9^R}$ and we have followed this synthetic procedure.[131] The reactivity between **8** and PR_3 ligands (where R = Ph, Me, ^{i}Pr and OPh) has been investigated. Changing the R groups of the PR_3 ligand, will change the steric and electronic properties at the ruthenium centre, and therefore will impact the structure of these complexes and impact their reactivity.[20]

3.3.1 Synthesis of $[Ru(\eta^5\text{-}C_5H_5)(PPh_3)(NCMe)_2][PF_6]$, $\mathbf{9^{Ph}}$

The reaction between **8** and a range of phosphorus-containing ligands has been investigated. The first example investigated was the reaction between **8** and triphenylphosphine. The alkenylation reaction of pyridine and TMS-substituted alkynes employs a ruthenium catalyst, **1** which contains triphenylphosphine to give 2-styrylpyridine derivatives.[253]

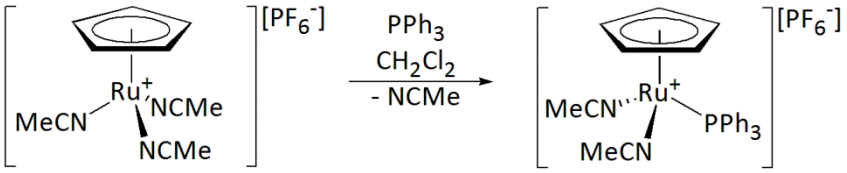

8 **9^{Ph}**

Scheme 3.4: Stoichiometric reaction of complex **8** with triphenylphosphine.

Complex $[Ru(\eta^5\text{-}C_5H_5)(PPh_3)(NCMe)_2][PF_6]$ $\mathbf{9^{Ph}}$, was synthesised as described by Kirchner *et al.*,[131] and the spectroscopic data compared to that reported (Scheme 3.4). The acetonitrile groups in the ^{1}H NMR spectrum appeared as a doublet due to the protons coupling with the phosphorus atom, at 2.05 ppm ($^5J_{HP}$ = 1.5 Hz), confirming that one triphenylphosphine ligand was coordinated to the ruthenium centre. In addition, the cyclopentadienyl protons exhibited a singlet resonance at 4.44 ppm. All aromatic

protons were between 7.28-7.50 ppm as multiplets, and integrated correctly to the cyclopentadienyl and acetonitrile protons. In the $^{31}P\{^{1}H\}$ NMR spectrum the $[PF_6]^-$ ion was seen at -143.0 ppm, and the triphenylphosphine ligand exhibited a singlet at 52.2 ppm. No evidence for the *bis*-substituted complex in the $^{31}P\{^{1}H\}$ NMR spectrum at 51.5 ppm was observed and this was corroborated by the ^{1}H NMR spectrum due to the absence of a triplet resonance for the acetonitrile ligands at 2.12 ppm. An accurate ESI-MS exhibited a ruthenium-containing peak with a *m/z* of 511.0889, which was identified as the cationic fragment $[Ru(\eta^5\text{-}C_5H_5)(PPh_3)(NCMe)_2]^+$ of $\mathbf{9^{Ph}}$. The data suggested that a mono-substitution reaction had occurred between **8** and triphenylphosphine.

3.3.2 Synthesis of $[Ru(\eta^5\text{-}C_5H_5)(PMe_3)(NCMe)_2][PF_6]$, $\mathbf{9^{Me}}$

To investigate the reactivity of the half-sandwich ruthenium complex of the type $[Ru(\eta^5\text{-}C_5H_5)(PR_3)(L)_2][PF_6]$ further, we expanded the library of phosphorus ligands by using trimethylphosphine. Trimethylphosphine is sterically smaller and more electron-donating in character than triphenylphosphine, hence investigation into the properties of these half-sandwich ruthenium complexes would be of great interest.

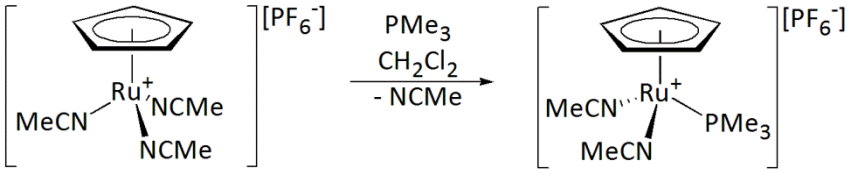

8 **9^{Me}**

Scheme 3.5: Stoichiometric reaction of complex **8** with trimethylphosphine.

The procedure for the synthesis of complex $[Ru(\eta^5\text{-}C_5H_5)(PMe_3)(NCMe)_2][PF_6]$ $\mathbf{9^{Me}}$, involved the stoichiometric addition of trimethylphosphine to **8** in dichloromethane as reported by Kirchner *et al.* (Scheme 3.5).[131] A colour change of the reaction mixture from orange to yellow indicated a reaction has occurred. The NMR spectra and ESI-MS data were compared to the reported literature to confirm the formation of complex $\mathbf{9^{Me}}$.

The ^{1}H NMR spectra displayed a doublet peak at 1.51 ppm with a $^{2}J_{HP}$ coupling of 9.6 Hz due to the methyl groups on the trimethylphosphine ligand. The peak at 1.51 ppm integrated as 9H with respect to peaks at 2.36 ppm ($^{5}J_{HP}$ = 1.6 Hz) which had an integration of 6H due to the methyl groups of the acetonitrile ligands, and at 4.46 ppm

which had an integration of 5H due to the cyclopentadienyl ligand protons. A singlet resonance at 7.6 ppm in the $^{31}P\{^{1}H\}$ NMR spectrum indicated only one trimethylphosphine ligand was present. Additionally, an accurate ESI-MS exhibited at peak with a *m/z* of 325.0406 with a ruthenium isotope pattern, this was identified as the cationic $[Ru(\eta^5\text{-}C_5H_5)(PMe_3)(NCMe)_2]^+$ fragment. These data combined indicated the formation of $\mathbf{9^{Me}}$ and that only the mono-substituted trimethylphosphine complex had been synthesised.

On changing the triphenylphosphine ligand to trimethylphosphine, a difference in the chemical shift of the methyl groups of the acetonitrile ligands is observed. There is a downfield shift from 2.05 ppm ($\mathbf{9^{Ph}}$) to 2.36 ppm ($\mathbf{9^{Me}}$).

3.3.3 Synthesis of $[Ru(\eta^5\text{-}C_5H_5)(P^iPr_3)(NCMe)_2][PF_6]$, $\mathbf{9^{iPr}}$

Triisopropylphosphine is a more electron-donating phosphorus ligand and has a larger cone angle than triphenylphosphine and trimethylphosphine. The reason for studying this ligand was to investigate the scope of the half-sandwich ruthenium complexes in the catalytic reaction of 2-styrylpyridine and look at the properties of the ruthenium complexes.

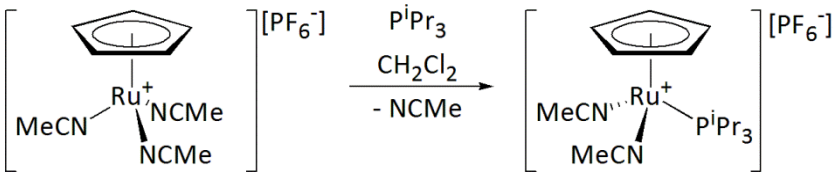

8 **$\mathbf{9^{iPr}}$**

Scheme 3.6: Stoichiometric reaction of complex **8** with triisopropylphosphine.

Following the same preparation method by Kirchner *et al.*,[131] the complex $[Ru(\eta^5\text{-}C_5H_5)(P^iPr_3)(NCMe)_2][PF_6]$ $\mathbf{9^{iPr}}$, was prepared from the stoichiometric addition of triisopropylphosphine to **8** (Scheme 3.6). The ^1H NMR data displayed resonances at 1.21 ppm and between 2.29-2.36 ppm with a multiplicity of a doublet of doublets and a multiplet respectively, due to the triisopropylphosphine ligand. Also, in the ^1H NMR spectrum a doublet ($^5J_{HP}$ = 1.1 Hz) at 2.37 ppm due to the methyl groups of the acetonitrile ligands was observed; the doublet is characteristic of a mono-substituted complex. The integration of the triisopropylphosphine ligand was 18H (1.21 ppm) and 3H (2.29-2.36 ppm) with respect to the acetonitrile ligands of 6H, which indicated mono-substitution by the triisopropylphosphine ligand at the ruthenium centre. The

$^{31}P\{^{1}H\}$ NMR spectrum only displayed two resonances at -143.0 and 57.4 ppm, as a septet due to the $[PF_6]^-$ anion and as a singlet due to the coordinated triisopropylphosphine ligand respectively.

3.3.4 Synthesis of $[Ru(\eta^5\text{-}C_5H_5)(P(OPh)_3)(NCMe)_2][PF_6]$, $\mathbf{9^{OPh}}$

The phosphorus ligands that have been mentioned all have greater electron-donating properties with respect to triphenylphosphine. To understand the effects of different electronic-properties of the phosphorus ligands triphenylphosphite an electron-withdrawing ligand was also trialled.

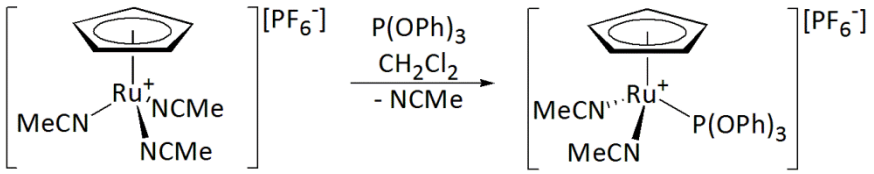

8 **9^{OPh}**

Scheme 3.7: Stoichiometric reaction of complex **8** with triphenylphosphite.

Following the synthetic preparation of Kirchner *et al.* complex $\mathbf{9^{OPh}}$ could be synthesised (Scheme 3.7).[131] There was no reported literature on the synthesis of $\mathbf{9^{OPh}}$, however the methodology to synthesise this complex was carried out in the same manner as all complexes $\mathbf{9^{R}}$. In the ^{1}H NMR spectrum the acetonitrile proton signals appeared at 2.22 ppm as a doublet ($^{5}J_{HP}$ = 1.2 Hz). In addition, the cyclopentadienyl protons also showed signs of coupling to the phosphite group which was not observed with any of the phosphine ligands, at 4.44 ppm ($^{3}J_{HP}$ = 0.6 Hz). The phenyl groups in the ^{1}H NMR spectrum were observed between 7.23-7.41 ppm as multiplets. The $^{31}P\{^{1}H\}$ NMR spectrum contained resonances for the $[PF_6]^-$ anion and the coordinated triphenylphosphite at -143.0 ppm (septet, $^{1}J_{PF}$ = 711 Hz) and 142.6 ppm (singlet).

3.4 Substitution of acetonitrile ligands in complexes 9^{R} with various N-containing heterocycles

Reactions of complexes $\mathbf{9^{R}}$ with various nitrogen-containing ligands has been carried out in order to try and obtain complexes $[Ru(\eta^5\text{-}C_5H_5)(PR_3)(L)_2][PF_6]$, (where R = Ph, OPh, ^{i}Pr, Me, and L = N-containing heterocycle). The N-containing heterocycles we have employed to coordinate to the cationic ruthenium complexes in this section are pyridine, 4-methylpyridine, 4-dimethylaminopyridine, 3-methylpyridine, 2-methylpyridine, 1-methylimidazole and ^{t}butylimidazole. Substituent effects have been studied extensively to determine effects on reaction rates and equilibria. A *para* methyl group donates electron density *via* an inductive effect, with a Hammett substituent effect (σ_p) of -0.17. Alternatively, a *meta* methyl substituent demonstrated a lower σ_m of -0.07. Whereas, a *para* dimethylamino group through a mesomeric effect, exhibits a larger σ_p of -0.83.[292-295]

3.4.1 Reactions of complex 9^{Ph} with N-Containing Heterocycles

3.4.1.1 Reaction of 9^{Ph} with pyridine for the preparation of complex 10^{H}

The independent synthesis of $\mathbf{10^{H}}$ was a significant finding, as this was the complex that we have hypothesised was present in the heated reaction mixture from the addition of d_5-pyridine to complex $[Ru(\eta^5\text{-}C_5H_5)(PPh_3)_2(=C=CHPh)][PF_6]$, $\mathbf{2^{Ph}}$ (Chapter 2).

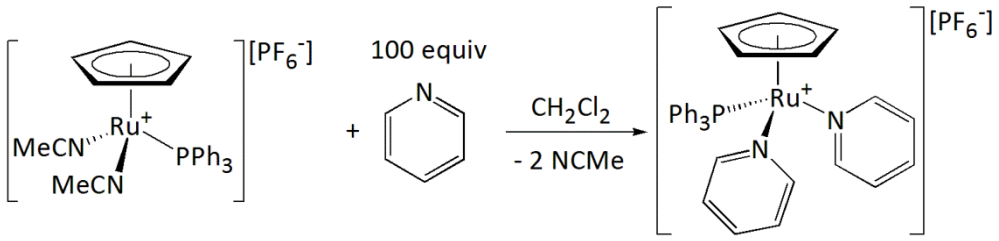

$\mathbf{9^{Ph}}$ $\mathbf{10^{H}}$

Scheme 3.8: Synthesis of complex $\mathbf{10^{H}}$.

The preparation of $\mathbf{10^{H}}$ involved the addition of an excess of pyridine (100 equivalents) to $\mathbf{9^{Ph}}$ in a dichloromethane solution (Scheme 3.8). The resulting orange crystals were air-sensitive and were stored under a nitrogen atmosphere. A high yield of the product $\mathbf{10^{H}}$ was collected (95 %).

The complex $[Ru(\eta^5\text{-}C_5H_5)(PPh_3)(NC_5H_5)_2][PF_6]$ $\mathbf{10^{H}}$, could be clearly identified by NMR spectroscopy in d_2-dichloromethane. A ^{1}H NMR spectrum revealed that the

cyclopentadienyl protons had shifted slightly upfield to 4.42 ppm from 4.44 ppm for complex **9^{Ph}**. In addition, the aromatic region had resonances for the phenyl groups of the triphenylphosphine and pyridine protons between 7.00-8.30 ppm. All coordinated and uncoordinated acetonitrile had been removed, as no signals were observed at 2.05 ppm or 1.97 ppm respectively, in the ^{1}H NMR spectrum. The ^{31}P{^{1}H} NMR spectrum contained peaks for the $[PF_6]^-$ anion and the triphenylphosphine ligand at -143.0 and 50.2 ppm respectively. A high resolution ESI-MS detected the complete cationic ruthenium complex $[Ru(\eta^5\text{-}C_5H_5)(PPh_3)(NC_5H_5)_2]^+$ with a peak of *m/z* 587.1190. Fragmentation peaks for $[Ru(\eta^5\text{-}C_5H_5)(PPh_3)(NC_5H_5)(NCCH_3)]^+$ and $[Ru(\eta^5\text{-}C_5H_5)(PPh_3)(NC_5H_5)]^+$ were detected at a *m/z* of 549.1037 and 508.0772 respectively. Under these conditions the pyridine ligands were extremely labile and could have been lost or substituted very easily within the spectrometer. This is due to the sample being prepared in an acetonitrile solution or the presence of acetonitrile within the spectrometer.

The complex **10^{H}** was dissolved in d_5-pyridine and ^{1}H and ^{31}P{^{1}H} NMR spectra collected. The ^{1}H NMR exhibited a resonance at 4.57 ppm as a singlet for the cyclopentadienyl protons and two multiplets at 7.36-7.42 and 7.47 ppm were observed for the triphenylphosphine ligand. In the ^{1}H NMR spectrum, the coordinated pyridine molecules were no longer observed as it is possible that they are exchanging with the uncoordinated d_5-pyridine solvent to give $[Ru(\eta^5\text{-}C_5H_5)(PPh_3)(NC_5D_5)_2][PF_6]$, **5**. The ^{31}P{^{1}H} NMR spectrum displayed only two resonances at -143.0 and 49.2 ppm as a septet and a singlet, for the $[PF_6]^-$ anion and the triphenylphosphine ligand respectively.

Attempts were made to carry out a one-pot reaction to obtain complex **10^{H}** from **8,** by stoichiometric addition of triphenylphosphine in a pyridine solution; however uncoordinated acetonitrile present in the reaction mixture competes with the pyridine. This creates an equilibrium between a mono-substituted pyridine complex $[Ru(\eta^5\text{-}C_5H_5)(PPh_3)(NC_5H_5)(NCMe)][PF_6]$ and the *bis*-substituted pyridine complex **10^{H}**. Therefore, it has been easier to isolate the pure product **10^{H}** from a stepwise procedure and isolating complex **9^{Ph}** as an intermediate.

Crystals suitable for X-ray crystallography were obtained by slow diffusion of either hexane or pentane into the reaction mixture containing complex **10^{H}** (Figure 3.2, Table 3.2). The bond angles of N(2)-Ru(1)-N(1), N(1)-Ru(1)-P(1) and N(2)-Ru(1)-P(1) were 88.12(7), 91.04(5) and 97.35(5) ° respectively, which suggests a distorted octahedral

geometry. The bond angle between the two coordinated pyridine molecules is the smallest, due to the steric requirements of the triphenylphosphine ligand. The ruthenium to cyclopentadienyl ligand bonding has been studied, and the bond lengths for C(3)-Ru(1) and C(4)-Ru(1) are 2.221(2) and 2.220(2) Å respectively, which is notably longer than the adjacent Ru-C bond lengths of C(2)-Ru(1) and C(5)-Ru(1) are 2.182(2) and 2.188(2) Å respectively. From studying the structure of the cation of **10^{H}** (Figure 3.2), the longer bond lengths could be attributed to the *trans* triphenylphosphine ligand which causes a destabilisation of these bonds as it has a higher *trans* influence than the nitrogen donor ligands. The P(1)-Ru(1) bond length was found to be 2.3181(6) Å. Additionally, the ruthenium to nitrogen bond lengths were statistically inequivalent, where the N(1)-Ru(1) of 2.1530(18) Å, was longer than N(2)-Ru(1) of 2.1293(19) Å. This could potentially be due to the pyridine fragment, containing N(1) being close in space to two phenyl rings of the triphenylphosphine ligand, where as the pyridine molecule belonging to N(2) is adjacent to only one phenyl ring.

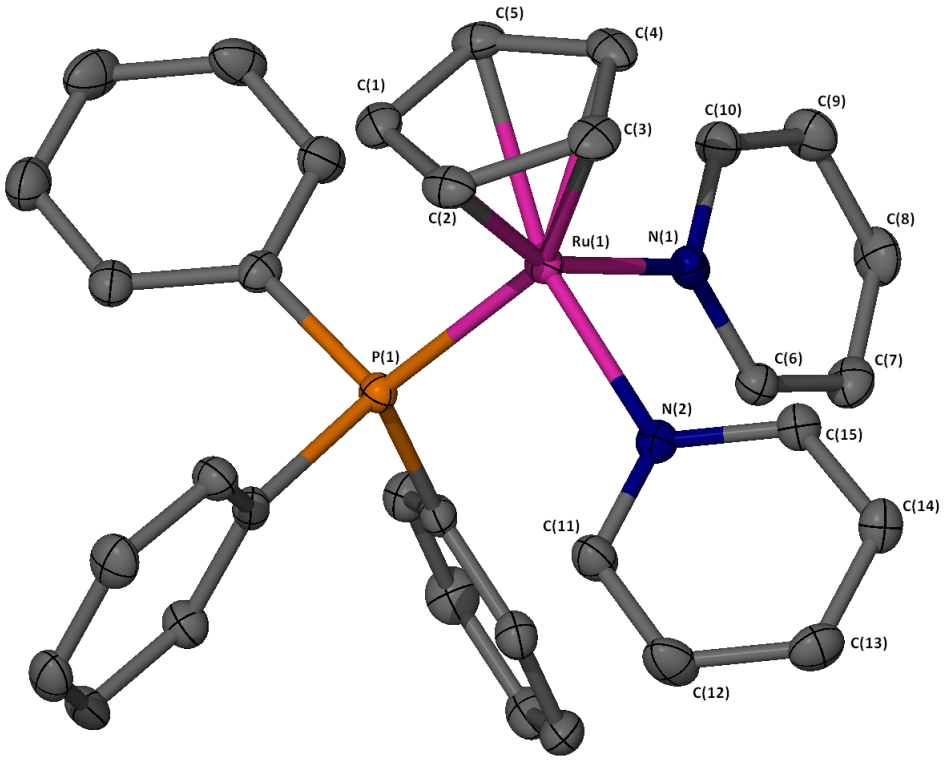

Figure 3.2: X-Seed diagram of the cation $[Ru(\eta^5\text{-}C_5H_5)(PPh_3)(NC_5H_5)_2]^+$ from complex **10^{H}**. Hydrogen atoms, a dichloromethane molecule and $[PF_6]^-$ anion have been omitted for clarity, and where shown the thermal ellipsoids are at a 50 % probability level. The $[PF_6]^-$ anion was disordered over two positions in a ratio of 3:1.

	Bond lengths (Å)		Bond angles (°)
C(1)-Ru(1)	2.220(2)	N(2)-Ru(1)-N(1)	88.12(7)
C(2)-Ru(1)	2.182(2)	N(1)-Ru(1)-P(1)	91.04(5)
C(3)-Ru(1)	2.221(2)	N(2)-Ru(1)-P(1)	97.35(5)
C(4)-Ru(1)	2.220(2)	C(6)-N(1)-C(10)	116.48(19)
C(5)-Ru(1)	2.188(2)	N(1)-C(6)-C(7)	123.3(2)
N(1)-Ru(1)	2.1530(18)	C(8)-C(7)-C(6)	119.7(2)
N(2)-Ru(1)	2.1293(19)	C(7)-C(8)-C(9)	117.7(2)
P(1)-Ru(1)	2.3181(6)	C(10)-C(9)-C(8)	119.4(2)
C(6)-N(1)	1.342(3)	N(1)-C(10)-C(9)	123.4(2)
C(10)-N(1)	1.351(3)	C(11)-N(2)-C(15)	117.0(2)
C(11)-N(2)	1.347(3)	N(2)-C(11)-C(12)	122.5(2)
C(15)-N(2)	1.351(3)	C(13)-C(12)-C(11)	119.8(2)
		C(12)-C(13)-C(14)	118.4(2)
		C(15)-C(14)-C(13)	118.9(2)
		N(2)-C(15)-C(14)	123.4(2)

Table 3.2: Selected bond lengths (Å) and angles (°) for complex **10^{H}**.

3.4.1.2 Reaction of 9^{Ph} with d_5- pyridine for the preparation of complex 5

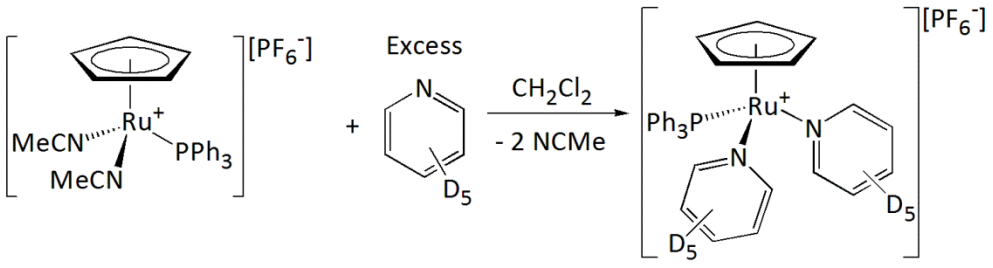

9^{Ph} **5**

Scheme 3.9: Synthesis of complex **5**.

The synthesis of $[Ru(\eta^5\text{-}C_5H_5)(PPh_3)(NC_5D_5)_2][PF_6]$, **5** was carried out in a similar fashion to the synthesis of **10^{H}** (Scheme 3.9). The product was collected in a high yield of 75 %, and ^1H and $^{31}P\{^1H\}$ NMR spectra used for the characterisation of **5**. The ^1H NMR spectrum of **5** in d_2-dichloromethane was similar to **10^{H}**, however resonances for the pyridine protons were absent. The $^{31}P\{^1H\}$ NMR spectrum revealed a slightly downfield chemical shift of 50.4 ppm. Additionally, a high resolution ESI-MS contained a *m/z* peak at 597.1823 for a ruthenium-containing complex, which was assigned as the cationic $[Ru(\eta^5\text{-}C_5H_5)(PPh_3)(NC_5D_5)_2]^+$ fragment.

3.4.1.3 Reaction of ***9^{Ph}*** *with 4-methylpyridine for the preparation of complex* ***10^{Me}***

The ability of 4-methylpyridine to act as a ligand at the ruthenium centre was evaluated. The methyl group in the 4-position of the N-containing heterocycle would change the electronic properties of the ligand and avoid any steric influences close to the ruthenium centre. The properties of coordinating a more electron-donating N-containing heterocycle to the ruthenium fragment $[Ru(\eta^5\text{-}C_5H_5)(PR_3)]^+$ was investigated and differences were observed in the synthesis of **10^{Me}**.

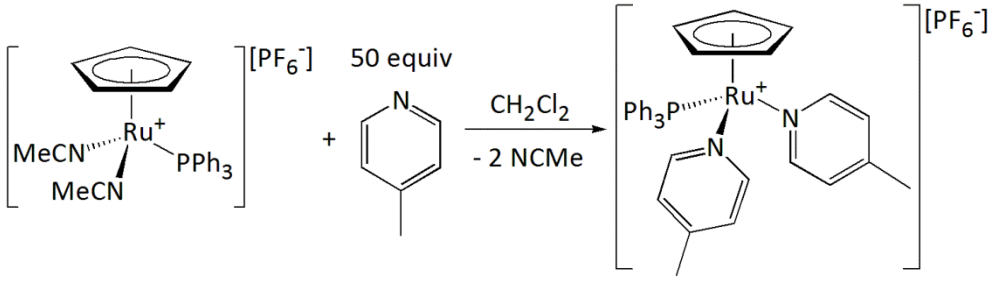

9^{Ph} **10^{Me}**

Scheme 3.10: Synthesis of complex **10^{Me}.**

Complex **10^{Me}** was synthesised *via* the addition of 50 equivalents of 4-methylpyridine to **9^{Ph}** in dichloromethane (Scheme 3.10) and was fully characterised through NMR spectroscopy, high resolution ESI-MS, elemental analysis and X-ray crystallography.

The ^{1}H NMR spectrum of **10^{Me}** in d_2-dichloromethane displayed a singlet resonance for the cyclopentadienyl protons at 4.36 ppm. The 4-methylpyridine resonances in the ^{1}H NMR spectrum were exhibited at 2.32 (singlet), 6.86 (doublet) and 8.10 (doublet) ppm, for the methyl, and the C-3/5 and C-2/6 positions protons respectively. The integration of the methyl group protons on the 4-methylpyridine was 6H with respect to the cyclopentadienyl resonance at 4.36 ppm which had an integration of 5H. In addition, the absence of any doublet resonance at approximately 2.05 ppm for the methyl protons of the acetonitrile ligands, suggested there was no acetonitrile present in the product. The ^{1}H NMR spectrum indicated that substitution of both the acetonitrile ligands by 4-methylpyridine had occurred. The ^{31}P{^{1}H} NMR spectrum displayed the triphenylphosphine resonance at 50.4 ppm (singlet). The signal for **9^{Ph}** at 52.2 ppm was not present in the final product, suggesting all of the starting material had reacted. The ^{13}C{^{1}H} NMR spectrum displayed a doublet resonance at 77.9 ppm with a $^2J_{CP}$ of 1.9 Hz for the cyclopentadienyl carbon atoms. The ^{13}C{^{1}H} NMR spectrum displayed a doublet resonance at 156.0 ppm with a $^3J_{CP}$ coupling of 2.0 Hz from the phosphorus atom of the triphenylphosphine ligand to the carbon atom at the C-2/6 positions of the

4-methylpyridine ligands. This suggested that there were two 4-methylpyridine ligands coordinated to the ruthenium centre in **10^{Me}**.

The high resolution ESI-MS contained an accurate *m/z* peak of 615.1503 with a ruthenium isotope pattern, which could be assigned to $[Ru(\eta^5\text{-}C_5H_5)(PPh_3)(NC_5H_4\text{-}4\text{-}Me)_2]^+$. In addition, a signal with a *m/z* of 563.1187 was due to $[Ru(\eta^5\text{-}C_5H_5)(PPh_3)(NC_5H_4\text{-}4\text{-}Me)(NCMe)]^+$, and a *m/z* of 522.0929 was assigned to the loss of a 4-methylpyridine molecule, $[Ru(\eta^5\text{-}C_5H_5)(PPh_3)(NC_5H_4\text{-}4\text{-}Me)]^+$.

Crystals of **10^{Me}** could be obtained from the slow diffusion of pentane into a layer of dichloromethane containing **10^{Me}** (Figure 3.3, Table 3.3). The cation of **10^{Me}** contained a cyclopentadienyl ruthenium fragment which was bonded to two 4-methylpyridine molecules through the nitrogen atoms and a triphenylphosphine ligand. The geometry of the ruthenium-containing cation was a distorted octahedral structure, where the bond angles for N(1)-Ru(1)-P(2), N(2)-Ru(1)-P(2), and N(2)-Ru(1)-N(1) were 90.10(9), 99.77(9), and 84.17(13) ° respectively. The latter bond angle between the two 4-methylpyridine molecules was the smallest, and could be attributed to the higher steric demands of the triphenylphosphine ligand. In comparison to **10^{H}**, the N-Ru-N bond angle for **10^{Me}** is 3.98 ° smaller. The η^5-bonding of the cyclopentadienyl ligand to the ruthenium centre is not uniform, the bond lengths of C(14)-Ru(1) and C(15)-Ru(1) are 2.211(4) and 2.208(4) Å respectively, which are longer than the other Ru-C bond lengths (range from 2.149(5) - 2.169(4) Å). The longer bond lengths are a result of the *trans* triphenylphosphine ligand. A statistical difference in the ruthenium to nitrogen bond lengths N(1)-Ru(1) and N(2)-Ru(1) of 2.181(3) and 2.125(3) Å respectively were observed. The N(1) atom was closer in proximity to the quaternary carbon atom of the triphenylphosphine ligand (3.359 Å), possibly causing a longer Ru-N bond length. The P(2)-Ru(1) bond length was found to be 2.3105(9) Å, which is very similar to complex **10^{H}**.

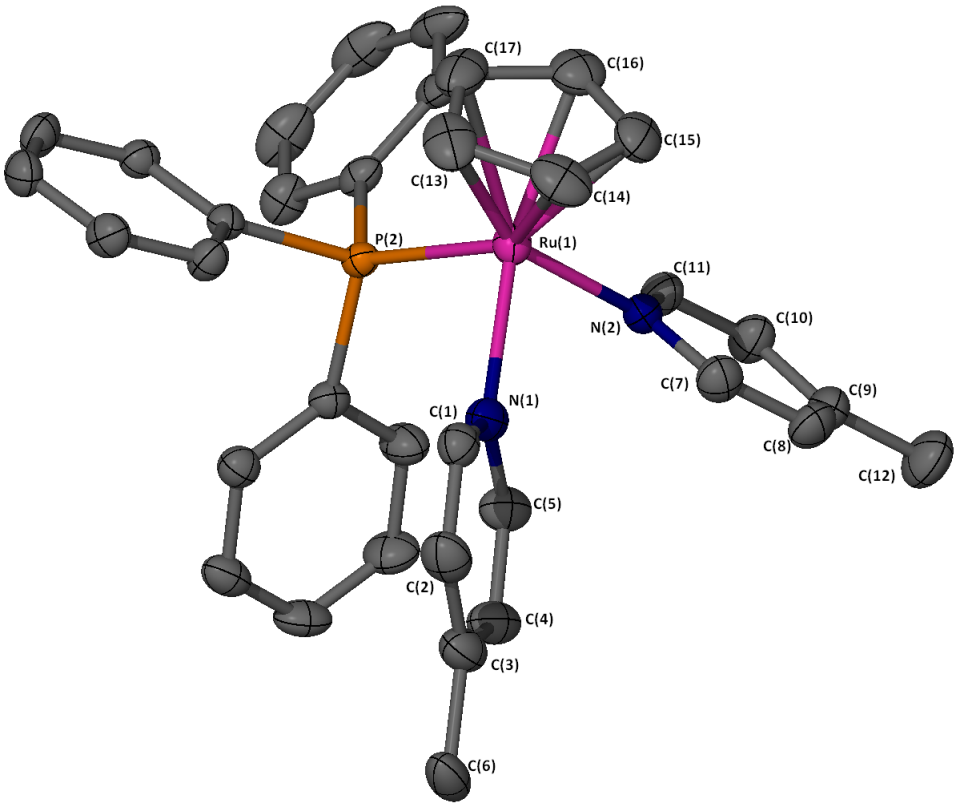

Figure 3.3: X-Seed diagram of the cation $[Ru(\eta^5\text{-}C_5H_5)(PPh_3)(NC_5H_4\text{-}p\text{-}Me)_2]^+$ from complex **10^{Me}**. Hydrogen atoms, a dichloromethane molecule and $[PF_6]^-$ anion have been omitted for clarity, and where shown the thermal ellipsoids are at a 50 % probability level. The $[PF_6]^-$ anion displayed disorder over two positions and was refined to a ratio of 74.2:25.8(9).

	Bond lengths (Å)		Bond angles (°)
C(13)-Ru(1)	2.169(4)	N(1)-Ru(1)-P(2)	90.10(9)
C(14)-Ru(1)	2.211(4)	N(2)-Ru(1)-P(2)	99.77(9)
C(15)-Ru(1)	2.208(4)	N(2)-Ru(1)-N(1)	84.17(13)
C(16)-Ru(1)	2.165(5)	C(1)-N(1)-C(5)	116.2(4)
C(17)-Ru(1)	2.149(5)	N(1)-C(1)-C(2)	123.2(4)
P(2)-Ru(1)	2.3105(9)	C(1)-C(2)-C(3)	120.3(4)
N(1)-Ru(1)	2.181(3)	C(4)-C(3)-C(2)	116.4(4)
N(2)-Ru(1)	2.125(3)	C(3)-C(4)-C(5)	119.4(4)
C(1)-N(1)	1.332(5)	N(1)-C(5)-C(4)	124.6(4)
C(5)-N(1)	1.357(5)	C(11)-N(2)-C(7)	116.6(3)
C(7)-N(2)	1.354(5)	N(2)-C(7)-C(8)	122.5(4)
C(11)-N(2)	1.332(5)	C(7)-C(8)-C(9)	120.4(4)
C(3)-C(6)	1.540(6)	C(8)-C(9)-C(10)	117.1(4)
C(9)-C(12)	1.494(6)	C(11)-C(10)-C(9)	119.3(4)
		N(2)-C(11)-C(10)	124.0(4)

Table 3.3: Selected bond lengths (Å) and angles (°) for complex **10^{Me}**.

3.4.1.4 Reaction of 9^{Ph} with 4-dimethylaminopyridine for the preparation of complex 10^{NMe2}

Coordination of the ligand 4-dimethylaminopyridine to complex $\mathbf{9^{Ph}}$ was also attempted. The substituent NMe_2 in the 4-position on the pyridine ligand contributes electron density to the aromatic system through conjugation from the lone pair on the NMe_2 group, specifically at the C-3/5 positions and the nitrogen atom , therefore creating an extremely good donor ligand.[29] The synthesis and properties of $\mathbf{10^{NMe2}}$ has been investigated.

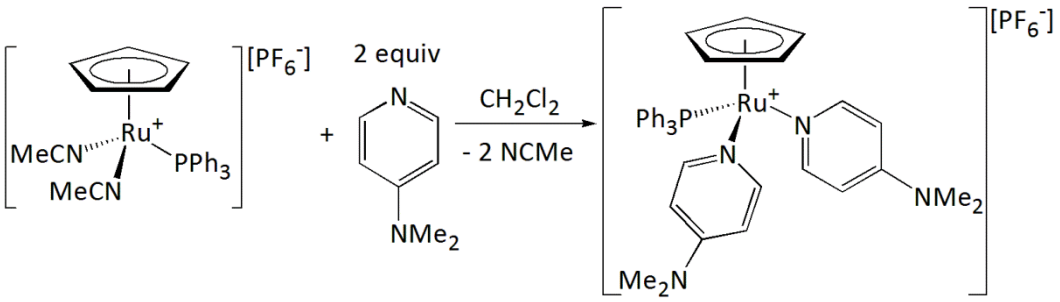

$\mathbf{9^{Ph}}$ $\mathbf{10^{NMe2}}$

Scheme 3.11: Synthesis of complex $\mathbf{10^{NMe2}}$.

The synthetic preparation of $\mathbf{10^{NMe2}}$ was similar to those of complexes $\mathbf{10^{H}}$ and $\mathbf{10^{Me}}$, however the addition of 4-dimethylaminopyridine was reduced to the exact equivalents required (two equivalents) (Scheme 3.11). Any excess 4-dimethylaminopyridine that remained in the reaction mixture was removed by washing the resulting precipitate with toluene. It was found that $\mathbf{10^{NMe2}}$ was more air-sensitive in nature, probably due to the increase of electron density at the ruthenium centre.

The ^{1}H NMR spectrum of $\mathbf{10^{NMe2}}$ in d_2-dichloromethane displayed resonances at 2.96 ppm for the methyl groups on the 4-dimethylaminopyridine ligands and at 4.25 ppm for the cyclopentadienyl protons; these resonances had relative integrations of 12H to 5H, which would only occur if two 4-dimethylaminopyridine ligands were coordinated to the ruthenium centre. The other peaks in the ^{1}H NMR spectrum were in the aromatic region between 6.16-7.73 ppm. The protons at the C-2/6 and C-3/5 positions of the 4-dimethylaminopyridine ligands displayed resonances at 7.73 and 6.16 ppm respectively, where both peaks integrated as 4H with respect to the cyclopentadienyl protons at 4.25 ppm. The ^{1}H NMR spectrum did not exhibit a resonance at 2.05 ppm for the methyl groups of the acetonitrile ligand, which strongly suggested substitution of both acetonitrile ligands with 4-dimethylaminopyridine. Peaks for uncoordinated DMAP at

2.97 ppm for the methyl groups, and at 6.48 and 8.16 ppm for the aromatic protons were not detected. The $^{31}P\{^{1}H\}$ NMR spectrum exhibited a resonance at 51.4 ppm as a singlet, due to the phosphorus atom of the triphenylphosphine ligand which was coordinated to the ruthenium centre. The $^{13}C\{^{1}H\}$ NMR data was consistent with what was observed in the ^{1}H and $^{31}P\{^{1}H\}$ NMR spectra. A doublet resonance at 77.0 ppm for the cyclopentadienyl ligand displayed a $^{2}J_{CP}$ of 2.6 Hz. In addition, the $^{13}C\{^{1}H\}$ NMR spectrum at 155.3 ppm displayed a doublet resonance with a $^{3}J_{CP}$ of 1.7 Hz for the carbon atom at the C-2/6 positions of the 4-dimethylaminopyridine ligand, where as the carbon atoms at the C-3/5 positions only displayed a singlet peak at 107.8 ppm.

The high resolution ESI-MS contained several cationic ruthenium complexes with *m/z* peaks of 673.2031, 592.1460 and 511.1205, which have been assigned as $[Ru(\eta^5\text{-}C_5H_5)(PPh_3)(NC_5H_4\text{-}4\text{-}NMe_2)_2]^+$, $[Ru(\eta^5\text{-}C_5H_5)(PPh_3)(NC_5H_4\text{-}4\text{-}NMe_2)(NCMe)]^+$, and $[Ru(\eta^5\text{-}C_5H_5)(PPh_3)(NCMe)]^+$ respectively.

Crystals suitable for single crystal X-ray crystallography of $\mathbf{10^{NMe2}}$ were obtained through slow diffusion of pentane into a solution of $\mathbf{10^{NMe2}}$ in dichloromethane. A distorted octahedral geometry was observed for the cation of $\mathbf{10^{NMe2}}$ where the bond angles of N(1)-Ru(1)-P(1), N(3)-Ru(1)-P(1) and N(3)-Ru(1)-N(1) were 97.35(4), 89.77(4) and 87.74(5) ° respectively. The smallest bond angle was N(3)-Ru(1)-N(1), which is probably due to the steric requirements of the triphenylphosphine ligand. However, the N(3)-Ru(1)-N(1) bond angle is closer to $\mathbf{10^{H}}$ than $\mathbf{10^{Me}}$. Similar to the previously mentioned X-ray structures, the Ru-C bond lengths of the cyclopentadienyl ligand *trans* to the triphenylphosphine ligand are significantly longer. The C(2)-Ru(1) and C(3)-Ru(1) bond lengths of 2.2229(17) and 2.2312(17) Å respectively, were longer than the other Ru-C bond lengths. For $\mathbf{10^{NMe2}}$ the Ru-N bond lengths were statistically equivalent.

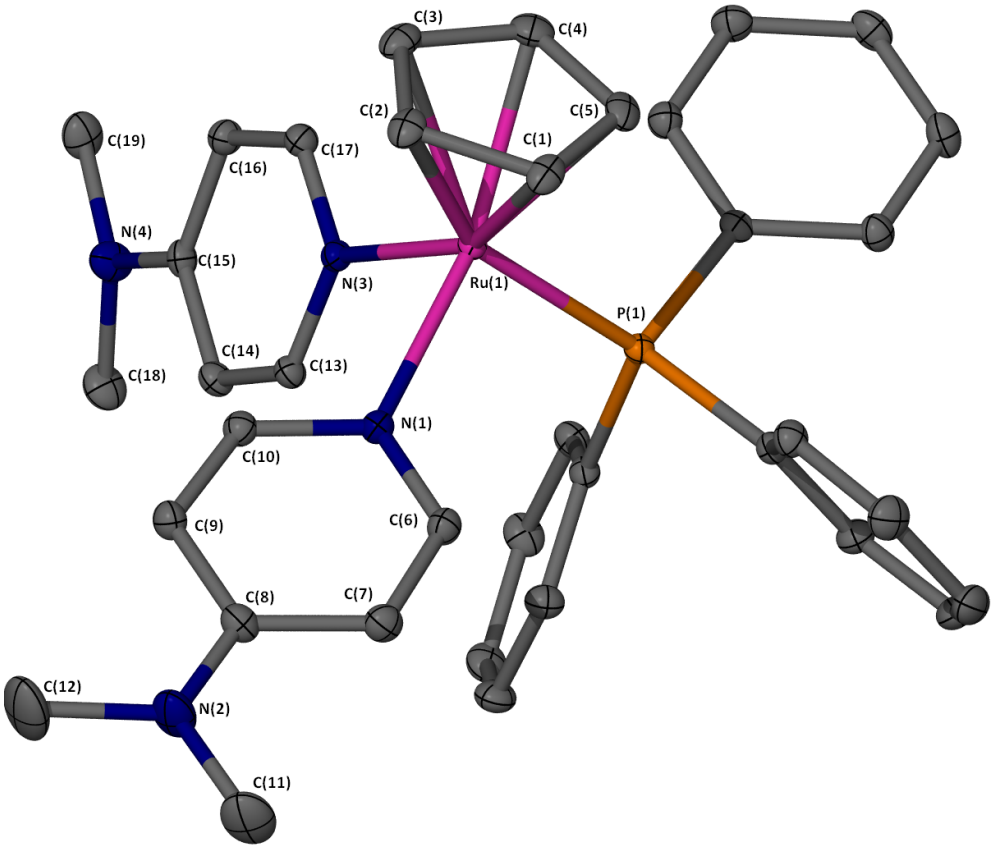

Figure 3.4: X-Seed diagram of the cation $[Ru(\eta^5\text{-}C_5H_5)(PPh_3)(NC_5H_4\text{-}4\text{-}NMe_2)_2]^+$ from complex **10**^{NMe2}. Hydrogen atoms, a dichloromethane molecule and $[PF_6]^-$ anion have been omitted for clarity, and where shown the thermal ellipsoids are at a 50 % probability level. . The $[PF_6]^-$ anion was in a special position which could not be modelled.

	Bond lengths (Å)		Bond angles (°)
C(1)-Ru(1)	2.1679(17)	N(1)-Ru(1)-P(1)	97.35(4)
C(2)-Ru(1)	2.2229(17)	N(3)-Ru(1)-P(1)	89.77(4)
C(3)-Ru(1)	2.2312(17)	N(3)-Ru(1)-N(1)	87.74(5)
C(4)-Ru(1)	2.1964(18)	C(10)-N(1)-C(6)	114.83(15)
C(5)-Ru(1)	2.1632(17)	N(1)-C(6)-C(7)	124.99(16)
P(1)-Ru(1)	2.3070(4)	C(6)-C(7)-C(8)	119.99(16)
N(1)-Ru(1)	2.1532(14)	C(7)-C(8)-C(9)	115.12(16)
N(3)-Ru(1)	2.1555(13)	C(8)-C(9)-C(10)	120.48(16)
C(6)-N(1)	1.358(2)	N(1)-C(10)-C(9)	124.57(15)
C(10)-N(1)	1.358(2)	C(13)-N(3)-C(17)	115.38(14)
C(13)-N(3)	1.351(2)	N(3)-C(13)-C(14)	124.51(15)
C(17)-N(3)	1.358(2)	C(13)-C(14)-C(15)	119.71(16)
		C(14)-C(15)-C(16)	116.16(15)
		C(15)-C(16)-C(17)	119.90(15)
		N(3)-C(17)-C(16)	124.28(16)

Table 3.4: Selected bond lengths (Å) and angles (°) for complex **10**^{NMe2}.

*3.4.1.5 Reaction of **9**^{Ph} with 3-methylpyridine for the preparation of complex **11***

Other substituent effects have also been investigated; including the location of the methyl group at the C-3 position of the pyridine molecule. The reason for studying the formation of **11** was to observe if the methyl group would have any steric influence at the ruthenium centre on synthesising the half-sandwich ruthenium complex. Also, if **11** was synthesised it would be of interest to explore if any selectivity is observed in the formation of the 2-styrylpyridine derivative from the alkenylation reaction.

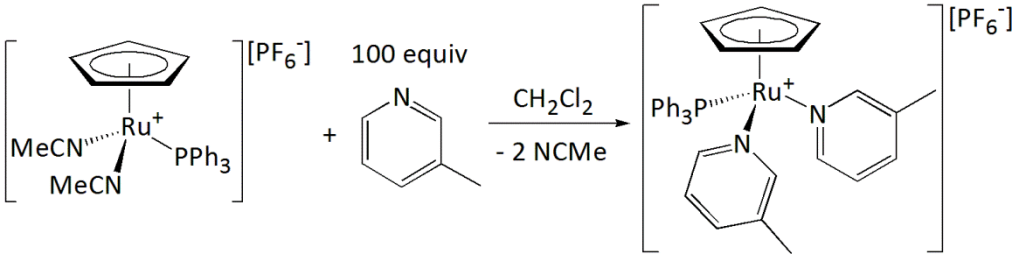

9^{Ph} **11**

Scheme 3.12: Synthesis of complex **11**.

Complex **11** was prepared from **9**^{Ph} in a similar manner to **10**^{H}, where an excess of 3-methylpyridine (100 equivalents) was added to a dichloromethane solution of **9**^{Ph} (Scheme 3.12). Orange air-sensitive crystals of the complex could be obtained through slow diffusion of pentane into a dichloromethane solution containing **11**, and isolated in a reasonable yield (67 %).

The ^{1}H NMR spectrum of **11** exhibited singlet resonances for the methyl group at 2.00 ppm and the cyclopentadienyl protons at 4.40 ppm, which integrated in a manner of 6H to 5H respectively. The aromatic hydrogen atoms on the 3-methylpyridine ligand exhibited individual resonances at 7.01, 7.49, 7.93 and 8.28 ppm, where they all integrate as 2H with respect to the cyclopentadienyl protons at 4.40 ppm (5H). The protons at the C-2/6 positions of the 3-methylpyridine were assigned at 7.93 and 8.28 ppm which had a singlet and doublet multiplicity respectively. The integrations suggest that there are two 3-methylpyridine molecules coordinated to the ruthenium centre. The ^{31}P{^{1}H} NMR spectrum displayed a singlet resonance at 49.1 ppm for the triphenylphosphine ligand coordinated to the ruthenium centre, in addition to the septet resonance at -144.4 ppm ($^{1}J_{PF}$ = 711 Hz) for the $[PF_6]^-$ anion. There are no other peaks for any other metal complexes. The ^{13}C{^{1}H} NMR spectrum displayed a peak at 18.4 ppm for the methyl carbon atoms of 3-methylpyridine. Additionally, in the ^{13}C{^{1}H} NMR spectrum at 78.1 ppm a doublet with a $^{2}J_{CP}$ of 1.9 Hz, was assigned as the

cyclopentadienyl carbon atoms. The carbon atoms at the C-2 and C-6 positions of the 3-methylpyridine ligands exhibited doublet signals at 154.1 and 156.7 ppm, with $^{3}J_{CP}$ of 1.9 and 2.4 Hz respectively. These data suggested that two 3-methylpyridine ligands were coordinated to the ruthenium complex as a coupling between the carbon atoms at the C-2 and C-6 positions and the triphenylphosphine phosphorus atom was observed.

The high resolution ESI-MS displayed a peak with a *m/z* of 615.1493 which is expected for $[Ru(\eta^5\text{-}C_5H_5)(PPh_3)(NC_5H_4\text{-}3\text{-}Me)_2]^+$ of **11**. Further fragmentation was observed at 563.1177 and 522.0916 for the cationic ruthenium complexes where the earlier species has lost a 3-methylpyridine ligand and been substituted by an acetonitrile ligand to give $[Ru(\eta^5\text{-}C_5H_5)(PPh_3)(NC_5H_4\text{-}3\text{-}Me)(NCMe)]^+$ and the latter has lost a 3-methylpyridine ligand to yield $[Ru(\eta^5\text{-}C_5H_5)(PPh_3)(NC_5H_4\text{-}3\text{-}Me)]^+$.

Crystals suitable for single crystal X-ray crystallography of **11** were obtained through slow diffusion of pentane into a solution of the species in dichloromethane (Figure 3.5, Table 3.5). In the ruthenium-containing cationic species, one of the phenyl rings of the triphenylphosphine ligand was disordered over two positions. The geometry of the ruthenium cation of **11**, can be described as a distorted octahedron where the ruthenium bond angles of N(1)-Ru(1)-P(1), N(2)-Ru(1)-P(1), and N(2)-Ru(1)-N(1) are 90.66(5), 96.07(5), and 89.41(7) ° respectively. The bond angle between the two 3-methylpyridine molecules of N(2)-Ru(1)-N(1) is 89.41(7) ° is the smallest in the structure. The ruthenium to cyclopentadienyl ligand bonding is not equivalent, as the C(31)-Ru(1), C(32)-Ru(1) and C(33)-Ru(1) bonds lengths are 2.195(2), 2.224(2) and 2.205(2) Å respectively, which are longer than the other Ru-C bond lengths. The bond lengths C(32)-Ru(1) and C(33)-Ru(1) are *trans* to a triphenylphosphine ligand. The two Ru-N bond lengths were not equivalent. The P(1)-Ru(1) bond length was found to be 2.3186(6) Å.

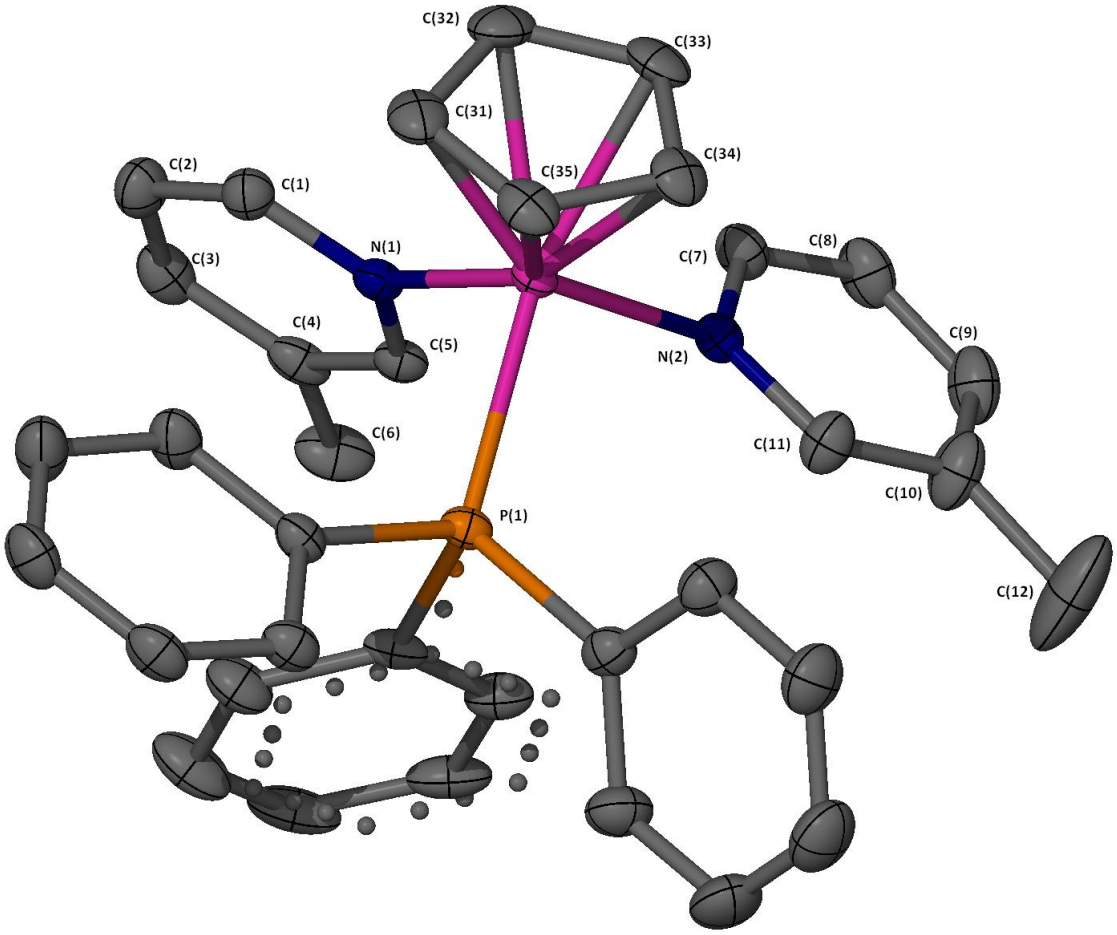

Figure 3.5: X-Seed diagram of the cation $[Ru(\eta^5\text{-}C_5H_5)(PPh_3)(NC_5H_4\text{-}3\text{-}Me)_2]^+$ from complex **11**. Hydrogen atoms, a dichloromethane molecule and $[PF_6]^-$ anion have been omitted for clarity, and where shown the thermal ellipsoids are at a 50 % probability level. The dichloromethane molecule was disordered over two positions with occupancies of 0.55629:0.44371. The $[PF_6]^-$ anion was disordered in two positions, and modelled with occupancies of 0.67953:0.32047. A phenyl group of the triphenylphosphine ligand is disordered in two positions (major and minor, in a 0.75304:0.24696 ratio respectively), where the minor component is shown as fragmented spheres.

	Bond lengths (Å)		Bond angles (°)
C(31)-Ru(1)	2.195(2)	N(1)-Ru(1)-P(1)	90.66(5)
C(32)-Ru(1)	2.224(2)	N(2)-Ru(1)-P(1)	96.07(5)
C(33)-Ru(1)	2.205(2)	N(2)-Ru(1)-N(1)	89.41(7)
C(34)-Ru(1)	2.166(2)	C(1)-N(1)-C(5)	117.0(2)
C(35)-Ru(1)	2.158(2)	N(1)-C(1)-C(2)	122.8(2)
P(1)-Ru(1)	2.3186(6)	C(1)-C(2)-C(3)	119.3(3)
N(1)-Ru(1)	2.1527(19)	C(4)-C(3)-C(2)	119.0(2)
N(2)-Ru(1)	2.135(2)	C(3)-C(4)-C(5)	118.0(2)
C(1)-N(1)	1.354(3)	N(1)-C(5)-C(4)	123.9(2)
C(5)-N(1)	1.347(3)	C(11)-N(2)-C(7)	117.1(2)
C(7)-N(2)	1.351(3)	N(2)-C(7)-C(8)	122.7(2)
C(11)-N(2)	1.340(3)	C(7)-C(8)-C(9)	119.1(3)
C(4)-C(6)	1.496(4)	C(8)-C(9)-C(10)	119.3(3)
C(10)-C(12)	1.512(5)	C(11)-C(10)-C(9)	117.7(3)
		N(2)-C(11)-C(10)	123.9(2)

Table 3.5: Selected bond lengths (Å) and angles (°) for complex **11**.

*3.4.1.6 Reaction of 9^{Ph} with 2-methylpyridine for the preparation of complex **12***

The addition of 2-methylpyridine to $\mathbf{9^{Ph}}$ in dichloromethane, was carried out in order to observe if the *bis*-substituted 2-methylpyridine could be synthesised. The methyl group in the C-2 position of the pyridine molecule provided a very clear steric hindrance with the nitrogen donor atom, and could inhibit the ligand from coordinating to the ruthenium centre.[212] A similar procedure to the preparation of complex $\mathbf{10^{H}}$ was followed (Scheme 3.13) where 2-methylpyridine (approximately 100 equivalents) was added to $\mathbf{9^{Ph}}$ in a dichloromethane solution and reaction mixture stirred for 16 hours, the product was precipitated, collected and analysed.

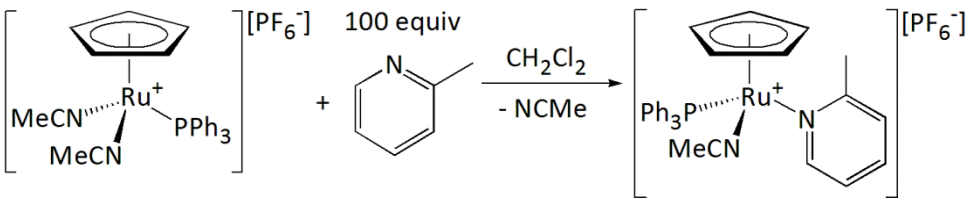

$\mathbf{9^{Ph}}$ **12**

Scheme 3.13: General synthesis of complex **12**.

After the addition of 2-methylpyridine to **9^{Ph}** for 16 hours, the reaction mixture had undergone a colour change from a yellow to a brown solution. The brown precipitate was collected and ^{1}H and ^{31}P{^{1}H} NMR spectra recorded, which displayed the presence of several ruthenium-containing products. The ^{1}H NMR spectrum indicated that there were three significant resonances for the cyclopentadienyl protons at 4.43 (two adjacent peaks) and 4.46 ppm. In addition, three sets of acetonitrile peaks were observed at 1.86, 2.05 and 2.06 ppm as doublets with $^{5}J_{HP}$ couplings of approximately 1.5 Hz and no uncoordinated acetonitrile protons were observed at 1.97 ppm. The ^{31}P{^{1}H} NMR spectrum exhibited four resonances at -143.0, 52.2, 52.3 and 54.3 ppm, whereas the former resonance was for the $[PF_6]^-$ anion and the remaining peaks belonged to triphenylphosphine ligands of different ruthenium containing complexes.

One of the complexes present in the reaction mixture was identified as the starting material **9^{Ph}** (in the ^{1}H NMR spectrum the cyclopentadienyl ligand at 4.43 ppm, acetonitrile ligands at 2.05 ppm; and in the ^{31}P{^{1}H} NMR spectrum at 52.2 ppm).

A major complex was identified in the reaction mixture from the NMR spectra. In the ^{1}H NMR spectrum, the major cyclopentadienyl resonance was seen at 4.46 ppm which integrated as 5H with respect to an acetonitrile ligand resonance at 1.86 ppm with an integration of 3H. Additionally, coordinated 2-methylpyridine aromatic resonances have cautiously been assigned at 6.82 (1H), ~7.20, ~7.55 (1H) and 8.81 (1H) ppm from a ^{1}H and 2D ^{1}H-^{1}H COSY NMR spectra, and a broad methyl resonance was observed at 2.54 ppm (3H). The major triphenylphosphine resonance was at 52.3 ppm in the ^{31}P{^{1}H} NMR spectrum. This species has been tentatively assigned as $[Ru(\eta^5\text{-}C_5H_5)(PPh_3)(NC_5H_4\text{-}2\text{-}Me)(NCMe)][PF_6]$, **12**. The literature reports the substitution of one acetonitrile ligand of $[Ru(\eta^5\text{-}C_5H_5)(NCMe)_3][PF_6]$, **8** with 2-methylpyridine.[296]

The final ruthenium-containing complex in the reaction mixture displayed in the ^{1}H NMR spectrum a cyclopentadienyl resonance at 4.43 ppm and a corroborating acetonitrile peak at 2.06 ppm. The ^{31}P{^{1}H} NMR spectrum exhibited a resonance at 54.3 ppm for a coordinated triphenylphosphine ligand. Unfortunately this species has not been fully characterised due to limited data. A report has noted that long reaction times of $[Ru(\eta^5\text{-}C_5H_5)(NC_5H_4\text{-}2\text{-}Me)(NCMe)_2]^+$ results in the formation of a π-coordinated 2-methylpyridine ligand, $[Ru(\eta^5\text{-}C_5H_5)(\pi\text{-}NC_5H_4\text{-}2\text{-}Me)]^+$ species and uncoordinated acetonitrile.[296]

A high resolution ESI-MS of the crude reaction mixture displayed *m/z* peaks at 470.0583 and 429.0315 were assigned as the cationic species $[Ru(\eta^5\text{-}C_5H_5)(PPh_3)(NCMe)]^+$ and $[Ru(\eta^5\text{-}C_5H_5)(PPh_3)]^+$ respectively. It should be noted that the cationic species of complex **12** has not been observed from ESI-MS. Interestingly, *m/z* peaks at 549.1048 and 508.0778 for the species $[Ru(\eta^5\text{-}C_5H_5)(PPh_3)(NCMe)(NC_5H_5)]^+$ and $[Ru(\eta^5\text{-}C_5H_5)(PPh_3)(NC_5H_5)]^+$ were observed.

Crystals of **12** suitable for X-ray diffraction were obtained from slow diffusion of pentane into a dichloromethane layer containing various ruthenium complexes (Figure 3.6). However, due to poor quality of the data, the interpretation needs to be approached cautiously as an R value of 8.1 % was obtained and data collection stopped prematurely. Although it is clear from the data that the structure of the species is $[Ru(\eta^5\text{-}C_5H_5)(PPh_3)(NC_5H_4\text{-}2\text{-}Me)(NCMe)][PF_6]$ and the 2-methylpyridine molecule is disordered over two positions.

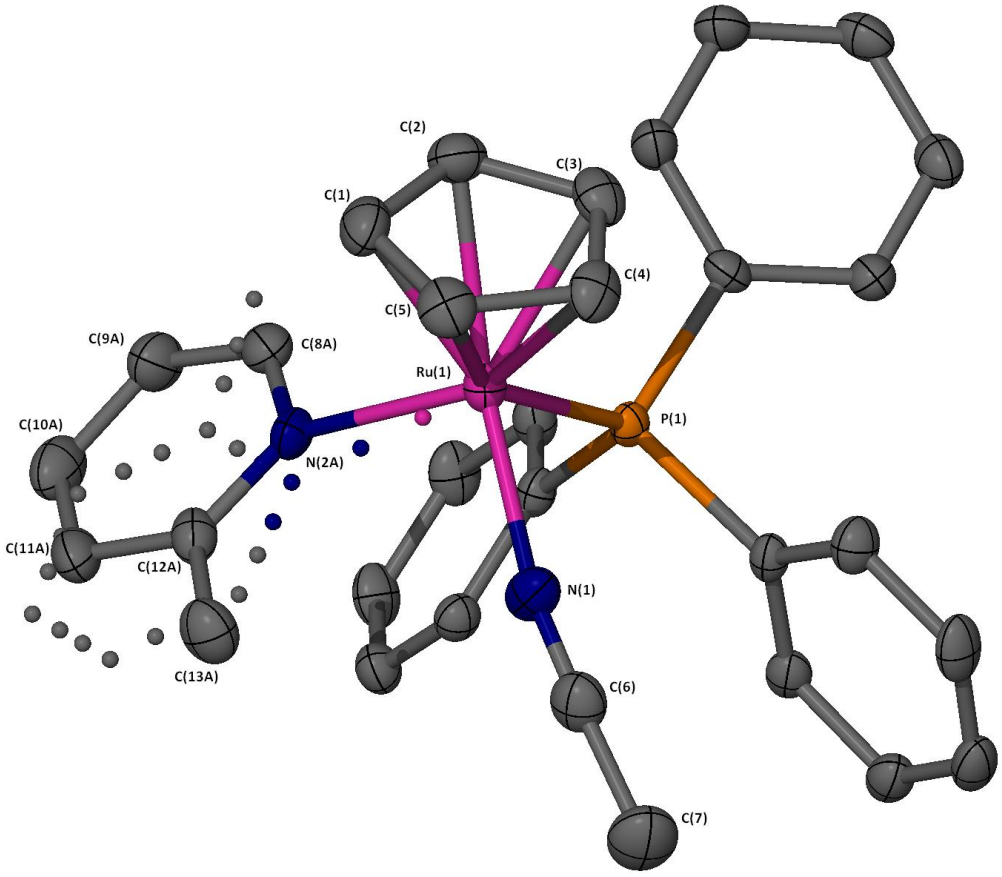

Figure 3.6: X-Seed diagram of the cation $[Ru(\eta^5\text{-}C_5H_5)(PPh_3)(NC_5H_4\text{-}2\text{-}Me)(NCMe)]^+$ from complex **12**. Hydrogen atoms and $[PF_6]^-$ anion have been omitted for clarity, and where shown the thermal ellipsoids are at a 50 % probability level. The $[PF_6]^-$ anion is disordered over two positions with a ratio of 0.668:0.332(11). The 2-methylpyridine molecule is disordered over two positions with a major and minor component in a ratio of 0.719:0.281(4) respectively.

From the data obtained from the different reaction conditions a range of ruthenium complexes have been formed from this reaction mixture. No evidence has been observed for the *bis*-substituted 2-methylpyridine complex, this could be attributed to the high steric demand at the ruthenium centre due to the methyl substituent.

3.4.1.7 Reaction of $\mathbf{9^{Ph}}$ with 1–methylimidazole for the preparation of complex $\mathbf{13^{Me}}$

We extended our library of potential nitrogen-containing heterocycles to complex to 1-methylimidazole, to observe if the disubstituted 1-methylimidazole complex **13^{Me}** could be synthesised in a similar way to **10^{H}**. If this stage of the reaction was successful it would be interesting to investigate if **13^{Me}** performed a catalytic alkenylation reaction as reported by Murakami and Hori.[253]

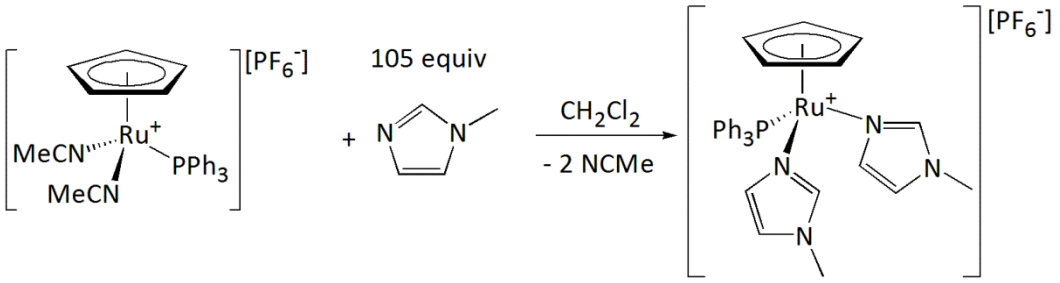

9^{Ph} **13^{Me}**

Scheme 3.14: Synthesis of complex **13^{Me}**.

The reaction to synthesise **13^{Me}** required the addition of 1-methylimidazole (105 equivalents) to **9^{Ph}** in dichloromethane (Scheme 3.14). From this procedure a reasonable yield of 63 % was obtained. The product was analysed using NMR spectroscopy, high resolution ESI-MS, IR spectroscopy, elemental analysis and X-ray crystallography.

The ^{1}H NMR spectrum of the product **13^{Me}** exhibited a singlet at 3.49 ppm and 4.26 ppm which integrated as 6H and 5H for the methyl groups of the imidazole ligands and the cyclopentadienyl protons respectively. The protons on the imidazole ligand exhibited a slightly more upfield chemical shift in comparison to the pyridine derivatives at 6.79-6.82 ppm as a multiplet and integration of 6H with respect to the cyclopentadienyl protons at 4.26 ppm. The remaining aromatic signals from 7.19-7.41 ppm were assigned to the triphenylphosphine ligand. The ^{31}P{^{1}H} NMR spectrum contained two resonances at -144.4 and 51.4 ppm as a septet for the $[PF_6]^-$ non-coordinating anion and a singlet for the phosphorus atom of the triphenylphosphine ligand respectively. There were no other triphenylphosphine peaks in the ^{31}P{^{1}H} NMR

spectrum which indicated that **13^{Me}** had been formed selectively. A $^{13}C\{^{1}H\}$ NMR spectrum for **13^{Me}** exhibited resonances for the methyl groups of the imidazole ligand at 34.6 ppm as a singlet and a doublet at 75.6 ppm with a $^{2}J_{CP}$ of 2.4 Hz for the cyclopentadienyl carbon atoms. The imidazole ring carbon atoms were identified at 121.6, 130.2 and 134.7 ppm as singlets. This is a different observation for **13^{Me}** as complexes **10^{R}** and **11** all displayed a $^{3}J_{CP}$ coupling between the phosphorus atom of the triphenylphosphine ligand and the carbon atoms at the C-2/6 positions. Unfortunately, exact assignment of these carbon atoms was not achieved, despite using a range of 2D NMR spectra such as COSY, HMQC and HMBC experiments.

An ESI-MS of the sample revealed a *m/z* peak of 593.1423 with a ruthenium isotope pattern which is expected for the cationic fragment $[Ru(\eta^5\text{-}C_5H_5)(PPh_3)(N_2C_4H_6)_2]^+$ of **13^{Me}**. Another *m/z* peak of 511.0900 was observed with a ruthenium isotope pattern which was identified as $[Ru(\eta^5\text{-}C_5H_5)(PPh_3)(NCMe)_2]^+$, where both 1-methylimidazole ligands had been substituted by acetonitrile ligands.

These data strongly suggest that **13^{Me}** has been synthesised and additionally an X-ray structure of **13^{Me}** has been obtained from the slow diffusion of pentane into a dichloromethane layer containing **13^{Me}** (Figure 3.7, Table 3.6). The cationic unit of **13^{Me}** indicated that the two 1-methylimidazole ligands were bound to the ruthenium centre through the nitrogen atoms N(1) and N(3). The geometry around the ruthenium centre could be described as a distorted octahedron, as the bond angles for N(1)-Ru(1)-P(1), N(3)-Ru(1)-P(1) and N(3)-Ru(1)-N(1) were found to be 95.70(6), 89.13(5) and 85.57(8) ° respectively. The smallest bond angle was N(3)-Ru(1)-N(1), which could be due to the steric requirements of the triphenylphosphine ligand. The η^5-coordination of the cyclopentadienyl ligand to the ruthenium centre was not equal, as three of the bond lengths for C(1)-Ru(1), C(2)-Ru(1) and C(5)-Ru(1) were 2.209(3), 2.196(3) and 2.192(3) Å respectively, which are longer than other Ru-C interactions (2.156(3) and 2.166(3) Å). The carbon atoms C(1) and C(2) are *trans* to the triphenylphosphine ligand. The ruthenium to nitrogen bond lengths for N(1)-Ru(1) and N(3)-Ru(1) were found to be 2.148(2) and 2.132(2) Å respectively. Again, a difference in the two Ru-N bond lengths was observed due to the orientation of the triphenylphosphine ligand. A Ru(1)-P(1) bond length of 2.3195(6) Å was found.

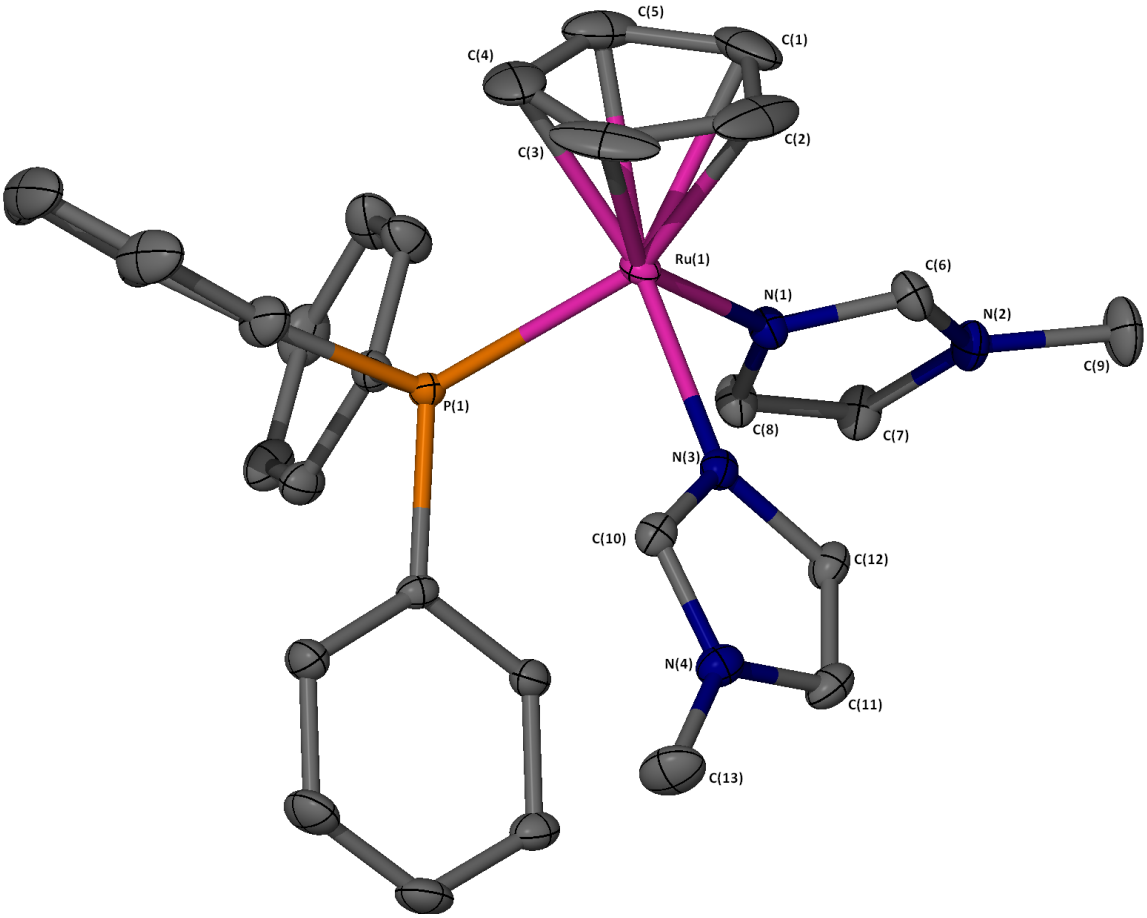

Figure 3.7: X-Seed diagram of the cation $[Ru(\eta^5\text{-}C_5H_5)(PPh_3)(N_2C_4H_6)_2]^+$ from complex **13**$^{\mathbf{Me}}$. Hydrogen atoms and $[PF_6]^-$ anion have been omitted for clarity, and where shown the thermal ellipsoids are at a 50 % probability level. The ADP of the cyclopentadienyl and one phenyl (C14-C19) were elongated. Inspection of the electron density map revealed that this was due to a continuous variation of the position of the carbons rather than the carbons occupying two discrete locations and so it would have been inappropriate to use a two-site model in these cases.

	Bond lengths (Å)		Bond angles (°)
C(1)-Ru(1)	2.209(3)	N(1)-Ru(1)-P(1)	95.70(6)
C(2)-Ru(1)	2.196(3)	N(3)-Ru(1)-P(1)	89.13(5)
C(3)-Ru(1)	2.156(3)	N(3)-Ru(1)-N(1)	85.57(8)
C(4)-Ru(1)	2.166(3)	C(6)-N(1)-C(8)	104.4(2)
C(5)-Ru(1)	2.192(3)	N(2)-C(6)-N(1)	111.7(2)
P(1)-Ru(1)	2.3195(6)	C(6)-N(2)-C(7)	107.4(2)
N(1)-Ru(1)	2.148(2)	C(8)-C(7)-N(2)	106.3(3)
N(3)-Ru(1)	2.132(2)	C(7)-C(8)-N(1)	110.1(2)
C(6)-N(1)	1.340(3)	C(10)-N(3)-C(12)	105.3(2)
C(6)-N(2)	1.335(4)	N(3)-C(10)-N(4)	111.3(3)
C(9)-N(2)	1.465(3)	C(10)-N(4)-C(11)	107.2(2)
C(7)-N(2)	1.372(3)	C(12)-C(11)-N(4)	106.8(2)
C(7)-C(8)	1.352(4)	C(11)-C(12)-N(3)	109.3(2)
C(8)-N(1)	1.381(4)		
C(10)-N(3)	1.326(3)		
C(10)-N(4)	1.342(3)		
C(13)-N(4)	1.466(3)		
C(11)-N(4)	1.366(4)		
C(11)-C(12)	1.351(4)		
C(12)-N(3)	1.383(3)		

Table 3.6: Selected bond lengths (Å) and angles (°) for complex $\mathbf{13^{Me}}$.

3.4.1.8 Reaction of $\boldsymbol{9^{Ph}}$ with t-butylimidazole for the preparation of complex $\boldsymbol{13^{tBu}}$

The ability of t-butylimidazole to coordinate to the ruthenium centre was investigated. The t-butyl group can donate more electron density though an inductive effect to the imidazole ring and is also a bulkier substituent than the methyl group. The synthetic preparation of synthesising a half-sandwich ruthenium complex coordinated to t-butylimidazole ligands was investigated.

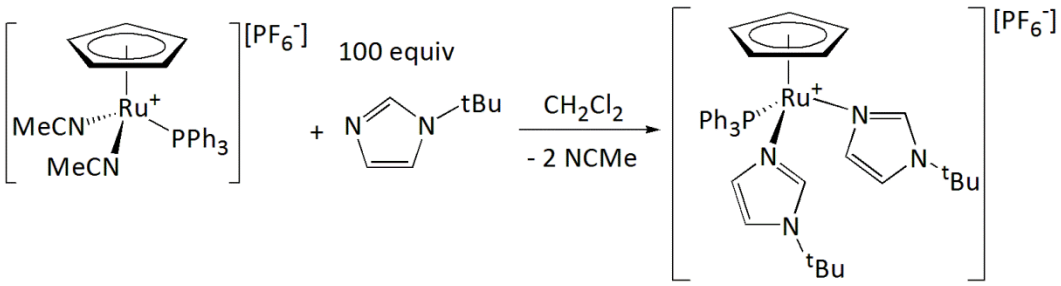

9^{Ph} **13^{tBu}**

Scheme 3.15: Synthesis of complex **13^{tBu}**.

In order to synthesise **13^{tBu}** a similar procedure to that for **10^{H}** was used. To complex **9^{Ph}** in dichloromethane, 100 equivalents of t-butylimidazole was added and the reaction mixture was left to stir for 16 hours (Scheme 3.15). A product was isolated through the slow diffusion of pentane in a dichloromethane layer containing the yellow complex.

The ^{1}H NMR spectrum displayed two singlet resonances at 1.28 and 4.29 ppm, which were assigned to the t-butyl group methyl substituents and the cyclopentadienyl protons respectively. The peaks at 1.28 and 4.29 ppm integrated in an 18H to 5H manner respectively, which is indicative of a disubstituted t-butylimidazole complex. The other hydrogen atoms in the ring of the t-butylimidazole molecule exhibited peaks at 6.91, 6.95 and 7.00 ppm with a triplet multiplicity due to J_{HH} couplings (a ^{1}H{^{31}P} NMR experiment did not change the multiplicity of these resonances). The remaining peaks in the aromatic region were assigned to the triphenylphosphine ligand protons between 7.11 and 7.42 ppm. The ^{31}P{^{1}H} NMR spectrum exhibited two resonances at -144.5 and 51.8 ppm as a septet and a singlet respectively. These peaks were assigned as the $[PF_6]^-$ anion and the latter as the phosphorus atom of the triphenylphosphine ligand coordinated to the ruthenium centre. The absence of a signal at 52.2 ppm for the triphenylphosphine ligand of complex **9^{Ph}** in the ^{31}P{^{1}H} NMR spectrum suggested that the reaction had gone to completion. A ^{13}C{^{1}H} NMR spectrum for **13^{tBu}** exhibited a resonance for the methyl carbon atoms at 30.1 ppm and the quartenary carbon atom at 56.6 ppm. At 75.9 ppm a doublet with a $^{2}J_{CP}$ of 2.2 Hz for the cyclopentadienyl carbon atoms was observed. The ^{13}C{^{1}H} NMR spectrum also exhibited peaks for the imidazole ring carbon atoms at 118.0 (singlet), 134.5 (singlet) and 139.1 (doublet with a J_{CP} = 2.6 Hz) ppm. This observation is different to **13^{Me}** where there is no coupling between the imidazole carbon atoms and the triphenylphosphine ligand.

The ESI-MS contained a *m/z* peak of 677.2334 which had a ruthenium isotope pattern, and was assigned to the cationic ruthenium fragment $[Ru(\eta^5\text{-}C_5H_5)(PPh_3)(N_2C_7H_{12})_2]^+$ of **13^{tBu}**. The NMR spectra and ESI-MS data combined provided supporting evidence for the formation of the ruthenium complex **13^{tBu}**.

In addition, an X-ray structure of **13^{tBu}** was obtained. Unfortunately, the crystal structure was not of sufficient quality to determine any structural data however a general diagram has been reported. The unit cell contained two molecules of **13^{tBu}**, where all atoms were approximately isotropically restrained. In both of the molecules, one of the *tert*-butyl substituents exhibited disorder over two positions, with refined occupancies of 0.540(13):0.460(13) and 0.537(19):0.463(19). One of the $[PF_6]^-$ anions was disordered over two positions, with occupancies of 0.781(11):0.219(11), and a dichloromethane molecule also displayed disorder and was modelled over three positions with refined occupancies of 0.526(9):0.276(14):0.199(13).

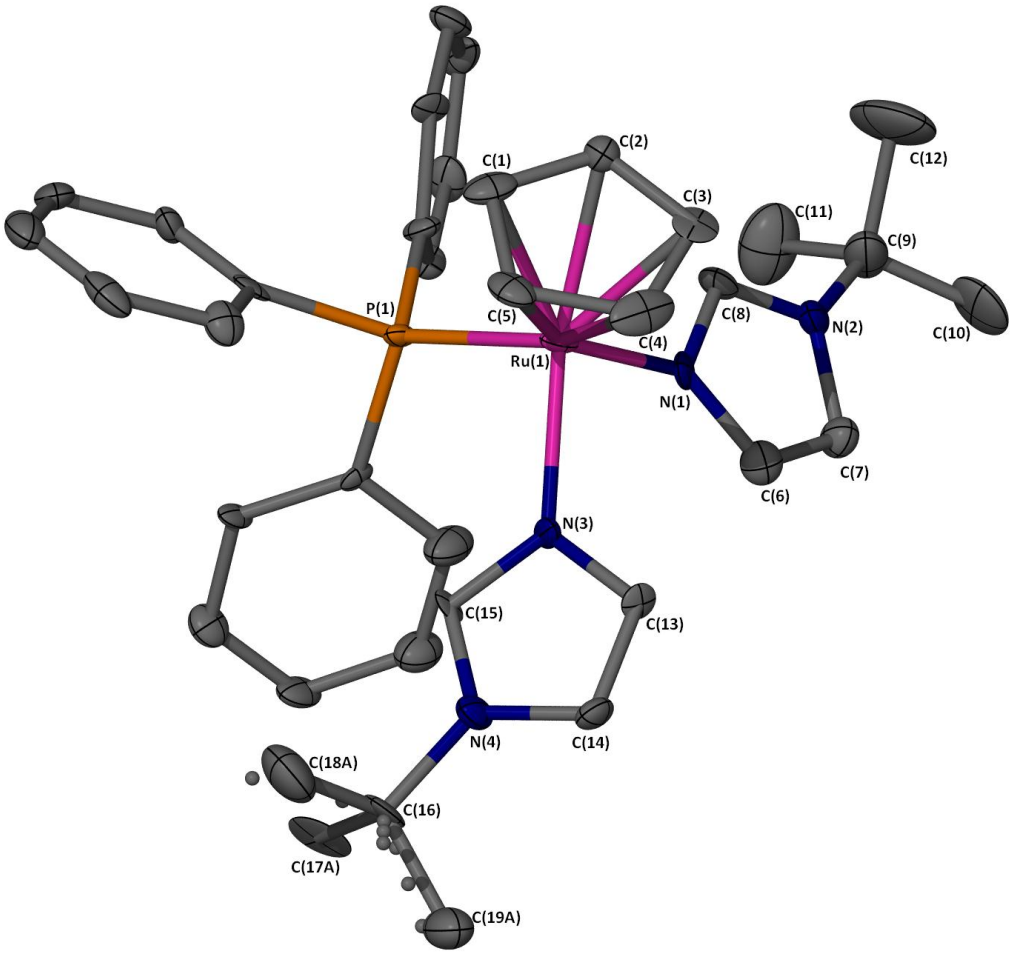

Figure 3.8: X-Seed diagram of one of the two independent cations of $[Ru(\eta^5\text{-}C_5H_5)(PPh_3)(N_2C_4H_{12})_2]^+$ from **13^{tBu}**, where hydrogen atoms, $[PF_6]^-$ anions and a dichloromethane molecule have been omitted for clarity, and where shown the thermal ellipsoids are at a 50 % probability level. One the t-butyl groups exhibited disorder over two positions, where the refined occupancies are 0.540(13):0.460(13), and the major component is displayed in a solid line.

3.4.2 Reaction of complex 9^{Me} with N-containing heterocycles

The range of phosphine ligands employed in this study was extended to include trimethylphosphine which has a smaller cone angle and more is electron-donating than triphenylphosphine.[20] The substitution of the acetonitrile ligands has been carried out with pyridine and 4-dimethylaminopyridine. The synthesis and properties of these complexes has been studied in detail.

3.4.2.1 Reaction of 9^{Me} with pyridine for the preparation of complex 14^{H}

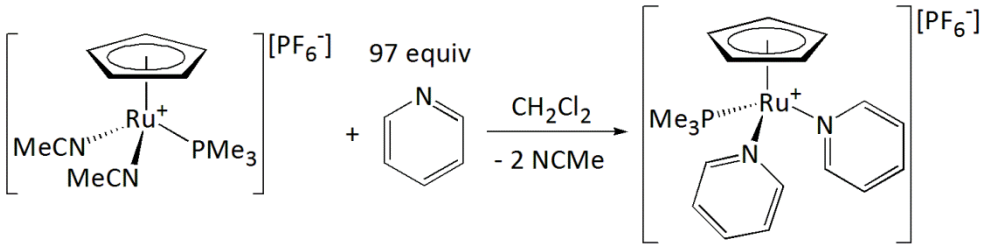

9^{Me} **14^{H}**

Scheme 3.16: Synthesis of complex **14^{H}**.

The reaction between complex **9^{Me}** and an excess of pyridine in dichloromethane was carried out in order to observe if the acetonitrile ligands could be substituted with pyridine in a similar manner to the reaction between complex **9^{Ph}** and pyridine (Scheme 3.16). The product was characterised using NMR spectroscopy, ESI-MS, elemental analysis and X-ray crystallography.

The ^{1}H NMR spectrum of the product displayed resonances at 1.40 and 4.39 ppm as a doublet with a $^{2}J_{HP}$ of 26.3 Hz and a singlet respectively, which were assigned as the methyl group resonances of the trimethylphosphine ligand and the cyclopentadienyl ligand respectively. Upon running a ^{1}H{^{31}P} NMR spectrum, the doublet resonance at 1.40 ppm simplified to reveal a singlet, confirming the nature of the doublet coupling, and is consistent with this resonance being due to the methyl groups of the phosphine ligand. In addition, the integration of the resonances at 1.40 and 4.39 ppm were 9H to 5H respectively. The pyridine resonances were observed in the aromatic region at 7.28, 7.81 and 8.41 ppm, with integrations of 4H, 2H and 4H respectively, with respect to the cyclopentadienyl protons at 4.39 ppm (5H), which is indicative of two pyridine molecules coordinated to the ruthenium centre. The absence of the acetonitrile ligand resonances at approximately 2.36 ppm, indicated the loss of the acetonitrile ligands from the ruthenium centre and the formation of the *bis*-substituted pyridine complex **14^{H}**. Additionally, the ^{31}P{^{1}H} NMR spectrum revealed only two resonances a -144.4

ppm and 3.1 ppm with a multiplicity of a septet and a singlet respectively, where the latter resonance was due to the phosphorus atom of the trimethylphosphine. The $^{13}C\{^{1}H\}$ NMR spectrum exhibited doublet resonances at 17.9 ppm and 76.0 ppm with a $^{1}J_{CP}$ of 26.3 Hz and a $^{2}J_{CP}$ of 2.3 Hz respectively, which were assigned as the methyl groups of the trimethylphosphine and the cyclopentadienyl ligands carbon atoms. Interestingly, the carbon atoms at the C-2/6 positions of the pyridine molecule at 156.7 ppm displayed a $^{3}J_{CP}$ of 2.8 Hz, which suggested that the pyridine molecules were coordinated at the ruthenium centre. The other pyridine resonances were observed at 126.0 and 137.4 ppm with a singlet multiplicity.

A high resolution ESI-MS displayed the presence of several ruthenium-containing complexes with a *m/z* of 401.0717, 363.0568 and 322.0336. These signals were assigned to the cationic species $[Ru(\eta^5\text{-}C_5H_5)(PMe_3)(NC_5H_5)_2]^+$, $[Ru(\eta^5\text{-}C_5H_5)(PMe_3)(NC_5H_5)(NCMe)]^+$ and $[Ru(\eta^5\text{-}C_5H_5)(PMe_3)(NC_5H_5)]^+$ respectively. The elemental analysis of the complex **14^{H}** was within an error of 0.2 %, and therefore is consistent with the formation of **14^{H}**.

Dark yellow air-sensitive crystals suitable for X-ray crystallography could be obtained of the product *via* slow diffusion of pentane into a dichloromethane layer containing the species **14^{H}** (Figure 3.9, Table 3.7). The cation of **14^{H}** can be described as having a distorted octahedral geometry, where the bond angles N(1)-Ru(1)-P(1), N(2)-Ru(1)-P(1) and N(2)-Ru(1)-N(1) are 88.13(3), 97.25(3) and 89.04(4) ° respectively. For trimethylphosphine, which has a smaller cone angle[20] than triphenylphosphine the N-Ru-N bond angle at the ruthenium centre is no longer the smallest (in **10^{H}** the N-Ru-N bond angle was 88.12(7) °) . The Ru-C bond lengths for the cyclopentadienyl ligand indicate that the η^5-interaction is not equivalent, as the C(3)-Ru(1) and C(4)-Ru(1) bonds lengths are 2.2155(14) and 2.2089(15) Å respectively, as the *trans* trimethylphosphine ligand causes a destabilisation of these bonds as it has a higher *trans* influence than the nitrogen donor ligands. The P(1)-Ru(1) bond length was 2.3063(4) Å. Bond lengths from the ruthenium centre to the two nitrogen atoms varied by a 0.019 Å. Additionally, the angle through which the pyridine molecules coordinate to the ruthenium is not planar, and was especially noticeable in the N(2) coordinated pyridine molecule, as the Ru(1)-N(2)-C(13) bond angle was 'tilted' and measured as 159.91 °, where as the Ru(1)-N(1)-C(8) bond angle was 177.08 °.

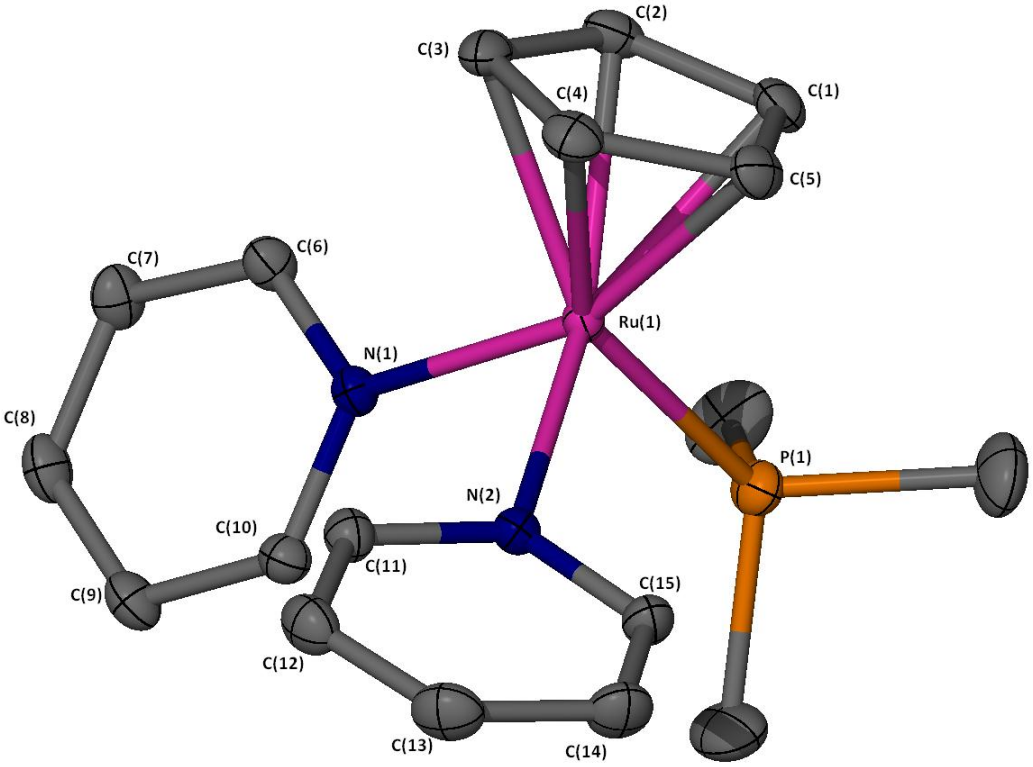

Figure 3.9: X-Seed diagram of the cation $[Ru(\eta^5\text{-}C_5H_5)(PMe_3)(NC_5H_5)_2]^+$ from complex **14^H**. Hydrogen atoms and $[PF_6]^-$ anion have been omitted for clarity, and where shown the thermal ellipsoids are at a 50 % probability level.

Bond lengths (Å)			Bond angles (°)
C(1)-Ru(1)	2.1659(14)	N(1)-Ru(1)-P(1)	88.13(3)
C(2)-Ru(1)	2.1839(14)	N(2)-Ru(1)-P(1)	97.25(3)
C(3)-Ru(1)	2.2155(14)	N(2)-Ru(1)-N(1)	89.04(4)
C(4)-Ru(1)	2.2089(15)	C(10)-N(1)-C(6)	116.71(12)
C(5)-Ru(1)	2.1766(14)	N(1)-C(6)-C(7)	123.25(13)
P(1)-Ru(1)	2.3063(4)	C(8)-C(7)-C(6)	119.22(14)
N(1)-Ru(1)	2.1399(12)	C(7)-C(8)-C(9)	118.31(14)
N(2)-Ru(1)	2.1208(12)	N(1)-C(10)-C(9)	123.03(14)
C(6)-N(1)	1.3523(18)	C(15)-N(2)-C(11)	117.27(13)
C(10)-N(1)	1.3517(17)	N(2)-C(11)-C(12)	122.63(14)
C(11)-N(2)	1.3551(18)	C(11)-C(12)-C(13)	119.37(15)
C(15)- N(2)	1.3473(18)	C(12)-C(13)-C(14)	118.56(15)
		C(15)-C(14)-C(13)	119.06(15)
		N(2)-C(15)-C(14)	123.08(14)

Table 3.7: Selected bond lengths (Å) and angles (°) for complex **14^H**.

3.4.2.2 Reaction of $\boldsymbol{9^{Me}}$ *with 4-dimethylaminopyridine for the preparation of* $\boldsymbol{14^{NMe2}}$

For $\mathbf{9^{Me}}$ two pyridine ligands were coordinated to give $\mathbf{14^{H}}$ and also in order to investigate the substituent effects, the effect of an NMe_2 group in the 4-position of the N-containing heterocycle was investigated. This section will discuss coordination of 4-dimethylaminopyridine to $\mathbf{9^{Me}}$.

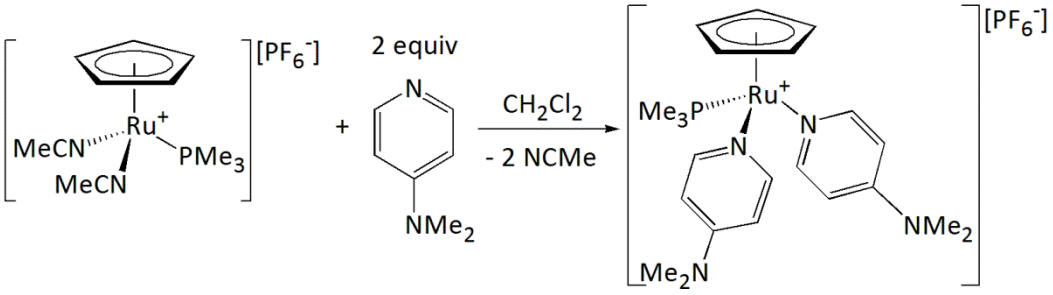

$\mathbf{9^{Me}}$ $\mathbf{14^{NMe2}}$

Scheme 3.17: Synthesis of complex $\mathbf{14^{NMe2}}$.

The synthesis of $\mathbf{14^{NMe2}}$ was similar to the preparation of $\mathbf{10^{NMe2}}$ (Scheme 3.17). The reaction was carried out through the addition of two equivalents of 4-dimethylaminopyridine to $\mathbf{9^{Me}}$ in dichloromethane. The product was purified through a crystallisation method involving slow diffusion of pentane into a dichloromethane layer containing the product $\mathbf{14^{NMe2}}$.

The ^{1}H NMR spectrum of $\mathbf{14^{NMe2}}$ in d_2-dichloromethane exhibited two sets of resonances in the aliphatic region at 1.35 and 3.01 ppm, with a doublet and singlet multiplicity respectively. The signals at 1.35 and 3.01 ppm have relative integrations of 9H and 12H, with respect to the cyclopentadienyl resonances at 4.24 ppm of 5H. The doublet resonance at 1.35 ppm with a $^{2}J_{HP}$ of 8.1 Hz, decoupled to a singlet peak when a $^{1}H\{^{31}P\}$ NMR spectrum was run on the sample. In the aromatic region of the ^{1}H NMR spectrum, there were only two doublet peaks with an identical $^{3}J_{HH}$ coupling of 6.6 Hz, at 6.38 and 7.83 ppm, both with an integration of 4H with respect to the cyclopentadienyl resonance at 4.24 ppm. These have been assigned as the protons at the C-3/5 positions (6.38 ppm) and the C-2/6 positions (7.83 ppm) of the 4-dimethylaminopyridine ligands. The $^{31}P\{^{1}H\}$ NMR spectrum displayed two resonances at -144.4 and 4.75 ppm as a septet and a singlet respectively. The peak at -144.4 ppm had a $^{1}J_{PF}$ of 710 Hz, which was due to the $[PF_6]^-$ non-coordinating anion, and the singlet signal at 4.75 ppm as the trimethylphosphine phosphorus atom. There were no other resonances present in the $^{31}P\{^{1}H\}$ NMR spectrum and this suggested there was only one ruthenium complex present which contained a trimethylphosphine ligand. A

$^{13}C\{^{1}H\}$ NMR spectrum exhibited a doublet resonance at 18.4 ppm with a $^{1}J_{CP}$ of 24.6 Hz for the methyl carbon atoms of the trimethylphosphine ligand. The cyclopentadienyl ligand displayed a doublet resonance at 74.5 ppm with a $^{2}J_{CP}$ of 2.5 Hz. The peaks for the 4-dimethylaminopyridine ligand were observed at 39.3, 108.1, 154.1 and 155.4 ppm. The latter resonance at 155.4 ppm was a doublet which was assigned as the carbon atoms at the C-2/6 positions of the 4-dimethylaminopyridine molecules and had a $^{3}J_{CP}$ of 2.4 Hz.

The ESI-MS displayed several peaks, which had a ruthenium isotope pattern. These peaks had an accurate *m/z* of 487.1571, 406.0975 and 365.0723 and were assigned as the cationic fragments of $[Ru(\eta^5\text{-}C_5H_5)(PMe_3)(NC_5H_4\text{-}4\text{-}NMe_2)_2]^+$, $[Ru(\eta^5\text{-}C_5H_5)(PMe_3)(NC_5H_4\text{-}4\text{-}NMe_2)(NCMe)]^+$, and $[Ru(\eta^5\text{-}C_5H_5)(PMe_3)(NC_5H_4\text{-}4\text{-}NMe_2)]^+$. The accurate *m/z* peak at 487.1571 for the molecular cationic species has been observed and within an error of 0.6 mDa, and therefore it is very likely that the **14**$^{\mathbf{NMe2}}$ has been synthesised. In addition, the elemental analysis obtained was within a 0.3 % limit of what would be expected for **14**$^{\mathbf{NMe2}}$.

An X-ray structure has been collected for **14**$^{\mathbf{NMe2}}$ *via* the slow diffusion of diethyl ether into a dichloromethane layer containing **14**$^{\mathbf{NMe2}}$ (Figure 3.10). Unfortunately, the structure was greatly disordered, however it is possible to determine that the ruthenium cation consists of two coordinated 4-dimethylaminopyridine molecules, a trimethylphosphine and cyclopentadienyl ligand. The unit cell contained two molecules of **14**$^{\mathbf{NMe2}}$, both of which were disordered over a mirror place in two positions. The trimethylphosphine and cyclopentadienyl ligands were modelled over two positions, where a methyl carbon atom was found to overlap with a cyclopentadienyl carbon.

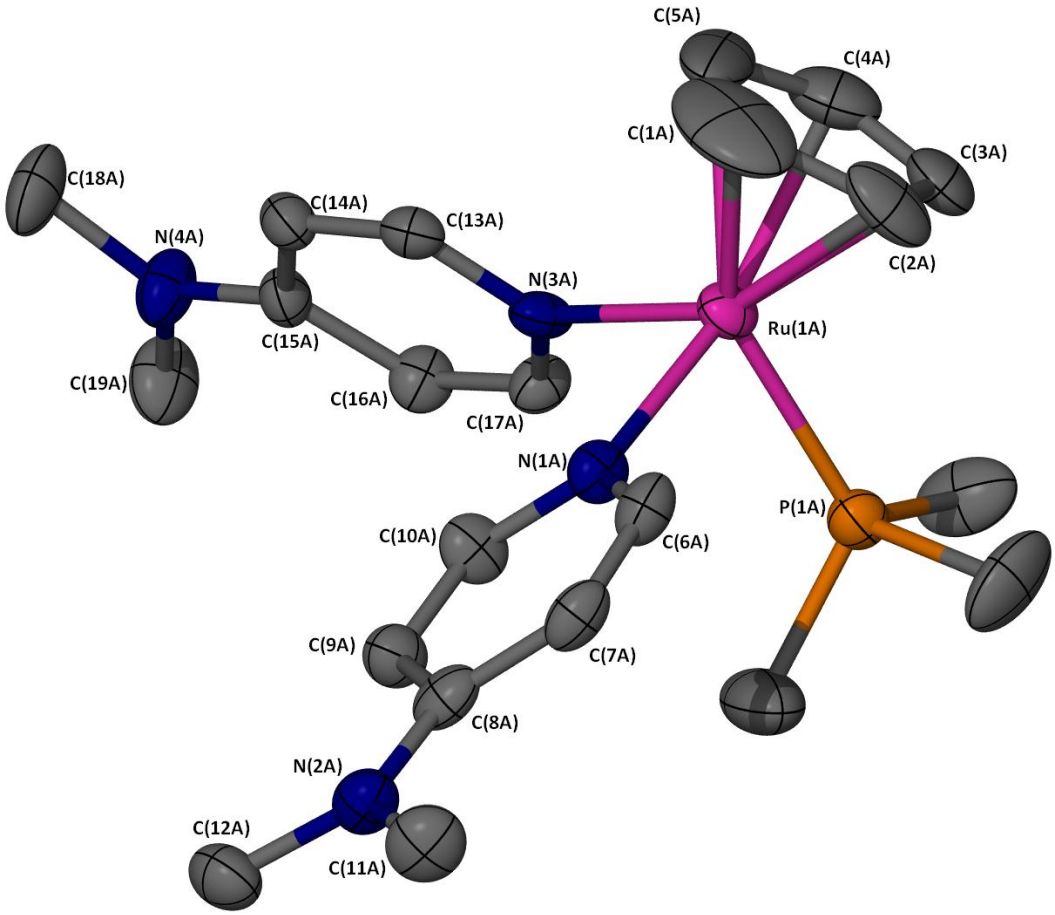

Figure 3.10: X-Seed diagram of one of the major cations $[Ru(\eta^5\text{-}C_5H_5)(PMe_3)(NC_5H_4\text{-}p\text{-}NMe_2)_2]^+$ from complex **14**^{NMe2} (with an occupancy of 0.7730(14)). Each structure contained two molecules of the complex, which were considerably disordered over two positions; the relative occupancies for one of these structures was 0.7730:0.2270(14); and for the other was 0.5095:0.4905(14). Molecules of dichloromethane and diethyl ether were overlapped over a mirror plane. The hydrogen atoms, two $[PF_6]^-$ anions, a $[Ru(\eta^5\text{-}C_5H_5)(PMe_3)(NC_5H_4\text{-}p\text{-}NMe_2)_2]^+$, a dichloromethane and a diethyl ether molecule have been omitted for clarity, and where shown the thermal ellipsoids are at a 50 % probability level.

3.4.3 Reaction of complex 9^{iPr} with pyridine

In order to understand the steric and electronic effects of the phosphorus ligands, the steric factor of the electron-donating groups was altered. This was investigated with the use of trimethylphosphine, a sterically small electron-donating phosphine ligand and triisopropylphosphine, a sterically bulky electron-donating phosphine ligand. The reaction conditions used were aimed to synthesise the *bis*-substituted pyridine complex from **9**^{iPr} (Scheme 3.18).

Three different sets of reactions were carried out to synthesise the *bis*-substituted ruthenium complex $[Ru(\eta^5\text{-}C_5H_5)(P^iPr_3)(NC_5H_5)_2][PF_6]$:

i) Addition of pyridine (approx. 50 equivalents)

ii) Addition of pyridine (approx. 50 equivalents), followed by precipitation of the reaction mixture and further addition of pyridine (approx. 50 equivalents)

iii) Addition of pyridine (10 equivalents)

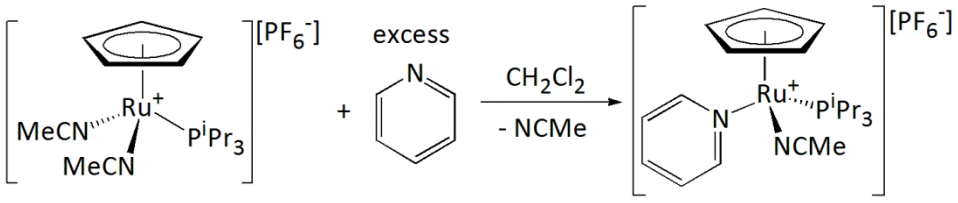

9^{iPr} **15**

Scheme 3.18: Synthesis of complex **15**.

In order to achieve substitution of both acetonitrile ligands from **9^{iPr}** a reaction was carried out involving the addition of excess pyridine (reaction conditions i) approximately 50 equivalents) in dichloromethane and allowing the reaction to stir for 16 hours. The crude reaction mixture was initially observed *via* NMR spectroscopy which demonstrated that a mixture of three ruthenium containing products were present. The resonances due to two products appeared sharp, while the resonances due to the other species was broad.

One of the products in the reaction mixture was characterised by using NMR spectroscopy as being complex [Ru(η^5-C_5H_5)(P^iPr_3)(NCMe)(NC_5H_5)][PF_6], **15**. The characterisation of complex **15** was based on ^{1}H and ^{31}P{^{1}H} NMR spectroscopy and ESI-MS. The ^{1}H NMR spectrum displayed resonances of the isopropyl group of the phosphorus ligand between 1.09-1.17 ppm and at 2.24 ppm, for the methyl groups and the CH group of the isopropylphosphine substituent. The resonances between 1.09-1.17 ppm and at 2.24 ppm, had integrations of 18H and 3H respectively, with respect to cyclopentadienyl protons at 4.51 (5H). A doublet resonance at 2.54 ppm had a $^5J_{HP}$ of 1.2 Hz, which was assigned to the methyl group of the acetonitrile ligand. In the aromatic region of the ^{1}H NMR spectrum resonances were identified at 7.29, 7.75 and 8.71 ppm with integrations of 2H, 1H and 2H respectively, relative to the cyclopentadienyl protons, which was due a coordinated pyridine ligand. This confirms the presence of one acetonitrile ligand and one pyridine ligand coordinated to the ruthenium centre. Additionally, a resonance at 52.8 ppm in the ^{31}P{^{1}H} NMR spectrum was identified as the phosphorus atom of the coordinated triisopropylphosphine to the ruthenium centre. A high resolution ESI-MS included a small peak with a *m/z* of

447.1492 which was assigned to the cationic fragment of **15** $[Ru(\eta^5\text{-}C_5H_5)(P^iPr_3)(NCMe)(NC_5H_5)]^+$. Other ESI-MS peaks with a ruthenium isotope pattern were observed with *m/z* peaks of 406.1228, 368.1053 and 325.0284 which were identified as the cationic units $[Ru(\eta^5\text{-}C_5H_5)(P^iPr_3)(NC_5H_5)]^+$, $[Ru(\eta^5\text{-}C_5H_5)(P^iPr_3)(NCMe)]^+$, and $[Ru(\eta^5\text{-}C_5H_5)(P^iPr_3)]^+$ respectively.

The reaction conditions were altered in an attempt to synthesise the pure *bis*-substituted ruthenium complex $[Ru[(\eta^5\text{-}C_5H_5)(P^iPr_3)(NC_5H_5)_2][PF_6]$ (using reaction conditions ii). The altered reaction conditions involved placing $\mathbf{9^{iPr}}$ in dichloromethane and adding an excess of pyridine (50 equivalents) and working up the reaction mixture to give a yellow-orange precipitate, followed by the further addition of pyridine (50 equivalents) to drive the reaction to completion. By altering the amount of excess pyridine added to $\mathbf{9^{iPr}}$ the quantity of products present in the crude reaction mixture changed. The more equivalents of pyridine added to the reaction mixture reduced the intensity of the set of resonances which had been identified as complex **15**. However, in the ^1H NMR spectrum an increase in intensity of the peaks at 4.15 (5H), 7.33 (6H), 7.83 (4H), and 8.47 (5H) ppm was observed, where the former peak can be assigned as the cyclopentadienyl ligand and the latter three resonances for the pyridine molecule. In addition, the $^{31}P\{^1H\}$ NMR spectrum does not display an increase in any of the phosphorus signals for the triisopropylphosphine ligand. This species from the ^1H NMR data could potentially be assigned as a *tris*-substituted pyridine complex $[Ru(\eta^5\text{-}C_5H_5)(NC_5H_5)_3]^+$. However, the integrations collected for the pyridine resonances in the ^1H NMR spectrum are not accurate due to underlying broad peaks, and in the ESI-MS the absence of the *m/z* peak at 404.07 for the $[Ru(\eta^5\text{-}C_5H_5)(NC_5H_5)_3]^+$ cation does not support this theory.

Under the set of reaction conditions iii, in the crude reaction mixture a mixture of ruthenium complexes were present even though fewer pyridine equivalents were used. In order to separate these complexes, purification of the crude reaction mixture was attempted by slow diffusion of pentane into the dichloromethane reaction mixture (which contained complex **15**). Analysis of the resulting crystals by single crystal X-ray diffraction demonstrated that $[Ru(\eta^5\text{-}C_5H_5)(P^iPr_3)(NCMe)(NC_5H_5)][PF_6]$, **15**, was present. However, the structure also exhibited an area of unresolved electron density which has been modelled as a $[MeP^iPr_3]^+$ cation with a $[PF_6]^-$ anion (Figure 3.11).

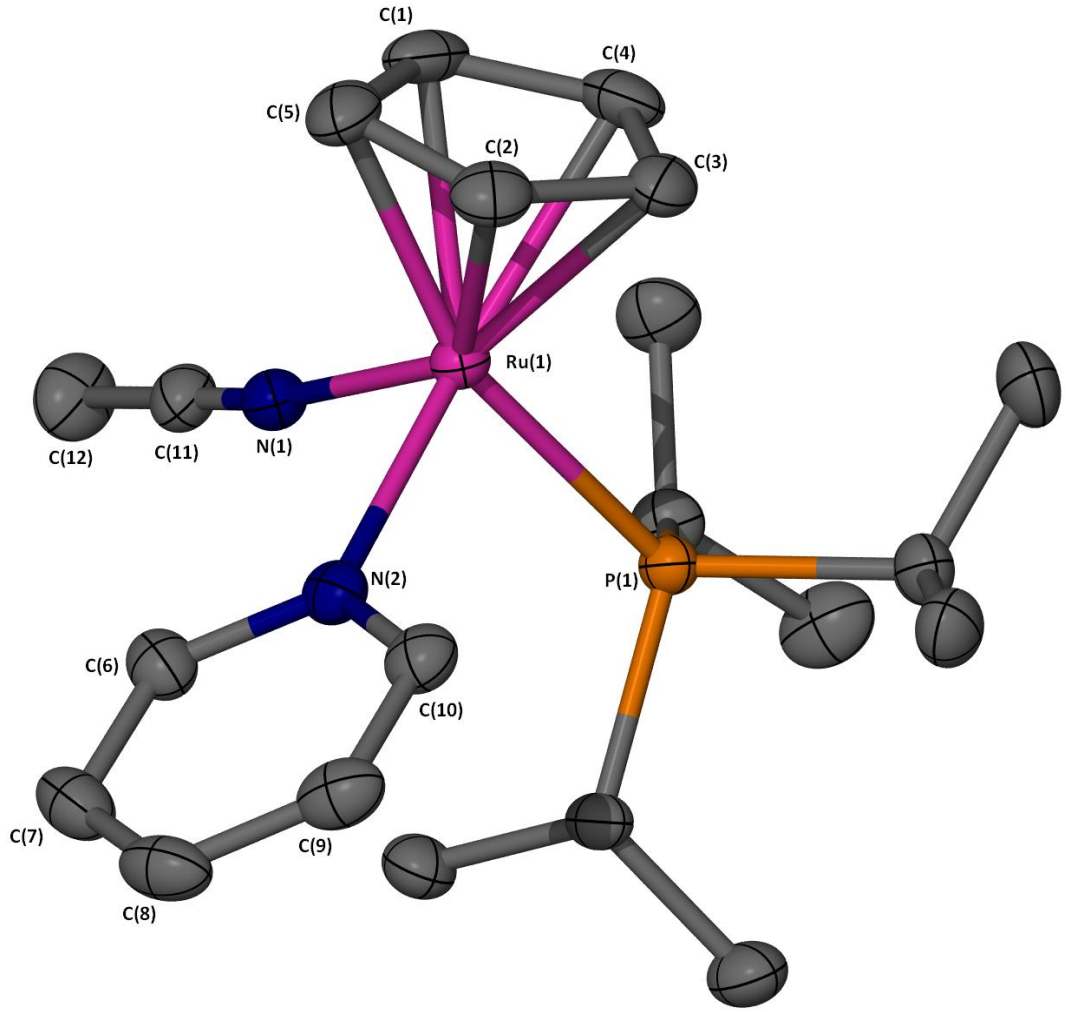

Figure 3.11: X-Seed diagram of the cation $[Ru(\eta^5\text{-}C_5H_5)(P^iPr_3)(NCMe)(NC_5H_5)]^+$ from complex **15**. Hydrogen atoms and a $[PF_6]^-$ anion have been omitted for clarity, and where shown the thermal ellipsoids are at a 50 % probability level. Additionally, a $[MeP^iPr_3][PF_6]$ species has been omitted.

The reaction of $\mathbf{9^{iPr}}$ with pyridine under a range of conditions has given several ruthenium complexes. One of these has been identified as the mono-pyridine substituted complex $[Ru(\eta^5\text{-}C_5H_5)(P^iPr_3)(NCMe)(NC_5H_5)][PF_6]$, **15**. Another species, could potentially be due to the *tris*-pyridine substituted complex $[Ru(\eta^5\text{-}C_5H_5)(NC_5H_5)_3][PF_6]$, although assignment of this species must be considered tentatively. The remaining resonances observed in the NMR spectra are broad in nature, indicating fluxional behaviour for this ruthenium-containing complex. Triisopropylphosphine has a larger cone angle of 160 ° than triphenylphosphine which has a cone angle of 145 ° and this may cause steric crowding at the ruthenium centre if two pyridine molecules were coordinated.[20] The broad resonances in the NMR spectrum may be a result of steric crowding at the ruthenium centre.

3.4.4 Reaction of complex 9^{OPh} with pyridine

In addition to using trimethylphosphine and triisopropylphosphine that are more electron-donating than triphenylphosphine, the effect of an electron-withdrawing phosphorus ligand, triphenylphosphite was also investigated. This section will look at the synthesis of the *bis*-substituted pyridine complex from $\mathbf{9^{OPh}}$.

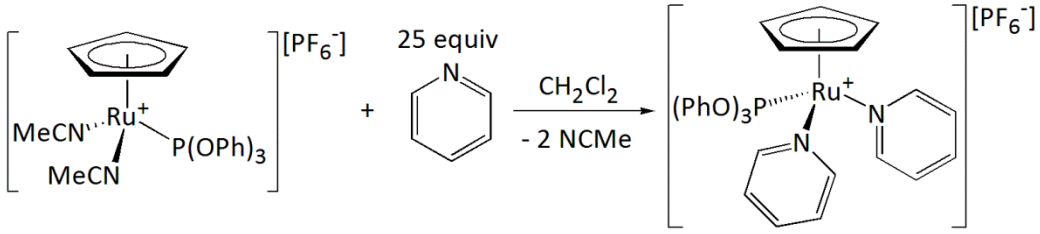

9^{OPh} **16**

Scheme 3.19: Synthesis of complex **16**.

The synthesis of **16** was achieved by the addition of 25 equivalents of pyridine to $\mathbf{9^{OPh}}$ in a dichloromethane solution which stirred for 16 hours at room temperature. Characterisation of **16** was achieved using NMR spectroscopy, high resolution ESI-MS, elemental analysis and X-ray crystallography.

The ^{1}H NMR spectrum of **16** in d_2-dichloromethane exhibited a singlet resonance at 4.39 ppm for the cyclopentadienyl protons. The remaining peaks were observed in the aromatic region between 7.03 and 8.41 ppm. The pyridine protons at the C-2/6 positions were observed at 8.41 ppm as doublet with a $^{3}J_{HH}$ of 5.2 Hz, which integrated as 4H with respect to the resonance for the cyclopentadienyl protons at 4.39 ppm with an integration of 5H. Additionally, the ^{31}P{^{1}H} NMR spectrum only displayed two resonances at -143.0 and 140.6 ppm as a septet with a $^{1}J_{PF}$ of 711 Hz, and a singlet respectively. The ^{13}C{^{1}H} NMR spectrum exhibited a doublet resonance at 80.1 ppm for the cyclopentadienyl ligand which had a $^{2}J_{CP}$ of 3.2 Hz. Interestingly, the pyridine carbon atoms at the C-2/6 positions were identified at 157.4 ppm as a doublet with a $^{3}J_{CP}$ of 2.1 Hz, suggesting the pyridine is coordinated to the ruthenium centre. The ^{1}H NMR spectrum of **16** was quite different to the acetonitrile analogue. The cyclopentadienyl protons for **16** had a singlet resonance at 4.39 ppm, where as in $\mathbf{9^{OPh}}$ the cyclopentadienyl protons appeared at 4.44 ppm as a doublet.

The ESI-MS contained peaks for several ruthenium-containing complexes with a *m/z* of 635.1041, 597.0871 and 556.0623 which were identified as the cationic complexes

$[Ru(\eta^5\text{-}C_5H_5)(P(OPh)_3)(NC_5H_5)_2]^+$, $[Ru(\eta^5\text{-}C_5H_5)(P(OPh)_3)(NC_5H_5)(NCMe)]^+$and the species $[Ru(\eta^5\text{-}C_5H_5)(P(OPh)_3)(NC_5H_5)]^+$respectively.

Block yellow crystals suitable for X-ray diffraction were grown by slow diffusion of pentane into a dichloromethane layer containing **16** (Figure 3.12). The crystal structure contained two areas of undefined electron density close to the ruthenium centre therefore lowering the reliability of this data. The X-ray data suggests that the *bis*-substituted pyridine complex has been synthesised.

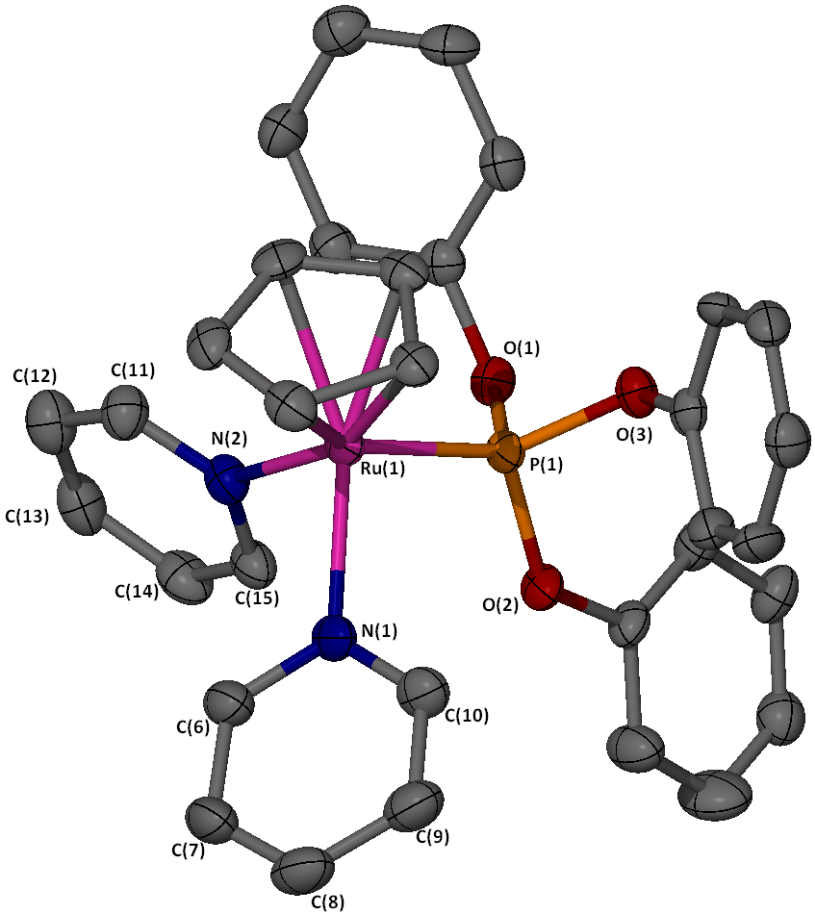

Figure 3.12: X-Seed diagram of the cation $[Ru(\eta^5\text{-}C_5H_5)(P(OPh)_3)(NC_5H_5)_2]^+$ from complex **16**. Hydrogen atoms and $[PF_6]^-$ anion have been omitted for clarity, and where shown the thermal ellipsoids are at a 50 % probability level. There were two large residual density peaks one close to Ru(1) (3.11 eA^{-3}) and one close to the P(1) (0.99 eA^{-3}) This is believed to be due to the presence of a minor non-merohedral twin of approximately 7% of the main crystal with the residual density corresponding to the sites of Ru(1) and P(1) of the twin.

3.5 Comparison of Half-Sandwich Ruthenium Complexes

3.5.1 Synthesis

The synthetic preparation of $\mathbf{10^{Me}}$ and $\mathbf{10^{NMe2}}$ with respect to $\mathbf{10^{H}}$ was compared. A key difference in the synthesis of complex $\mathbf{10^{Me}}$ and $\mathbf{10^{NMe2}}$ was that they required fewer equivalents of the N-containing heterocycle (4-methylpyridine required 50 equivalents and 4-dimethylaminopyridine required 2 equivalents) in order to obtain the *bis*-substituted heterocyclic complexes. For the synthesis of $\mathbf{10^{H}}$, 100 equivalents of pyridine were required in order for the reaction to go to completion. This could be attributed to the stronger electronic donor properties of the N-containing heterocycle, where this has been demonstrated by Hammett substituent effects.[292-295] Similar requirements were found for the synthesis of $\mathbf{14^{H}}$ and $\mathbf{14^{NMe2}}$.

3.5.2 NMR spectroscopic data

3.5.2.1 Effects of the substituents at the 4-positions

The spectroscopic parameters for complexes $\mathbf{10^{R}}$ (where R = H, Me and NMe_2) were analysed. For $\mathbf{10^{Me}}$, the NMR data displayed significant changes in the chemical shifts of certain protons and of the phosphorus atom. The ^{1}H NMR data from complexes $\mathbf{10^{H}}$, $\mathbf{10^{Me}}$ and $\mathbf{10^{NMe2}}$ displayed an upfield shift in the cyclopentadienyl ligands resonances to 4.42, 4.36 and 4.25 ppm respectively. A similar pattern is observed in the chemical shifts of the protons at the C-2/6 positions of the N-containing heterocycles at 8.29, 8.10 and 7.73 ppm for where the R substituents are H, Me and NMe_2 respectively. The $^{31}P\{^{1}H\}$ NMR chemical shifts for the triphenylphosphine ligands in complexes $\mathbf{10^{R}}$ were 50.3, 50.4 and 51.4 ppm, for the R groups H, Me and NMe_2 respectively, where there appears to be a downfield shift. Similar observations have been made in the literature of cyclopentadienyl ruthenium complexes.[287, 288, 297]

The differences in chemical shifts between complexes $\mathbf{10^{H}}$ and $\mathbf{10^{Me}}$ are more subtle ($\Delta\delta_H$ for the cyclopentadienyl ligands was 0.06 ppm; $\Delta\delta_H$ for the protons at the C-2/6 of the N-containing heterocycles was 0.19 ppm; and $\Delta\delta_P$ for triphenylphosphine ligand was 0.1 ppm). However, on going from $\mathbf{10^{Me}}$ to $\mathbf{10^{NMe2}}$ there are larger differences in the chemical shifts ($\Delta\delta_H$ for the cyclopentadienyl ligands was 0.11 ppm; $\Delta\delta_H$ for the protons at the C-2/6 positions of the N-containing heterocycles was 0.37 ppm; and $\Delta\delta_P$ for triphenylphosphine ligand was 1.0 ppm). This could be attributed to the different methods through which the methyl group and dimethylamino group donate electron

density to the six-membered ring. The 4-methyl group donates electron density through an inductive method. However, the 4-dimethylamino substituent is a more powerful electron-donating group as it donates electron density through conjugation (towards the nitrogen atom and the C-3 and 5 positions of the heterocycle).[29]

The spectroscopic data for complexes **14^{R}** was compared. The cyclopentadienyl ligand in the NMR spectra exhibited an upfield shift from complex **14^{H}** to **14^{NMe2}**, in the ^{1}H NMR spectra from 4.39 to 4.24 ppm respectively, and in the ^{13}C{^{1}H} NMR spectra from 76.0 to 74.5 ppm respectively. This can be explained by the presence of the NMe_2 group in the 4-position of the six-membered N-containing heterocycle, which through conjugation places additional electron density at the C3/5 positions and N-donor atom of the heterocycle. This therefore places additional electron density at the ruthenium centre which can be donated the cyclopentadienyl ligand. A similar effect was seen in complexes **10^{R}** (where R= H, Me, and NMe_2).

3.5.2.2 Position of methyl substituent

The attempted synthesises for the *bis*-substituted N-containing complexes of the 3-methylpyridine and 2-methylpyridine complexes were analysed. The addition of 2-methylpyridine to **9^{Ph}** did not generate the *bis*-substituted complex, possibly due to the steric effects of the methyl group hindering coordination of the second heterocycle.

The data belonging to **11** was compared to complexes **10^{H}** and **10^{Me}** to look at the effects of the methyl substituent. The cyclopentadienyl protons chemical shifts in the ^{1}H NMR spectrum for complex **11**, **10^{Me}** and **10^{H}** were 4.40, 4.36 and 4.42 ppm respectively. The cyclopentadienyl chemical shift for complex **11** is downfield of **10^{Me}**. which is due to the inductive effect of the methyl group.

3.5.2.3 Imidazole substituents

The complexes **13^{R}** (where R= Me or ^{t}Bu) have been synthesised where the substituent on the nitrogen atom has been changed. There are a few differences in the NMR spectra of complex **13^{R}**, where the cyclopentadienyl ligand displays a slight downfield shift in the ^{1}H and ^{13}C{^{1}H} NMR spectra on changing the R group from Me to ^{t}Bu, due to the ligand being deshielded. The next stage was to investigate the reactivity of these complexes with terminal alkynes.

3.5.3 X-ray crystallography data

General trends observed with all of the X-ray structures reported in this chapter included an unequal coordination mode of the η^5-cyclopentadienyl ligand to the ruthenium centre, due to the higher *trans* influence of the phosphorus ligand with respect to the nitrogen donor ligands, which destabilises the *trans* Ru-C bonds to the phosphorus. Similar observations have been reported by Kirchner *et al*. for the [Ru(η^5-C_5H_5)(PR_3)($NCMe)_2$][PF_6] species, where R = Ph and Cy.[131] Also distorted octahedron geometries around the ruthenium centres were observed, which is seen for other cyclopentadienyl ruthenium complexes.[287, 288, 297]

The Ru-P bond lengths ranged between 2.3063(4) and 2.3186(6) Å, which are slightly shorter than the average Ru-P bond length for six coordinate ruthenium complexes.[298] In comparison to **9^{Ph}**, a mono-substituted triphenylphosphine complex where the Ru-P bond length was 2.294(1) Å, our reported structures have a slightly longer Ru-P bond length.[131] For the complexes with two coordinated N-containing heterocycles, the Ru-N bond lengths generally exhibited one short and one long bond length (except for **10^{NMe2}**, which was attributed to the stronger donor properties of the 4-dimethylamino substituent). The shorter Ru-N bond lengths ranged between 2.1208(12) and 2.135(2) Å, which are between the expected range for a ruthenium-pyridine complex.[298]

A comparison of the N-Ru-N bond angles has been conducted. For **11**, an increase in the N-Ru-N bond angle of 5.24 ° (where the N(2)-Ru(1)-N(1) was 89.41(7) °) with respect to complex **10^{Me}** (where the N(2)-Ru(1)-N(1) was 84.17(13) °) was observed. This could be due to a steric influence of the methyl groups in the C-3 position of the pyridine molecule in **11**. However, for **10^{H}** (where the N(2)-Ru(1)-N(1) was 88.12(7) °) the N-Ru-N bond angle is larger than that observed for **10^{Me}**. Additionally, differences were observed with the PR_3 ligands (where R = Ph and Me). The N-Ru-N bond angles for the ruthenium triphenylphosphine complexes (**10^{R}** (where R = H, Me and NMe_2), **11**) were smaller than for the ruthenium trimethylphosphine complex **14^{H}**, due to the smaller cone angle of the trimethylphosphine ligand.

3.6 Conclusions

In this chapter the synthesis of half-sandwich ruthenium complexes with the formula $[Ru(\eta^5\text{-}C_5H_5)(PR_3)(L)_2][PF_6]$ (where R = Ph, OPh, ^{i}Pr, Me, and L = N-containing ligand) have been achieved. A range of phosphorus ligands have been coordinated to give the $[Ru(\eta^5\text{-}C_5H_5)(PR_3)]^+$ fragment and the complexes $\mathbf{9^R}$ isolated and characterised, following the synthetic preparation method mentioned by Kirchner *et al.*[131] The stoichiometric addition of the phosphorus ligands must be exact, as it was found that due to the labile nature of the acetonitrile ligands it is easy to synthesise the *bis*-substituted fragment $[Ru(\eta^5\text{-}C_5H_5)(PR_3)_2]^+$.

The N-containing heterocycle, pyridine has been reacted with complexes $\mathbf{9^R}$ (where R = Ph, OPh, ^{i}Pr, Me). The synthesis of the *bis*-substituted pyridine complex $[Ru(\eta^5\text{-}C_5H_5)(PR_3)(NC_5H_5)_2][PF_6]$ has been carried out successfully when R = Ph, OPh and Me. However, in the case of the P^iPr_3 ligand a range of ruthenium complexes were synthesised and the major species identified as a mono-substituted pyridine complex $[Ru(\eta^5\text{-}C_5H_5)(P^iPr_3)(NC_5H_5)(NCMe)][PF_6]$, **15**. A reason for the failure to synthesise the *bis*-substituted pyridine complex with triisopropylphosphine could be due to the large cone angle of 160 °, which will cause steric crowding around the ruthenium centre. The complex $\mathbf{9^{Me}}$ has also been reacted with 4-dimethylaminopyridine to give $\mathbf{14^{NMe2}}$.

Complex $\mathbf{9^{Ph}}$ has been reacted with a range of N-containing heterocycles including 4-methylpyridine, 4-dimethylaminopyridine, 3-methylpyridine, 2-methylpyridine, 1-methylimidazole and ^{t}butylimidazole. With the exception of 2-methylpyridine, all of the other N-containing heterocycles have given the *bis*-substituted complexes. The methyl group in the 2-position of 2-methylpyridine causes a steric clash with the metal centre makes it difficult for the nitrogen atom to coordinate. This reactivity has been exploited by Carmona[206-208] and Esteruelas[142, 223, 225] to give the 2-carbene tautomers of the N-containing heterocycles.

The next stage was to investigate the reactivity of these complexes with various terminal alkynes to understand the mechanism through which the alkenylation reaction of pyridine takes place. From investigating the reaction pathway, we are aiming to understand the role of the ruthenium species and improve the catalytic reaction conditions.

Chapter 4. Coordination and Properties of the 2-Styrylpyridine Derivatives to Half-Sandwich Ruthenium Complexes

4.1 Introduction

Transition metal complexes are often employed as catalysts to reduce energy barriers of reaction pathways, provide a more atom economical and cleaner route to the desired products.[7, 254, 299] However, the efficiency of a catalyst is challenged by catalyst stability and deactivation. Deactivation of transition metal complexes in homogeneous catalysis could occur through several potential methods, including the precipitation of the metal and/or ligand; reaction of the metal centre with ligands, substrates, products or impurities and the formation of dimers.[300, 301] From undertaking a mechanistic approach and understanding the reaction pathway, there is a possibility of improving the catalytic method and developing new systems.[254]

The alkenylation of pyridine by half-sandwich ruthenium complexes generates 2-styrylpyridine compounds,[253] therefore understanding the bonding and properties between 2-styrylpyridine and the ruthenium centre is essential for the turnover of the product and regeneration of the catalyst. Mechanistic investigations into the coordination and reactivity of 2-styrylpyridine to the cationic ruthenium fragments $[Ru(\eta^5\text{-}C_5H_5)(PR_3)]^+$ (where R = Ph, Me) and of *E*-2-(4-(trifluoromethyl)styryl)pyridine to $[Ru(\eta^5\text{-}C_5H_5)(PPh_3)]^+$ were performed.

4.2 Reaction between 9^{Ph} and 2-styrylpyridine

The reactivity between 2-styrylpyridine derivatives and half-sandwich ruthenium complexes $[Ru(\eta^5\text{-}C_5H_5)(PR_3)(NCMe)_2][PF_6]$, where R = Ph and Me has been investigated. The synthesis and properties of these complexes are interesting due to their relevance in the catalytic cycle for the alkenylation of 2-styrylpyridine,[253] and therefore the coordination of 2-styrylpyridine derivatives to the fragments $[Ru(\eta^5\text{-}C_5H_5)(PR_3)]^+$ has been studied.

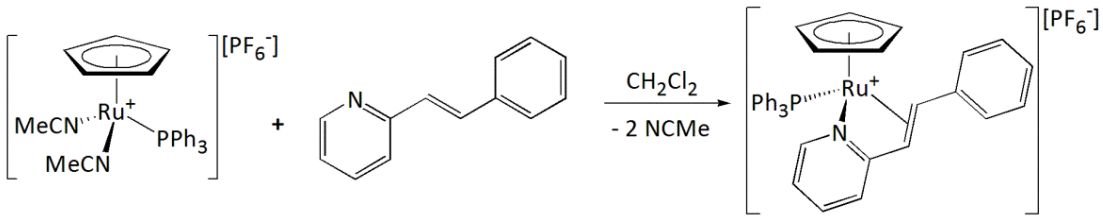

9^{Ph} **17^{H}**

Scheme 4.1: Reaction of complex **9^{Ph}** with 2-styrylpyridine.

4.2.1 Experimental studies

The reactivity between 2-styrylpyridine and $[Ru(\eta^5\text{-}C_5H_5)(PPh_3)(NCMe)_2][PF_6]$, **$9^{Ph}$** was investigated. In order to substitute the acetonitrile ligands from **9^{Ph}**, 2-styrylpyridine was added in a stoichiometric quantity in d_2-dichloromethane. The reaction was monitored *via* ^1H and $^{31}P\{^1H\}$ NMR spectroscopy. The ^1H NMR spectrum exhibited resonances in the cyclopentadienyl region at 4.43 and 4.74 ppm due to complexes **9^{Ph}** and **17^{H}**. Additionally, the ^1H NMR spectrum displayed a resonance at 8.57 ppm for the proton at the C-6 position of uncoordinated 2-styrylpyridine. The reaction appeared to reach equilibrium between **9^{Ph}**, uncoordinated 2-styrylpyridine and **17^{H}**.

The NMR scale reaction indicated that the reaction had not gone to completion as the starting material **9^{Ph}** and uncoordinated 2-styrylpyridine were still observed in the ^1H and $^{31}P\{^1H\}$ NMR spectra. To ensure the reaction had reached completion a reaction procedure was developed which involved the stoichiometric addition of 2-styrylpyridine to **9^{Ph}** in dichloromethane. The solvent was removed under vacuum to remove any uncoordinated acetonitrile and therefore when the reaction mixture was re-dissolved in dichloromethane to allow the equilibrium to favour the formation of **17^{H}** (Scheme 4.1). This process was repeated between 4-5 times to ensure the reaction went to completion,

and success was confirmed using NMR spectroscopy by the absence of the acetonitrile methyl groups resonances at 2.05 ppm (doublet, with a $^5J_{HP}$ of 1.5 Hz) and at 1.97 ppm (singlet) for coordinated or uncoordinated ligands.

All resonances for the expected product **17^H** were broad in the ^{1}H and ^{31}P{^{1}H} NMR spectra, displaying fluxional behaviour. Some of the resonances in the ^{13}C{^{1}H} NMR spectrum were broad, however this still supported the theory that **17^H** was exhibiting fluxional behaviour in solution. The cyclopentadienyl region displayed a broad resonance for the cyclopentadienyl protons at 4.73 ppm. In the ^{1}P{^{1}H} NMR spectrum, the resonance for the phosphorus atom of the triphenylphosphine ligand at 47.7 ppm was broad. The ESI-MS analysis displayed a peak with a *m/z* of 610.13 for the cationic ruthenium fragment of **17^H**. An elemental analysis of the product agreed within 0.3 % for complex **17^H**, containing 0.2 equivalents of CH_2Cl_2 and the solvent content was verified by NMR spectroscopy.

A variable temperature ^{1}H and ^{31}P{^{1}H} NMR experiment was conducted on **17^H** in a d_2-dichloromethane solution from 300 K to 220 K. The temperature was decreased in 20 K steps where NMR spectra were recorded at these intervals (Figure 4.1). The ^{1}H and ^{31}P{^{1}H} NMR spectra appeared to get broader until 260 K, and below this point until 220 K the resonances began to get sharper. Both the ^{1}H and ^{31}P{^{1}H} NMR spectra displayed the presence of two species in equilibrium in a ratio of ~5: 1. In the ^{31}P{^{1}H} NMR spectrum three resonances were observed at -143.0, 47.2 and 55.0 ppm, as a septet ($^1J_{PF}$ = 711 Hz) for the $[PF_6]^-$ and two singlets respectively. The triphenylphosphine resonance at 47.2 ppm was determined to be the major species as this had the greatest integration, in comparison to the resonance at 55.0 ppm which belonged to the minor complex. The difference in the free energy of the major and minor complexes was calculated at 220 K, using the equation $\Delta G = -RT\ln K$. The difference in Gibbs free energy at 220 K of the two species in solution was calculated as 4.3 kJ mol^{-1}.

$$\Delta G = - 8.314 \text{ J K}^{-1} \text{ mol}^{-1} \text{ x } 220 \text{ K x } \ln(1/4.53)$$

$$\Delta G_{220} = 4{,}357 \text{ J mol}^{-1} = 4.3 \text{ kJ mol}^{-1}$$

Equation 4.1: Calculating the Gibbs free energy.

The ^{1}H NMR spectrum at 220 K exhibits peaks for the major species at 4.28, 4.75, and 6.08 ppm with relative integrations of 1H:5H:1H. The cyclopentadienyl protons were

assigned as the resonance at 4.75 ppm (singlet). The peaks at 4.28 and 6.08 ppm had a multiplicity of an apparent triplet and a doublet with $^{3}J_{HH} = {}^{3}J_{HP}$ of 11.1 Hz, and $^{3}J_{HH}$ of 10.6 Hz respectively, were assigned to the alkene functional group of 2-styrylpyridine. The coupling to phosphorus demonstrated this group was bound to the ruthenium centre. In the ^{1}H NMR spectrum at 220 K, aromatic resonances were observed between 6.51-7.74 ppm. However, there were more than the expected peaks in this region for the major complex in addition to the 2-styrylpyridine protons and this was due to there being an individual environment for each of the phenyl rings on the triphenylphosphine ligand. From these data the structure of the major species is thought to be **17^{H}**, where the 2-styrylpyridine is bound to the ruthenium centre *via* both the alkene bond and the nitrogen atom.

The identity of the minor form of **17^{H}** was determined through combined experimental NMR data and DFT calculations. From the low variable temperature ^{1}H NMR experimental data the minor species displayed resonances at 4.67 ppm (apparent triplet, $^{3}J_{HH}$, $^{3}J_{HP}$ of 9.3 Hz) and 6.45 ppm (doublet, $^{3}J_{HH}$ of 10.1 Hz) with a relative integration of 1:1 respectively. These resonances were assigned to the alkene protons. Additionally, the proton at the C-6 position of the pyridine ring has shifted downfield in comparison to the major complex **17^{H}**, to a chemical shift of 8.25 ppm, which indicates a different environment (proton at the C-6 position of 2-styrylpyridine resonance is observed at approximately 7.6 ppm for the major species **17^{H}**, and 8.57 for uncoordinated 2-styrylpyridine). From the NMR spectra it is reasonable to conclude that the alkene bond is still coordinated to the ruthenium centre as the chemical shifts are characteristic of alkene groups bound to a ruthenium centre, and the difference in environment of the pyridine proton at the C-6 position of 2-styrylpyridine suggested that the nitrogen atom was now closer to being uncoordinated to the ruthenium centre. The ^{31}P{^{1}H} NMR spectrum at 220 K reveals the minor species triphenylphosphine resonance is at 55.0 ppm. The variable temperature NMR experiment suggested that there are two complexes in equilibrium with each other, as upon cooling the sample two sets of resonances were observed.

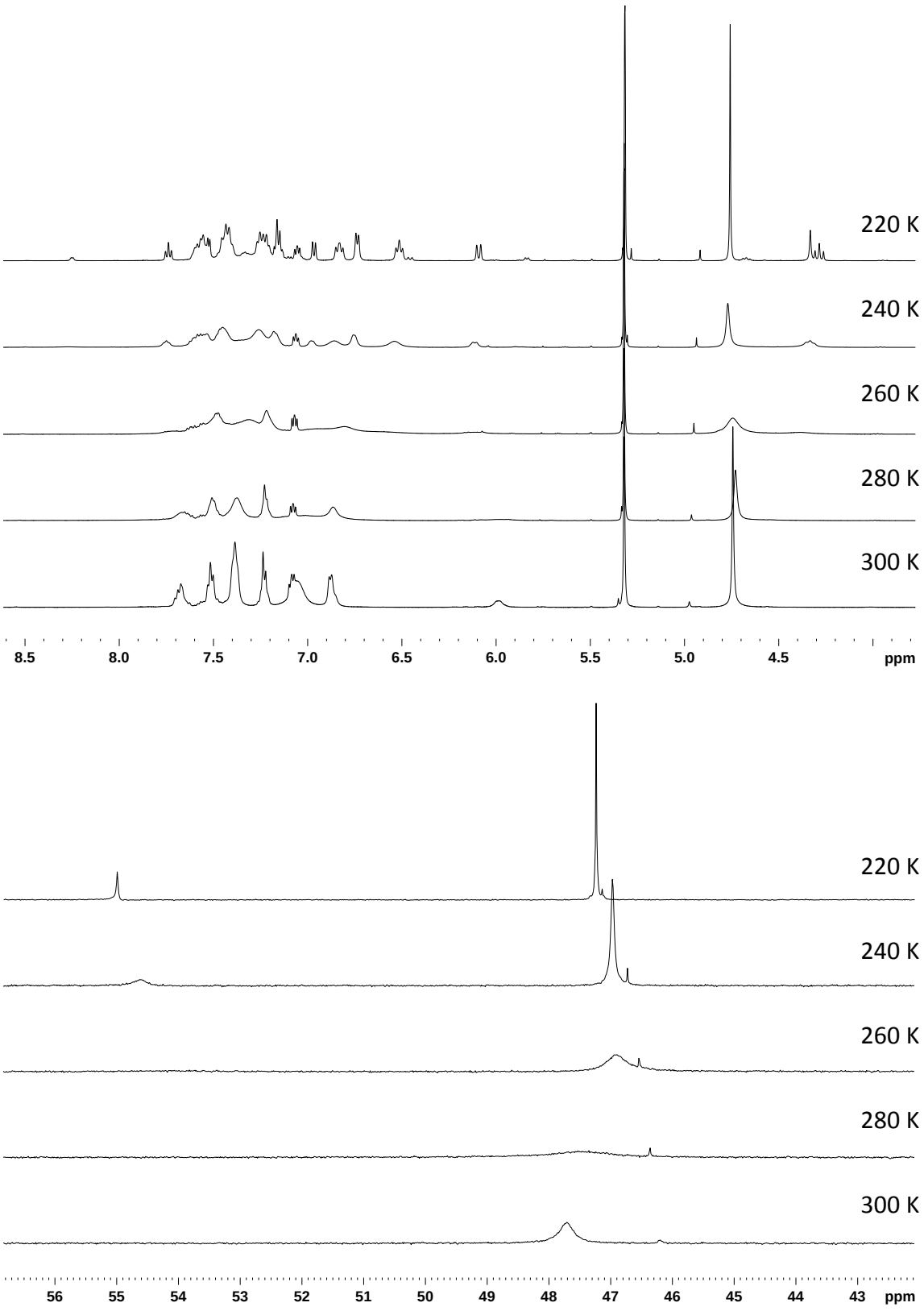

Figure 4.1: ^{1}H NMR (top) and $^{31}P\{^{1}H\}$(bottom) spectra of **17^{H}** at 300 K, 280 K, 260 K, 240 K and 220 K.

Crystals of **17^{H}** suitable for X-ray diffraction were grown by slow diffusion of pentane into a dichloromethane solution containing **17^{H}** (Figure 4.2, Table 4.1). The structure allowed us to determine that 2-styrylpyridine was coordinated to the ruthenium centre *via* the nitrogen atom and the alkene bond of the molecule. The P(1)-Ru(1) bond length was 2.3498(4) Å. The ruthenium coordination to the 2-styrylpyridine molecule bond lengths of N(1)-Ru(1) was 2.1195(12) Å and to the alkene functional group for C(6)-Ru(1) and C(7)-Ru(1) were 2.2074(16) and 2.2928(16) Å respectively. For the coordinated 2-styrylpyridine molecule of **17^{H}**, the C(6)-C(7) bond length was 1.399(2) Å; whereas the two adjacent bonds C(5)-C(6) and C(7)-C(8) were longer at 1.478(2) and 1.484(2) Å respectively. This indicates there is still some double bond character for the alkene bond. An independent crystal structure of uncoordinated 2-styrylpyridine has been reported and the alkene bond length was found to be 1.321(8) Å.[302] Thus the alkene bond in **17^{H}** is elongated, where the longer bond length could probably be attributed to electron density from the ruthenium centre being donated into the anti-bonding orbital and also donation from the π orbital to the metal. In the uncoordinated 2-styrylpyridine crystal structure, the adjacent bond lengths to the alkene bond were found to be 1.486(8) and 1.462(8) Å.[302]

The coordination of 2-vinylpyridine ligands to osmium and ruthenium centres has been investigated by Esteruelas *et al*. for the synthesis of complexes [M(Tp)($P^{i}Pr_3$)($NC_5H_4CH=CH_2$)][BF_4] (where Tp = hydridotris(pyrazolyl)borate and M = Os, Ru).[142] The alkene chemical shifts of the ruthenium complex were at a lower field than the osmium complexes. The ruthenium complex in the ^{1}H NMR spectrum exhibited alkene chemical shifts at 6.26 (CH), 4.56 and 3.86 (CH_2) ppm, which is consistent with our NMR spectroscopic data. The carbon-carbon bond length for transition metal η^2-coordinated alkene complexes was reported to be between 1.340 and 1.445 Å.[303] For example, the osmium complex [OsCl($P^{i}Pr_3$)($NC_5H_4CH=CH$) ($NC_5H_4CH=CH_2$)], exhibited a carbon-carbon bond length for the η^2-coordinated alkene at 1.401(4) Å and osmium-carbon bond lengths of 2.162(2) and 2.170(3) Å.[304] Complexes **17^{R}** (where R = H and CF_3) exhibited carbon-carbon bond lengths for the η^2-coordinated alkene of 1.399(2) and 1.408(4) respectively, which is in the middle of the previously reported range.

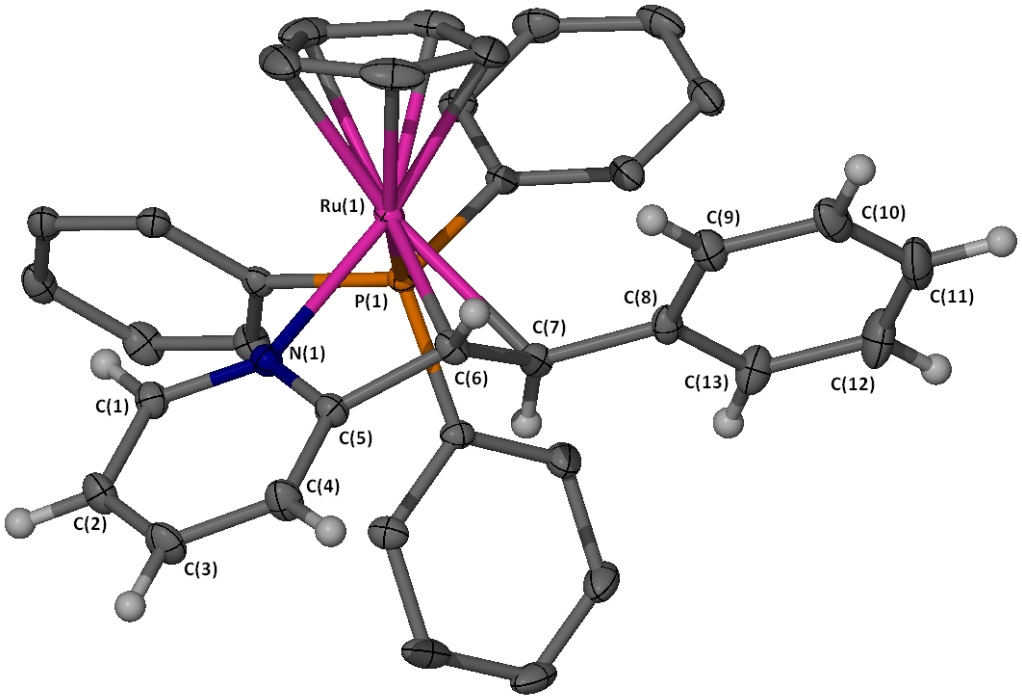

Figure 4.2: X-Seed diagram of the cation $[Ru(\eta^5\text{-}C_5H_5)(PPh_3)(NC_{13}H_{11})]^+$ from complex **17^H**. Selected hydrogen atoms, a dichloromethane molecule and $[PF_6]^-$ anion have been omitted for clarity, and where shown the thermal ellipsoids are at a 50 % probability level.

	Bond lengths (Å)		Bond angles (°)
P(1)-Ru(1)	2.3498(4)	N(1)-Ru(1)-P(1)	91.71(4)
N(1)-Ru(1)	2.1195(12)	C(6)-Ru(1)-P(1)	116.98(4)
C(6)-Ru(1)	2.2074(16)	C(7)-Ru(1)-P(1)	87.55(4)
C(7)-Ru(1)	2.2928(16)	N(1)-Ru(1)-C(6)	63.63(5)
C(1)-N(1)	1.3408(19)	C(5)-N(1)-Ru(1)	97.84(9)
C(1)-C(2)	1.388(2)	N(1)-C(5)-C(6)	107.64(13)
C(2)-C(3)	1.386(2)	C(5)-C(6)-Ru(1)	90.27(10)
C(3)-C(4)	1.394(2)	C(4)-C(5)-C(6)	129.41(15)
C(4)-C(5)	1.384(2)	C(7)-C(6)-C(5)	120.18(14)
C(5)-N(1)	1.348(2)	C(6)-C(7)-Ru(1)	68.59(9)
C(5)-C(6)	1.478(2)	C(6)-C(7)-C(8)	121.13(14)
C(6)-C(7)	1.399(2)	C(1)-N(1)-C(5)	119.76(13)
C(7)-C(8)	1.484(2)		

Table 4.1: Selected bond lengths (Å) and angles (°) for complex **17^H**.

4.2.2 DFT studies

The DFT structures of **17^{H}** were modelled by David Johnson, using an initial optimisation at the (RI)-BP86/SV(P) level and a further single point calculation at the PBE0/def2-TZVPP level, to provide insight in to the nature of the minor species. A structure where the nitrogen atom of 2-styrylpyridine was uncoordinated and a chlorine atom from the dichloromethane solvent was coordinated to the ruthenium centre was modelled, and found to be 89 kJ mol^{-1} higher in enthalpy than the major species. This enthalpy was not consistent with experimental evidence and therefore disregarded.

Also, the propeller direction of the phenyl rings in the PPh_3 ligand was rotated and modelled in a similar fashion. This indicated that there was a small difference in the enthalpy of 9 kJ mol^{-1} relative to the major complex, and could possibly explain the fluxional behaviour observed. However, it does not explain completely the differences observed for the chemical shifts for the pyridine protons at the C-6 position of 2-styrylpyridine.

A final possibility was modelled using DFT which involved changing the coordination mode of 2-styrylpyridine. If 2-styrylpyridine was to rotate around the carbon-carbon bond adjacent to the alkene bond and re-coordinate through the nitrogen atom of the pyridine ring it would create another orientation for the ligand to coordinate at the ruthenium centre (Figure 4.3). A difference in enthalpy of -16 kJ mol^{-1} was calculated and a difference in Gibbs free energy at 298 K was -16 kJ mol^{-1} between the two complexes, where the major complex was more stable and therefore lower in energy. This seemed like the most reasonable explanation for the minor species from the reaction in Scheme 4.1. From these calculations, the two conformers are the most likely explanation for the fluxional behaviour.

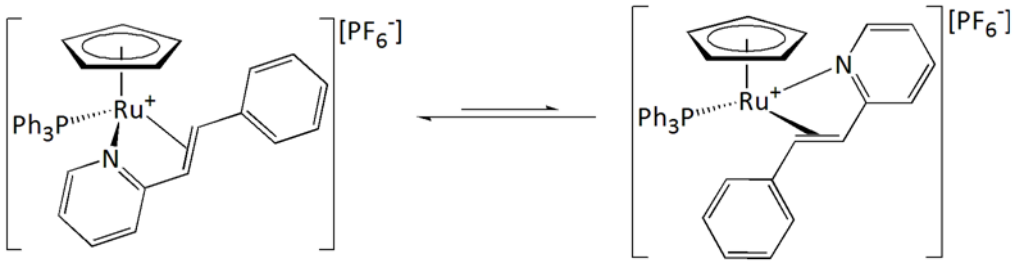

Major complex **17^{H}** Minor complex

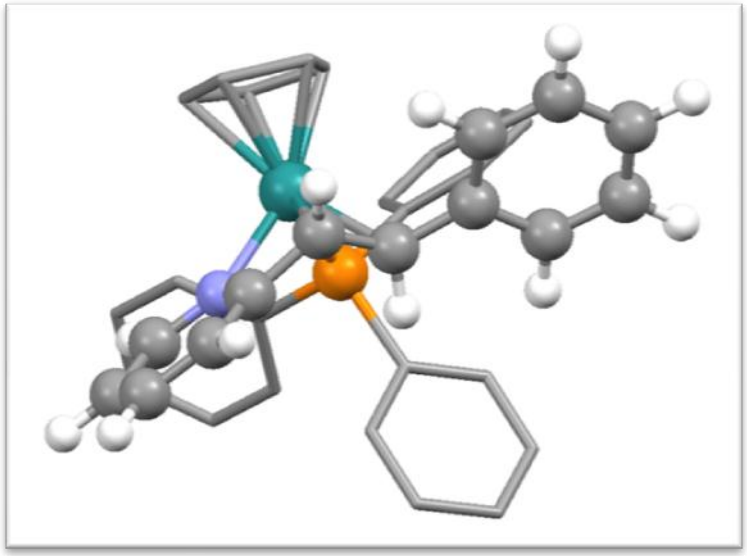

DFT calculated structure of major complex **17^{H}**

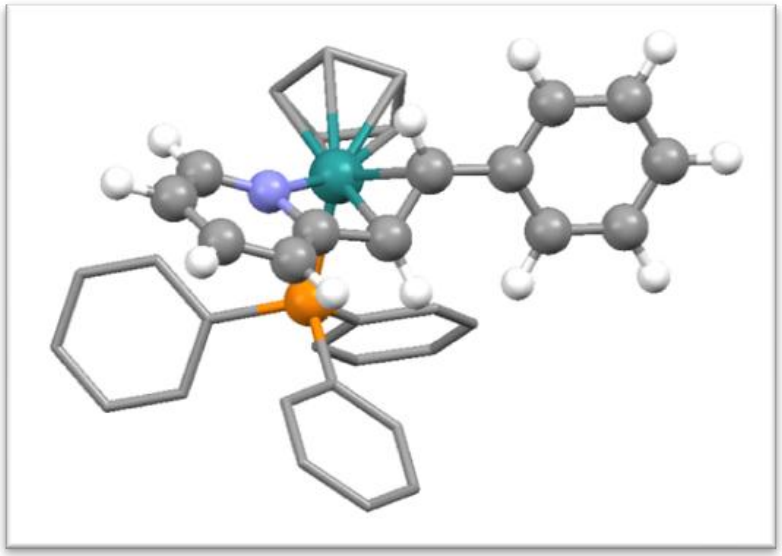

DFT calculated structure of minor complex

Figure 4.3: DFT calculation structures of major and minor complexes of complex **17^{H}**.

4.2.3 Reactivity observed with 17^{H} in d_5- pyridine

In the catalytic reaction reported by Murakami and Hori, 2-styrylpyridine was the alkenylation product formed from the catalytic reaction between the half-sandwich ruthenium complex [Ru(η^5-C_5H_5)(PPh_3)$_2$Cl], **1**, $NaPF_6$ and a TMS-substituted alkyne in pyridine.[253] During the course of the catalytic cycle, 2-styrylpyridine would be coordinated to the ruthenium centre and it is therefore important to understand how **17^{H}** behaves in the presence of pyridine (the catalytic reaction medium).

Complex **17^{H}** was dissolved in an excess of d_5-pyridine and the reaction was monitored *via* NMR spectroscopy (Scheme 4.2). The ^{1}H NMR and ^{31}P{^{1}H} NMR spectra revealed that there were no broad resonances belonging to **17^{H}** in the reaction mixture. In fact, the ^{1}H NMR spectrum exhibited a sharp resonance at 4.57 ppm for cyclopentadienyl protons of a new complex and the ^{31}P{^{1}H} NMR spectrum displayed a new triphenylphosphine resonance at 49.1 ppm and the $[PF_6]^-$ anion at -143.0 ppm. These resonances matched those for **5**, when compared to an authentic sample. Also, the ^{1}H NMR spectrum displayed a doublet resonance at 8.03 ppm with a $^{3}J_{HH}$ of 16.0 Hz, which is characteristic of an alkene proton of uncoordinated 2-styrylpyridine. These observations suggested that the pyridine molecules have substituted the 2-styrylpyridine from **17^{H}**.

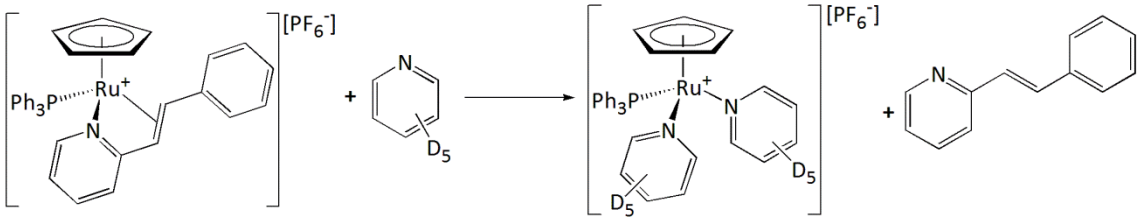

17^{H} **5**

Scheme 4.2: Addition of excess d_5-pyridine to complex **17^{H}**.

4.3 Reaction between *E*-2-(4-(trifluoromethyl)styryl)pyridine and 9^{Ph}

The substituent effects from a CF_3 group in the 4-position of the phenyl ring in the compound 2-styrylpyridine was also investigated, to observe any differences in the coordination of *E*-2-(4-(trifluoromethyl)styryl)pyridine to the cationic ruthenium fragment $[Ru(\eta^5\text{-}C_5H_5)(PPh_3)]^+$. Furthermore, the CF_3 substituent was used to monitor the catalytic reactions observed in Chapter 5, and therefore it would be useful to determine if the coordination of *E*-2-(4-(trifluoromethyl)styryl)pyridine was similar to 2-styrylpyridine.

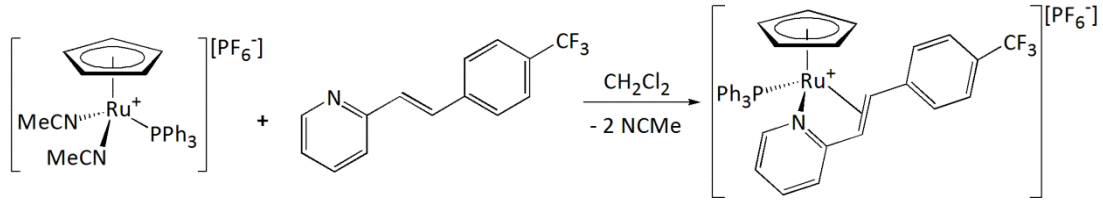

9^{Ph} **17^{CF3}**

Scheme 4.3: Reaction of complex **9^{Ph}** with *E*-2-(4-(trifluoromethyl)styryl)pyridine.

A similar method to the synthesis of **17^{H}** was used to prepare **17^{CF3}** (Scheme 4.3). The addition of *E*-2-(4-(trifluoromethyl)styryl)pyridine to a solution of **9^{Ph}** in dichloromethane resulted in coordination of *E*-2-(4-(trifluoromethyl)styryl)pyridine through the nitrogen atom and the alkene functional group. The product was characterised by variable temperature NMR spectroscopy, ESI-MS, elemental analysis and X-ray crystallography.

At 295 K, the ^1H and $^{31}P\{^1H\}$ NMR spectra in d_2-dichloromethane revealed only broad resonances for the final product, consistent with fluxional behaviour on the NMR timescale. This was similar to the properties of the solution of **17^{H}** at 295 K in d_2-dichloromethane. In the ^1H NMR spectrum at 295 K, broad signals at 4.50 and 6.51 ppm could be observed for the alkene protons. The $^{31}P\{^1H\}$ NMR spectrum exhibited two peaks at -143.0 ppm (septet) and at 46.7 ppm (broad) for the $[PF_6]^-$ anion and triphenylphosphine ligand respectively. An ESI-MS displayed a *m/z* peak of 678.11 with a ruthenium isotope pattern, which was assigned to the cationic ruthenium fragment $[M^+]$ of **17^{CF3}**. Also, elemental analysis of the species **17^{CF3}** was within an error of 0.5 % when a molecule of CH_2Cl_2 was included. This is not unusual

considering crystals of **17^{CF3}** were submitted for analysis and the crystals may contain a solvent molecule.

A variable temperature ^{1}H and ^{31}P{^{1}H} NMR experiment was conducted on **17^{CF3}** from 300 K to 220 K and spectra were recorded in 20 K intervals (Figure 4.4). In a similar fashion to **17^{H}**, on lowering the temperature of the sample for complex **17^{CF3}** the resonances got broader until 260 K and below this temperature the peaks began to get sharper. At 240 K, it was apparent that there were two species in the reaction mixture, a major and minor complex being observed in the ^{1}H and ^{31}P{^{1}H} NMR spectra. At 220 K, the peaks were all well-defined. The ratio of major and minor species from the ^{1}H NMR spectrum was found to be approximately 11:1. This was consistent with the ^{31}P{^{1}H} NMR spectrum at 220 K, where three resonances at -143.0, 46.9 and 54.6 ppm were observed for the $[PF_6]^-$ anion and the triphenylphosphine ligand of the major and minor complexes respectively. The CF_3 substituent in the 4-position of the phenyl group favours the major complex **17^{CF3}** in solution. The difference in Gibbs free energy of the two species solution at 220 K has been calculated and found to be 2.7 kJ mol^{-1}.

$$\Delta G = - 8.314 \text{ J K}^{-1} \text{ mol}^{-1} \text{ x } 220 \text{ K x ln}(1/10.83)$$

$$\Delta G_{220} = 2{,}763 \text{ J mol}^{-1} = 2.7 \text{ kJ mol}^{-1}$$

Equation 4.2 : Calculating the Gibbs free energy.

From the information gathered on **17^{H}** and the similarities observed between the complexes **17^{H}** and **17^{CF3}** the minor complex could potentially be where the ligand *E*-2-(4-(trifluoromethyl)styryl)pyridine has rotated around the alkene bond and has coordinated in two different modes to give the two isomers (Figure 4.3).

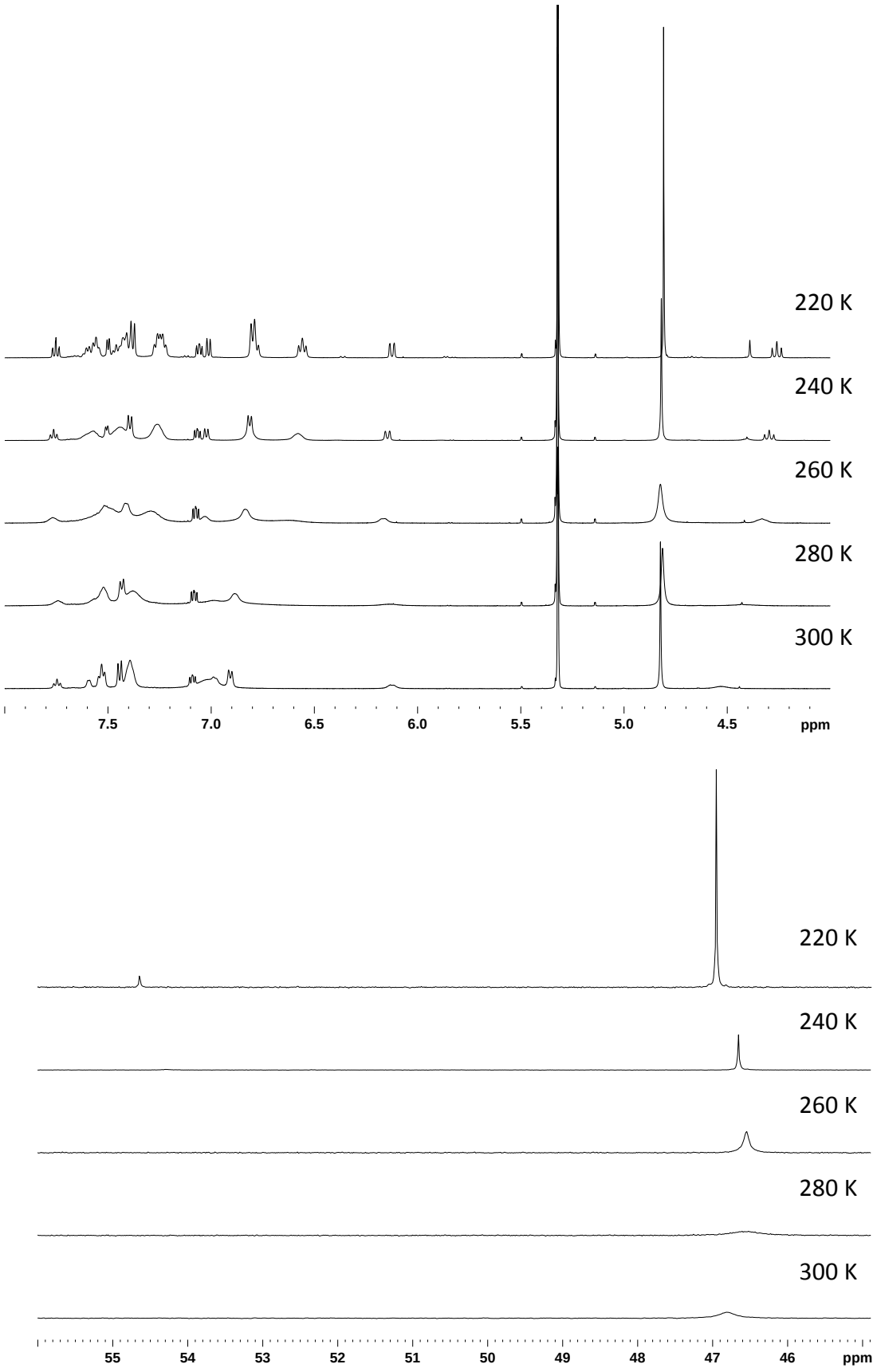

Figure 4.4: ^{1}H NMR (top) and ^{31}P{^{1}H}NMR (bottom) spectra of **17**$^{\mathbf{CF3}}$ at 300 K, 280 K, 260 K, 240 K and 220K.

Crystals of **17**^{CF3} suitable for X-ray diffraction were grown by slow diffusion of pentane into a dichloromethane solution containing the complex. An R value of 6 % was determined and therefore the ESDs within this structure were larger. The molecule *E*-2-(4-(trifluoromethyl)styryl)pyridine was found to coordinate to the $[Ru(\eta^5\text{-}C_5H_5)(PPh_3)]^+$ fragment through the nitrogen atom and the alkene bond. A P(1)-Ru(1) bond length was 2.3445(8) Å. The bond lengths of the ruthenium centre to *E*-2-(4-(trifluoromethyl)styryl)pyridine of N(1)-Ru(1), C(6)-Ru(1) and C(7)-Ru(1) were found to be 2.091(3), 2.189(3), and 2.272(3) Å respectively. In comparison to **17**^{H} these bond lengths were found to be significantly shorter. The shorter bond lengths in **17**^{CF3} could indicate stronger coordination of the 2-styrylpyridine derivative to the ruthenium centre.

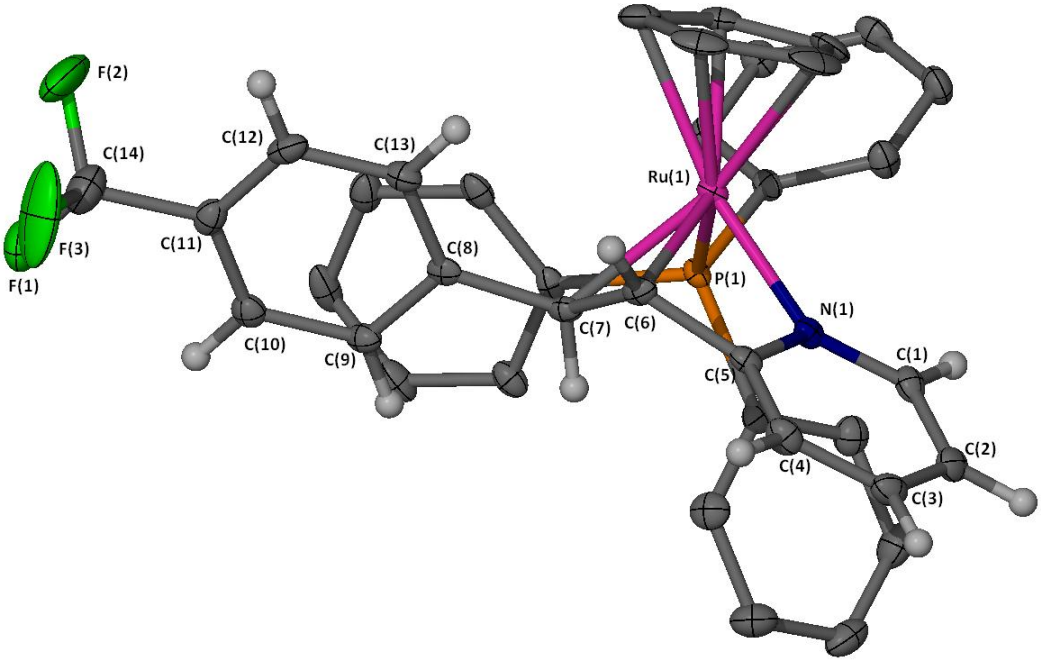

Figure 4.5: X-Seed diagram of the cation $[Ru(\eta^5\text{-}C_5H_5)(PPh_3)(NC_{14}H_{10}F_3)]^+$ from complex **17**^{CF3}. Selected hydrogen atoms, a dichloromethane molecule and $[PF_6]^-$ anion have been omitted for clarity, and where shown the thermal ellipsoids are at a 50 % probability level.

	Bond lengths (Å)		Bond angles (°)
P(1)-Ru(1)	2.3445(8)	N(1)-Ru(1)-P(1)	90.24(7)
N(1)-Ru(1)	2.091(3)	C(6)-Ru(1)-P(1)	116.55(9)
C(6)-Ru(1)	2.189(3)	C(7)-Ru(1)-P(1)	85.81(8)
C(7)-Ru(1)	2.272(3)	N(1)-Ru(1)-C(6)	64.02(11)
C(1)-N(1)	1.336(4)	C(5)-N(1)-Ru(1)	97.9(2)
C(1)-C(2)	1.376(5)	N(1)-C(5)-C(6)	106.6(3)
C(2)-C(3)	1.398(5)	C(5)-C(6)-Ru(1)	90.14(19)
C(3)-C(4)	1.384(5)	C(4)-C(5)-C(6)	131.3(3)
C(4)-C(5)	1.378(4)	C(7)-C(6)-C(5)	118.3(3)
C(5)-N(1)	1.354(4)	C(6)-C(7)-Ru(1)	68.43(17)
C(5)-C(6)	1.476(4)	C(6)-C(7)-C(8)	123.3(3)
C(6)-C(7)	1.408(4)	C(1)-N(1)-C(5)	120.2(3)
C(7)-C(8)	1.477(4)		

Table 4.2: Selected bond lengths (Å) and angles (°) for complex **17**^{CF3}.

4.4 Reaction between 9^{Me} and 2-styrylpyridine

Coordination of 2-styrylpyridine to a half-sandwich ruthenium complex, with a different phosphine ligand was also investigated. The triphenylphosphine ligand was substituted with trimethylphosphine. In Chapter 7, the ability of **14**^{H} to perform the catalytic transformation of phenylacetylene and pyridine to give 2-styrylpyridine in an alkenylation reaction was investigated, therefore it is important to understand how the compound 2-styrylpyridine coordinates to the fragment $[Ru(\eta^5\text{-}C_5H_5)(PMe_3)]^+$.

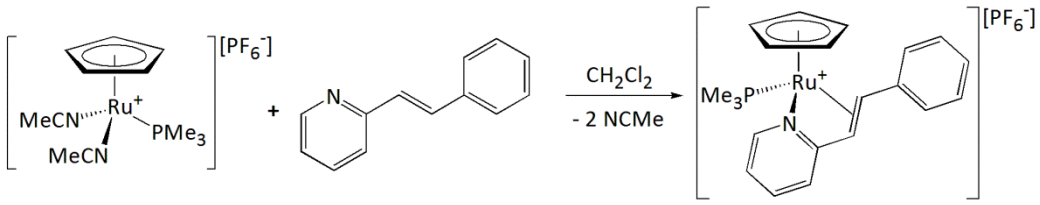

9^{Me} **18**

Scheme 4.4: Reaction of complex **9**^{Me} with 2-styrylpyridine.

The preparation of **18** involved the addition of 2-styrylpyridine to **9**^{Me} in a dichloromethane solution. A similar procedure for the synthesis of complexes **17**^{R} was used for **18**. The resulting yellow precipitate was washed with hexane, and a yield of 60

% was collected. The solubility of **18** in dichloromethane was poor, as the addition of 20 mg of **18** was not fully soluble in approximately 0.6 ml of d_2-dichloromethane. Approximately 10 mg of **18** was fully soluble in approximately 0.6 ml of d_2-dichloromethane. The product was characterised by NMR spectroscopy, ESI-MS, elemental analysis and X-ray crystallography.

The ^{1}H NMR spectrum displayed a peak at 1.63 ppm as a doublet with a 9H integration with respect to a broad singlet resonance at 4.84 ppm with an integration of 5H, which could be assigned as the methyl groups of the trimethylphosphine ligand and the cyclopentadienyl protons respectively. In addition, a $^{1}H\{^{31}P\}$ NMR spectrum revealed that the resonance at 1.63 ppm simplified to a singlet resonance. The aromatic signals for the protons of 2-styrylpyridine were observed between 6.98 and 7.88 ppm. Interestingly, only two resonances at 4.22 and 5.77 ppm were broad and both had an integration of 1H with respect to the cyclopentadienyl protons at 4.84 ppm, these were assigned to the alkene functional group of 2-styrylpyridine. Similar observations were found in the $^{13}C\{^{1}H\}$ NMR spectrum for the alkene resonances at 44.7 and 71.1 ppm which were also broad. The $^{31}P\{^{1}H\}$ NMR spectrum of **18** contained two sharp resonances at -143.0 ppm as a septet and 11.2 ppm as a singlet, for the $[PF_6]^-$ anion and the trimethylphosphine ligand.

The ESI-MS exhibited two peaks with a ruthenium isotope pattern, with a *m/z* of 424.07 and 325.04, which were assigned to being the $[M^+]$ and $[M^+ - C_{14}H_{10}F_3N]$ fragments respectively. In addition, an elemental analysis of crystals collected of complex **18** were within a 0.6 % error of the calculated product **18** containing 0.15 equivalents of CH_2Cl_2, which was confirmed by NMR spectroscopy.

Several variable temperature NMR experiments were conducted of **18** and spectra recorded in 20 K steps, including a low temperature experiment in d_2-dichloromethane between 295 and 215 K; and a high temperature experiment in d_2-tetrachloroethane between 295 and 355 K (Figure 4.6). The low temperature variable temperature ^{1}H and $^{31}P\{^{1}H\}$ NMR spectra revealed fascinating properties belonging to the cyclopentadienyl and alkene protons. On cooling the sample, the $^{31}P\{^{1}H\}$ NMR spectrum between 295 and 215 K exhibited only one trimethylphosphine resonance, however there is a large change in the chemical shift of the singlet peak from 11.2 ppm to 13.8 ppm. The ^{1}H NMR spectra are consistent with the $^{31}P\{^{1}H\}$ NMR spectra, as they only display one cyclopentadienyl resonance. Between 295 and 275 K, the cyclopentadienyl ligand and

the two alkene protons appear to get broader, and below 275 K to 215 K, the resonances get sharper. The alkene peak at 4.22 ppm (broad, 295 K), develops in to a doublet of doublets at 4.02 ppm with a $^{3}J_{HH}$ of 9.5 Hz and $^{3}J_{HP}$ of 13.4 Hz. The other alkene resonance at 5.77 ppm (broad, 295 K), changes into a sharp doublet resonance at 5.83 ppm with $^{3}J_{HH}$ of 9.5 Hz. A high variable temperature NMR experiment between 295 K and 355 K of **18** in d_2-tetrachloroethane displayed the broad alkene and cyclopentadienyl resonances becoming sharper upon raising the temperature. The resonance for the alkene protons at 4.16 ppm (broad, 295 K) became an apparent triplet at 4.38 ppm with a $^{3}J_{HP}$, $^{3}J_{HH}$ of 10.7 Hz when heated to 355 K. The other alkene proton at 5.72 ppm (broad, 295 K), upon heating to 355 K exhibited at 5.76 ppm a doublet resonance with a $^{3}J_{HH}$ of 9.9 Hz. Heating the sample above 355 K was not possible, as the sample had already begun to thermally decompose and new resonances were observed in the ^{1}H NMR spectrum. The variable temperature ^{1}H NMR experiments displayed that the broad alkene resonances get sharper upon cooling and heating the sample, exhibited one environment for these protons.

The ^{1}H and ^{31}P{^{1}H} NMR spectra of **18** were different to the complexes **17^{R}**. For complexes **17^{R}** in a d_2-dichloromethane solution they possessed broad resonances for all proton environments and for the triphenylphosphine ligand in the ^{31}P{^{1}H} NMR spectrum. A precise reason has not yet been identified for the NMR spectroscopy observations of **18**. However, potential reasons could involve steric and electronic factors. The Tolman cone angles[20] of trimethylphosphine and triphenylphosphine are 118 ° and 145 ° respectively. The smaller cone angle of trimethylphosphine ligand would provide fewer steric demands at the ruthenium centre, and therefore allow stronger coordination of 2-styrylpyridine to the metal centre. Alternatively, a similar justification for what was observed for complexes **17^{R}** could also be occurring for **18**, where there is an equilibrium between a major and minor species. However, in the case of **18** the minor species has not been detected by NMR spectroscopy.

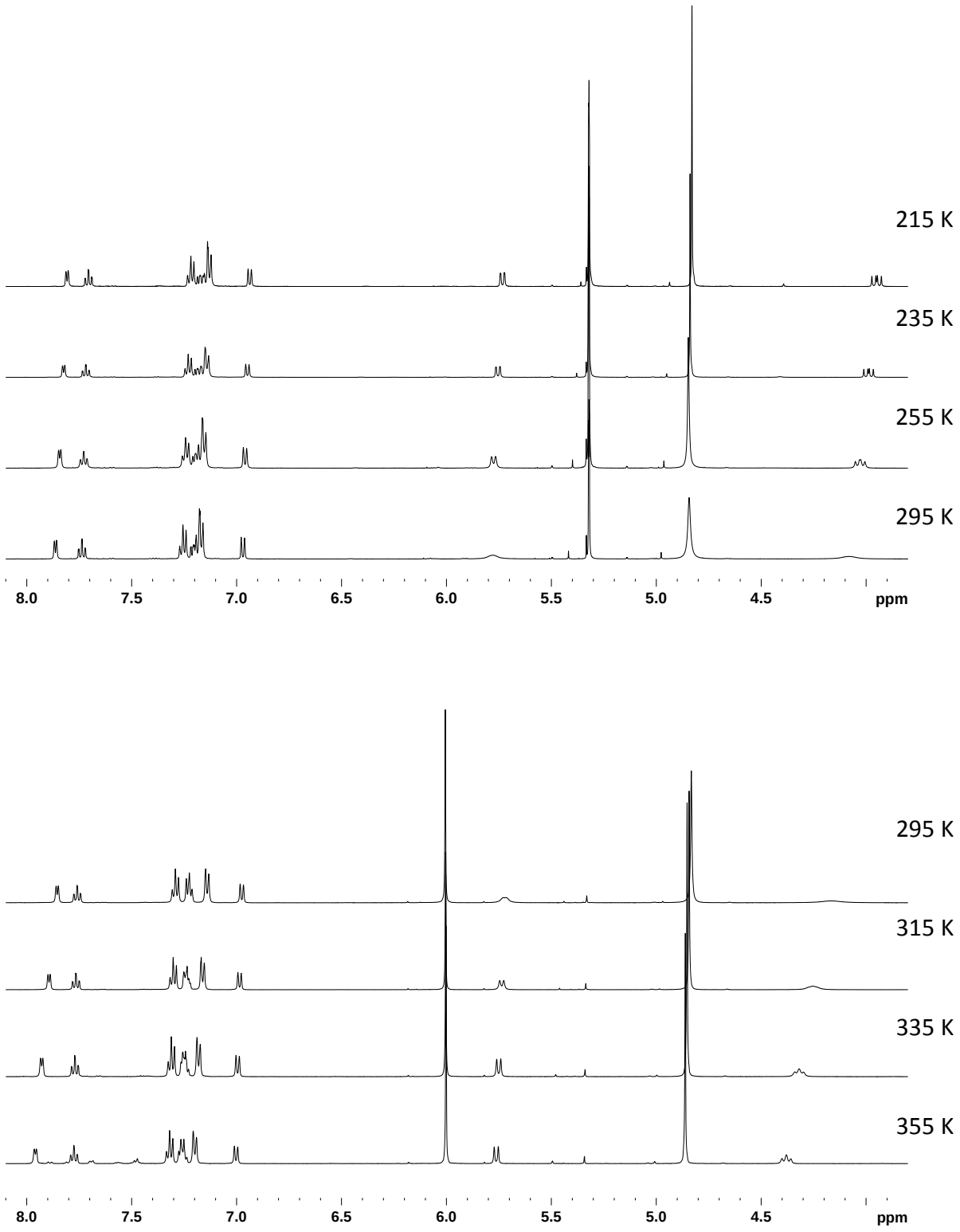

Figure 4.6: Variable temperature ^{1}H NMR spectra of complex **18** (top set of spectra: low temperature NMR spectra in CD_2Cl_2 at 215 K, 235 K, 255 K, 275 K, and 295 K; bottom set of spectra: high temperature NMR spectra in $C_2D_2Cl_4$ at 295 K, 315 K, 335 K and 355 K).

Crystals suitable for X-ray crystallography were grown by the slow diffusion of pentane in to a dichloromethane solution containing **18**. Unfortunately the crystal displayed merohedral twinning characteristics, and therefore any structural data obtained has not been discussed. However, we can determine that **18** has been synthesised where the 2-styrylpyridine is coordinated *via* the nitrogen atom and an alkene bond.

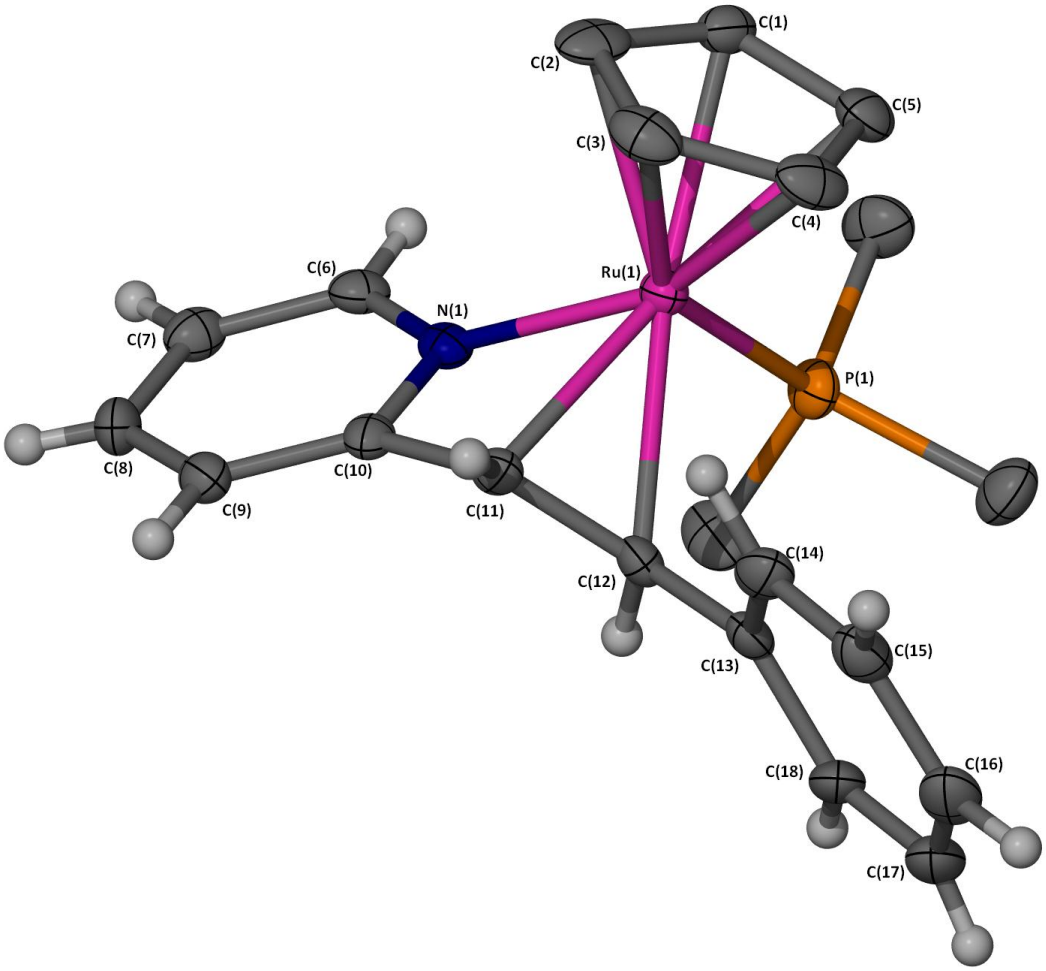

Figure 4.7: X-Seed diagram of the major cation $[Ru(\eta^5\text{-}C_5H_5)(PPh_3)(NC_{13}H_{11})]^+$ from complex **18**. Disorder was observed for both the ruthenium cation and the $[PF_6]^-$ anion. The $[Ru(\eta^5\text{-}C_5H_5)(PPh_3)(NC_{13}H_{11})]^+$ species was modelled over two locations with relative occupancies of 0.9105:0.0895. The minor form atoms were modelled isotropically. Selected hydrogen atoms, a dichloromethane molecule and $[PF_6]^-$ anion have been omitted for clarity, and where shown the thermal ellipsoids are at a 50 % probability level.

4.5 Conclusions

The compounds 2-styrylpyridine and *E*-2-(4-(trifluoromethyl)styryl)pyridine were reacted with $\mathbf{9^{Ph}}$ to give $\mathbf{17^{R}}$ (where R = H and CF_3) and 2-styrylpyridine with $\mathbf{9^{Me}}$ to yield **18**. The formation of complexes $\mathbf{17^{R}}$ and **18** is extremely important from a mechanistic point, as the coordination of the 2-styrylpyridine derivatives defines the end point in the catalytic cycle in the alkenylation reaction of pyridine to TMS-substituted alkynes. It was imperative to demonstrate that the catalyst deactivation was not occurring due to strong coordination of the product.

The coordination of the 2-styrylpyridine derivatives to $\mathbf{9^{Ph}}$ to generate $\mathbf{17^{R}}$ (where R = H and CF_3) suggested fluxional behaviour on an NMR timescale. From a combination of experimental and DFT calculations it was proposed that there were two conformational isomers of the ruthenium complexes $\mathbf{17^{R}}$. The addition of excess d_5-pyridine to complex $\mathbf{17^{H}}$, gives uncoordinated 2-styrylpyridine and **5**. This is an extremely promising finding as it indicates that the 2-styrylpyridine product does not hinder the regeneration of **5**; which we have found from our mechanistic studies (Chapter 2), is a key intermediate from the reaction mixture of $[Ru(\eta^5\text{-}C_5H_5)(PPh_3)_2(=C=CHR)][PF_6]$ in d_5-pyridine. In the literature, the coordination of 2-vinylpyridine was compared to benzophenone imine at the ruthenium centre, $[RuPhCl(CO)(P^iPr_3)_2]$ where substitution by 2-vinylpyridine was not favoured due to its higher steric demands at the metal centre, which supports our findings.[305]

The coordination of 2-styrylpyridine to $\mathbf{9^{Me}}$ produced **18**, which unlike $\mathbf{17^{R}}$ (where R = H and CF_3) did not exhibit complete fluxional behaviour in solution. Only the alkene resonances displayed broad characteristics in the ^{1}H NMR spectrum, which is due to the differences in coordination of the trimethylphosphine with respect to triphenylphosphine. A reason for this behaviour has not been fully identified.

Chapter 5. Reactivity of Half-Sandwich Ruthenium Complexes: Part I

5.1 Introduction

The once thought inert C-H bond can be activated using transition metal centres.[4] Organometallic chemistry is therefore a useful tool for the selective C-H functionalisation of the substrates, as it presents an atom economical route to synthesise new carbon-carbon or carbon-heteroatom bonds for applications in organic synthesis and catalysis.[4, 6, 7, 166, 306] By understanding the mechanisms of transition metal centres in stoichiometric chemistry, novel catalytic systems can be developed. A mechanistic approach was employed by Bergman *et al.*, where they exploited rhodium C-H bond activation for the synthesis of various biologically relevant structures.[167, 168, 175, 178, 307, 308] Focussing on the C-H alkylation of N-containing heterocycles they successfully reported the synthesis of the alkaloid (-)-incarvillateine, which is used in pain relief.[309] In 2006, they highlighted that the formation an N-heterocyclic carbene ligand at a rhodium centre could potentially be used further in coupling reactions.[178]

Our goal to understand the mechanism for the alkenylation of pyridine *via* the half-sandwich ruthenium complexes lead to a set of mechanistic investigations in d_2-dichloromethane.[253] Since the ruthenium complex $[Ru(\eta^5\text{-}C_5H_5)(PPh_3)(NC_5D_5)_2][PF_6]$, **5** was the major species observed in the reaction mixtures of complexes $\mathbf{2^R}$ in d_5-pyridine, our aim was to study the reactivity of these types of complexes. In Chapter 3, a general synthetic procedure for the synthesis of a range of ruthenium complexes was reported. Now, the stoichiometric chemistry of $\mathbf{10^H}$ (protio- version of **5**) will be described in this chapter. The reactivity of complexes $[Ru(\eta^5\text{-}C_5H_5)(PR_3)(L)_2][PF_6]$, (where R = Ph, Me, ^{i}Pr, OPh) with various terminal alkynes in a dichloromethane solution was also investigated and is reported in the following chapter. This approach will allow us to gain further mechanistic insight into the role of these species. This chapter will focus on the reactivity of $\mathbf{10^H}$ with various alkynes in d_2-dichloromethane and the reactions monitored *via* NMR spectroscopy under a nitrogen atmosphere.

5.2 Reactivity of complex 10^{H} with terminal aryl alkynes

The initial mechanistic studies in Chapter 2 identified the *bis*-d_5-pyridine complex **5** as the major new ruthenium-containing species in the reaction mixture. The protio- version of **5** is $\mathbf{10^{H}}$ and was synthesised independently in Chapter 3. This section will describe the reactions between $\mathbf{10^{H}}$ and various alkynes in a dichloromethane solution.

The alkenylation reactions reported by Murakami and Hori[253] have the potential to be 100 % atom efficient with respect to the starting materials required, which could be obtained by the removal of the TMS group of the alkyne 1-phenyl-2-trimethylsilylacetylene. We have therefore studied the behaviour of terminal alkynes with $\mathbf{10^{H}}$ in a dichloromethane solution. The full range of terminal alkynes studied included aryl substituents (phenylacetylene, 1-ethynyl-4-fluorobenzene, 4-ethynyl-α,α,α-trifluorotoluene) and alkyl substituents (*tert*-butylacetylene, 1-hexyne). The reactivity of TMS-substituted alkynes 1-phenyl-2-trimethylsilylacetylene and trimethylsilylacetylene have also been investigated.

This chapter will discuss the reactivity of $\mathbf{10^{H}}$ with aryl terminal alkynes and a further deuterium labelling study in order to provide further mechanistic information. The following chapter will describe substituent effects, including the differences observed in the reactivity when alkyl and TMS-substituted alkynes are used with $\mathbf{10^{H}}$. The mechanistic studies will hopefully provide an insight into how the ruthenium centre is involved in the alkenylation reaction of pyridine.[253]

5.2.1 Reaction between complex 10^{H} with phenylacetylene

The stoichiometric addition of phenylacetylene to $[Ru(\eta^5\text{-}C_5H_5)(PPh_3)(NC_5H_5)_2][PF_6]$, $\mathbf{10^{H}}$ in d_2-dichloromethane was investigated. The reactions were carried out with phenylacetylene, and repeated with a ^{13}C-label, $H^{13}C{\equiv}CPh$ to give more information on how the reaction proceeded (Figure 5.1). The reaction mixtures were monitored by NMR spectroscopy at room temperature until no more changes were observed.

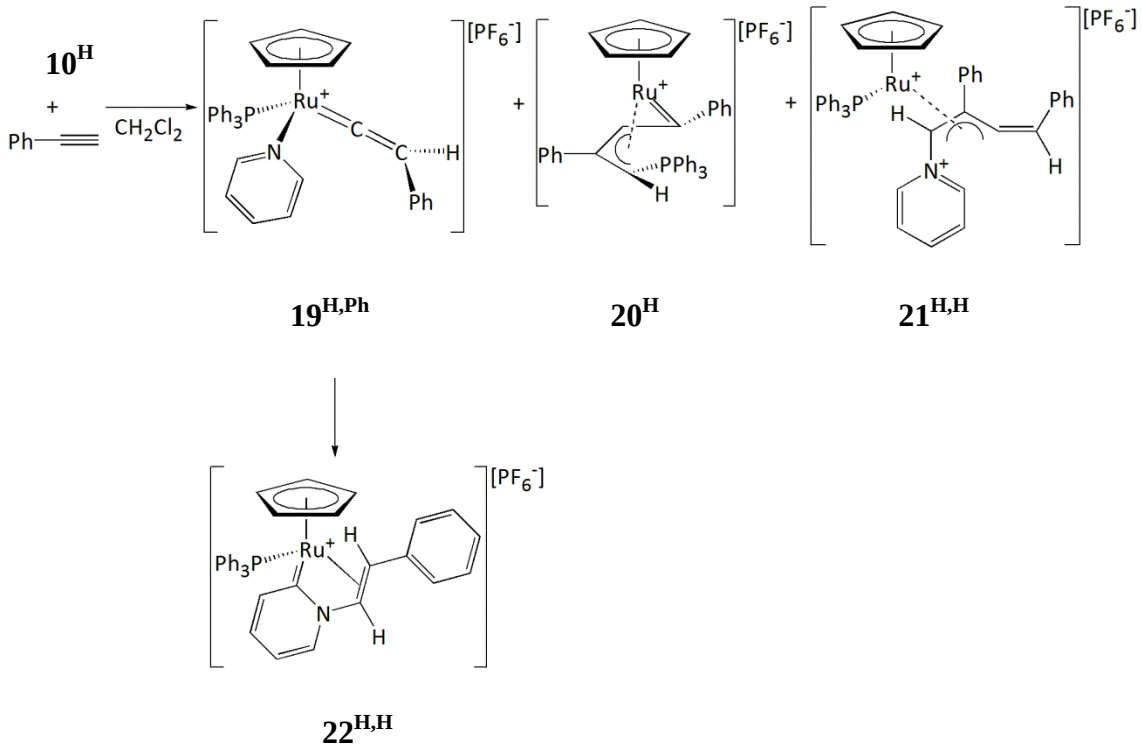

Scheme 5.1: Reaction of **5** with phenylacetylene in d_2-dichloromethane.

The stoichiometric reaction between phenylacetylene and $\mathbf{10^H}$ resulted in a reaction mixture in which initially three new products ($\mathbf{19^{H,Ph}}$, $\mathbf{20^H}$, and a minor unknown species which is short-lived and only present in the initial NMR spectra) could be observed *via* ^{1}H and ^{31}P{^{1}H} NMR spectroscopy. After 16 hours a set of NMR spectra were recorded which exhibited new resonances belonging to two more ruthenium complexes ($\mathbf{21^{H,H}}$ and $\mathbf{22^{H,H}}$). In total there were five new ruthenium species formed from this reaction mixture, four of which have been identified. The discussion will firstly involve the characterisation of complexes $\mathbf{19^{H,Ph}}$, $\mathbf{20^H}$ and $\mathbf{21^{H,H}}$; followed by how complex $\mathbf{22^{H,H}}$ was identified.

The initial NMR spectra of the starting material $\mathbf{10^H}$ exhibited cyclopentadienyl proton resonances at 4.42 ppm in the ^{1}H NMR spectrum, and the triphenylphosphine ligand at 50.2 ppm in the ^{31}P{^{1}H} NMR spectrum. Uncoordinated pyridine displayed resonances at 8.58 (*ortho* protons), 7.68, and 7.28 ppm and uncoordinated phenylacetylene in the ^{1}H NMR spectrum in d_2-dichloromethane. The ^{31}P{^{1}H} NMR spectrum did not show any signs of uncoordinated triphenylphosphine or triphenylphosphine oxide. The pyridine ligands from $\mathbf{10^H}$ appeared to be labile and were being substituted by phenylacetylene.

The reaction was left to continue at room temperature and monitored regularly *via* NMR spectroscopy. The reaction appeared to proceed slowly as the phenylacetylene proton resonance at 3.12 ppm was still present in the ^{1}H NMR spectrum after approximately 10 days. After 13 days, the majority of phenylacetylene had reacted, however **10^{H}** was still present in the reaction mixture and this suggested that more than one equivalent of phenylacetylene had been consumed with respect to **10^{H}**.

Overall, five new cyclopentadienyl ligand singlet resonances were observed: 5.48, 5.10, 4.97, 4.95 and 4.55 ppm alongside the resonances for **10^{H}** in the ^{1}H NMR spectrum and five new triphenylphosphine resonances: 51.8, 29.7, 53.6, 53.5 and 48.0 ppm respectively in the ^{31}P{^{1}H} NMR spectrum. Integration was used to help identify the respective cyclopentadienyl resonances from the ^{1}H NMR spectrum with the triphenylphosphine resonances in the ^{31}P{^{1}H} NMR spectrum. The manner in which the relative integrations of peaks changed over time was recorded from both the ^{1}H and ^{31}P{^{1}H} NMR spectra. Unfortunately due to the number of ruthenium complexes present in the reaction mixture, the aromatic region in the ^{1}H NMR spectrum was extremely complex and hence any resonances from between 7.00 – 7.75 ppm were not useful in the determination of the nature of the products.

The reaction conditions were changed in order to optimise the formation of certain ruthenium complexes, the reasons will be explained throughout this section. The different reaction conditions employed between **10^{H}** and phenylacetylene in dichloromethane include:

i) Stoichiometric addition of phenylacetylene to **10^{H}** in d_2-dichloromethane;
ii) Stoichiometric addition of ^{13}C-labelled phenylacetylene to **10^{H}** in d_2-dichloromethane;
iii) Stoichiometric addition of phenylacetylene to **10^{H}** in the presence of two equivalents of pyridine in d_2-dichloromethane;
iv) Addition of four equivalents of phenylacetylene to **10^{H}** in the presence of four equivalents of pyridine in dichloromethane.

The ratio of the complexes **10^{H}**, **20^{H}**, **21^{H,H}** and **22^{H,H}** has been calculated from the different reaction conditions (Table 5.1).

Reaction conditions	Ratio of complexes			
	10^{H}	**20^{H}**	**21^{H,H}**	**22^{H,H}**
i	1.0	1.5	1.5	7.0
ii	1.0	1.0	1.0	5.0
iii	-	-	1.0	5.7
iv	-	-	1.0	1.0

Table 5.1: Ratio of complexes present in the reaction mixture from different conditions.

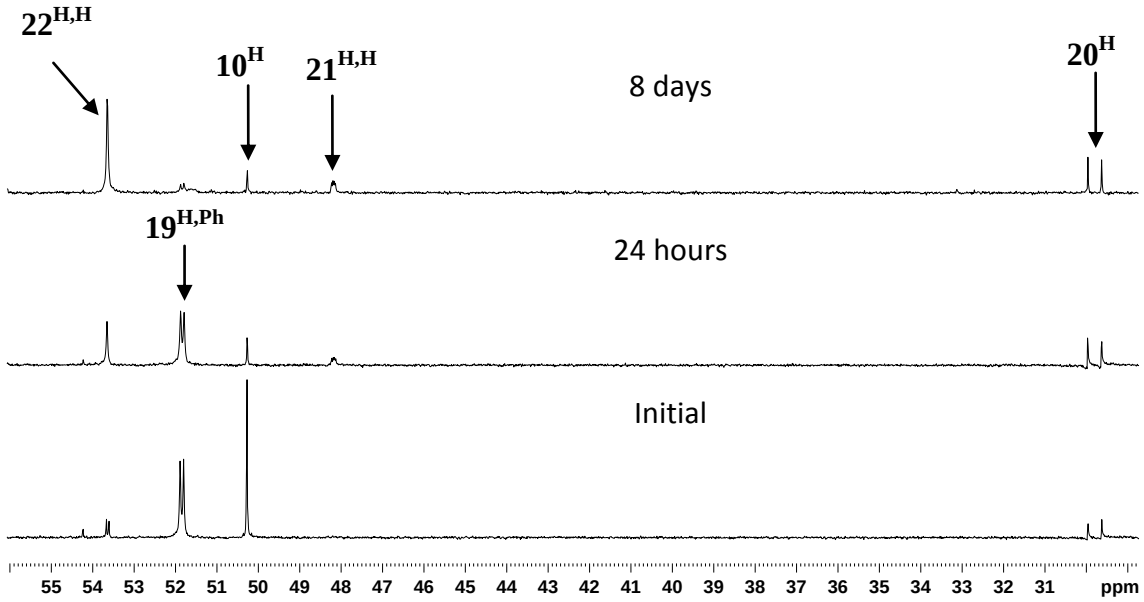

Figure 5.1: The $^{31}P\{^{1}H\}$ NMR spectra of reaction conditions ii proceeding over time.

5.2.1.1 The minor unknown species present in the initial reaction mixture

A minor unknown species was observed in the initial ^{1}H and $^{31}P\{^{1}H\}$ NMR spectra, and the NMR spectra recorded after 16 hours resulted in the loss of the resonances associated with this complex. The ^{1}H NMR spectrum contained resonances for the cyclopentadienyl protons at 4.97 ppm, and in the $^{31}P\{^{1}H\}$ NMR spectrum at 53.6 ppm. When $H^{13}C{\equiv}CPh$ was used the $^{31}P\{^{1}H\}$ NMR spectrum displayed a doublet at 53.6 ppm with a J_{PC} of 12.3 Hz. Due to its short-lived presence in the reaction mixture more information on this species has not been obtained.

*5.2.1.2 Identification of complex **19^{H,Ph}***

After the addition of phenylacetylene to **10^{H}** (reaction conditions i), there appeared to be one major new ruthenium species in the reaction mixture. The ^{1}H NMR spectrum displayed a broad resonance for the cyclopentadienyl protons at 5.48 ppm (5H) and there was also a broad resonance at 5.14 ppm (1H). In the aromatic region of the ^{1}H NMR spectrum, a pyridine signal was observed at 8.40 ppm as a multiplet which

integrated to 2H for the C-2/6 proton positions; when a $^{1}H\{^{31}P\}$ experiment was run this resonance simplified to a doublet, which suggested there is one pyridine molecule coordinated to the ruthenium centre. The major species in the $^{31}P\{^{1}H\}$ NMR spectrum had a singlet resonance at 51.8 ppm. This suggested that one pyridine ligand had dissociated from **10^{H}**; and the triphenylphosphine ligand was still coordinated to the ruthenium centre. It also implied that a phenylacetylene molecule must have substituted one of the pyridine ligands at the ruthenium centre.

The reaction was repeated with a ^{13}C-label to give more information on the nature of the species. The reaction between $H^{13}C{\equiv}CPh$ and **10^{H}** resulted in a change in the multiplicity of the resonances for **19^{H,Ph}**. In the $^{31}P\{^{1}H\}$ NMR spectrum the resonance at 51.8 ppm was a doublet with a $^{2}J_{PC}$ of 16.9 Hz. In addition, a $^{13}C\{^{1}H\}$ NMR spectrum revealed more information on the nature of this complex, as a doublet peak at 355.2 ppm, with a $^{2}J_{PC}$ of 16.9 Hz was observed. The chemical shift strongly suggests that **19^{H,Ph}** is a vinylidene-containing species.[54] The ^{1}H NMR spectrum still contained broad resonances at 5.48 and 5.14 ppm with an integration of 5H and 1H respectively, where these resonances have been assigned as the cyclopentadienyl ligand and the vinylidene proton respectively.

The data are consistent with **19^{H,Ph}** being a vinylidene-containing complex, where the other ligands at the ruthenium centre are a pyridine molecule, a triphenylphosphine ligand and the cyclopentadienyl ligand. However, after 24 hours the resonances for the vinylidene-containing complex **19^{H,Ph}** began to decrease, and after 10 days could no longer be detected. As the resonances for complex **19^{H,Ph}** decreased in intensity, resonances for another ruthenium-containing complex **22^{H,H}** increased in intensity.

*5.2.1.3 Identification of complex **20^{H}***

The initial reaction mixture of phenylacetylene to **10^{H}** (reaction conditions i) contained resonances for the cyclopentadienyl proton at 5.10 ppm (singlet, 5H) in the ^{1}H NMR spectrum. A doublet resonance at 5.82 ppm (1H) with a $^{2}J_{HP}$ of 9.8 Hz for a single proton coupled to a phosphorus atom was also observed. The $^{31}P\{^{1}H\}$ NMR spectrum displayed the corresponding triphenylphosphine group at 29.7 ppm (singlet). Further spectra recorded after this point did not indicate any change in the amount of this product, suggesting that the formation of **20^{H}** was complete within 30 minutes. The resonances belonging to **20^{H}** were found to change in the reaction mixture dependant on the reaction conditions (Section 1.5).

When the reaction was repeated with the ^{13}C-labelled species, H^{13}C≡CPh (reaction conditions ii), the ^{31}P{^{1}H} NMR spectrum exhibited a doublet at 29.7 ppm with a $^{1}J_{PC}$ of 67.2 Hz. This indicated that the phosphorus atom of the triphenylphosphine was coupling to the ^{13}C-labelled atom.

The resonances for **20^{H}** were very similar to those reported by Kirchner *et al.* for the product formed in the reaction between [Ru(η^{5}-C$_5$H$_5$)(PR$_3$)(NCMe)$_2$][PF$_6$] and two equivalents of alkyne (where R = Me, Ph or Cy).[132, 136, 138, 139] The alkyne molecules react in a head-to-tail fashion at the ruthenium centre and the phosphine group migrates, where the newly formed organic ligand at the ruthenium centre is an η^{3}-allyl carbene species. These reactions were reported to occur within a few minutes, consistent with observations made in our reactions. Kirchner *et al.* reported that when [Ru(η^{5}-C$_5$H$_5$)(PMe$_3$)(NCMe)$_2$][PF$_6$], **9^{Me}** is treated with two equivalents of phenylacetylene, the ^{31}P{^{1}H} NMR spectrum displayed a resonance at 31.5 ppm for the PMe$_3$ group; and the cyclopentadienyl protons at 5.33 ppm in the ^{1}H NMR spectrum. These results were very similar to what was observed in our reaction (Scheme 5.1). The reaction between [Ru(η^{5}-C$_5$H$_5$)(PPh$_3$)(NCMe)$_2$][PF$_6$], **9^{Ph}** and two molecules of phenylacetylene yielded the respective η^{3}-allyl carbene complex **20^{H}**.[132] However, **20^{H}** was unstable and over time converted to give a η^{4}-butadiene complex containing an orthometallated phenyl ligand of the triphenylphosphine ligand (Section 1.5).[139] Therefore was no reported experimental literature on **20^{H}** due to its unstable nature and therefore to confirm the presence of this species in the reaction mixture, an independent synthesis was conducted. Using the procedure reported by Kirchner *et al.*,[136] the resonances obtained from the independent reaction of **9^{Ph}** with two equivalents of phenylacetylene in d$_2$-dichloromethane were found to match the peaks belonging to **20^{H}**.

Complex **20^{H}** was removed from the reaction mixture by washing with pentane, or by changing the reaction conditions. If the stoichiometric reaction was conducted in the presence of two equivalents of pyridine, the formation of **20^{H}** was prevented (reaction conditions iii). The competing reaction pathway to synthesise **20^{H}** required two coordination sites at the ruthenium centre where both alkyne molecules could coordinate to form of a metallocyclopentatriene species and generate **20^{H}**.[132] This reaction pathway was now inhibited due to the presence of excess pyridine in the system.

This implied that $[Ru(\eta^5\text{-}C_5H_5)(PPh_3)(NC_5H_5)_2][PF_6]$, **10^{H}** had similar properties to the complexes $[Ru(\eta^5\text{-}C_5H_5)(PR_3)(NCMe)_2][PF_6]$ (where R = Me, Ph or Cy). However, it also appears that changing the labile acetonitrile ligands to pyridine molecules changes the reactivity seen with respect to terminal alkynes, as another reaction pathway is preferred to the formation of η^3-allyl carbene complex (since **20^{H}** is no longer the major complex in the reaction mixture). Additionally, this explained why there was unreacted **10^{H}** in the reaction mixture, as from the stoichiometric addition of phenylacetylene to **10^{H}** to form the η^3-allyl carbene complex **20^{H}**, the reaction required two equivalents of phenylacetylene per ruthenium complex.

*5.2.1.4 Identification of complex **21^{H,H}***

The resonances belonging to **21^{H,H}** were observed in the NMR spectra 16 hours after the stoichiometric addition of phenylacetylene to **10^{H}** (reaction conditions i). The formation of **21^{H,H}** in the reaction mixture was minor and did not increase after the 16 hours. However, by changing to the reaction conditions iv, a higher quantity of **21^{H,H}** was observed in the reaction mixture, which was determined *via* NMR spectroscopy. The % conversions to give **21^{H,H}** following reaction conditions i was approximately 10 %, alternatively with reaction conditions iv, an approximate 50 % conversion was observed.

The ^{1}H NMR spectrum exhibited a cyclopentadienyl ligand resonance at 4.55 ppm (singlet), and the triphenylphosphine resonance was observed at 48.0 ppm (singlet) for **21^{H,H}** in the $^{31}P\{^{1}H\}$ NMR spectrum. An ESI-MS of the reaction mixture with phenylacetylene resulted in a peak with a *m/z* of 712.17 and was interpreted to include the $[Ru(\eta^5\text{-}C_5H_5)(PPh_3)]^+$, NC_5H_5 and two HC≡CPh fragments.

In the equivalent experiment where $H^{13}C{\equiv}CPh$ was used (reaction conditions ii), a difference in the $^{31}P\{^{1}H\}$ NMR spectrum for the resonance at 48.0 ppm was observed. A resonance at 48.1 ppm was now a broad doublet of doublets which exhibited $^{2}J_{PC}$ couplings of 12.2 and 6.3 Hz between the triphenylphosphine ligand and two ^{13}C atoms. The $^{13}C\{^{1}H\}$ NMR spectrum of this species in the reaction mixture, exhibited two ^{13}C-labelled enriched signals at 67.1 and 170.8 ppm as doublets with a $^{2}J_{CP}$ of 7.7 and 12.9 Hz respectively. These coupling values are very similar to those observed in the $^{31}P\{^{1}H\}$ NMR spectrum for the resonance at 48.1 ppm. An ESI-MS of the crude reaction mixture exhibited a ruthenium containing peak with a *m/z* of 714.17 which was interpreted as a complex which contained the cationic fragment $[Ru(\eta^5\text{-}C_5H_5)(PPh_3)]^+$,

NC_5H_5 and two $H^{13}C{\equiv}CPh$ units. An organic fragment was also observed in the ESI-MS with a *m/z* of 286.15 which matched the formula $[C_{19}{}^{13}C_2H_{18}N]^+$. This suggested that the pyridine molecule was coordinated to two $H^{13}C{\equiv}CPh$ units.

Several methods were developed in order to purify and characterise **21^{H,H}**. The complex **21^{H,H}** was isolated from the reaction where conditions iv were employed, by the slow diffusion of pentane into a dichloromethane layer containing the product. Alternatively, following the reaction conditions iii, only two ruthenium species remained **21^{H,H}** and **22^{H,H}**. Complex **22^{H,H}** could be removed from the reaction mixture by the addition of base (Section 5.2.1.6), leaving behind **21^{H,H}**.

Although an analytically pure sample of **21^{H,H}** could not be obtained, the ^{1}H NMR spectrum of **21^{H,H}** exhibited broad resonances in the aromatic region suggesting fluxional behaviour in solution at room temperature. The $^{13}C\{^1H\}$ NMR spectrum of **21^{H,H}** also exhibited broad peaks between approximately 120 – 140 ppm. A variable temperature NMR experiment was conducted on a sample of **21^{H,H}** in d_2-dichloromethane. A set of ^{1}H and $^{31}P\{^1H\}$ NMR spectra were recorded at 20 K intervals from 295 K. Upon cooling the sample to 215 K, the broad resonances that were present at 295 K became sharper. Due to impurities in the sample, full characterisation of these peaks was not possible; however this complex displays fluxional behaviour at room temperature and cooling the sample resolves these resonances (Figure 5.2).

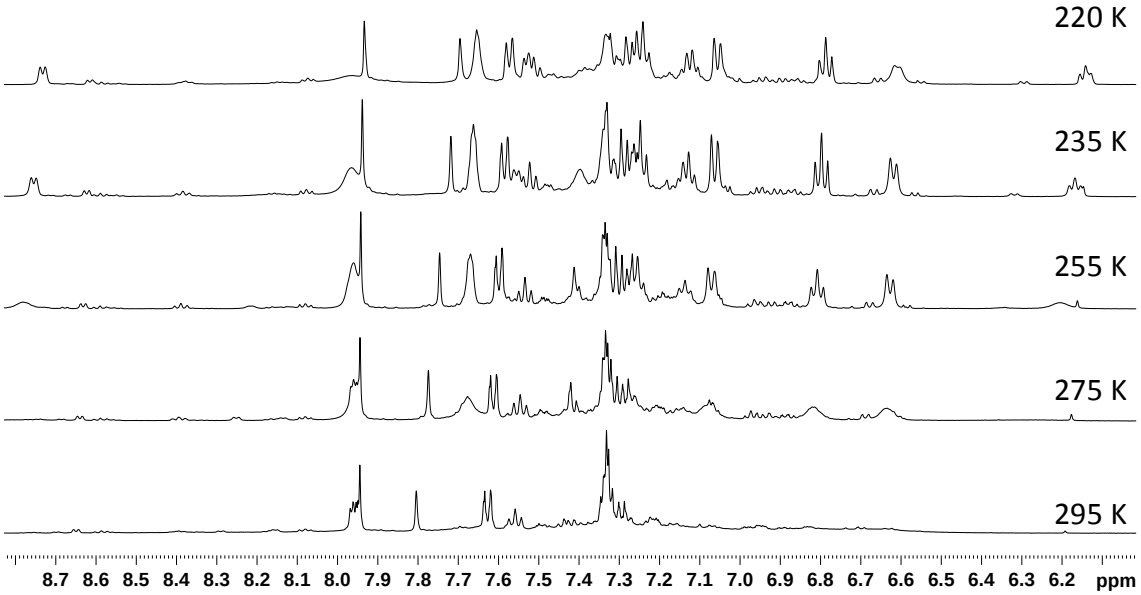

Figure 5.2: Low variable temperature ^{1}H NMR spectra of the aromatic region of **21^{H,H}** at 295 K, 275 K, 255 K, 235 K and 220 K.

Crystals suitable for X-ray diffraction indicated that **21^{H,H}** contained a pyridinium butadienyl fragment, which was coordinated through an η^3-bonding mode of the butadienyl group (Figure 5.3, Table 5.2). The structure of **21^{H,H}** revealed that new C-C and N-C bonds have been formed between two alkyne molecules and a pyridine molecule. The η^3-allylic group maintains an *exo* orientation with respect to the η^5-cyclopentadienyl ligand.[310-313] The structural data demonstrated the bond lengths of the ruthenium centre to the η^3-allyl group were not equivalent as the C(37)-Ru(1) bond of 2.086(7) Å was significantly shorter than the C(29)-Ru(1) and C(30)-Ru(1) bond lengths of 2.141(9) and 2.142(7) Å respectively. This trend has been observed in many η^3-butadienyl complexes, where Bruce *et al.* have noted that the shorter Ru-C bond is dependent on the substituents on the vinylic group and more pronounced differences are observed between Ru-C allylic bond lengths when stronger electron-withdrawing groups are present on the vinyl group.[314] The η^3-allylic group C(37)-C(30) and C(29)-C(30) bond lengths were 1.432(9) and 1.437(10) Å respectively, where these bond lengths were found to similar and could be attributed to delocalisation of the π electrons of the allyl group and are similar to bond lengths expected for an allyl group.[314, 315] However the vinyl -C=CHPh group displayed a significantly shorter bond length between C(37)-C(38) of 1.344(9) Å, which suggested that there is multiple bond character between these two carbon atoms. Additionally, the structure displayed the C=CHPh group is bent out of the plane of the allylic group C(29)-C(30)-C(37) where C(38) is bent away from the ruthenium centre and where the torsion angle between the allylic and vinyl group was -140.1(8) °. This suggested that the π orbitals of the allyl system are not conjugated with the vinylic C=CHPh π-system. It is common for the 1,2,3-η^3-butadienyl complexes to contain two π systems, as the energy for a η^3-butadienyl molybedenum complex has previously been calculated and was found to be more stable than the conjugated system.[316] These are common observations for η^3-butadienyl complexes and have been reported for a range of 1,2,3-η^3-butadienyl complexes by Brisdon and Walton.[317]

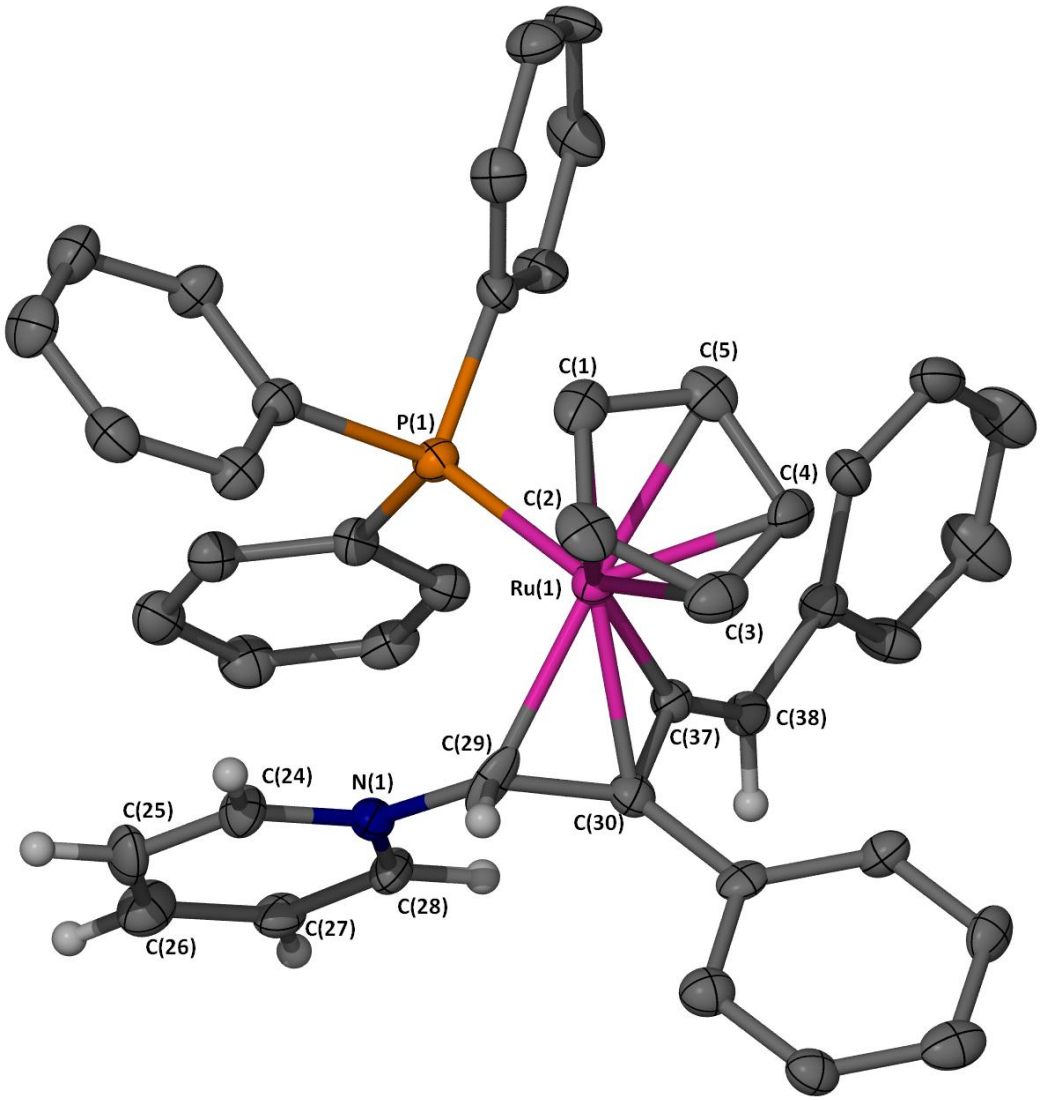

Figure 5.3: X-Seed diagram of $[Ru(\eta^5\text{-}C_5H_5)(PPh_3)(\eta^3\text{-}CH(NC_5H_5)C(C_6H_5)C{=}CH(C_6H_5)]^+$ from complex $\mathbf{21^{H,H}}$. Selected hydrogen atoms, dichloromethane molecule, pentane molecule and $[PF_6]^-$ anion have been omitted for clarity, and where shown the thermal ellipsoids are at a 50 % probability level. The $[PF_6]^-$ anion was disordered over two positions which differed in the location of the fluorine atoms.

	Bond lengths (Å)		Bond angles (°)
C(29)-Ru(1)	2.141(9)	C(29)-Ru(1)-P(1)	97.87(18)
C(30)-Ru(1)	2.142(7)	C(37)-Ru(1)-P(1)	94.03(18)
C(37)-Ru(1)	2.086(7)	N(1)-C(29)-C(30)	119.8(6)
C(37)-C(38)	1.344(9)	C(29)-C(30)-C(37)	116.1(6)
C(37)-C(30)	1.432(9)	C(30)-C(37)-C(38)	134.3(6)
C(29)-C(30)	1.437(10)		
C(29)-N(1)	1.495(9)		
P(1)-Ru(1)	2.3535(18)		

Table 5.2: Selected bond lengths (Å) and angles (°) for complex $\mathbf{21^{H,H}}$.

5.2.1.5 Identification of complex $\mathbf{22^{H,H}}$

The species $\mathbf{22^{H,H}}$ was observed in the reaction mixture, from the addition of phenylacetylene to $\mathbf{10^{H}}$. However in order to obtain a full characterisation of this species a range of purification methods were attempted. This section will describe the purification methods employed to obtain $\mathbf{22^{H,H}}$ from the other ruthenium-containing complexes. The initial spectroscopic observations of $\mathbf{22^{H,H}}$ will then be discussed from reaction conditions i and ii, followed by full characterisation from a pure sample of $\mathbf{22^{H,H}}$.

The purification of $\mathbf{22^{H,H}}$ was developed by employing reaction conditions iii, where the excess pyridine in the system competes for coordination at the ruthenium centre and therefore prevents the formation of complex $\mathbf{20^{H}}$. However, the presence of the excess pyridine in the reaction mixture also meant that the formation of the vinylidene-containing species $\mathbf{19^{H,H}}$ was hindered, as the initial ^{1}H NMR spectrum (taken approximately 4 hours from the addition of phenylacetylene) displayed smaller intensities for the resonances belonging to $\mathbf{19^{H,H}}$ than reaction conditions i. Due to the slow nature of these reactions, the reaction mixture was heated at 50 °C for 16 hours.

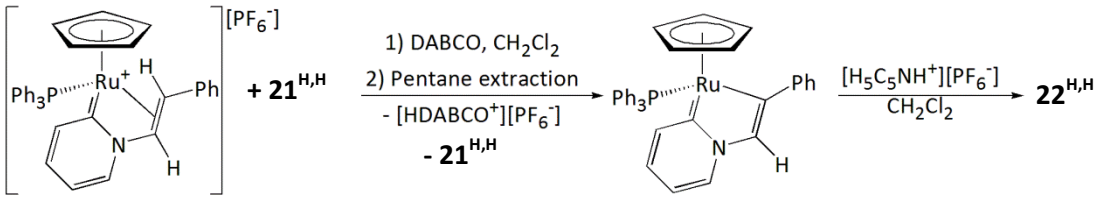

$\mathbf{22^{H,H}}$ $\mathbf{23^{H,H}}$

Scheme 5.2: Purification of complex $\mathbf{22^{H,H}}$.

The crude reaction mixture therefore contained two ruthenium-containing complexes $\mathbf{21^{H,H}}$ and $\mathbf{22^{H,H}}$, and several methods were attempted in order to obtain a pure sample of $\mathbf{22^{H,H}}$. Firstly crystallisation techniques of the reaction mixtures containing complexes $\mathbf{22^{H,H}}$ and $\mathbf{21^{H,H}}$ yielded two different looking crystals either clear yellow block, or orange 'feathery-type' crystals respectively. From this the appropriate crystals could be selected. Alternatively, the addition of 1,4-diazabicyclo[2.2.2]octane (DABCO) to a reaction mixture containing complexes $\mathbf{22^{H,H}}$ and $\mathbf{21^{H,H}}$ results in selective deprotonation of $\mathbf{22^{H,H}}$ to give $\mathbf{23^{H,H}}$ (Section 5.2.1.6) and a pentane extraction isolates $\mathbf{23^{H,H}}$. Then a simple reprotonation of $\mathbf{23^{H,H}}$ with pyridinium hexafluorophosphate gives $\mathbf{22^{H,H}}$ (Scheme 5.2).

Employing reaction conditions i, resonances for **22^{H,H}** were observed in the NMR spectra after approximately 24 hours, and the formation of this species originated from the cationic vinylidene-containing complex **19^{H,H}**. In the ^{1}H NMR spectrum a resonance was observed at 4.95 ppm (singlet, 5H) for a cyclopentadienyl ligand. Furthermore two resonances at 3.64 ppm (apparent triplet, 1H) and 6.68 ppm (doublet, $^{3}J_{HH}$ = 7.6 Hz, 1H) were displayed in the ^{1}H NMR spectrum; where a 2D ^{1}H-^{1}H COSY experiment revealed a strong coupling between these two peaks. A ^{1}H{^{31}P} NMR experiment showed that the resonance at 3.64 ppm decoupled to give a doublet ($^{3}J_{HH}$ = 7.5 Hz). The ^{31}P{^{1}H} NMR spectrum exhibited a singlet peak at 53.4 ppm for **22^{H,H}**.

The reaction mixture involving H^{13}C≡CPh displayed differences to the unlabelled experiment. In the ^{1}H NMR spectrum the resonance at 6.68 ppm was now a doublet of doublets, which contained a $^{1}J_{HC}$ of 183 Hz and a $^{3}J_{HH}$ of 7.5 Hz. In the ^{31}P{^{1}H} NMR spectrum, the resonance at 53.4 ppm remained as a singlet, suggesting the ^{13}C-label was not coupling with the triphenylphosphine ligand. The ESI-MS of the reaction mixture where H^{13}C≡CPh was used included a peak with a ruthenium isotope pattern with a *m/z* 611.13, which was consistent with the species containing the fragments [Ru(η^5-C_5H_5)(PPh_3)]$^+$, NC_5H_5 and PhC^{13}CH. In addition, an organic fragment with a peak of *m/z* 183.09 which contains [$C_{12}{}^{13}CH_{11}N$ + H]$^+$ was observed. This was an extremely interesting result, as this was the mass expected for the ^{13}C-labelled 2-styrylpyridine species in the mass spectrum. However, its exact structure could not yet be determined.

A pure sample of **22^{H,H}** was obtained therefore allowing analysis of the aromatic region of the ^{1}H NMR spectrum. The aromatic resonances between 6.83 and 7.94 ppm contained both sharp and broad resonances therefore making it difficult to integrate the peaks accurately. There were four sharp resonances for the nitrogen heterocycle that were identified and were observed at 7.06, 7.15, 7.36 and 7.94 ppm, and confirmed *via* a 2D ^{1}H-^{1}H COSY experiment. The broad peaks in the ^{1}H NMR spectrum were determined to be due to the phenyl groups of the triphenylphosphine ligand. The ^{13}C{^{1}H} NMR spectrum displayed singlet resonances for the alkene carbon atoms at 55.2 and 69.4 ppm. The most downfield resonance was a broad peak at 180.7 ppm, this was shown through a long range 2D ^{1}H-^{13}C HMBC experiment to couple to protons within the pyridine resonances. This suggested that one of the carbon atoms on the pyridine did not contain a C-H bond. Additionally, in the ^{13}C{^{1}H} NMR spectrum broad resonances were observed for the carbon atoms of the triphenylphosphine ligand. An ESI-MS of **22^{H,H}** exhibited peaks with a *m/z* of 610.12 and 182.09 which were assigned

as the cationic fragment of **22^{H,H}** and the organic species $[C_{13}H_{12}N]^+$. An elemental analysis of **22^{H,H}** was within an error of 0.2 % when a molecule of dichloromethane was included.

A low variable temperature NMR experiment was conducted on a sample of **22^{H,H}** between 295 K and 225 K and ^{1}H and ^{31}P{^{1}H} NMR spectra recorded in 10 K intervals (Figure 5.4). The ^{1}H NMR spectrum exhibited that the broad resonances in the aromatic region became flatter and broader until 275 K, and below this temperature the peaks became more resolved. At 225 K, peaks for the phenyl ligands of the triphenylphosphine ligand displayed individual resonances for each phenyl ring. This is due to each of the phenyl rings experiencing an individual environment around the ruthenium centre due to restricted rotation around the Ru-P bond. The ^{31}P{^{1}H} NMR spectrum did not display any changes in the triphenylphosphine and $[PF_6]^-$ anion resonances.

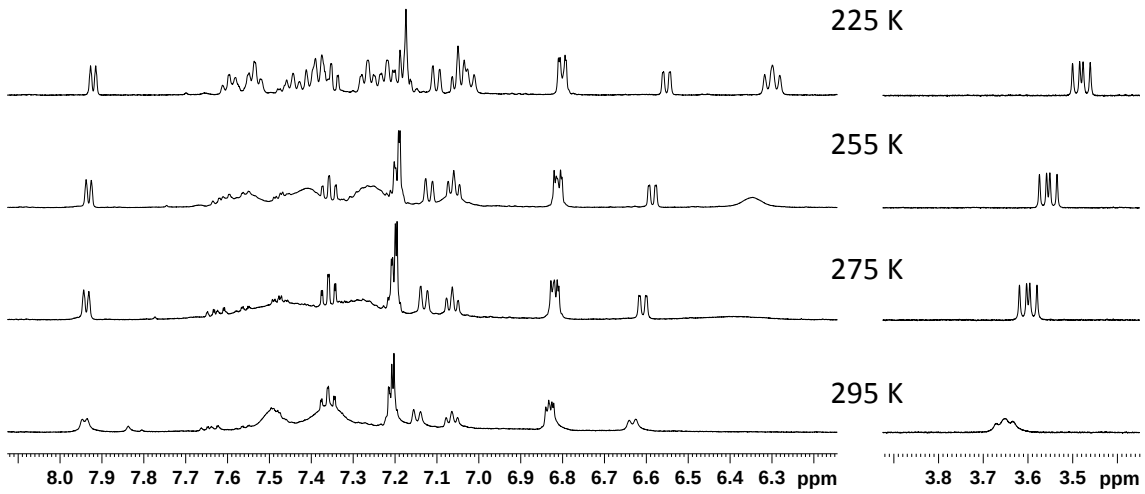

Figure 5.4: Low variable temperature ^{1}H NMR spectra of **22^{H,H}** at 295, 275, 255 and 225 K.

Crystals suitable for X-ray diffraction were grown by the slow diffusion of pentane into a dichloromethane layer containing **22^{H,H}**, and the data demonstrated that the phenylacetylene had formed a bond to the pyridine moiety *via* the nitrogen atom; the carbon-hydrogen bond had been C-H functionalised to generate a new Ru-C(2) bond (Figure 5.5, Table 5.3). It would be interesting to note that this was an isomer of the intermediate in the proposed mechanism by Murakami and Hori.[253]

The geometry of the cation of **22^{H,H}** could be described as a distorted octahedron, as the C(6)-Ru(1)-C(12), C(6)-Ru(1)-P(1) and C(12)-Ru(1)-P(1) were found to be 84.00(7), 90.66(5) and 87.45(5) ° respectively. The Ru-C bonds to the cyclopentadienyl ligand were found to be generally statistically equivalent with an average bond length of 2.240

Å. The organic fragment at the ruthenium centre could be regarded as a pyridylidene ligand, where the C(6)-Ru(1) bond length was 2.0390(19) Å (Section 6.14). The bond lengths around the pyridylidene ring were not equivalent as the bond lengths of C(6)-N(1) and C(10)-N(1) were 1.359(2) and 1.349(2) Å respectively, which was significantly shorter than the adjacent bonds C(6)-C(7) and C(9)-C(10) where the bond lengths were 1.406(3) and 1.373(3) Å respectively. The Ru-C bond lengths to the alkene component was not equivalent, as the C(11)-Ru(1) was 2.152(2) Å, which was shorter than the C(12)-Ru(1) bond of 2.2575(19) Å. This distortion has been explained by Eisenstein and Hoffmann where a transition metal centres can move towards one of the carbon atoms of the alkene bond.[318, 319] The alkene bond length C(11)-C(12) was 1.405(3) Å and found to be significantly shorter than the adjacent bonds and is consistent with coordinated alkene bond lengths.[298] The Ru(1)-P(1) bond length was 2.3367(5) Å.

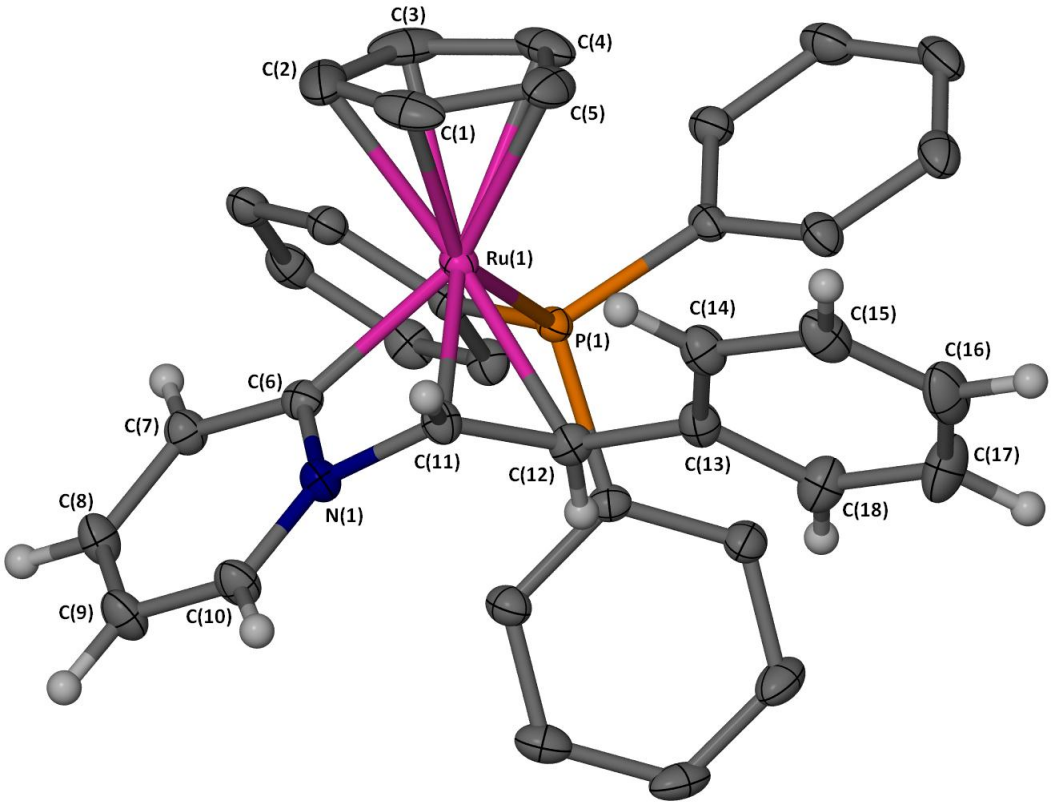

Figure 5.5: X-Seed diagram of $[Ru(\eta^5\text{-}C_5H_5)(PPh_3)(\kappa^3\text{-}C_3\text{-}C_5H_4NCH{=}CH(C_6H_5)]^+$ from complex **22**^{H,H}. Selected hydrogen atoms, a dichloromethane molecule and $[PF_6]^-$ anion have been omitted for clarity, and where shown the thermal ellipsoids are at a 50 % probability level.

	Bond lengths (Å)		Bond angles (°)
C(1)-Ru(1)	2.233(2)	C(6)-Ru(1)-C(12)	84.00(7)
C(2)-Ru(1)	2.243(2)	C(6)-Ru(1)-C(11)	63.86(7)
C(3)-Ru(1)	2.224(2)	C(6)-Ru(1)-P(1)	90.66(5)
C(4)-Ru(1)	2.247(2)	C(12)-Ru(1)-P(1)	87.45(5)
C(5)-Ru(1)	2.249(2)	N(1)-C(6)-Ru(1)	99.98(12)
C(6)-Ru(1)	2.0390(19)	C(6)-N(1)-C(11)	104.09(15)
C(6)-N(1)	1.359(2)	N(1)-C(11)-Ru(1)	92.03(11)
C(6)-C(7)	1.406(3)	C(12)-C(11)-N(1)	118.05(16)
C(7)-C(8)	1.388(3)	C(11)-C(12)-Ru(1)	67.40(11)
C(8)-C(9)	1.402(3)	C(11)-C(12)-C(13)	120.38(17)
C(9)-C(10)	1.373(3)	N(1)-C(6)-C(7)	115.06(17)
C(10)-N(1)	1.349(2)	C(8)-C(7)-C(6)	119.96(18)
C(11)-N(1)	1.453(2)	C(7)-C(8)-C(9)	121.01(18)
C(11)-Ru(1)	2.152(2)	C(10)-C(9)-C(8)	119.01(19)
C(11)-C(12)	1.405(3)	N(1)-C(10)-C(9)	117.43(18)
C(12)-Ru(1)	2.2575(19)		
C(12)-C(13)	1.486(3)		
P(1)-Ru(1)	2.3367(5)		

Table 5.3: Selected bond lengths (Å) and angles (°) for complex **22^{H,H}**.

5.2.1.6 Deprotonation/ Addition of pyridine to complex 22^{H,H}

An investigation in to the properties of **22^{H,H}** in pyridine was conducted due to this being the major ruthenium-containing complex present in the reaction mixture from the addition of phenylacetylene to **10^{H}**.

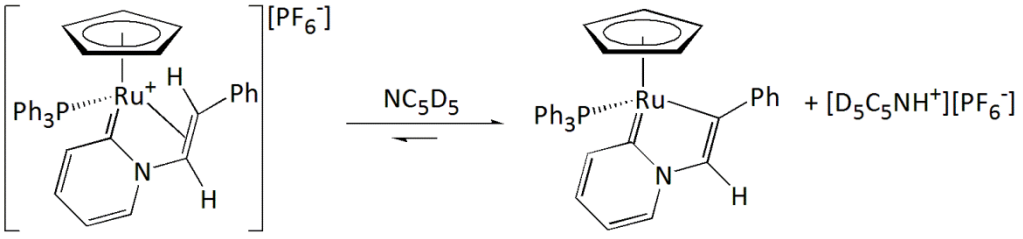

22^{H,H} **23^{H,H}**

Scheme 5.3: Addition of d_5-pyridine to complex **22^{H,H}**.

The addition of d_5-pyridine to **22^{H,H}** resulted in an immediate colour change from a pale yellow precipitate to deep red solution (Scheme 5.3). A set of ^{1}H and $^{31}P\{^{1}H\}$ NMR

spectra were recorded of the solution. The ^{1}H NMR spectrum displayed two sets of broad resonances, however one of these sets was slightly sharper in nature. The ^{1}H NMR spectrum exhibited a downfield peak at 16.78 ppm (broad), due to $[H\text{-}NC_5H_5]^+$. The ^{1}H NMR spectrum also displayed two cyclopentadienyl resonances at 4.65 (less broad) and 5.12 (broader) ppm. The two alkene resonances for **22^{H,H}** (3.64 and 6.68 ppm) were no longer be observed in the ^{1}H NMR spectrum. In the ^{31}P{^{1}H} NMR spectrum, only two resonances at -144.3 (septet) and at 52.2 (singlet) were observed for the $[PF_6]^-$ and **22^{H,H}** respectively. Another broad resonance was expected in the ^{31}P{^{1}H} NMR spectrum for **23^{H,H}**, however it was not detected, this could be due to an equilibrium between **22^{H,H}** and **23^{H,H}**. It is possible that pyridine is acting as a base towards **22^{H,H}** to form a deprotonated species **23^{H,H}** and therefore exhibits fluxional behaviour in solution on the NMR timescale.

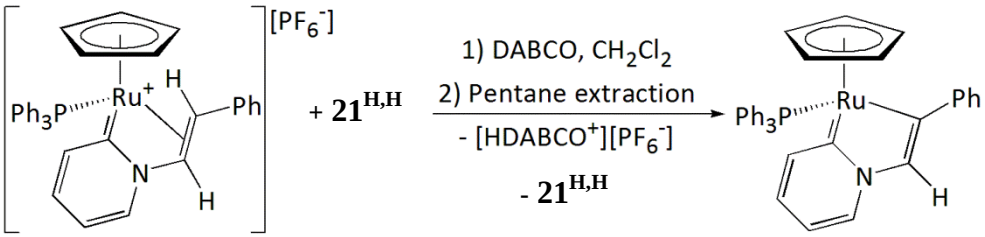

22^{H,H} **23^{H,H}**

Scheme 5.4: Deprotonation of **22^{H,H}** with DABCO in dichloromethane.

Subsequently, the addition of DABCO to a dichloromethane solution containing **22^{H,H}** resulted in a similar colour change from a yellow to red solution. The product was found to be partially soluble in pentane, and when stored at -20 °C, red crystals of the new species **23^{H,H}** were collected. The ^{1}H NMR spectrum of **23^{H,H}** displayed a cyclopentadienyl peak at 4.75 ppm (singlet) which integrated as 5H with respect to the pyridine ring protons at 6.51, 6.56, 7.83 and 8.15 ppm which all had an integration of 1H. The alkene resonances belonging to **22^{H,H}** were not present, indicating that DABCO may have deprotonated one of the alkene protons. The ^{31}P{^{1}H} NMR spectrum possessed one resonance at 60.3 ppm as a broad singlet for the triphenylphosphine ligand. A ^{13}C{^{1}H} NMR spectrum of **23^{H,H}** exhibited a resonance for the carbon atoms of the cyclopentadienyl ligand at 83.0 ppm as a doublet with a $^{2}J_{CP}$ of 1.8 Hz. Interestingly, two quaternary carbon atoms were observed at 192.9 and 218.3 ppm as doublets with $^{2}J_{CP}$ couplings of 12.7 Hz and 15.3 Hz respectively. This suggested that there were now two Ru-C bonds in **23^{H,H}**. The ESI-MS of the product displayed a

ruthenium-containing peak with a *m/z* of 610.1228 which was consistent with the reprotonation of **23^{H,H}** within the mass spectrometer.

5.2.2 Reaction between complex 10^{H} with 1-ethynyl-4-fluorobenzene

The range of aryl terminal alkynes was extended by investigating the effects of a *para* substituent on the aryl group. A fluorine atom in the *para* position of the phenyl ring has an overall electron-withdrawing effect (there is a electron-withdrawing inductive effect and electron density is donated *via* a mesomeric effect).[29] The Hammett constant of a *para* fluorine substituent was +0.06.[292-295] The aim was to investigate the ruthenium-containing complexes formed from the stoichiometric addition of 1-ethynyl-4-fluorobenzene and determine if there were any changes in the reactivity towards **10^{H}**.

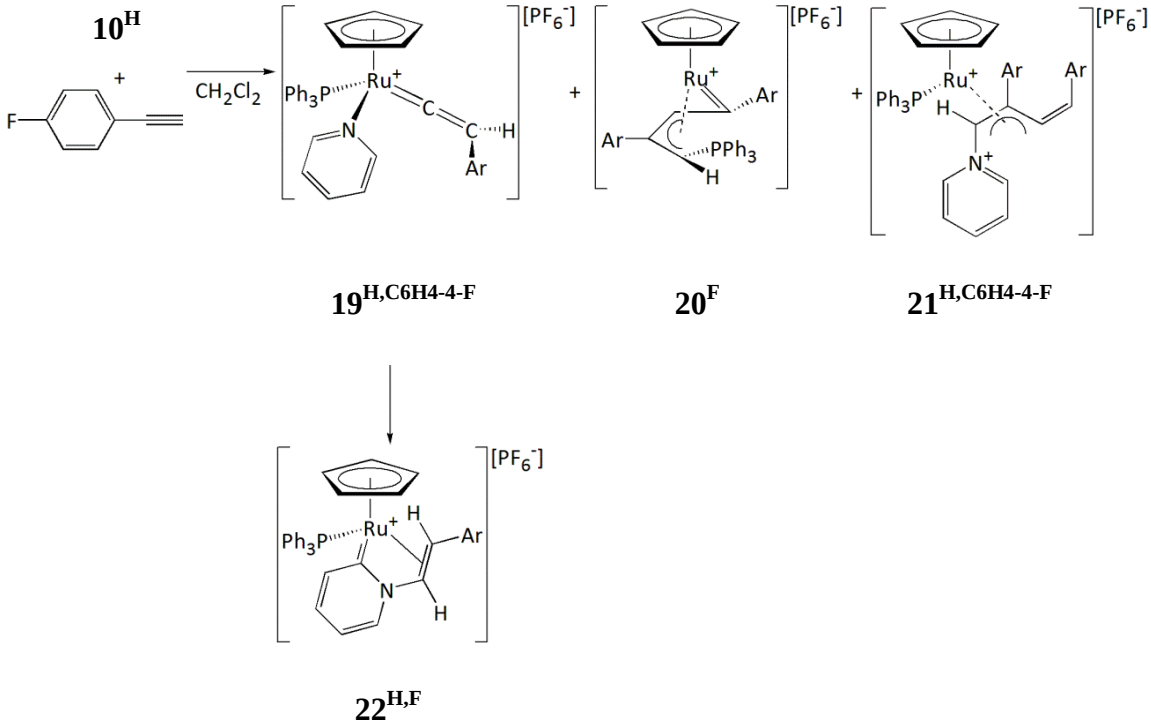

Scheme 5.5: Reaction of **10^{H}** with 1-ethynyl-4-fluorobenzene, where Ar = C_6H_4-4-F in d_2-dichloromethane.

The addition of 1-ethynyl-4-fluorobenzene to **10^{H}** in d_2-dichlormethane was monitored *via* NMR spectroscopy (Scheme 5.5). From the ^{1}H NMR spectrum the reaction initially contained 0.5 equivalent of 1-ethynyl-4-fluorobenzene and once this was consumed, a further one equivalent was added.

The ^{1}H and ^{31}P{^{1}H} NMR spectra for the addition of 1-ethynyl-4-fluorobenzene to **10^{H}**, displayed similar resonances for the reaction between **10^{H}** and phenylacetylene. Overall,

from the NMR experiment five new ruthenium-containing complexes were detected, two of these species were short-lived intermediates (a minor unknown species and **19**$^{H,C6H4\text{-}4\text{-}F}$) and three of these complexes remained in the final reaction mixture (complexes **20**^{F}, **21**^{H,F} , **22**^{H,F}).

5.2.2.1 The minor unknown species present in the initial reaction mixture

The NMR spectra exhibited peaks for the unknown complex only after initial addition of the alkyne and were only present in a very small quantity. In the ^{1}H NMR spectrum the only peak for the minor species was observed in the cyclopentadienyl region at 4.97 ppm. The ^{31}P{^{1}H} NMR spectrum displayed a resonance at 53.7 ppm as a singlet for the triphenylphosphine ligand.

*5.2.2.2 Identification of complex **19**$^{H,C6H4\text{-}4\text{-}F}$*

The other short-lived intermediate in the reaction mixture was characterised by NMR spectroscopy, and displayed very similar resonances and behaviour to the vinylidene-containing complex, **19**^{H,Ph}. In the ^{1}H NMR spectrum broad resonances were observed at 5.49 (5H) and 5.14 (1H) ppm for the cyclopentadienyl ligand and the vinylidene proton respectively. The aromatic region of the ^{1}H NMR spectrum was complex and therefore the pyridine ligand resonances that were identified according to integrations at different times within the NMR spectrum were observed at 7.57 (1H) and 8.25 (2H) ppm for the C-4 and C-2/6 protons on the coordinated pyridine ligand respectively. The ^{31}P{^{1}H} NMR spectrum exhibited a triphenylphosphine ligand peak at 51.7 ppm.

*5.2.2.3 Observations for **20**^{F}*

The reaction mixture contained resonances that were similar to those observed for **20**^{H}. The ^{1}H NMR spectrum exhibited a cyclopentadienyl resonance at 5.09 ppm, and the ^{31}P{^{1}H} NMR spectrum displayed a peak at 29.9 ppm for a triphenylphosphine ligand. The information gathered from the previous study from the addition of phenylacetylene to **10**^{H} in d_2-dichloromethane was used to determine the species present in this reaction mixture.

*5.2.2.4 Observations for **21**^{H,F}*

Characterisation of **21**^{H,F} was based on the previous reaction between **10**^{H} and phenylacetylene. The resonances that were observed in the NMR spectra for **21**^{H,F} were at a similar chemical shift for **21**^{H,H}. The ^{1}H NMR spectrum displayed the cyclopentadienyl ligand with a resonance at 4.57 ppm, and the ^{31}P{^{1}H} NMR spectrum displayed a peak at 47.7 ppm for a triphenylphosphine ligand.

5.2.2.5 Observations for $\boldsymbol{22^{H,F}}$

The formation of $\mathbf{22^{H,F}}$ in the reaction mixture was observed to increase in intensity when resonances belonging to $\mathbf{19^{H,C6H4\text{-}4\text{-}F}}$ began to decrease. In the ^{1}H NMR spectrum peaks at 3.62 ppm (broad dd, $^{3}J_{HP}$ = 10.7 Hz, $^{3}J_{HP}$ = 8.2 Hz), 6.66 (doublet, $^{3}J_{HP}$ = 8.2 Hz) and 4.95 ppm (singlet) ppm were observed for the two alkene protons and the cyclopentadienyl ligand respectively. A resonance in the ^{31}P{^{1}H} NMR spectrum at 53.6 ppm for the coordinated triphenylphosphine ligand of $\mathbf{22^{H,F}}$ was observed.

Crystals suitable for X-ray diffraction of $\mathbf{22^{H,F}}$ were obtained by the slow diffusion of pentane into the reaction mixture (Figure 5.6, Table 5.4). The organic fragment of the molecule contained a C-H functionalised pyridine molecule, where the nitrogen atom had formed a bond with a carbon atom of the alkyne molecule to yield a pyridylidene-alkene species. The geometry of the ruthenium complex could be described as a distorted octahedral, where the C(6)-Ru(1)-C(12), C(6)-Ru(1)-P(1) and C(12)-Ru(1)-P(1) bond angles were 84.44(8), 90.23(6) and 88.18(5) ° respectively. The alkene bond C(25)-C(26) had a bond length of 1.413(3) Å, which was significantly shorter than the adjacent bonds C(11)-N(1) and C(13)-C(12) of 1.449(3) and 1.474(3) Å respectively. The C(6)-N(1) bond length was 1.352(3) Å, which was shorter than C(7)-C(6) bond length of 1.409(3) Å. The P(1)-Ru(1) bond length was found to be 2.3317(5) Å.

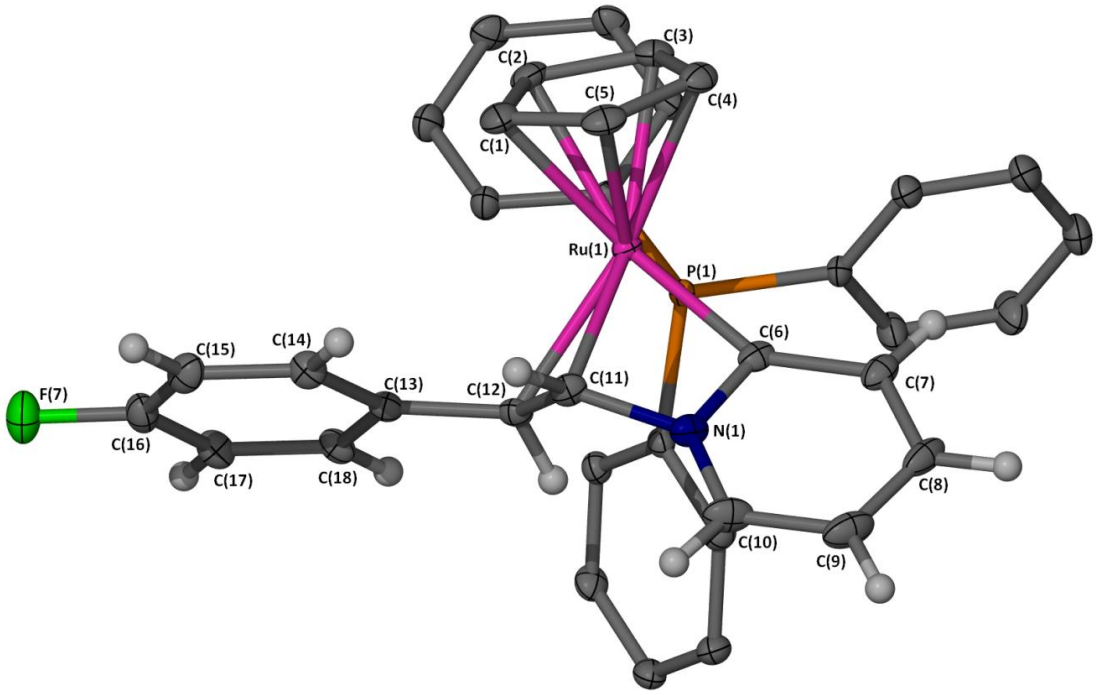

Figure 5.6: X-Seed diagram of $[Ru(\eta^{5}\text{-}C_5H_5)(PPh_3)(\kappa^{3}\text{-}C_3\text{-}C_5H_4NCH{=}CH(C_6H_4\text{-}4\text{-}F)]^{+}$ from complex $\mathbf{22^{H,F}}$. Selected hydrogen atoms, a dichloromethane molecule and $[PF_6]^{-}$ anion have been omitted for clarity, and where shown the thermal ellipsoids are at a 50 % probability level. The dichloromethane molecule was disordered over two positions in a ratio of 0.543:0.457(15).

	Bond lengths (Å)		Bond angles (°)
C(1)-Ru(1)	2.224(2)	C(6)-Ru(1)-C(11)	64.06(8)
C(5)-Ru(1)	2.216(2)	C(6)-N(1)-C(11)	104.53(16)
C(4)-Ru(1)	2.250(2)	N(1)-C(11)-Ru(1)	91.97(13)
C(3)-Ru(1)	2.247(2)	N(1)-C(6)-Ru(1)	99.39(13)
C(2)-Ru(1)	2.2605(19)	C(6)-Ru(1)-C(12)	84.44(8)
C(6)-Ru(1)	2.0384(19)	C(12)-C(11)-N(1)	118.16(17)
C(6)-N(1)	1.352(3)	C(11)-C(12)-C(13)	121.62(18)
C(10)-N(1)	1.355(3)	C(6)-Ru(1)-P(1)	90.23(6)
C(10)-C(9)	1.370(4)	C(11)-Ru(1)-P(1)	117.79(6)
C(9)-C(8)	1.399(4)	C(12)-Ru(1)-P(1)	88.18(5)
C(8)-C(7)	1.379(3)	N(1)-C(6)-C(7)	115.59(19)
C(6)-C(7)	1.409(3)	C(8)-C(7)-C(6)	119.5(2)
C(11)-Ru(1)	2.137(2)	C(7)-C(8)-C(9)	121.6(2)
C(11)-N(1)	1.449(3)	C(10)-C(9)-C(8)	118.7(2)
C(12)-C(11)	1.413(3)	N(1)-C(10)-C(9)	117.6(2)
C(12)-Ru(1)	2.247(2)	C(6)-N(1)-C(10)	127.0(2)
C(12)-C(13)	1.474(3)		
P(1)-Ru(1)	2.3317(5)		

Table 5.4: Selected bond lengths (Å) and angles (°) for complex **22**$^{\mathbf{H,F}}$.

5.2.2.6 Summary

From screening the stoichiometric reaction between 1-ethynyl-4-fluorobenzene and **10**$^{\mathbf{H}}$ we have observed the same number of ruthenium-containing complexes from the reaction of **10**$^{\mathbf{H}}$ and phenylacetylene. The presence of **20**$^{\mathbf{H}}$ can be excluded from the reaction mixture by addition of excess pyridine, however due to the difficult separation of complexes **21**$^{\mathbf{H,F}}$ and **22**$^{\mathbf{H,F}}$, a decision was made to investigate the effects of alternative substituents on the phenyl ring of the terminal alkynes.

5.2.3 Reaction between complex 10^{H} with 4-ethynyl-α,α,α-trifluorotoluene

The effect of the trifluoromethyl substituent in the 4-position of the phenyl ring with **10^{H}** was investigated. The presence of additional fluorine atoms will mean a stronger electron-withdrawing effect through induction. The Hammett substituent effects for a *para* trifluoromethyl group was stated as +0.54. This value is significantly larger than for a *para* fluorine (+0.06).[292-295] A change in reactivity is therefore possible with respect to the previous examples of phenylacetylene and 1-ethynyl-4-fluorobenzene.

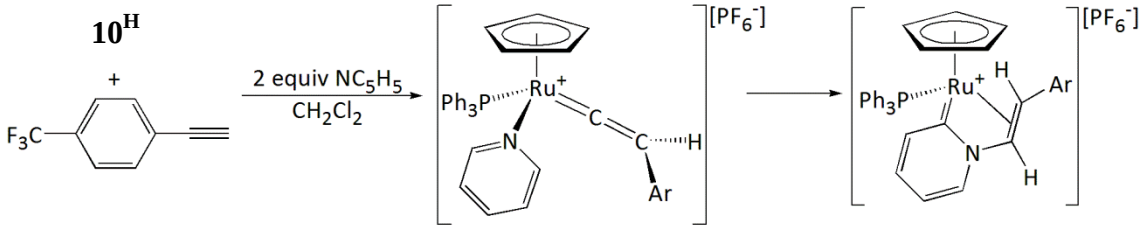

$19^{H,C6H4-4-CF3}$ **$22^{H,CF3}$**

Scheme 5.6: Reaction of **10^{H}** with 4-ethynyl-α,α,α-trifluorobenzene, where Ar = C_6H_4-4-CF_3.

The stoichiometric addition of 4-ethynyl-α,α,α-trifluorobenzene to **10^{H}** in the presence of two equivalents of pyridine in a d_2-dichloromethane solution was monitored by NMR spectroscopy (Scheme 5.6). The initial NMR spectra exhibited a set of resonances for a major ruthenium-containing complex **$19^{H,C6H4-4-CF3}$**; this species was an intermediate and reacted further to give resonances for a new ruthenium-containing complex **$22^{H,CF3}$**. This reaction was the most selective as the excess pyridine in the reaction mixture had prevented the formation of the π-allyl carbene complex **20** and the presence of the trifluoromethyl group on the phenyl ring of the terminal alkyne appeared to inhibit the formation of the pyridinium η^3-butadienyl species **21**.

5.2.3.1 Identification of ***$19^{H,C6H4-4-CF3}$***

The intermediate **$19^{H,C6H4-4-CF3}$** was observed *via* NMR spectroscopy. The ^{1}H NMR spectrum exhibited peaks at 5.17 and 5.53 ppm with integration values of 1H and 5H respectively, which were assigned to the vinylidene ligand proton and the cyclopentadienyl ligand respectively. In addition, in the aromatic region resonances were exhibited at 6.99 (2H), 7.57 (1H) and 8.36 (2H) ppm for a coordinated pyridine ligand. The $^{31}P\{^{1}H\}$ NMR spectrum displayed a broad singlet at 51.0 ppm for the triphenylphosphine ligand of the intermediate species.

Interestingly, the 4-trifluoromethyl group has promoted the formation of **19$^{H,C6H4-4-CF3}$** as this is the major species over several days and therefore the trifluoromethyl group appears to stabilise the vinylidene-containing intermediate. The equivalent reaction carried out with phenylacetylene displayed the largest quantity of the vinylidene-containing species **19^{H,Ph}** was after initial addition and after one day the concentration of the vinylidene species had decreased in solution.

*5.2.3.2 Identification of **22^{H,CF3}***

The complex **22^{H,CF3}** was the major ruthenium-containing complex at the end of the reaction, and was isolated *via* the slow diffusion of pentane or hexane into a dichloromethane layer containing **22^{H,CF3}**, and the product was isolated as pale yellow crystals.

The ^{1}H NMR spectrum of **22^{H,CF3}** exhibited resonances at 4.99 (s), 3.60 (dd, $^{3}J_{HP}$ = 11.4 Hz, $^{3}J_{HH}$ = 7.9 Hz) and 6.77 (d, $^{3}J_{HH}$ = 7.9 Hz) ppm, with integrations of 5H, 1H and 1H, for the cyclopentadienyl ligand and the two alkene protons respectively. The aromatic region of the ^{1}H NMR spectrum displayed sharp and broad resonances, where the sharper peaks were due to the pyridylidene fragment $C_5H_4NCH{=}CHC_6H_4$-4-CF_3. The ^{1}H NMR spectrum displayed four resonances at 8.00, 7.37, 7.12 and 7.08 ppm which were found to couple to each other through a 2D ^{1}H-^{1}H COSY experiment. In the ^{1}H NMR spectrum the broad peaks in the aromatic region were due to the phenyl rings of the triphenylphosphine ligand. The ^{31}P{^{1}H} NMR spectrum exhibited a singlet peak at 52.8 ppm for the triphenylphosphine ligand. A ^{13}C{^{1}H} NMR spectrum displayed a doublet at 179.6 ppm with a $^{2}J_{CP}$ of 19 Hz, this suggested a Ru-C bond was present within this structure. A set of 2D ^{1}H-^{13}C HMQC and HSQC experiments demonstrated that the peak at 179.6 ppm was part of the nitrogen heterocycle, therefore indicating a C-H bond had been functionalised. The ^{13}C{^{1}H} NMR spectrum also exhibited quartet peaks due to the CF_3 substituent where a $^{1}J_{CF}$ of 272 Hz was observed at 124.5 ppm.

A high resolution ESI-MS of **22^{H,CF3}** exhibited a *m/z* peak a 678.1135 which had a ruthenium isotope pattern was equivalent to $[C_{37}H_{30}NF_3PRu]^{+}$, and a fragment with a *m/z* of 250.0832 was observed for the organic fragment $[C_{14}H_{11}F_3N]^{+}$. Elemental analysis of the resulting pale yellow crystals were found to be accurate within an error of 0.3 %, when containing half a molecule of dichloromethane.

A low variable temperature ^{1}H and ^{31}P{^{1}H} NMR experiment was conducted on **22^{H,CF3}** in d_2-dichloromethane (Figure 5.7). The ^{31}P{^{1}H} NMR spectra for the

triphenylphosphine resonance at low temperatures did not exhibit any changes. The ^{1}H NMR spectra displayed broadening of the resonances until 280 K, and below this temperature the peaks began to get sharper. The ^{1}H NMR spectra in the aromatic region displayed that the triphenylphosphine ligand had an individual environment for each of the phenyl groups. This is due to restricted rotation of the triphenylphosphine ligand at the ruthenium centre in solution on the NMR timescale.

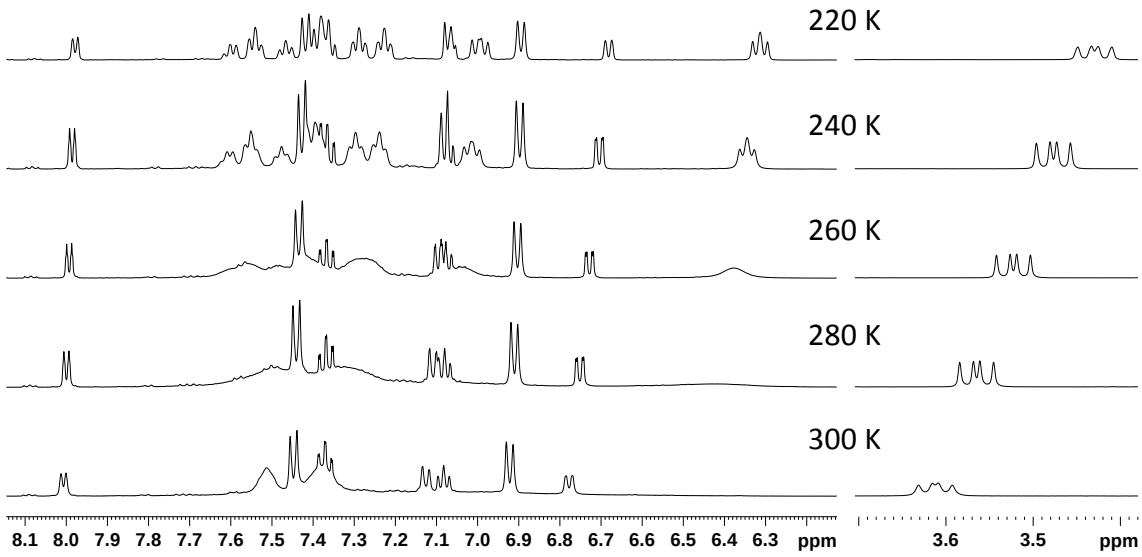

Figure 5.7: Low variable temperature ^{1}H NMR spectra of **22^{H,CF3}** at 300 K, 280 K, 260 K, 240 K and 220 K.

Pale yellow crystals of **22^{H,CF3}** suitable for X-ray diffraction were obtained by the slow diffusion of pentane into a dichloromethane solution of **22^{H,CF3}**. The structure of **22^{H,CF3}** revealed that the pyridine molecule had undergone a C-H functionalisation reaction to give a pyridylidene ligand. The cation of **22^{H,CF3}** was a distorted octahedron, where the bond angles C(6)-Ru(1)-C(12), C(6)-Ru(1)-P(1) and C(12)-Ru(1)-P(1) were 83.61(10), 88.60(7) and 85.76(7) ° respectively. The C(6)-Ru(1) bond length was 2.029(3) Å, which is consistent with literature for a pyridylidene ligand (Section 6.14). The Ru-C bonds to the alkene functional group, C(11)-Ru(1) and C(12)-Ru(1) were 2.127(3) and 2.245(3) Å respectively (Section 5.2.1.5). The bond length of C(11)-C(12) was 1.411(4) Å which is consistent for a C=C bond.[298] A P(1)-Ru(1) bond length of 2.3365(7) Å was found.

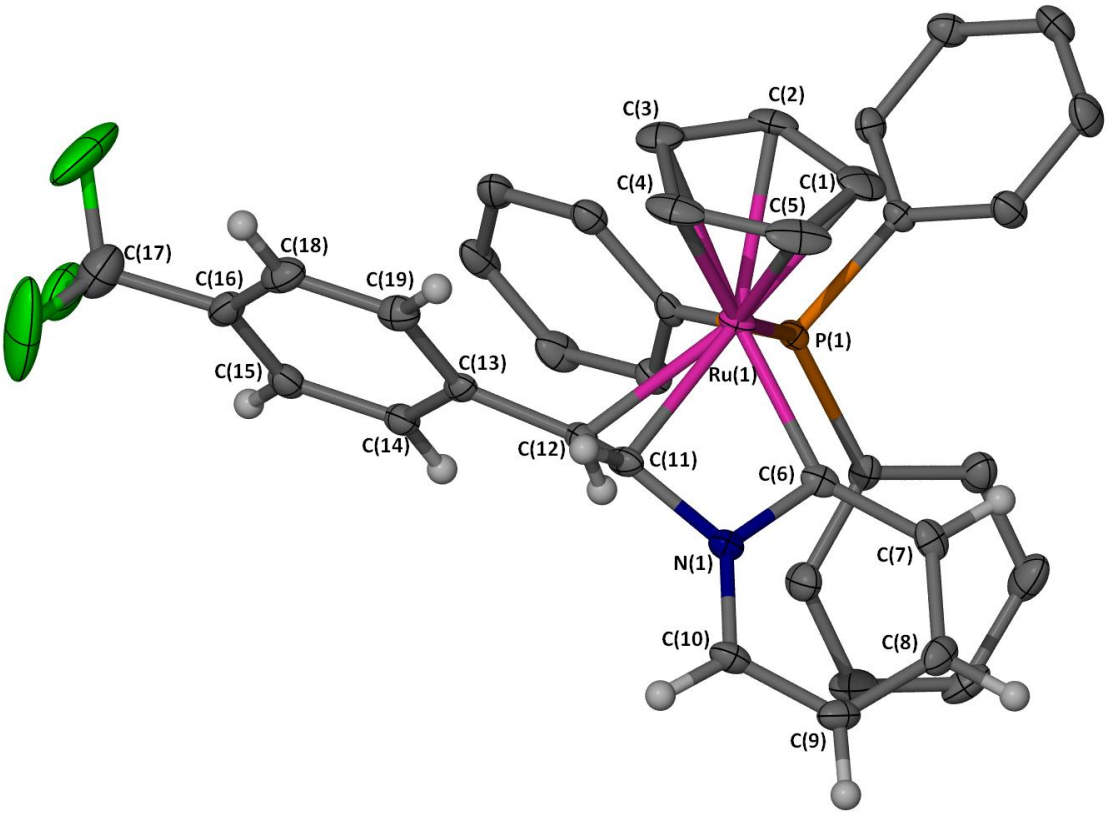

Figure 5.8: X-Seed diagram of $[Ru(\eta^5\text{-}C_5H_5)(PPh_3)(\kappa^3\text{-}C_3\text{-}C_5H_4NCH{=}CH(C_6H_4\text{-}4\text{-}CF_3)]^+$ from complex $\mathbf{22}^{\mathbf{H,CF3}}$. Selected hydrogen atoms, a dichloromethane molecule and $[PF_6]^-$ anion have been omitted for clarity, and where shown the thermal ellipsoids are at a 50 % probability level.

	Bond lengths (Å)		Bond angles (°)
C(4)-Ru(1)	2.295(3)	C(6)-Ru(1)-C(11)	64.36(11)
C(3)-Ru(1)	2.243(3)	C(6)-N(1)-C(11)	103.5(2)
C(2)-Ru(1)	2.203(3)	N(1)-C(6)-Ru(1)	99.72(18)
C(1)-Ru(1)	2.212(3)	N(1)-C(11)-Ru(1)	92.25(16)
C(5)-Ru(1)	2.253(3)	C(6)-Ru(1)-C(12)	83.61(10)
C(6)-Ru(1)	2.029(3)	C(6)-Ru(1)-P(1)	88.60(7)
C(6)-N(1)	1.360(3)	C(11)-Ru(1)-P(1)	115.80(8)
C(10)-N(1)	1.353(3)	C(12)-Ru(1)-P(1)	85.76(7)
C(10)-C(9)	1.367(4)	C(12)-C(11)-N(1)	116.9(2)
C(9)-C(8)	1.405(4)	C(11)-C(12)-C(13)	122.9(2)
C(8)-C(7)	1.380(4)	C(10)-N(1)-C(6)	126.6(2)
C(6)-C(7)	1.401(4)	N(1)-C(10)-C(9)	117.6(3)
C(11)-N(1)	1.459(3)	C(10)-C(9)-C(8)	119.1(3)
C(11)-Ru(1)	2.127(3)	C(7)-C(8)-C(9)	121.2(3)
C(12)-C(11)	1.411(4)	C(8)-C(7)-C(6)	119.6(3)
C(12)-Ru(1)	2.245(3)	N(1)-C(6)-C(7)	115.9(2)
C(12)-C(13)	1.474(4)		
P(1)-Ru(1)	2.3365(7)		

Table 5.5: Selected bond lengths (Å) and angles (°) for complex **22**^{H,CF3}.

5.2.3.3 Deprotonation of 22^{H,CF3}

The properties of isolated **22**^{H,CF3} in d_5-pyridine was investigated, as the ruthenium-containing species contained an isomer of the 2-styrylpyridine derivative. The behaviour of **22**^{H,CF3} in d_5-pyridine would therefore give information on the role of the ruthenium centre in the reaction medium of the catalytic cycle (pyridine).

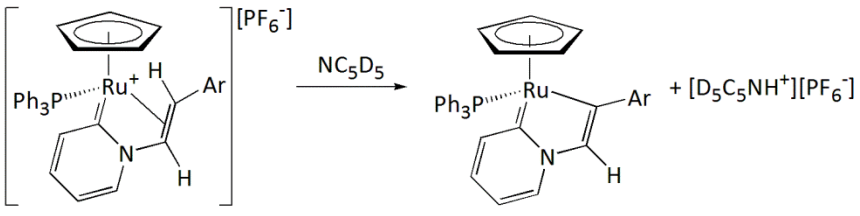

22^{H,CF3} **23**^{H,CF3}

Scheme 5.7: Addition of d_5-pyridine to **22**^{H,CF3}, where Ar = C_6H_4-4-CF_3.

The complex **22**^{H,CF3} was placed in d_5-pyridine, and the pale yellow product changed to a deep red solution indicative for the formation of **23**^{H,CF3}. The reaction was monitored

by NMR spectroscopy. The ^{1}H NMR spectrum of the species indicated that a new ruthenium species was present in the reaction mixture, as the alkene resonances for **22^{H,CF3}** were absent. In the ^{1}H NMR spectrum a broad resonance at 17.4 ppm was observed, which is characteristic of $[H\text{-}NC_5H_5]^+$ and a 2D ^{1}H-^{1}H COSY NMR experiment displayed that this peak did not couple to any of the resonances belonging to the new ruthenium complex. The integration of the remaining resonances in the ^{1}H NMR spectrum of the new ruthenium species in the sample suggested that there was one fewer proton present. In the ^{1}H NMR spectrum, the four protons belonging to the pyridylidene ligand were exhibited at 8.36, 8.09, 6.61 and 6.56 ppm, each with an integration of 1H with respect to the cyclopentadienyl ligand at 4.98 ppm (5H). Also, in the ^{1}H NMR spectrum the peaks for the phenyl groups of the triphenylphosphine ligand were sharp, suggesting there was no longer restricted rotation of the triphenylphosphine ligand around the Ru-P bond on the NMR timescale. The ^{31}P{^{1}H} NMR spectrum of the reaction mixture displayed two sets of peaks at -142.8 and 60.4 ppm as a septet and a singlet for the $[PF_6]^-$ anion and the triphenylphosphine ligand respectively. A ^{13}C{^{1}H} NMR spectrum exhibited two doublets at 190.8 and 219.4 ppm with a $^{2}J_{CP}$ of 13.2 and 15.6 Hz; this could be attributed to two Ru-C bonds in **23^{H,CF3}**. The NMR data for **23^{H,CF3}** suggested the d_5-pyridine had acted as base to deprotonate **22^{H,CF3}**, the proton had been abstracted from the alkene functional group to yield the metallacyclic species, **23^{H,CF3}**.

Attempts were made to deprotonate **22^{H,CF3}** in a dichloromethane solution using the base, $NaN(SiMe_3)_2$. The crude reaction mixture included resonances belonging to **23^{H,CF3}**, however there were also unidentified ruthenium-containing species present.

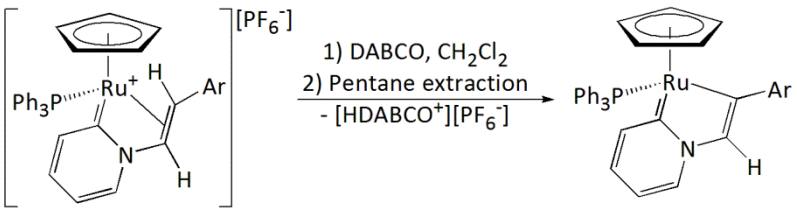

22^{H,CF3} **23^{H,CF3}**

Scheme 5.8: Deprotonation of **22^{H,CF3}** with DABCO in dichloromethane, where Ar = C_6H_4-4-CF_3.

A more successful route involved the stoichiometric addition of DABCO to **22^{H,CF3}** in dichloromethane, and resulted in a clean reaction to produce only one ruthenium-containing complex, **23^{H,CF3}**. The red product was extracted with pentane, the solvent

was reduced and stored at -20 °C. Crystals of **23^{H,CF3}** were obtained under these conditions. Complex **23^{H,CF3}** was placed in d_2-dichloromethane as the d_5-pyridine resonances in the aromatic region made it difficult to fully assign all the peaks belonging to **23^{H,CF3}**. However, differences were observed in the NMR spectra from changing the NMR solvent. The ^{1}H NMR spectrum was similar to the sample of **23^{H,CF3}** in d_5-pyridine and was consistent with the loss of a proton from **22^{H,CF3}**. A ^{1}H{^{31}P} NMR experiment revealed a broad singlet at 6.93 ppm, with a 1H integration with respect to the cyclopentadienyl ligand resonance. This peak was assigned as the proton on the metallacycle. Interestingly, the ^{31}P{^{1}H} NMR spectrum of **23^{H,CF3}** in d_2-dichloromethane displayed only one broad peak at 61.2 ppm for the triphenylphosphine ligand of **23^{H,CF3}**. This was different from the sharp peak observed for **23^{H,CF3}** in d_5-pyridine, and could potentially be due to the slightly acidic nature of the d_2-dichloromethane solvent, which therefore causes an equilibrium between the deprotonated species **23^{H,CF3}** and the protonated version **22^{H,CF3}** in solution. This was also observed in the ^{13}C{^{1}H} NMR spectrum, as the two quaternary carbon atoms at 190.2 and 219.3 ppm were broad. Unfortunately, one of the carbon atoms in the metallacycle (-Ru-C-*C*H-N-C-) could not be observed in the ^{13}C{^{1}H} NMR spectrum. A range of NMR experiments (DEPT 135, ^{1}H-^{13}C HSQC, ^{1}H-^{13}C HMBC and a quantitative ^{13}C{^{1}H} NMR spectra) did not exhibit any conclusive information on the chemical shift of this carbon atom. The carbon atom in the metallacycle -Ru-C-*C*H-N-C- could have been broad due to an equilibrium existing in the d_2-dichloromethane solution. An elemental analysis of **23^{H,CF3}** was within a 0.3 % error, and consistent with other spectroscopic data that a deprotonation reaction had occurred.

Red crystals of **23^{H,CF3}** suitable for X-ray diffraction were grown from a pentane solution at -16 °C and displayed that a second C-H functionalisation reaction had occurred at the alkene functional group of **22^{H,CF3}**, to yield a five-membered metallacyclic species, 1-ruthanaindolizine. The geometry of **23^{H,CF3}** can be described as distorted octahedral, where the bond angles of C(6)-Ru(1)-P(1), C(12)-Ru(1)-P(1) and C(6)-Ru(1)-C(12) are 86.20(6), 92.32(6) and 77.76(9) ° respectively, where the smallest bond angle was due to the metallacyclic ligand. The adjacent bond angles for the metallacycle were wider, where C(11)-C(12)-Ru(1) and N(1)-C(6)-Ru(1) had similar bond angles of 116.83(16) and 116.90(15) ° respectively. The Ru-C bond lengths C(6)-Ru(1) and C(12)-Ru(1) for the C-H functionalised carbon atoms were 1.996(2) and 2.046(2) Å respectively (Section 6.14). The pyridylidene ligand displayed significantly

different bond lengths around the ring, as the C(6)-C(7) and C(8)-C(9) were found to be significantly longer than the adjacent bonds C(6)-N(1), C(7)-C(8) and C(9)-C(10). The Ru-C cyclopentadienyl ligand bond lengths ranged from 2.231(2) to 2.274(2) Å and the P(1)-Ru(1) bond length was 2.2791(5) Å.

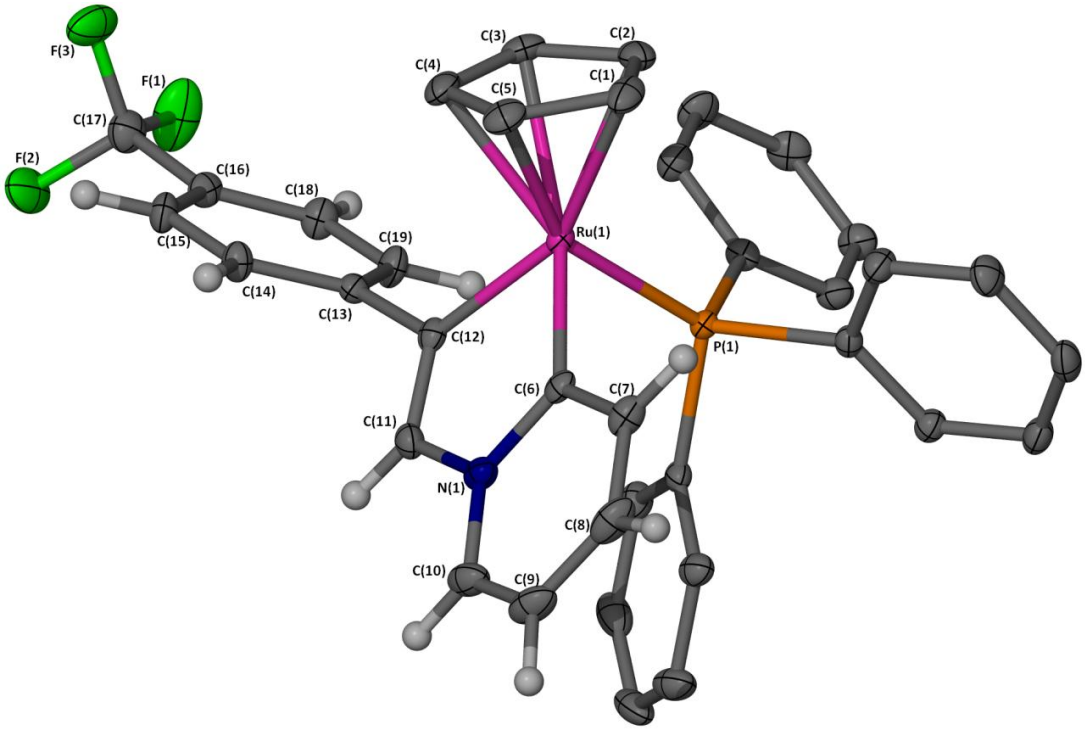

Figure 5.9: X-Seed diagram of complex **23**^{H,CF3}. Selected hydrogen atoms and a pentane molecule have been omitted for clarity, and where shown the thermal ellipsoids are at a 50 % probability level.

	Bond lengths (Å)		Bond angles (°)
C(5)-Ru(1)	2.240(2)	C(6)-Ru(1)-P(1)	86.20(6)
C(1)-Ru(1)	2.284(2)	C(12)-Ru(1)-P(1)	92.32(6)
C(2)-Ru(1)	2.264(2)	C(6)-Ru(1)-C(12)	77.76(9)
C(3)-Ru(1)	2.274(2)	C(11)-C(12)-Ru(1)	116.83(16)
C(4)-Ru(1)	2.231(2)	C(12)-C(11)-N(1)	114.8(2)
C(6)-Ru(1)	1.996(2)	C(6)-N(1)-C(11)	113.72(18)
C(6)-N(1)	1.394(3)	N(1)-C(6)-Ru(1)	116.90(15)
C(11)-N(1)	1.415(3)	N(1)-C(6)-C(7)	113.94(19)
C(11)-C(12)	1.339(3)	C(10)-N(1)-C(6)	124.2(2)
C(12)-Ru(1)	2.046(2)	C(9)-C(10)-N(1)	120.5(2)
C(12)-C(13)	1.481(3)	C(10)-C(9)-C(3)	118.9(2)
C(10)-N(1)	1.368(3)	C(7)-C(8)-C(9)	119.8(2)
C(9)-C(10)	1.353(4)	C(8)-C(7)-C(6)	122.5(2)
C(8)-C(9)	1.406(4)	N(1)-C(6)-C(7)	113.94(19)
C(7)-C(8)	1.375(3)		
C(6)-C(7)	1.420(3)		
P(1)-Ru(1)	2.2791(5)		

Table 5.6: Selected bond lengths (Å) and angles (°) for complex **23^{H,CF3}**.

5.2.3.4 Investigating the properties of 23^{H,CF3}

The properties of **23^{H,CF3}** in d_5-pyridine were investigated under two different reaction conditions:

i) Heating **23^{H,CF3}** at 50, 100 and 150 °C in the presence of a stoichiometric equivalent of a pyridinium hexafluorophosphate;

ii) Heating **23^{H,CF3}** at 50 and 100 °C in the absence of the pyridinium hexafluorophosphate.

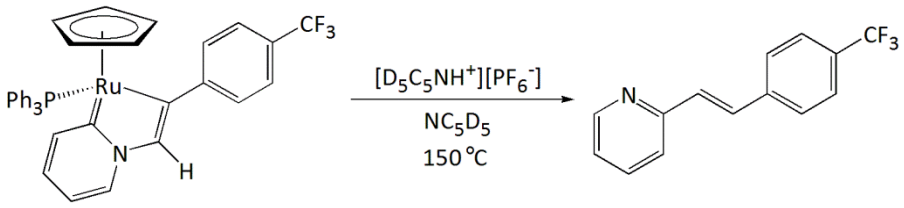

23^{H,CF3}

Scheme 5.9: Reaction upon heating **23^{H,CF3}** with $[D_5C_5NH][PF_6]$ in d_5-pyridine at 150 °C.

Following reaction conditions i, the reaction mixture was heated at 50, 100 and 150 °C and the reaction followed by NMR spectroscopy. After heating the sample at 50 and 100 °C over several days, the NMR spectra of the reaction mixture displayed very few changes. However, when the reaction mixture was heated at 150 °C the ^{1}H NMR spectrum exhibited significant changes, including the reduction in the peaks for **23^{H,CF3}**. There was also a set of new resonances at 8.76 ppm for a proton at the C-6 of the pyridine ring and at 8.00 ppm an alkene peak was observed for the organic species *E*-2-(4-trifluoromethyl)styrylpyridine. The ^{31}P{^{1}H} NMR spectrum of the reaction mixture displayed the reduction in the resonance at 60.4 ppm and there was increase in intensity at -5.4 ppm for uncoordinated triphenylphosphine. Additionally, due to the high temperatures employed degradation of the $[PF_6]^-$ anion was observed as triplet resonances at -13.3 and -14.4 ppm with a J_{PF} of 953 and 947 Hz coupling were observed respectively for several PF_2 containing species. There was no evidence for the regeneration of **5** in the NMR spectra, however this may be due to the high temperatures employed and the absence of the non-coordinating anion, $[PF_6]^-$.

The reaction conditions ii, involved heating **23^{H,CF3}** in d_5-pyridine in the absence of the pyridinium hexafluorophosphate at 50 and 100 °C. When heated at 50 °C, no changes were observed in the NMR spectra. However, when the sample was heated at 100 °C a set of resonances were observed for a new ruthenium-containing complex. The reaction however stopped at 50 % conversion. In the ^{1}H NMR spectrum a cyclopentadienyl resonance was observed at 4.92 ppm and the ^{31}P{^{1}H} NMR spectrum exhibited peaks at 58.9 and at -5.4 ppm for the triphenylphosphine ligand of a new ruthenium-containing complex and uncoordinated triphenylphosphine. Unfortunately, this species could not be identified. However resonances for the organic species *E*-2-(4-trifluromethyl)styrylpyridine were not observed, therefore highlighting that pyridinium hexafluorophosphate is required in order for the C-C coupling reaction to occur

.

5.3 Reactivity of complex 5 with alkynes

To gain further mechanistic insight into the formation of complexes **22^{R1,R2}** a deuterium labelling study was carried out. In order to study the location of the C-H functionalised proton from the pyridine moiety in complexes **22^{R1,R2}** a reaction was designed involving stoichiometric addition of either phenylacetylene or 4-ethynyl-α,α,α-trifluorobenzene to **5** in the presence of two equivalents of d_5-pyridine in a d_2-dichloromethane solution and the reaction was monitored *via* NMR spectroscopy.

5.3.1 Reaction between complex 5 with phenylacetylene

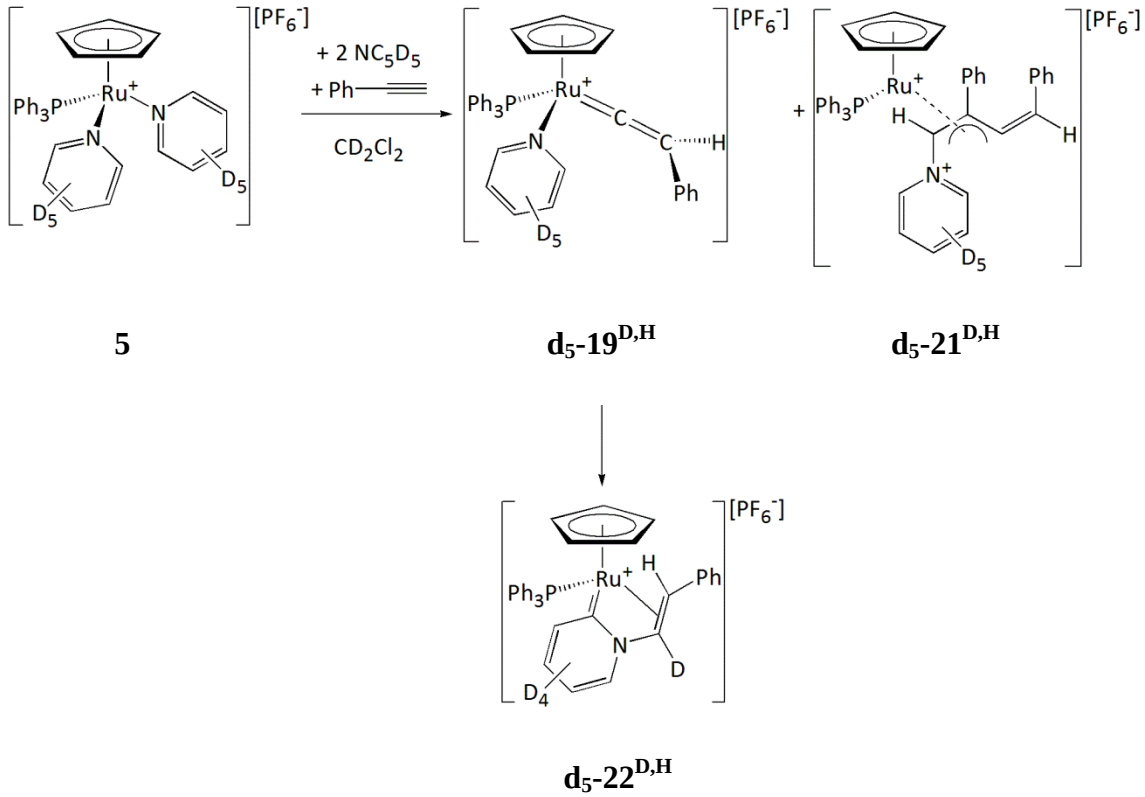

5 **d$_5$-19^{D,H}** **d$_5$-21^{D,H}**

d$_5$-22^{D,H}

Scheme 5.10: Stoichiometric reaction of **5** with phenylacetylene in the presence of two equivalents of d_5-pyridine.

The stoichiometric addition of phenylacetylene to **5** and two equivalents of d_5-pyridine in a d_2-dichloromethane solution was monitored *via* NMR spectroscopy (Scheme 5.10). The initial NMR spectra of the reaction mixture displayed resonances belonging to the vinylidene-containing species **d$_5$-19^{D,H}**, where the ^{1}H NMR spectrum exhibited broad peaks at 5.48 and 5.15 ppm for the cyclopentadienyl protons and the vinylidene proton respectively. The pyridine resonances were not observed due to deuteration. The ^{31}P{^{1}H} spectrum displayed a broad resonance at 51.9 ppm for the triphenylphosphine ligand.

After 24 hours the reaction mixture displayed resonances for the deuterated complex **d_5-22^{D,H}**. In the ^{1}H NMR spectrum at 4.95 ppm the cyclopentadienyl resonance was observed. The alkene resonances were of particular interest as these would reveal where the deuterium atom was incorporated. The species **22^{H,H}** exhibited the alkene peaks at 3.65 ppm (apparent t, 1H, $^3J_{HH}$, $^3J_{HP}$ = 9.5 Hz) and at 6.63 ppm (d, 1H, $^3J_{HH}$ = 7.8 Hz). The ^{1}H NMR spectrum of **d_5-22^{D,H}** from the deuterium labelling study exhibited a broad doublet peak at 3.65 ppm and the peak at 6.63 ppm was absent, which suggested deuterium incorporation has occurred at the resonance at 6.63 ppm. At this point, these data demonstrated that **A** was the species formed (Figure 5.10). A ^{1}H{^{31}P} NMR experiment revealed that the peak at 3.65 ppm decoupled to a broad singlet. The ^{31}P{^{1}H} NMR spectrum displayed the triphenylphosphine resonance at 53.7 ppm.

The ^{1}H NMR spectrum recorded after 5 days exhibited a doublet resonance at 6.68 ppm. A ^{1}H-^{1}H 2D COSY experiment revealed that this peak coupled strongly to the other alkene resonance at 3.65 ppm. The chemical shift of the alkene proton at 6.68 ppm was shifted slightly downfield and integration of this peak was difficult due to a noisy baseline. However, from these observations it is possible to conclude that over time deuterium scrambling was occurring. After 5 days, in the ^{31}P{^{1}H} NMR spectrum the resonance at 53.7 ppm had a shoulder, which could be due to similar species, but with different amounts of deuterium incorporation.

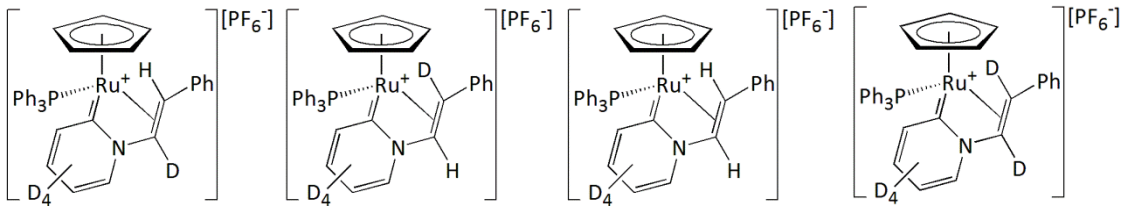

A **B** **C** **D**

d_5-22^{D,H} **d_5-22^{D,H}** **d_4-22^{D,H}** **d_6-22^{D,H}**

Figure 5.10: Potential isotopomers that could exist due to deuterium scrambling.

After leaving the reaction mixture for 7 days, the NMR spectra became increasingly noisy. This made integration of the peaks difficult as many new ruthenium-containing species that had not been observed previously were now present (Figure 5.10).

5.3.2 Reaction between complex 5 with 4-ethynyl-α,α,α-trifluorotoluene

Since the reaction between **5** and phenylacetylene gave many ruthenium-containing species making it difficult to integrate the alkene resonances. The reaction of **5** with 4-ethynyl-α,α,α-trifluorotoluene was investigated. The reaction of $\mathbf{10^{H}}$ and 4-ethynyl-α,α,α-trifluorotoluene was more selective as it yielded one major species, $\mathbf{22^{H,CF3}}$ and would hopefully give more details on the formation of $\mathbf{22^{H,CF3}}$.

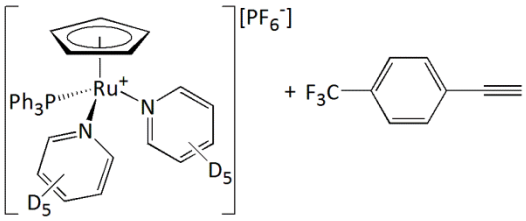

5

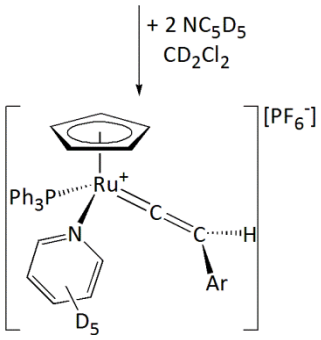

$\mathbf{d_5\text{-}19^{D,C6H4\text{-}4\text{-}CF3}}$

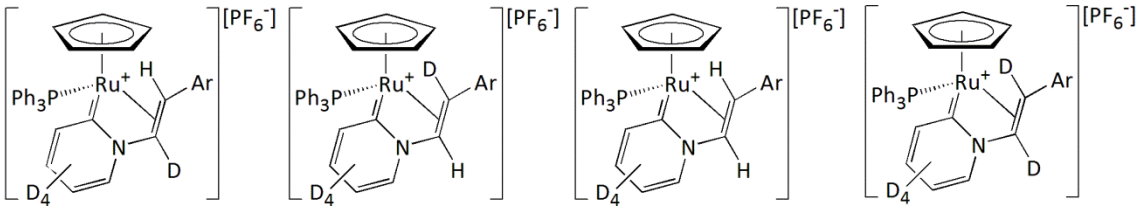

E **F** **G** **H**

$\mathbf{d_5\text{-}22^{D,CF3}}$ $\mathbf{d_5\text{-}22^{D,CF3}}$ $\mathbf{d_4\text{-}22^{D,CF3}}$ $\mathbf{d_6\text{-}22^{D,CF3}}$

Scheme 5.11: Stoichiometric reaction of **5** with 4-ethynyl-α,α,α-trifluorotoluene in the presence of two equivalents of d_5-pyridine.

The stoichiometric addition of 4-ethynyl-α,α,α-trifluorotoluene to **5** in the presence of two equivalents of d_5-pyridine in a d_2-dichloromethane solution was monitored *via* NMR spectroscopy. The initial ^{1}H NMR spectrum after the addition of 4-ethynyl-α,α,α-trifluorobenzene exhibited broad resonances for the vinylidene-containing complex **d_5-19^{D,CF3}** at 5.51 and 5.17 ppm for the cyclopentadienyl ligand and the vinylidene proton on the β-carbon atom respectively. This was consistent with the reaction of **10^{H}** and 4-ethynyl-α,α,α-trifluorotoluene in d_2-dichloromethane.

After 24 hours, the ^{1}H NMR spectrum displayed resonances for the C-H functionalised species **22^{D,CF3}** at 4.98 and 3.60 ppm in the cyclopentadienyl and alkene region respectively. Interestingly, these resonances had a more complicated multiplicity, as the cyclopentadienyl peak at 4.98 ppm appeared to have three peaks at this chemical shift, suggesting three ruthenium isotopomers **E**, **G** and **H** were present in the reaction mixture. The ratio of these complexes could not be determined as the resonances of the isotopomers overlapped. This was also observed at 3.60 ppm where the multiplicity could be reported to be an apparent doublet of triplets. However, this was actually due to two distinct alkene peaks; where one of these peaks was a doublet of doublets ($^3J_{HP}$ = 11.4 Hz, $^3J_{HH}$ = 7.9 Hz) for **G**, and the other was a doublet ($^3J_{HP}$ = 11.4 Hz) for **E**. The ^{1}H NMR spectrum also exhibited a doublet peak at 6.77 ppm ($^3J_{HH}$ = 7.9 Hz) due to the one of the alkene protons of **G**. The doublet at 3.60 ppm was assigned to the isotopomer **E**, where the other alkene resonance was deuterated and therefore was absent. As there were three isotopic isomers present in the reaction mixture and two of these have been observed in the ^{1}H NMR spectrum, it is possible that the third species has double deuterium incorporation at the alkene bond for **H**, and is consistent with the absence of any other alkene resonances in the ^{1}H NMR spectrum. In the ^{31}P{^{1}H} NMR spectrum a peak at 53.0 ppm was observed for the triphenylphosphine ligand, where the peak appeared to have a shoulder for the isotopic isomers of **22^{D,CF3}**.

As the reaction proceeded over several weeks, deuterium scrambling occurred in the reaction mixture and the ratio of the isotopomers changed. This was observed in the ^{31}P{^{1}H} NMR spectrum as shoulder of the resonance at 53.0 ppm began to increase in intensity until both peaks were of equal intensity. Also in the ^{1}H NMR spectrum the integrations changed over time if all the cyclopentadienyl ligand resonances at 4.98 ppm were integrated as 5H and compared with the alkene peaks at 3.60 ppm. After 24 hours the resonance at 3.60 ppm integrated to 0.7 H, and after 16 days the integration was 0.5 H with respect to the cyclopentadienyl ligand. These observations are consistent with

deuterium scrambling occurring over time.[178] Unfortunately, due to deuterium scrambling and difficulties in obtaining single integration values the kinetic isotope effect has not been determined.

A high resolution ESI-MS of the reaction mixture after 16 days provided information on the deuterium incorporated complexes. A peak with a *m/z* of 683.1443 was observed, but the ruthenium isotope pattern was not consistent with one single complex. This was interpreted as three different ruthenium complexes which differed in the amount of deuterium atoms incorporated, where the highest *m/z* peaks were observed at 682.1423, 683.1443 and 684.1443 for the cationic fragments of $[C_{37}H_{26}D_4F_3NPRu]^+$, $[C_{37}H_{25}D_5F_3NPRu]^+$ and $[C_{37}H_{24}D_6F_3NPRu]^+$ respectively. These data are not conclusive, as ruthenium contains many isotopes which can distort the shape of the isotope pattern observed. However, the fragmentation of these species were observed with *m/z* peaks of 254.1081, 255.1141 and 256.1196 for the organic fragments $[C_{14}H_7D_4F_3N]^+$, $[C_{14}H_6D_5F_3N]^+$ and $[C_{14}H_5D_6F_3N]^+$ respectively. The differences between these *m/z* peaks were 1.0060 and 1.0055 respectively, which is consistent with changing the amount of deuterium atoms present in the structure. Therefore from the high resolution ESI-MS there are three different products present from the reaction between **5** and 4-ethynyl-α,α,α-trifluorotoluene; one of these is a complex where one deuterium atom has been incorporated at the alkene position (*m/z* peaks of 683.1443 and 255.1141); the other being where both of the alkene sites contain a C-H bond (*m/z* peaks of 682.1423 and 254.10810; and the last species is where both alkene sites have a C-D bond (*m/z* peaks of 684.1443 and 256.1196).

5.3.3 Summary of deuterium labelling studies

The deuterium labelling studies have exhibited that initial deuterium incorporation occurred at the alkene carbon atom that was bonded to the nitrogen atom. Despite deuterium scrambling, the initial results are consistent with the formation of the pyridylidene-containing complex resulting from further reactivity of the vinylidene-containing complex.

5.4 Conclusions

The reactivity of the half-sandwich ruthenium complex **10^{H}** has been investigated in a dichloromethane solution with various aryl terminal alkynes. The stoichiometric addition with phenylacetylene resulted in the formation of several ruthenium complexes (**20^{H}**, **21^{H,H}** and **22^{H,H}**). The reaction conditions were optimised to avoid the formation of **20^{H}**. The intermediate vinylidene-containing species **19^{H,Ph}** reacted further to yield **22^{H,H}**.

The major ruthenium-containing species was **22^{H,H}** which contained a pyridylidene ligand, where a C-H functionalisation had occurred at the 2-position of the N-containing heterocycle and the nitrogen atom was bound to a pendant alkene group. The stoichiometric reaction with 4-ethynyl-α,α,α-trifluorotoluene in the presence of two equivalents of pyridine resulted in a selective reaction to give the corroborating pyridylidene-containing complex **22^{H,CF3}**. The properties of the pyridylidene-containing complex were of interest as the pyridylidene-alkene fragments were isomers of the carbon-carbon coupled 2-styrylpyridine derivatives. There are few examples in the literature of parent pyridine yielding a pyridylidene complex, since the N-bound version is usually more stable. Carmona *et al.* reported the formation of a pyridylidene complex from pyridine using the species [Tp$^{Ms''}$Ir(N_2)].[207] Our studies therefore have exhibited quite a unique type of reactivity.

A deprotonation reaction occurred upon the addition of **22^{H,CF3}** to an excess of pyridine to yield a 1-ruthenaindolizine species, **23^{H,CF3}** and pyridinium hexafluorophosphate. The reactivity of **23^{H,CF3}** was probed by heating the reaction mixture. No changes were observed when the reaction mixture was heated at 50 and 100 °C. However, the 2-styrylpyridine derivative was formed when higher reaction temperatures of 150 °C were employed. This suggested **23^{H,CF3}** was a thermodynamic sink in the formation of the 2-styrylpyridine compounds.

A deuterium labelling study between **5** and the terminal alkynes phenylacetylene and 4-ethynyl-α,α,α-trifluorotoluene in a dichloromethane solution resulted in the formation of the pyridylidene-containing complexes **22** *via* the vinylidene-containing complexes **19**. Initial deuterium incorporation for **22** was observed at the alkene carbon atom which was bonded to the nitrogen atom. The findings were consistent the vinylidene-containing complexes **19** being intermediates for the formation of **22**.

Chapter 6. Reactivity of Half-Sandwich Ruthenium Complexes: Part II

6.1 Introduction

The reactivity exhibited by transition metal complexes can be tuned depending on the ligands present. The Hammett equation has been useful in determining trends in reaction rates and equilibria.[295] The Hammett values were determined by analysis of substituted benzoic acids to give information on the electronic effects. The substituent constants reported have been extensively studied and methods developed to improve the accuracy.[292-295, 320] By screening and understanding substituents effects, it is possible that more efficient catalytic systems may be developed.

The previous chapter discussed the reactions of **10^{H}** with aryl terminal alkynes (phenylacetylene, 1-ethynyl-4-fluorobenzene, 4-ethynyl-α,α,α-trifluorotoluene) in a dichloromethane solution, where one of the most characteristic products generated a ruthenium pyridylidene complexes. This chapter continues from the previous chapter to explore the role of substituent effects (alkynes, N-containing heterocycles and phosphorus ligands). Several aspects will be investigated:

1. The reactivity of **10^{H}** with alkyl and TMS-substituted alkynes.
2. The reactivity of ruthenium complexes $[Ru(\eta^5\text{-}C_5H_5)(PPh_3)(NC_5H_4R)_2][PF_6]$ with different N-containing heterocycles (4-methyl, 4-dimethylamino and 3-methyl) towards terminal alkynes.
3. The reactivity of ruthenium complexes $[Ru(\eta^5\text{-}C_5H_5)(PR_3)(NC_5H_5)_2][PF_6]$, **$14^{H}$**, **16** and $[Ru(\eta^5\text{-}C_5H_5)(P^iPr_3)(NC_5H_5)(NCMe)][PF_6]$, **15** with different phosphorus ligands (trimethylphosphine, triisopropylphosphine and triphenylphosphite) towards terminal alkynes.
4. The reactivity of $[Ru(\eta^5\text{-}C_5H_5)(PPh_3)_2(L)][PF_6]$ (where L = NCMe, NC_5H_5) with phenylacetylene will be briefly discussed.
5. The final section in this chapter will summarise the substituent effects with respect to the data (NMR and X-ray crystallography).

6.2 Reactivity of 10^{H} with alkyl- and TMS-substituted alkynes

The reactivity of **10^{H}** with alkyl and TMS-substituted alkynes in a dichloromethane solution was investigated and the reactions monitored using NMR spectroscopy. The role of the terminal alkyl substituents (*tert*-butyl, n-butyl) and the TMS-substituted alkynes (trimethylsilylacetylene, 1-phenyl-2-trimethylsilylacetylene) were determined.

6.2.1 Reaction between complex 10^{H} with *tert*-butylacetylene

The range of terminal alkynes was extended from aryl to alkyl substituents. The reactivity of *tert*-butylacetylene towards complex **10^{H}** in d_2-dichloromethane was investigated. Murakami and Hori have reported that the alkyne ^{t}BuC≡CTMS does not undergo the alkenylation reaction with pyridine.[253] By investigating the reaction between **10^{H}** and *tert*-butylacetylene and observing any potential ruthenium complexes formed, it may provide further mechanistic insight into how the C-C bond formation reaction proceeds. Also, it would be of interest to observe if any similar ruthenium complexes observed in the reactions between **10^{H}** and the aryl terminal alkynes are present with the alkyl substituents.

The reaction of **10^{H}** with *tert*-butylacetylene was investigated under different reaction conditions:

i) Stoichiometric addition of *tert*-butylacetylene to **10^{H}** in d_2-dichloromethane;

ii) Addition of five equivalents of *tert*-butylacetylene to **10^{H}** in d_2-dichloromethane.

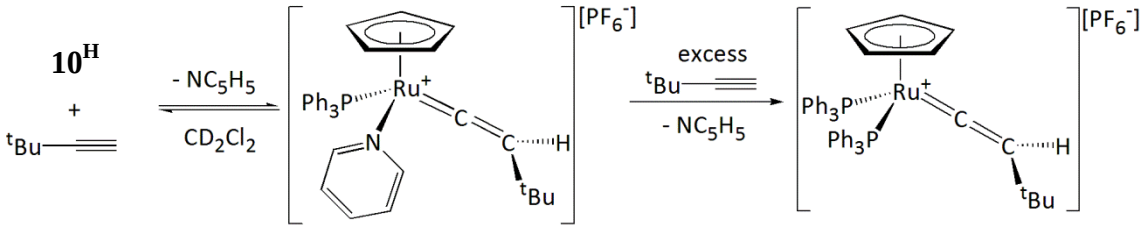

$19^{H,tBu}$ **2^{tBu}**

Scheme 6.1: Addition of *tert*-butylacetylene to **10^{H}**.

The stoichiometric addition of *tert*-butylacetylene to **10^{H}** was monitored using NMR spectroscopy (reaction conditions i, Scheme 6.1). The NMR spectra displayed a set of resonances for a new ruthenium species, and after 24 hours the reaction appeared to be in equilibrium between **10^{H}**, *tert*-butylacetylene and a new complex **19^{H,tBu}** in a 1:1 ratio. The ^{1}H NMR spectrum still exhibited resonances for **10^{H}** as the cyclopentadienyl protons at 4.42 ppm, and the protons at the C-2/6 positions on the coordinated pyridine ligands at 8.30 ppm were observed. In the ^{1}H NMR spectrum the new ruthenium complex, **19^{H,tBu}** exhibited a singlet resonance at 5.31 ppm and a doublet peak at 3.97 ppm ($^{4}J_{HP}$ = 3.0 Hz). A ^{1}H{^{31}P} NMR experiment revealed that the doublet resonance at 3.97 ppm decoupled to a singlet, this is characteristic of the proton on the β-carbon atom of the vinylidene ligand. In addition, the ^{1}H NMR spectrum the protons at the C-2/6 positions of uncoordinated pyridine had resonances at 8.58 ppm with an integration of 2H and the methyl groups of the *tert*-butyl group at 1.17 ppm had an integration of 9H relative to the resonance at 3.97 ppm of 1H. The ^{31}P{^{1}H} NMR spectrum of **19^{H,tBu}** exhibited a resonance for the triphenylphosphine ligand at 53.5 ppm (singlet). Based on the NMR spectra the new species in the reaction mixture was assigned as the ruthenium vinylidene-containing complex [Ru(η^{5}-C_5H_5)(=C=CH^{t}Bu)(PPh_3)(NC_5H_5)][PF_6], **19^{H,tBu}**.

The reaction conditions were changed in order to try and change the equilibrium position to favour the formation of **19^{H,tBu}** (reaction conditions ii). The addition of excess *tert*-butylacetylene (5 equivalents) to **10^{H}** was monitored by NMR spectroscopy (Scheme 6.1). The reaction mixture initially displayed resonances for three ruthenium-containing complexes, as in the ^{31}P{^{1}H} NMR spectrum peaks at 42.7, 50.2 and 53.5 ppm were observed. These species were identified as complexes **10^{H}**, **19^{H,tBu}** and **2^{tBu}**, where confirmation of **10^{H}** and **2^{tBu}** were supported by authentic samples. After heating the reaction mixture for 4 days, the major species present in the reaction mixture was **2^{tBu}**, as the ^{1}H NMR spectrum exhibited resonances at 5.11 ppm (singlet), and the proton on the β-carbon atom of the vinylidene ligand displayed a resonance at 4.24 ppm (triplet, $^{4}J_{HP}$ of 2.8 Hz) for **2^{tBu}**. The ^{31}P{^{1}H} NMR spectrum included a peak at 42.7 ppm (singlet) for both triphenylphosphine ligands at the ruthenium centre of **2^{tBu}**. At this stage there still remained an excess of *tert*-butylacetylene in the reaction mixture.

The behaviour of **19^{H,tBu}** within the reaction mixture upon heating suggested that it is converted to the more thermodynamically stable complex, **2^{tBu}**. Attempts were made to purify and isolate the species **19^{H,tBu}** *via* many different crystallisation methods.

Unfortunately none of these attempts were successful, and therefore there is limited data for **19^{H,tBu}**.

The other reactions of **10^{H}** with terminal alkynes results in the vinylidene species **19^{R1,R2}** that are short-lived intermediates. This data potentially supports the observations reported by Murakami and Hori, since they have reported that the *tert*-butyl substitent does not generate the alkenylation product. Since **19^{H,tBu}** remains in solution and not reacting further with pyridine, it therefore indicates that the carbon-carbon bond formation reaction requires the vinylidene–containing intermediate to react further with pyridine.

6.2.2 Reaction between complex 10^{H} with 1-hexyne

The effect of changing the alkyl substituent of the terminal alkyne to a less sterically demanding substituent (n-butyl) was investigated. The reaction of **10^{H}** with 1-hexyne was monitored *via* NMR spectroscopy. Several reaction conditions were investigated:

i) Stoichiometric addition of 1-hexyne to **10^{H}** in a d_2-dichloromethane solution;

ii) Stoichiometric addition of 1-hexyne to **10^{H}** in the presence of two equivalents of pyridine in a d_2-dichloromethane solution.

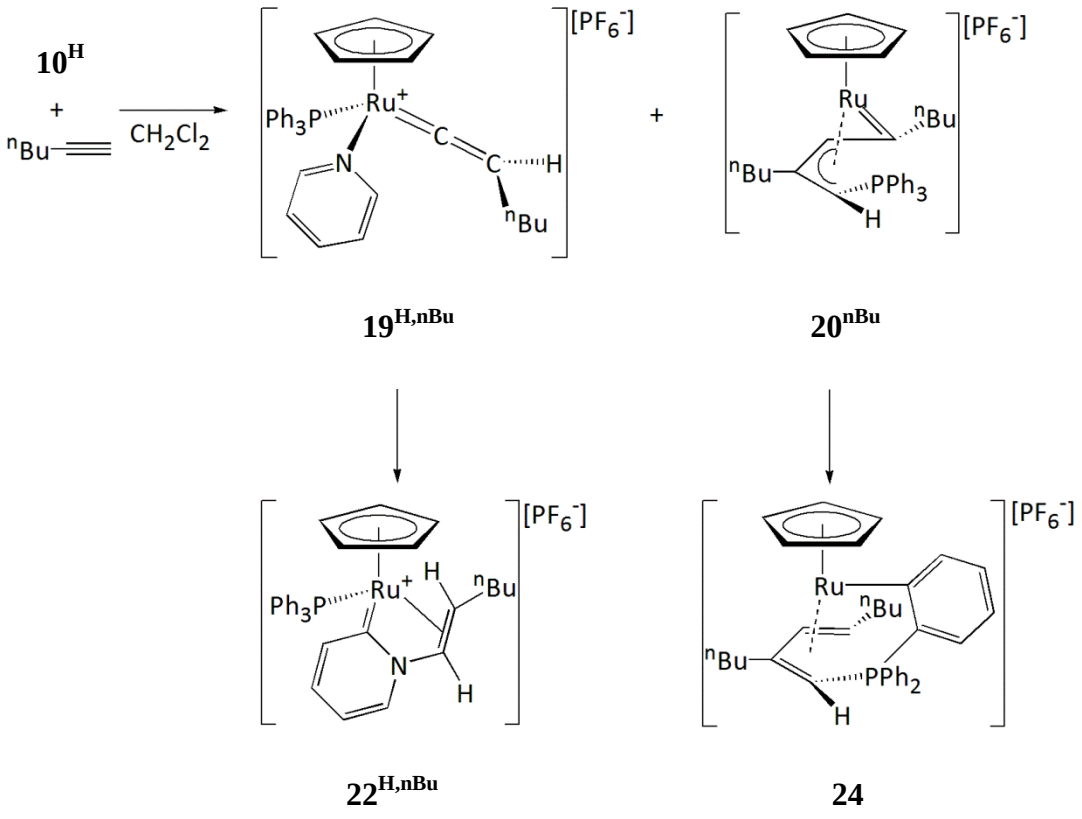

Scheme 6.2: Reaction between **10^{H}** and 1-hexyne in dichloromethane, reaction conditions i.

Following reaction conditions i, the initial NMR spectrum exhibited resonances for two new ruthenium complexes which have cautiously been assigned as **19^{H,nBu}** and **20^{nBu}**, where **19^{H,nBu}** was a short-lived intermediate. Once the reaction had gone to completion there were four new ruthenium complexes present in the reaction mixture (Scheme 6.2).

Under reaction conditions ii, the reaction proceeded to give the same resonances that were observed under reaction conditions i, however different quantities of the species are formed. The reaction proceeded more slowly than the reaction without excess pyridine and therefore was heated at 50 °C for 16 hours.

*6.2.2.1 Identification of **19^{H,nBu}***

Employing reaction conditions i, resonances were tentatively assigned as the vinylidene-containing complex **19^{H,nBu}** were only observed in the initial NMR spectra and after 24 hours were no longer present. The initial $^{31}P\{^{1}H\}$ NMR spectrum exhibited a peak at 53.3 ppm for a triphenylphosphine ligand. In the ^{1}H NMR spectrum a resonance for the cyclopentadienyl ligand could not be observed, as it is possible that this peak lies underneath the d_2-dichlormethane resonance. The resonance at 5.32 ppm was integrated with respect to the grease peak at 0.8 ppm (as this remained constant) and after 24 hours the integration of yhis peak decreases in intensity. Additionally, the cyclopentadienyl ligand resonance for **19^{H,tBu}** appeared at 5.31 ppm, which indicates that the cyclopentadienyl ligand of **19^{H,nBu}** may be at a similar chemical shift. The ^{1}H NMR spectrum exhibited a resonance at 4.21 ppm as a triplet of doublets, with coupling constants of $^{3}J_{HH}$ of 8.3 Hz and a $^{4}J_{HP}$ of 2.9 Hz for the vinylidene proton. A $^{1}H\{^{31}P\}$ NMR experiment revealed that the resonance at 4.21 ppm simplified to a triplet peak. If the complex **19^{H,nBu}** was present in the reaction mixture, the vinylidene proton would be expected to have this multiplicity.

*6.2.2.2 Identification of **20^{nBu}** and its further reactivity to give **24***

Under reaction conditions i, the initial NMR spectra exhibited major new resonances for a species which has cautiously been assigned as **20^{H,nBu}**. The ^{1}H NMR spectrum displayed a peak at 4.97 ppm for the cyclopentadienyl ligand. The protons on the allyl backbone were observed at 4.78 (broad, 1H) and 5.30 (doublet) ppm with respect to the cyclopentadienyl ligand at 4.97 ppm (5H) for the =C-C*H*-C(^{n}Bu)-CHPPh_3 and =C-CH-C(^{n}Bu)-C*H*PPh_3 protons respectively. Unfortunately the resonance at 5.30 ppm overlaps with the d_2-dichloromethane peak and therefore integration of this peak was not possible, however a $^{1}H\{^{31}P\}$ NMR spectrum revealed that this peak decouples to a

singlet peak. The $^{31}P\{^{1}H\}$ NMR spectrum displayed a peak at 31.6 ppm for the triphenylphosphine ligand of **20^{nBu}**.

After 24 hours the resonances for **20^{nBu}** began to decrease in the NMR spectra and a new set of peaks were observed in the NMR spectra for **24**. The ^{1}H NMR spectrum exhibited a peak at 4.17 ppm (5H) for a new cyclopentadienyl resonance and a doublet resonances at 3.68 (1H, $^{2}J_{HP}$ = 14.0 Hz) and 4.05 (1H, $^{4}J_{HH}$ = 4.9 Hz) ppm for the allyl hydrogen atoms. The $^{31}P\{^{1}H\}$ NMR spectrum displayed a peak at 31.1 ppm for a new triphenylphosphine ligand, as **20^{nBu}** converted to a new unidentified complex. The work reported by Kirchner *et al.* indicates a further C-H functionalisation reaction of **20^{nBu}** occurring at the phenyl ring of the triphenylphosphine ligand reaction of the π-allyl carbene complex to give the species $[Ru(\eta^5\text{-}C_5H_5)(\eta^4\text{-}CH(^{n}Bu)CHC(^{n}Bu)CH\text{-}PPh_2(\eta^1\text{-}C_6H_4))][PF_6]$ **24** (Section 1.5.2). The resonances from the reaction mixture were compared with the literature data to confirm this assignment.[132, 138]

When the reaction conditions ii were followed, the set of resonances belonging to the π-allyl carbene complex reduced in intensity, suggesting that the excess pyridine in the reaction mixture was inhibiting the formation of this species due to the pyridine competing for a coordination site at the ruthenium centre. This is consistent with the findings in previous reactions of phenylacetylene with **10^{H}** (Section 5.2).

*6.2.2.3 Identification of **22^{H,nBu}***

From the reaction of 1-hexyne it is possible that **22^{H,nBu}** is generated, however there is limited evidence for this compound and therefore should be considered cautiously. Over the course of 8 days, the $^{31}P\{^{1}H\}$ NMR spectrum exhibited a signal at 56.6 ppm which increased in intensity. A set of corresponding resonances in the ^{1}H NMR spectrum became evident at 5.02 (s, 5H), 2.73 (1H, broad) and 5.82 (d, 1H, $^{3}J_{HH}$ = 7.8 Hz) ppm for a cyclopentadienyl ligand, and two alkene protons respectively. A 2D ^{1}H-^{1}H COSY NMR experiment exhibited a strong coupling between the resonances at 2.73 and 5.82 ppm, which is consistent for two alkene protons. With reaction conditions ii, the major resonances observed were those that were assigned tentatively as **22^{H,nBu}**.

6.2.2.4 Other unknown species

Not all of the resonances in the NMR spectra have been assigned. Another major species was present in the reaction mixture after 5 days. The ^{1}H NMR spectrum exhibited a cyclopentadienyl ligand peak at 4.29 ppm, and in the $^{31}P\{^{1}H\}$ NMR

spectrum a resonance at 35.8 ppm was observed for the corresponding triphenylphosphine ligand.

6.2.3 Reaction between complex 10^{H} with TMS-substituted alkynes

Murakami and Hori reported the carbon-carbon bond formation reactions of TMS-substituted alkynes and pyridine with the pre-catalyst [Ru(η^5-C_5H_5)Cl(PPh_3)$_2$], **1**. They reported the role of the TMS group was to prevent alkyne dimerisation.[253] An investigation into the reactivity between $\mathbf{10^{H}}$ and TMS-containing alkynes in d_2-dichloromethane was conducted.

6.2.3.1 Reaction between 10^{H} and 1-phenyl-2-trimethylsilylacetylene

The stoichiometric addition of 1-phenyl-2-trimethylsilylacetylene to complex $\mathbf{10^{H}}$ in d_2-dichloromethane was monitored by NMR spectroscopy at room temperature for 6 days, followed subsequently by heating for 16 hours at 50 °C.

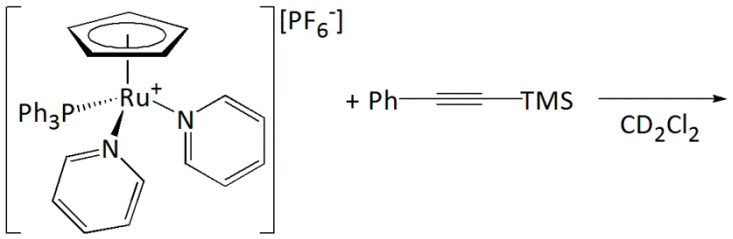

$\mathbf{10^{H}}$

Scheme 6.3: Stoichiometric addition of 1-phenyl-2-trimethylsilylacetylene to $\mathbf{10^{H}}$.

Initial ^{1}H and ^{31}P{^{1}H} NMR spectra were recorded within 30 minutes of alkyne addition and indicated the formation of three new ruthenium-containing species. The ^{31}P{^{1}H} NMR spectrum for the triphenylphosphine resonances of the three new complexes were observed at 43.4, 51.6 and 61.8 ppm The ^{1}H NMR spectrum also displayed resonances at 4.42 ppm for the cyclopentadienyl protons of $\mathbf{10^{H}}$, and the TMS group of the alkyne at 0.24 ppm.

The ^{31}P{^{1}H} NMR spectrum after 5 days demonstrated decomposition of the $[PF_6]^-$ anion had occurred. A broad sextet resonance at -143.0 ppm with a $^1J_{PF}$ of 796 Hz was observed, which is due to a species containing a PF_5 fragment. The ^{1}H NMR spectrum in the TMS region displayed many unknown peaks. It is possible that a fluorine atom has been abstracted from the $[PF_6]^-$ anion by the silicon atom, due to a thermodynamic

driving force for the formation of a Si-F bond.[321-323] The decomposition of the $[PF_6]^-$ anion indicated that this was not a suitable anion for this reaction.

After 5 days the $^{31}P\{^1H\}$ NMR spectrum the peak at 61.8 ppm was no longer observed and a new resonance at 40.3 ppm began to increase in intensity. The ^1H NMR spectrum had a corroborating cyclopentadienyl resonance at 4.10 ppm. This new complex was assigned as the species $[Ru(\eta^5\text{-}C_5H_5)Cl(PPh_3)_2]$, **1**. The unknown ruthenium species in the reaction mixture were unstable in nature with respect to **1** and therefore a chloride atom could have been abstracted from the d_2-dichloromethane solvent, to give **1** which is a more thermodynamically stable complex. Unfortunately the other ruthenium complexes present in the reaction mixture have not been identified.

*6.2.3.2 Reaction between complex **10^H** with trimethylsilylactylene*

The addition of trimethylsilylacetylene to **10^H** was investigated, as research by Kirchner *et al.* demonstrated that a vinylidene-containing complex $[Ru(\eta^5\text{-}C_5H_5)(=C=CHSiMe_3)(PPh_3)(NCMe)][PF_6]$ was generated from a reaction between $[Ru(\eta^5\text{-}C_5H_5)(PPh_3)(NCMe)_2][PF_6]$, **9^{Ph}** and trimethylsilylactylene. The vinylidene species they identified was not isolated, as during the work-up the product decomposed.[132]

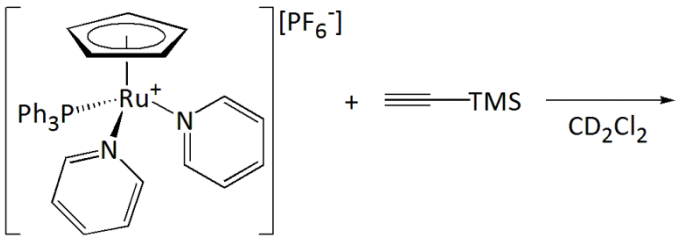

10^H

Scheme 6.4: Stoichiometric addition of trimethylsilylacetylene to **10^H**.

The stoichiometric reaction between **10^H** and trimethylsilylactylene was carried out on an NMR scale at room temperature in d_2-dichloromethane. ^1H and $^{31}P\{^1H\}$ NMR spectra were recorded within one hour of alkyne addition. From the $^{31}P\{^1H\}$ NMR spectrum it appeared that four new phosphorus-containing products were present at 54.9, 54.2, 52.7 and 31.3 ppm. In the ^1H NMR spectrum in the cyclopentadienyl proton region there were new resonances at 5.35, 5.23, 5.03, and 4.85 ppm. Unfortunately, the resonances between the two spectra could not be correlated. Also, in the ^1H NMR spectrum, uncoordinated pyridine was detected with resonances observed at 8.58, 7.68 and 7.28 ppm. After 24 hours, all resonances observed after initial alkyne addition were no longer present and many were displaced by different resonances. In a similar fashion

to the reaction with 1-phenyl-2-trimethylsilylacetylene, the $^{31}P\{^{1}H\}$ NMR spectrum displayed a new resonance at -143.0 ppm (broad sextet, $^{1}J_{PF}$ = 796 Hz) for a species that contained a PF_5 group. This was attributed to the formation of Si-F bonds, where the fluorine atoms are abstracted from the $[PF_6]^-$ anion.[321-323]

This reaction gave a multitude of species, none of which could be identified. The presence of the TMS group and a $[PF_6]^-$ anion suggested that a different non-coordinating anion is required to stabilise any potential ruthenium intermediates due to the formation of Si-F bonds. The further study of the TMS-substituted alkynes was therefore discontinued.

6.3 Reactivity of complex 10^{Me} with alkynes

Previously, in this chapter the reactivity of *bis*-substituted pyridine complexes $\mathbf{10^{H}}$ and **5** (NC_5H_5 or NC_5D_5) with various alkynes has been described. This chapter will now progress on to substituent effects, and the following section will look at the reactivity of a different N-containing heterocycle, 4-methylpyridine. The ligand, 4-methylpyridine is a stronger nitrogen donor atom than pyridine due to the inductive effect of the methyl substituent, and this could change the reactivity towards the terminal alkynes phenylacetylene and 4-ethynyl-α,α,α-trifluorotoluene.

6.3.1 Reaction between complex 10^{Me} with phenylacetylene

The stoichiometric addition of phenylacetylene to $\mathbf{10^{Me}}$ in d_2-dichloromethane was monitored by NMR spectroscopy (Scheme 6.5). The initial NMR spectra were recorded after approximately 30 minutes to reveal resonances present for three new ruthenium-containing complexes in the reaction mixture: a minor unknown species, $\mathbf{19^{Me,Ph}}$ and $\mathbf{20^{H}}$. The minor unknown species and $\mathbf{19^{Me,Ph}}$ were short-lived intermediates. After 24 hours, the reaction mixture displayed peaks for an additional two new ruthenium-containing complexes $\mathbf{21^{Me,H}}$, $\mathbf{22^{Me,H}}$. After five days $\mathbf{10^{Me}}$ was still present in the reaction mixture, therefore a further aliquot of phenylacetylene was added to the reaction mixture to drive the reaction to completion. This reaction followed a very similar pattern to the stoichiometric reaction of phenylacetylene and $\mathbf{10^{H}}$. In the ^{1}H NMR spectrum, resonances for uncoordinated 4-methylpyridine were observed at 2.34 (3H), 7.10 (2H) and 8.41 (2H) ppm and were assigned to the methyl group and protons at the C-3/5 and C-2/6 positions respectively.

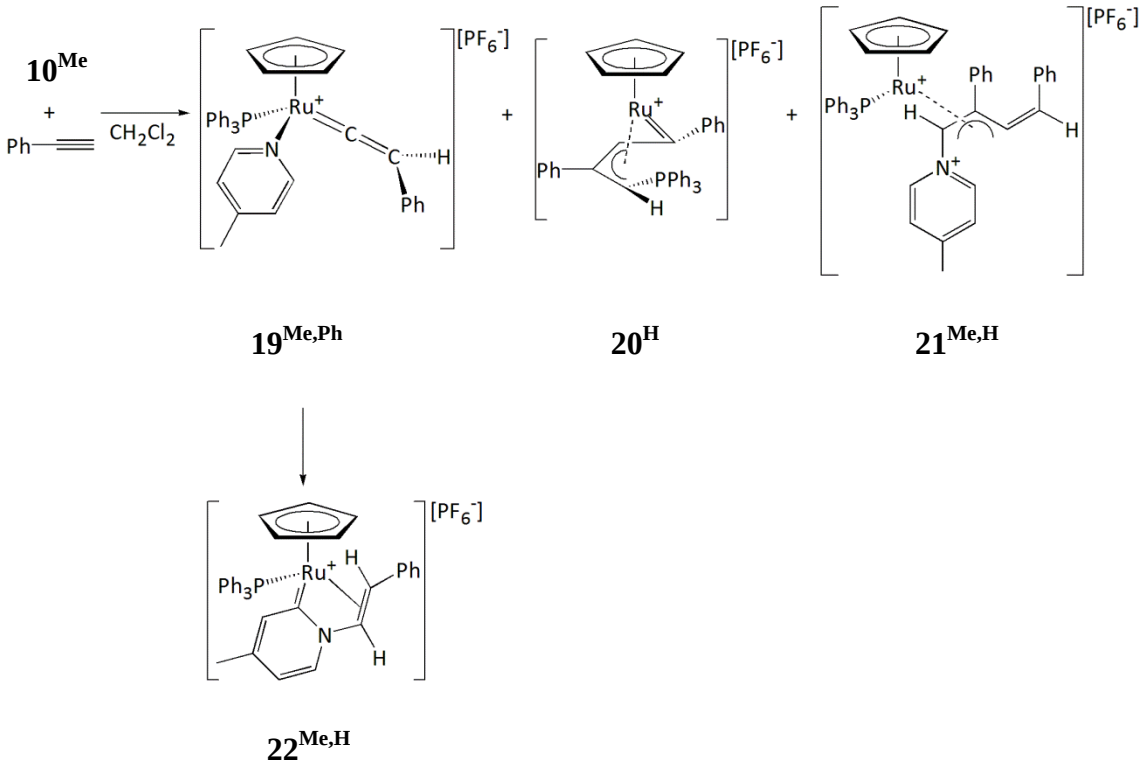

Scheme 6.5: Stoichiometric reaction between **10**$^{\mathbf{Me}}$ and phenylacetylene in dichloromethane.

6.3.1.1 Identification of the minor unknown species

The minor unknown species was observed in the initial ^{1}H and ^{31}P{^{1}H} NMR spectra, however spectra recorded after 24 hours did not display these resonances suggesting it was a short-lived species. The ^{1}H NMR spectrum contained a resonance at 4.94 ppm for the cyclopentadienyl ligand. The ^{31}P{^{1}H} NMR spectrum exhibited a corresponding peak at 53.6 ppm for the triphenylphosphine ligand.

*6.3.1.2 Identification of complex **19**$^{\mathbf{Me,Ph}}$*

The initial NMR spectra exhibited that the major new ruthenium-containing complex in the reaction mixture was **19**$^{\mathbf{Me,Ph}}$. The ^{1}H NMR spectrum exhibited broad peaks at 5.13 and 5.47 ppm with integrations of 1H and 5H for the vinylidene ligand proton and the cyclopentadienyl ligand respectively. Additionally, the ^{1}H NMR spectrum exhibited a set of resonances at 2.23 (s, 3H), 6.77 (d, 2H, $^{3}J_{HH}$ = 6.2 Hz) and 8.17 (d, 2H, $^{3}J_{HH}$ = 6.2 Hz) ppm, which were assigned to the methyl group and the protons at the C-3/5 and C-2/6 positions respectively, of a coordinated 4-methylpyridine ligand. The ^{31}P{^{1}H} NMR spectrum exhibited a broad singlet resonance at 51.9 ppm for the triphenylphosphine ligand.

6.3.1.3 Identification and formation of $\mathbf{20^H}$

The identification of $\mathbf{20^H}$ was confirmed through an independent reaction (Section 5.2). However, unlike the reaction of $\mathbf{10^H}$ with phenylacetylene, this reaction was not complete within 30 minutes. The peaks belonging to $\mathbf{20^H}$ continued to increase in intensity for 24 hours. This could be attributed to 4-methylpyridine containing a better donor atom than pyridine and therefore dissociation from ruthenium is less favourable.

6.3.1.4 Identification of $\mathbf{21^{Me,H}}$

The presence of $\mathbf{21^{Me,H}}$ in the reaction mixture was tentatively assigned based on the previous reaction of $\mathbf{10^H}$ with phenylacetylene. The ^{1}H NMR spectrum displayed a resonance at 4.54 ppm for the cyclopentadienyl ligand and the ^{31}P{^{1}H} NMR spectrum exhibited a singlet at 48.0 ppm for the triphenylphosphine ligand. These are similar chemical shifts to $\mathbf{21^{H,H}}$ and therefore the assignment must be approached cautiously. This was a minor side-product from the reaction and therefore was not explored further.

6.3.1.5 Identification of $\mathbf{22^{Me,H}}$

The major species present in the reaction mixture at the end of the reaction between $\mathbf{10^{Me}}$ and phenylacetylene was $\mathbf{22^{Me,H}}$. The product was purified either *via* the slow diffusion of pentane in to the reaction mixture to afford pale yellow crystals or through the addition of DABCO to the crude reaction mixture to afford $\mathbf{23^{Me,H}}$ which was extracted with pentane and then reprotonated using pyridinium hexafluorophosphate to yield a pale yellow precipitate (Scheme 6.6). The complex $\mathbf{22^{Me,H}}$ was characterised fully using ^{1}H NMR spectroscopy and high resolution ESI-MS. The ^{31}P{^{1}H} and ^{13}C{^{1}H} NMR spectra contained unknown impurities and the elemental analysis data presented was from one run.

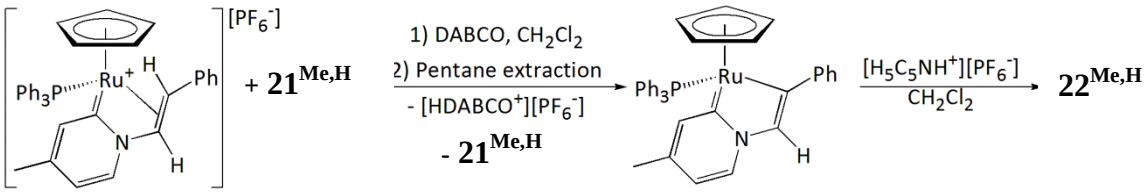

$\mathbf{22^{Me,H}}$ $\mathbf{23^{Me,H}}$

Scheme 6.6: Purification technique for complex $\mathbf{22^{Me,H}}$.

The ^{1}H NMR spectrum of $\mathbf{22^{Me,H}}$ in d_2-dichloromethane, exhibited peaks at 4.92 (singlet, 5H), 3.68 (multiplet, 1H) and 6.47 (doublet, $^3J_{HH}$ = 7.8 Hz) ppm for the cyclopentadienyl ligand and the two alkene protons respectively. Additionally a methyl

resonance at 2.13 ppm (singlet, 3H) for **22^{Me,H}** was observed, and other resonances originating from the 4-methylpyridine ligand were exhibited at 6.84 (multiplet, 2H) and 7.72 (doublet, 1H, $^{3}J_{HH}$ = 6.4 Hz) ppm. The integrations suggested that there was one fewer proton on the N-containing heterocycle, which is consistent for a C-H functionalisation having occurred. The aromatic region of the ^{1}H NMR spectrum contained broad peaks for the phenyl groups of the triphenylphosphine ligand (similar to **22^{H,H}**). The ^{31}P{^{1}H} NMR spectrum exhibited a major peak at 52.3 ppm for the triphenylphosphine ligand of **22^{Me,H}**. The ^{13}C{^{1}H} NMR spectrum contained impurities, however the relevant resonances belonging to **22^{Me,H}** were identified with 2D ^{1}H-^{13}C HSQC and ^{1}H-^{13}C HMBC NMR experiments. The ^{13}C{^{1}H} NMR spectrum exhibited broad signals at 54.7 and 68.6 ppm for the alkene carbon atoms. Interestingly a doublet peak at 178.2 ppm with a $^{2}J_{CP}$ of 18.4 Hz was observed, and found to show a long range ^{1}H-^{13}C coupling to the methyl group at 2.13 ppm, suggesting a Ru-C bond was present in **22^{Me,H}**. This data supports the theory that a C-H functionalisation reaction has occurred. A high resolution ESI-MS on a pure sample of **22^{Me,H}** displayed a ruthenium-containing complex with a *m/z* of 624.1394 consistent with the cationic species of **22^{Me,H}**.

Crystals suitable for X-ray diffraction were obtained *via* the slow diffusion of pentane into a dichloromethane layer containing **22^{Me,H}** (Figure 6.1, Table 6.1). The structure of **22^{Me,H}** was found to contain a C-H functionalised pyridine ring in the form of a pyridylidene ligand, where the nitrogen atom was coordinated to an alkene functional group which came from the phenylacetylene molecule. The bond angles at the ruthenium centre of **22^{Me,H}** for C(6)-Ru(1)-P(1), C(12)-Ru(1)-P(1) and C(6)-Ru(1)-C(12) were 90.79(5), 84.86(5) and 83.26(7) ° respectively, indicating that geometry could be described as a distorted octahedron. The C(6)-Ru(1) bond length to the pyridylidene fragment was 2.0183(19) Å. The coordination of the ruthenium centre to the alkene group was not equivalent, as the C(12)-Ru(1) and C(11)-Ru(1) bond lengths were 2.272(2) and 2.1435(19) Å respectively. The significantly unequal ruthenium to alkene bond lengths have been observed by Eisentstein and Hoffmann.[318, 319] The C(11)-C(12) bond length was 1.410(3) Å which was significantly shorter than the adjacent bonds, suggesting multiple bond character and characteristic of an alkene bond length.[298] The P(1)-Ru(1) bond length was found to be 2.3215(5) Å.

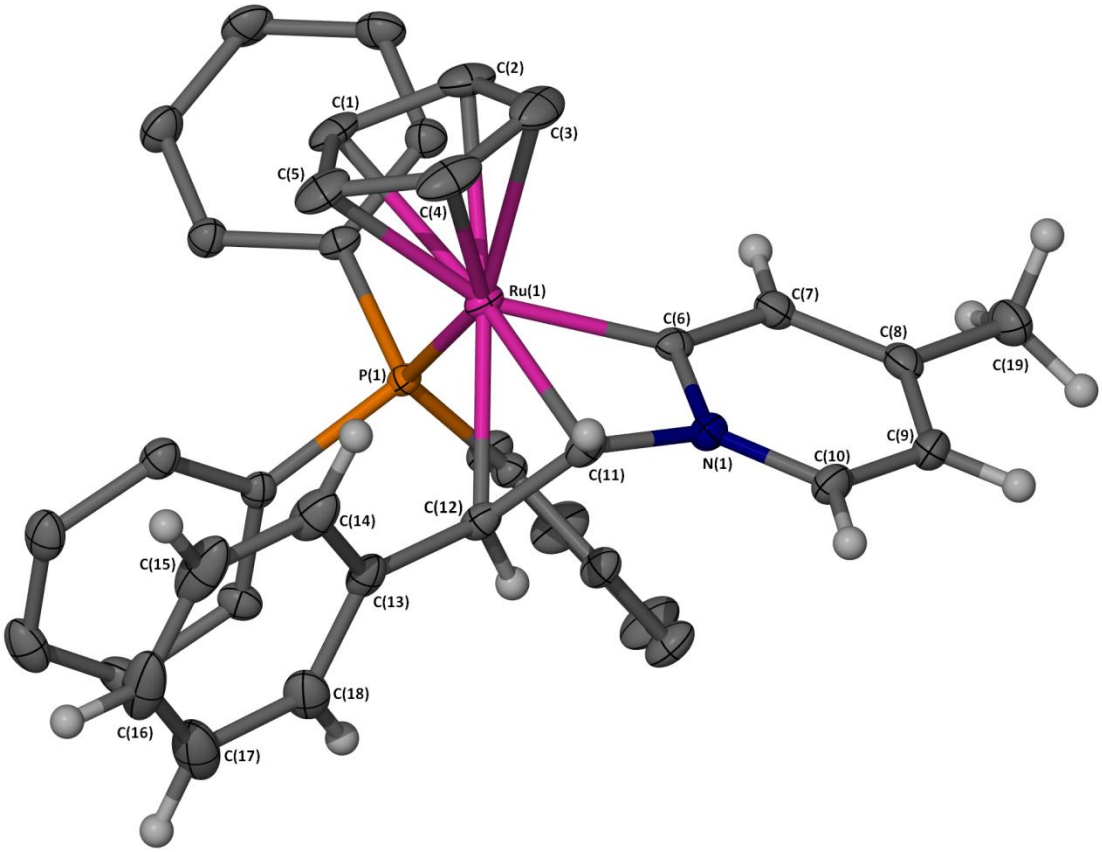

Figure 6.1: X-Seed diagram of $[Ru(\eta^5\text{-}C_5H_5)(PPh_3)(\kappa^3\text{-}C_3\text{-}(4\text{-}Me\text{-}C_5H_3N)CH{=}CH(C_6H_5)]^+$ from complex **22**$^{\mathbf{Me,H}}$. Selected hydrogen atoms, a dichloromethane molecule and $[PF_6]^-$ anion have been omitted for clarity, and where shown the thermal ellipsoids are at a 50 % probability level. The $[PF_6]^-$ anion was disordered, where the fluorine atoms were in two positions.

	Bond lengths (Å)		Bond angles (°)
C(3)-Ru(1)	2.217(2)	C(6)-Ru(1)-P(1)	90.79(5)
C(2)-Ru(1)	2.213(2)	C(12)-Ru(1)-P(1)	84.86(5)
C(1)-Ru(1)	2.251(2)	C(6)-Ru(1)-C(12)	83.26(7)
C(5)-Ru(1)	2.294(2)	C(12)-C(11)-N(1)	117.03(17)
C(4)-Ru(1)	2.250(2)	C(6)-N(1)-C(11)	103.73(15)
C(6)-Ru(1)	2.0183(19)	N(1)-C(6)-Ru(1)	100.20(13)
C(6)-N(1)	1.360(2)	N(1)-C(11)-Ru(1)	91.62(11)
C(11)-N(1)	1.457(2)	N(1)-C(6)-C(7)	116.31(17)
C(11)-C(12)	1.410(3)	C(10)-N(1)-C(6)	125.87(17)
C(12)-Ru(1)	2.272(2)	C(9)-C(10)-N(1)	117.69(19)
C(11)-Ru(1)	2.1435(19)	C(10)-C(9)-C(8)	120.29(19)
C(12)-C(13)	1.478(3)	C(7)-C(8)-C(9)	119.27(19)
C(10)-N(1)	1.351(2)	C(8)-C(7)-C(6)	120.53(19)
C(9)-C(10)	1.370(3)		
C(8)-C(9)	1.408(3)		
C(7)-C(8)	1.387(3)		
C(6)- C(7)	1.400(3)		
P(1)-Ru(1)	2.3215(5)		

Table 6.1: Selected bond lengths (Å) and angles (°) for complex **22^{Me,H}**.

6.3.2 Reaction between complex 10^{Me} with 4-ethynyl-α,α,α-trifluorotoluene

In the previous studies with **10^{H}** and terminal alkynes, 4-ethynyl-α,α,α-trifluorotoluene displayed the highest selectivity as it yielded one major ruthenium-containing complex **22^{H,CF3}**. The effect of a 4-CF_3 substituent on the phenyl ring of the terminal alkyne was investigated and compared with the analogous reaction with **10^{H}**.

The stoichiometric addition of 4-ethynyl-α,α,α-trifluorotoluene to **10^{Me}** in d_2-dichloromethane was monitored *via* NMR spectroscopy (Scheme 6.7). The initial NMR spectra recorded exhibited resonances for three new ruthenium-containing complexes, a minor unknown complex, **19$^{Me,C6H4-4-CF3}$** and **20^{CF3}**. After 24 hours the reaction mixture displayed a new set of resonances belonging to a new ruthenium-containing complex **22^{Me,CF3}**, and after 7 days **22^{Me,CF3}** was the major species.

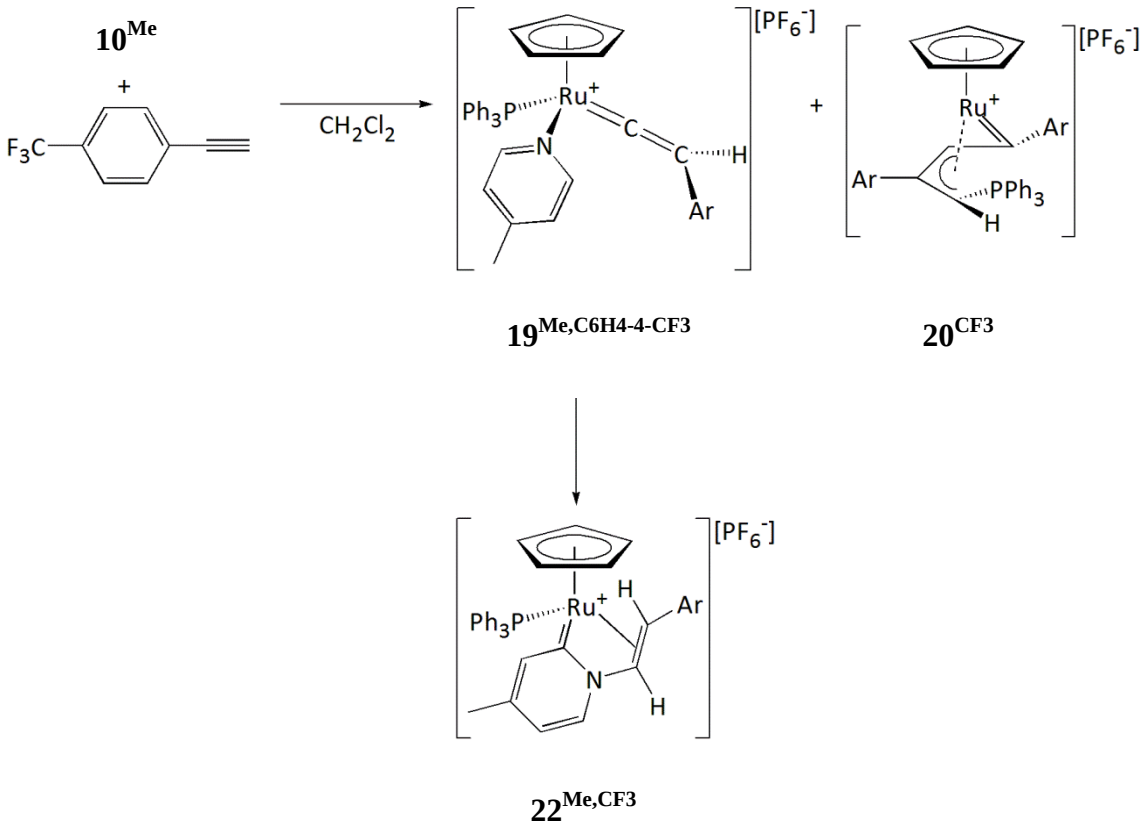

Scheme 6.7: Stoichiometric reaction between **10**$^{\mathbf{Me}}$ and 4-ethynyl-α,α,α-trifluorotoluene in dichloromethane, where Ar = C_6H_4-4-CF_3.

6.3.2.1 Identification of the minor unknown species

The minor unknown species was only observed in the initial NMR spectra. In the ^{1}H NMR spectrum a singlet signal at 4.98 ppm due to the cyclopentadienyl ligand of this complex. The ^{31}P{^{1}H} NMR spectrum exhibited a resonance at 53.1 ppm for the corresponding triphenylphosphine ligand. The minor unknown species was a short-lived intermediate and displayed similar characteristics to the previous reactions.

*6.3.2.2 Identification of complex **19**$^{Me,C6H4-4-CF3}$*

The NMR spectra exhibited resonances characteristic of a vinylidene-containing complex **19**$^{\mathbf{Me,\ C6H4-4-CF3}}$. The ^{1}H NMR spectrum exhibited broad peaks at 5.51 (5H) and 5.14 (1H) ppm for the cyclopentadienyl ligand and the vinylidene proton on the β carbon atom respectively. A set of resonances at 2.25 (s, 3H), 6.79 (d, 2H, $^3J_{HH}$ = 6.0 Hz) and 8.14 (d, 2H, $^3J_{HH}$ = 6.0 Hz) were integrated with respect to the peak at 5.51 ppm, and were assigned as a coordinated 4-methylpyridine ligand. The ^{31}P{^{1}H} NMR spectrum exhibited a resonance at 51.9 ppm for a coordinated triphenylphosphine ligand of **19**$^{\mathbf{Me,C6H4-4-CF3}}$. The complex **19**$^{\mathbf{Me,C6H4-4-CF3}}$ was the major new ruthenium-containing species in the reaction mixture, however it could not be isolated as it was a short-lived intermediate and reacted further to give **22**$^{\mathbf{Me,CF3}}$.

6.3.2.3 Identification of complex $\boldsymbol{20^{CF3}}$

The reaction was conducted in the absence of excess 4-methylpyridine, and due to this resonances similar to $\mathbf{20^{H}}$ were observed in the crude reaction mixture. This species was thought to be $\mathbf{20^{CF3}}$, and the assignment was based on the earlier observations with $\mathbf{20^{H}}$. Since $\mathbf{20^{CF3}}$ was a side-product, it has been tentatively assigned. The initial ^{1}H NMR spectrum exhibited a resonance at 5.18 ppm in the cyclopentadienyl region. Additionally, the ^{31}P{^{1}H} NMR spectrum displayed a peak at 31.1 ppm for the triphenylphosphine ligand, and this chemical shift is similar for the π-allyl carbene complex, $\mathbf{20^{H}}$.[132, 136, 139] After 7 days, the resonances belonging to $\mathbf{20^{CF3}}$ began to decrease in intensity. This is similar to what was previously observed for $\mathbf{20^{H}}$ by Kirchner *et al.*[136]

6.3.2.4 Identification of $\boldsymbol{22^{Me,CF3}}$

When the reaction reached completion, $\mathbf{22^{Me,CF3}}$ was the major-ruthenium-containing species present in the crude reaction mixture. The product $\mathbf{22^{Me,CF3}}$ was purified *via* the slow diffusion of pentane into a dichloromethane layer containing $\mathbf{22^{Me,CF3}}$ to yield a pale yellow precipitate which was fully characterised by NMR spectroscopy, high resolution ESI-MS and elemental analysis.

The ^{1}H NMR spectrum of $\mathbf{22^{Me,CF3}}$ displayed resonances at 4.96 (s, 5H), 3.62 (dd, 1H, $^{3}J_{HP}$ = 11.6 Hz, $^{3}J_{HH}$ = 7.7 Hz) and 6.68 (d, 1H, $^{3}J_{HH}$ = 7.7 Hz) ppm for the cyclopentadienyl ligand and the two alkene protons respectively. The aromatic region of the ^{1}H NMR spectrum contained both sharp and broad peaks. Through a set of 2D experiments ^{1}H-^{1}H COSY, ^{1}H-^{13}C HSQC and ^{1}H-^{13}C HMBC, a set of three sharp peaks were found to couple to each other at 7.82 (d, 1H, $^{3}J_{HH}$ = 6.8 Hz), 6.85 and 6.81 (s, 1H) ppm. These resonances originated from the 4-methylpyridine ligand; however $\mathbf{22^{Me,CF3}}$ was missing a proton from the proton at the C-2 position of the N-containing heterocycle. The broad peaks were assigned to the triphenylphosphine ligand, based on the behaviour of previous complexes $\mathbf{22^{H,H}}$ and $\mathbf{22^{H,CF3}}$. The ^{31}P{^{1}H} NMR spectrum exhibited a singlet peak at 52.9 ppm for a coordinated triphenylphosphine ligand of $\mathbf{22^{Me,CF3}}$. A ^{13}C{^{1}H} NMR spectrum of $\mathbf{22^{Me,CF3}}$ displayed a doublet at 177.1 ppm with a $^{2}J_{CP}$ = ~18 Hz, due to a Ru-C bond present in $\mathbf{22^{Me,CF3}}$. A broad peak at 65.9 ppm was assigned to an alkene carbon atom, unfortunately the other alkene atom was not observed in the ^{13}C{^{1}H} NMR spectrum and therefore a 2D ^{1}H-^{13}C HSQC experiment was used to identify a cross-peak at approximately 54.1 ppm. The data suggested that a

C-H functionalisation reaction had occurred creating a new Ru-C bond, where the proton has been abstracted from a 4-methylpyridine ligand at the C-2 position.

The high resolution ESI-MS displayed a *m/z* peak with a ruthenium isotope pattern at 692.1188, this was interpreted as the cationic species $[Ru(\eta^5\text{-}C_5H_5)(PPh_3)(4\text{-}CH_3\text{-}C_5H_3NCHCHC_6H_4\text{-}4\text{-}CF_3)]^+$ of **22**$^{\mathbf{Me,CF3}}$, and was found to be within an error 0.7 mDa. An elemental analysis of the resulting pale yellow precipitate was within an error of 0.3 %.

Crystals suitable for X-ray diffraction were obtained *via* the slow diffusion of pentane into a dichloromethane layer containing **22**$^{\mathbf{Me,CF3}}$, where the unit cell contained two **22**$^{\mathbf{Me,CF3}}$ structures. The structure was found to contain a pyridylidene ligand, which was coordinated to an alkene group *via* the nitrogen atom. The geometry around the ruthenium centre could be described as a distorted octahedral structure, as the C(6)-Ru(1)-P(1), C(12)-Ru(1)-P(1) and C(6)-Ru(1)-C(12) bond angles were found to be 90.64(12), 83.71(11) and 83.91(15) ° respectively. The ruthenium to cyclopentadienyl ligand bond lengths ranged from 2.219(4) to 2.260(5) Å. The bond length of the ruthenium to pyridylidene ligand, C(6)-Ru(1) was 2.028(4) Å. The P(1)-Ru(1) bond length was 2.3167(11) Å.

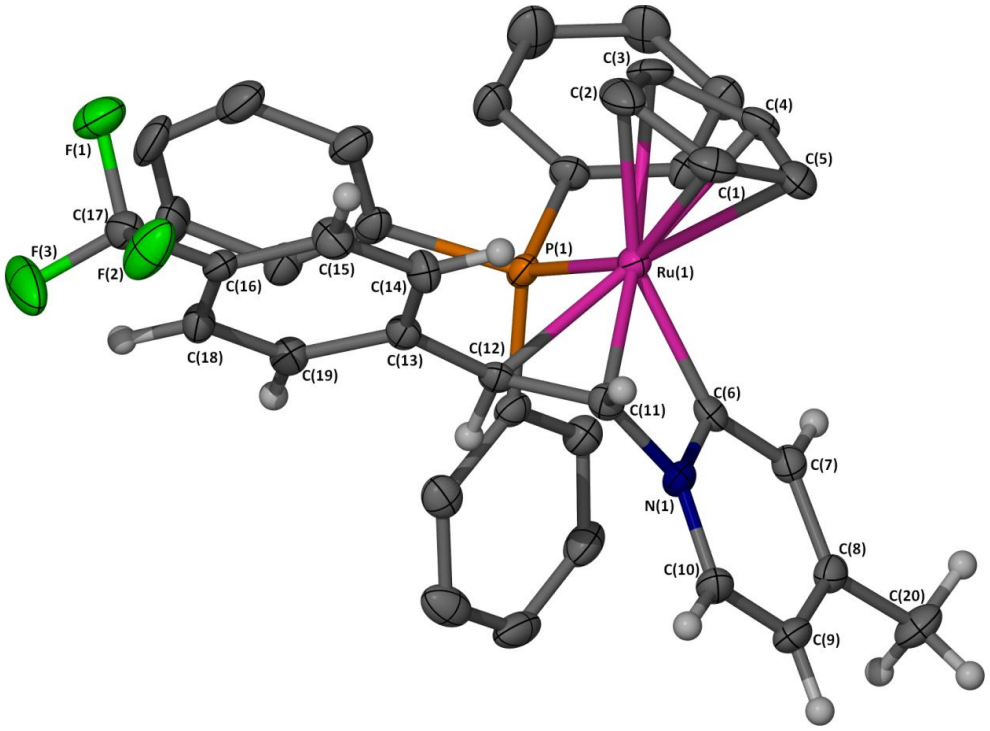

Figure 6.2: X-Seed diagram of $[Ru(\eta^5\text{-}C_5H_5)(PPh_3)(\kappa^3\text{-}C_3\text{-}(4\text{-}Me\text{-}C_5H_3N)CH{=}CH(C_6H_4\text{-}4\text{-}CF_3)]^+$ from complex **22**$^{\mathbf{Me,CF3}}$. The unit cell contains two structures of **22**$^{\mathbf{Me,CF3}}$, where only one of these has been displayed. Selected hydrogen atoms and the $[PF_6]^-$ anion have been omitted for clarity, and where shown the thermal ellipsoids are at a 50 % probability level.

	Bond lengths (Å)		Bond angles (°)
C(3)-Ru(1)	2.224(4)	C(6)-Ru(1)-P(1)	90.64(12)
C(2)-Ru(1)	2.260(5)	C(12)-Ru(1)-P(1)	83.71(11)
C(1)-Ru(1)	2.247(4)	C(6)-Ru(1)-C(12)	83.91(15
C(5)-Ru(1)	2.239(4)	C(12)-C(11)-N(1)	117.2(4)
C(4)-Ru(1)	2.219(4)	C(6)-N(1)-C(11)	103.7(3)
C(6)-Ru(1)	2.028(4)	N(1)-C(6)-Ru(1)	100.0(3)
C(6)-N(1)	1.359(5)	N(1)-C(11)-Ru(1)	91.9(2)
C(11)-N(1)	1.463(5)	N(1)-C(6)-C(7)	115.6(4)
C(11)-C(12)	1.408(6)	C(10)-N(1)-C(6)	126.9(4)
C(12)-Ru(1)	2.252(4)	C(9)-C(10)-N(1)	117.5(4)
C(11)-Ru(1)	2.138(4)	C(10)-C(9)-C(8)	119.8(4)
C(12)-C(13)	1.476(6)	C(7)-C(8)-C(9)	119.8(4)
C(10)-N(1)	1.341(5)	C(8)-C(7)-C(6)	120.4(4)
C(9)-C(10)	1.372(6)		
C(8)-C(9)	1.403(6)		
C(7)-C(8)	1.389(6)		
C(6)-C(7)	1.396(6)		
P(1)-Ru(1)	2.3246(12)		

Table 6.2: Selected bond lengths (Å) and angles (°) for complex **22**$^{\mathbf{Me,CF3}}$.

6.3.2.5 Deprotonation of 22^{Me,CF3}

The addition of DABCO to a dichloromethane solution containing **22**$^{\mathbf{Me,CF3}}$ resulted in the formation of **23**$^{\mathbf{Me,CF3}}$. The complex **23**$^{\mathbf{Me,CF3}}$ was fully characterised using NMR spectroscopy, high resolution ESI-MS, elemental analysis and single crystal X-ray crystallography.

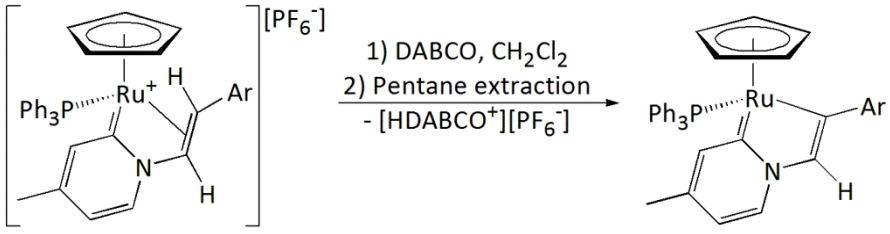

22$^{\mathbf{Me,CF3}}$ **23**$^{\mathbf{Me,CF3}}$

Scheme 6.8: Deprotonation of **22**$^{\mathbf{Me,CF3}}$ with DABCO in dichloromethane, where Ar = C_6H_4-4-CF_3.

The ^{1}H NMR spectrum exhibited similar resonances to the species **23^{Me,H}**. In the ^{1}H NMR spectrum the alkene peaks were no longer observed at 3.62 and 6.68 ppm, the total integration of the protons present in the new complex had reduced by 1H, suggesting a deprotonation reaction had occurred at the alkene functional group. In the ^{1}H NMR spectrum the resonances belonging to the N-containing heterocycle were observed at 2.17 (s, 3H), 6.36 (dd, 1H, $^{3}J_{HH}$ = 6.5 Hz, $^{4}J_{HH}$ = 1.7 Hz), 7.72 (d, 1H, $^{3}J_{HH}$ = 6.4 Hz) and 7.96 (s, 1H) ppm, which indicated the C-H functionalisation species was still present. Also a doublet peak with at 6.98 ppm with $^{4}J_{HP}$ of 2.4 Hz was observed with an integration of 1H, this was assigned to the proton of the metallacycle. Interestingly the aromatic region of the ^{1}H NMR spectrum now exhibited sharp resonances for the triphenylphosphine ligand indicating there was no longer restricted rotation of the Ru-P bond in **23^{Me,CF3}**. The ^{31}P{^{1}H} NMR spectrum displayed a downfield shift for the triphenylphosphine ligand, as a singlet at 61.7 ppm was observed. The ^{13}C{^{1}H}NMR spectrum displayed two doublets at 187.9 and 217.8 ppm with $^{2}J_{CP}$ of 13.2 and 15.8 Hz respectively. The data suggested that there were two Ru-C bonds in **23^{Me,CF3}**. The other carbon atom on the metallacycle was bonded to a hydrogen atom and was observed at 132.4 ppm. The CF_3 substituent at the 4-position of the phenyl ring displayed quartet couplings in the ^{13}C{^{1}H}NMR spectrum at 125.5 (q, $^{1}J_{CF}$ = 271 Hz), 126.1 (q, $^{2}J_{CF}$ = 32.0 Hz) and 124.2 (q, $^{3}J_{CF}$ = 3.7 Hz) ppm.

A high resolution ESI-MS of **23^{Me,CF3}** displayed a ruthenium isotope pattern for a *m/z* peak at 691.1188 which was assigned as the complex $[Ru(\eta^{5}\text{-}C_5H_5)(PPh_3)(4\text{-}Me\text{-}C_5H_3NCHCC_6H_4\text{-}4\text{-}CF_3)]^{+}$ and was consistent with a deprotonation reaction. An elemental analysis of the red precipitate was found to be within an error of 0.3 %.

Crystals suitable for X-ray diffraction of **23^{Me,CF3}** were obtained by cooling a pentane solution of the product at -20 °C. The structure confirmed that a proton has been abstracted from the alkene functional group to give a five-membered metallacyclic complex. The data obtained for **23^{Me,CF3}** was not of sufficient quality to permit a discussion of the structural metrics.

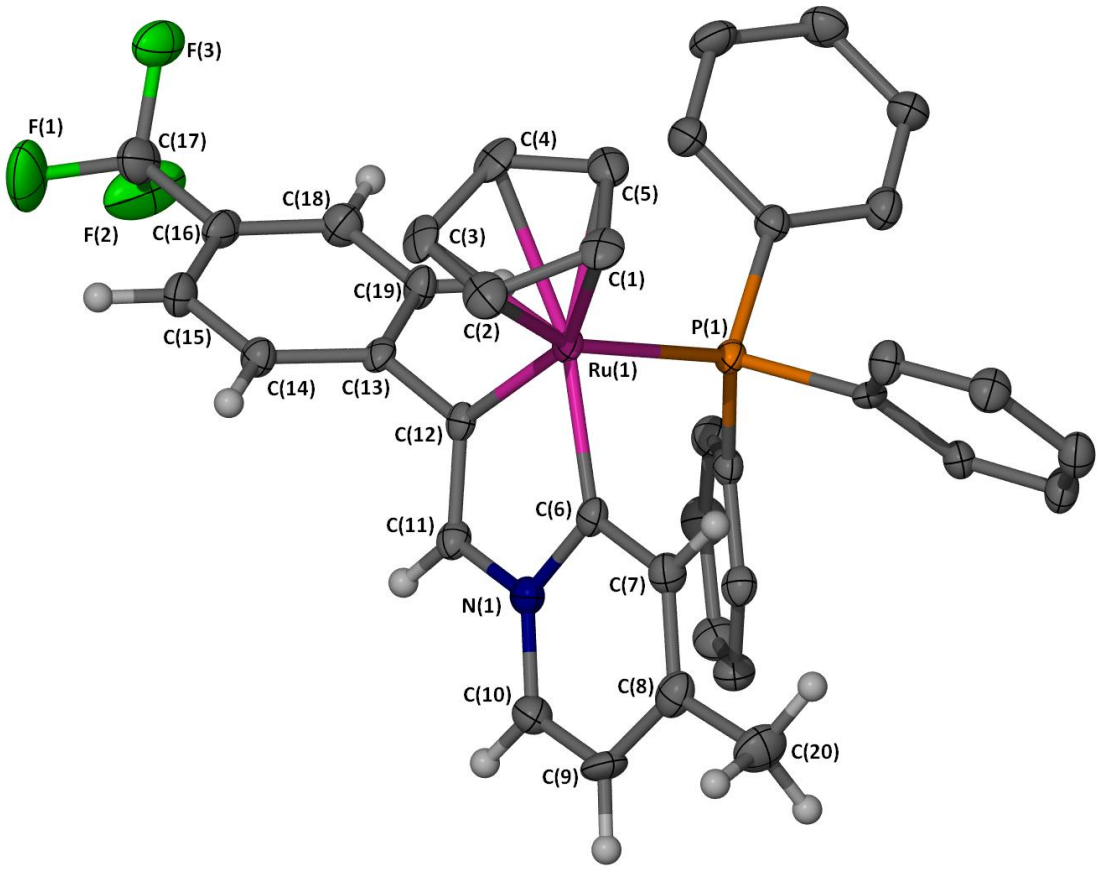

Figure 6.3: X-Seed diagram of complex **23**^{Me,CF3}. Selected hydrogen atoms and a pentane molecule have been omitted for clarity, and where shown the thermal ellipsoids are at a 50 % probability level.

6.4 Reactivity of complex 10^{NMe2} with alkynes

The previous N-containing heterocycles studied are pyridine and 4-methylpyridine, where the N-containing ligand is more electron-donating due to an inductive effect. The N-containing heterocycle 4-dimethylaminopyridine, has an NMe_2 group in the 4-position of the aromatic ring, and through conjugation donates electron density to the C-3/5 positions and the nitrogen atom, which makes it an extremely good donating ligand. The reactivity of $\mathbf{10^{NMe2}}$ with various terminal alkynes has been investigated.

6.4.1 Reaction between complex 10^{NMe2} with phenylacetylene

The stoichiometric addition of phenylacetylene to $\mathbf{10^{NMe2}}$ in d_2-dichloromethane was monitored *via* NMR spectroscopy (Scheme 6.9). The reaction mixture exhibited many resonances belonging to different unidentified ruthenium-containing complexes; and some of the resonances were cautiously assigned to some of the ruthenium-containing species observed previously. However, the reaction did yield one major ruthenium-containing complex. The reaction was repeated with the stoichiometric addition of ^{13}C-phenylacetylene to $\mathbf{10^{NMe2}}$ in d_2-dichloromethane to obtain further information.

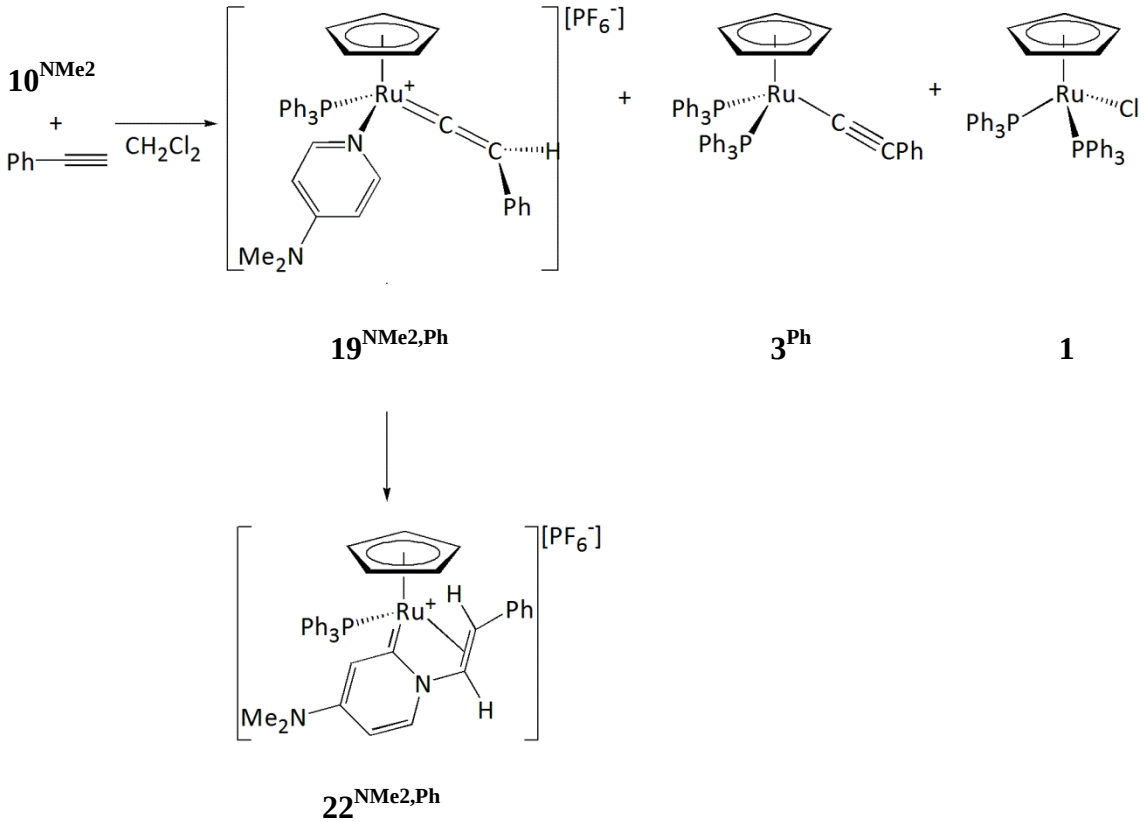

Scheme 6.9: Stoichiometric reaction between $\mathbf{10^{NMe2}}$ and phenylacetylene in dichloromethane.

The initial NMR spectra were recorded within two hours from the addition of phenylacetylene, resonances for a minor unknown species and vinylidene-containing species **19**$^{\mathbf{NMe2,Ph}}$ were observed. After 10 days the NMR spectra displayed peaks for a major ruthenium-containing complex **22**$^{\mathbf{NMe2,H}}$.

There were also several other ruthenium-containing complexes present in the reaction mixture as the reaction proceeded. In the ^{1}H NMR spectrum after 10 days, the cyclopentadienyl region displayed peaks at 4.09 (1.3H), 4.30 (0.4 H), 4.32 (0.9 H), 4.51 (0.4 H) and 4.70 (0.9 H) ppm with respect to the major cyclopentadienyl peak at 4.86 ppm (5H). The ^{31}P{^{1}H} NMR spectrum exhibited resonances at 17.2, 40.3, 43.6, 51.6 and 57.7 ppm. One of these species was identified as [Ru(η^5-C_5H_5)(PPh_3)$_2$Cl], **1** where resonances in the ^{1}H NMR spectrum at 4.09 ppm and in the ^{31}P{^{1}H} NMR spectrum at 40.3 ppm for the triphenylphosphine ligands were observed to increase in intensity after 48 hours. Additionally, an acetylide-containing complex was identified as [Ru(η^5-C_5H_5)(C≡CPh)(PPh_3)$_2$] **3**$^{\mathbf{Ph}}$ where the resonances were observed in the ^{1}H NMR spectrum at 4.32 ppm for the cyclopentadienyl ligand, and in the ^{31}P{^{1}H} NMR spectrum at 51.6 ppm for the triphenylphosphine ligands. The reaction with ^{13}C-phenylacetylene displayed a doublet at 51.6 ppm with a $^{2}J_{PC}$ = 24.3 Hz and the ^{13}C{^{1}H} NMR spectrum exhibited a small triplet at 116.7 ppm with a $^{2}J_{CP}$ = 24.3 Hz.

The reaction yielded several ruthenium-containing species and therefore different reaction conditions were investigated in order to avoid the formation of **1** and **3**$^{\mathbf{Ph}}$ in the reaction mixture. In the NMR scale reactions, the reaction was left to proceed at room temperature and the intensity of **1** increased over time (48 hours) as this was a thermodynamic sink. Hence in order to avoid the formation of **1**, the reaction mixture of the stoichiometric addition of phenylacetylene to **10**$^{\mathbf{NMe2}}$ in dichloromethane was heated at 50 °C for 22 hours. Unfortunately, under these reaction conditions there was an increase of **1** in the reaction mixture.

A difference in reactivity was observed in **10**$^{\mathbf{NMe2}}$ in comparison to **10**$^{\mathbf{H}}$ and **10**$^{\mathbf{Me}}$ as the stoichiometric addition of phenylacetylene to **10**$^{\mathbf{NMe2}}$ did not yield the species **20**$^{\mathbf{H}}$ or **21**$^{\mathbf{NMe2,H}}$. The reaction pathway for **20**$^{\mathbf{H}}$ requires two alkyne molecules to coordinate at the ruthenium centre (Section 1.5) and as 4-dimethylaminopyridine is a stronger donor ligand this presumably indicates that both of the N-containing heterocycles do not dissociate from the ruthenium centre.[132, 138]

6.4.1.1 Identification of the minor unknown species

The NMR spectra displayed resonances for a short-lived complex from the addition of phenylacetylene to **10**$^{\mathbf{NMe2}}$, which was only observed in the initial NMR spectra. The ^{1}H NMR spectrum exhibited a peak at 4.85 ppm for the cyclopentadienyl ligand of this species. The ^{31}P{^{1}H} NMR spectrum displayed a singlet at 53.9 ppm for a coordinated triphenylphosphine ligand. When the reaction was repeated with ^{13}C-phenylacetylene the ^{31}P{^{1}H} NMR spectrum contained a doublet resonance at 53.9 ppm with a J_{PC} = 12.5 Hz.

*6.4.1.2 Identification of complex **19**$^{NMe2, Ph}$*

From the initial NMR spectra recorded within two hours after alkyne addition, the ^{1}H NMR spectrum exhibited broad peaks at 5.40 and 5.04 ppm with integrations of 5H and 1H respectively. The ^{31}P{^{1}H} NMR spectrum exhibited a minor broad peak 52.7 ppm for the triphenylphosphine. This data should be considered cautiously as proof of the species **19**$^{\mathbf{NMe2,Ph}}$ as these resonances were extremely minor in the reaction mixture and were not observed after 24 hours.

From the reaction of ^{13}C-phenylacetylene with **10**$^{\mathbf{NMe2}}$, the initial ^{31}P{^{1}H} and ^{13}C{^{1}H} NMR spectra did not display resonances for the α-carbon atom of the vinylidene ligand of **^{13}C-19**$^{\mathbf{NMe2,Ph}}$. However, upon running a ^{13}C{^{1}H} NMR spectrum with additional scans (4096 scans) three resonances were observed at 349.4 (d, $^{2}J_{PC}$ = 18.3 Hz), 351.4 (broad) and 353.6 (d, $^{2}J_{PC}$ = 16.8 Hz) ppm . This could potentially be due to different conformations of **^{13}C-19**$^{\mathbf{NMe2,Ph}}$ in solution, where either the vinylidene or 4-dimethylaminopyridine ligands are undergoing slow rotation at the ruthenium centre. The ^{13}C{^{1}H} NMR spectra conducted later on the reaction mixture all required 4096 scans to observe the α-carbon atom of the vinylidene ligand. After 24 hours, the ^{13}C{^{1}H} NMR spectrum only displayed one resonance at 353.6 ppm for the α-carbon atom of the vinylidene ligand. The ^{31}P{^{1}H} NMR spectrum after 24 hours displayed a minor peak at 52.8 ppm as a doublet with a $^{2}J_{PC}$ of ~16 Hz.

These data suggest that a vinylidene-containing species is present in the reaction mixture, and is most likely **19**$^{\mathbf{NMe2,Ph}}$ (based on previous findings). However, the vinylidene-containing complex was only a very minor part of the reaction mixture. The difference in reactivity of **10**$^{\mathbf{NMe2}}$ in comparison to **10**$^{\mathbf{H}}$ and **10**$^{\mathbf{Me}}$ could be due to the strong ligand donor properties of the 4-dimethylaminopyridine ligand.

6.4.1.3 Identification of $\mathbf{22^{NMe2,Ph}}$

After 10 days there appeared to be one major ruthenium-containing complex, $\mathbf{22^{NMe2,Ph}}$ present in the reaction mixture. The product was purified *via* the slow diffusion of pentane into a dichloromethane layer containing $\mathbf{22^{NMe2,Ph}}$ and the resulting pale yellow crystals were collected. Unfortunately, due to the number of ruthenium complexes present in the crude reaction mixture pure isolation of this species was not possible.

The ^{1}H NMR spectrum exhibited a resonance at 4.86 ppm for the cyclopentadienyl ligand. In addition in the ^{1}H NMR spectrum resonances at 3.55 (dd, 1H, $^{3}J_{HP}$ = 11.7 Hz, $^{3}J_{HH}$ = 7.9 Hz) and at 6.32 (dd, 1H, $^{3}J_{HH}$ = 7.9 Hz, , $^{4}J_{HP}$ = 1.6 Hz) ppm were assigned to the alkene protons of $\mathbf{22^{NMe2,Ph}}$ and found to couple in a 2D ^{1}H-^{1}H COSY experiment. When the reaction was repeated using ^{13}C-phenylacetylene, the alkene peak at 6.32 ppm now exhibited a large $^{1}J_{HC}$ coupling of ~185 Hz. The aromatic region of $\mathbf{22^{NMe2,Ph}}$ contained many resonances, however the 2D ^{1}H-^{1}H COSY experiment assisted in identifying the protons belonging to the N-containing heterocycle at 5.81 (1H), 6.23 (1H) and 7.34 ppm. This suggested that an aromatic proton was missing from the originating 4-dimethylaminopyridine ligand. Interestingly, in the ^{1}H NMR spectrum the methyl substituents of the NMe_2 group displayed a broad peak at 2.82 ppm (6H), indicating fluxional behaviour on the NMR timescale. This behaviour could potentially be attributed to each of the methyl groups experiencing a different environment due to restricted rotation around the C-N bond. The ^{31}P{^{1}H} NMR spectrum exhibited a singlet resonance at 55.3 ppm for the coordinated triphenylphosphine ligand, and this resonance remained a singlet in the reaction where ^{13}C-phenylacetylene was employed.

A high resolution ESI-MS of a reaction mixture containing $\mathbf{22^{NMe2,Ph}}$ displayed a *m/z* peak with a ruthenium isotope pattern of 653.1655 which was consistent with the cationic fragment of $[Ru(\eta^5\text{-}C_5H_5)(PPh_3)(4\text{-}NMe_2\text{-}C_5H_3NCHCHC_6H_5)]^+$ and was found to be within in an error of 0.5 mDa.

Crystals suitable for X-ray diffraction were obtained *via* the slow diffusion of pentane into a dichloromethane layer containing $\mathbf{22^{NMe2,Ph}}$. The structure of $\mathbf{22^{NMe2,Ph}}$ revealed that the 4-dimethylaminopyridine molecule had undergone a C-H functionalisation reaction to give a pyridylidene ligand which was bonded through the nitrogen atom to an alkene group. The bond angles around the ruthenium centre C(6)-Ru(1)-P(1), C(12)-Ru(1)-P(1) and C(6)-Ru(1)-C(12) were 89.63(6), 88.70(6) and 83.83(9) ° respectively, therefore making the geometry of the ruthenium complex a distorted octahedron. The

ruthenium to cyclopentadienyl ligand bonds on average were 2.2382 Å. The ruthenium to alkene bond lengths C(11)-Ru(1) and C(12)-Ru(1) were 2.140(2) and 2.242(2) Å respectively and significantly unequal.[318, 319] A P(1)-Ru(1) bond length of 2.3302(6) was found. There were significantly shorter carbon-carbon bond lengths in the pyridylidene fragment of C(7)-C(6) and C(10)-C(9). Similar observations were made by Bercaw *et al*. where a 4-NMe_2 substituent on a pyridylidene ligand was present.[188]

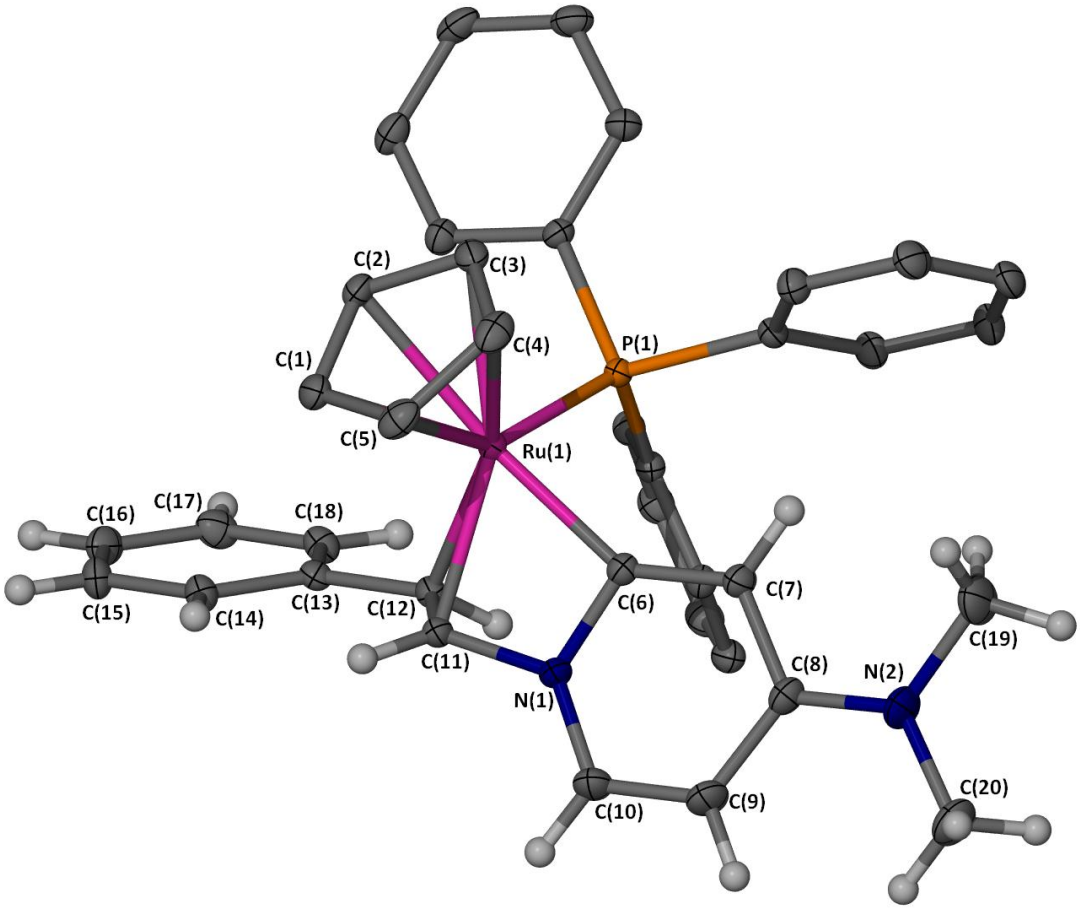

Figure 6.4: X-Seed diagram of $[Ru(\eta^5\text{-}C_5H_5)(PPh_3)(\kappa^3\text{-}C_3\text{-}(4\text{-}NMe_2\text{-}C_5H_4N)CH{=}CH(C_6H_5)]^+$ from complex **22**$^{\mathbf{NMe2,H}}$. Selected hydrogen atoms, two dichloromethane molecules and the $[PF_6]^-$ anion have been omitted for clarity, and where shown the thermal ellipsoids are at a 50 % probability level. Both of the dichloromethane molecules were disordered over two positions, the first was disordered in a ratio of 88:12 and the second was constrained to a disorder of 50:50.

	Bond lengths (Å)		Bond angles (°)
C(4)-Ru(1)	2.248(2)	C(6)-Ru(1)-P(1)	89.63(6)
C(5)-Ru(1)	2.214(2)	C(12)-Ru(1)-P(1)	88.70(6)
C(1)-Ru(1)	2.226(2)	C(6)-Ru(1)-C(12)	83.83(9)
C(3)-Ru(1)	2.241(2)	C(6)-Ru(1)-C(11)	64.37(8)
C(2)-Ru(1)	2.262(2)	N(1)-C(6)-Ru(1)	98.80(14)
C(6)-Ru(1)	2.043(2)	C(6)-N(1)-C(11)	104.88(17)
C(11)-Ru(1)	2.140(2)	C(12)-C(11)-N(1)	117.0(2)
C(12)-Ru(1)	2.242(2)	C(11)-C(12)-C(13)	124.1(2)
C(13)-C(12)	1.479(3)	C(10)-N(1)-C(6)	124.7(2)
C(27)-C(11)	1.407(3)	N(1)-C(10)-C(9)	119.2(2)
C(11)-N(1)	1.449(3)	C(10)-C(9)-C(8)	120.2(2)
C(6)-N(1)	1.363(3)	C(7)-C(8)-C(9)	117.6(2)
C(6)-C(7)	1.380(3)	C(6)-C(7)-C(8)	121.0(2)
C(7)-C(8)	1.418(3)		
C(8)-C(9)	1.425(4)		
C(9)-C(10)	1.360(4)		
C(10)-N(1)	1.350(3)		
C(8)-N(2)	1.349(3)		
P(1)-Ru(1)	2.3302(6)		

Table 6.3: Selected bond lengths (Å) and angles (°) for complex **22**$^{\mathbf{NMe2,H}}$.

6.4.2 Reaction between complex 10^{NMe2} with 4-ethynyl-α,α,α-trifluorotoluene

The stoichiometric addition of 4-ethynyl-α,α,α-trifluorotoluene to **10**^{NMe2} in a d_2-dichloromethane solution was monitored *via* NMR spectroscopy (Scheme 6.10). As the reaction proceeded six different ruthenium-containing species were observed, however not all of these were identified. The species **1** was identified to be present in the reaction mixture, as the ^{1}H NMR spectrum exhibited a resonance at 4.09 ppm for the cyclopentadienyl ligand and the ^{31}P{^{1}H} NMR spectrum a singlet peak at 40.3 ppm for the triphenylphosphine ligands. The other resonances in the ^{31}P{^{1}H} NMR spectrum were seen at 51.6, 55.2, 57.7 and 64.1 ppm for the unknown complexes.

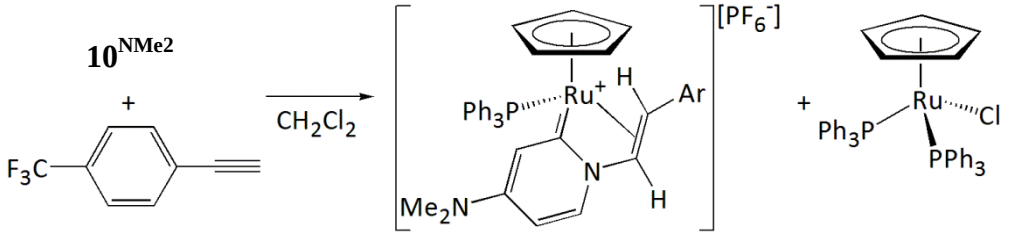

22^{NMe2,CF3} **1**

Scheme 6.10: Stoichiometric addition of 4-ethynyl-α,α,α-trifluorotoluene to **10**^{NMe2} in d_2-dichloromethane.

6.4.2.1 Identification of ***22***^{NMe2,CF3}

By studying the NMR spectra the resonances for the species **22**^{NMe2,CF3} were identified *in situ* as the major species. However, due to numerous minor side products from the reaction **22**^{NMe2,CF3} was not obtained pure and therefore not fully characterised. The ^{1}H NMR spectrum displayed resonances at 4.90, 3.48 (dd, $^{3}J_{HP}$ = 11.7 Hz, $^{3}J_{HH}$ = 7.8 Hz) and 6.44 (dd, $^{3}J_{HH}$ = 7.8 Hz, $^{3}J_{HP}$ = 1.7 Hz) ppm with relative integrations of 5:1:1 and therefore the peaks were assigned as the cyclopentadienyl ligand and the two alkene protons respectively. The protons around the nitrogen-containing heterocycle were observed at 2.80 (broad, lies underneath other peaks), 5.79 (m, 1H) and 6.25 (dd, $^{3}J_{HH}$ = 7.3 Hz, $^{4}J_{HH}$ = 2.8 Hz) ppm, where the final hydrogen atom on the ring was hidden in the aromatic region. These peaks are characteristic of the C-H functionalised species **22**^{NMe2,Ph}. The aromatic region of the ^{1}H NMR spectrum contained broad resonances probably due to the restricted rotation of the triphenylphosphine ligand (Section 5.2.1.5). The ^{31}P{^{1}H} NMR spectrum exhibited a singlet resonance at 54.7 ppm for the coordinated triphenylphosphine ligand of **22**^{NMe2,CF3}.

6.4.3 Reaction between complex $\mathbf{10^{NMe2}}$ with *tert*-butylacetylene

The stoichiometric addition of *tert*-butylacetylene to $\mathbf{10^{NMe2}}$ in d_2-dichloromethane was monitored *via* NMR spectroscopy to determine if $\mathbf{10^{NMe2}}$ displayed a similar reactivity to $\mathbf{10^{H}}$. The reaction was monitored over 18 days where few changes were observed in the ^{1}H and $^{31}P\{^{1}H\}$ NMR spectra. After 18 days, $\mathbf{10^{NMe2}}$ was the major ruthenium-containing complex. The ^{1}H NMR spectrum exhibited a resonance at 4.25 ppm for the cyclopentadienyl ligand and in the $^{31}P\{^{1}H\}$ NMR spectrum a peak at 51.4 ppm for the triphenylphosphine ligand. The peaks for *tert*-butylacetylene were observed in the ^{1}H NMR spectrum at 2.09 (1H) and 1.23 (9H) ppm for the alkyne proton and the methyl substituents respectively. Minor resonances were observed in the ^{1}H NMR spectrum at 4.09 ppm for cyclopentadienyl protons and in the $^{31}P\{^{1}H\}$ NMR spectrum at 40.4 ppm for the coordinated triphenylphosphine ligand of **1**.

6.4.4 Reaction between complex $\mathbf{10^{NMe2}}$ with 1-hexyne

The stoichiometric addition of 1-hexyne to $\mathbf{10^{NMe2}}$ in d_2-dichloromethane was monitored *via* NMR spectroscopy to determine if similar reactivity to $\mathbf{10^{H}}$ could be observed. Unfortunately the reaction gave a large number of unidentified ruthenium-containing complexes and no useful data was obtained on the nature of the species formed. One of the minor ruthenium-containing species present in the reaction mixture was identified as **1**.

6.5 Reactivity of complex 11 with alkynes

The reaction between terminal alkynes and complex **11** in d_2-dichloromethane was investigated. The 3-methylpyridine ligands introduced the concept of regioselectivity, as the C-H functionalisation could occur potentially at two locations of the N-containing heterocycle. It would be of particular interest to study as Murakami and Hori stated that the alkenylation reaction with 3-methylpyridine was regioselective with alkenylation only occurring at the C-6 position.[253]

6.5.1 Reaction between complex 11 with phenylacetylene

The stoichiometric addition of phenylacetylene to **11** in d_2-dichloromethane was monitored *via* NMR spectroscopy. The initial NMR spectra exhibited resonances for three new species $\mathbf{20^H}$, $\mathbf{25^H}$ and a minor unknown species, where the latter two complexes were short-lived intermediates. The identity of $\mathbf{20^H}$ was confirmed by comparison with the literature (Section 5.2.1.3).[139] After 24 hours the reaction mixture displayed further new resonances for **26** and $\mathbf{27a^H}$ and $\mathbf{27b^H}$. Once the reaction had reached completion there were four ruthenium-containing complexes present in the reaction mixture (Scheme 6.11).

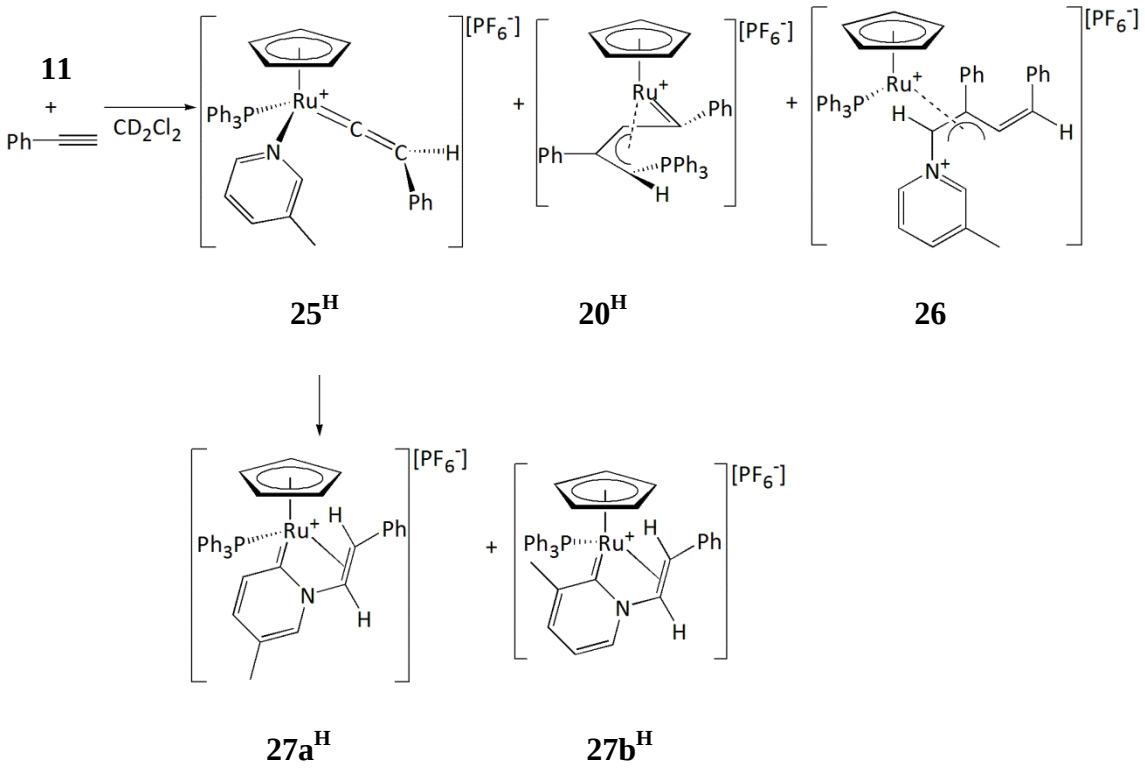

Scheme 6.11: Stoichiometric reaction between **11** and phenylacetylene in d_2-dichloromethane.

*6.5.1.1 Identification of **25^{H}***

The complex **25^{H}** was a short-lived intermediate and was characteristic of a vinylidene-containing complex. The ^{1}H NMR spectrum displayed broad resonances at 5.49 and 5.12 ppm with relative integrations of 5H and 1H, which were assigned as the cyclopentadienyl ligand and vinylidene proton on the β-carbon atom respectively. Additionally, the ^{1}H NMR spectrum displayed peaks at 1.87 (s, 3H), 6.93 (apparent t, 1H), 7.98 (s, 1H) and 8.27 (d, 1H) ppm for the coordinated 3-methylpyridine ligand. The ^{31}P{^{1}H} NMR spectrum exhibited a broad singlet resonance at 52.0 ppm for the coordinated triphenylphosphine ligand of **25^{H}**. The set of resonances belonging to **25** after 24 hours began to decrease as peaks for **27a^{H}** and **27b^{H}** increased.

*6.5.1.2 Identification of **26***

The species **26** was characteristic of the pyridinium η^{3}-butadienyl complexes, where the ^{1}H NMR spectrum exhibited a singlet peak at 4.55 ppm for a cyclopentadienyl ligand, and in the ^{31}P{^{1}H} NMR spectrum a singlet peak at 48.5 ppm was observed. A high resolution ESI-MS of the reaction mixture exhibited a ruthenium isotope peak with a *m/z* of 726.1871 which was consistent with the expected formula $[C_{45}H_{39}NPRu]^{+}$ (error of 1.3 mDa) and was equivalent to containing the fragments $[Ru(\eta^{5}\text{-}C_5H_5)(PPh_3)]^{+}$, NC_5H_5 and two PhC≡CH molecules. This species has been cautiously assigned as **26** based on similar spectroscopic characteristics to **21^{H,H}** (Section 5.2.1.4).

*6.5.1.3 Identification of complexes **27a^{H}** and **27b^{H}***

The complexes **27a^{H}** and **27b^{H}** were observed *via* ^{1}H NMR spectroscopy in the reaction mixture after 24 hours. The ^{1}H NMR spectrum exhibited two resonances at 5.07 and 4.92 ppm, where the former peak was sharp and the latter broad for the two cyclopentadienyl ligands. It is possible that the broad resonance is due to the more sterically hindered C-H functionalised species, where the 3-methyl substituent is closer to the ruthenium centre. Also in the ^{1}H NMR spectrum the alkene resonances exhibited sharp and broad features. The sharp alkene peaks were observed at 3.47 (1H, dd, $^{3}J_{HP}$ = 12.3 Hz, $^{3}J_{HH}$ = 8.0 Hz) and 6.51 (1H, dd, $^{3}J_{HH}$ = 8.0 Hz, $^{3}J_{HP}$ = 1.5 Hz) ppm with respect to the peak at 5.07 ppm. The broad alkene signals were exhibited at 3.62 (1H, broad m) and 6.62 (1H, broad d, $^{3}J_{HH}$ = 8.2 Hz) ppm with respect to the peak at 4.92 ppm. The ^{31}P{^{1}H} NMR spectrum exhibited the resonances for the triphenylphosphine ligands at 51.2 (sharp) and 53.7 (broad). A high resolution ESI displayed a *m/z* peak of 624.1387 with a ruthenium isotope pattern and was consistent with a $[Ru(\eta^{5}\text{-}C_5H_5)(PPh_3)(\kappa3\text{-}C_3\text{-}MeC_5H_3NCH{=}CHC_6H_5)]^{+}$ species.

Purification of complexes **27a**$^{\mathbf{H}}$ and **27b**$^{\mathbf{H}}$ was difficult due to the presence of complex **26** (as both of these complexes have similar solubilities, Section 5.2). Reactions with 4-ethynyl-α,α,α-trifluorotoluene were then conducted, as previous reactions indicate the absence of a pyridinium η^3-butadienyl complex with this alkyne.

6.5.2 Reaction between complex 11 with 4-ethynyl-α,α,α-trifluorotoluene

In previous reactions the 4-CF_3 substituent on the phenyl ring of the terminal alkyne has displayed a more selective reaction and the complexes of the type **21** were not observed. The stoichiometric addition of 4-ethynyl-α,α,α-trifluorotoluene to **11** to a d_2-dichloromethane solution in the presence of two equivalents of 3-methylpyridine was monitored *via* NMR spectroscopy.

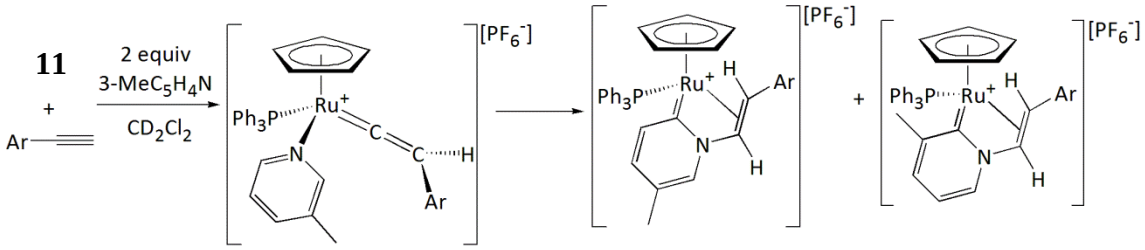

25$^{\mathbf{CF3}}$ **27a**$^{\mathbf{CF3}}$ **27b**$^{\mathbf{CF3}}$

Scheme 6.12: Stoichiometric reaction between **11** and 4-ethynyl-α,α,α-trifluorotoluene in d_2-dichloromethane in the presence of two equivalents of 3-methylpyridine.

The initial NMR spectra exhibited a set of resonances for a new ruthenium-containing complex **25**$^{\mathbf{CF3}}$. This species was found to be short-lived in solution and therefore as the resonances for **25**$^{\mathbf{CF3}}$ decreased, resonances for **27a**$^{\mathbf{CF3}}$ and **27b**$^{\mathbf{CF3}}$ increased in intensity.

6.5.2.1 Identification of 25^{CF3}

The species **25**$^{\mathbf{CF3}}$ was characteristic of a vinylidene-containing complex, as the ^{1}H NMR spectrum exhibited broad peaks at 5.52 and 5.14 ppm with integrations of 5H and 1H, which were assigned as the cyclopentadienyl ligand and the vinylidene proton on the β-carbon atom respectively. In addition, the ^{1}H NMR spectrum exhibited peaks at 8.27 (1H, d), 7.96 (1H, s), 6.96 (1H, dd) and 1.88 (3H, s) ppm for a coordinated 3-methylpyridine ligand. The ^{31}P{^{1}H} NMR spectrum displayed a broad peak at 51.2 ppm for the triphenylphosphine ligand of **25**$^{\mathbf{CF3}}$.

*6.5.2.2 Identification of complexes **27a**^{CF3} and **27b**^{CF3}*

There were two sets of resonances for **27a**^{CF3} and **27b**^{CF3} in the NMR spectra (similar to the reaction of **11** with phenylacetylene), where one of the species had a broader set of peaks. The ^{1}H NMR spectrum exhibited sharp peaks at 5.10 (s), 3.44 (dd, $^{3}J_{HP}$ = 12.3 Hz, $^{3}J_{HH}$ = 7.9 Hz) and 6.61 (dd, $^{3}J_{HP}$ = 1.7 Hz, $^{3}J_{HH}$ = 7.9 Hz) ppm for the cyclopentadienyl ligand and the two alkene protons respectively. The corroborating 3-methylpyridine displayed peaks at 6.30 (broad, 1H), 7.86 (s, 1H) ppm, where one other aromatic hydrogen atom was in the multiplet range 7.12-7.58 ppm. This suggested a C-H functionalisation reaction had occurred at the 3-methylpyridine ligand on the less hindered side to give a pyridylidene species **27a**^{CF3}. The ^{31}P{^{1}H} NMR spectrum displayed a sharp singlet at 50.5 ppm for the triphenylphosphine ligand of **27a**^{CF3}.

The broader resonances were consistent with the species **27b**^{CF3} and was confirmed by the ^{1}H NMR spectrum in the aromatic region as the pyridylidene ligand displayed the three protons on the aromatic ring at 7.82 (d, $^{3}J_{HH}$ = 6.0 Hz) and in the multiplets 7.12-7.58 and 6.93-7.05 ppm. The absence of the singlet resonance for the protons at the C-2 position on the 3-methylpyridine ligand is indicative that the isomer **27b**^{CF3} is present. The ^{31}P{^{1}H} NMR spectrum exhibited a broad peak at 53.0 ppm for the triphenylphosphine ligand of **27b**^{CF3}.

A ^{13}C{^{1}H} NMR spectrum exhibited resonances for the two C-H functionalised carbon atoms at 173.9 (d, $^{2}J_{CP}$ = 18.9 Hz) and 179.9 (d, $^{2}J_{CP}$ = 16.6 Hz) ppm for the two isomers **27a**^{CF3} and **27b**^{CF3} respectively. A high resolution ESI-MS displayed a peak with *m/z* of 692.1229 for the cationic fragment $[Ru(\eta^5\text{-}C_5H_5)(PPh_3)(\kappa^3\text{-}C_3\text{-}(Me\text{-}C_5H_3N)CH{=}CH(C_6H_4\text{-}4\text{-}CF_3)]^+$ of **27a**^{CF3} and **27b**^{CF3}.

A low variable temperature NMR study was conducted on a sample containing **27a**^{CF3} and **27b**^{CF3} in d_2-dichloromethane at 295 K and from 280 to 220 K in 20 K intervals (Figure 6.5). The ^{1}H NMR spectrum displayed sharper resonances in the aromatic region upon cooling, due to the restricted rotation around the ruthenium-phosphorus bond of the triphenylphosphine ligand. Interestingly, the two isomers displayed different rates of rotation and this could potentially be attributed to the differences in the steric properties around the metal centre. The ^{31}P{^{1}H} NMR spectrum did not display any significant changes.

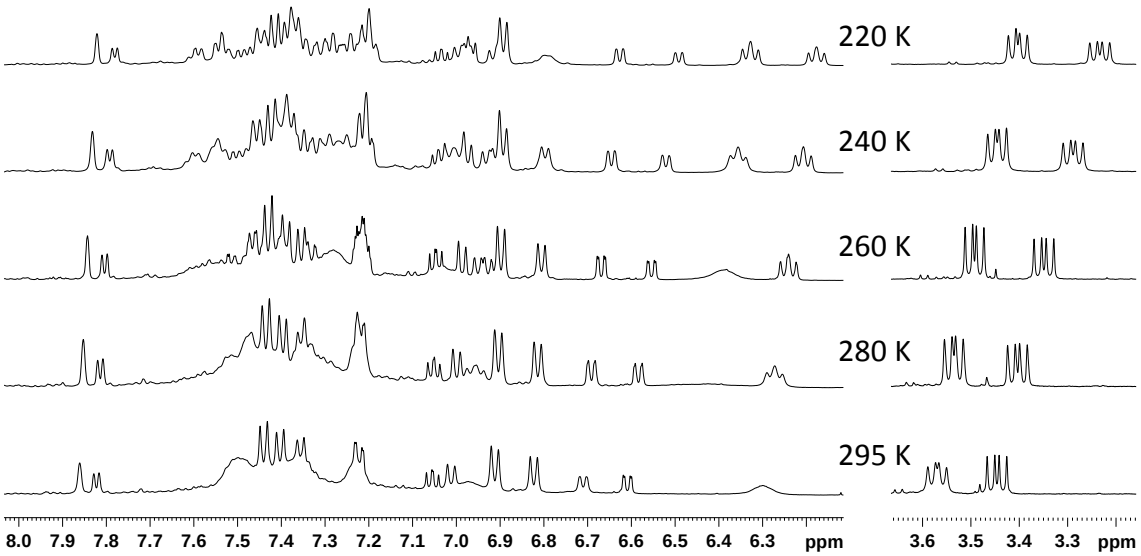

Figure 6.5: Low variable temperature ^{1}H NMR experiment of **27a**^{CF3} and **27b**^{CF3} in d_2-dichloromethane at 295, 280, 260, 240 and 220 K.

Crystals suitable for X-ray diffraction were obtained by the slow diffusion of pentane in to a dichloromethane layer containing **27a**^{CF3} (Figure 6.6). The unit cell contained two structures of **27a**^{CF3} and only one of these has been represented in the diagram. The crystal was twinned and therefore there are areas of electron density that have not been modelled, however the structure of **27a**^{CF3} clearly illustrates that a C-H functionalisation reaction at the 3-methylpyridine ligand has occurred yielding a pyridylidene complex where the nitrogen atom is coordinated to an alkene functional group.

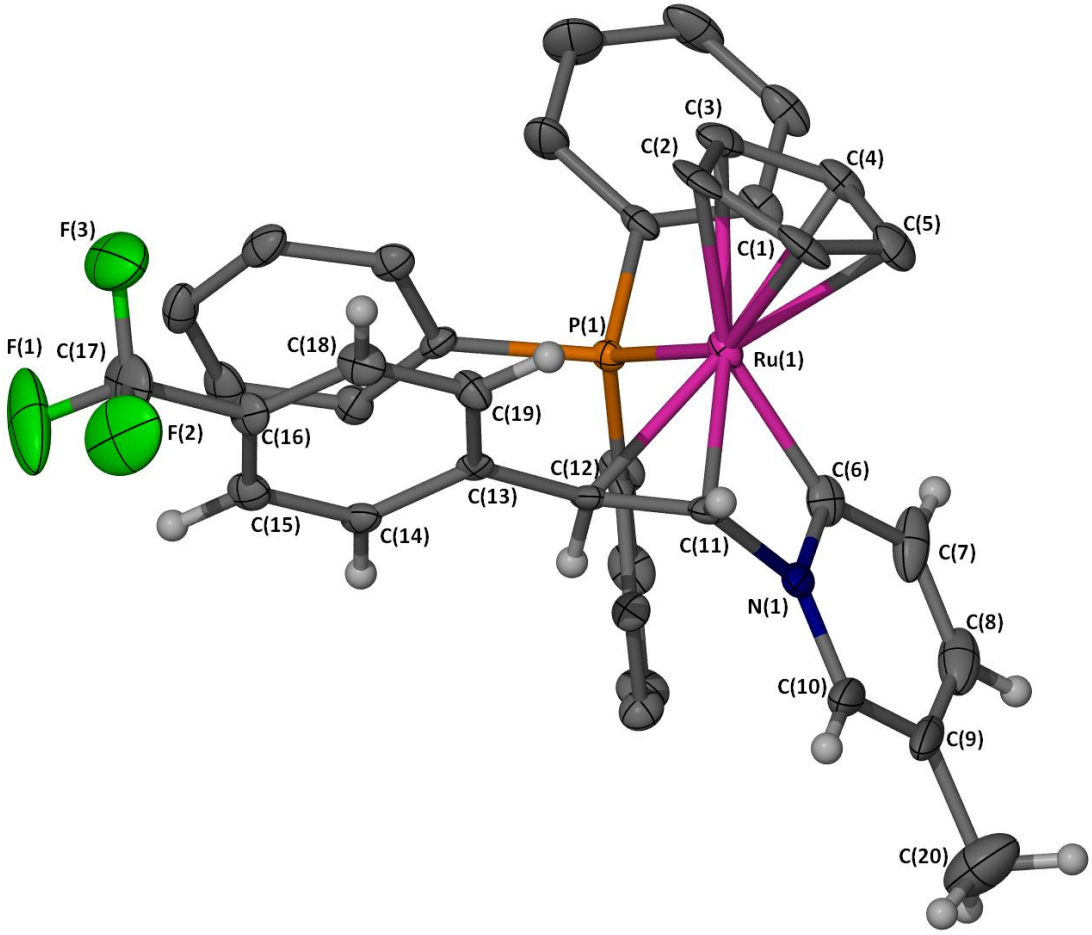

Figure 6.6: X-Seed diagram of $[Ru(\eta^5\text{-}C_5H_5)(PPh_3)(\kappa^3\text{-}C_3\text{-}(Me\text{-}C_5H_3N)CH{=}CH(C_6H_4\text{-}4\text{-}CF_3)]^+$ from complex **27a**^{CF3}. Selected hydrogen atoms and the $[PF_6]^-$ anion have been omitted for clarity, and where shown the thermal ellipsoids are at a 50 % probability level. The crystal was twinned and was modelled as two independent components. There are also minor components that have not been modelled and may explain the residual electron density.

6.6 Reactivity of complex 13^{Me} with alkynes

The reaction of the imidazole-containing complexes $\mathbf{13^R}$ was investigated. The previous reactions of complexes $\mathbf{10^R}$ with terminal alkynes have displayed the formation of the N-heterocyclic carbene ligands at the two position of the six-membered N-containing heterocycles. The reaction of the imidazole-containing complexes $\mathbf{13^R}$ with terminal alkynes was of interest as potentially the imidazole ring could undergo a C-H functionalisation reaction to give an *N*-heterocyclic carbene ligand at the ruthenium centre.

6.6.1 Reaction between complex 13^{Me} with phenylacetylene

The stoichiometric addition of phenylacetylene to $\mathbf{13^{Me}}$ in d_2-dichloromethane was monitored *via* NMR spectroscopy, and the reaction was repeated with ^{13}C-labelled phenylacetylene to provide additional information on the reaction mechanism.

In the reaction with phenylacetylene, after 24 hours, the resonances for one new minor ruthenium-containing complex $\mathbf{28^{Me,H}}$ were observed. Additionally after 24 hours peaks for uncoordinated 1-methylimidazole were observed in the ^{1}H NMR at 3.66, 6.90, 6,97 and 7.37 ppm, and these resonances increased in intensity as $\mathbf{13^{Me}}$ reacted further. No major changes were observed in the NMR spectra after 48 hours and therefore the reaction mixture was heated at 50 °C for 16 hours (Scheme 6.13).

The complex $\mathbf{28^{Me,H}}$ was partially characterised *via* NMR spectroscopy and hypothesised to be a vinylidene-containing complex. The ^{1}H NMR spectrum displayed two broad peaks at 5.43 and 5.09 ppm which had an integration of 5:1, and were assigned as the cyclopentadienyl protons and the hydrogen atoms at the β-carbon atom of the vinylidene ligand respectively. Additionally in the ^{1}H NMR spectrum, singlet resonances at 3.39, 6.61 and 6.64 ppm with integrations of 3:1:1 with respect to the cyclopentadienyl ligand and were assigned to one coordinated 1-methylimidazole ligand. The ^{31}P{^{1}H} NMR spectrum exhibited a broad peak at 53.0 ppm for a coordinated triphenylphosphine ligand. Further resonances for this species could not be identified as the aromatic region was too complex. The reaction with PhC≡^{13}CH displayed in the ^{13}C{^{1}H} NMR spectrum a ^{13}C-labelled enriched peak at 351.3 ppm (doublet, $^2J_{CP}$ = 17.6 Hz) which was characteristic of the α-carbon atom of a vinylidene ligand. Additionally, this corroborated with the ^{31}P{^{1}H} NMR spectrum at 53.0 ppm, as a doublet with a $^2J_{CP}$ of 17.6 Hz was observed for the triphenylphosphine ligand.

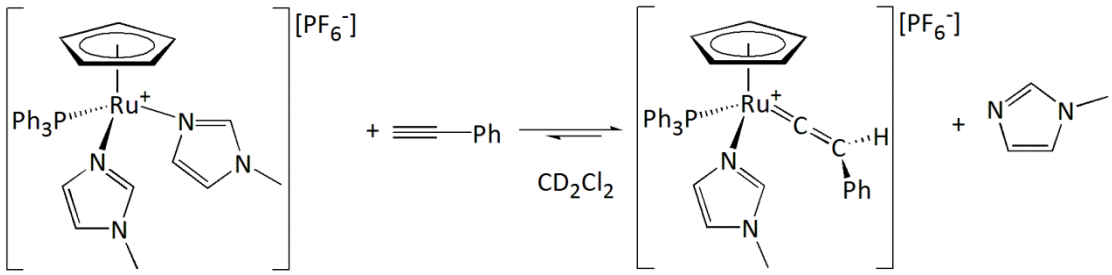

13^{Me} **28^{Me,H}**

Scheme 6.13: Stoichiometric addition of phenylacetylene to **13^{Me}** in d_2-dichloromethane at room temperature.

After heating the reaction mixture containing phenylacetylene the major species was still the starting material **13^{Me}**, however resonances in the $^{31}P\{^{1}H\}$ NMR spectrum displayed the presence of two minor unknown triphenylphosphine containing species at 43.2 and 51.7 ppm and the resonances belonging to **28^{Me,H}** were now absent. After heating the reaction mixture the ^{1}H NMR spectrum exhibited the absence of peaks for uncoordinated phenylacetylene, which suggested that all the alkyne had reacted which only required a sub-stoichiometric quantity of **13^{Me}**. A further five equivalents of phenylacetylene were added to the reaction mixture and heated at 50 °C for 16 hours. The NMR spectra displayed that resonances for **13^{Me}** were absent. The major ruthenium-containing species present in the $^{31}P\{^{1}H\}$ NMR spectrum was at 51.7 ppm, however there was still uncoordinated phenylacetylene present in the reaction mixture.

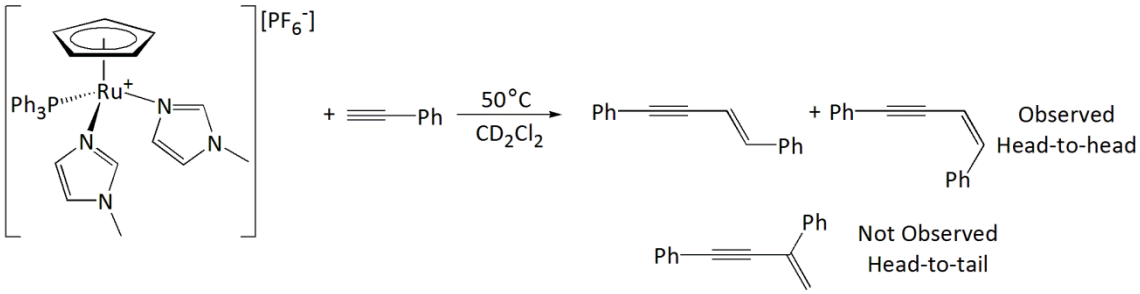

13^{Me}

Scheme 6.14: Reaction of phenylacetylene with **13^{Me}** in d_2-dichloromethane after heating at 50 °C.

The ^{1}H NMR spectrum displayed doublet peaks at 6.42 and 7.06 ppm with a $^{3}J_{HH}$ of 16.2 Hz for the *E*-1,4-diphenylbut-1-ene-3-yne compound, and another set of doublet resonances were observed at 5.94 and 6.73 ppm with a $^{3}J_{HH}$ of 12.0 Hz due to the *Z*-1,4-diphenylbut-1-ene-3-yne molecule, where the resonances were compared to those stated in the literature.[87, 91] The ratio of the *E*:*Z* butenyne present in the reaction mixture was approximately 1:0.3 respectively. This suggested that both of the coordinated 1-methylimidazole ligands of **13^{Me}** were dissociating from the ruthenium centre and therefore creating two vacant coordination sites where the dimerisation reaction of the phenylacetylene molecules could occur.[87, 91] On heating the reaction mixture containing ^{13}C-labelled phenylacetylene, the ^{13}C{^{1}H} NMR spectrum displayed enhancements for two doublet resonances 108.3 and 89.2 ppm with a $^{2}J_{CC}$ of 91.9 Hz and another set of doublet resonances at 107.5 and 88.5 ppm with $^{2}J_{CC}$ of 88.7 Hz. The resonances are characteristic of the *E* and *Z* butenyne species.

From the reaction mixture employing phenylacetylene, a high resolution ESI-MS exhibited a peak with a *m/z* of 185.1076 which was assigned for a $[C_{12}H_{12}N_2]^+$ fragment, which would account for a 1-methylimidazole and phenylacetylene molecule. Additionally, a TOF-EI MS was also carried out on a sample of the reaction mixture where a *m/z* peak was observed at 204.09401 which corresponds to a $[C_{16}H_{12}]^+$ species and was assigned to a disubstituted butenyne molecule.

6.6.2 Reaction between complex 13^{Me} with 4-ethynyl-α,α,α-trifluorotoluene

The reaction of 4-ethynyl-α,α,α-trifluorotoluene with **13^{Me}** in d_2-dichloromethane was investigated. The 4-CF_3 substituent of the phenyl ring of the terminal alkyne has previously changed the reactivity observed in the reactions of **10^{R}** with aryl terminal alkynes (Section 5.2.3).

The stoichiometric addition of 4-ethynyl-α,α,α-trifluorotoluene to **13^{Me}** in a d_2-dichloromethane solution was monitored using NMR spectroscopy. The NMR spectra after 24 hours displayed the resonance for the presence of a minor ruthenium-containing complex **28^{Me,CF3}** and the major ruthenium-containing species was still **13^{Me}** (Scheme 6.15).

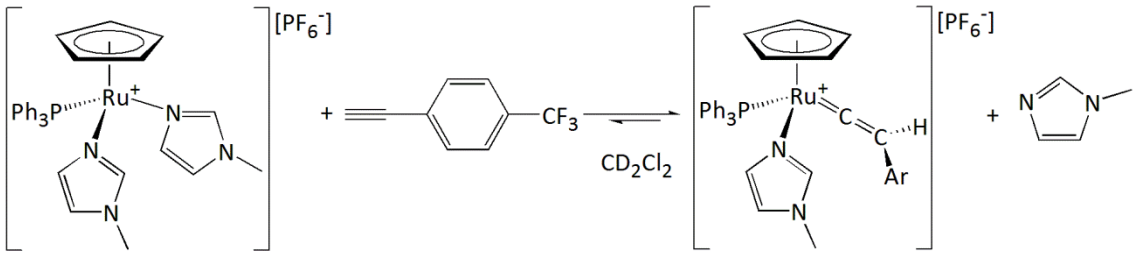

13^{Me} **28^{Me,CF3}**

Scheme 6.15: Stoichiometric addition of 4-ethynyl-α,α,α-trifluorotoluene with **13^{Me}** in d_2-dichloromethane at room temperature, where Ar = C_6H_4-4-CF_3.

The complex **28^{Me,CF3}** was hypothesised to be a vinylidene-containing complex as similar resonances were observed to those reported previously in this chapter. The ^{1}H NMR spectrum exhibited broad signals at 5.11 and 5.47 ppm with relative integrations of 1H and 5H, and were assigned as the vinylidene hydrogen atom on the β carbon atom and the cyclopentadienyl ligand respectively. There were also resonances at 3.42 (3H), 6.60 (1H) and 6.63 (1H) ppm with integrations relative to the cyclopentadienyl ligand for a coordinated 1-methylimidazole ligand.

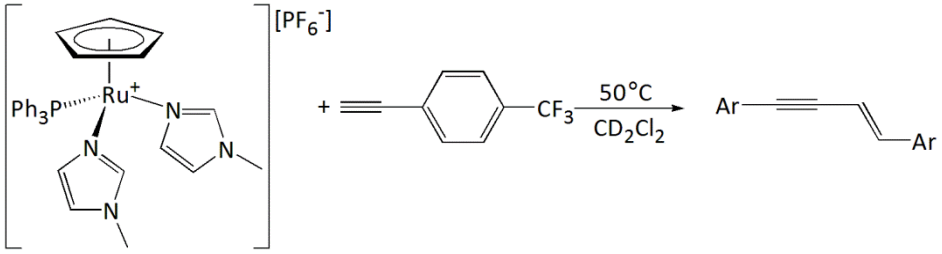

13^{Me}

Scheme 6.16: Reaction of 4-ethynyl-α,α,α-trifluorotoluene with **13^{Me}** in d_2-dichloromethane after heating at 50 °C, where Ar = C_6H_4-4-CF_3.

After 24 hours minor changes were observed in the NMR spectra, therefore the reaction mixture was heated at 50 °C for 16 hours (Scheme 6.16). The ^{1}H NMR spectrum exhibited the absence of the peak at 3.28 ppm for the terminal proton of the 4-ethynyl-α,α,α-trifluorotoluene molecule. The major species present in the reaction mixture was **13^{Me}** and resonances for **28^{Me,CF3}** were also present. A further equivalent of 4-ethynyl-α,α,α-trifluorotoluene was added to the reaction mixture and heated for an additional 16 hours. The NMR spectra of the reaction mixture at this stage demonstrated that **13^{Me}** was the major ruthenium-containing complex, and **28^{Me,CF3}** was present as a minor species among many other minor unknown compounds. The ^{1}H NMR spectrum

displayed a doublet resonance at 6.52 ppm with a $^{3}J_{HH}$ of 16.3 Hz and was assigned as *E*-1,4-di-4-trifluoromethylphenylbut-1-ene-3-yne.

A high resolution ESI-MS of the reaction mixture revealed a *m/z* peak at 253.0934, which was assigned to a $[C_{13}H_{12}F_3N_2]^+$ fragment and corresponds to a 1-methylimidazole and 4-ethynyl-α,α,α-trifluorotoluene molecule. The ESI-MS also exhibited *m/z* peaks with a ruthenium-isotope pattern at 593.1421 and 681.1232 which were assigned to $[Ru(\eta^5\text{-}C_5H_5)(PPh_3)(N_2C_4H_6)_2]^+$ and $[Ru(\eta^5\text{-}C_5H_5)(PPh_3)(N_2C_4H_6)(C_2HC_6H_4\text{-}4\text{-}CF_3)]^+$ respectively. Two further *m/z* peaks were also observed with a ruthenium-isotope pattern at 773.1794 and 861.1606, which could not assigned to a reasonable ruthenium-containing fragment.

6.6.3 Summary

The complex **13^{Me}** exhibited initial similar reactivity to complexes **10^{R}** as the vinylidene-containing complexes were observed. However, the vinylidene-containing complexes **28^{Me,H}** and **28^{Me,CF3}** were only minor species in the reaction mixture, and did not appear to react further. Further heating of the system lead to dissociation of both 1-methylimidazole ligands and therefore allowed for the dimerisation of phenylacetylene to occur. From these studies, we can determine that the 1-methylimidazole ligands are stronger nitrogen donors at the ruthenium centre than pyridine, since upon addition of the terminal alkynes the major species present in the reaction mixture is **13^{Me}**. This could be due to the 1-methylimidazole have a higher *p*K_a value than pyridine.[29] Potential reasons for the lack of the NHC ligand could have been due to steric and electronic effects, as it has been found in the literature that substituents coordinated to the imidazole ring can stabilise the NHC tautomer, and therefore the methyl substituent was substituted for a *tert*-butyl group (Section 6.7).[164]

6.7 Reactivity of 13^{tBu} with 4-ethynyl-α,α,α-trifluorotoluene

The reaction of **13^{tBu}** with 4-ethynyl-α,α,α-trifluorotoluene was probed to observe if changing the methyl group to a *tert*-butyl substituent on the nitrogen atom would change the reactivity. The *tert*-butyl group is more sterically bulky and donates more electron density to the imidazole ring *via* an inductive effect than a methyl substituent.

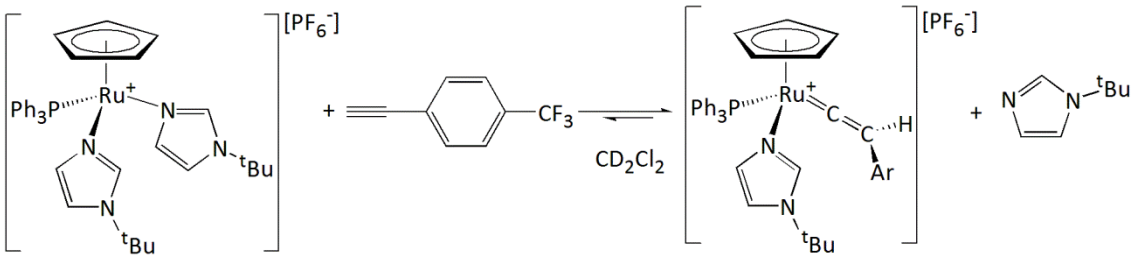

13^{tBu} **$28^{tBu,CF3}$**

Scheme 6.17: Stoichiometric addition of 4-ethynyl-α,α,α-trifluorotoluene with **13^{tBu}** in d_2-dichloromethane at room temperature, where Ar = C_6H_4-4-CF_3.

The stoichiometric addition of 4-ethynyl-α,α,α-trifluorotoluene to **13^{tBu}** in d_2-dichloromethane was monitored *via* NMR spectroscopy. The initial NMR spectra were recorded within an hour from the addition of phenylacetylene and did not display any new resonances. The reaction mixture was left at room temperature for 24 hours and the subsequent NMR spectra displayed a set of resonances for a new minor ruthenium-containing species **$28^{tBu,CF3}$**, however **13^{tBu}** was still the major species (Scheme 6.17).

The ^{1}H NMR spectrum displayed peaks for a minor species **$28^{tBu,CF3}$** which was characteristic of containing a vinylidene ligand with broad peaks at 5.14 and 5.48 ppm with integrations of 1H and 5H which was assigned as the vinylidene ligand proton on the β carbon atom and the cyclopentadienyl ligand respectively. Additionally, in the ^{1}H NMR spectrum the peaks at 1.17 (9H), 6.76 (1H) and 6.84 (1H) ppm were assigned to a coordinated *tert*-butylimidazole. The ^{31}P{^{1}H} NMR spectrum exhibited a broad peak at 52.5 ppm for a coordinated triphenylphosphine ligand.

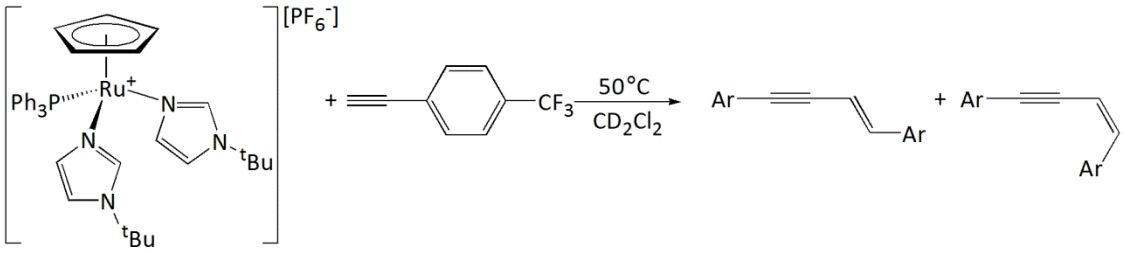

13^{tBu}

Scheme 6.18: Reaction of 4-ethynyl-α,α,α-trifluorotoluene with **13^{tBu}** in d_2-dichloromethane after heating at 50 °C, where Ar = C_6H_4-4-CF_3.

After 6 days, (since no changes were observed in the NMR spectra) the reaction mixture was heated at 50 °C for 16 hours where the NMR spectra exhibited resonances for **13^{tBu}** (major), **28^{tBu,CF3}** (minor) amongst many minor unknown ruthenium-containing species (Scheme 6.18). Interesting, after heating the reaction mixture the ^{1}H NMR spectrum displayed peaks for uncoordinated 4-ethynyl-α,α,α-trifluorotoluene in the reaction mixture at 3.28 ppm. Based upon these observations the reaction mixture was heated for a further 16 hours at 50 °C. The major species present in the reaction mixture once all the 4-ethynyl-α,α,α-trifluorotoluene was consumed was **13^{tBu}** amongst many other unknown species. The ^{1}H NMR spectrum displayed doublet resonances at 6.52 and 6.51 ppm with a $^3J_{HH}$ of 16.3 and 16.2 Hz, for the *E*- and *Z*- 1,4-di-4-trifluoromethyl phenylbut-ene-3-yne respectively, where the major isomer was the *E*-disubstituted butenyne.

A high resolution ESI-MS of the reaction mixture displayed *m/z* peaks with ruthenium isotope patterns at 677.2355 and 723.1723 which were assigned as the species $[Ru(\eta^5\text{-}C_5H_5)(PPh_3)(N_2C_3H_3CH_3)_2]^+$ and $[Ru(\eta^5\text{-}C_5H_5)(PPh_3)(N_2C_3H_3CH_3)(C_2HC_6H_4\text{-}4\text{-}CF_3)]^+$ respectively.

6.7.1 Summary

The difference in the reactivity of the **13^{Me}** and **13^{tBu}** was observed when heating the reaction mixture at 50 °C for 16 hours, as the phenylacetylene all reacts in the system with **13^{Me}** under these conditions, however the analogous reaction with **13^{tBu}** required further heating. This could be due to the *tert*-butyl group donating more electron density to the imidazole ring and therefore creating a stronger nitrogen donor atom than 1-methylimidazole.

6.8 Reactivity of complex 14^{H} with alkynes

The reactivity of the trimethylphosphine-substituted complexes **14^{H}** and **14^{NMe2}** with terminal alkynes was investigated. The trimethylphosphine ligand is smaller and more electron donating than triphenylphosphine and therefore the change in the steric and electronic properties of the phosphorus ligand will be expected to change the reactivity observed towards terminal alkynes.

6.8.1 Reaction between complex 14^{H} with phenylacetylene

6.8.1.1 Reactivity observed in d_2-dichloromethane

The stoichiometric addition of phenylacetylene to **14^{H}** in a d_2-dichloromethane was monitored *via* NMR spectroscopy (Scheme 6.19). The initial NMR spectra indicated that most of the starting complex **14^{H}** had reacted, and the one major species was observed in the NMR spectra, **29** (Section 1.5). A further stoichiometric equivalent of phenylacetylene was added to the reaction mixture to drive the reaction to completion. The reaction mixture was monitored after 24 hours and the resonance belonging to **29** had decreased in intensity and a set of peaks for a new unknown ruthenium complex was observed in the NMR spectra. The initial ^{1}H NMR spectrum also exhibited resonances for uncoordinated pyridine at 8.58, 7.68 and 7.28 ppm for the protons at the C-2/6, C-4 and C-3/5 positions respectively.

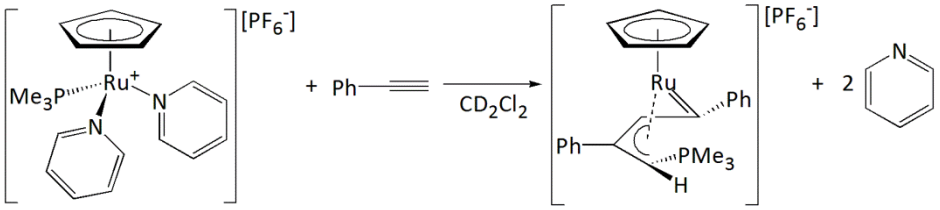

14^{H} **29**

Scheme 6.19: Reaction between **14^{H}** and phenylacetylene in d_2-dichloromethane.

The ^{1}H NMR spectrum exhibited a peak at 5.24 ppm (5H) for the cyclopentadienyl ligand, and signals at 5.79 (s, 1H) and 5.12 (d, J_{HP} = 10.7 Hz) ppm were assigned to the allyl hydrogen atoms of **29**. A doublet resonance at 1.33 ppm with a $^{2}J_{HP}$ of 13.3 Hz was observed for the methyl groups of the trimethylphosphine ligand. In the ^{31}P{^{1}H} NMR spectrum a peak at 33.2 ppm for the triphenylphosphine ligand was observed. The resonances observed in the initial NMR spectra were compared to the literature data of **29** to confirm the presence of this complex. Additionally Kirchner *et al.* reported that

the formation of **29** is fast from **14^{H}** and complete within a few minutes and this is consistent with our findings.[136]

The resonances for the new unknown ruthenium complex were observed in the ^{1}H NMR spectrum at 5.12 ppm for the cyclopentadienyl ligand. The $^{31}P\{^{1}H\}$ NMR spectrum displayed a peak at 34.2 ppm for a triphenylphosphine ligand. Interestingly the resonances for uncoordinated pyridine in the reaction mixture decreased after 24 hours. This could have been due to the nitrogen lone pair coordinating at the ruthenium centre of **29** , as it has been established by Kirchner *et al.* that two electron donor ligands (e.g CF_3COO^-, PPh_3), can coordinate to the metal centre.[136, 139] This is only a hypothesis and should be considered cautiously.

The reaction of **14^{H}** and phenylacetylene in d_2-dichloromethane did not indicate the presence of the C-H functionalised species in the reaction mixture, as was observed in the reaction of **10^{H}** and terminal alkynes. The major product formed in the reaction was **29** and a possible reason for this observation in reactivity could be attributed to the more electron-donating trimethylphosphine ligand in **14^{H}** and therefore the pyridine ligands are more labile in nature. It is possible that in the presence of phenylacetylene, both pyridine molecules are substituted by the alkyne which prefers the reaction pathway to form **29** (Section 1.5). Alternatively, the smaller cone angle of trimethylphosphine may allow for easier coordination of the alkyne molecules. The reaction conditions were consequently changed to account for these observations by carrying out the stoichiometric addition of phenylacetylene to **14^{H}** in a pyridine solution.

6.8.1.2 Reactivity observed in d_5-pyridine and pyridine

The stoichiometric addition of phenylacetylene to **14^{H}** in d_5-pyridine (55 equivalents with respect to the alkyne) was monitored using NMR spectroscopy. The reaction was left to proceed at room temperature for 48 hours, however no changes were observed and therefore the sample was heated at 50 °C for 16 hours. The ^{1}H NMR spectrum after heating for 16 hours demonstrated that the resonances for phenylacetylene were no longer present. The NMR spectra after heating the reaction still exhibited peaks belonging to **14^{H}** in d_5-pyridine, however there were peaks present for a new ruthenium-containing species **30^{D,H}**. In an attempt to drive the reaction to completion a further equivalent of phenylacetylene was added to the reaction mixture and the resonances for **30^{D,H}** were observed to increase in intensity. The ^{1}H NMR spectrum exhibited additional resonances to **30^{D,H}** including a doublet peak at 8.03 ppm with a $^{3}J_{HH}$ of 16.0

Hz; through a 2D ^{1}H-^{1}H COSY experiment this peak was found to couple to a resonance at 7.45 ppm under a multiplet. These resonances were characteristic of a *trans* alkene proton. Other aromatic peaks were observed at 7.30, 7.38 and 7.61 ppm for a phenyl ring. Since there were no additional resonances for a cyclopentadienyl ligand and trimethylphosphine ligand in the ^{1}H and ^{31}P{^{1}H} NMR spectra, this suggested that the species must have been of an organic nature. A comparison of the ^{1}H NMR spectra with an authentic sample of 2-styrylpyridine confirmed the presence of the compound in the reaction mixture. The resonances which were expected for the pyridine fragment of 2-styrylpyridine were not observed as these were deuterated. An ESI-MS of the reaction mixture displayed *m/z* peaks at 186.1167, 187.1229 and 188.1287 which were assigned as $[C_{13}H_8D_4N]^+$, $[C_{13}H_7D_5N]^+$ and $[C_{13}H_6D_6N]^+$ respectively, and were due to different levels of deuterium incorporation. These are the expected *m/z* peaks for the 2-styrylpyridine compounds or the N-bound isomer. The stoichiometric addition of phenylacetylene to **14^{H}** in d_5-pyridine gave the deuterated analogues of 2-styrylpyridine and **30^{H,H}**. This therefore explained the observation that a further equivalent of phenylacetylene was required to form **30^{H,H}**.

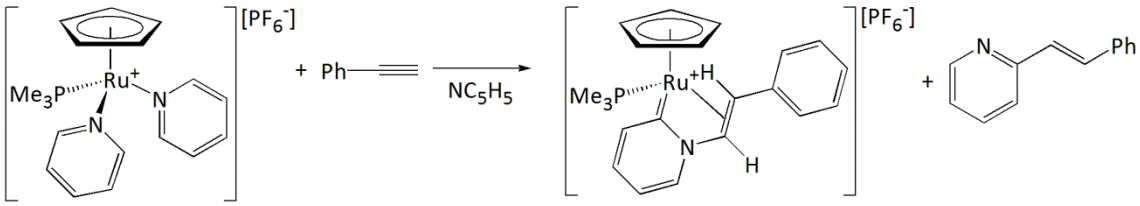

14^{H} **30^{H,H}**

Scheme 6.20: Reaction between **14^{H}** and phenylacetylene in pyridine.

The reaction was also repeated with pyridine instead of d_5-pyridine to avoid deuterium incorporation in to the final products (Scheme 6.20). The excess solvent was removed under vacuum and **30^{H,H}** isolated by the slow diffusion of pentane into a dichloromethane layer containing **30^{H,H}**. The identification of **30^{H,H}** was based on NMR spectroscopy, ESI-MS and X-ray crystallography. Many attempts were made to purify **30^{H,H}** unfortunately due to the air-sensitive nature of the species in solution, purification was difficult and therefore full characterisation was not obtained.

The ^{1}H NMR spectrum exhibited the resonances for **30^{H,H}** in d_2-dichloromethane at 1.54 (d, 9H, $^{2}J_{HP}$ = 9.6 Hz) and 4.99 (s, 5H) ppm for the trimethylphosphine and cyclopentadienyl ligands at the ruthenium centre respectively. A 2D 1H-1H COSY exhibited a strong coupling between the resonances at 3.57 (dd, 1H, $^{3}J_{HP}$ = 12.9 Hz,

$^{2}J_{HH}$ = 7.0 Hz) and 6.37 (dd, $^{2}J_{HP}$ = 7.0 Hz, $^{3}J_{HP}$ = 1.3 Hz) ppm which were assigned as to the two alkene protons. The $^{31}P\{^{1}H\}$ NMR spectrum displayed resonances at -143.0 (sept, $^{1}J_{PF}$ = 710 Hz) and 14.8 (s) ppm for the $[PF_6]^-$ anion and the trimethylphosphine ligand respectively. The $^{13}C\{^{1}H\}$ NMR spectrum displayed peaks at 62.1 (d, $^{2}J_{CP}$ = 4.6 Hz), 76.1 (d, $^{2}J_{CP}$ = 2.4 Hz) and 87.5 (d, $^{2}J_{CP}$ = 1.4 Hz) ppm for the two alkene carbon atoms and the cyclopentadienyl ligand respectively. The $^{13}C\{^{1}H\}$ NMR spectrum displayed a set of peaks at 142.7, 118.2, 137.3, 136.7 (d, $^{3}J_{CP}$ = 3.6 Hz) and 182.3 (d, $^{2}J_{CP}$ = 19.9 Hz) ppm for the pyridylidene fragment, where the latter signal was due to the C-H functionalised carbon atom. A high resolution ESI-MS contained a *m/z* peak with a ruthenium isotope pattern at 424.0756 which was assigned to the cationic fragment of **30**$^{\mathbf{H,H}}$.

Crystals suitable for X-ray diffraction were obtained by the slow diffusion of pentane or hexane into a dichloromethane layer containing **30**$^{\mathbf{H,H}}$. The structure of **30**$^{\mathbf{H,H}}$ contained a C-H functionalised pyridine molecule in the form of a pyridylidene ligand which was bonded through the nitrogen atom to an alkene fragment. The geometry of **30**$^{\mathbf{H,H}}$ could be described as a distorted octahedral as the bond angles of C(6)-Ru(1)-P(1), C(12)-Ru(1)-P(1) and C(6)-Ru(1)-C(12) were 86.20(6), 84.51(6) and 84.52(8) ° respectively. The P(1)-Ru(1) bond length was 2.2940(6) Å. The C(6)-Ru(1) bond to the pyridylidene ligand was 2.0101(19) Å. The bonds around the pyridylidene ligand displayed significantly longer bond lengths for C(6)-C(7) and C(8)-C(9) than the adjacent bonds. The alkene bond length C(11)-C(12) was 1.414(3) Å, which was shorter than the adjacent bond lengths suggesting multiple bond character.

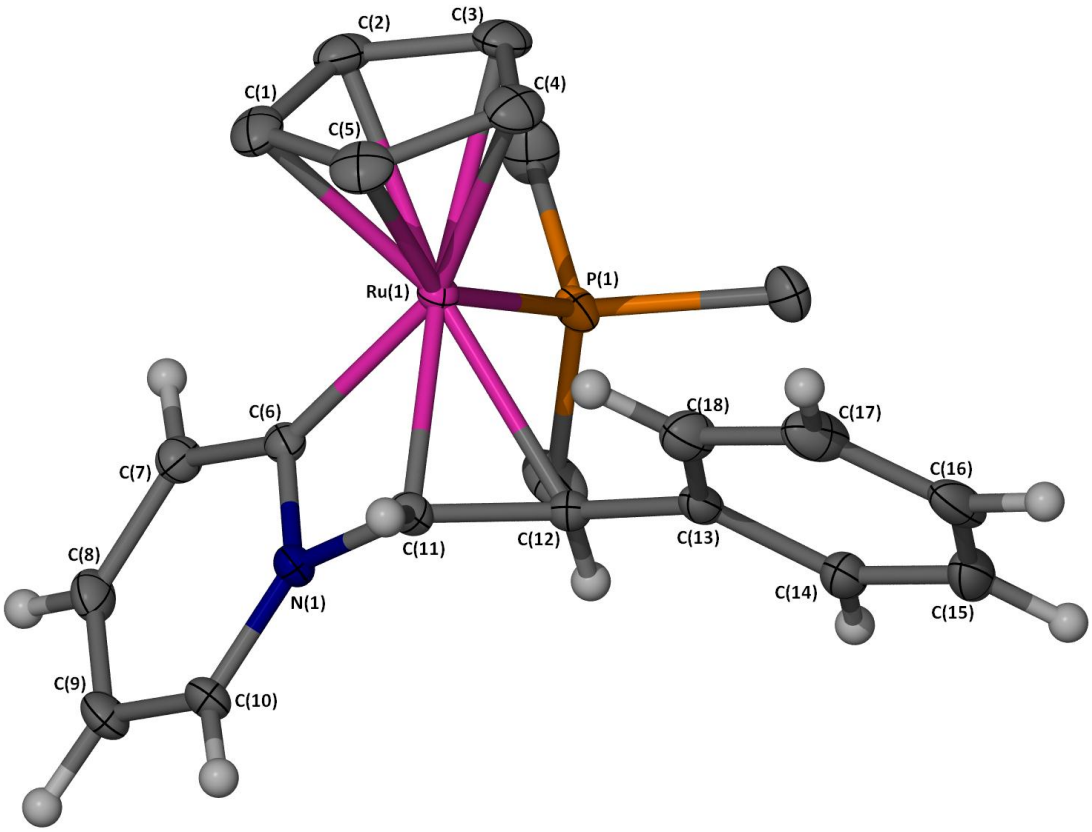

Figure 6.7: X-Seed diagram of $[Ru(\eta^5\text{-}C_5H_5)(PMe_3)(\kappa^3\text{-}C_3\text{-}C_5H_4N)CH{=}CH(C_6H_5)]^+$ from complex $\mathbf{30}^{\mathbf{H,H}}$. Selected hydrogen atoms and the $[PF_6]^-$ anion have been omitted for clarity, and where shown the thermal ellipsoids are at a 50 % probability level. The fluorine atoms of the $[PF_6]^-$ anion were disordered over two positions in a ratio of 0.6807:0.3193. There were two large electron density peaks Q1 and Q2 present, due to a non-merahedrol twin element that was too weak to model.

	Bond lengths (Å)		Bond angles (°)
C(1)-Ru(1)	2.218(2)	C(6)-Ru(1)-P(1)	86.20(6)
C(2)-Ru(1)	2.199(2)	C(12)-Ru(1)-P(1)	84.51(6)
C(3)-Ru(1)	2.242(2)	C(6)-Ru(1)-C(12)	84.52(8)
C(4)-Ru(1)	2.273(2)	C(6)-Ru(1)-C(11)	64.26(8)
C(5)-Ru(1)	2.243(2)	N(1)-C(6)-Ru(1)	100.20(13)
C(6)-Ru(1)	2.0101(19)	C(12)-C(13)-N(1)	117.14(18)
C(11)-Ru(1)	2.120(2)	C(11)-C(12)-C(13)	121.32(19)
C(12)-Ru(1)	2.224(2)	C(10)-N(1)-C(6)	126.49(18)
C(11)-C(12)	1.414(3)	N(1)-C(10)-C(9)	117.6(2)
C(12)-C(13)	1.484(3)	C(10)-C(9)-C(8)	119.1(2)
C(11)-N(1)	1.449(2)	C(7)-C(8)-C(9)	121.5(2)
C(6)-N(1)	1.355(3)	C(8)-C(9)-C(10)	119.1(2)
C(6)-C(7)	1.397(3)	N(1)-C(6)-C(7)	116.16(18)
C(7)-C(8)	1.377(3)		
C(8)-C(9)	1.397(3)		
C(9)-C(10)	1.360(3)		
C(10)-N(1)	1.348(3)		
P(1)-Ru(1)	2.2940(6)		

Table 6.4: Selected bond lengths (Å) and angles (°) for complex **30**$^{\mathbf{H,H}}$.

In comparison to the reactions conducted with triphenylphosphine, the reaction of **14**$^{\mathbf{H}}$ (containing trimethylphosphine) with phenylacetylene requires the presence of excess pyridine in the system to generate the C-H activated product. Pyridine ligands are more labile when the phosphine ligand is trimethylphosphine and therefore additional pyridine was required. In the reactions with **14**$^{\mathbf{H}}$ a vinylidene-containing species was not observed. This could potentially be due to vinylidene species being less favoured in a basic medium, due to the vinylidene proton being electrophilic in nature.[54] In reactions where the *in situ* vinylidene-containing species **19**$^{\mathbf{H,Ph}}$ was placed in a pyridine solution to observe its reactivity, **19**$^{\mathbf{H,Ph}}$ returned to **10**$^{\mathbf{H}}$ (equilibrium favours the formation of **10**$^{\mathbf{H}}$). This may possibly explain why the only ruthenium-containing complexes observed in these reactions are **14**$^{\mathbf{H}}$ and **30**$^{\mathbf{H,H}}$.

6.8.2 Reaction between complex 14^{H} with 4-ethynyl-α,α,α-trifluorotoluene

Using the understanding gained from the reaction of **14^{H}** with phenylacetylene in d_2-dichloromethane the stoichiometric addition of 4-ethynyl-α,α,α-trifluorotoluene to **14^{H}** was conducted in a pyridine solution to avoid the formation of the π-allyl carbene complexes reported by Kirchner *et al.*[136] The reaction mixture was heated at 50 °C for 16 hours and a small aliquot placed in d_2-dichloromethane to observe how the reaction proceeded *via* NMR spectroscopy. After heating the reaction mixture for 16 hours at 50 °C, a set of resonances for **$30^{H,CF3}$** were observed in the NMR spectra, however resonances for **14^{H}** and 4-ethynyl-α,α,α-trifluorotoluene were still present and therefore was heated for an additional 16 hours (Scheme 6.21). The characterisation of **$30^{H,CF3}$** has been based on the NMR spectra from this reaction mixture and has been assigned cautiously. Further attempts to characterise this species were not conducted due to time constraints.

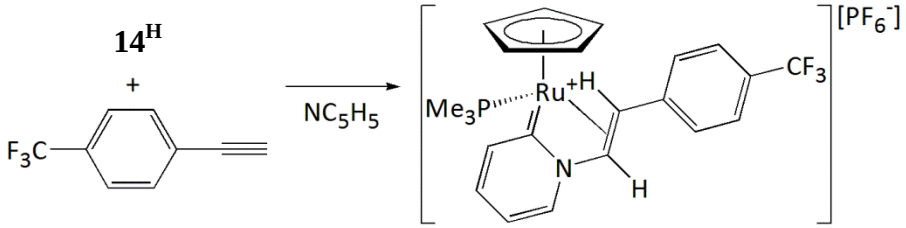

$30^{H,CF3}$

Scheme 6.21: Reaction between **14^{H}** and 4-ethynyl-α,α,α-trifluorotoluene in pyridine.

The resonances observed in the ^{1}H NMR spectrum in d_2-dichloromethane that have been assigned to **$30^{H,CF3}$** were observed at 1.52 (d, 9H, $^{2}J_{HP}$ = 9.7 Hz) and 5.00 (s, 5H) ppm for the trimethylphosphine and cyclopentadienyl ligands respectively. The resonances at 3.55 (dd, 1H, $^{3}J_{HP}$ = 12.9 Hz, $^{3}J_{HH}$ = 6.8Hz) and 6.48 (dd, 1H, $^{3}J_{HH}$ = 6.8 Hz, $^{3}J_{HP}$ = 1.5 Hz) ppm were assigned to the alkene protons of **$30^{H,CF3}$**. The ^{31}P{^{1}H} NMR spectrum displayed resonances at -143.0 (sept, $^{1}J_{PF}$ = 710 Hz) and 14.2 (s) ppm for the $[PF_6]^-$ anion and the trimethylphosphine ligand respectively. From the ^{1}H NMR spectrum it was not possible to determine if the organic species, *E*-2-(4-trifluoromethyl)styrylpyridine was present in the reaction mixture.

6.9 Reactivity of complex 14^{NMe2} with terminal alkynes

The observations from the reaction of $\mathbf{14^{H}}$ with phenylacetylene in d_2-dichloromethane suggested that the pyridine ligands were extremely labile, as the formation of **29** required the coordination of two phenylacetylene molecules at the ruthenium centre and is due to the fragment $[Ru(\eta^5\text{-}C_5H_5)(PMe_3)]^+$ being accessible in solution. The coordination of 4-dimethylaminopyridine molecules to $[Ru(\eta^5\text{-}C_5H_5)(PMe_3)]^+$ to give $\mathbf{14^{NMe2}}$ would therefore control the reactivity to favour the formation of the pyridylidene species, since 4-dimethylaminopyridine is a more strongly donating ligand than pyridine. The reactivity of $\mathbf{14^{NMe2}}$ with terminal alkynes phenylacetylene and 4-ethynyl-α,α,α-trifluorotoluene has been investigated.

6.9.1 Reaction between complex 14^{NMe2} with phenylacetylene

The addition of phenylacetylene to $\mathbf{14^{NMe2}}$ in d_2-dichloromethane was carried out under several different reaction conditions at room temperature and monitored *via* NMR spectroscopy:

i) Stoichiometric addition of phenylacetylene to $\mathbf{14^{NMe2}}$ in d_2-dichloromethane;
ii) Stoichiometric addition of phenylacetylene to $\mathbf{14^{NMe2}}$ in d_2-dichloromethane in the presence of two equivalents of 4-dimethylaminopyridine.

Following reaction conditions i, three ruthenium-containing complexes were observed in the NMR spectra **29**, $\mathbf{30^{NMe2,H}}$ and an unknown species. When the reaction conditions ii were employed, the reaction was more selective and only exhibited resonances for $\mathbf{30^{NMe2,H}}$.

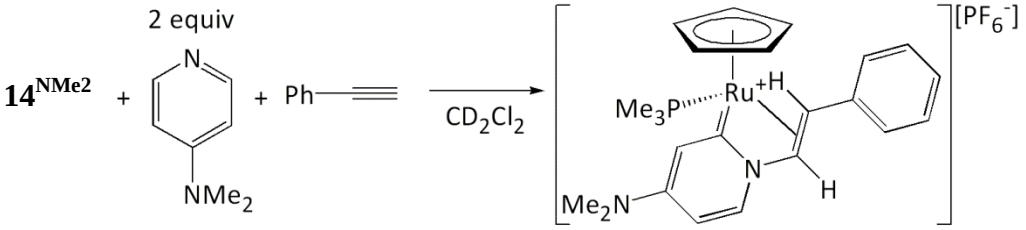

$\mathbf{30^{NMe2,H}}$

Scheme 6.22: Reaction between $\mathbf{14^{NMe2}}$ and phenylacetylene in the presence of two equivalents of 4-dimethylaminopyridine in d_2-dichloromethane.

The resonances for **29** were observed in the ^{1}H NMR spectrum at 5.14 (d, 1H, J_{HP} = 10.7 Hz), 5.79 (s, 1H) and 5.24 (s, 5H) ppm for the two allyl hydrogen atoms and cyclopentadienyl ligand respectively. The $^{31}P\{^1H\}$ NMR spectrum contained a singlet

peak at 33.3 ppm for the trimethylphosphine ligand of **29**. To confirm the presence of **29** in the reaction mixture, the spectra were compared to the literature data.[136]

From the NMR spectra for reaction conditions ii, the ^{1}H NMR spectrum exhibited peaks for **30**$^{\mathbf{NMe2,H}}$ and all the protons were assigned. The ^{1}H NMR spectrum exhibited resonances at 1.55 (d, $^{2}J_{HP}$ = 9.5 Hz) and 3.04 (s) ppm for the methyl substituents of the trimethylphosphine and the NMe_2 groups respectively. The two alkene protons were observed at 3.47 (dd, $^{3}J_{HP}$ = 13.1 Hz, $^{3}J_{HH}$ = 6.9 Hz) and 6.10 (dd, 1H, $^{3}J_{HP}$ = 1.1 Hz, $^{3}J_{HH}$ = 6.9 Hz) ppm, which both integrated as 1H with respect to the cyclopentadienyl ligand at 4.90 (5H) ppm. Three protons for the aromatic ring of the 4-dimethylaminopyridine ligand were observed at 6.20, 6.30 and 7.35 ppm, where the peak at 6.30 ppm did not display the expected doublet coupling, suggesting that a proton at the C-2 position was not present and a C-H functionalisation reaction had occurred. This is consistent with previous observations made with the 4-methylpyridine and 4-dimethylaminopyridine N-containing heterocycles. The ^{31}P{^{1}H} NMR spectrum displayed a singlet peak at 16.1 ppm for the trimethylphosphine ligand. A high resolution ESI-MS of the reaction mixture exhibited a *m/z* peak at 467.1195 which matched the cation $[Ru(\eta^5\text{-}C_5H_5)(\kappa^3\text{-}C_3\text{-}(4\text{-}NMe_2)C_5H_3N\text{-}C_2H_2C_6H_5)]^+$ of **30**$^{\mathbf{NMe2,H}}$.

Crystals of **30**$^{\mathbf{NMe2,H}}$ were grown and found to be suitable for X-ray diffraction by the slow diffusion of pentane into a dichloromethane layer containing **30**$^{\mathbf{NMe2,H}}$ (Figure 6.8, Table 6.5). The crystal data displayed a large amount of disorder as both the cation and anion were disordered over two positions. The structure shown below confirms the formation of a pyridylidene ligand which is bonded to an alkene functional group through the nitrogen atom. A distorted octahedral geometry around the ruthenium centre was observed, where the C(6)-Ru(1)-P(1), C(12)-Ru(1)-P(1) and were 89.15(6), 83.32(5) and 84.75(7) ° respectively. The ruthenium centre exhibited an unequal coordination to the alkene bond where C(11)-Ru(1) and C(12)- Ru(1) were found to 2.1332(18) and 2.2460(18) Å respectively. The C(6)-Ru(1) bond length was 2.0323(19) Å to the pyridylidene ligand. The C(7)-C(6) and C(10)-C(9) bond lengths of the pyridylidene fragment were significantly shorter than the adjacent carbon-carbon bonds. A set of platinium (II) complexes with chelate pyridine-pyridylidene ligands were studied *via* X-ray crystallography, where the derivative containing a 4-NMe_2 substituent at the pyridylidene fragment exhibited similar patterns to those observed for **30**$^{\mathbf{NMe2,H}}$.[188]

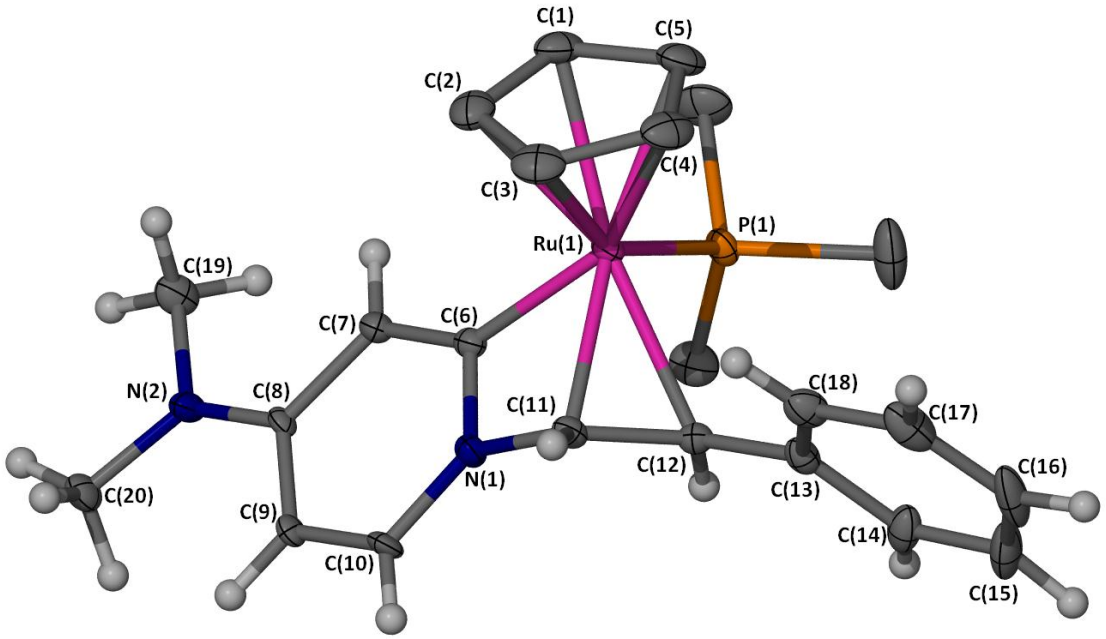

Figure 6.8: X-Seed diagram of $[Ru(\eta^5\text{-}C_5H_5)(PMe_3)(\kappa^3\text{-}C_3\text{-}(4\text{-}NMe_2)C_5H_4N)CH{=}CH(C_6H_5)]^+$ from complex **30**^{NMe2,H}. Selected hydrogen atoms and the $[PF_6]^-$ anion have been omitted for clarity, and where shown the thermal ellipsoids are at a 50 % probability level. Both the cation and anion were completely disordered over two positions, with refined occupancies of 0.9148:0.0852 (6). The cation of the largest occupancy has been displayed.

	Bond lengths (Å)		Bond angles (°)
C(1)-Ru(1)	2.209(2)	C(6)-Ru(1)-P(1)	89.15(6)
C(2)-Ru(1)	2.235(2)	C(12)-Ru(1)-P(1)	83.32(5)
C(3)-Ru(1)	2.256(2)	C(6)-Ru(1)-C(12)	84.75(7)
C(4)-Ru(1)	2.277(2)	C(6)-N(1)-C(11)	104.42(15)
C(5)-Ru(1)	2.246(2)	C(12)-C(11)-N(1)	117.02(17)
C(6)-Ru(1)	2.0323(19)	C(11)-C(12)-C(13)	121.34(18)
C(6)-N(1)	1.365(2)	C(10)-N(1)-C(6)	124.16(19)
C(7)-C(6)	1.379(3)	N(1)-C(6)-C(7)	118.12(18)
C(8)-C(7)	1.424(3)	C(6)-C(7)-C(8)	120.4(2)
C(9)-C(8)	1.430(3)	C(7)-C(8)-C(9)	117.7(2)
C(10)-C(9)	1.354(3)	C(10)-C(9)-C(8)	120.6(2)
C(10)-N(1)	1.362(3)	C(9)-C(10)-N(1)	119.1(2)
C(11)-N(1)	1.451(2)		
C(11)-C(12)	1.423(3)		
C(11)-Ru(1)	2.1332(18)		
C(12)- Ru(1)	2.2460(18)		
P(1)-Ru(1)	2.2978(6)		

Table 6.5: Selected bond lengths (Å) and angles (°) for complex **30**^{NMe2,H} .

6.9.2 Reaction of complex 14^{NMe2} with 4-ethynyl-α,α,α-trifluorotoluene

The stoichiometric addition of 4-ethynyl-α,α,α-trifluorotoluene to **14^{NMe2}** in the presence of two equivalents of 4-dimethylaminopyridine in d_2-dichloromethane was investigated (Scheme 6.23). The reaction was allowed to proceed at room temperature and was monitored *via* NMR spectroscopy. One major ruthenium containing complex **$30^{NMe2,CF3}$** was observed, amongst many minor unidentified species.

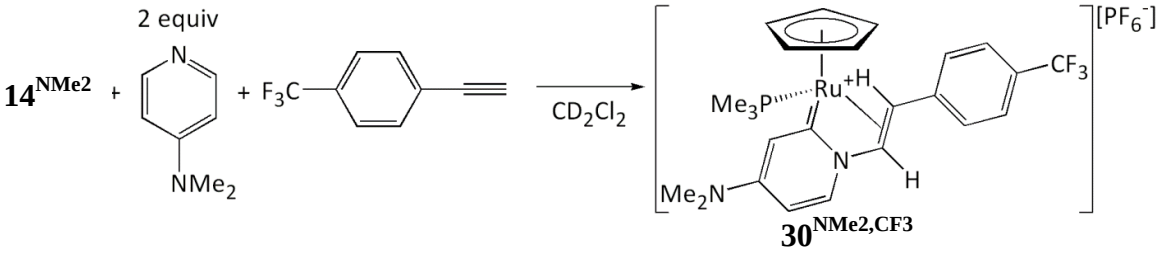

Scheme 6.23: Reaction between **14^{NMe2}** and 4-ethynyl-α,α,α-trifluorotoluene in the presence of two equivalents of 4-dimethylaminopyridine in d_2-dichloromethane.

The species **$30^{NMe2,CF3}$** was identified in the reaction mixture from the ^{1}H and ^{31}P{^{1}H} NMR spectra. Since the reaction produced many minor unknown species the purification of **$30^{NMe2,CF3}$** was challenging and not obtained. The ^{1}H NMR spectrum exhibited the alkene proton resonances at 3.45 and 6.17 ppm where both peaks had an integration of 1H with respect to the cyclopentadienyl ligand peak at 4.92 ppm (s, 5H). Similarly to the previous pyridylidene ligands, only three protons were observed on the heterocycle at 6.21 (d, $^3J_{HH}$ = 6.8 Hz), 6.30 (m) and 7.40 (d, $^3J_{HH}$ = 7.2 Hz) ppm, where each signal had an integration of 1H with respect to the cyclopentadienyl ligand resonance. The ^{31}P{^{1}H} NMR spectrum displayed a peak at 15.6 ppm for the coordinated trimethylphosphine ligand. The ESI-MS of the reaction mixture exhibited many ruthenium-containing *m/z* peaks, however a *m/z* peak at 535.1074 was observed and could be assigned to the cationic fragment $[Ru(\eta^5\text{-}C_5H_5)(\kappa^3\text{-}C_3\text{-}(4\text{-}NMe_2)C_5H_3N\text{-}C_2H_2(4\text{-}CF_3\text{-}C_6H_4))]^+$ of **$30^{NMe2,CF3}$**.

Interestingly, there has been no evidence for a vinylidene-containing complex in the reactions where **14^{NMe2}** has been reacted with terminal alkynes. This could be an effect of the 4-dimethylaminopyridine ligand, as it is a much strongly coordinating ligand due to the conjugation effect of the NMe_2 group in the 4-position of the heterocycle. It is possible that the vinylidene-containing complex is only a minor component of the reaction mixture. This corroborates with the reactions of **10^{NMe2}** and phenylacetylene (Section 6.4).

6.10 Reactivity of complex 15 with phenylacetylene

The reaction of **15** with phenylacetylene in d_2-dichloromethane was investigated. The role of a more electron-donating phosphine ligand with a larger cone angle than triphenylphosphine was explored. The reactivity of **15** was of particular interest as attempts to synthesise the *bis*-pyridine complex was not successful due to the steric constraints at the ruthenium centre, and therefore this may impact the reactivity observed towards phenylacetylene.

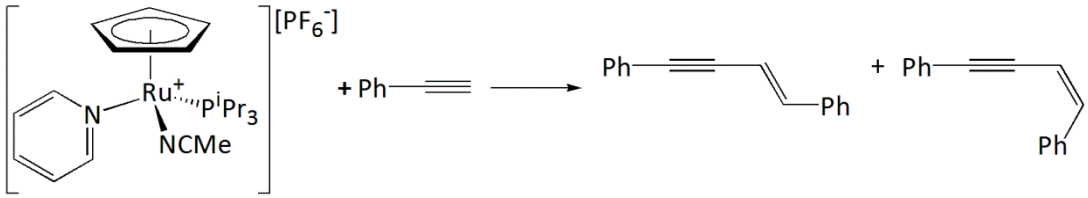

15

Scheme 6.24: Addition of phenylacetylene to **15** in d_2-dichloromethane.

Since **15** could not be obtained pure, a reaction mixture where **15** was the major species was used. The initial NMR spectra from the stoichiometric addition of phenylacetylene to **15** were recorded within one hour. The NMR spectra indicated the presence of two short-lived unknown complexes, where one was a major complex and the other a minor complex that was only present in the initial NMR spectra. The major ruthenium-containing species in the initial ^{1}H NMR spectrum was observed at 5.64 ppm for a potential cyclopentadienyl ligand, and in the ^{31}P{^{1}H} NMR spectrum the resonance for the coordinated triisopropylphosphine ligand was observed at 64.8 ppm. The minor initial unknown species in the ^{31}P{^{1}H} NMR spectrum exhibited a minor broad peak at 61.7 ppm for a triisopropylphosphine ligand.

After 24 hours, the ^{1}H NMR spectrum exhibited no resonances for uncoordinated phenylacetylene at 3.12 ppm. In the ^{1}H NMR spectrum a resonance at 8.58 ppm (broad) was seen for the protons at the C-2/6 positions for uncoordinated pyridine, and also uncoordinated acetonitrile at 1.97 ppm (singlet). However, after 24 hours the resonances for the major complex decreased in intensity, as the peaks for two new unidentified species at 75.8 and 58.8 ppm were observed in the ^{31}P{^{1}H} NMR spectrum. A 2D ^{1}H-^{1}H COSY experiment displayed a strong coupling between two peaks at 2.01 (d, J = 8.3 Hz) and at 6.61 (dd, J = 8.3 Hz, J = 0.9 Hz) ppm where these peaks had an equal integration. Unfortunately, the nature of these complexes is unknown, however it may

be possible that they are metal-containing intermediates in the formation of 1,4-butenyne species.

Additionally, the ^{1}H NMR spectrum after 24 hours exhibited resonances for the dimerisation products *E* and *Z*- 1,4-diphenylbut-1-ene-3-yne compounds. Where the vinyl protons for these compounds were displayed at 6.42 ppm (doublet, $^{3}J_{HH}$ = 16.2 Hz) for *E*-butenyne and at 6.73 and 5.98 ppm (doublet, $^{3}J_{HH}$ = 12.0 Hz) for *Z*-butenyne.[87, 91]

A high resolution ESI-MS of the crude reaction mixture displayed one major ruthenium-containing peak with a *m/z* of 531.1756, which was assigned to a cationic fragment $[Ru(\eta^{5}\text{-}C_5H_5)(P^{i}Pr_3)(CCHPh)_2]^{+}$. This is consistent with the ruthenium-containing species that are responsible for the dimerisation of phenylacetylene (Section 1.4.1).

The reaction of phenylacetylene with **15** resulted in multiple unidentified ruthenium-containing complexes; however it is possible that some of these species are related to the formation of the butenyne compounds. The triisopropylphosphine ligand at the ruthenium centre displayed extremely different reactivity towards terminal alkynes than the triphenylphosphine and trimethylphosphine containing complexes. Since trimethylphosphine is a more electron-donating ligand than triphenylphosphine, the difference in reactivity difference may not be due to electronic effects. A potential reason for the differences in reactivity of **15** in comparison to $\mathbf{10^{H}}$ could be due to the steric influence of the isopropyl substituents, as the triphenylphosphine-pyridylidene complexes **22** exhibit steric interactions at the ruthenium centre around the Ru-P bond. Additionally, it was not possible to synthesise a bis-substituted pyridine complex with a triisopropylphosphine ligand. It is therefore possible that there may a steric factor involved at the ruthenium centre for the coordination and reactivity of the pyridine and phenylacetylene molecules.

6.11 Reactivity of complex 16 with phenylacetylene

The complex $[Ru(\eta^5\text{-}C_5H_5)(P(OPh)_3)(NC_5H_5)_2][PF_6]$, **16** contained an electron-withdrawing phosphorus ligand, triphenylphosphite. The triphenylphosphite ligand changes the electronic properties of the ruthenium complex, as less electron density is present at the ruthenium centre in comparison to the triphenylphosphine analogue $\mathbf{10^H}$. The reactivity of **16** towards a stoichiometric quantity of ^{13}C-phenylacetylene in d_2-dichloromethane was investigated to determine if a similar reaction of $\mathbf{10^H}$ with phenylacetylene occurred (Scheme 6.25).

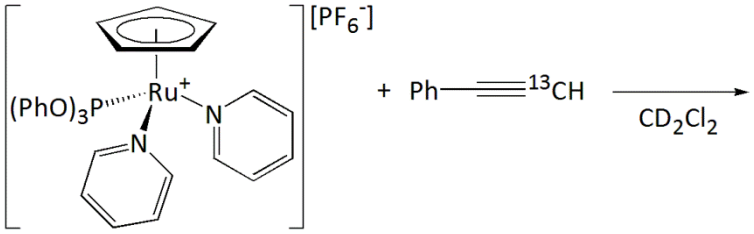

16

Scheme 6.25: Stoichiometric addition of ^{13}C-phenylacetylene to **16**.

The initial NMR spectra recorded after two hours at room temperature only exhibited resonances due to the starting materials, where the ^{1}H NMR spectrum displayed a singlet peak at 4.39 ppm for the cyclopentadienyl ligand of **16** at a doublet peak at 3.12 ppm with a $^1J_{HC}$ of 251 Hz for the terminal proton of ^{13}C-phenylacetylene. Also the ^{1}H NMR spectrum did not exhibit peaks for uncoordinated pyridine. The ^{31}P{^{1}H} NMR spectrum exhibited a singlet peak at 140.6 ppm for the phosphorus atom of the triphenylphosphite ligand. A ^{13}C{^{1}H} NMR spectrum displayed a singlet peak at 77.6 ppm for the ^{13}C label of ^{13}C-phenylacetylene. The reaction appeared to proceed slowly and was therefore heated for 24 hours at 50 °C. After heating the reaction mixture, the ^{1}H and ^{13}C{^{1}H} NMR spectra no longer displayed the peaks for ^{13}C-phenylacetylene indicating the alkyne had all reacted. Unfortunately, from the ^{13}C{^{1}H} NMR spectrum, there was no major resonance for the ^{13}C label, suggesting there was no major species in the reaction mixture. The ^{1}H and ^{31}P{^{1}H} NMR spectra suggested there were three minor new ruthenium-containing species, as in the ^{1}H NMR spectrum the cyclopentadienyl region contained singlet peaks at 4.74, 4.82 and 4.88 ppm, and in the ^{31}P{^{1}H} NMR spectrum there were resonances at 171.4, 174.0 (d, J_{PC} = 13.4 Hz) and 198.3 ppm for the phosphorus atom of the triphenylphosphite ligand. However, the

major resonances in the NMR spectra belonged to **16**. This data suggested that more than one equivalent of phenylacetylene was being consumed per ruthenium complex.

A further reaction involving the addition of 10 equivalents of phenylacetylene to a d_2-dichloromethane solution of **16** was heated for 16 hours at 50 °C and monitored using NMR spectroscopy. The NMR spectra of the reaction mixture demonstrated the absence of the resonances belonging to **16** and multiple resonances for unidentified species. Only one set of peaks from the previous stoichiometric reaction was present in the NMR spectra, in the ^{1}H NMR spectrum at 4.74 ppm for the cyclopentadienyl ligand and in the ^{31}P{^{1}H} NMR spectra at 198.3 ppm for the triphenylphosphite ligand.

A difference in the reactivity towards phenylacetylene is observed between complexes **16** and **10^{H}**. The electron-withdrawing effect of the triphenylphosphite ligand changed the reactivity observed when compared to triphenylphosphine. The major ruthenium complex initially formed upon the addition of phenylacetylene to **10^{H}** is the vinylidene-containing species **19^{H,Ph}**, this complex then reacts further to yield **22^{H,H}**. However the addition of phenylacetylene to **16** did not exhibit any evidence for a vinylidene-containing complex, this could be due to the ruthenium centre being electron-deficient in nature. Fischer type vinylidene complexes require an electron rich metal centre to stabilise an electron deficient vinylidene ligand (Section 1.3.2).[324] The absence of a vinylidene-containing complex from the reaction of **16** with phenylacetylene suggests that the ruthenium centre does not possess enough electron density to stabilise a vinylidene ligand at the ruthenium centre or the pyridine ligand may not be as labile.

6.12 Reactivity of $[Ru(\eta^5\text{-}C_5H_5)(PPh_3)_2]^+$ with phenylacetylene

The addition of phenylacetylene to complexes $\mathbf{9^{Ph}}$ and **31** in a d_2-dichloromethane solution was explored. The formation of the vinylidene-containing complexes $\mathbf{2^{Ph}}$ from the stoichiometric addition of phenylacetylene to the complexes $[Ru(\eta^5\text{-}C_5H_5)(PPh_3)_2(L)][PF_6]$ (where L = NCMe, NC_5H_5) was analysed *in situ*.

6.12.1 Reaction of $[Ru(\eta^5\text{-}C_5H_5)(PPh_3)_2(NCMe)][PF_6]$, 9^{Ph} with phenylacetylene

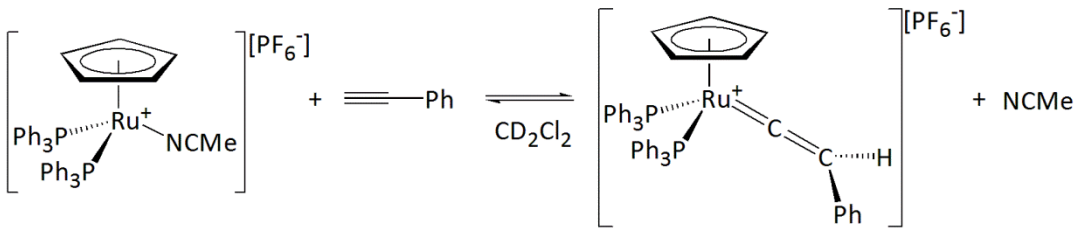

$\mathbf{9^{Ph}}$ $\mathbf{2^{Ph}}$

Scheme 6.26: Stoichiometric addition of phenylacetylene to $\mathbf{9^{Ph}}$ in d_2-dichloromethane.

The stoichiometric addition of phenylacetylene to $\mathbf{9^{Ph}}$ was monitored *via* NMR spectroscopy at different time periods (Scheme 6.26). The NMR spectra exhibited resonances for the formation of $\mathbf{2^{Ph}}$ in the reaction mixture. The ^{1}H NMR spectrum exhibited broad resonances at 5.27 (5H) and 5.43 (1H) ppm, for the cyclopentadienyl ligand and the proton of β carbon atom of the vinylidene ligand respectively. The $^{31}P\{^1H\}$ NMR spectrum displayed a peak at 43.9 ppm for the triphenylphosphine ligands of $\mathbf{2^{Ph}}$. The characterisation of this species was confirmed against an authentic sample of $\mathbf{2^{Ph}}$.

The ^{1}H NMR spectra over 1, 2, 3 and 10 days exhibited changes in the intensities for the resonances at 2.12 and 1.97 ppm for the acetonitrile methyl substituents of $\mathbf{9^{Ph}}$ and the uncoordinated species respectively. The reaction mixture displayed an increase in the quantity of uncoordinated acetonitrile over time (Table 6.6). The reaction reached equilibrium between $\mathbf{9^{Ph}}$ and $\mathbf{2^{Ph}}$ as resonances for phenylacetylene were observed in the ^{1}H NMR spectrum at 3.13 ppm.

Days	Relative integrations of methyl substituents of acetonitrile	
	$\mathbf{9^{Ph}}$	Uncoordinated
1	1.0	0.2
2	1.0	2.8
3	1.0	4.0
10	1.0	5.5

Table 6.6: Relative integrations of acetonitrile methyl substituents of reaction mixture.

6.12.2 Reaction of $[Ru(\eta^5\text{-}C_5H_5)(PPh_3)_2(NC_5H_5)][PF_6]$, 31 with phenylacetylene

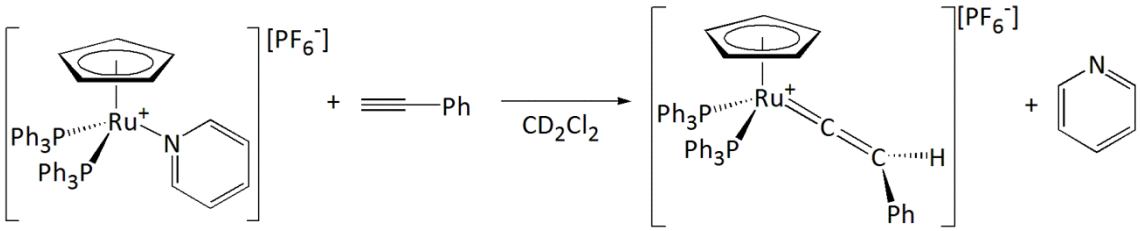

31 **$\mathbf{2^{Ph}}$**

Scheme 6.27: Stoichiometric addition of phenylacetylene to **31** in d_2-dichloromethane.

The stoichiometric addition of phenylacetylene to $[Ru(\eta^5\text{-}C_5H_5)(PPh_3)_2(NC_5H_5)][PF_6]$ was monitored *via* NMR spectroscopy and found to give resonances belonging to $\mathbf{2^{Ph}}$ by comparison with an authentic sample. In the ^1H NMR spectrum the cyclopentadienyl resonances at 4.42 ppm and in the $^{31}P\{^1H\}$ NMR spectrum for the triphenylphosphine ligand at 43.4 ppm belonging to **31** were found to be absent after two days suggesting the reaction had gone to completion. Additionally, the ^1H NMR spectrum displayed resonances at 7.70 (1H) and 8.58 (2H) ppm for uncoordinated pyridine in the reaction mixture.

6.12.3 Comparison of the reaction of $\mathbf{9^{Ph}}$ and 31 with phenylacetylene

The vinylidene-containing complex $\mathbf{2^{Ph}}$ was generated from the addition of phenylacetylene to complexes $\mathbf{9^{Ph}}$ and **31**. The related reaction of $\mathbf{9^{Ph}}$ remained in equilibrium after 10 days, however the reaction of **31** went to completion within two days. This difference in reactivity suggests that it is possible that the pyridine molecule is more labile on the $[Ru(\eta^5\text{-}C_5H_5)(PPh_3)_2]^+$ fragment, and could be due to the higher steric demand of the heterocycle.

6.13 Properties of the vinylidene-containing complexes $19^{R1,R2}$ and $28^{R1,R2}$

The spectroscopic properties of complexes $\mathbf{19^{R1,R2}}$ and $\mathbf{28^{R1,R2}}$ will be discussed as they have exhibited similar behaviour in a dichloromethane solution upon the addition of terminal alkynes and the substituent effects will be briefly described.

The addition of the terminal alkynes (phenylacetylene, 1-ethynyl-4-fluorobenzene, 4-ethynyl-α,α,α-trifluorotoluene) to complexes $\mathbf{10^{R}}$ or $\mathbf{13^{R}}$ in dichloromethane resulted in the formation of the vinylidene-containing complexes $\mathbf{19^{R1,R2}}$ and $\mathbf{28^{R1,R2}}$ where the NMR spectra displayed broad resonances for these short-lived intermediates. The formation of $\mathbf{19^{R1,R2}}$ and $\mathbf{28^{R1,R2}}$ in the dichloromethane solution required the coordination of the terminal alkyne and dissociation of the N-containing heterocycles. In the literature it is well established that the vinylidene proton at the β-carbon atom is readily deprotonated in a basic medium,[54] and therefore upon formation of the species $\mathbf{19^{R1,R2}}$ and $\mathbf{28^{R1,R2}}$ an uncoordinated equivalent of the basic N-containing heterocycles will be present in the reaction mixture. In solution it is possible that an equilibrium exists between the vinylidene-containing species and the acetylide complex, where the N-containing heterocycles are acting as a base to deprotonated the vinylidene proton at the β-carbon atom. The only vinylidene-containing species that remained in solution was $\mathbf{19^{H,tBu}}$ and this could potentially be attributed to the bulkiness of the *tert*-butyl group.

The presence of the electron-withdrawing groups on the phenyl ring of $\mathbf{19^{R1,R2}}$ and $\mathbf{28^{R1,R2}}$ has displayed a change in the δ_P of the triphenylphosphine ligands, as when the groups change from H, F, CF_3 the chemical shifts move further upfield. For example the δ_P of $\mathbf{19^{H,H}}$,$\mathbf{19^{H,C6H4\text{-}4\text{-}F}}$ and $\mathbf{19^{H,C6H4\text{-}4\text{-}CF3}}$ are exhibited at 51.8, 51.7 and 51.0 ppm respectively, where the largest difference in the chemical shifts is observed between the F and the CF_3 groups. This can be attributed to the additional fluorine atoms which through an inductive effect withdraw electron density from the complex.

6.14 Determining properties of the pyridylidene complexes

The type of bonding in the C-H functionalised complexes could either be considered as a pyridinium- or carbene-type of ligand is discussed. Existing pyridylidene-containing transition metal complexes exhibit characteristic spectroscopic properties. A comparison of the spectroscopic data for the pyridylidene-containing complexes **22**$^{\mathbf{R1,R2}}$, **23**$^{\mathbf{R1,R2}}$, **27**$^{\mathbf{R1,R2}}$ and **30**$^{\mathbf{R1,R2}}$ will be conducted. The X-ray crystallography data obtained for the complexes will also be compared to the established literature of pyridylidene-containing complexes.

6.14.1 General NMR spectroscopy data of the pyridylidene complexes

To determine the coordination of the C-H functionalised N-containing heterocycle, some of the key spectroscopic data for the pyridylidene-alkene complexes have been presented (Table 6.7, Table 6.8 and Table 6.9). The $^{13}C\{^{1}H\}$, ^{1}H and $^{13}P\{^{1}H\}$ NMR data are discussed in this section. The carbon atom of the C-H functionalised pyridylidene ligands of **22**$^{\mathbf{R1,R2}}$, **27**$^{\mathbf{R1,R2}}$ and **30**$^{\mathbf{R1,R2}}$ were observed in the $^{13}C\{^{1}H\}$ NMR spectrum between 167.2 –182.3 ppm as doublets, where a $^{2}J_{CP}$ of approximately 19 Hz was observed. The downfield shift from pyridine suggests a more carbene-type of character is present. The reported ruthenium pyridylidene ligands in the literature exhibit a δ_C for the carbene carbon atom between 205 – 220 ppm.[221-223] However, higher field chemical shifts have been observed for the iridium and osmium pyridylidene complexes between 170 – 200 ppm.[211] The complexes synthesised in this thesis are therefore consistent with those presented in the literature (Section 1.8).

The ^{1}H NMR spectra of **22**$^{\mathbf{R1,R2}}$, **27**$^{\mathbf{R1,R2}}$ and **30**$^{\mathbf{R1,R2}}$ for the coordinated alkene group at the ruthenium centre exhibited peaks at approximately 3.6 and 6.6 ppm, where the resonances at approximately 3.6 ppm displayed larger $^{3}J_{HP}$ coupling constants at around 12 Hz, where as the resonances at approximately 6.6 ppm displayed smaller $^{3}J_{HP}$ values of ~1.5 Hz. Similar observations have been reported in the literature for the η^2-coordination of an alkene to transition metal centres.[325-328] To analyse the metal to alkene bonding interaction through NMR spectroscopy, the change in the chemical shifts of the coordinated and uncoordinated alkene proton and carbon atoms can be calculated.[140, 318, 319] The larger the difference in the chemical shifts suggests a stronger donation of electron density from the metal centre to the alkene.[140] The significant upfield shift of one of the alkene atoms has been reported, where the shielded effect is

due to additional electron density from the metal centre being donated to the alkene group.[94, 325, 329]

Additionally, in the ^{1}H NMR spectra of **22**$^{\mathbf{R1,R2}}$ and **27**$^{\mathbf{R1,R2}}$ the aromatic region displayed broad resonances for the phenyl rings of the triphenylphosphine ligand, this was due to the restricted rotation of the Ru-P bond on the NMR timescale and therefore each of the phenyl rings experienced an individual environment. For complexes **30**$^{\mathbf{R1,R2}}$ there were no broad resonances were observed for the methyl substituents of the trimethylphosphine ligands, suggesting these species were less sterically hindered around the ruthenium centre.

The ^{31}P{^{1}H} NMR chemical shifts for **22**$^{\mathbf{R1,R2}}$ and **27**$^{\mathbf{R1,R2}}$ were observed between 50.5 – 54.7 ppm for the coordinated triphenylphosphine ligand and for the **30**$^{\mathbf{R1,R2}}$ complexes the resonances were observed at approximately 15 ppm for the trimethylphosphine ligand.

The spectroscopic data for the 1-ruthanaindolizine complexes **23**$^{\mathbf{R1,R2}}$ were compared to the complexes **22**$^{\mathbf{R1,R2}}$. The δ_C for the Ru-C bonds to the pyridylidene fragment of **23**$^{\mathbf{R1,R2}}$ shifted further downfield and observed between 217.8 – 219.3 ppm where a $^{2}J_{HP}$ of approximately 15.5 Hz was found. The other Ru-C bond in the ^{13}C{^{1}H} NMR spectrum were observed at ~190 ppm with a smaller $^{2}J_{HP}$ of approximately 12.9 Hz. Interestingly, the δ_P for the triphenylphosphine ligands of **23**$^{\mathbf{R1,R2}}$ were seen at a higher chemical shift of approximately 60 ppm in comparison to complexes **22**$^{\mathbf{R1,R2}}$.

The NMR spectroscopic data for the reported pyridylidene complexes in this chapter were compared and the substituent effects have been studied (Table 6.7 and Table 6.8). The Hammett constants have assisted in determining the electronic properties of the substituents.[292-295] In all complexes **22**$^{\mathbf{R1,R2}}$, **27**$^{\mathbf{R1,R2}}$ and **30**$^{\mathbf{R1,R2}}$ the resonances for the alkene protons, the phosphine ligand and the carbon of the pyridylidene ligand have been evaluated with regards to:

i) The presence of a 4-CF_3 group on the phenyl group of the terminal alkyne;
ii) The substituents at the 4-position of the N-containing heterocycles (e.g. H, Me, NMe_2)

On changing the substituent at the 4-position of the terminal alkyne from H to CF_3, the effect of an electron-withdrawing group was investigated and changes were observed in the ^{1}H and ^{31}P{^{1}H} NMR spectra.[292-295] In the ^{1}H NMR spectrum the resonances

belonging to the alkene resonances at ~3.6 ppm all shifted upfield, where as the other alkene proton resonances are further downfield at ~6.6 ppm. The resonances at ~3.6 ppm are for the alkene protons that are more closely bonded to the aryl group (Ph or 4-CF_3-C_6H_4). The presence of the 4-CF_3 substituent has shielded the alkene protons at ~3.6 ppm, which suggests that additional electron density is donated into the metal to alkene bond.[140] Additionally, the $^{31}P\{^1H\}$ chemical shifts have shifted further upfield upon the presence of a 4-CF_3 substituent.

Alternatively, more electron-donating substituents on the N-containing heterocycles were introduced at the 4-position (H, Me and NMe_2) where the C-3/5 and nitrogen donor atom positions are activated on the ring.[292-295] The methyl substituent activates positions around the phenyl ring *via* an inductive effect, where as the NMe_2 group strongly activates the positions due to conjugation. The $^{31}P\{^1H\}$ NMR chemical shifts as the substituents became more electron-donating all shifted further downfield, where the a larger difference in the chemical shifts were observed on going from Me to NMe_2 (opposite effect to the electron-withdrawing substituents above). The $^{13}C\{^1H\}$ NMR chemical shifts for the C-H functionalised carbon atom on the pyridylidene ligand shifted upfield, indicating that the carbon atoms were shielded as the substituents on the N-containing heterocycle became more electron-donating. Similar trends were reported by Bercaw *et al.*, when studying the effects of electron-releasing groups.[188]

Complex	δ_H Ru-(CH(pyr)=C*H*(Ar))	δ_H Ru-(C*H*(pyr)=CH(Ar))	δ_P PR_3
22^{H,H}	3.65 (app t, $^3J_{HH}$, $^3J_{HP}$ = 9.5 Hz)	6.63 (d, $^3J_{HH}$ = 7.8 Hz)	53.5
22^{H,CF3}	3.60 (dd, $^3J_{HP}$ = 11.4 Hz, $^3J_{HH}$ = 7.9 Hz)	6.77 (d, $^3J_{HH}$ = 7.9 Hz)	52.8
22^{Me,H}	3.68 (m)	6.47 (d, $^3J_{HH}$ = 7.8 Hz)	53.6
22^{Me,CF3}	3.62 (dd, $^3J_{HP}$ = 11.6 Hz, $^3J_{HH}$ = 7.7 Hz)	6.68 (d, $^3J_{HH}$ = 7.7 Hz)	52.9
22^{NMe2,H}	3.55 (dd, $^3J_{HP}$ = 11.7 Hz, $^3J_{HH}$ = 7.9 Hz)	6.32 (dd, $^3J_{HH}$ = 7.9 Hz, $^3J_{HP}$ = 1.6 Hz)	55.3
22^{NMe2,CF3}	3.48 (dd, $^3J_{HP}$ = 11.7 Hz, $^3J_{HH}$ = 7.8 Hz)	6.44 (dd, $^3J_{HH}$ = 7.8 Hz, $^3J_{HP}$ = 1.7 Hz)	54.7
27a^{H}	3.47 (dd, $^3J_{HP}$ = 12.3 Hz, $^3J_{HH}$ = 8.0 Hz)	6.51 (dd, $^3J_{HH}$ = 8.0 Hz, $^3J_{HP}$ = 1.5 Hz)	51.2
27b^{H}	3.62 (broad)	6.62 (broad d, $^3J_{HH}$ = 8.2 Hz)	53.7
27a^{CF3}	3.44 (dd, $^3J_{HP}$ = 12.3 Hz, $^3J_{HH}$ = 7.9 Hz)	6.61 (dd, $^3J_{HH}$ = 7.9 Hz, $^3J_{HP}$ = 1.7 Hz)	50.5
27b^{CF3}	3.57 (dd, 1H, $^3J_{HP}$ = 11.4 Hz, $^3J_{HH}$ = 7.9 Hz	6.71 (dd, $^3J_{HH}$ = 7.9 Hz, $^3J_{HP}$ = 0.9 Hz)	53.0
30^{H,H}	3.57 (dd, $^3J_{HP}$ = 12.9 Hz, $^2J_{HH}$ = 7.0 Hz)	6.37 (dd, $^2J_{HP}$ = 7.0 Hz, $^3J_{HP}$ = 1.3 Hz)	14.8
30^{H,CF3}	3.55 (dd, $^3J_{HP}$ = 12.9 Hz, $^3J_{HH}$ = 6.8Hz)	6.48 (dd, $^3J_{HH}$ = 6.8 Hz, $^3J_{HP}$ = 1.5 Hz)	14.2
30^{NMe2,H}	3.47 (dd, $^3J_{HP}$ = 13.1 Hz, $^3J_{HH}$ = 6.9 Hz)	6.10 (dd, $^3J_{HH}$ = 6.9 Hz, $^3J_{HP}$ = 1.1 Hz)	16.1
30^{NMe2,CF3}	3.45 (dd, $^3J_{HP}$ = 13.1 Hz, $^3J_{HH}$ = 6.8 Hz)	6.17 (dd, $^3J_{HH}$ = 6.8 Hz, $^3J_{HP}$ = 1.5 Hz)	15.6

Table 6.7: Comparison of the ^{1}H and ^{13}P{^{1}H} NMR spectroscopic data for the pyridylidene-containing complexes **22^{R1,R2}**, **27^{R1,R2}** and **30^{R1,R2}**.

Complex	δ_C Ru-C (alkene)	δ_C Ru-C (pyridylidene)
22^{H,H}	55.2 (s) and 69.4 (s)	180.7 (broad)
22^{H,CF3}	66.6 (d, $^2J_{CP}$ = 3 Hz) and 54.8 (s)	179.6 (d, $^2J_{CP}$ = 19 Hz)
22^{Me,H}	54.7 (broad), 68.6 (s)	178.2 (d, $^2J_{CP}$ = 18.4 Hz)
22^{Me,CF3}	~54.1 (lies underneath CD_2Cl_2 peak), 65.9 (broad)	177.1 (d, $^2J_{CP}$ = 18 Hz)
22^{NMe2,H}	53.1 (s), 68.4 (d, $^3J_{CP}$ = 2.6 Hz),	167.2 (d, $^2J_{CP}$ = 20.5 Hz)
27a^{CF3}, 27b^{CF3}		173.9 (d, $^2J_{CP}$ = 18.9 Hz) and 179.9 (d, $^2J_{CP}$ = 16.6 Hz)
30^{H,H}	62.1 (d, $^2J_{CP}$ = 4.6 Hz), 76.1 (d, $^2J_{CP}$ = 2.4 Hz)	182.3 (d, $^2J_{CP}$ = 19.9 Hz)

Table 6.8: Comparison of $^{13}C\{^1H\}$ NMR spectroscopic data for the pyridylidene-containing complexes **22^{R1,R2}**, **27^{R1,R2}** and **30^{R1,R2}**.

Complex	δ_C Ru-C	δ_C Ru-C (pyridylidene)	δ_P PR_3
23^{H,H}	192.9 (d, $^2J_{CP}$ = 12.7 Hz))	218.3 (d, $^2J_{CP}$ = 15.3 Hz)	60.3
23^{H,CF3}	190.2 (broad)	219.3 (broad)	61.2
23^{Me,CF3}	187.9 (d, $^2J_{CP}$ = 13 Hz)	217.8 (d, $^2J_{CP}$ = 16 Hz)	61.7

Table 6.9: Comparison of spectroscopic data for the pyridylidene-containing complexes **23^{R1,R2}**.

6.14.2 Analysis of the crystallographic data

The X-ray data for the pyridylidene complexes mentioned in this chapter have been compared with the relevant literature data for iridium[206-210, 213, 217, 218] and osmium[214, 221-224, 227, 330] complexes where the major contributions are from the research groups of Carmona and Esteruelas (Figure 6.9, Table 6.10). This will give an indication on the properties of these complexes.

The ruthenium-carbon bond length to the pyridylidene ligand was studied to provide information on the nature of the bonding interaction. For the complexes containing pyridylidene-alkene ligands $\mathbf{22^{R1,R2}}$ and $\mathbf{30^{R1,R2}}$, the ruthenium-carbon bonds ranged between 2.0101(19) - 2.043(2) Å, where these bond lengths are longer than for the iridium and osmium complexes apart from complex ***i*** (Table 6.10). This suggested that there may be more carbene character in the complexes in the literature complexes. A comparison of the ruthenium-carbon bond lengths to complexes containing the more traditional NHC ligands has also been included.[155, 331, 332] Theoretical studies calculated a ruthenium-carbon (carbene) bond length of 2.108 Å for the complex $[Ru(CO)_4(nNHC)]$ (where nNHC = imidazol-2-ylidene).[161] Additionally, an X-ray structure of a ruthenium NHC complex from Whittlesey *et al.* demonstrated that the ruthenium-carbon (carbene) bond length was 2.1282(18) Å.[333] A set of ruthenium NHC complexes exhibited ruthenium-carbon (carbene) bond lengths of 2.045(2), 1.93(2), 2.087(2) and 2.188(2) Å.[334] Generally, the ruthenium-carbon bond lengths of the complexes $\mathbf{22^{R1,R2}}$ and $\mathbf{30^{R1,R2}}$ display shorter bond lengths in comparison to the already existing ruthenium NHC complexes present in the literature. This suggests there is a carbene-like property in the $\mathbf{22^{R1,R2}}$ and $\mathbf{30^{R1,R2}}$ complexes and therefore can be described as a pyridylidene ligand.

The structural features from the coordination of the alkene group in the complexes $\mathbf{22^{R1,R2}}$ and $\mathbf{30^{R1,R2}}$ was compared to several species reported in the literature. The C(11)-C(12) bond lengths for the complexes $\mathbf{22^{R1,R2}}$ and $\mathbf{30^{R1,R2}}$ fall in the range for other metal η^2-alkene complexes (carbon-carbon bond lengths are reported to range between 1.40 – 1.46 Å).[218, 335] The C(11)-C(12) bond lengths are between those expected for a carbon-carbon single and double bond.[335] Additionally, there is significant difference in the ruthenium to carbon bond lengths of the alkene group. In cases where there is a strong interaction the metal-alkene coordination can be described as a metallacyclopropane. There are two key interactions: donation of the alkene π

electrons to the metal d orbitals and a metal to alkene π* back-bonding interaction. The geometry of cyclopentadienyl transition metal complexes with an η^2-coordinated alkene group is hypothesised to be due to both electronic and steric factors, in comparison to octahedral species where electronic factors are more dominant.[140, 336] A stabilisation is found to occur upon the metal fragment moving towards one end of the alkene bond, which results in the LUMO decreasing in energy and therefore becoming localised on the further carbon atom.[318, 319] The NMR spectroscopic and X-ray crystallographic data are both consistent with the pyridylidene-alkene fragment in the half-sandwich ruthenium complexes **22**$^{\mathbf{R1,R2}}$ and **30**$^{\mathbf{R1,R2}}$.

The 1-ruthanaindolizine complex **23**$^{\mathbf{H,CF3}}$ displayed a shorter ruthenium-carbon bond length (1.996(2) Å) in comparison to the pyridylidene-alkene containing complexes, and can be interpreted as the species having additional carbene character. Interestingly, the C(6)-N and C(6)-C(7) bond length are now significantly longer. This is also observed in the $^{13}C\{^1H\}$ NMR spectrum as the carbon atom on the pyridylidene ligand exhibits a more downfield resonance at 219.3 ppm. The C(11)-C(12) bond length for **23**$^{\mathbf{H,CF3}}$ was shorter (1.339(3) Å) and therefore suggests this bond has more multiple bond character than in complexes **22**$^{\mathbf{R1,R2}}$ and **30**$^{\mathbf{R1,R2}}$. The C(11)-C(12) bond length of **23**$^{\mathbf{H,CF3}}$ was closer to ***f*** than ***d***, which corroborates the carbon-carbon double bond structure. Similar 3-ruthanaindolizine and 3-osmaindolizine complexes have been reported by Esteruelas *et al.*[142, 143] which display that there is a significant amount of delocalisation in their systems due to the shortening of the metal-carbon and metal-nitrogen bond lengths. Based upon bond lengths around the ruthenacycle it is reasonable to suggest that delocalisation in **23**$^{\mathbf{H,CF3}}$ exists.

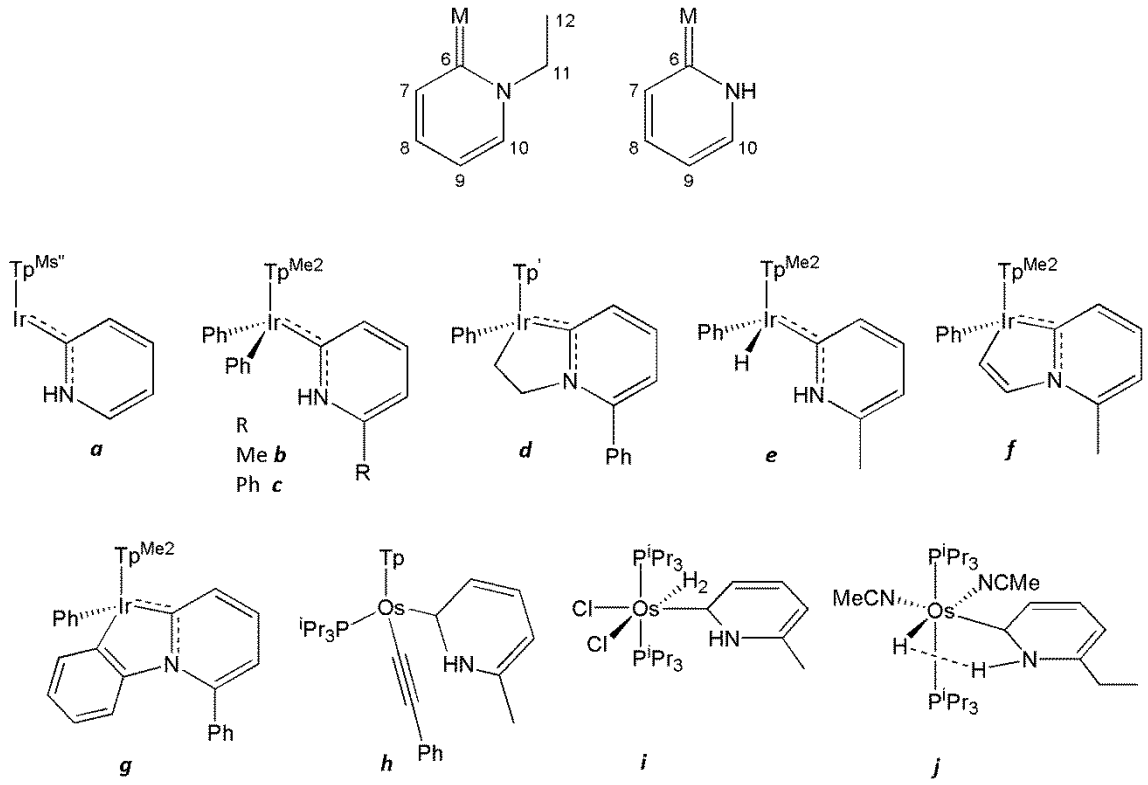

Figure 6.9: Pyridylidene schematics and labels for Table 6.10.

	M-C(6)	C(6)-N	C(6)-C(7)	C(7)-C(8)	C(8)-C(9)	C(9)-C(10)	C(10)-N	C(11)-N	C(11)-C(12)	M-C(11)	M-C(12)
22^{H,H}	2.0390(19)	1.359(2)	1.406(3)	1.388(3)	1.402(3)	1.373(3)	1.349(2)	1.453(2)	1.405(3)	2.152(2)	2.2575(19)
22^{H,F}	2.0384(19)	1.352(3)	1.409(3)	1.379(3)	1.399(4)	1.370(4)	1.355(3)	1.449(3)	1.413(3)	2.137(2)	2.247(2)
22^{H,CF3}	2.029(3)	1.360(3)	1.401(4)	1.380(4)	1.405(4)	1.367(4)	1.353(3)	1.459(3)	1.411(4)	2.127(3)	2.245(3)
22^{Me,H}	2.0183(19)	1.360(2)	1.360(2)	1.387(3)	1.408(3)	1.370(3)	1.351(2)	1.457(2)	1.410(3)	2.1435(19)	2.272(2)
22^{Me,CF3}	2.024(4)	1.355(5)	1.387(6)	1.385(6)	1.409(6)	1.356(6)	1.355(5)	1.448(5)	1.410(6)	2.128(4)	2.256(4)
22^{NMe2,H}	2.043(2)	1.363(3)	1.380(3)	1.418(3)	1.425(4)	1.360(4)	1.350(3)	1.449(3)	1.407(3)	2.140(2)	2.242(2)
30^{H,H}	2.0101(19)	1.355(3)	1.397(3)	1.377(3)	1.397(3)	1.360(3)	1.348(3)	1.449(2)	1.414(3)	2.120(2)	2.224(2)
30^{NMe2,H}	2.0323(19)	1.365(2)	1.379(3)	1.424(3)	1.430(3)	1.354(3)	1.451(2)	1.451(2)	1.423(3)	2.1332(18)	2.2460(18)
23^{H,CF3}	1.996(2)	1.394(3)	1.420(3)	1.375(3)	1.406(4)	1.353(4)	1.368(3)	1.415(3)	1.339(3)		2.046(2)
***a*^{207}**	1.975(2)	1.368(3)	1.423(4)	1.369(4)	1.402(3)	1.363(4)	1.361(4)				
***b*$^{206, 208}$**	1.982(2)	1.366(3)	1.422(2)	1.373(3)	1.402(3)	1.358(3)	1.364(2)				
***c*$^{206, 208}$**	1.978(3)	1.369(4)	1.431(4)	1.379(4)	1.397(6)	1.366(5)	1.396(5)				
***d*^{217}**	1.949(3)	1.384(4)	1.414(4)	1.369(5)	1.402(6)	1.371(5)	1.375(4)	1.500(4)	1.533(4)		2.063(3)
***e*^{213}**	1.983(9)	1.347(11)	1.414(12)	1.375(13)	1.417(15)	1.356(15)	1.365(13)				
***f*^{213}**	1.989(4)	1.387(6)	1.408(6)	1.366(7)	1.386(7)	1.368(7)	1.379(6)	1.428(6)	1.327(7)		2.004(5)
***g*^{218}**	1.959(4)	1.397(5)	1.395(6)	1.395(6)	1.384(7)	1.353(7)	1.390(5)	1.462(6)	1.402(6)		
***h*^{227}**	1.994(3)	1.379(4)	1.435(4)	1.361(5)	1.404(5)	1.363(5)	1.360(4)				
***i*^{223}**	2.055(8)	1.366(9)	1.41(1)	1.37(1)	1.39(1)	1.35(1)	1.39(1)				
***j*^{224}**	1.993(6)	1.392(7)	1.420(8)	1.374(9)	1.415(10)	1.344(9)	1.363(7)				

Table 6.10: Comparison of X-ray crystallography data for the pyridylidene-alkene complexes.

6.15 Conclusions

The reactivity of complexes **10^{H}** with terminal alkynes (aryl and alkyl substituents) and TMS-substituted alkynes in dichloromethane has been investigated. The reactions of **10^{H}** with *tert*-butylacetylene provided significant mechanistic evidence and suggested that the vinylidene-containing intermediates were important in the further reactivity of the half-sandwich ruthenium complexes. Reactions conducted with the TMS-substituted alkynes unfortunately yielded many unknown complexes and further reactivity of the $[PF_6]^-$ anion. However, these studies displayed that the choice of anions was important in extending the lifetime of the catalyst.

Further investigations were made into substituent effects at the N-containing heterocycle and the terminal aryl alkynes. The reactivity of **10^{Me}** was very similar that of **10^{H}**, where the formation of complexes **20**, **21** and **22** was observed. However, more selective reactions were observed upon the reaction of **10^{NMe2}** to generate **22^{NMe2,R2}**. Unfortunately, purification of these reactions were challenging due to the formation of the more thermodynamically stable, $[Ru(\eta^5\text{-}C_5H_5)(PPh_3)_2Cl]$ **1**. These reactions generated the novel pyridylidene-alkene complexes **22** and data gathered supports the proposed structures. Reactions of **11** with terminal alkynes produced both isomers of the pyridylidene-alkene complexes **27**, therefore exhibiting that there is not a significant selective route for the C-H functionalisation to occur. Upon the reaction of complexes **13** with terminal alkynes the major products observed were those belonging to alkyne dimerisation. The formation of an NHC ligand from the imidazole rings suggested was not observed. The spectroscopic data of these complexes has been analysed.

Other factors investigated included altering the phosphorus-containing ligands. The reactivity of complexes **14** with terminal alkynes generated the pyridylidene-alkene containing complexes, **30**. The deprotonation of one of the alkene protons to generate the respective 1-ruthanaindolizine species was not obtained. Additionally, reactions where triisopropylphosphine and triphenylphosphite were employed did not generate similar products.

Overall, a range of novel pyridylidene-containing ruthenium complexes have been synthesised and their properties compared to the existing literature. The scope of these reactions has been tested and also provided significant mechanistic data for determining the potential energy surface.

Chapter 7. Catalysis

7.1 Introduction

The extensive role of $[Ru(\eta^5\text{-}C_5H_5)Cl(PPh_3)_2]$, **1** and other $[Ru(\eta^5\text{-}C_5H_5)]^+$ species for catalysis was described in a review by Trost.[40] Bruce *et al.* reported the synthesis of ruthenium vinylidene complexes from terminal alkynes.[54] The formation of ruthenium vinylidene complexes introduces a bond polarity to the carbon-carbon double bond and therefore induces selectivity in reaction products, alongside the advantage of atom economy from activation of the C-H bond.[46]

Murakami and Hori employed $[Ru(\eta^5\text{-}C_5H_5)Cl(PPh_3)_2]$, **1** and $NaPF_6$ as a more convenient alternative to the cationic complex $[Ru(\eta^5\text{-}C_5H_5)(PPh_3)_2(=C=CHPh)][PF_6]$, $\mathbf{2^{Ph}}$ for the alkenylation reaction of pyridine with TMS-substituted alkynes. To understand the catalytic process, it is imperative to observe the reactivity of **1** in solution. When mentioning the reaction conditions employed by Murakami and Hori throughout this chapter it will be in reference to the paper published in 2003.[253]

Previous chapters have discussed the mechanistic findings from stoichiometric studies of $[Ru(\eta^5\text{-}C_5H_5)(PPh_3)(NC_5H_5)_2][PF_6]$, $\mathbf{10^H}$ with various alkynes in a dichloromethane solution. To build on the knowledge gained from this system, catalytic reaction conditions will be screened. This chapter addresses the catalytic reactions for the synthesis of 2-styrylpyridine derivatives. The first part of this chapter will investigate the role of different half-sandwich ruthenium complexes as potential catalysts for the alkenylation reactions. The roles of $[Ru(\eta^5\text{-}C_5H_5)Cl(PPh_3)_2]$ **1**, $[Ru(\eta^5\text{-}C_5H_5)(C{\equiv}CPh)(PPh_3)_2]$ $\mathbf{3^{Ph}}$, $[Ru(\eta^5\text{-}C_5H_5)(PPh_3)_2(NC_5H_5)][PF_6]$ **31** and $[Ru(\eta^5\text{-}C_5H_5)(PPh_3)(NC_5H_5)_2][PF_6]$ $\mathbf{10^H}$ with TMS-substituted alkynes in a pyridine solution have been explored. The second half of the chapter looks at the development of the catalytic conditions originally reported by Murakami and Hori. The effects of terminal alkynes, lower temperatures, addition of alkynes to the reaction mixture, reduced catalyst loadings, changes in the reaction volume and application of microwave heating have been investigated.

7.2 Investigating the catalytic activity of complex 1

The role of [Ru(η^5-C_5H_5)Cl(PPh_3)$_2$], **1** in the alkenylation reaction of pyridine and TMS-substituted alkynes has been investigated. The original procedure reported for the alkenylation reaction to give 2-styrylpyridine has been repeated in our laboratory to provide a benchmark on the expected yields with respect to the literature. Additionally, the role of **1** in a mechanistic study has been explored and has offered information on how the reaction mechanism proceeds.

7.2.1 Repeating the reported catalytic conditions from Murakami and Hori

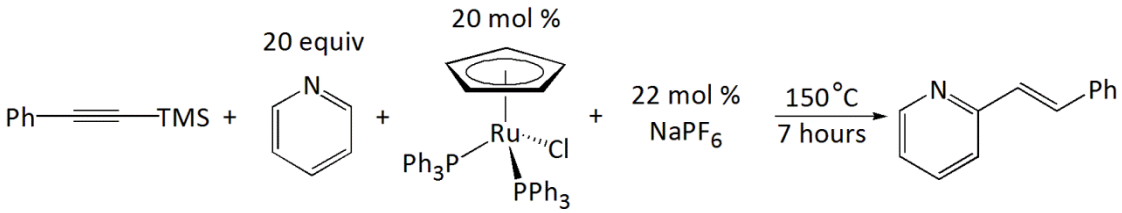

1

Scheme 7.1: Catalytic reaction conditions reported by Murakami and Hori.[253]

The alkenylation reaction by Murakami and Hori was repeated as reported in the literature, where the reaction required 20 mol % of the pre-catalyst [Ru(η^5-C_5H_5)Cl (PPh_3)$_2$], **1** in the presence of a halide scavenger $NaPF_6$ to perform the carbon-carbon coupling reaction between 1-phenyl-2-trimethylsilylacetylene and pyridine.[253] The reaction mixture was heated at 150 °C for 7 hours and the product, 2-styrylpyridine isolated *via* a preparative TLC method in a 12 % yield (Scheme 7.1). The isolated yield was significantly lower than reported in the literature (87 %), and although the reaction was repeated several times the isolated yield did not improve.

The alkenylation reaction of 4-methylphenyl(trimethylsilyl)ethyne was also repeated under the reported reaction conditions mentioned by Murakami and Hori and a higher isolated yield of 22 % was collected. Unfortunately again this was significantly lower than the literature reported yield of 92 %.

Murakami and Hori stated that when a 10 mol % catalyst loading of **1** was used the isolated yield of 2-styrylpyridine dropped to 24 %. This displayed that a high catalyst loading is required in the alkenylation reactions; however the discrepancy between the literature and experimental findings required further investigation in order to understand how the reaction proceeds.

7.2.2 Determining the role of 1 in the alkenylation reaction

To understand the role of **1** in the catalytic cycle to form 2-styrylpyridine, the catalytic quantities were recreated in d_5-pyridine. The TMS-substituted alkyne was replaced with the terminal alkyne $H^{13}C{\equiv}CPh$, to gather more information and the reaction was carried out employing aerobic conditions where the reagents were used as supplied. The reaction was monitored *via* NMR spectroscopy (Scheme 7.2, Figure 7.1).

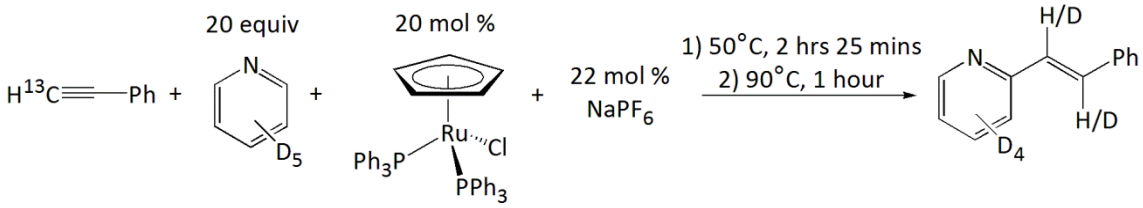

1

Scheme 7.2: A mechanistic insight into the catalytic reaction between $PhC^{13}CH$ and d_5-pyridine with **1**.

The initial NMR spectra after addition of the reagents did not display any changes at room temperature, and therefore the reaction mixture was heated at 50 °C for 25 minutes. The ^1H and $^{31}P\{^1H\}$ NMR spectra recorded after heating indicated that a reaction was occurring. Several ruthenium-containing products were identified in the reaction mixture from the NMR spectra as $[Ru(\eta^5\text{-}C_5H_5)(^{13}C{\equiv}CPh)(PPh_3)_2]$ $\mathbf{3^{Ph}}$, $Ru[(\eta^5\text{-}C_5H_5)(PPh_3)_2(NC_5H_5)][PF_6]$ **31**, and $[Ru(\eta^5\text{-}C_5H_5)(PPh_3)(NC_5H_5)_2][PF_6]$ $\mathbf{10^H}$ through comparisons with authentic samples. Additionally, the $^{31}P\{^1H\}$ NMR spectrum also displayed resonances for uncoordinated triphenylphosphine and triphenylphosphine oxide at -5.6 ppm and 26.4 ppm respectively.

Evidence for the acetylide species $\mathbf{3^{Ph}}$ in the ^1H NMR spectrum was determined by comparison with an authentic sample of the species in d_5-pyridine; the species $\mathbf{3^{Ph}}$ displayed a peak at 4.59 ppm for the cyclopentadienyl ligand and in addition the aromatic signals were also present in the reaction mixture. The $^{31}P\{^1H\}$ NMR spectrum exhibited a doublet signal at 50.3 ppm with a $^2J_{PC}$ of 24.8 Hz, due to the triphenylphosphine ligands coupling with the ^{13}C label. Additionally, this matched signals observed in the initial mechanistic studies where the cationic ruthenium vinylidene was added to d_5-pyridine (Chapter 2).

The reaction mixture was left at room temperature for 16 hours and no further reaction was observed. The sample was heated for a further two hours at 50 °C, and the NMR

spectra exhibited that the major species was **3**$^{\mathbf{Ph}}$, and that other ruthenium-containing species were present in minor quantities. Further heating of the sample within the NMR spectrometer at 90 °C for one hour did not result in any significant changes.

The complex **10**$^{\mathbf{H}}$ was present in the reaction mixture however it was only observed in the NMR spectra after heating for 25 minutes at 50 °C, further heating of reaction mixture at 90 °C for one hour displayed that **10**$^{\mathbf{H}}$ had reacted further. It is possible that under the catalytic conditions **10**$^{\mathbf{H}}$ reacts with additional phenylacetylene and that the two species are reacting further. As the ^{1}H NMR spectrum exhibited a doublet peak at 8.03 ppm with a $^{3}J_{HH}$ of 16.0 Hz, which is characteristic for one the alkene protons of 2-styrylpyridine. An ESI-MS of the reaction mixture exhibited *m/z* peaks at 187.1, 188.1 and 189.1 which were assigned as the species $[C_{12}{}^{13}CH_8D_4N]^+$, $[C_{12}{}^{13}CH_7D_5N]^+$ and $[C_{12}{}^{13}CH_6D_6N]^+$ respectively, where different levels of deuterium incorporation had occurred. The *m/z* peaks were consistent with either 2-styrylpyridine or the pyridylidene-alkene fragment from **22**$^{\mathbf{H,H}}$.

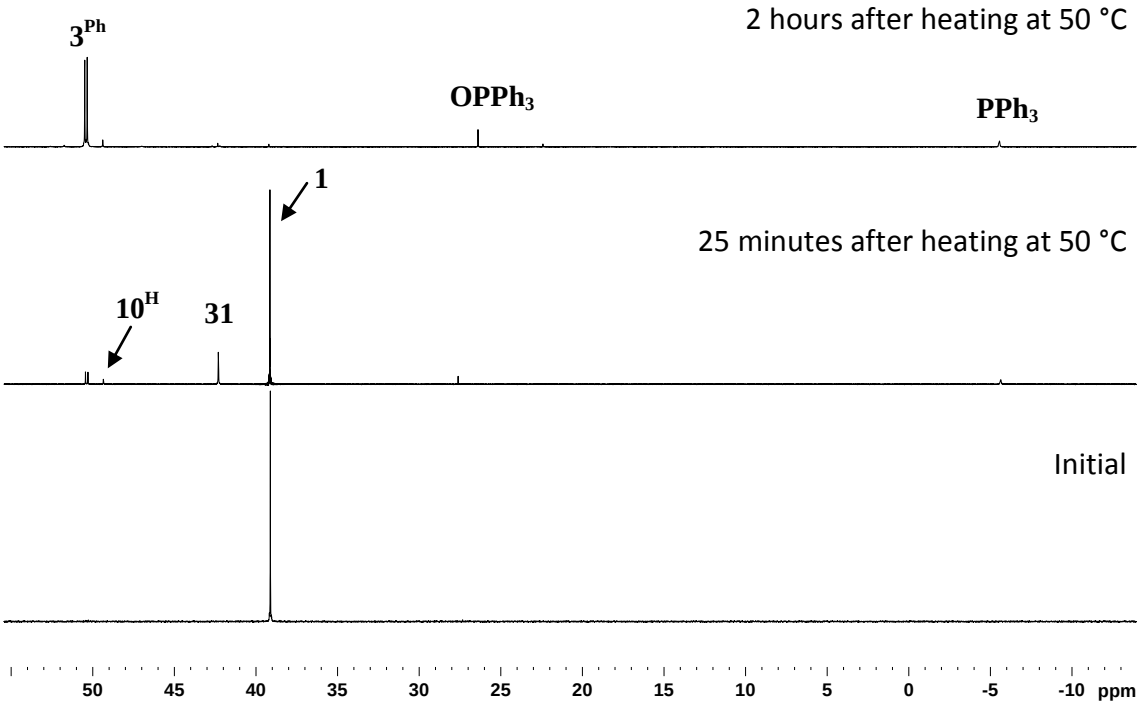

Figure 7.1: $^{31}P\{^{1}H\}$ NMR spectra of catalytic reaction of **1**, $NaPF_6$, $PhC^{13}CH$ and d_5-pyridine at different times.

7.3 Investigating the potential catalytic activity of $[Ru(\eta^5\text{-}C_5H_5)(C{\equiv}CPh)(PPh_3)_2]$, $\mathbf{3^{Ph}}$

The involvement of $\mathbf{3^{Ph}}$ as a potential catalyst in the alkenylation reaction of 2-styrylpyridine has been investigated with and without the presence of pyridinium tetrafluoroborate to determine if $\mathbf{3^{Ph}}$ was catalytically active. The activity of $\mathbf{3^{Ph}}$ was also investigated by Murakami and Hori, where they reported this species does not produce the alkenylation product, 2-styrylpyridine.[253]

7.3.1.1 In the absence of pyridinium tetrafluoroborate

A sample of $\mathbf{3^{Ph}}$ in d_5-pyridine was heated at 90 °C for 72 hours under aerobic conditions. The reaction mixture was analysed by NMR spectroscopy and ESI-MS. The NMR spectra after heating the reaction mixture revealed that the major species was $\mathbf{3^{Ph}}$, where the ^{1}H NMR spectrum displayed a singlet peak at 4.59 ppm for the cyclopentadienyl proton and the $^{31}P\{^1H\}$ NMR spectrum exhibited a singlet peak at 50.3 ppm for the triphenylphosphine ligands. Additionally, the $^{31}P\{^1H\}$ NMR spectrum exhibited a minor resonance at 25.5 ppm due to triphenylphosphine oxide. The ESI-MS of the reaction mixture did not display a peak for 2-styrylpyridine. The data suggested that the alkenylation reaction to give 2-styrylpyridine had not occurred, and therefore the reaction may require the presence of a proton in order to observe the formation of 2-styrylpyridine.

7.3.1.2 In the presence of pyridinium tetrafluoroborate

The stoichiometric addition of pyridinium tetrafluoroborate to $\mathbf{3^{Ph}}$ in d_5-pyridine was investigated by heating the reaction at 50 °C at various intervals over a total of 30 hours. No air-sensitive measures were employed and the reaction was monitored *via* NMR spectroscopy in order to observe if the presence of a proton in the reaction mixture resulted in the formation of 2-styrylpyridine.

After heating the reaction mixture for 30 hours at 50 °C, the NMR spectra exhibited that the reaction mixture contained several ruthenium-containing species and two major resonances in the $^{31}P\{^1H\}$ NMR spectrum exhibited peaks at 50.3 and 42.0 ppm for $\mathbf{3^{Ph}}$ and **4** respectively. The $^{31}P\{^1H\}$ NMR spectrum also displayed a peak at 25.5 ppm for triphenylphosphine oxide. The ESI-MS contained ruthenium isotope peaks with a *m/z* of 793.2 and 719.1, which were assigned as the cationic fragments $[Ru(\eta^5\text{-}C_5H_5)(PPh_3)_2(C_2HPh)]^+$ and $[Ru(\eta^5\text{-}C_5H_5)(PPh_3)_2(CO)]^+$ respectively. An IR spectrum of the reaction

mixture also displayed peaks at 2072.9 and 1975.2 cm^{-1} and were assigned as the $\nu_{C\equiv C}$ and ν_{CO} of $\mathbf{3^{Ph}}$ and **4** respectively.

The presence of protons in the reaction mixture would lead to an equilibrium exisiting in the reaction mixture between $\mathbf{3^{Ph}}$ and the vinylidene-containing complex, $\mathbf{2^{Ph}}$, where the reaction of $\mathbf{2^{Ph}}$ with air or water would give **4** (Section 1.4.3). The reaction mixture was analysed by ESI-MS and did not display any peaks for 2-styrylpyridine which was consistent with the ^{1}H NMR spectrum.

Pyridinium tetrafluoroborate did not allow the alkenylation reaction for the formation of 2-styrylpyridine. The anion dependence of reaction has not been investigated and it is possible that the $[PF_6]^-$ anion may cause a change in the reactivity. The reaction could be repeated with pyridinium hexafluorophosphate in order to observe if 2-styrylpyridine was synthesised under these reaction conditions. However, in the successful alkenylation reactions the NMR spectra display resonances for uncoordinated alkyne which has not been observed under these reaction conditions

7.4 Investigating the potential catalytic activity of $[Ru(\eta^5\text{-}C_5H_5)(PPh_3)_2(NC_5H_5)][PF_6]$, 31

The role of **31** as a potential catalyst was determined as in the catalytic reaction carried out previously (Section 7.2.2) this species was identified in the reaction mixture. To determine if **31** was catalytically active in the formation of 2-styrylpyridine, a catalytic reaction was conducted between 1-phenyl-2-trimethylsilylacetylene and pyridine where 20 mol % of **31** was used and the reaction mixture heated at 150 °C for 3 hours under non air-sensitive conditions. The reaction mixture was analysed by ESI-MS.

The ESI-MS of the reaction mixture did not display the expected *m/z* peak at 182.1 for 2-styrylpyridine. The ESI-MS revealed several ruthenium-containing peaks with *m/z* of 719.1 and 536.1 were present and were assigned as the cationic fragments $[Ru(\eta^5\text{-}C_5H_5)(PPh_3)_2(CO)]^+$ and $[Ru(\eta^5\text{-}C_5H_5)(PPh_3)(CO)(NC_5H_5)]^+$ respectively, and a *m/z* signal at 279.1 was due to triphenylphosphine oxide. The data from this experiment demonstrated that **31** was not a catalytically active species.

7.5 Investigating the potential catalytic activity of $[Ru(\eta^5\text{-}C_5H_5)(PPh_3)(NC_5H_5)_2][PF_6]$, 10^H

The reactivity of TMS-substituted alkynes with $\mathbf{10^H}$ in a pyridine solution under catalytic quantities was investigated, in order to evaluate the role of the TMS group. The reaction mixtures were studied extensively by ESI-MS.

7.5.1.1 Catalytic reaction with 1-phenyl-2-trimethylsilylacetylene

The ability of $\mathbf{10^H}$ to perform the alkenylation reaction between 1-phenyl-2-trimethylsilylacetylene and pyridine with 20 mol % of $\mathbf{10^H}$ was investigated under a nitrogen atmosphere. The reaction mixture was heated at 120 °C for 16 hours and the crude reaction mixture analysed *via* ESI-MS and NMR spectroscopy (Scheme 7.3).

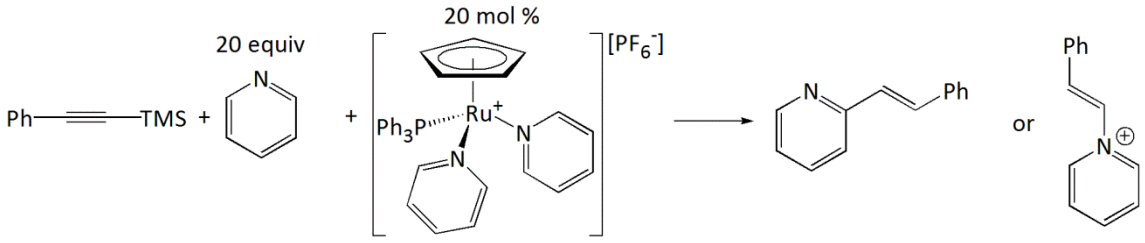

$\mathbf{10^H}$

Scheme 7.3: Investigating the catalytic activity of $\mathbf{10^H}$.

A high resolution ESI-MS displayed *m/z* peaks at 80.0502, 263.0985, and 279.0937 which indicated the presence of pyridine, triphenylphosphine, and triphenylphosphine oxide respectively. There was a *m/z* peak at 182.0966 with the correct isotope pattern for a $[C_{13}H_{12}N]^+$ species and this may have been due to the formation of 2-styrylpyridine or an isomer. In addition to this several peaks with a ruthenium isotope pattern were observed with a *m/z* peak of 793.1753 and 691.1289 which were assigned as the $[Ru(\eta^5\text{-}C_5H_5)(PPh_3)_2(C_2HPh)]^+$ and $[Ru(\eta^5\text{-}C_5H_5)(PPh_3)_2]^+$ fragments. Interestingly, a species with a *m/z* peak at 617.1289 was observed, where the isotope pattern was not consistent with it being a single ruthenium-containing complex (*m/z* peaks ranged between 610.1-626.1). However, it is likely that there are several ruthenium-containing fragments around the peak at 617 and therefore this created an unusual isotope pattern. Further experiments to characterise the peak at 617.1289 using an ESI-MS-MS method were employed, however it was not possible to isolate a single ruthenium-containing complex and therefore these species remain unidentified. It is also

important to note if the pyridylidene species **22** was present in the reaction mixture, then a *m/z* peak at 610.1242 would be expected.

An aliquot of the crude reaction mixture was analysed *via* NMR spectroscopy in d_2-dichloromethane. The ^{1}H NMR spectrum indicated that many side reactions occurred due to the presence of the TMS group on the alkyne, as there were multiple resonances around 0 ppm. The $^{31}P\{^{1}H\}$ NMR spectrum exhibited resonances for uncoordinated triphenylphosphine at -3.4 ppm and triphenylphosphine oxide at 28.6 ppm. There are also two major resonances at 40.4 and 51.7 ppm which have not been identified. The $[PF_6]^-$ resonance at -143.0 ppm is distorted, and there appears to be a broad sextet at -143.0 ppm, for a PF_5^--containing complex. The NMR spectra do not exhibit any peaks for the $\mathbf{2^{Ph}}$ or $\mathbf{3^{Ph}}$ in the reaction mixture, and therefore it is possible that these species may only be present in a minor quantity in the reaction mixture.

This catalytic reaction suggested that 2-styrylpyridine may potentially have been formed during the reaction, unfortunately there were many unidentified species present in the reaction mixture and therefore no conclusive results have been obtained The presence of the TMS group has resulted in the degradation of the non-coordinating anion $[PF_6]^-$. The absence of the $[PF_6]^-$ anion in the reaction mixture, could lead to the difficulties in regeneration of a cationic catalyst and therefore these reaction conditions are not sustainable.

The previous stoichiometric reaction between $\mathbf{10^{H}}$ and the TMS-substituted alkynes in a d_2-dichloromethane solution demonstrated that multiple unidentified ruthenium-containing species were formed and that the $[PF_6]^-$ anion was reacting further to yield a PF_2-containing compound (Chapter 5). These studies are both consistent with the fact that the $[PF_6]^-$ anion is not suitable for these studies and perhaps a more robust non-coordinating anion should be implemented to allow for fewer side-products being generated.

7.5.1.2 Catalytic reaction with 1-[(trimethylsilyl)ethynyl]-4-trifluorotoluene

A catalytic reaction between 1-[(trimethylsilyl)ethynyl]-4-trifluorotoluene and pyridine with 20 mol % of **10^{H}** and was carried out under aerobic conditions. The reaction mixture was heated at 150 °C for 7 hours. The reaction mixture was analysed with NMR spectroscopy and ESI-MS.

An aliquot of the crude reaction mixture was placed in $CDCl_3$ for analysis by NMR spectroscopy. The $^{31}P\{^{1}H\}$ NMR spectrum displayed peaks at 30.6 and -4.1 ppm for triphenylphosphine oxide and uncoordinated triphenylphosphine. A high resolution ESI-MS displayed a *m/z* peak at 250.0835 which is consistent with the cationic fragment $[C_{14}H_{11}F_3N]^+$ and could be interpreted as *E*-2-(4-trifluoromethyl)styrylpyridine.

In order to purify the alkenylation species *E*-2-(4-trifluoromethyl)styrylpyridine preparative TLC was employed. The collected product (impure, as shown by NMR spectroscopy) was characterised with NMR spectroscopy in $CDCl_3$. The ^{1}H NMR spectrum displayed characteristic resonances in the aromatic region at 8.63 (1H, d, $^{3}J_{HH}$ = 4.7 Hz), 7.40 (1H, d, $^{3}J_{HH}$ = 7.8 Hz) and 7.19 (1H, m) ppm for the protons at the 6-, 3- and 4-position around the pyridine ring of *E*-2-(4-(trifluoromethyl)styrylpyridine.

7.6 Developing the catalytic reactions between terminal alkynes and $[Ru(\eta^5\text{-}C_5H_5)(PPh_3)(NC_5H_5)_2][PF_6]$, $\mathbf{10^H}$

A range of catalytic reactions between terminal alkynes and pyridine with $\mathbf{10^H}$ have been investigated under a nitrogen atmosphere. An NMR-based method was developed to calculate the percentage conversion of the alkyne to the 2-styrylpyridine derivatives. The catalytic reaction conditions have been altered and either percentage yields or conversions calculated for the alkenylation product and the state of the ruthenium species at the end of the reaction mixture.

7.6.1 Determining the percentage conversion

A method to calculate the percentage conversion of the catalytic reactions was investigated as isolation of the alkenylation products resulted in significantly lower yields than those reported in the literature. The percentage conversion of the alkynes to the 2-styrylpyridine derivatives should have indicated whether the isolated yields for the catalytic reactions were representative. The catalyst loading in the reaction mixture was confirmed through the ^{1}H NMR spectra where the cyclopentadienyl ligand of $\mathbf{10^H}$ and the terminal proton of the alkyne were integrated with respect to each other. The catalytic reactions which employed 4-ethynyl-α,α,α-trifluorotoluene provided an additional NMR handle as the relative integrations of the CF_3 substituent and $[PF_6]^-$ anion in the ^{19}F NMR spectra provided information on the catalyst loading and these data should corroborate with the ^{1}H NMR spectra. In order to accurately measure the percentage conversions for the catalytic reactions using NMR spectroscopy, a set of T_1 (inversion recovery) measurements were conducted on a sample to containing $\mathbf{10^H}$ and 4-ethynyl-α,α,α-trifluorotoluene containing pyridine in a d_2-dichloromethane solution. In the ^{1}H NMR spectrum, a set of T_1 measurements on the cyclopentadienyl protons of $\mathbf{10^H}$ at 4.57 ppm had a T_1 of 4.2 seconds. However, the terminal proton did not display a measurable value of T_1, as when a maximum time delay between the pulses was set to 120 seconds, the intensity of the peak at 3.59 ppm still increased, and therefore an approximate value of 94 seconds was obtained. The percentage conversion data was therefore only meaningful when using 4-ethynyl-α,α,α-trifluorotoluene as the ^{19}F NMR spectra could be used to confirm the catalyst loading. However, the NMR experiments suggested that a longer delay time between pulses (d_1) was required and due to time constraints, the delay was increased to 60 seconds.

7.6.2 Overview of reaction conditions

A summary of the general reaction conditions that have been investigated are shown below (Scheme 7.4, Table 7.1). The entries are of stoichiometric and catalytic reactions conditions where differences include the method of addition of the alkyne to the reaction mixture, changing the catalytic loading, changing the reaction volumes and exploring the effect of irradiating the reaction mixture. Further discussion of the entries has been included in the following sections.

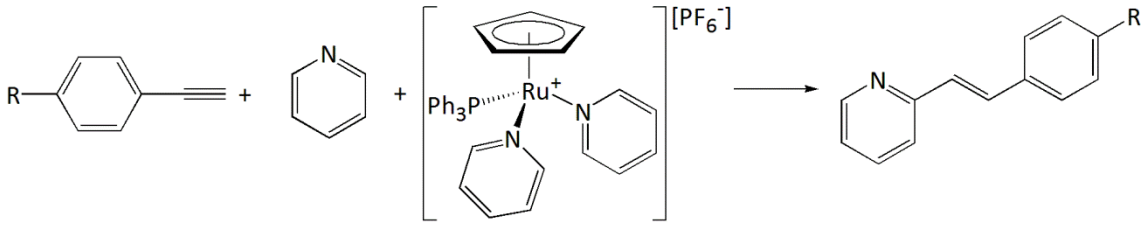

Scheme 7.4: General schematic of reagents used in developing the catalytic reaction for the synthesis of 2-styrylpyridine derivatives, where R = H or CF_3.

Entry	Alkyne	10^{H} (mol %)	Pyridine equivalents	Reaction conditions	Time (hrs)	Percentage Yield / Conversion
1	PhC≡CH	20	20	50 °C	32	14
2	4-CF_3-C_6H_4C≡CH	20	20	50 °C	32	19
3	4-CF_3-C_6H_4C≡CH	100	55	50 °C	72	48[a]
4	5 x 1 equiv PhC≡CH	20	55	50 °C	5 x 24	33[a]
5	5 x 1 equiv 4-CF_3-C_6H_4C≡CH	20	55	50 °C	5 x 24	17[a]
6	4-CF_3-C_6H_4C≡CH	5	20	50 °C	24	2.5[b]
7	4-CF_3-C_6H_4C≡CH	20	55	50 °C	72	49[b]
8	4-CF_3-C_6H_4C≡CH	20	20	50 °C, CH_2Cl_2	48	24[a]
9	4-CF_3-C_6H_4C≡CH	20	20	μwave, 50 °C, CH_2Cl_2	1	7[b]
10	4-CF_3-C_6H_4C≡CH	20	20	μwave, 100 °C	0.5	9[b]

Table 7.1: Summary of different reaction conditions for pyridine alkenylation reactions, where [a] is the percentage isolated yield, and [b] is the percentage conversion which has been calculated relative to the $[PF_6]^-$ anion. The relative mol % and pyridine equivalents used are relative to the alkyne employed.

7.6.3 Investigating the catalytic reaction between 10^{H} and terminal alkynes

The reported literature from Murakami and Hori employed TMS-substituted alkynes as these compounds avoided the dimerisation observed with terminal alkynes. The effects of using terminal alkynes (phenylacetylene and 4-ethynyl-α,α,α-trifluorotoluene) have been investigated, as this will avoid the degradation of the $[PF_6]^-$ and may potentially provide a more atom efficient alkenylation reaction. Following the catalytic reaction quantities mentioned by Murakami and Hori for the synthesis of the 2-styrylpyridine derivatives,[253] the entries **1** and **2** (Table 7.1) are discussed in this section.

7.6.3.1 Standard catalytic reactions with phenylacetylene

The catalytic reaction conditions to synthesise 2-styrylpyridine are in entry **1**. The reaction required phenylacetylene (1 equivalent), pyridine (20 equivalents) with $\mathbf{10^{H}}$ (20 mol %) and was heated at 50 °C over two 16 hours periods. The reaction was monitored by removing aliquots from the reaction mixture and placed in d_2-dichloromethane, where the analysis was carried out by NMR spectroscopy (Scheme 7.5).

The reaction mixture of entry **1** was heated at 50 °C for 16 hours and an aliquot analysed. The ^{1}H NMR spectrum exhibited a peak at 3.12 ppm for the terminal proton of uncoordinated phenylacetylene and therefore the reaction mixture was heated for an additional 16 hours at 50 °C and a further aliquot removed from the reaction mixture and placed in d_2-dichloromethane. The ^{1}H NMR spectrum no longer exhibited resonances for uncoordinated phenylacetylene suggesting that all starting material had been consumed. Additionally, the ^{1}H NMR spectrum exhibited that in the cyclopentadienyl region the resonances for $\mathbf{10^{H}}$ had decreased in intensity and several new ruthenium-containing species were formed. The major ruthenium-containing species present was identified as $\mathbf{22^{H,H}}$, which displayed a resonance at 4.95 ppm for the cyclopentadienyl ligand and this was consistent with the ^{31}P{^{1}H} NMR spectrum as a peak at 53.5 ppm for the triphenylphosphine ligand was observed. The reaction mixture was also analysed *via* TLC against an authentic sample of 2-styrylpyridine, which confirmed this compound was in the catalytic reaction.

An ESI-MS of the reaction mixture displayed a *m/z* peak at 182.0966 for a $[C_{13}H_{12}N]^+$ species, which could be interpreted as 2-styrylpyridine or an isomer. The ESI-MS also displayed peaks for several ruthenium-containing complexes with a *m/z* of 610.1232, 712.1733 and 793.1761. The *m/z* peak at 610.1232 displayed the expected mass for the cationic fragment of $\mathbf{22^{H,H}}$, however it did not display the correct isotope pattern. It is

possible that the deprotonated species **23^{H,H}** was present in the reaction mixture and therefore these two peaks are overlapping. The other *m/z* signals at 712.1733 and 793.1761 were due to cationic fragments of **21^{H,H}** and **3^{Ph}** respectively. An isolated yield of 2-styrylpyridine 14 % was collected.

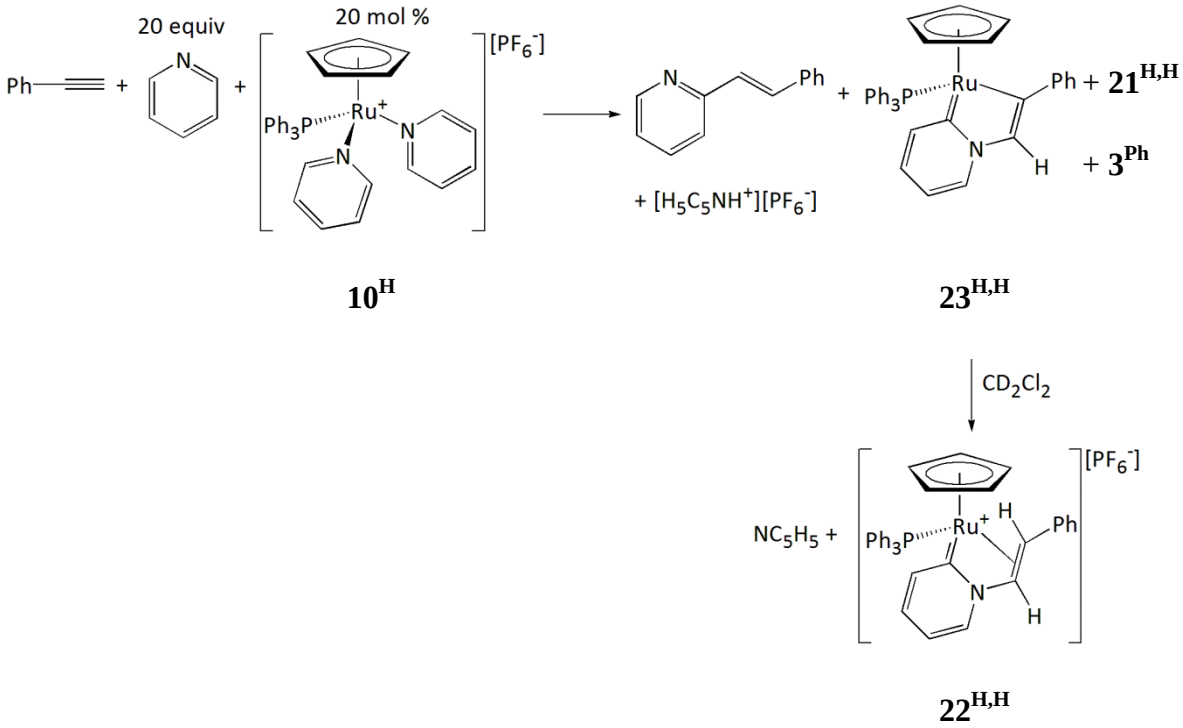

Scheme 7.5: Catalytic reaction conditions from entry 1 displaying the formation of various ruthenium complexes.

The reaction conditions mentioned in entry **1** were repeated with d_5-pyridine and the reaction was left to proceed at room temperature. The reaction was monitored *via* NMR spectroscopy at various intervals over a period of 23 days at room temperature. After 24 hours a doublet peak at 8.03 ppm was observed with a $^3J_{HH}$ of 16.0 Hz which was assigned to the one of the alkene resonances of 2-styrylpyridine and this resonance increased in intensity over time. The NMR spectra also displayed a new set of resonances for a new ruthenium-containing complex, where the ^{1}H NMR spectrum displayed a peak at 5.00 ppm and in the ^{31}P{^{1}H} NMR spectrum exhibited a resonance at 60.5 ppm for coordinated triphenylphosphine. This new species was assigned as **23^{H,H}** and as the reaction proceeded these resonances increased in intensity to become the major species, as the peaks belonging to **10^{H}** decreased. In addition, other minor ruthenium-containing species were observed in the NMR spectra, where one of these species was identified as **3^{Ph}**. In d_2-dichloromethane the major species observed was **22^{H,H}**. The species **22^{H,H}** and **23^{H,H}** are easily accessible *via* a protonation/

deprotonation step and therefore in a more basic reaction medium the equilibrium favours the deprotonated species **23^{H,H}**.

*7.6.3.2 Catalytic reactions between **10^{H}** and 4-ethynyl-α,α,α-trifluorotoluene*

The catalytic alkenylation reaction of 4-ethynyl-α,α,α-trifluorotoluene with pyridine was investigated (entry **2**). The 4-CF_3 substituent provided an additional NMR handle on how the reaction proceeded. In addition, the stoichiometric studies between **10^{H}** and 4-ethynyl-α,α,α-trifluorotoluene in d_2-dichloromethane had demonstrated that a more selective reaction pathway had occurred (Chapter 5). The reaction conditions mentioned in entry **2** required 4-ethynyl-α,α,α-trifluorotoluene (1 equivalent) and pyridine (20 equivalents) with **10^{H}** (20 mol %) and was heated at 50 °C for two 16 hour periods. The aliquots of the reaction mixture were placed in d_2-dichloromethane and monitored *via* NMR spectroscopy.

Using reaction conditions from entry **2** and after heating the reaction mixture at 50 °C for 16 hours, the ^{1}H and ^{19}F NMR spectra displayed peaks for uncoordinated 4-ethynyl-α,α,α-trifluorotoluene at 4.30 and -64.4 ppm respectively. The peaks for **10^{H}** were no longer present in the NMR spectra and the major ruthenium-containing complex in d_2-dichloromethane was found to be **22^{H,CF3}**. A TLC plate of the reaction mixture at this point confirmed that the 2-styrylpyridine derivative had been synthesised. The reaction mixture was heated for an additional 16 hours at 50 °C, however further conversion of the alkyne to in *E*-2-(4-trifluoromethyl)styrylpyridine was not observed. The ^{19}F NMR spectrum suggested that only approximately 50 % of the alkyne had reacted. This corroborates with previous data which suggests that the pyridylidene-containing complexes **22** are the deactivation products. A high resolution ESI-MS of the reaction mixture displayed a *m/z* peak at 250.0827 which was due to a $[C_{14}H_{11}F_3N]^+$ species, which is either due to *E*-2-(4-trifluoromethyl)styrylpyridine or the pyridylidene fragment of **22^{H,CF3}**. An isolated yield of *E*-2-(4-trifluoromethyl)styrylpyridine 19 % was collected.

The catalytic reaction conditions mentioned for entry **2** were repeated with d_5-pyridine and the reaction was monitored *via* NMR spectroscopy at room temperature until no further changed were observed and then heated at 150 °C for 16 hours. From leaving the reaction mixture at room temperature after 6 days, the reaction mixture displayed that the resonance in ^{31}P{^{1}H} NMR spectrum for **10^{H}** was no longer present and therefore had all reacted. The ^{1}H NMR spectrum displayed a doublet peak at 7.99 ppm with a

$^{3}J_{HH}$ of 16.0 Hz, which is characteristic of one of the alkene protons of *E*-2-(4-trifluoromethyl)styrylpyridine. Interestingly, the ^{1}H NMR spectrum demonstrated that the resonances for 4-ethynyl-α,α,α-trifluorotoluene were still present, as the terminal alkyne proton was observed at 4.30 ppm. The resonances for the alkyne remained in the reaction mixture even after heating the reaction mixture for 16 hours at 150 °C. This suggested that the reaction mixture no longer contained the active catalyst and therefore the alkenylation reaction was not occurring. These data suggests that the catalyst had been rendered inactive, and from studying the NMR spectra it appears that there is one major ruthenium-containing complex (amongst some minor species). The ^{1}H NMR spectrum displayed a peak at 4.98 ppm for the cyclopentadienyl ligand and in the ^{31}P{^{1}H} NMR spectrum a resonance at 60.2 ppm for the triphenylphosphine ligand which was identified as **23^{H,CF3}**. The reaction mixture was heated for 16 hours at 150 °C and analysed *via* NMR spectroscopy and ESI-MS. The ^{1}H and ^{31}P{^{1}H} NMR spectra no longer displayed peaks belonging to **23^{H,CF3}** and the major resonances present in the ^{1}H NMR spectrum was at 4.36 ppm for a cyclopentadienyl ligand and in the ^{31}P{^{1}H} NMR spectrum at 39.3 ppm for the triphenylphosphine ligand, which is consistent with the formation of **1**. The chloride atom has presumably been abstracted from dichloromethane present in the reaction mixture. Additionally, the ^{31}P{^{1}H} NMR spectrum displayed resonances at -5.3 (singlet) and -13.7 (triplet, J_{PF} = 945 Hz) ppm for a uncoordinated triphenylphosphine and an unknown PF_2-containing species. A high resolution ESI-MS of the reaction mixture after heating at 150 °C displayed a *m/z* peak of 255.1140 and was consistent with a $[C_{14}H_6D_5F_3N]^+$ compound for the 2-styrylpyridine derivative and there were also additional peaks with a *m/z* difference of ±1 due to different amounts of deuterium incorporation.

7.6.3.3 Summary

These reactions are extremely promising when compared to Murakami and Hori's original catalytic conditions[253] as it has been demonstrated that the alkenylation reaction has occurred at lower reaction temperatures of 50 °C, and that the use of terminal alkynes has created a more atom economical route to the 2-styrylpyridine derivatives. The lower reaction temperatures could potentially be attributed to using **10^{H}** where the relatively more labile pyridine molecules can be substituted with alkyne molecules in comparison to when **2^{Ph}** was employed. There was also evidence of dimerisation of the alkynes to give the butenyne compounds, however this was a minor part of the final

reaction mixture and not a major component as was found under the reaction conditions reported by Murakami and Hori.

7.6.4 Investigating the stoichiometric addition of terminal alkynes to 10^{H} in a pyridine solution

The low isolated yields in the previously mentioned catalytic reactions has meant further investigations into the stoichiometric effect of terminal alkynes (phenylacetylene and 4-ethynyl-α,α,α-trifluorotoluene) to **10^{H}** in pyridine solutions was probed. The reaction mixtures were heated at 50 °C and the formation of the 2-styrylpyridine derivatives monitored with respect to the amount of **10^{H}** present in the reaction mixture, where this section refers to entries **3**, **4** and **5** (Table 7.1).

7.6.4.1 Stoichiometric addition of phenylacetylene to 10^{H}

The stoichiometric addition of phenylacetylene to **10^{H}** in a pyridine solution (271 equivalents with respect to **10^{H}**) was heated at 50 °C for 24 hours. After which time an aliquot of the reaction mixture was placed in d_2-dichloromethane and examined by NMR spectroscopy. The reaction mixture of entry **4** after a single stoichiometric reaction with phenylacetylene displayed peaks for 2-styrylpyridine in the ^{1}H NMR spectrum. The ^{1}H and ^{31}P{^{1}H} NMR spectra exhibited a set of resonances for a major new ruthenium-containing complex **$22^{H,H}$** in the reaction mixture where the ratio of **10^{H}** and **$22^{H,H}$** was found to be approximately 1:0.3.

A further two stoichiometric equivalents of phenylacetylene were added to the reaction mixture and further aliquots of the reaction mixture taken at each interval. Upon further stoichiometric addition of phenylacetylene the resonances belonging to **$22^{H,H}$** increased in intensity. After the addition of five equivalents of phenylacetylene the NMR spectra indicated that the major ruthenium-containing species present in the reaction mixture was **$22^{H,H}$** and resonances for **10^{H}** were no longer present. Additionally, the ^{1}H NMR spectrum displayed a peak at 3.12 ppm due to uncoordinated phenylacetylene suggesting the reaction had not gone to completion. This is consistent with previous data (Chapter 5) as it suggests that **$22^{H,H}$** is a deactivation product and therefore the alkenylation reaction is not occurring when this is the major species in the reaction mixture.

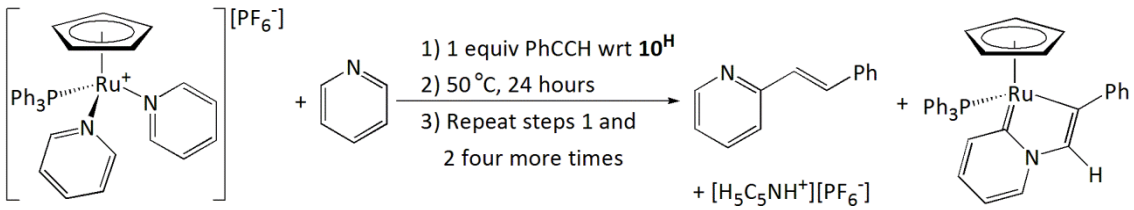

10^{H} **$23^{H,H}$**

Scheme 7.6: Stoichiometric addition of phenylacetylene to **10^{H}** in a pyridine solution.

The stoichiometric addition of phenylacetylene to **10^{H}** in a pyridine solution was heated at 50 °C for 24 hours. A further four stoichiometric quantities of the alkyne were added to the reaction mixture in a similar fashion (Entry **4**). The 2-styrylpyridine product was purified *via* a preparative TLC method and the product confirmed by ^{1}H NMR spectroscopy where an isolated yield of 33 % was obtained.

*7.6.4.2 Stoichiometric addition of 4-ethynyl-α,α,α-trifluorotoluene to **10^{H}***

The stoichiometric addition of 4-ethynyl-α,α,α-trifluorotoluene to **10^{H}** was investigated *via* NMR spectroscopy where the role of the ruthenium complex was monitored with respect to the formation of *E*-2-(4-trifluoromethyl)styrylpyridine. The stoichiometric addition of 4-ethynyl-α,α,α-trifluorotoluene to **10^{H}** in a pyridine solution (271 equivalents with respect to **10^{H}**) was heated at 50 °C for 24 hours and an aliquot of the reaction mixture placed in d_2-dichloromethane. The ^{1}H and ^{19}F NMR spectra recorded after the initial stoichiometric reaction displayed that 4-ethynyl-α,α,α-trifluorotoluene had reacted, where the ^{19}F NMR spectrum displayed quantitative conversion of the alkyne to *E*-2-(4-trifluoromethyl)styrylpyridine with respect to the $[PF_6]^-$ signals. The ^{1}H and ^{31}P{^{1}H} NMR spectra demonstrated that the major ruthenium complex present in the reaction mixture was **10^{H}** and resonances for **$22^{H,CF3}$** were very minor.

A further two stoichiometric equivalents of alkyne were added and aliquots taken from the reaction mixture. Upon further addition of 4-ethynyl-α,α,α-trifluorotoluene an increase in the resonances for the alkenylation product and for **$22^{H,CF3}$** were observed. This was followed by the addition of five equivalents of alkyne to the reaction mixture and a final aliquot taken from the reaction mixture. After the addition of five equivalents of 4-ethynyl-α,α,α-trifluorotoluene, the major ruthenium complex in the reaction mixture was **$22^{H,CF3}$** and the formation of the 2-styrylpyridine derivative ceased.

A stoichiometric reaction between **10^{H}** and 4-ethynyl-α,α,α-trifluorotoluene in a pyridine solution was heated at 50 °C for 72 hours (Entry **3**), and the reaction mixture purified by preparative TLC for the alkenylation product, *E*-2-(4-trifluoromethyl)styrylpyridine. An isolated yield of 48 % was obtained and the product characterised by NMR spectroscopy.

A reaction involving five stoichiometric additions of 4-ethynyl-α,α,α-trifluorotoluene to **10^{H}** in a pyridine solution every 24 hours whilst heating the reaction mixture at 50 °C was conducted (Entry **5**). The pure species *E*-2-(4-trifluoromethyl)styrylpyridine was obtained using a preparative TLC method in a 17 % yield.

7.6.4.3 Summary

From these reactions it is possible to demonstrate that **10^{H}** is still present after the stoichiometric addition of the terminal alkyne. However, further addition of alkyne results in the formation of the pyridylidene complexes **22** and **23** which do not perform the alkenylation reaction. After the addition of five equivalents of alkyne with respect to **10^{H}** to the reaction mixture, **10^{H}** is no longer present in the reaction mixture. The catalytic reaction conditions therefore need to be adapted to ensure a higher conversion to the 2-styrylpyridine derivatives can be achieved.

7.6.5 Optimising the catalytic conditions with 10^{H} and of 4-ethynyl-α,α,α-trifluorotoluene

The catalytic reactions reported previously have displayed low yields and therefore a range of different reaction conditions have been explored to determine if a higher yield can be obtained. The conditions that have been changed include the catalyst loading, larger reaction volumes (additional pyridine or increasing the reaction volume with dichloromethane) and microwave reactions. The results of these variations are reported in this section.

7.6.5.1 Catalyst loading

The catalyst loading of 20 mol % has been used as an initial starting point as these were the ideal reaction conditions reported by Murakami and Hori.[253] A more economical reaction could be achieved if the catalyst loading could be reduced therefore a lower catalyst loading of 5 mol % has been employed in the reaction between 4-ethynyl-α,α,α-trifluorotoluene and 20 equivalents of pyridine (Entry **6**). The reaction mixture was heated at 50 °C for 24 hours and was monitored using NMR spectroscopy, ESI-MS and TLC.

A TLC of the reaction mixture displayed that *E*-2-(4-trifluoromethyl)styrylpyridine and unreacted 4-ethynyl-α,α,α-trifluorotoluene were present in the reaction mixture after 24 hours.

An aliquot of the reaction mixture was placed in d_2-dichloromethane and the ^{19}F NMR spectrum of the reaction mixture displayed the major fluorine-containing species was 4-ethynyl-α,α,α-trifluorotoluene and there were many minor unknown fluorine resonances, where one of the minor peaks was due to alkenylation product, and a percentage conversion of approximately 2.5 % was calculated. The ^{1}H NMR spectrum displayed many unknown ruthenium-containing species in the cyclopentadienyl region where a peak at 4.70 ppm was the major unidentified ruthenium-containing complex. The ^{1}H NMR spectrum also displayed peaks for $\mathbf{22^{H,CF3}}$, however this was a minor part of the reaction mixture.

A high resolution ESI-MS of the final reaction mixture displayed a *m/z* peak at 250.0828 due to the cationic species $[C_{14}H_{11}F_3N]^+$, which could either be due to the 2-styrylpyridine derivative or an isomer. An peak with a ruthenium isotope pattern at *m/z* 678.1112 was assigned as the cationic fragment of $\mathbf{22^{H,CF3}}$. Interestingly, peaks that had

not been observed previously at *m/z* 420.1183 and 590.1518 were assigned to the cationic fragments $[C_{23}H_{15}F_6N]^+$ and $[C_{32}H_{20}F_9N]^+$ and corroborated with the initial species containing one pyridine molecule and two alkyne molecules and the second species containing one pyridine molecule and three alkyne molecules. These fragments were found to originate from $[Ru(\eta^5\text{-}C_5H_5)(PPh_3)]^+$ species, as *m/z* peaks at 848.1440 and 1018.1798 were found with a ruthenium isotope pattern. These complexes have never previously been observed in the reactions of 4-ethynyl-α,α,α-trifluorotoluene with **10^{H}** and further information of these species is required before confirming their identity.

7.6.5.2 Additional pyridine equivalents

A catalytic reaction employing 20 mol % of **10^{H}** and 4-ethynyl-α,α,α-trifluorotoluene in a pyridine solution (55 equivalents with respect to alkyne) was heated at 50 °C for 72 hours (Entry **7**). The reaction was followed by NMR spectroscopy where aliquots were taken of the initial reaction mixture and after heating for 72 hours and placed in d_2-dichloromethane.

The final reaction mixture in the ^{19}F NMR spectrum demonstrated that the major species was *E*-2-(4-trifluoromethyl)styrylpyridine and the resonance for 4-ethynyl-α,α,α-trifluorotoluene was not present and therefore had been consumed. Approximately 49 percentage conversion to *E*-2-(4-trifluoromethyl)styrylpyridine was found, where the remaining alkyne had reacted to give other species. The ^1H and $^{31}P\{^1H\}$ NMR spectra exhibited that there were several ruthenium-containing complexes present, where two of these have been identified as **10^{H}** and **22^{H,CF3}**. Interestingly, under these reaction conditions **10^{H}** is still present at the end of the reaction and therefore this reaction mixture could perform further catalysis.

An increase in pyridine equivalents in the reaction mixture has reduced the amount of the deactivation species **22^{H,CF3}** formed and it is likely in these reactions that the additional pyridine equivalents favours the formation of **10^{H}**.

7.6.5.3 Increasing reaction volume

A catalytic reaction between 4-ethynyl-α,α,α-trifluorotoluene, pyridine (20 equivalents), **10^{H}** (20 mol %) in a dichloromethane solution (271 equivalents relative to the alkyne) was heated at 50 °C for 48 hours. The reaction mixture was analysed by NMR spectroscopy and the product purified using column chromatography (Entry **8**)

An aliquot of the reaction mixture taken after 24 hours was placed in d_2-dichloromethane. The ^{1}H and ^{19}F NMR spectra demonstrated that the reaction had not gone to completion as resonances belonging to 4-ethynyl-α,α,α-trifluorotoluene were still present. The reaction mixture was heated for an additional 24 hours after which time the NMR spectra demonstrated that the peaks belonging to 4-ethynyl-α,α,α-trifluorotoluene were absent suggesting the reaction had gone to completion. The ^{19}F NMR spectrum displayed that the reaction had given approximately a 50 % conversion to *E*-2-(4-trifluoromethyl)styrylpyridine.

Different unsuccessful purification methods were attempted to try and purify the organic product, involving:

i) Acid washes with 1M HCl and extraction of ruthenium complexes with dichloromethane, followed by neutralisation of the aqueous phase with $NaHCO_3$, and a dichloromethane extraction of the organic species;
ii) Acid washing the reaction mixture to remove excess pyridine, followed by column chromatography on a base washed column with 5 % triethylamine with ethyl acetate and hexane (1: 3 respectively).

However, the product was successfully purified using silica column chromatography where a 5 % triethylamine base wash was used and a solvent mixture of ethyl acetate and hexane (1: 10 respectively), and the pure product collected in a 24 % yield.

An increase in the reaction volume has allowed all the alkyne to be consumed due to the change in the ratio between the alkyne: pyridine: **10^{H}**. The ratio between **10^{H}** and alkyne has been reduced resulting in less of the deactivation species **23^{H,CF3}** being formed.

7.6.5.4 Microwave reactions

Two sets of microwave reaction conditions were employed to see if irradiating the catalytic reaction mixtures would reduce the long reaction times that were required with conventional heating and display a similar conversion to the alkenylation product (Entries **9** and **10**).

Entry **9** explored using the reaction quantities from Entry **8** and the sample was irradiated for 60 minutes at 50 °C. An aliquot of the reaction mixture was taken before and after heating and placed in d_2-dichloromethane for analysis by NMR spectroscopy. The ^{1}H and ^{19}F NMR spectra demonstrated that approximately 50 % of the alkyne remained unreacted and the ^{19}F NMR spectrum exhibited a 7 % conversion to the alkenylation product. The ^{1}H NMR spectrum exhibited resonances for several ruthenium-containing complexes, where $\mathbf{10^{H}}$ and $\mathbf{22^{H,CF3}}$ were the major species.

Entry **10** employed the catalytic quantities mentioned in Entry **2** but the reaction mixture was irradiated at 100 °C for 30 minutes. Aliquots of the reaction mixture were taken before and after irradiating the sample and placed in d_2-dichloromethane. The ^{19}F NMR spectrum demonstrated that approximately 20 % of the alkyne remained unreacted and a 9 % conversion to the alkenylation product had occurred. The ^{1}H NMR spectrum displayed a doublet peak at 6.52 ppm with a $^{3}J_{HH}$ of 16.3 Hz and due to dimerisation product *E*-1,4-di-(4-trifluoromethylphenyl)but-1-ene-3-yne. The higher reaction temperatures favour the dimerisation reaction pathway as the pyridine ligand under these condition is probably more labile and therefore two alkyne molecules can coordinate at the ruthenium centre. The lower reaction temperature of 50 °C has therefore created a more atom economical reaction as the TMS-substituted alkyne is not required.

7.7 Conclusion

The initial part of this chapter describes the screening of a range of potential half-sandwich ruthenium complexes as catalysts for the synthesis of 2-styrylpyridine. The role of **1** as a pre-catalyst was investigated mechanistically with ^{13}C-labelled phenylacetylene and from this reaction a variety of ruthenium complexes were observed. These complexes included $\mathbf{3^{Ph}}$, **31** and $\mathbf{10^{H}}$. The complexes $\mathbf{3^{Ph}}$ and **31** did not display any of the desired reactivity to give 2-styrylpyridine. However, the reactivity of $\mathbf{10^{H}}$ in pyridine with TMS-substituted alkynes displayed potential as there appeared to be evidence of the alkenylation reaction occurring. When the reaction mixture was analysed by ESI-MS the ruthenium-containing complexes were difficult to identify. The NMR spectra of the crude reaction mixture exhibited degradation of the $[PF_6]^-$ non-coordinating anion and many TMS-containing by-products. The presence of the TMS group made it difficult to understand the reaction mixture from a mechanistic point, and therefore catalytic reactions employing terminal alkynes were explored.

The reactivity of terminal alkynes in a pyridine solution with $\mathbf{10^{H}}$ gave the 2-styrylpyridine compounds. This route was atom-economical and required lower reaction temperature of 50 °C, than the reported 150 °C in the literature. The isolated yields following the original catalytic quantities were found to be 14 and 19 %. When the reaction was conducted with 4-ethynyl-α,α,α-trifluorotoluene, only 50 % of the alkyne was consumed and $\mathbf{10^{H}}$ was absent in the reaction mixture. The major ruthenium-containing complex formed these reactions were the pyridylidene-containing species (**22** in d_2-dichloromethane and **23** in d_5-pyridine) and upon further heating of the reaction mixture no additional organic product was observed. Based on these observations the reaction conditions needed to be further optimised in order to collect a higher yield of the 2-styrylpyridine compounds and avoid formation of the deactivation products **22** and **23**.

To improve the reaction conditions and to optimise the lifetime of $\mathbf{10^{H}}$ in the reaction mixture a range of catalytic conditions were investigated. A stoichiometric study exhibited that upon addition of further equivalents of alkyne, the quantity of the deactivation species **22** or **23** increased. As this occurred lower conversion of the alkyne to the 2-styrylpyridine compounds was observed. The most promising results were found when the reaction volume was increased as it is likely that the ratio between the alkyne and $\mathbf{10^{H}}$ decreases. The following chapter will discuss this in further detail.

Chapter 8. Determining the Mechanism and Final Conclusions

8.1 Introduction

The development of novel catalysts can be achieved through a fundamental understanding of how the reaction mechanism proceeds. One successful example of where this methodology has been applied is in the development of catalysts for olefin metathesis. The development of the ruthenium catalysts lead to higher activity and synthesis of a phosphine-free system.[9-12] A similar approach has been adopted in order to improve the reported alkenylation reaction of pyridine.[253]

The previous chapters have described the experimental findings from mechanistic studies. A range of techniques including NMR and mass spectroscopy, single crystal X-ray crystallography and isotopic labelling studies have provided valuable information. The experimental findings from the mechanistic and catalytic studies have been summarised in the earlier part of this chapter. This will progress onto DFT calculations for potential reaction pathways. The theoretical calculations have been based upon experimental observations to determine the reaction mechanism.

The initial mechanistic findings (Chapter 2) offered useful guidelines on the reaction mechanism and therefore assisted in the initial theoretical DFT calculations. The stoichiometric reactions from addition of alkynes to $\mathbf{10^H}$ in dichloromethane and catalytic reactions provided further mechanistic insight. The full reaction mechanism was determined in a collaborative fashion with both experimental and theoretical findings providing an insight into the role of the half-sandwich ruthenium complexes in the alkenylation reaction of pyridine. Finally, conclusions will be drawn for this entire project and how this relates to current literature. It should be noted that all theoretical calculations mentioned were conducted by David Johnson.

8.2 Key experimental observations

The important mechanistic findings from the previous chapters for the alkenylation of pyridine to give the 2-styrylpyridine derivatives are summarised below. These points have provided a framework for the DFT investigations and helped define the reaction mechanism and shall be referred to within this chapter.

1. The reaction mixture of **2**^{Ph} in d_5-pyridine generated **3**^{Ph}, pyrididium hexafluorophosphate and a carbonyl complex. On heating the reaction mixture at 90 °C resonances belonging to **5** were exhibited and for 2-styrylpyridine (Section 2.3).

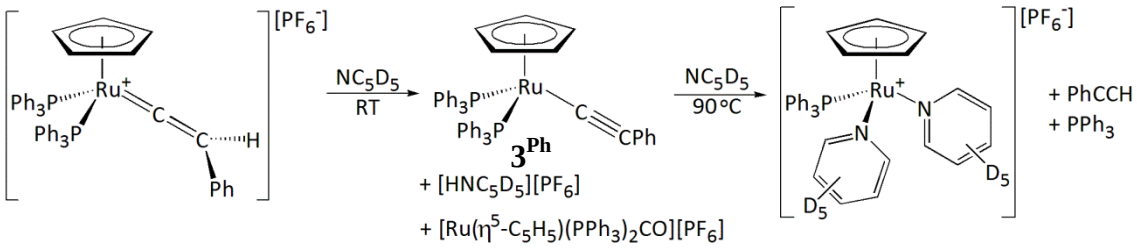

2^{Ph} **5**

2. The reaction of **10**^{H} and terminal alkynes in a dichloromethane solution gave the vinylidene-containing complexes **19** and **25**, which are short-lived intermediates (Section 5.2).

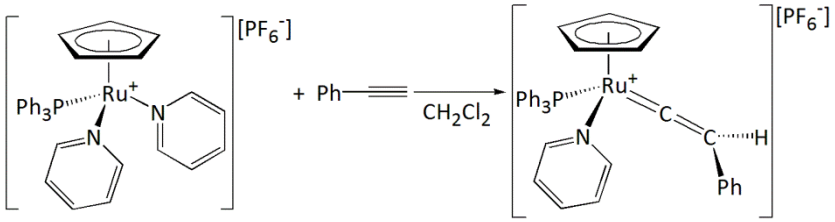

10^{H} **19**^{H,Ph}

3. The vinylidene-containing complexes **19** and **25** in a dichloromethane solution react further, to afford the pyridylidene-containing complexes **22**, **27** and **30** (Section 5.2).

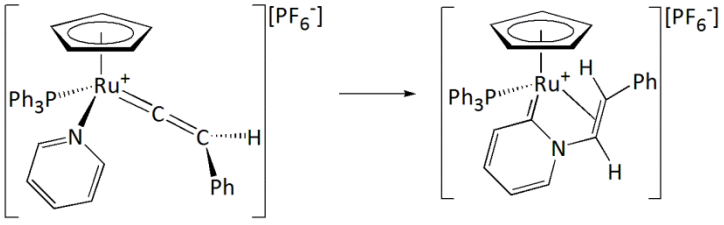

19^{H,Ph} **22**^{H,H}

4. A deuterium labelling study for the formation of **d_5-22^{H,H}** in dichloromethane exhibited initial selective deuterium incorporation at the α-carbon atom of the alkene functional group (Section 5.3).

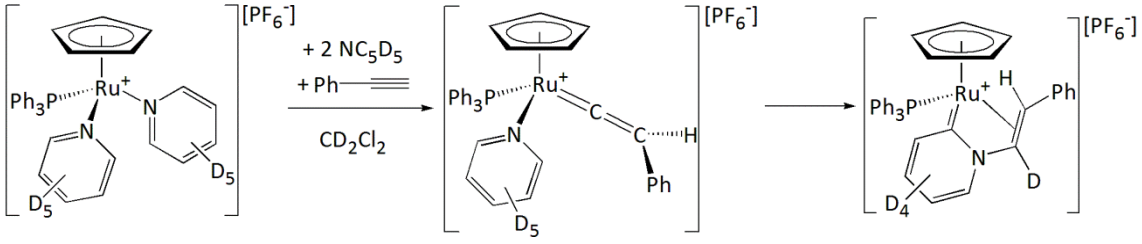

5 **19^{D,Ph}** **22^{D,H}**

5. The addition of excess pyridine to the pyridylidene-alkene containing complexes **22** results in the deprotonation of one of the alkene protons to give 1-ruthanaindolizine complexes **23** and pyridinium hexafluorophosphate (Section 5.2.1.6).

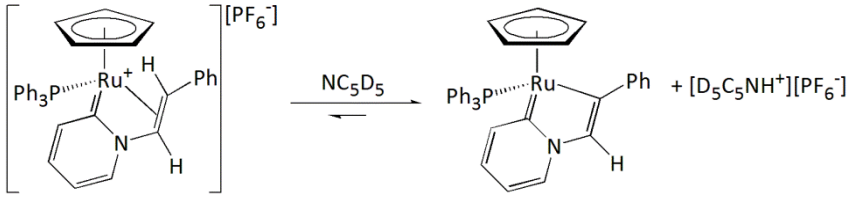

22^{H,H} **23^{H,H}**

6. A reaction mixture of **23^{H,CF3}** and pyridinium hexafluorophosphate in a d_5-pyridine solution when heated at 150 °C yielded *E*-2-(4-trifluoromethyl)styrylpyridine (at lower reaction temperatures of 50 and 100 °C the alkenylation reaction does not occur) (Section 5.2.3.4).

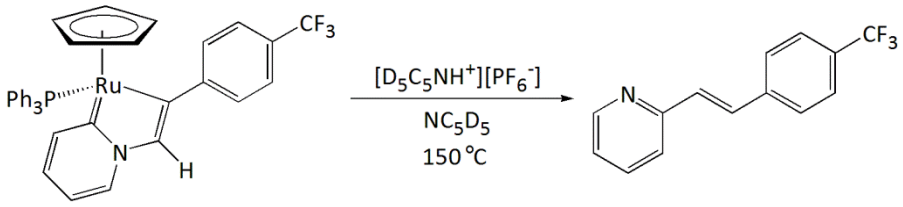

23^{H,CF3}

7. The sub-stoichiometric reactions between terminal alkynes and **10^{H}** in a pyridine solution (when heated at 50 °C) gave the 2-styrylpyridine compounds. At the end of the catalytic reaction the major ruthenium-containing species was the pyridylidene complexes **23** (Section 7.6.4).

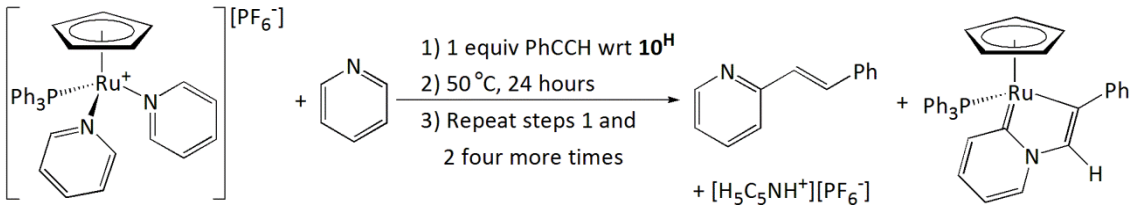

10^{H} **23^{H,H}**

8. The N-bound 2-styrylpyridine complexes **17** displayed fluxional behaviour between two isomers in a dichloromethane solution at room temperature on the NMR timescale and dissolution in d_5-pyridine resulted in formation of **5** (Section 4.2.3).

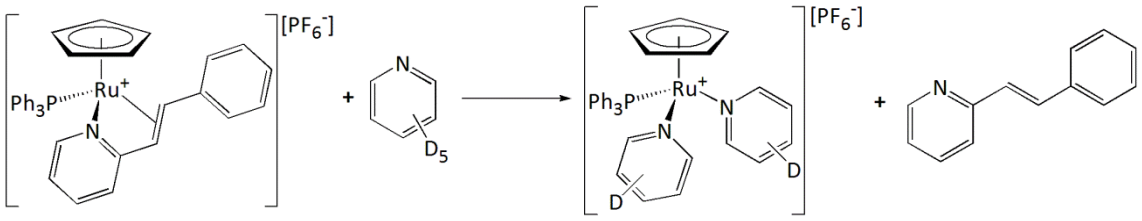

17^{H} **5**

8.3 Theoretical calculations

An extensive DFT investigation in collaboration with David Johnson and John Slattery has been carried on the reactions of the cation of $\mathbf{10^H}$ with terminal alkynes in a dichloromethane and pyridine solution.[337] The data presented in this section will refer to ZPE-corrected SCF energies ($E_{SCF+ZPE}$) and Gibbs free energies in pyridine solution (approximated using the COSMO solvation method and a dielectric constant of 13.26 for pyridine) and are reported in kJ mol^{-1}. For the calculations, models of the cationic complexes were studied with the weakly coordinating anion $[PF_6]^-$ excluded and no simplifications of the substituents were made. All the theoretical species have been numbered with capital letters (e.g. $[A]^+$) and if the computed species have been observed experimentally, the label will be denoted with a * to indicate that this species has been modelled without the weakly coordinating anion $[PF_6]^-$. All energies reported are relative to $[\mathbf{*10^H}]^+$, unless otherwise stated.

The initial section will look at the formation of the vinylidene-containing complex $[\mathbf{*19^{H,H}}]^+$ as this is shared by all three reaction pathways that were investigated. Then two potential mechanisms are discussed for the formation of 2-styrylpyridine and finally the catalyst deactivation process. Three potential energy surface pathways were explored to give a detailed explanation of the role of the ruthenium complexes in a pyridine solution. The pathways include the formation of:

A. 2-styrylpyridine from the proposed Murakami and Hori reaction mechanism.[253]
B. the pyridylidene-containing complexes $\mathbf{22^{H,H}}$ and $\mathbf{23^{H,H}}$ that leads to catalyst deactivation.[337]
C. 2-styrylpyridine from our experimental and theoretical observations.[337]

8.3.1 Formation of the vinylidene-containing complex $[\mathbf{*19^{H,H}}]^+$

The experimental findings demonstrated that the reaction of $\mathbf{10^H}$ with phenylacetylene yielded the vinylidene-containing complex $\mathbf{19^{H,H}}$ in a dichloromethane solution. All of the potential energy surfaces modelled began in a similar route with the formation of the vinylidene-containing complex $\mathbf{19^{H,H}}$. The theoretical models of $\mathbf{10^H}$ and $\mathbf{19^{H,H}}$ are referred to as $[\mathbf{*10^H}]^+$ and $[\mathbf{*19^{H,H}}]^+$ respectively. After formation of $[\mathbf{*19^{H,H}}]^+$ the potential energy surfaces for the other three reaction mechanisms differ and have been described individually in the following sections.

The formation of the vinylidene-containing complex [***19**^{H,H}]$^+$ was modelled to occur *via* the initial η^2-coordination of the alkyne [A]$^+$. This slips to the σ coordination of the C-H bond to give [B]$^+$. The formation of [***19**^{H,H}]$^+$ was achieved through a 1,2-hydrogen migration transition state at + 76 kJ mol^{-1} relative to [***10**^{H}]$^+$. The $\Delta E_{SCF+ZPE}$ of [***19**^{H,H}]$^+$ was -14 kJ mol^{-1} relative to [***10**^{H}]$^+$, therefore more energetically favourable and consistent with experimental findings. The 1,2-hydrogen migration mechanism for the formation of vinylidene-containing complexes is well established in the literature (Section 1.3.2.4).[45] Silvestre and Hoffman reported an activation barrier of 121 kJ mol^{-1}.[35] Additionally, De Angelis *et al.* reported activation barriers between 77 and 114 kJ mol^{-1} for a 1,2-hydrogen migration pathway.[65, 66] Our reported findings are therefore comparable to those found in the literature.

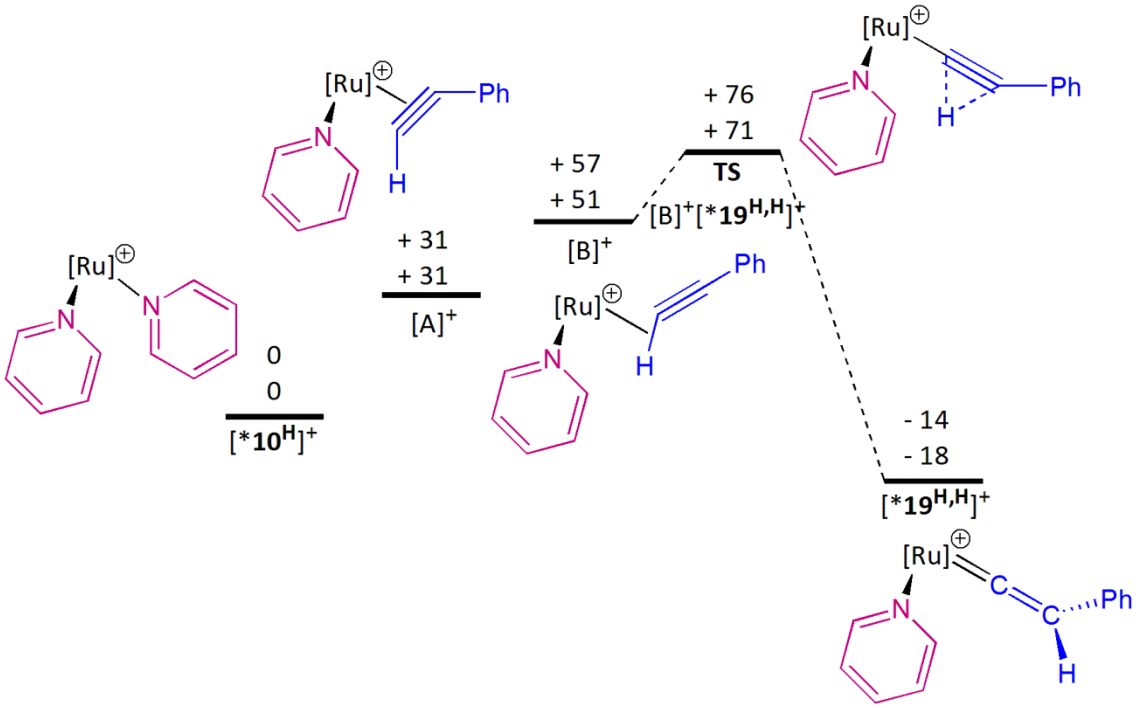

Figure 8.1: Potential energy surface for the formation [***19**^{H,H}]$^+$ where [Ru] = [Ru(η^5-C_5H_5)(PPh_3)] and the relative $E_{SCF+ZPE}$ (top) and Gibbs free energy (bottom) in pyridine are displayed in kJ mol^{-1}.

The formation of the vinylidene-containing complex **19**^{H,H} was proposed in the reaction mechanism for the formation of 2-styrylpyridine by Murakami and Hori.[253] Our experimental findings have confirmed the presence of this species in the reaction mixture and theoretical studies display this species is thermodynamically favourable relative to [***10**^{H}]$^+$ and alkyne.

8.3.2 Pathway A: Proposed reaction mechanism by Murakami and Hori[253]

The reaction mechanism proposed by Murakami and Hori was investigated to probe the energies of the intermediates and transition states required for the formation of 2-styrylpyridine (Figure 8.2). All energies reported are relative to $[\mathbf{*10^{H}}]^{+}$.

In the proposed mechanism, the vinylidene-containing complex $[\mathbf{*19^{H,H}}]^{+}$ undergoes an electrophilic substitution reaction between then the α-carbon atom of the vinylidene ligand and the proton at the C-2 position of the pyridine ligand to directly form a carbon-carbon bond to give $[C]^{+}$ (+ 136 kJ mol^{-1}) This process involved a high energy transition state $\mathbf{TS}[\mathbf{*19^{H,H}}]^{+}[C]^{+}$ that was + 154 kJ mol^{-1} relative to $[\mathbf{*10^{H}}]^{+}$.

From $[C]^{+}$ two potential pathways were investigated to afford $[E]^{+}$, where $[E]^{+}$ contained a coordinated 2-styrylpyridine molecule *via* the nitrogen atom and an agostic interaction of the α C-H bond from the alkene. The formation of $[E]^{+}$ was energetically favourable at - 99 kJ mol^{-1}. The first of these pathways involved deprotonation of the proton at the C-2 position of the N-containing heterocycle by a pyridine molecule to give [D] (- 61 kJ mol^{-1}), followed by reprotonation at the alkenyl carbon atom bound to the ruthenium centre to afford $[E]^{+}$. The second pathway from $[C]^{+}$ involved a higher energy transition state $\mathbf{TS}[C]^{+}[E]^{+}$ of + 149 kJ mol^{-1}, where the hydrogen atom migrated from the N-containing heterocycle to the alkenyl ligand to afford $[E]^{+}$.

From $[E]^{+}$ the agostic C-H interaction was cleaved to give $[F]^{+}$ (- 92 kJ mol^{-1}) and coordination of the alkene bond to the ruthenium centre yielded the more stable $[\mathbf{*17^{H}}]^{+}$ (- 148 kJ mol^{-1}). The regeneration of the starting ruthenium complex $[\mathbf{*10^{H}}]^{+}$ and 2-styrylpyridine ***G** was relatively more favourable at – 172 kJ mol^{-1}. This final step is consistent with our experimental findings where the addition of excess pyridine to $\mathbf{17^{H}}$ regenerates $\mathbf{10^{H}}$ and uncoordinated 2-styrylpyridine.

The relatively high energy turnover-determining transition state (TDTS) of + 154 kJ mol^{-1} means that from $[C]^{+}$ there is a large energetic span of + 168 kJ mol^{-1}. Under the experimental conditions mentioned by Murakami and Hori where reaction temperatures of 150 °C are employed for the formation of 2-styrylpyridine.[253] However, our experimental studies have determined that the alkenylation reaction can occur at a lower temperature of 50 °C and therefore the energetic span is too large for the relative rate of reaction at room temperature.

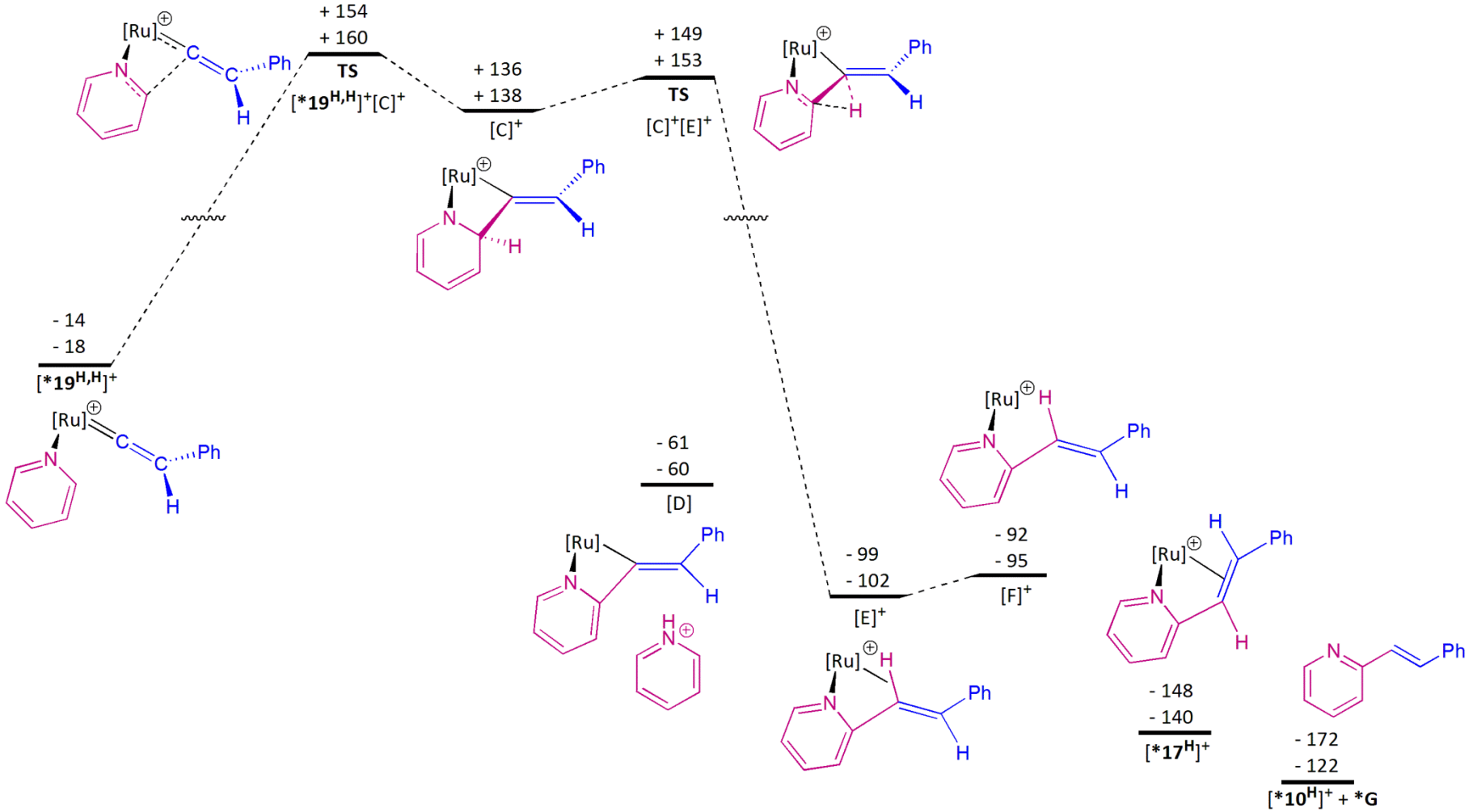

Figure 8.2: Potential energy surface for the formation of [***10**$^{\mathbf{H}}$]$^{+}$ and ***G** following reaction mechanism proposed by Murakami and Hori, where [Ru] = [Ru(η^5-C_5H_5)(PPh_3)] and the relative $E_{SCF+ZPE}$ (top) and Gibbs free energy (bottom) in pyridine are displayed in kJ mol^{-1}.

8.3.3 Pathway B: Formation of the deactivation pyridylidene-complexes[337]

The reaction pathway for the formation of the pyridylidene-containing complexes $\mathbf{22^{H,H}}$ and $\mathbf{23^{H,H}}$ were investigated, as these were the major ruthenium-containing species present at the end of the catalytic reaction and further conversion to the alkenylation products was inhibited by their presence (Figure 8.3). The potential energy surface from $[\mathbf{*19^{H,H}}]^+$ explored the properties of the vinylidene ligand, since when coordinated to a Ru(II) centre, the α carbon atom is electrophilic in nature. All energies reported are relative to $[\mathbf{*10^{H}}]^+$, unless otherwise stated.

The attack at the α-carbon atom by uncoordinated pyridine of $[\mathbf{*19^{H,H}}]^+$ resulted in the formation of $[H]^+$ (- 8 kJ mol^{-1}). The loss of the nitrogen coordinated pyridine ligand resulted in $[I]^+$. The C-H bond at the C-2 position of the pyridine molecule formed an agostic interaction with the ruthenium centre to give $[J]^+$ due to the vacant coordination site, which was at + 29 kJ mol^{-1}. The following step involved oxidative addition of the C-H agostic bond to the metal centre, from $[J]^+$ to give $[K]^+$ (+ 55 kJ mol^{-1}), a complex containing a hydride ligand and where the new ruthenium-carbon bond was interpreted as a pyridylidene ligand. The formation of $[K]^+$ involves the transition state $\mathbf{TS}[J]^+[K]^+$ of + 58 kJ mol^{-1} where the C-H bond undergoes a formal oxidative addition reaction at the ruthenium centre. (Note: An alternative C-H activation step is responsible for the formation of 2-styrylpyridine, Section 8.3.4). From $[K]^+$ the hydride ligand migrates to the alkenyl carbon atom coordinated to the ruthenium centre *via* the transition state $\mathbf{TS}[K]^+[L]^+$ (+ 56 kJ mol^{-1}) to give $[L]^+$ (- 3 kJ mol^{-1}). The species $[L]^+$ contained a pyridylidene-alkenyl ligand where the C-H bond of the alkene bond is agostically coordinated to the metal centre. The cleavage of the metal agostic C-H interaction and coordination *via* the alkene group to give $[\mathbf{*22^{H,H}}]^+$ was thermodynamically more stable at - 84 kJ mol^{-1}. Deprotonation to give $[\mathbf{*23^{H,H}}]$ was found to be – 42 kJ mol^{-1}. Although formation of $[\mathbf{*22^{H,H}}]^+$ was favourable, it is not as favourable as the formation of 2-styrylpyridine and regeneration of $[\mathbf{*10^{H}}]^+$. This suggests that the formation of $[\mathbf{*22^{H,H}}]^+$ is the kinetic product and is consistent as there is a smaller energetic span relative to the formation of 2-styrylpyridine (Section 8.3.4).

The formation of 2-styrylpyridine from $[\mathbf{*23^{H,H}}]$ was explored, and two reaction pathways were found to be potentially viable. The initial pathway involved breaking the C-N bond through a high energy transition state $\mathbf{TS}[\mathbf{*23^{H,H}}][M]$ (+ 187 kJ mol^{-1}) to give [M], where [M] is a pyridyl alkynyl complex. The alkynyl ligand of [M] could

isomerise to a vinylidene ligand to give [P] which is responsible for the formation of 2-styrylpyridine (Section 8.3.4). Alternatively, a second option would be the reprotonation of [***23**^{H,H}] to give [***22**^{H,H}]$^{+}$ which could slip back to [J]$^{+}$ and a different C-H activation step occur. Following this reaction pathway to 2-styrylpyridine the turnover determining transition state is **TS**[P][D] which is + 95 kJ mol^{-1}, therefore making the energetic span for this pathway + 179 kJ mol^{-1}. Both of the routes display high energy barriers to the formation of 2-styrylpyridine.

When considering the theoretical results it was important to observe if these findings corroborated with the experimental results. The potential energy surface for the formation of **22**^{H,H} is consistent with the experimental deuterium labelling observations, as the location of the hydrogen atom from the C-H activation step is at the α-carbon atom of the alkene group. Additionally, a high barrier to access 2-styrylpyridine from [***23**^{H,H}] was consistent with experimental findings since experimentally a high reaction temperature of 150 °C was required. Both the experimental and theoretical studies suggest that the pyridylidene-containing complexes **22**^{H,H} and **23**^{H,H} are catalyst deactivation products.

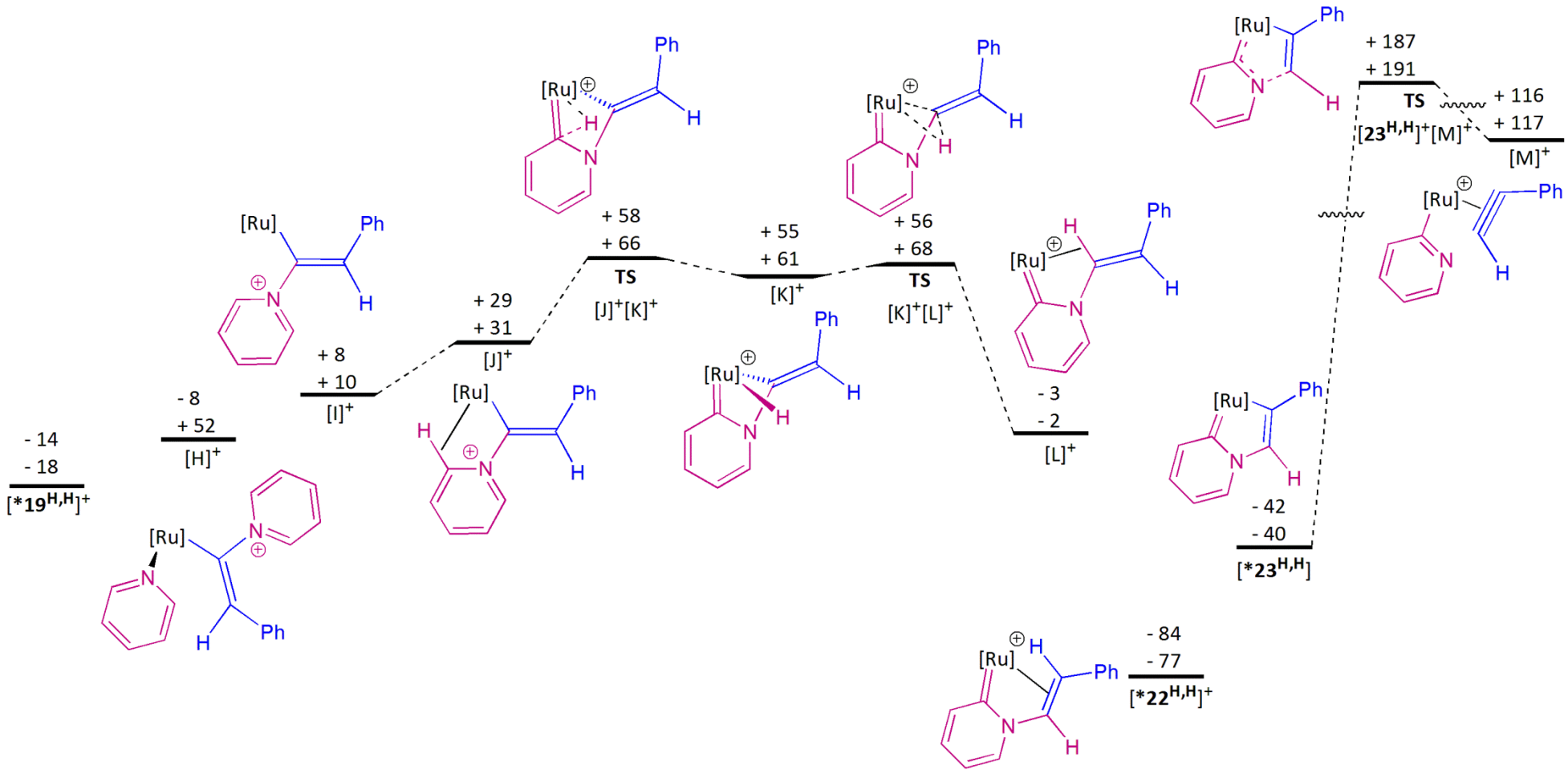

Figure 8.3: Potential energy surface on the formation of the deactivation pyridylidene complexes [***22**^{H,H}]$^+$ and [***23**^{H,H}]$^+$, where [Ru] = [Ru(η^5-C_5H_5)(PPh_3)] and the relative $E_{SCF+ZPE}$ (top) and Gibbs free energy (bottom) in pyridine are displayed in kJ mol^{-1}.

8.3.4 Pathway C: Pyridylidene ligands in the formation of 2-styrylpyridine[337]

The final potential energy surface to consider is the role of the pyridylidene ligands in the formation of 2-styrylpyridine based upon our experimental findings (Figure 8.4). The route proposed by Murakami and Hori displayed high energy barriers for the formation of 2-styrylpyridine, which is not consistent with experimental observations where 2-styrylpyridine formation has been observed at lower reaction temperatures of 50 °C. This suggested that there must another reaction pathway for the formation of 2-styrylpyridine and the experimental observations suggested that pyridylidene ligands may play a crucial role.

The formation of $[J]^+$ from $[\mathbf{*22^{H,H}}]^+$ followed the same route as mentioned previously. An alternative formal oxidative addition of the C-H bond from $[J]^+$ (from a different isomer) can occur to give a different pyridylidene-hydride containing complex $[N]^+$ at + 8 kJ mol^{-1} *via* the transition state **TS**$[J]^+[N]^+$ (+ 25 kJ mol^{-1}) which can be considered to be isoenergetic with $[J]^+$. The deprotonation of $[N]^+$ by uncoordinated pyridine yielded [O] at – 3 kJ mol^{-1}. To obtain a new carbon-carbon bond, the carbon-nitrogen bond must first be cleaved *via* the transitions state **TS**[O][P] at + 94 kJ mol^{-1}. The resulting complex [P] contains a pyridyl and a vinylidene ligand, which is + 62 kJ mol^{-1}. This can undergo a carbon-carbon bond coupling step through a pyridyl migration *via* transition state **TS**[P][D] which has an $E_{SCF+ZPE}$ of + 95 kJ mol^{-1} to give [D]. The remaining process to obtain $[\mathbf{*17^{H}}]^+$ has been mentioned previously in Pathway A.

Alternatively, 2-styrylpyridine may be accessed *via* pyridylidene intermediates, by the protonation of the nitrogen atom of [P] to give $[Q]^+$ (- 2 kJ mol^{-1}). A pyridylidene migration to the α-carbon atom of the vinylidene-containing ligand *via* the transition state **TS**$[Q]^+[R]^+$ (+ 77 kJ mol^{-1}) gives $[R]^+$ at – 50 kJ mol^{-1}. A deprotonation and reprotonation at the ruthenium-carbon alkenyl bond will then give $[\mathbf{*17^{H}}]^+$ which can regenerate the species $[\mathbf{*10^{H}}]^+$ and 2-styrylpyridine.

The experimental results displayed that *E*-stereoselectivity for 2-styrylpyridine was the only species observed. This has been explained from the theoretical studies as the two stereoisomers *E*-(*proE*) and *Z*-(*proZ*) pathways were investigated. The key feature of this investigation displayed that the transition state **TS**[P][D] was 19 kJ mol^{-1} (this is the TDTS for *E*-2-styrylpyridine formation) lower in energy than the *proZ* pathway as it avoids steric interactions between the phenyl ring and the pyridyl ligand.

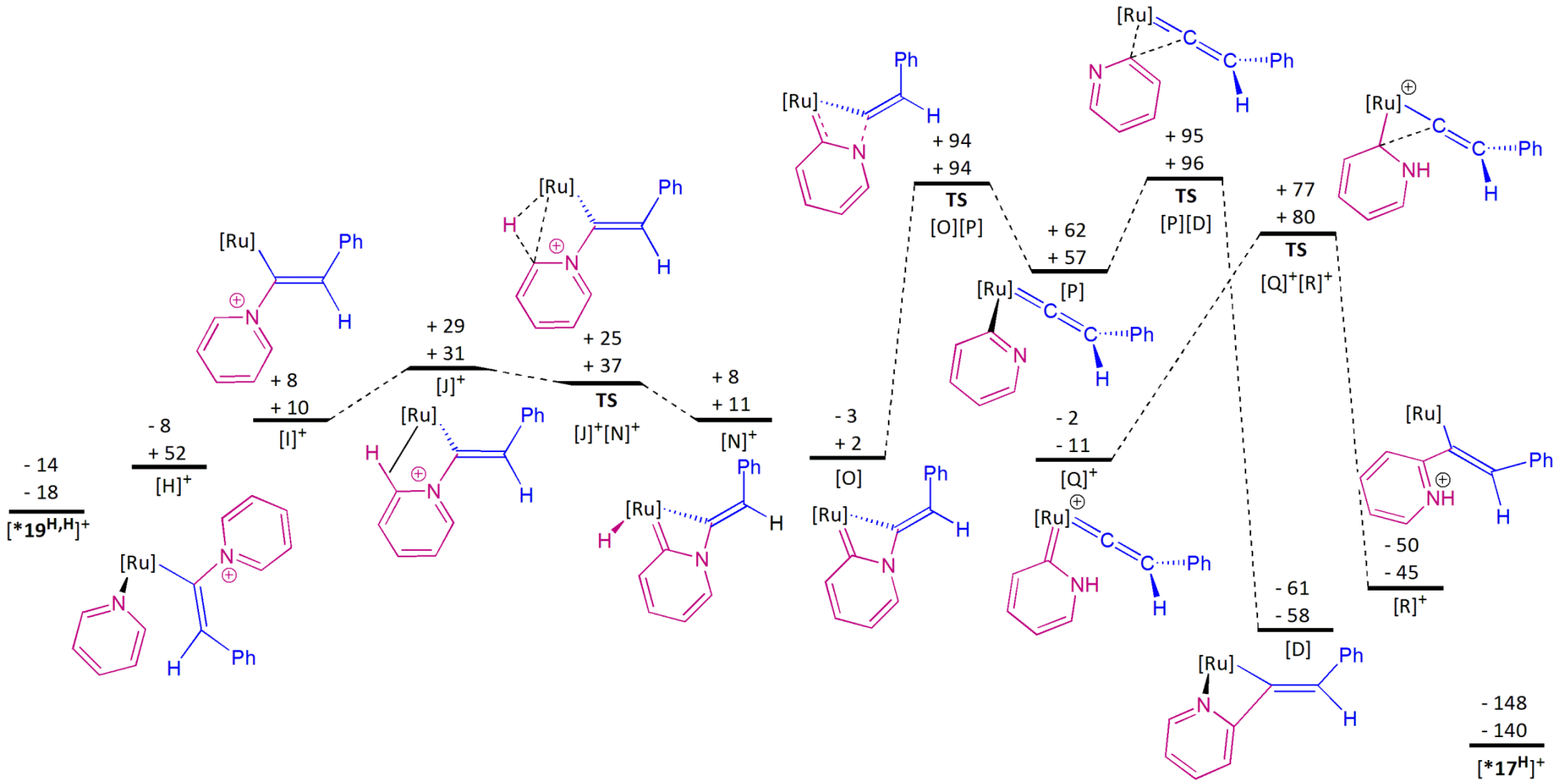

Figure 8.4: Potential energy surface on the role of pyridylidene ligands in the formation of 2-styrylpyridine, where [Ru] = [Ru(η^5-C_5H_5)(PPh_3)] and the relative $E_{SCF+ZPE}$ (top) and Gibbs free energy (bottom) in pyridine are displayed in kJ mol^{-1}.

8.4 Summary of theoretical studies

A combined theoretical and experimental investigation has been conducted on the formation of 2-styrylpyridine complexes. The potential energy surfaces have been calculated by David Johnson. Overall, three major pathways have been explored (A: proposed mechanism by Murakami and Hori, B: formation of the pyridylidene complexes $\mathbf{22^{H,H}}$ and $\mathbf{23^{H,H}}$ and C: the role of pyridylidene ligands in the formation of 2-styrylpyridine).

The mechanism proposed by Murakami and Hori[253] displayed a high TDTS (+ 154 kJ mol^{-1}) and a large energetic span (+ 168 kJ mol^{-1}) which was not consistent with our experimental observations that have found that 2-styrylpyridine is present in a reaction when heated a much lower reaction temperature of 50 °C. This suggested another reaction pathway might be responsible for the alkenylation of pyridine.

Further investigations were made into the formation of the pyridylidene-containing complexes $\mathbf{22^{H,H}}$ and $\mathbf{23^{H,H}}$ from the vinylidene-containing complex $\mathbf{19^{H,H}}$. It was apparent that the reactivity of the Ru(II) vinylidene ligand was exploited, since the α-carbon atom of the vinylidene undergoes nucleophilic attack by uncoordinated pyridine in the reaction mixture, to give $[H]^+$. The close proximity of the C-H bond at the 2 position of the pyridine molecule allowed an agostic interaction to form between the ruthenium centre, $[J]^+$. This paved the way to the formation of the $[\mathbf{*22^{H,H}}]^+$ which was a relatively low energy pathway in comparison to pathways A and C, where the energetic span for route was + 72 kJ mol^{-1} (TDI was $[\mathbf{*19^{H,H}}]$ and TDTS was $\mathbf{TS}[J]^+[K]^+$). The pyridylidene-containing complexes $[\mathbf{*22^{H,H}}]^+$ and $[\mathbf{*23^{H,H}}]$ are kinetic products and the transition states for the formation of 2-styrylpyridine from these species have been found to be relatively high energy (from $[\mathbf{*22^{H,H}}]^+$ of – 84 kJ mol^{-1} a transition state of + 95 kJ mol^{-1} and from $[\mathbf{*23^{H,H}}]$ of – 42 kJ mol^{-1} a transition state of + 187 kJ mol^{-1} were required). This corroborated with experimental findings where high temperatures of 150 °C were required to obtain 2-styrylpyridine.

The final reaction pathway C explored the role of pyridylidene ligands in the alkenylation reaction of pyridine. The reaction pathway displayed that cleavage of the C-N bond in [O] required a transition state with a + 94 kJ mol^{-1} to give either pyridyl or pyridylidene vinylidene-containing complexes [P] or $[Q]^+$ respectively. The energetic span from $[\mathbf{*10^{H}}]^+$ to generate 2-styrylpyridine was + 109 kJ mol^{-1} and therefore smaller

than the reaction mechanism proposed by Murakami and Hori. These complexes then underwent a carbon-carbon coupling reaction by either pyridyl or pyridylidene migration which followed by subsequent deprotonation/ reprotonation yielded [***17**$^{\mathbf{H}}$]$^{+}$. These results corroborated with experimental findings where the organic product was observed after heating at lower reaction temperatures of 50 °C.

The difference in reactivity observed experimentally in dichloromethane (preference for **22**$^{\mathbf{H,H}}$) or pyridine (preference for 2-styrylpyridine) solutions can be explained with reference to the theoretical pathways. The catalyst deactivation species **22**$^{\mathbf{H,H}}$ is preferred in a dichloromethane solution as there are fewer equivalents of uncoordinated pyridine present in the reaction mixture and therefore the hydride complex [K]$^{+}$ is not deprotonated in solution and can migrate to generate **22**$^{\mathbf{H,H}}$. However, in a pyridine solution the hydridric species [N]$^{+}$ (where PABOON calculations suggest that the hydride has a partial charge more consistent with a protic species) is more likely to be deprotonated, which leads to the alkenylation reaction pathway being favoured.

8.5 Final conclusions

This chapter has summarised the significant experimental findings obtained from previous chapters. The findings have been supported by theoretical studies which have allowed us to construct a realistic picture of the potential energy surface for the alkenylation of pyridine with terminal alkynes. A final catalytic cycle has been proposed (Scheme 8.1) for the alkenylation of pyridine to afford 2-styrylpyridine. From our mechanistic studies it was established that $\mathbf{10^{H}}$ was the active ruthenium complex. In the presence of a terminal alkyne, the vinylidene-containing complex $\mathbf{19^{H,H}}$ was obtained. Uncoordinated pyridine acts as a Lewis base towards the α-carbon atom of the vinylidene ligand to yield $[H]^+$ and therefore brings the α C-H bond of the N-containing heterocycle into close proximity of the ruthenium centre to afford $[J]^+$. Subsequent C-H activation leads to $[N]^+$ or $[K]^+$, where $[K]^+$ leads to the formation of the kinetically favoured deactivation complexes, $\mathbf{22^{H,H}}$ or $\mathbf{23^{H,H}}$. Alternatively, deprotonation (likely to occur in a basic reaction medium) gives [O]. A C-N bond cleavage followed by a carbon-carbon bond formation step *via* either the pyridyl or pyridylidene complexes [P] or $[Q]^+$ leads to 2-styrylpyridine, which can be released regenerating $\mathbf{10^{H}}$.

The formation of iridium-pyridylidene ligands in the literature has been reported by Carmona *et al.*[208] In the case of pyridine it has been found through theoretical calculations that the 2-carbene tautomer is 17 kJ mol^{-1} less stable than the nitrogen bound complex. However with the 2-substituted pyridine complexes (2-methylpyridine and 2-phenylpyridine) the iridium centre stabilises the 2-carbene complex with respect to the N-bound tautomer and therefore the carbon bound adduct is the thermodynamic product. This highlights the unique qualities of our system as in order to access the 2-carbene tautomer of pyridine a substituent at the C-6 position was not required.

There are several literature mechanisms that have explored the potential energy surfaces for the formation of pyridylidene complexes. Carmona *et al.* have reported a mechanism for the formation of iridium N-heterocyclic carbene complexes.[208] Their theoretical studies suggested that a σ-CAM mechanism was responsible for the formation of the 2-carbene tautomers. An initial σ C-H bond interaction at the 2-position of the N-containing heterocycle and the iridium centre is assisted by a phenyl ligand which abstracts the hydrogen atom and replaces it at the nitrogen atom to give the pyridylidene complex.

Esteruelas *et al*. have also investigated the formation of osmium-pyridylidene complexes for 2-methylpyridine.[223] In their proposed mechanism the osmium hydride complexes allow for an initial intermolecular hydrogen migration from the metal complex to the nitrogen atom of the N-containing heterocycle. This undergoes C-H activation at the α bond of the N-containing heterocycle resulting in a dihydride complex and is followed by a dihydride-dihydrogen tautomerisation process. The C-H activation mechanism in these complexes required an intermolecular exchange of hydrogen atoms in order to stabilise the NH tautomer.

Lastly, a detailed mechanistic study by Bergman *et al*. studied the C-H activation mechanism of N-containing heterocycles at a rhodium centre to give a N-heterocyclic carbene ligand.[178] From DFT calculation it was determined that different orientations of the C-H bond of the N-containing heterocycle yielded two different reaction pathways, however the C–H oxidative addition stages were the rate-limiting in these mechanisms.

The mechanisms mentioned above highlight different methods for the synthesis of N-heterocyclic carbene ligands. These mechanisms differ from our findings as in our system the role of the vinylidene ligand shapes the potential energy surface as it brings the α C-H bond of the pyridine ligand in to close proximity of the ruthenium centre and hence access to the pyridylidene ligands.

Additionally, substituent effects from various phosphorus-containing ligands, nitrogen-containing ligands and alkynes were investigated from a mechanistic perspective. Altering the electronic and steric factors was found to change the reactivity of the ruthenium centre. Trimethylphosphine is considered to increase electron density at metal centres with respect to PH_3.[20] In these cases, similar reactivity observed in both the stoichiometric chemistry in a dichloromethane solution where the formation of complexes **22** was observed. Alternatively, reducing electron density at the metal centre (with triphenylphosphite) ceased the formation of the ruthenium vinylidene-containing complex $[Ru(\eta^5\text{-}C_5H_5)(PR_3)(L)(=C=CHPh)][PF_6]$ and promoted a different reaction pathway.

Increasing the steric influence of ligands close to the metal centre (with triisopropylphosphine and 2-methylpyridine) inhibited the formation of the complexes $[Ru(\eta^5\text{-}C_5H_5)(PR_3)(L)_2][PF_6]$ (where R = Ph or ^{i}Pr and L = N-containing heterocycle). Stronger electron-donating N-containing heterocycles with respect to pyridine were screened. The reported ligands Hammett values of 3-methylpyridine, 4-methylpyridine

and 4-dimethylaminopyridine were -0.07, -0.17 and -0.83 respectively.[292, 294, 295] The earlier two ligands exhibited similar observations to pyridine, where the vinylidene-containing complexes $[Ru(\eta^5\text{-}C_5H_5)(PPh_3)(L)(=C=CHR)][PF_6]$ could be observed. However, this intermediate was not detected for 4-dimethylaminopyridine which has a stronger electron donating ability *via* conjugation. In all of these cases, the formation of the pyridylidene-alkene complexes was observed.

The substituents at the 4-position of the phenyl ring of terminal alkynes has included H, F and CF_3. The electron-withdrawing effects of F and CF_3 with Hammett values were 0.06 and 0.54 respectively, therefore demonstrating that the CF_3 group has a much larger effect.[292, 294, 295] This was observed in the stoichiometric reactions of $\mathbf{10^H}$ and aryl terminal alkynes in a dichloromethane solution, where reactions with the 4-CF_3 substituent were more selective to only generate complexes **22**, due to a preference for the generating the vinylidene complexes **19**.

To conclude, the reaction pathway for the alkenylation of pyridine with terminal alkynes by $\mathbf{10^H}$ has been investigated. The alkenylation reaction is 100 % atom efficient with respect to the starting materials employed and the reaction is preferred at lower temperatures of 50 °C. A set of novel ruthenium pyridylidene-alkene complexes have been identified; where the role of the pyridylidene ligands have been demonstrated to lead to catalyst deactivation.

8.6 Future Work

The research on the alkenylation of pyridine by $\mathbf{10^H}$ has been extensively studied and a potential energy surface proposed. Based upon the knowledge gained it is possible to extend the research into new fields. The development of the catalytic system has been extended to include a wider variety of N-containing heterocycles. Additionally, the easier to handle, air-stable complex $[Ru(\eta^5\text{-}C_5H_5)(\text{naphthalene})][PF_6]$ can be employed to generate an *in situ* catalyst and prevent an extra synthetic step for formation of the catalyst for the alkenylation of pyridine.[282, 296, 338] A more mechanistic approach to catalyst development, will include the use of non-covalent interactions to assist in the alkenylation reaction pathway. For example, the presence of a pyridyl group at the phosphorus ligand may exhibit enhanced features due to the close proximity of the nitrogen donor group.[112, 117]

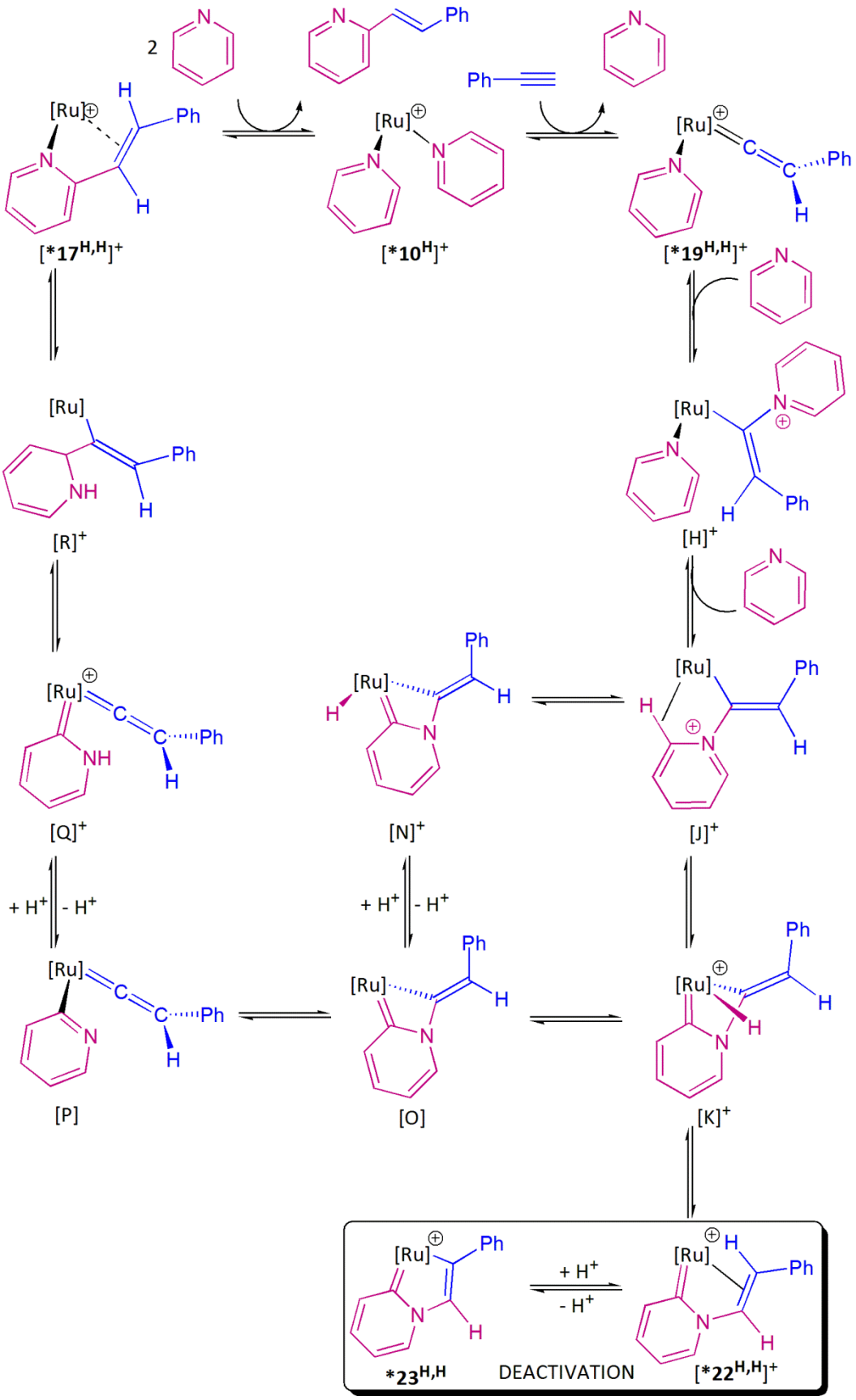

Scheme 8.1: The proposed catalytic cycle for the alkenylation of pyridine with terminal alkynes, where [Ru] = $[Ru(\eta^5\text{-}C_5H_5)(PPh_3)]^+$.

Chapter 9. Experimental

9.1 General Considerations

All experimental procedures were performed under an atmosphere of dinitrogen using standard Schlenk Line and Glove Box techniques. Dichloromethane, pentane, hexane, and toluene were purified with the aid of an Innovative Technologies anhydrous solvent engineering system. Diethyl ether was dried over sodium under argon. Pyridine 99.5 % was Acros Organics "Extra Dry" which was stored under nitrogen and handled in a Glove Box. The CD_2Cl_2 used for NMR experiments was dried over CaH_2 and degassed with three freeze-pump-thaw cycles. The solvent was then transferred into NMR tubes fitted with PTFE Young's taps or kept under a nitrogen atmosphere in the Glove Box. Unless mentioned otherwise d_5-pyridine was purchased from Sigma-Aldrich and dried over molecular sieves 4 Å, and degassed with three freeze-pump-thaw cycles. The solvent was then stored under a nitrogen atmosphere in the Glove Box. Microwave reactions were heated in a CEM Discover Microwave. Phenylacetylene (Acros Organics) and purified by passage through an alumina column and degassed by three freeze-pump-thaw cycles. $RuCl_3.3H_2O$ was supplied from Precious Metals Online. 4-Ethynyl-α,α,α-trifluorobenzene was purchased from Sigma-Aldrich and used as supplied. $[Ru(\eta^5\text{-}C_5H_5)(NCMe)_3][PF_6]$ was supplied by Sigma-Aldrich, and kept at -20 °C under a nitrogen atmosphere in the Glove Box. 4-Methylpyridine was degassed with three freeze-pump-thaw cycles and stored under a nitrogen atmosphere. 3-Methylpyridine and 2-methylpyridine were deoxygenated from bubbling nitrogen gas through the solvent. 4-Dimethylaminopyridine was purchased from Sigma-Aldrich and used as supplied. 1-Methylimidazole ≥99%, purified by re-distillation was purchased from Sigma-Aldrich, and was deoxygenated by bubbling nitrogen gas through the solvent.

NMR spectra were acquired where mentioned either on a JEOL 400 (Operating frequencies ^1H 400 MHz, ^{19}F 376.17 MHz, ^{31}P 162 MHz, ^{13}C 100 MHz); a Bruker AVANCE 500 (Operating frequencies ^1H 500.23 MHz, ^{31}P 202.50 MHz, ^{13}C 125.77 MHz, ^{19}F 470.68 MHz); or a Bruker AV700 (Operating frequencies ^1H 700.13 MHz, ^{13}C 176.04 MHz). The $^{31}P\{^1H\}$ and $^{13}C\{^1H\}$ spectra were recorded with proton decoupling. Accurate mass, ESI-MS results were recorded on a Bruker micrOTOF mass

spectrometer, coupled to an Agilent 1200 series LC system. EI-MS was recorded on a Waters GCT Premier mass spectrometer, coupled to an Agilent 7890 GC system to provide GC-EI-MS. IR spectra were acquired either on a Thermo-Nicolet Avatar 370 FTIR spectrometer using CsCl solution cells, or on a Unicam RS 10000 FTIR instrument using the ATR function under aerobic conditions. Diffraction data was either collected at 110(2) K on a Bruker Smart Apex diffractometer with Mo-K_α radiation (λ = 0.71073 Å) using a SMART CCD camera or on an Oxford Diffraction SuperNova diffractometer with Mo-K_α radiation (λ = 0.71073 Å) using a EOS CCD camera, where the crystal was cooled with an Oxford Instruments Cryojet.

9.2 Synthesis of Half Sandwich Ruthenium Complexes of the Type $[Ru(\eta^5\text{-}C_5H_5)(PPh_3)_2]$

9.2.1 Synthesis of $[Ru(\eta^5\text{-}C_5H_5)Cl(PPh_3)_2]$, 1.[265]

A distillation set-up was used to crack dicyclopentadiene (45 mL). The round bottom flask containing the dimer was stirred whilst being slowly heated, the temperature at the top of the Vigreux column was maintained at 35 °C.

Ethanol (1 L) was deoxygenated (2 hours) with nitrogen, and fitted with a reflux condenser. In a 2 L round bottom flask triphenylphosphine (21.0 g, 0.08 mol), and anti-bumping granules were added, and the mixture heated to reflux.

$RuCl_3.3H_2O$ (4.98 g, 0.02 mol) was dissolved in deoxygenated ethanol (80 mL). The freshly distilled cyclopentadiene (10 mL) was added to ethanol (10 mL) under nitrogen.

The $RuCl_3.3H_2O$ solution was transferred to the round bottom flask (2 L) *via* a cannula transfer; followed similarly by the cyclopentadienyl solution. The reaction mixture was heated at reflux (1 hour). The solution was cooled to room temperature, and stored at -20 °C for 16 hours to give bright red crystals. The product was air stable, and washed with ethanol (4 x 25 mL) and diethyl ether (4 x 25 mL). A second batch of orange precipitate could be collected when the solvent was reduced. (Yield: 10.44 g, 72%)

Characterisation Data

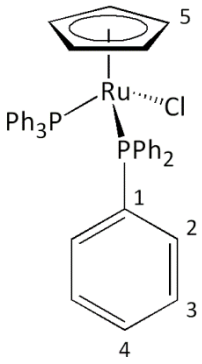

Figure 9.1: Labelled diagram of complex **1**.

^{1}H NMR (CD_2Cl_2, 400 MHz, 295 K): 4.09 (s, 5H, H_5), 7.14 (apparent t, 12H, $^{3}J_{HH}$ = 7.2 Hz, H_2), 7.25 (t, 6H, $^{3}J_{HH}$ = 7.4 Hz, H_4), 7.32-7.36 (m, 12H, H_3)

^{31}P{^{1}H} NMR (CD_2Cl_2, 162 MHz, 295 K): 39.5 (s, PPh_3)

^{13}C{^{1}H} NMR (CD_2Cl_2, 100 MHz, 295 K): 81.7 (t, $^{2}J_{CP}$ = 2.4 Hz, C_5), 127.8 (t, $^{1}J_{CP}$ + $^{3}J_{CP}$ = 9.2 Hz, C_2), 129.1 (s, C_4), 134.1 (t, $^{1}J_{CP}$ + $^{3}J_{CP}$ = 10.2 Hz, C_3), 138.8 (m, $^{1}J_{CP}$ + $^{3}J_{CP}$ = 39.7 Hz, C_1)

ESI-MS (MeOH, *m/z*): Observed 732.1573 [M^+ –Cl +NCMe], Expected $C_{43}H_{38}NP_2{}^{102}Ru$ 732.1532, Error = 4.1 mDa; Observed 691.1286 [M^+ -Cl], Expected $C_{41}H_{35}P_2{}^{102}Ru$ 691.1257, Error = 2.9 mDa.

IR (CH_2Cl_2, ν /cm^{-1}): 1027.8 (broad m), 1089.8 (m), 1185.6 (w), 1257.8 (s), 1266.3 (s), 1275.5 (s), 1434.5 (m), 1456 (m), 1480.3 (w), 1506.3 (m), 1558.8 (w), 1575.7 (m), 1635.3 (w), 1652.8 (m), 1700.0 (m), 1733.9 (w), 2854.6 (broad w), 2926.7 (broad m), 2961.6 (broad m), 3046.4 (w), 3060.8 (w)

^{1}H NMR (NC_5D_5, 400 MHz, 295 K): 4.35 (s, 5H, H_5), 7.19 (m), 7.28 (m, 6H, H_4), 7.70 (m, 6H)

^{31}P{^{1}H} NMR (NC_5D_2, 162 MHz, 295 K): 39.8 (s, PPh_3)

9.2.2 Preparation of $[Ru(\eta^5\text{-}C_5H_5)(PPh_3)_2(=C=CHPh)][PF_6]$, 2^{Ph}. [54]

$[Ru(\eta^5\text{-}C_5H_5)Cl(PPh_3)_2]$, **1** (241 mg, 0.33 mmol) was suspended in methanol (20 mL). Under nitrogen NH_4PF_6 (170 mg, 1.0 mmol) and phenylacetylene (55 µl, 5.0 mmol) were added. The bright orange reaction mixture was stirred and heated to reflux (60 °C, 10 minutes). A colour change to a bright red indicated the completion of the reaction. The cooled reaction mixture was filtered to give a red solution, and the solvent was removed under vacuum. The red product was dissolved in dichloromethane (5 mL), and filtered into excess diethyl ether (20 mL) to give a red precipitate. The excess solvent was removed by filtration and the pale red product dried under vacuum. Limited data for yields.

Characterisation Data

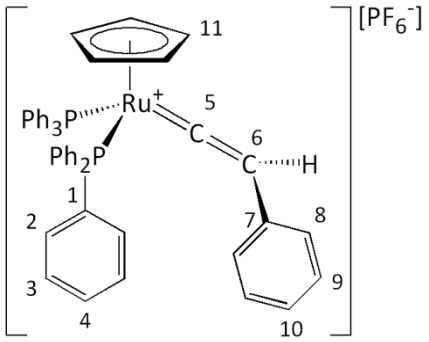

Figure 9.2: Labelled diagram of $\mathbf{2^{Ph}}$.

^{1}H NMR (CD_2Cl_2, 400 MHz, 295 K): 5.27 (s, 5H, H_{11}), 5.43 (t, 1H, $^4J_{HP}$ = 2.4 Hz, H_6), 7.01-7.09 (m, 14H, H_2, H_8), 7.16 (tt, 1H, $^3J_{HH}$ = 7.4 Hz, $^4J_{HH}$ = 1.2 Hz, H_{10}), 7.21-7.29 (m, 14H, H_3, H_9), 7.40-7.45 (m, 6H, H_4)

$^{31}P\{^1H\}$ NMR (CD_2Cl_2, 162 MHz, 295 K): -143.0 (sept, $^1J_{PF}$ = 710 Hz, PF_6^-), 43.9 (s, PPh_3)

$^{13}C\{^1H\}$ NMR (CD_2Cl_2, 125 MHz, 295 K): 95.3 (s, C_{11}), 119.9 (s, C_6), 127.5 (s), 127.5 (s), 127.8 (s), 129.1 (m), 129.4 (s), 131.5 (s), 133.4 (m), 133.9 (m), 354.4 (t, $^2J_{CP}$ = 15.6 Hz, C_5)

ESI-MS (MeOH, *m/z*): Observed 793.1721 [M^+], Expected $C_{49}H_{41}P_2{}^{102}Ru$ 793.1735, Error = 1.4 mDa; Observed 691.1266 [M^+ - HCCPh], Expected $C_{41}H_{35}P_2{}^{102}Ru$ 691.1257, Error = 0.9 mDa; Observed 429.0333 [M^+ - HCCPh – PPh_3], Expected $C_{23}H_{20}P^{102}Ru$ 429.0341, Error = 0.8 mDa.

9.2.3 Preparation of [Ru(η^5-C_5H_5)(PPh_3)$_2$(=^{13}C=CHPh)][PF_6], ^{13}C-2^{Ph}. [54]

[Ru(η^5-C_5H_5)Cl(PPh_3)$_2$], **1** (253 mg, 0.35 mmol) was suspended in methanol (20 mL). Under nitrogen NH_4PF_6 (173 mg, 1.0 mmol) and ^{13}C-phenylacetylene (50 µl, 4.5 mmol) were added. The bright orange reaction mixture was stirred and heated to reflux (60 °C, 10 minutes). The cooled reaction mixture was filtered to give a red solution and the solvent removed under vacuum. The red product was dissolved in dichloromethane (5 mL), and filtered into excess diethyl ether (20 mL) to give a red precipitate. The excess solvent was removed by filtration and the pale red product dried under vacuum. Limited data for yields.

Characterisation Data

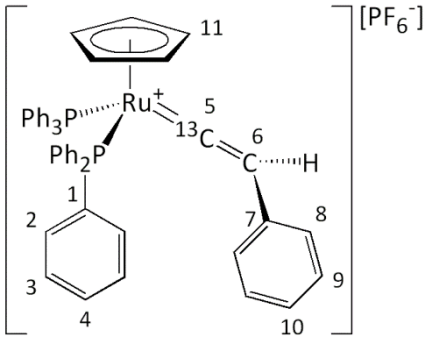

Figure 9.3: Labelled diagram of **^{13}C-2^{Ph}**.

^{1}H NMR (CD_2Cl_2, 400 MHz, 295 K): 5.27 (6, 5H, $^4J_{HH}$ = 1.2 Hz, H_{11}), 5.43 (m, 1H, H_6), 7.01-7.09 (m, 14H, H_2, H_8), 7.16 (m, 1H, H_{10}), 7.21-7.29 (m, 14H, H_3, H_9), 7.40-7.45 (m, 6H, H_4)

^{31}P{^{1}H} NMR (CD_2Cl_2, 162 MHz, 295 K): -143.0 (sept, $^1J_{PF}$ = 710 Hz, PF_6^-), 43.4 (d, $^2J_{PC}$ = 15.5 Hz, PPh_3)

^{13}C{^{1}H} NMR (CD_2Cl_2, 100 MHz, 295 K): 95.3 (s, C_{11}), 127.5 (s), 127.5 (s), 127.8 (s), 129.1 (m), 129.4 (s), 131.5 (s), 133.4 (m), 133.7 (s), 354.4 (t, $^2J_{CP}$ = 15.5 Hz, C_5) (Did not observe C_6)

ESI-MS (MeOH, *m/z*): Observed 794.1745 [M^+], Expected $C_{48}{}^{13}CH_{41}P_2{}^{102}Ru$ 794.1768, Error = 1.0 mDa.

9.2.4 Preparation of $[Ru(\eta^5\text{-}C_5H_5)(PPh_3)_2(=C=CH(p\text{-}MeC_6H_4)][PF_6]$, $2^{C6H4\text{-}p\text{-}Me}$. [54]

$[Ru(\eta^5\text{-}C_5H_5)Cl(PPh_3)_2]$, **1** (247 mg, 0.34 mmol) was suspended in methanol (20 mL). 4-ethynyltoluene (60 µL, 0.47 mmol) and NH_4PF_6 (345 mg, 2.1 mmol) were added and the reaction mixture heated to reflux (10 minutes). The cooled reaction mixture was filtered and the red solution collected. The solvent was removed under vacuum. The product was extracted with dichloromethane (5 mL), and the filtrate added to an excess of diethyl ether. A red precipitate was collected. Limited data for yields.

Characterisation Data

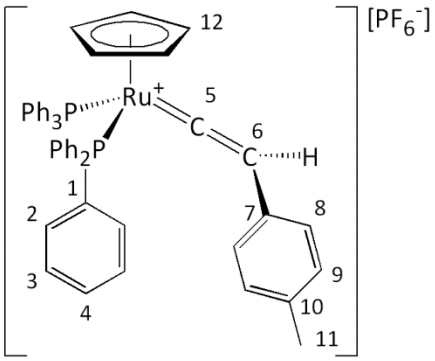

Figure 9.4: Labelled diagram of $\mathbf{2}^{C6H4\text{-}p\text{-}Me}$.

^1H NMR (CD_2Cl_2, 500 MHz, 295 K): 2.35 (s, 3H, H_{11}), 5.27 (s, 5H, H_{12}), 5.43 (t, 1H, $^4J_{HP}$ = 2.4 Hz, H_6), 6.99 – 7.12 (m, 16H, H_2, H_8, H_9), 7.25 (td, 12H, $^3J_{HH}$ = 7.7 Hz, $^4J_{HP}$ = 1.8 Hz, H_3), 7.43 (t, 6H, $^3J_{HH}$ = 7.4 Hz, H_4)

$^{31}P\{^1H\}$ NMR (CD_2Cl_2, 162 MHz, 295 K): -143.5 (sept, $^1J_{PF}$ = 710 Hz, PF_6^-), 43.6 (s, PPh_3)

$^{13}C\{^1H\}$ NMR (CD_2Cl_2, 125 MHz, 295 K): 21.1 (s, C_{11}), 95.2 (s, C_{12}), 119.7 (s, C_6), 124.9 (s), 127.4 (s), 129.0 (m), 130.1 (s), 131.4 (s), 133.4 (m), 134.0 (m), 137.6 (s), 355.5 (t, $^2J_{CP}$ = 15.4 Hz, C_5)

Low Resolution ESI-MS (CH_2Cl_2, *m/z*): Observed 807.2 [M^+], Expected $C_{50}H_{43}P_2{}^{102}Ru$ 807.1878; Observed 691.1 [M^+ - HCCPh], Expected $C_{41}H_{35}P_2{}^{102}Ru$ 691.1257.

9.2.5 Synthesis of $[Ru(\eta^5\text{-}C_5H_5)(PPh_3)_2(=C=CH^tBu)][PF_6]$, 2^{tBu}. [54]

$[Ru(\eta^5\text{-}C_5H_5)Cl(PPh_3)_2]$, **1** (252 mg, 0.35 mmol) was suspended in methanol (20 mL). NH_4PF_6 (186 mg, 1.1 mmol) and tert-butylacetylene (64 µl, 5.2 mmol) were added. The reaction mixture was heated to reflux (60 °C, 15 minutes). The colour change to a bright orange solution indicated the completion of the reaction. The cooled reaction mixture was filtered to give a red solution. The solvent was removed under vacuum. The red product was dissolved in dichloromethane (5 mL), and filtered into excess diethyl ether (20 mL). The excess solvent was removed by filtration and the orange product dried under vacuum. Limited data for yields.

Characterisation Data

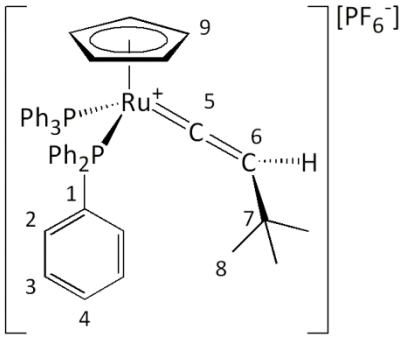

Figure 9.5: Labelled diagram of $\mathbf{2^{tBu}}$.

^{1}H NMR (CD_2Cl_2, 500 MHz, 295 K): 1.17 (s, 9H, H_8), 4.24 (t, 1H, $^4J_{HP}$ = 2.8 Hz, H_6), 5.11 (s, 5H, H_9), 7.02-7.06 (m, 12H, H_2), 7.26-7.29 (m, 12H, H_3), 7.44 (t, 6H, $^3J_{HH}$ = 7.2 Hz)

^{31}P{^{1}H} NMR (CD_2Cl_2, 202 MHz, 295 K): -143.0 (sept, $^1J_{PF}$ = 711 Hz, PF_6^-), 42.8 (s, PPh_3)

ESI-MS (*m/z*): Observed 773.2096 [M^+], Expected $C_{47}H_{45}P_2{}^{102}Ru$ 773.2034, Error = 6.2 mDa

9.2.6 Synthesis of [(Ru(η^5-C_5H_5)(C≡CPh)(PPh_3)$_2$], **3^{Ph}**. [54]

[Ru(η^5-C_5H_5)Cl(PPh_3)$_2$], **1** (243 mg, 0.33 mmol) was suspended in methanol (10 mL). Phenylacetylene (55 µl, 51 mg, 0.50 mmol) was added using a microsyringe and the reaction mixture heated to reflux (45 minutes). A solution of NaOMe (27 mg, 0.50 mmol) in methanol (1 mL) was added to the cooled reaction mixture, and the bright red solution turned yellow. Excess solvent was removed *via* filtration, and the product dried under vacuum. Yield (208 mg, 77 %).

Characterisation Data

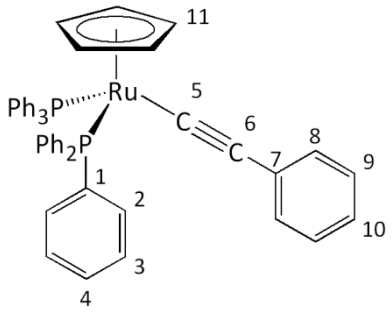

Figure 9.6: Labelled diagram of **3^{Ph}**.

^{1}H NMR (CD_2Cl_2, 400 MHz, 295 K): 4.32 (s, 5H, H_{11}), 7.08- 7.16 (m, 17H, Ph), 7.22 (t, 6H, H_4), 7.45- 7.50 (m, 12H, Ph)

^{31}P{^{1}H} NMR (CD_2Cl_2, 162 MHz, 295 K): 50.9 (s, PPh_3)

^{13}C{^{1}H} NMR (CD_2Cl_2, 100 MHz, 295 K): 85.5 (t, $^3J_{CP}$ = 2.2 Hz, C_{11}), 114.6 (s), 116.9 (broad), 123.3 (s), 127.6 (m), 128.0 (s), 128.8 (s), 130.6 (m), 132.2 (s), 134.1 (m), 139.3 (m, $^1J_{CP}$ + $^3J_{CP}$ = 41.7 Hz, C_1)

ESI-MS (*m/z*): Observed 793.1750 [M + H]$^+$, Expected $C_{49}H_{41}P_2{}^{102}Ru$ 793.1721, Error = 2.9 mDa.

IR (CH_2Cl_2, ν /cm^{-1}): 2072 (C≡C stretching)

^{1}H NMR (NC_5D_5, 400 MHz, 295 K): 4.59 (s, 5H, H_{11}), 7.12 (t, 1H, $^3J_{HH}$ = 7.3 Hz, H_{10}), 7.15- 7.21 (m, 12H, Ph), 7.26 (t, 6H, H_4), 7.34 (t, 2H, $^3J_{HH}$ = 7.6 Hz, H_9), 7.61 (d, 2H, $^3J_{HH}$ = 7.3 Hz, H_8), 7.76- 7.81 (m, 12H, Ph)

^{31}P{^{1}H} NMR (CD_5N_5, 162 MHz, 295 K): 50.4 (s, PPh_3)

9.2.7 Synthesis of $[Ru(\eta^5\text{-}C_5H_5)(C{\equiv}C(p\text{-}Me(C_5H_4))(PPh_3)_2]$, $3^{C6H4\text{-}p\text{-}Me}$. [54]

$[Ru(\eta^5\text{-}C_5H_5)Cl(PPh_3)_2]$, **1** (247 mg, 0.34 mmol), 4-ethynyltoluene (60 mg, 0.52 mmol) and methanol (15 mL) were stirred and heated to reflux (45 minutes). A solution of NaOMe (28 mg, 0.52 mmol) in methanol (2 mL) was added to the cooled reaction mixture, and the bright red solution turned yellow. Excess solvent was removed by filtration, and the product dried under vacuum. Yield (202 mg, 74 %).

Characterisation Data

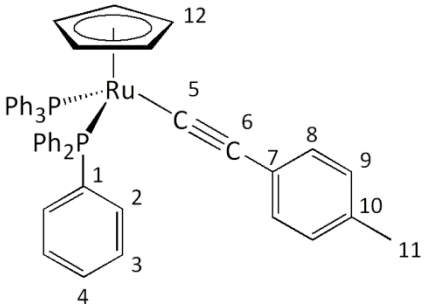

Figure 9.7: Labelled diagram of $\mathbf{3}^{C6H4\text{-}p\text{-}Me}$.

^{1}H NMR (CD_2Cl_2, 400 MHz, 295 K): 2.30 (s, 3H, H_{11}), 4.32 (s, 5H, H_{12}), 7.00 (m, 4H, $H_{8,}$ H_{9}), 7.11 (t, 12H, $^3J_{HH}$ = 7.2 Hz, Ph), 7.20- 7.24 (t, 6H, $^3J_{HH}$ = 7.2 Hz, H_4), 7.47-7.51 (m, 12H, Ph)

$^{31}P\{^1H\}$ NMR (CD_2Cl_2, 162 MHz, 295 K): 50.8 (s, PPh_3)

$^{13}C\{^1H\}$ NMR (CD_2Cl_2, 100 MHz, 295 K): 21.2 (s, C_{11}), 85.5 (t, $^2J_{CP}$ = 2.2 Hz, C_{12}), 114.3 (s), 114.4 (s), 127.6 (m), 128.1 (m), 128.8 (s), 130.5 (m), 132.9 (s), 134.1 (m), 139.4 (m, $^1J_{CP}$ + $^3J_{CP}$ = 41.6 Hz, C_1)

ESI-MS (*m/z*): Observed 807.1877 [M^+ + H], Expected $C_{50}H_{43}P_2{}^{102}Ru$ 807.1878, Error = 0.1 mDa; Observed 691.1254 [$M^+ - C_9H_7$], Expected $C_{41}H_{35}P_2{}^{102}Ru$ 691.1257, Error = 0.3 mDa

^{1}H NMR (NC_5D_5, 400 MHz, 295 K): 2.23 (s, 3H, H_{11}), 4.58 (s, 5H, H_{12}), 7.11-7.20 (m, 14H, Ph), 7.26 (t, 6H, $^3J_{HH}$ = 6.8 Hz, H_4), 7.53 (d, 2H, $^3J_{HH}$ = 7.9 Hz, H_8), 7.77-7.81 (m, 12H, Ph)

$^{31}P\{^1H\}$ NMR (CD_5N_5, 162 MHz, 295 K): 51.1 (s, PPh_3)

9.2.8 Synthesis of the $[Ru(\eta^5\text{-}C_5H_5)(PPh_3)_2(NC_5H_5)][PF_6]$, 31.

$[Ru(\eta^5\text{-}C_5H_5)Cl(PPh_3)_2]$, **1** (238 mg, 0.33 mmol) and $NaPF_6$ (170 mg, 1.0 mmol) were suspended in methanol (20 mL) stirred. Pyridine (140 µL, 1.73 mmol) was added. The reaction mixture was heated to reflux (1 hour), until it appeared yellow. The reaction mixture was cooled, and the solution filtered to give a yellow precipitate. The precipitate was dissolved in a minimum amount of dichloromethane (5 mL). Diethyl ether (20 mL) was added to give a yellow precipitate. The excess solution was removed by filtration, and the precipitate dried under vacuum. Yield (166 mg, 56 %)

Characterisation Data

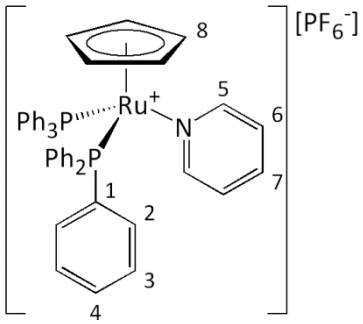

Figure 9.8: Labelled diagram of **31**.

^{1}H NMR (CD_2Cl_2, 500 MHz, 295 K): 4.43 (s, 5H, H_8), 6.71 (m, 2H, H_6), 7.08 (m, 12H, H_3), 7.28 (t, 12H, $^3J_{HP}$ = 7.21 Hz, H_2), 7.44 (m, 7H, H_4 + H_7), 8.21 (dd, 2H, $^3J_{HH}$ = 6.3 Hz, $^4J_{HP}$ = 1.2 Hz, H_5)

^{31}P{^{1}H} NMR (CD_2Cl_2, 202 MHz, 295 K): -143.0 (sept, $^1J_{PF}$ = 710 Hz, PF_6^-), 43.5 (s, PPh_3)

^{13}C{^{1}H} NMR (CD_2Cl_2, 100 MHz, 295 K): 83.6 (t, $^3J_{CP}$ = 2.0 Hz, C_8), 125.3 (s, C_7), 128.8 (m, $C_{2/3}$), 130.7 (t, $^4J_{CP}$ = 1.1 Hz, C_6), 134.0 (m, $C_{2/3}$), 135.3 (m, $^1J_{CP}$ + $^3J_{CP}$ = 40.5 Hz, C_1), 136.9 (s, C_4), 158.1 (t, $^3J_{CP}$ = 3.2 Hz, C_5)

ESI-MS: Observed 770.1675 [M^+], Expected $C_{46}H_{40}NP_2{}^{102}Ru$ 770.1686, Error = 0.1 mDa; Observed 691.1253 [M^+ - NC_5H_5], Expected $C_{41}H_{35}P_2{}^{102}Ru$ 691.1252, Error = 0.1 mDa.

IR (CH_2Cl_2, ν /cm^{-1}): 3054, 1480, 1435, 1268 (s), 1266 (s), 1260 (s), 1089

Elemental Analysis: Anal. $C_{47}H_{42}F_6NP_3Ru$: Calc. C(60.40) H(4.41) N (1.53), Found C(60.28) H(4.79) N (1.44)

In d_5-pyridine the pyridine ligand must be exchanging as it can't be detected.

^{1}H NMR (CD_5N_5, 400 MHz, 295 K): 4.72 (s, 5H, H_8), 7.25- 7.29 (m, 12H, Ph), 7.31-7.35 (m, 12H, Ph), 7.48 (t, 6H, $^3J_{HH}$ = 7.22 Hz, H_4)

^{31}P{^{1}H} NMR (CD_2Cl_2, 162 MHz, 295 K): -143.5 (sept, $^1J_{PF}$ = 710 Hz, PF_6^-), 41.6 (s, PPh_3)

9.2.9 Synthesis of $[Ru(\eta^5\text{-}C_5H_5)(PPh_3)_2(CO)][PF_6]$, 4.

$[Ru(\eta^5\text{-}C_5H_5)Cl(PPh_3)_2]$, **1** (202 mg, 0.28 mmol), NH_4PF_6 (133 mg, 0.82 mmol) were suspended in methanol (10 mL). The nitrogen atmosphere was removed under vacuum, and the vessel placed under a CO atmosphere, sealed and stirred for 40 hours. The solvent was removed under vacuum. The yellow solid was placed in dichloromethane (5 mL) and filtered into an excess of diethyl ether. The excess solvent was removed by filtration and a pale yellow solid dried under vacuum. Yield (0.12 g, 49 %).

Characterisation Data

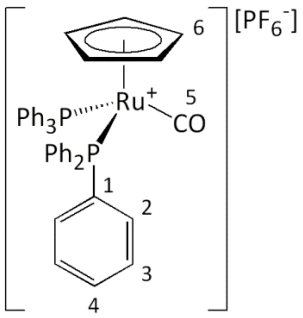

Figure 9.9: Labelled diagram of **4**.

^{1}H NMR (CD_2Cl_2, 400 MHz, 295 K): 5.30 (s, 5H, H_6), 7.06-7.12 (m, 12H, Ph), 7.29-7.33 (m, 12H, Ph), 7.43-7.48 (m, 6H, H_4)

^{31}P{^{1}H} NMR (CD_2Cl_2, 162 MHz, 295 K): -143.0 (sept, $^1J_{PF}$ = 711 Hz, PF_6^-), 43.2 (s, PPh_3)

^{13}C{^{1}H} NMR (CD_2Cl_2, 100 MHz, 295 K): 91.2 (t, $^3J_{CP}$ = 1.4 Hz, C_6), 129.4 (m, $^1J_{CP}$ + $^3J_{CP}$ = 10.7 Hz, $C_{2/3}$), 131.7 (m, $^1J_{CP}$ + $^3J_{CP}$ = 2.3 Hz, C_4), 133.5 (m, $^1J_{CP}$ + $^3J_{CP}$ = 10.6 Hz, $C_{2/3}$), 134.2 (m, $^1J_{CP}$ + $^3J_{CP}$ = 51.0 Hz, C_1)

ESI-MS (*m/z*): Observed 719.120 [M^+], Expected $C_{42}H_{35}OP_2{}^{102}Ru$ 719.1212, Error = 0.7 mDa.

IR (MeOH, ν /cm^{-1}): 1558 (s), 1576 (m), 16161.5 (m), 1635 (w), 1652.6 (m), 1684.5 (m), 1695.6 (s), 1700.9 (s), 1717.3 (s), 1734.2 (w), 1980.5 (CO stretching), 2926.3 (broad m)

^{1}H NMR (CD_5N_5, 400 MHz, 295 K): 5.30 (s, 5H, H_6), 7.25 (m, 12H), 7.33 (m, 12H), 7.47 (m, 6H, H_4)

$^{31}P\{^{1}H\}$ NMR (CD_2Cl_2, 162 MHz, 295 K): -143.0 (sept, $^{1}J_{PF}$ = 711 Hz, PF_6^-), 41.8 (s, PPh_3)

9.3 Synthesis of Half Sandwich Ruthenium Complexes

9.3.1 Preparation of Ruthenocene, 6. [281]

Freshly distilled cyclopentadiene was obtained from a distillation of dicyclopentadiene (50 mL), where the temperature in the Vigreux column did not exceed 40 °C.

Degassed ethanol (100 mL) and $RuCl_3.3H_2O$ (5.20 g, 20.0 mmol) were stirred under nitrogen and freshly distilled cyclopentadiene (25 mL) was added. The reaction mixture was cooled in an ice bath, whilst zinc (13.1 g, 200 mmol) was slowly added. The reaction mixture was warmed to room temperature, and stirred (20 hours).

The crude reaction mixture was filtered through a plug of Celite and the yellow filtrate collected and solvent removed. The crude product was dissolved in toluene (400 mL) and passed through a short silica plug. The solvent was removed to give yellow crystalline ruthenocene. Yield (3.65 g, 79 %).

Characterisation Data

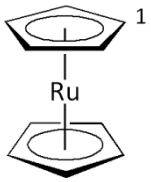

Figure 9.10: Labelled diagram of **6**.

^{1}H NMR ($CDCl_3$, 400 MHz, 295K): 4.55 (s, H_1)

$^{13}C\{^{1}H\}$ NMR ($CDCl_3$, 100 MHz, 295K): 70.2 (s, C_1)

9.3.2 Preparation of [Ru(η^5-C_5H_5)(naphthalene)][PF_6], 7. [281]

Ruthenocene, **6** (2.33 g, 10 mmol), naphthalene (2.55 g, 20.0 mmol), fine powder Al (0.135 g, 5.0 mmol) were placed in a microwave vial with a stirrer bar. The microwave vial and lid were pumped into the Glove Box where $AlCl_3$ (0.260 g, 1.9 mmol) was added, and the microwave lid used to seal the reaction vessel. $TiCl_4$ (0.55 mL, 5.0 mmol) placed in a sample vial with a subaseal top and sealed. The samples were removed from the Glove Box.

Degassed decalin (15 mL) was added to the added to the microwave vial, and stirred. $TiCl_4$ was added to the reaction mixture and stirred (5 minutes). The microwave vial was irradiated (15 mins, 194 °C).

The cooled reaction mixture was poured into an ice bath (80 mL), HCl (32%, 20 mL), H_2O_2 (30%, 20 mL) mixture and stirred (10 minutes). The reaction mixture was extracted with pentane (3 x 200mL). The organic layers were combined and extracted with water (2 x 100 mL). All aqueous layers were combined and stirred. KPF_6 (2.78 g, 15 mmol) was added and the reaction mixture stirred (15 minutes) to afford a light brown precipitate.

The reaction mixture was extracted with dichloromethane (4 x 200 mL), and the organic layers dried with $MgSO_4$. The yellow solution was reduced to give a orange-brown solid. The crude product was redissolved in dichloromethane (60 mL), and filtered through a plug of Celite. The Ceilte was washed with dichloromethane till washing became colourless. The solvent was reduced to approximately 10 mL, and poured into stirring diethyl ether (100 mL). The light brown precipitate was collected, and washed with diethyl ether (2 x 20 mL), pentane (2 x 20 mL).

Crystals suitable for X-ray diffraction were grown unintentionally from a reaction mixture containing complex **7** in furan and d_2-dichloromethane.

Characterisation Data

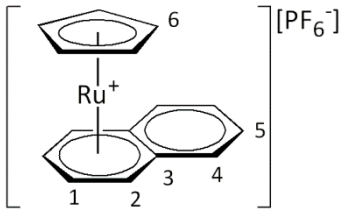

Figure 9.11: Labelled diagram of **7**.

^{1}H NMR ($CDCl_3$, 400 MHz, 295K): 5.00 (s, 5H, H_6), 6.31-6.33 (m, 2H), 6.97-6.99 (m, 2H), 7.57-7.60 (m, 2H), 7.70-7.73 (m, 2H)

^{31}P{^{1}H} NMR ($CDCl_3$, 162 MHz, 295K): -143.5 (sept, $^{1}J_{PF}$ = 711 Hz, PF_6^-)

Low Resolution ESI-MS (*m/z*): Observed 295.0 [M^+], Expected $C_{15}H_{13}{}^{102}Ru$ 295.0055.

9.3.3 Synthesis of $[Ru(\eta^5\text{-}C_5H_5)(NCMe)_3][PF_6]$, 8. [281]

$[Ru(\eta^5\text{-}C_5H_5)(naphthalene)][PF_6]$ (1.02 g, 2.3 mmol) was added and acetonitrile (10 mL) and the reaction mixture was stirred (24 hrs). The reaction mixture was washed with pentane (3 x10 mL). The reaction mixture was stirred (24 hrs), and was with pentane (4 x 5 mL). The solvent was removed under vacuum. Yield (0.50 g, 50 %).

Characterisation Data

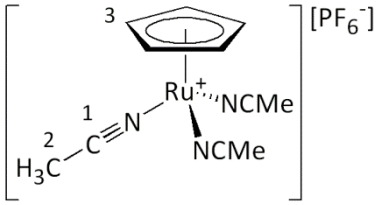

Figure 9.12: Labelled diagram of **8**.

^{1}H NMR (CD_2Cl_2, 500 MHz, 295 K): 2.37 (s, 12H, H_2), 4.25 (s, 5H, H_3)

^{31}P{^{1}H} NMR (CD_2Cl_2, 202 MHz, 295 K): -143.0 (sept, $^{1}J_{PF}$ = 711 Hz, PF_6^-)

ESI-MS (*m/z*): Observed 363.0716; 317.0593; 299.0377; Observed 248.9974 [M^+ - NCMe], Expected $C_9H_{11}N_2{}^{102}Ru$ 248.9960, Error = 1.4 mDa; Observed 235.9755; 222.9569; Observed 207.9705 [M^+ - 2 NCMe], Expected $C_7H_8N^{102}Ru$ 207.9695, Error = 1.0 mDa.

9.3.4 Synthesis of $[Ru(\eta^5\text{-}C_5H_5)(PPh_3)(NCMe)_2][PF_6]$, $\mathbf{9^{Ph}}$. [131]

To a solution of $[Ru(\eta^5\text{-}C_5H_5)(NCMe)_3][PF_6]$, **8** (96 mg, 0.22 mmol) and dichloromethane (10 mL) triphenylphosphine (56 mg, 0.21 mmol) was added, and the yellow reaction mixture stirred (3 hours). The solvent was removed under vacuum and a yellow product was collected. (135 mg, 96 %)

Characterisation Data

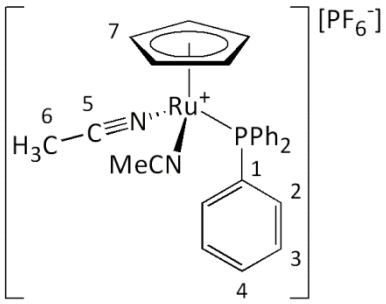

Figure 9.13: Labelled diagram of $\mathbf{9^{Ph}}$.

^{1}H NMR (CD_2Cl_2, 500 MHz, 295 K): 2.05 (d, 6H, $^5J_{HP}$ = 1.5 Hz, H_6), 4.44 (s, 5H, H_7), 7.28-7.31 (m, 6H, Ph), 7.42-7.50 (m, 9H, Ph)

^{31}P{^{1}H} NMR (CD_2Cl_2, 202 MHz, 295 K): -143.0 (sept, $^1J_{PF}$ = 711 Hz, PF_6^-), 52.2 (s, PPh_3)

^{13}C{^{1}H} NMR (CD_2Cl_2, 125 MHz, 295 K): 3.97 (s, C_6), 77.3 (d, $^3J_{CP}$ = 2.0 Hz, C_7), 127.5 (C_5), 128.9 (d, $^3J_{CP}$ = 9.9 Hz, C_3), 130.7 (d, $^4J_{CP}$ = 2.3 Hz, C_4), 133.8 (d, $^2J_{CP}$ = 11.1 Hz, C_2), 133.9 (d, $^1J_{CP}$ = 42.5, C_1)

ESI-MS (*m/z*): Observed 511.0889 [M^+], Expected $C_{27}H_{26}N_2P^{102}Ru$ 511.0879, Error = 1.1 mDa; 470.0616 [M^+ - NCMe], Expected $C_{25}H_{23}NP^{102}Ru$ 470.0606, Error = 1.0 mDa.

9.3.5 Synthesis of $[Ru(\eta^5\text{-}C_5H_5)(PMe_3)(NCMe)_2][PF_6]$, 9^{Me}. [131]

To a solution of $[Ru(\eta^5\text{-}C_5H_5)(NCMe)_3][PF_6]$, **8** (201 mg, 0.46 mmol) and dichloromethane (10 mL), trimethylphosphine (47 µL, 0.46 mmol, 1 equiv) was added. The reaction mixture stirred (2 hours) and the colour of the reaction mixture changed from orange to yellow. The solvent was removed under vacuum and a yellow product was collected. Yield (167 mg, 77 %).

Characterisation Data

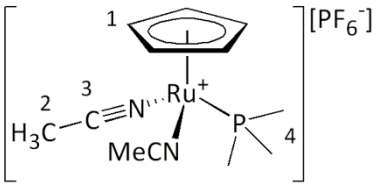

Figure 9.14: Labelled diagram of $\mathbf{9^{Me}}$.

^{1}H NMR (CD_2Cl_2, 500 MHz, 295 K): 1.51 (d, 9H, $^2J_{HP}$ = 9.6 Hz, H_4), 2.36 (d, 6H, $^5J_{HP}$ = 1.6 Hz, C_2), 4.46 (s, 5H, H_1)

^{31}P{^{1}H} NMR (CD_2Cl_2, 202 MHz, 295 K): -143.0 (sept, $^1J_{PF}$ = 707 Hz, PF_6^-), 7.64 (s, PMe_3)

^{13}C{^{1}H} NMR (125 MHz, 295 K, CD_2Cl_2): 4.27 (s, C_2), 18.3 (d, $^1J_{CP}$ = 28.4 Hz, C_4), 75.4 (s, C_1), 126.6 (s, C_3)

ESI-MS (*m/z*): Observed 325.0406 [M^+], Expected $C_{12}H_{20}N_2P^{102}Ru$ 325.0405, Error = 0.1 mDa

9.3.6 Synthesis of $[Ru(\eta^5\text{-}C_5H_5)(P^iPr_3)(NCMe)_2][PF_6]$, 9^{iPr}.

$[Ru(\eta^5\text{-}C_5H_5)(NCMe)_3][PF_6]$, **8** (100 mg, 0.23 mmol) was placed in dichloromethane (5 mL). Tri-isopropylphosphine (44 µl, 0.23 mmol) was added using a microsyringe and the yellow reaction mixture stirred (18 hours).The solvent removed under vacuum, and a yellow product collected. (120 mg, 94 %)

Characterisation Data

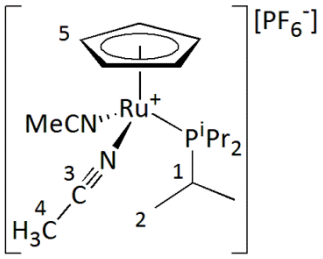

Figure 9.15: Labelled diagram of $\mathbf{9^{iPr}}$.

^{1}H NMR (CD_2Cl_2, 500 MHz, 295 K): 1.21 (dd, 18H, $^3J_{HP}$ = 13.2 Hz, $^3J_{HH}$ = 7.2 Hz, H_2), 2.29-2.36 (m, 3H, H_1), 2.37 (d, 6H, $^4J_{HP}$ = 1.1 Hz, H_4), 4.55 (s, 5H, H_5)

$^{31}P\{^1H\}$ NMR (CD_2Cl_2, 202 MHz, 295 K): -143.0 (sept, PF_6^-), 57.4 (s, P^iPr_3)

$^{13}C\{^1H\}$ NMR (CD_2Cl_2, 125 MHz, 295 K): 4.4 (s, C_4), 19.8 (s, C_2), 26.9 (d, $^1J_{CP}$ = 19.2 Hz, C_1), 75.4 (d, $^2J_{CP}$ = 1.4 Hz), 128.3 (s, C_3)

9.3.7 Preparation for $[Ru(\eta^5\text{-}C_5H_5)(P(OPh)_3)(NCMe)_2][PF_6]$, $\mathbf{9^{OPh}}$.

To a solution of $[Ru(\eta^5\text{-}C_5H_5)(NCMe)_3][PF_6]$, **8** (70 mg, 0.16 mmol) and dichloromethane (10 mL), triphenylphosphite (47 mg, 0.15 mmol) was added, and the reaction mixture stirred (16 hours). The solvent was removed under vacuum and the product was collected. Yield (75 mg, 66 %).

Characterisation Data

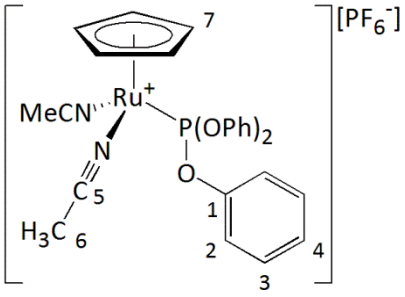

Figure 9.16: Labelled diagram of $\mathbf{9^{OPh}}$.

^{1}H NMR (CD_2Cl_2, 500 MHz, 295 K): 2.22 (d, 6H, $^5J_{HP}$ = 1.2 Hz, H_6), 4.44 (d, 5H, $^3J_{HP}$ = 0.6 Hz, H_7), 7.23-7.26 (m, 9H, Ph), 7.38-7.41 (m, 6H, Ph)

^{31}P{^{1}H} NMR (CD_2Cl_2, 202 MHz, 295 K): -143.0 (sept, $^1J_{PF}$ = 711 Hz, PF_6^-), 142.6 (s, $P(OPh)_3$)

^{13}C{^{1}H} NMR (CD_2Cl_2, 125 MHz, 295 K): 4.2 (s, C_6), 78.9 (d, $^2J_{CP}$ = 2.9 Hz, C_7), 121.2 (d, $^3J_{CP}$ = 5.1 Hz, C_2), 125.5 (s, C_3), 128.2 (s, C_5), 130.2 (s, C_4), 151.7 (d, $^2J_{CP}$ = 6.7 Hz, C_1)

9.3.8 Synthesis of $[Ru(\eta^5\text{-}C_5H_5)(PPh_3)(NC_5H_5)_2][PF_6]$, $\mathbf{10^H}$.

To a solution of $[Ru(\eta^5\text{-}C_5H_5)(PPh_3)(NCMe)_2][PF_6]$, $\mathbf{9^{Ph}}$ (80 mg, 0.12 mmol) in dichloromethane (10 mL), pyridine (0.98 mL, 12 mmol) was added and the reaction mixture stirred (18 hours). The reaction mixture was layered with either pentane or hexane to give orange crystals, suitable for X-ray diffraction. The excess solvent was removed by filtration and the air-sensitive product dried under vacuum. Yield (85 mg, 95%)

Characterisation Data

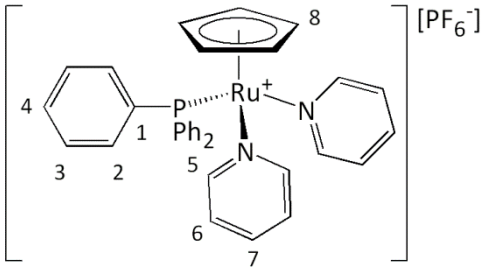

Figure 9.17: Labelled diagram of $\mathbf{10^H}$.

^{1}H NMR (CD_2Cl_2, 500 MHz, 295 K): 4.42 (s, 5H, H_8), 7.05-7.08 (m, 4H, H_6), 7.17-7.20 (m, 6H, H_2), 7.33-7.36 (m, 6H, H_3), 7.42-7.46 (m, 3H, H_4), 7.70 (tt, 2H, $^3J_{HH}$ = 7.6 Hz, $^4J_{HH}$ = 1.5 Hz, H_7), 8.29 (m, 4H, H_5)

^{31}P{^{1}H} NMR (CD_2Cl_2, 202 MHz, 295 K): -143.0 (sept, $^1J_{PF}$ = 711 Hz, PF_6^-), 50.3 (s, PPh_3)

^{13}C{^{1}H} NMR (CD_2Cl_2, 125 MHz, 295 K): 78.2 (d, $^2J_{CP}$ =2.2 Hz, C_8), 125.6 (s, C_6), 129.1 (d, $^3J_{CP}$ = 9.5 Hz, C_3), 130.7 (d, $^4J_{CP}$ =1.7 Hz, C_4), 133.7 (d, $^2J_{CP}$ = 10.9 Hz, C_2), 134.2 (d, $^1J_{CP}$ = 39.9 Hz, C_1), 137.4 (s, C_7), 156.7 (d, $^3J_{CP}$ = 2.5 Hz, C_5)

ESI-MS (*m/z*): Observed 587.1190 [M^+], Expected $C_{33}H_{30}N_2P^{102}Ru$ 587.1193, Error = 0.3 mDa; Observed 549.1037 [M^+ -NC_5H_5 +NCMe], Expected $C_{30}H_{28}N_2P^{102}Ru$ 549.1036, Error = 0.1 mDa; Observed 508.0772 [M^+ -NC_5H_5], Expected $C_{28}H_{25}NP^{102}Ru$ 508.0770, Error = 0.2 mDa.

ATR IR (ν /cm^{-1}): 607.5 (s), 698.1 (m), 749.2 (m), 836.0 (s), 1089.6 (w), 1433.8 (w), 1480.1 (w), 1600.7 (w), 2891.8 (w), 3067.2 (w)

Elemental Analysis: Anal. $C_{34}H_{30}F_6N_2P_2Ru$ + 1.0 CH_2Cl_2: Calc. C(50.01) H(3.95) N(3.43), Found C(49.95) H(3.92) N(3.32)

When complex **10^{H}** is placed in d_5-pyridine the resonances belonging to the coordinated pyridine molecules are no longer observed, as these are exchanging with uncoordinated d_5-pyridine.

^{1}H NMR (NC_5D_5, 500 MHz, 295 K): 4.57 (s, 5H, H_8), 7.36-7.42 (m, 12H, PPh_3), 7.47 (m, 3H, PPh_3)

^{31}P{^{1}H} NMR (NC_5D_5, 202 MHz, 295 K): -143.0 (sept, $^{1}J_{PF}$ = 711 Hz, PF_6^-), 49.2 (s, PPh_3)

9.3.9 Synthesis of [Ru(η^5-C$_5$H$_5$)(PPh$_3$)(NC$_5$D$_5$)$_2$][PF$_6$], 5.

To a solution [Ru(η^5-C_5H_5)(PPh_3)$(NCMe)_2$][PF_6], **9^{Ph}** (75 mg, 0.11 mmol) in dichloromethane (10 mL), d_5-pyridine (0.70 mL, 8.7 mmol, 76 equiv) was added and the reaction mixture stirred (48 hours). Slow diffusion of hexane in to the reaction mixture afforded orange crystals. The solvent was removed by filtration and the air-sensitive product dried under vacuum. Yield (64 mg, 75 %).

Characterisation Data

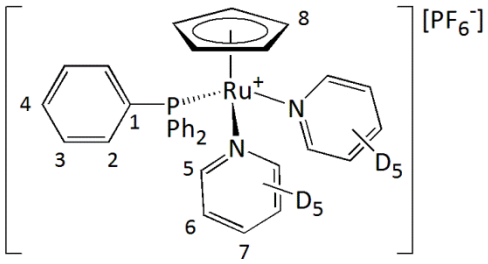

Figure 9.18: Labelled diagram of **5**.

^{1}H NMR (CD_2Cl_2, 500 MHz, 295 K): 4.42 (s, 5H, H_8), 7.19 (m, 6H, H2), 7.34 (td, 6H, $^{3}J_{HH}$ = 7.6 Hz, $^{4}J_{HP}$ = 1.9 Hz, H_3), 7.44 (td, 3H, $^{3}J_{HH}$ = 7.5 Hz, $^{4}J_{HP}$ = 1.3 Hz, H_4)

^{31}P{^{1}H} NMR (CD_2Cl_2, 202 MHz, 295 K): -143.0 (sept, $^{1}J_{PF}$ = 711 Hz, PF_6^-), 50.4 (s, PPh_3)

ESI-MS (*m/z*): Observed 597.1823 [M^+], Expected $C_{33}H_{20}D_{10}N_2P^{102}Ru$ 597.1821, Error = 0.2 mDa; Observed 554.1356 [M^+ -NC_5H_5 +NCMe], Expected $C_{30}H_{23}D_5N_2P^{102}Ru$ 554.1337, Error = 1.9 mDa; Observed 513.1056 [M^+ -NC_5H_5], Expected $C_{28}H_{20}D_5NP^{102}Ru$ 513.1071, Error = 1.5 mDa.

Elemental Analysis: Anal. $C_{33}H_{20}D_{10}F_6N_2P_2Ru$ + 1.0 CH_2Cl_2: Calc. C(49.40) H(5.12) N(3.39), Found C(49.78) H(3.89) N(3.52)

9.3.10 Synthesis of complex $[Ru(\eta^5\text{-}C_5H_5)(PPh_3)(4\text{-methylpyridine})_2][PF_6]$, $\mathbf{10^{Me}}$.

To a solution of $[Ru(\eta^5\text{-}C_5H_5)(PPh_3)(NCMe)_2][PF_6]$, $\mathbf{9^{Ph}}$ (250 mg, 0.38 mmol) in dichloromethane (10 mL), 4-methylpyridine (1.85 mL, 19 mmol, 50 equiv) was added and the reaction mixture stirred (6 hours). Slow diffusion of pentane in to the reaction mixture afforded orange crystals suitable for X-ray diffraction. The solvent was removed by filtration and the air-sensitive product dried under vacuum. Yield (177 mg, 61 %)

Characterisation Data

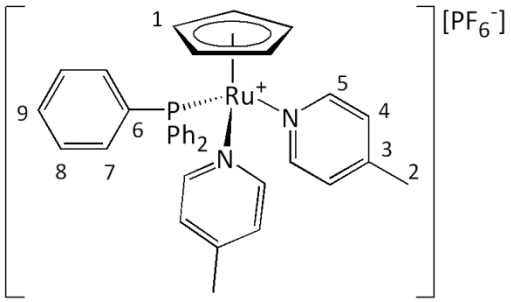

Figure 9.19: Labelled diagram of $\mathbf{10^{Me}}$.

^{1}H NMR (500 MHz, 295 K, CD_2Cl_2): 2.32 (s, 6H, H_2), 4.36 (s, 5H, H_1), 6.86 (d, 4H, $^3J_{HH}$ = 6.3 Hz, H_4), 7.18 (t, 6H, $^3J_{HH}$, $^3J_{HP}$ = 8.9Hz, H_7), 7.33 (td, 6H, $^3J_{HH}$ = 7.6 Hz, $^4J_{HP}$ = 1.6 Hz, H_8), 7.43 (td, 3H, $^3J_{HH}$ = 7.3 Hz, $^5J_{HP}$ = 1.3 Hz, H_9), 8.10 (d, 4H, $^3J_{HH}$ = 6.4 Hz, H_5)

^{31}P{^{1}H} NMR (202 MHz, 295 K, CD_2Cl_2): -143.0 (sept, 711 Hz, PF_6^-), 50.4 (s, PPh_3)

^{13}C{^{1}H} NMR (125 MHz, 295 K, CD_2Cl_2): 20.9 (s, C_2), 77.9 (d, $^2J_{CP}$ = 1.9 Hz, C_1), 126.5 (s, C_4), 128.9 (d, $^3J_{CP}$ = 9.6 Hz, C_8), 130.6 (d, $^4J_{CP}$ = 1.7 Hz, C_9), 133.7 (d, $^2J_{CP}$ = 10.6 Hz, C_7), 134.5 (d, $^1J_{CP}$ = 38.9 Hz, C_6), 149.7 (s, C_3), 156.0 (d, $^3J_{CP}$ = 2.0 Hz, C_5)

ESI-MS (*m/z*): Observed 615.1503 [M^+], Expected $C_{35}H_{34}N_2P^{102}Ru$ 615.1498, Error = 0.5 mDa; Observed 563.1187 [M^+ -NC_6H_7 +NCMe], Expected $C_{31}H_{30}N_2P^{102}Ru$ 563.1185, Error = 0.2 mDa; Observed 522.0929 [M^+ -NC_6H_7], Expected $C_{29}H_{27}NP^{102}Ru$ 522.0919, Error = 1.0 mDa.

Elemental Analysis: Anal. $C_{35}H_{34}F_6N_2P_2Ru$ + 0.25 CH_2Cl_2: Calc. C(54.22) H(4.45) N(3.59), Found C(54.45) H(4.10) N(3.39)

9.3.11 Synthesis of $[Ru(\eta^5\text{-}C_5H_5)(PPh_3)(DMAP)_2][PF_6]$, $\mathbf{10^{NMe2}}$.

To a solution of $[Ru(\eta^5\text{-}C_5H_5)(PPh_3)(NCMe)_2][PF_6]$, $\mathbf{9^{Ph}}$ (40 mg, 61 µmol) in dichloromethane (10 mL), 4-(dimethylamino)pyridine (15 mg, 122 µmol) was added to the yellow solution and the reaction mixture was stirred (48 hours). The excess solvent was removed under vacuum, and the yellow product collected. Excess 4-(dimethylamino)pyridine was removed by washing with toluene (5 mL), and then washed with pentane (2 x 15 mL), and the product dried under vacuum. Crystals suitable for X-ray diffraction were grown by slow diffusion of pentane into a layer of dichloromethane containing the product. Yield (35 mg, 70%)

Characterisation Data

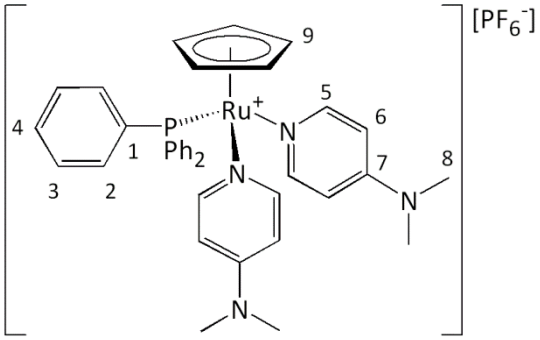

Figure 9.20: Labelled diagram of $\mathbf{10^{NMe2}}$.

^{1}H NMR (CD_2Cl_2, 500 MHz, 295 K): 2.96 (s, 12H, H_8), 4.25 (s, 5H, H_9), 6.16-6.17 (m, 4H, H_6), 7.20-7.24 (m, 6H, H_2), 7.32 (td, 6H, $^3J_{HH}$ = 7.3 Hz, $^4J_{HP}$ = 1.6 Hz, H_3), 7.39-7.41 (m, 3H, H_4), 7.73 (m, 4H, H_5)

^{31}P{^{1}H} NMR (CD_2Cl_2, 202 MHz, 295 K): -143.0 (sept, $^1J_{PF}$ = 711 Hz, PF_6^-), 51.4 (s, PPh_3)

^{13}C{^{1}H} NMR (125 MHz, 295 K, CD_2Cl_2): 39.2 (s, C_8), 77.0 (d, $^2J_{CP}$ = 2.6 Hz, C_9), 107.8 (s, C_6), 128.7 (d, $^3J_{CP}$ = 9.2 Hz, C_3), 130.2 (d, $^4J_{CP}$ = 1.7 Hz, C_4), 133.8 (d, $^2J_{CP}$ = 10.7 Hz, C_2), 135.5 (d, $^1J_{CP}$ = 37.5 Hz, C_1), 154.0 (s, C_7), 155.3 (d, $^3J_{CP}$ = 1.7 Hz, C_5)

ESI-MS (*m/z*): Observed 673.2031 [M^+], Expected $C_{37}H_{40}N_4P^{102}Ru$ 673.2029, Error = 0.2 mDa; Observed 592.1460 [M^+ -DMAP + NCMe], Expected $C_{32}H_{33}N_3P^{102}Ru$ 592.1450, Error = 1.0 mDa; Observed 551.1205 [M^+ -DMAP], Expected $C_{30}H_{30}N_2P^{102}Ru$ 551.1185, Error = 2.0 mDa.

ATR IR (ν /cm^{-1}): 610.4 (s), 695.2 (m), 737.7 (w), 749.2 (w), 810.0 (m), 837.0 (s), 950.8 (w), 1014.4 (w), 1062.6 (w), 1090.6 (w), 1182.2 (w), 1225.6 (w), 1384.7 (w), 1433.8 (w), 1479.2 (w), 1530.3 (m), 1619.0 (m), 2906.2 (w), 3066.3 (w)

Elemental Analysis: Anal. $C_{37}H_{40}F_6N_4P_2Ru$ + 1 CH_2Cl_2: Calc. C(50.56) H(4.69) N(6.21), Found C(50.29) H(4.63) N(6.47)

9.3.12 Synthesis of $[Ru(\eta^5\text{-}C_5H_5)(PPh_3)(3\text{-methylpyridine})_2][PF_6]$, 11.

To a solution of $[Ru(\eta^5\text{-}C_5H_5)(PPh_3)(NCMe)_2][PF_6]$, **9^{Ph}** (103 mg, 0.15 mmol) in dichloromethane (5 mL), 3-methylpyridine (1.5 mL, 15 mmol, 100 equiv) was added and the reaction mixture stirred (16 hours). Slow diffusion of pentane in to the reaction mixture afforded orange crystals, suitable for X-ray diffraction. The solvent was removed by filtration and the air-sensitive product dried under vacuum. Yield (80 mg, 67 %)

Characterisation Data

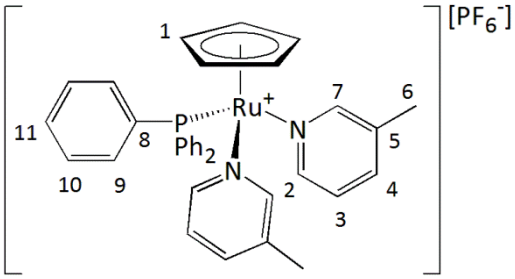

Figure 9.21: Labelled diagram of **11**.

^{1}H NMR (CD_2Cl_2, 500 MHz, 295 K): 2.00 (s, 6H, H_6), 4.40 (s, 5H, H_1), 7.01 (dd, 2H, $^3J_{HH}$ = 7.6 Hz, $^3J_{HH}$ = 5.6 Hz, H_3), 7.18 (m, 6H, H_9), 7.34 (m, 6H, H_{10}), 7.43 (m, 3H, H_{11}), 7.49 (d, 2H, $^3J_{HH}$ = 7.7 Hz, H_4), 7.93 (s, 2H, H_7), 8.28 (d, 2H, $^3J_{HH}$ = 5.6 Hz, H_2)

^{31}P{^{1}H} NMR (CD_2Cl_2, 202 MHz, 295 K): -144.4 (sept, $^1J_{PF}$ = 711 Hz, PF_6^-), 49.1 (s, PPh_3)

^{13}C{^{1}H} NMR (125 MHz, 295 K, CD_2Cl_2): 18.4 (s, C_6), 78.1 (d, $^2J_{CP}$ = 1.9 Hz, C_1), 124.9 (s, C_3), 129.0 (d, $^3J_{CP}$ = 9.3 Hz, C_{10}), 130.7 (d, $^4J_{CP}$ = 1.7 Hz, C_{11}), 133.6 (d, $^2J_{CP}$ = 10.6 Hz, C_9), 134.2 (d, $^1J_{CP}$ = 38.9 Hz, C_8), 135.8 (s, C_5), 138.0 (s, C_4), 154.1 (d, $^3J_{CP}$ = 1.9 Hz, C_7), 156.7 (d, $^3J_{CP}$ = 2.4 Hz, C_2)

ESI-MS (*m/z*): Observed 615.1493 [M^+], Expected $C_{35}H_{34}N_2P^{102}Ru$ 615.1507, Error = 1.4 mDa; Observed 563.1177 [M^+ -NC_6H_7 +NCMe], Expected $C_{31}H_{30}N_2P^{102}Ru$ 563.1185, Error = 0.8 mDa; Observed 522.0916 [M^+ -NC_6H_7], Expected $C_{29}H_{27}NP^{102}Ru$ 522.0919, Error = 0.3 mDa.

ATR IR (ν /cm^{-1}): 699.1 (s), 748.3 (m), 757.9 (m), 803.2 (m), 837.0 (s), 1088.6 (w), 1184.1 (w), 1238.1 (w), 1436.7 (w), 1479.2 (w), 1581.4 (w), 2933.2 (w), 2962.1 (w)

Elemental Analysis: Anal $C_{35}H_{34}F_6N_2P_2Ru$ + 0.5 CH_2Cl_2: Calc. C(53.10) H(4.40) N(3.49), Found C(52.90) H(4.50) N(3.39)

9.3.13 Synthesis of [Ru(η^5-C_5H_5)(PPh_3)(NCMe)(2-methylpyridine)][PF_6], 12.

To a solution of [Ru(η^5-C_5H_5)(PPh_3)$(NCMe)_2$][PF_6], **9^{Ph}** (53 mg, 0.08 mmol) in dichloromethane (5 mL), 2-methylpyridine (0.75 mL, 7.6 mmol, 95 equiv) was added and the reaction mixture stirred (16 hours). The solvent was reduced, and an excess of pentane added (20 mL). The solvent was removed *via* filtration and the precipitate was dried under vacuum. The reaction mixture contained three ruthenium containing species. Crystals of **12** were suitable for X-ray diffraction and were grown by slow diffusion of pentane into a layer of dichloromethane containing **12**.

Characterisation Data

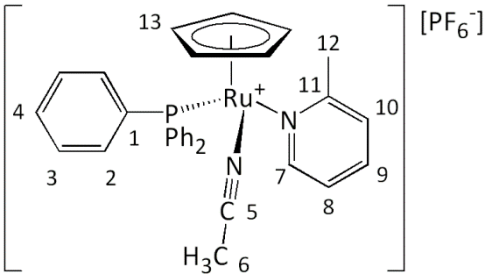

Figure 9.22: Labelled diagram of **12**.

^{1}H NMR (CD_2Cl_2, 500 MHz, 295 K): 1.86 (d, 3H, $^5J_{HP}$ = 1.5 Hz, H_6), 2.54 (broad, 3H, H_{12}), 4.46 (s, 5H, H_{13}), 6.83 (broad, 1H, H_8), 7.02-7.14 (m, 14H, PPh_3, H_{10} + impurity), 7.30-7.38 (m, 11.6H, PPh_3 + impurity), 7.41-7.47 (m, 7.5H, PPh_3 + impurity), 7.54 (td, 1H, $^3J_{HH}$ = 7.6 Hz, $^4J_{HH}$ = 1.5 Hz, H_9), 8.81 (d, 1H, $^3J_{HH}$ = 4.7 Hz, H_7).

Other peaks not belonging to **9^{Ph}**: 2.06 (d, $^5J_{HP}$ = 1.5 Hz), 7.02-7.14 (m), 7.30-7.38 (m), 7.41-7.47 (m), 7.61 (m), 8.45 (m)

^{31}P{^{1}H} NMR (CD_2Cl_2, 202 MHz, 295 K): -143.0 (sept, $^1J_{PF}$ = 711 Hz, PF_6^-), , 52.3 (broad).

Other peaks not belonging to **9^{Ph}**: 54.3 (s)

ESI-MS (*m/z*): Observed 549.1048 [Ru(η^5-C_5H_5)(PPh_3)(NCMe)(NC_5H_5)]$^+$, Expected $C_{30}H_{28}N_2P^{102}Ru$ 549.1028, Error = 2.0 mDa; Observed 508.0778 [Ru(η^5-C_5H_5)(PPh_3)(NC_5H_5)]$^+$, Expected $C_{28}H_{25}NP^{102}Ru$ 508.0763, Error = 1.5 mDa; Observed 470.0616 [Ru(η^5-C_5H_5)(PPh_3)(NCMe)]$^+$, Expected $C_{25}H_{23}NP^{102}Ru$ 470.0612, Error = 0.4 mDa; Observed 429.0351 [Ru(η^5-C_5H_5)(PPh_3)]$^+$, Expected $C_{23}H_{20}P^{102}Ru$ 429.0346, Error = 0.5 mDa.

An impurity present in the 2-methylpyridine lead to the formation of [Ru(η^5-C_5H_5)(PPh_3)($C_{12}H_{21}N_2$)][PF_6], which has been identified using X-ray crystallography.

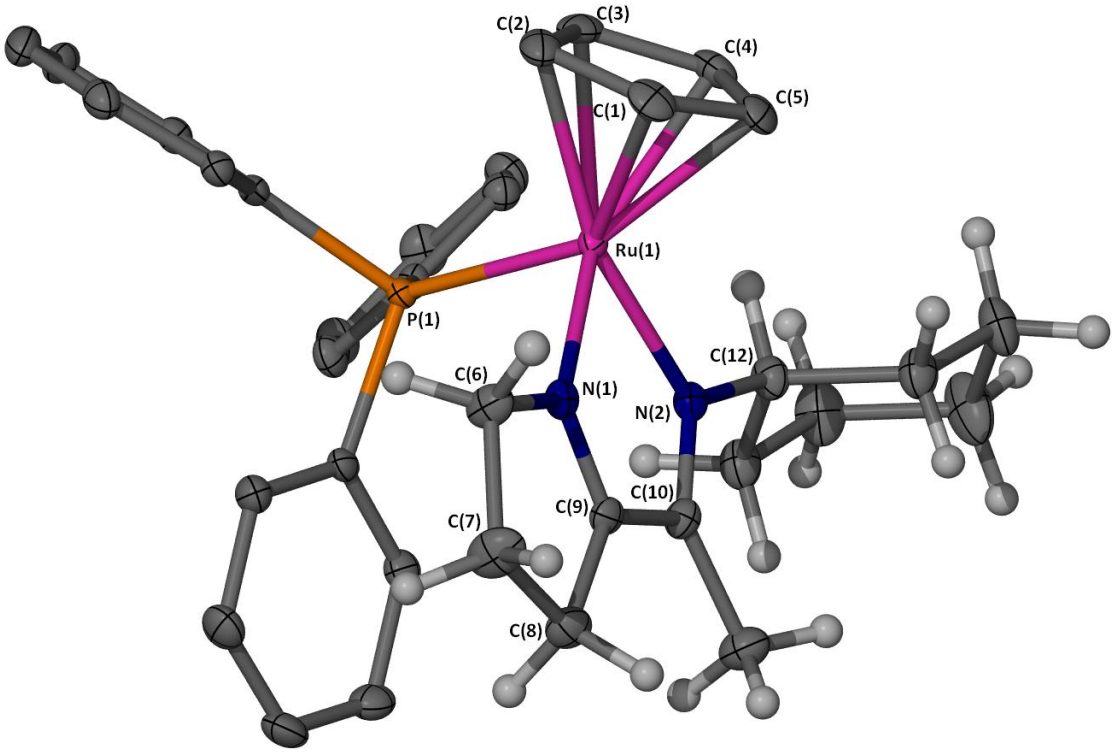

Figure 9.23: X-Seed diagram of the cation [Ru(η^5-C_5H_5)(PPh_3)($C_{12}H_{21}N_2$)]$^+$. Selected hydrogen atoms and [PF_6]$^-$ anion have been omitted for clarity, and where shown the thermal ellipsoids are at a 50 % probability level. The [PF_6]$^-$ anion was disordered over two positions.

9.3.14 Synthesis of $[Ru(\eta^5\text{-}C_5H_5)(PPh_3)(1\text{-methylimidazole})_2][PF_6]$, $\mathbf{13^{Me}}$.

To a solution of $[Ru(\eta^5\text{-}C_5H_5)(PPh_3)(NCMe)_2][PF_6]$, $\mathbf{9^{Ph}}$ (199 mg, 0.30 mmol) in dichloromethane (5 mL), 1-methylimidazole (2.5 mL, 31.3 mmol, 105 equiv) was added and the reaction mixture stirred (16 hours). Slow diffusion of pentane in to the reaction mixture afforded orange crystals of the product. The solvent was removed by filtration and the air-sensitive product dried under vacuum. Yield (141 mg, 63 %).

Characterisation Data

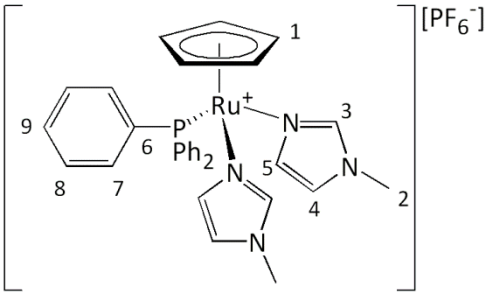

Figure 9.24: Labelled diagram of $\mathbf{13^{Me}}$.

^{1}H NMR (CD_2Cl_2, 500 MHz, 295 K): 3.49 (s, 6H, H_2), 4.26 (s, 5H, H_1), 6.79-6.82 (m, 6H, H_3, H_4, H_5), 7.19 (m, 6H, H_7), 7.33 (m, 6H, H_8), 7.41 (m, 3H, H_9)

^{31}P{^{1}H} NMR (CD_2Cl_2, 202 MHz, 295 K): -144.4 (sept, $^1J_{PF}$ = 711 Hz, PF_6^-), 51.4 (s, PPh_3)

^{13}C{^{1}H} NMR (125 MHz, 295 K, CD_2Cl_2): 34.6 (s, C_2), 75.9 (d, $^2J_{CP}$ = 2.4 Hz, C_1), 121.6 (s, $C_{3/4/5}$), 128.6 (d, $^3J_{CP}$ = 9.9 Hz, C_8), 130.2 (s, $C_{3/4/5}$), 133.8 (d, $^2J_{CP}$ = 11.0 Hz, C_7), 134.7 (s, $C_{3/4/5}$), 135.9 (d, $^1J_{CP}$ = 37.1 Hz, C_6), 142.2 (d, $^4J_{CP}$ = 2.0 Hz, C_9)

ESI-MS (*m/z*): Observed 593.1423 [M^+], Expected $C_{31}H_{32}N_4P^{102}Ru$ 593.1411, Error = 1.2 mDa; Observed 511.0900 [M^+ - (2 $N_2C_4H_6$) + (2 $NCCH_3$)], Expected $C_{27}H_{26}N_2P^{102}Ru$ 511.0879, Error = 1.1 mDa.

ATR IR (ν /cm^{-1}): 697.2 (s), 734.8 (m), 754.1 (w), 759 (w), 818.7 (s), 835.1 (s), 847.6 (s), 1090.6 (m), 1168.7 (w), 1235.3 (w), 1260.4 (w), 1284.5 (w), 1421.4 (w), 1433.0 (w), 1479.3 (w), 1535.2 (w), 1580.5 (w), 3159.2 (broad)

Elemental Analysis: Anal $C_{31}H_{32}F_6N_4P_2Ru$ + 0.14 CH_2Cl_2: Calc. C(49.90) H(4.34) N(7.48), Found C(49.77) H(4.27) N(7.66)

9.3.15 Synthesis of $[Ru(\eta^5\text{-}C_5H_5)(PPh_3)(\text{t-butylimidazole})_2][PF_6]$, $\mathbf{13^{tBu}}$.

To a solution of $[Ru(\eta^5\text{-}C_5H_5)(PPh_3)(NCMe)_2][PF_6]$, $\mathbf{9^{Ph}}$ (48 mg, 73 μmol) in dichloromethane (5 mL), t-butylimidazole (0.91 mg, 7.3 mmol, 100 equiv) was added and the reaction mixture stirred (16 hours). Slow diffusion of pentane in to the reaction mixture afforded orange crystals suitable for X-ray diffraction. The solvent was removed by filtration and the air-sensitive product dried under vacuum. Yield (22 mg, 37 %)

Characterisation Data

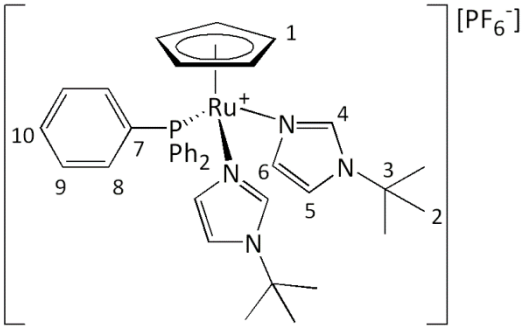

Figure 9.25: Labelled diagram of $\mathbf{13^{tBu}}$.

^{1}H NMR (CD_2Cl_2, 500 MHz, 295 K): 1.28 (s, 18H, H_2), 4.29 (s, 5H, H_1), 6.91 (t, 2H, $^XJ_{HH}$ = 1.3 Hz, imidazole), 6.95 (t, 2H, J_{HH} = 1.3 Hz, imidazole), 7.00 (t, 2H, J_{HH} = 1.4 Hz, imidazole), 7.11 (m, 6H, H_8), 7.33 (m, 6H, H_9), 7.42 (m, 3H, H_{10})

^{31}P{^{1}H} NMR (CD_2Cl_2, 202 MHz, 295 K): -144.5 (sept, $^1J_{PF}$ = 711 Hz, PF_6^-), 51.8 (s, PPh_3)

^{13}C{^{1}H} NMR (125 MHz, 295 K, CD_2Cl_2): 30.1 (s, C_2), 56.6 (s, C_3), 75.9 (d, $^2J_{CP}$ = 2.2 Hz, C_1), 118.0 (s, imidazole), 128.8 (d, $^3J_{CP}$ = 9.4 Hz, C_9), 130.3 (d, $^4J_{CP}$ = 1.8 Hz, C_{10}), 133.7 (d, $^2J_{CP}$ = 11.1 Hz, C_8), 134.5 (s, imidazole), 136.0 (d, $^1J_{CP}$ = 37.1 Hz, C_7), 139.1 (d, $^xJ_{CH}$ = 2.6 Hz, imidazole)

ESI-MS (*m/z*): Observed 677.2334 [M^+], Expected $C_{37}H_{44}N_4P^{102}Ru$ 677.2351, Error = 1.7 mDa.

ATR IR (ν /cm^{-1}): 611.3 (s), 647.0 (m), 663.4 (m), 702.0 (s), 737.7 (m), 754.1 (m), 814.8 (s), 822 (s), 1006.7 (w), 1091.5 (m), 1237.1 (m), 1271.8 (w), 1376.0 (w), 1433.8 (w), 1467.6 (w), 1480.1 (w), 1503.3 (w), 1625.7 (broad), 2980.8 (w), 3407.0 (broad)

Elemental Analysis: Anal. $C_{37}H_{44}F_6N_4P_2Ru$ + 0.25 CH_2Cl_2: Calc. C(53.07) H(5.32) N(6.65), Found C(52.33) H(5.39) N(6.57)

9.3.16 Synthesis of $[Ru(\eta^5\text{-}C_5H_5)(PMe_3)(NC_5H_5)_2][PF_6]$, $\mathbf{14^H}$.

To a solution of $[Ru(\eta^5\text{-}C_5H_5)(PMe_3)(NCMe)_2][PF_6]$, $\mathbf{9^{Me}}$ (108 mg, 0.23 mmol) in dichloromethane (5 mL), pyridine (1.8 mL, 22 mmol, 97 equiv) was added and the reaction mixture stirred (3 hours). Slow diffusion of pentane in to the reaction mixture afforded orange crystals, suitable for X-ray crystallography. The solvent was removed by filtration and the air-sensitive product dried under vacuum. Yield (83 mg, 66 %).

Characterisation Data

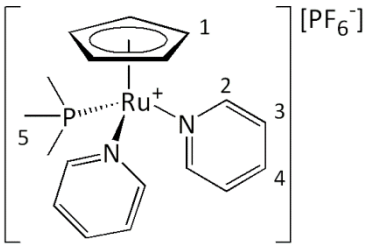

Figure 9.26: Labelled diagram of $\mathbf{14^H}$.

^{1}H NMR (CD_2Cl_2, 500 MHz, 295 K): 1.40 (d, 9H, $^2J_{HP}$ = 26.3 Hz, H_5), 4.39 (s, 5H, H_1), 7.28 (m, 4H, H_3), 7.81 (tt, 2H, $^3J_{HH}$ = 7.6 Hz, $^4J_{HH}$ = 1.5 Hz, H_4), 8.41 (m, 4H, H_2)

^{31}P{^{1}H} NMR (CD_2Cl_2, 202 MHz, 295 K): -144.4 (sept, $^1J_{PF}$ = 710 Hz, PF_6^-), 3.1 (s, PMe_3)

^{13}C{^{1}H} NMR (125 MHz, 295 K, CD_2Cl_2): 17.9 (d, $^1J_{CP}$ = 26.3 Hz, C_5), 76.0 (d, $^2J_{CP}$ = 2.3 Hz, C_1), 126.0 (s, C_3), 137.4 (s, C_4), 156.7 (d, $^3J_{CP}$ = 2.8 Hz, C_2)

ESI-MS (*m/z*): Observed 401.0717 [M^+], Expected $C_{18}H_{24}N_2P^{102}Ru$ 401.0720, Error = 0.3 mDa; Observed 363.0568 [M^+ -NC_5H_5 +NCMe], Expected $C_{15}H_{22}N_2P^{102}Ru$ 363.0559, Error = 0.9 mDa; Observed 322.0336, Expected $C_{13}H_{19}NP^{102}Ru$ 322.0293, Error = 4.3 mDa.

ATR IR (ν /cm^{-1}): 700.1 (s), 757.9 (s), 824.4 (s), 837.9 (s), 879.4 (w), 953.7 (w), 1025.0 (w), 1060.7 (w), 1100.2 (w), 1214.0 (w), 1261.2 (w), 1285.3 (w), 1351.9 (w), 1427.1 (w), 1445.4 (w), 1483.0 (w), 2359.5 (w), 2966.0 (w)

Elemental Analysis: Anal. $C_{18}H_{24}F_6N_2P_2Ru$: Calc. C(39.64) H(4.44) N(5.14), Found C(39.53) H(4.32) N(5.02)

9.3.17 Synthesis of $[Ru(\eta^5\text{-}C_5H_5)(PMe_3)(DMAP)_2][PF_6]$, $\mathbf{14^{NMe2}}$.

To a solution of $[Ru(\eta^5\text{-}C_5H_5)(PMe_3)(NCMe)_2][PF_6]$, $\mathbf{9^{Me}}$ (103 mg, 0.22 mmol) in dichloromethane (10 mL), 4-dimethylaminopyridine (53 mg, 0.43 mmol, 2 equiv) was added and the reaction mixture stirred (16 hours). The solvent was reduced under vacuum (5 mL) and excess of pentane (20 mL) added to the reaction mixture to yield a dark yellow precipitate. The product was washed with pentane (10 mL) and the air-sensitive product dried under vacuum. Slow diffusion of pentane in to a solution of the product in dichloromethane mixture afforded orange crystals, which were suitable for X-ray crystallography. Yield (81 mg, 59 %).

Characterisation Data

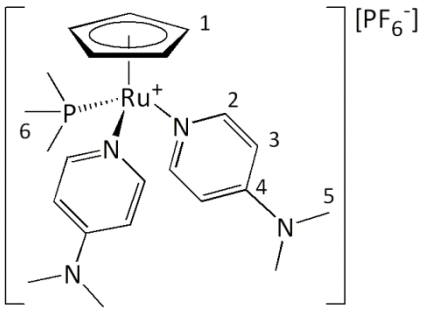

Figure 9.27: Labelled diagram of $\mathbf{14^{NMe2}}$.

^{1}H NMR (CD_2Cl_2, 500 MHz, 295 K): 1.35 (d, 9H, $^2J_{HP}$ = 8.1 Hz, H_6), 3.01 (s, 12H, H_5), 4.24 (s, 5H, H_1), 6.38 (d, 4H, $^3J_{HH}$ = 6.6 Hz, H_3), 7.83 (d, 4H, $^3J_{HH}$ = 6.6 Hz, H_2)

^{31}P{^{1}H} NMR (CD_2Cl_2, 202 MHz, 295 K): -144.4 (sept, $^1J_{PF}$ = 710 Hz, PF_6^-), 4.75 (s, PMe_3)

^{13}C{^{1}H} NMR (125 MHz, 295 K, CD_2Cl_2): 18.4 (d, $^1J_{CP}$ = 24.6 Hz, C_6), 39.3 (s, C_5), 74.5 (d, $^2J_{CP}$ = 2.5 Hz, C_1), 108.1 (s, C_3), 154.1 (s, C_4), 155.4 (d, $^3J_{CP}$ = 2.4 Hz, C_2)

ESI-MS (*m/z*): Observed 487.1571 [M^+], Expected $C_{22}H_{34}N_4P^{102}Ru$ 487.1565, Error = 0.6 mDa; Observed 406.0975 [M^+ -$N_2C_7H_{10}$ +NCMe], Expected $C_{17}H_{27}N_3P^{102}Ru$ 406.0981, Error = 0.6 mDa; Observed 365.0723 [M^+ -$N_2C_7H_{10}$], Expected $C_{15}H_{24}N_2P^{102}Ru$ 365.0715, Error = 0.8 mDa.

Elemental Analysis: Anal. $C_{22}H_{34}F_6N_4P_2Ru$: Calc. C(41.84) H(5.43) N(8.86), Found C(41.81) H(5.45) N(8.52)

9.3.18 Synthesis of $[Ru(\eta^5\text{-}C_5H_5)(P^iPr_3)(NCMe)(NC_5H_5)][PF_6]$, 15.

$[Ru(\eta^5\text{-}C_5H_5)(P^iPr_3)(NCMe)_2][PF_6]$, **9^{iPr}** (120 mg, 0.22 mmol) was placed in dichloromethane (5 mL). Pyridine (0.91 mL, 11.5 mmol, 50 equiv) was added to give an orange reaction mixture which was stirred (16 hours). The solvent was removed under vacuum. The reaction gave a mixture of products. The slow diffusion of pentane into a dichloromethane layer containing a mixture of ruthenium complexes afforded crystals of **15** suitable for X-ray diffraction.

Characterisation Data

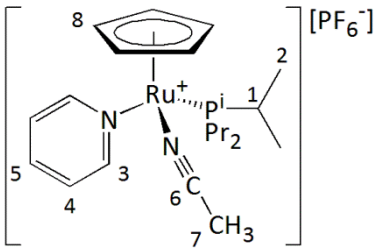

Figure 9.28: Labelled diagram of **15**.

^{1}H NMR (CD_2Cl_2, 500 MHz, 295 K): 1.09-1.17 (m, 18H, H_2), 2.24 (sept, 3H, $^3J_{HH}$ = 7.3 Hz, H_1), 2.54 (d, 3H, $^5J_{HP}$ = 1.2 Hz, H_7), 4.51 (s, 5H, H_8), 7.27-7.30 (m, 2H, H_4), 7.75 (tt, 1H, H_5), 8.70-8.72 (m, 2H, H_3)

Other ^{1}H NMR signals: 1.15, 1.38, 2.31, 4.15, 4.17, 4.43, 7.33, 7.67, 7.84, 8.48

^{31}P{^{1}H} NMR (CD_2Cl_2, 202 MHz, 295 K): -143.0 (sept, $^1J_{PF}$ = 711 Hz, PF_6^-), 52.8 (s, P^iPr_3)

Other ^{31}P{^{1}H} NMR signals: 43.8, 45.8, 50.7

ESI-MS (*m/z*): Observed 447.1492 [M^+], Expected $C_{21}H_{34}N_2P^{102}Ru$ 447.1503, Error = 1.1 mDa; Observed 406.1228 [M^+ - NCMe], Expected $C_{19}H_{31}NP^{102}Ru$ 406.1232, Error = 0.4 mDa; Observed 368.1053 [M^+ - NC_5H_5], Expected $C_{16}H_{29}NP^{102}Ru$ 406.1232, Error = 2.3 mDa; Observed 325.0284 $[Ru(\eta^5\text{-}C_5H_5)(NC_5H_5)_2]^+$, Expected $C_{15}H_{15}N_2{}^{102}Ru$ 325.0273, Error = 1.2 mDa.

9.3.19 Preparation for $[Ru(\eta^5\text{-}C_5H_5)(P(OPh)_3)(NC_5H_5)_2][PF_6]$, 16.

$[Ru(\eta^5\text{-}C_5H_5)(P(OPh)_3)(NCMe)_2][PF_6]$, **9^{OPh}** (56 mg, 79.5 µmol) was placed in dichloromethane (10 mL). Pyridine (0.16 mL, 2.0 mmol, 25 equiv) was added and the reaction mixture stirred (16 hours). The solvent was removed under vacuum. Slow diffusion of pentane in to a layer of dichloromethane containing the product yielded crystals suitable for X-ray crystallography. Yield (46 mg, 74 %).

Characterisation Data

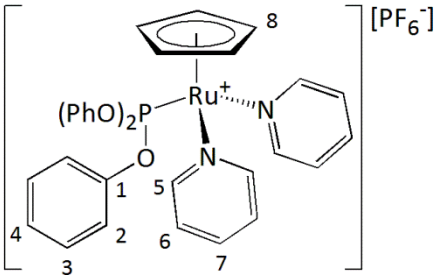

Figure 9.29: Labelled diagram of **16**.

^{1}H NMR (CD_2Cl_2, 500 MHz, 295 K): 4.39 (s, 5H, H_8), 7.03 (d, 6H, $^3J_{HH}$ = 8.2 Hz, H_2), 7.21 (t, 4H, $^3J_{HH}$ = 7.4 Hz, H_6), 7.28-7.32 (m, 9H, H_3 H_4), 7.86 (t, 2H, $^3J_{HH}$ = 7.6 Hz, H_7), 8.41 (d, 4H, $^3J_{HH}$ = 5.2 Hz, H_5)

^{31}P{^{1}H} NMR (CD_2Cl_2, 202 MHz, 295 K): -143.0 (sept, $^1J_{PF}$ = 711 Hz, PF_6^-), 140.6 (s, $P(OPh)_3$)

^{13}C{^{1}H} NMR (CD_2Cl_2, 125 MHz, 295 K): 80.1 (d, $^2J_{CP}$ = 3.2 Hz, C_8), 121.2 (d, $^3J_{CP}$ = 4.4 Hz, C_2), 125.6 (s, C_6), 126.2 (s, $C_{3/4}$), 130.3 (s, $C_{3/4}$), 138.3 (s, C_7), 151.5 (d, $^2J_{CP}$ = 9.1 Hz, C_1), 157.4 (d, $^3J_{CP}$ = 2.1 Hz, C_5)

ESI-MS (*m/z*): Observed 635.1041 [M^+], Expected $C_{33}H_{30}N_2O_3P^{102}Ru$ 635.1041, Error = 0.1 mDa; Observed 597.0871 [M^+ -NC_5H_5 +NCMe], Expected $C_{30}H_{28}N_2O_3P^{102}Ru$ 597.0876, Error = 0.5 mDa; Observed 556.0623 [M^+ -NC_5H_5], Expected $C_{28}H_{25}NO_3P^{102}Ru$ 556.0610, Error = 1.3 mDa.

ATR IR (ν /cm^{-1}): 694.3 (m), 756.0 (m), 779.4 (m), 780.1 (m), ~800 (s), 877.5 (m), 905.4 (m), 1024.0 (w), 1071.3 (w), 1095.4 (w), 1162.9 (w), 1188.0 (m), 1215.0 (w), 1261.2 (w), 1445.4 (w), 1485.9 (m), 1588.1 (w), 2967.0 (broad w)

Elemental Analysis: Anal. $C_{33}H_{30}F_6N_2O_3P_2Ru$ + 0.15 CH_2Cl_2: Calc. C(50.15) H(3.85) N(3.54), Found C(49.82) H(3.82) N(3.25)

9.4 Synthesis of Half Sandwich Ruthenium Complexes of the Type [Ru(η^5-C_5H_5)(PR_3)(2-Styrylpyridine)]

9.4.1 Synthesis of [Ru(η^5-C_5H_5)(PPh_3)(2-styrylpyridine)][PF_6], 17^H.

In a Schlenk 2-styrylpyridine (14 mg, 0.07 mmol) and [Ru(η^5-C_5H_5)(PPh_3)(NCMe)][PF_6], $\mathbf{9^{Ph}}$ (46 mg, 0.07 mmol) were added. Dichloromethane (5 mL) was added under nitrogen, and the reaction mixture stirred (1 hour). The solvent was removed under vacuum, and the reaction mixture re-dissolved in dichloromethane (5 mL). This process was repeated 4-5 times, in order to drive the reaction to completion. Crystals suitable for X-ray diffraction were grown by the slow diffusion of pentane in to a dichloromethane solution containing the complex [Ru(η^5-C_5H_5)(PPh_3)($NC_{13}H_{11}$)][PF_6]. Yield (35 mg, 66 %).

Characterisation Data

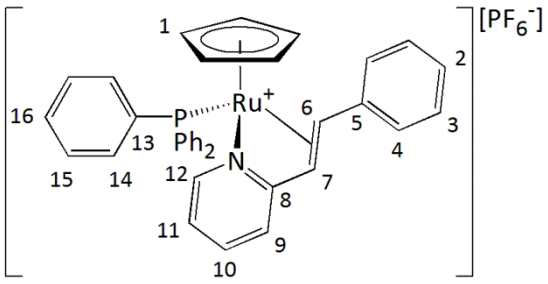

Figure 9.30: Labelled diagram of $\mathbf{17^H}$.

^{1}H NMR (CD_2Cl_2, 500 MHz, 295 K): 4.73 (broad s, 5H), 5.97 (broad s, 1H), 6.87 (broad m, 3H), 7.07 (broad m, 5H), 7.23 (m, 3H), 7.38 (m, 5H), 7.51 (broad m, 3H), 7.68 (broad m, 2H)

^{31}P{^{1}H} NMR (CD_2Cl_2, 202 MHz, 295 K): -143.0 (sept, $^1J_{PF}$ = 711 Hz, PF_6^-), 47.7 (broad s, PPh_3)

^{13}C{^{1}H} NMR (CD_2Cl_2, 125 MHz, 295 K): 51.1 (broad, $C_{6/7}$), 79.4 (broad, $C_{6/7}$), 84.5 (s, C_1), 122.8 (s), 125.0 (s), 125.9 (s), 128.1 (s), 129.2 (s), 129.4 (d, J_{CP} = 9.8 Hz, $C_{14/15}$), 131.5 (s, $^4J_{CP}$ = 2.1 Hz, C_{16}), 132.6 (d, $^1J_{CP}$ = 42.6 Hz, C_{13}), 133.8 (broad d, J_{CP} = 7.9 Hz, $C_{14/15}$), 138.0 (s), 139.9 (s), 152.4 (s), 164.1 (s, C_8)

ESI-MS (*m/z*): Observed 610.1316 [M^+], Expected $C_{36}H_{31}NP^{102}Ru$ 610.1242, Error = 0.7 mDa; Observed 511.0880 [M^+ - $C_{13}H_{11}N$ + 2 NCMe] Expected $C_{27}H_{26}N_2P^{102}Ru$ 511.0879, Error = 0.1 mDa; Observed: 470.0618 [M^+ - $C_{13}H_{11}N$ + $NCCH_3$], Expected

$C_{25}H_{23}NP^{102}Ru$ 470.0613, Error = 0.5 mDa; Observed 182.0891 [$C_{13}H_{11}N$ +H^+], Expected $C_{13}H_{12}N$ 182.0964, Error = 0.7 mDa.

Elemental Analysis: Anal. $C_{36}H_{31}F_6NP_2Ru$ + 0.2 CH_2Cl_2: Calc. C(56.58) H(4.11) N(1.83), Found C(56.55) H(4.06) N(1.76)

220 K

Chenical Shift, δ_H	**Multiplicity**	**Integration**	**Isomer**	**Assignment**
4.28	Apparent t ($^3J_{HH}$, $^3J_{HP}$ = 11.1 Hz)	1 H	Major	H_7
4.33	s	1 H	Minor	H_1
4.67	Apparent t ($^3J_{HH}$ =$^3J_{HP}$ = *ca*. 9 Hz)	0.2 H	Minor	H_6/H_7
4.75	s	5H	Major	H_1
5.84	d (7.3 Hz)	0.2 H	Minor	
6.08	d ($^3J_{HH}$ = 10.6 Hz)	1 H	Major	H_6
6.45	d ($^3J_{HH}$ = 10.2 Hz)	0.2 H	Minor	H_6/H_7
6.51	t ($^3J_{HH}$ = 8.7 Hz)	2 H	Major	H_4
6.73	d (6.8 Hz)	2 H	Major	PPh_3
6.83	dd (9.5 Hz)	2 H	Major	PPh_3
6.96	d (7.8 Hz)	1 H	Major	H_9/H_{12}
7.01-7.07	multiplet	1.2 H	Major + Minor	H_{10}/H_{11}
7.09	d (7.3 Hz)	0.2 H	Minor	
7.15	multiplet	3.2 H	Major + Major	PPh_3
7.23	multiplet	5.2 H	Major	H_3+ phenyl
7.33	multiplet	1.5 H	Minor + Minor	PPh_3
7.43	multiplet	6.2 H		
7.51-7.63	multiplet	5.4 H	Major	H_9/H_{12}
7.74	t ($^3J_{HH}$ = 7.7 Hz)	1 H	Major	H_{10}/H_{11}
8.25	d ($^3J_{HH}$ = 4.7 Hz)	0.2 H	Minor	H_9/H_{12}

$^{31}P\{^1H\}$ NMR (CD_2Cl_2, 202 MHz, 220 K): -143.0 (sept, $^1J_{PF}$ = 711 Hz, PF_6^-), 47.2 (s, major species, PPh_3), 55.0 (s, minor species, PPh_3)

9.4.2 Synthesis of [Ru(η^5-C_5H_5)(PPh_3)(*E*-2-(4-(trifluoromethyl)styrylpyridine))][PF_6].

[Ru(η^5-C_5H_5)(PPh_3)($NCMe)_2$][PF_6], **9^{Ph}** (50 mg, 0.07 mmol) was placed in dichloromethane (3 mL). *E*-2-(4-trifluoromethyl)styrylpyridine (27 mg, 0.1 mmol) was added to the reaction mixture under nitrogen and stirred (1-2 hours). The solvent was removed under vacuum, and re-dissolved in dichloromethane (5 mL). This cycle was repeated 4-5 times, and then washed with pentane. The yellow-green reaction mixture was placed in dichloromethane, and slow diffusion of pentane in to this solution obtained crystals suitable for X-ray diffraction. Yield (26 mg, 41 %).

Characterisation Data

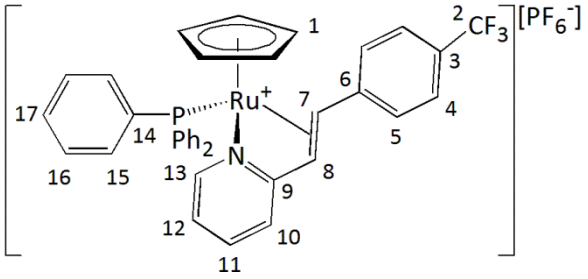

Figure 9.31: Labelled diagram of **17^{CF3}**.

^{1}H NMR (CD_2Cl_2, 500 MHz, 295 K): 4.50 (broad s, 1H), 4.82 (s, 5H), 6.12 (broad s, 1H), 6.89 (broad d, 3H), 6.98 (broad s, 4H), 7.08 (m, 2H), 7.39 (broad s, 6H), 7.44 (broad d, 3H), 7.53 (broad t, 4 H), 7.58 (broad s, 1H), 7.74 (broad t, 1H)

^{31}P{^{1}H} NMR (CD_2Cl_2, 202 MHz, 295 K): -143.0 (sept, $^1J_{PF}$ = 711 Hz, PF_6^-), 46.7 (PPh_3)

^{13}C{^{1}H} NMR (CD_2Cl_2, 125 MHz, 295 K): 75.2 (broad alkene), 85.1 (s, C_1), 122.8 (s, CH pyridine), 124.6 (q, $^1J_{CF}$ = 271 Hz, C_2), 125.2 (s, CH pyridine), 126.0 (s, C_5), 126.1 (q, $^3J_{CF}$ = 3 Hz, C_4), 128.8 (broad alkene), 129.0 (q, $^2J_{CF}$ = 32 Hz, C_3), 129.5 (d, J_{CP} = 9.5 Hz, $C_{15/16}$), 131.7 (s, C_{17}), 132.3 (broad m, C_{14}), 133.7 (broad s, $C_{15/16}$), 138.4 (s, CH pyridine), 144.7 (s, C_6), 152.4 (s, CH pyridine), 164.1 (s, C_9)

ESI-MS (*m/z*): Observed 678.1118 [M^+], Expected $C_{37}H_{30}NF_3P^{102}Ru$ 678.1116, Error = 0.2 mDa

Elemental Analysis: Anal. $C_{37}H_{30}F_9NP_2Ru$ + 1 CH_2Cl_2: Calc. C(50.29) H(3.55) N(1.54), Found C(50.80) H(3.59) N(1.65)

220 K

Chemical Shift, δ_H	Multiplicity	Integration	Isomer	Assignment
4.25	t ($^3J_{HH}$, $^3J_{HP}$ =11.1 Hz)	1 H	Major	H_7
4.39	s	0.46 H	Minor	H_1
4.67	t	0.09 H	Minor	H_7/H_8
4.80	s	5 H	Major	H_1
5.86	d	0.07	Minor???	
6.12	d ($^3J_{HH}$ = 10.5 Hz)	1 H	Major	H_8
6.36	d	0.09	Minor	H_7/H_8
6.55	t	2 H	Major	PPh_3
6.78	m	4 H	Major + Major	H_5 + PPh_3
7.02	d	1 H	Major	H_{11}/H_{12}
7.05	m	H	Major + Minor	H_{11}/H_{12}
7.12	m	0.2 H	Minor	
7.24	m	4.6 H	Major + Major	PPh_3
7.35-7.48	m	6.80 H	Major	H_4 + PPh_3
7.49	d	1.17 H	Major	H_{10}/H_{13}
7.54-7.70	m	3.62 H	Major	PPh_3
7.75	t	1 H	Major	H_{10}/H_{13}
8.25	d	0.07 H	Minor	

$^{31}P\{^1H\}$ NMR (CD_2Cl_2, 202 MHz, 220 K): -143.0 (sept, $^1J_{PF}$ = 711 Hz, PF_6^-), 46.9(s, major species, PPh_3), 54.6 (s, minor species, PPh_3)

9.4.3 Synthesis of [Ru(η^5-C_5H_5)(PMe_3)(2-styrylpyridine)][PF_6].

[Ru(η^5-C_5H_5)(PMe_3)(NCMe)][PF_6], **9^{Me}** (95 mg, 0.20 mmol) and 2-styrylpyridine (48 mg, 0.26 mmol) were added to a Schlenk. Dichloromethane (5 mL) was added under nitrogen, and the reaction mixture stirred (30 mins). The solvent was removed under vacuum, and the reaction mixture re-dissolved in dichloromethane (15 mL). This process was repeated 4-5 times, in order to drive the reaction to completion. Crystals suitable for X-ray diffraction were grown by the slow diffusion of pentane in to a dichloromethane solution containing the complex [Ru(η^5-C_5H_5)(PMe_3)($NC_{13}H_{11}$)][PF_6]. Yield (69 mg, 60 %).

Characterisation Data

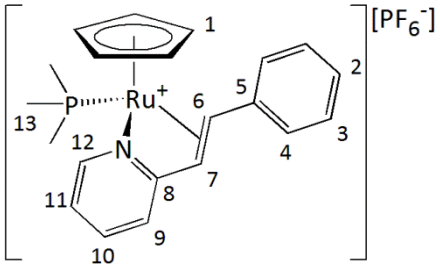

Figure 9.32: Labelled diagram of **18**.

^{1}H NMR (CD_2Cl_2, 500 MHz, 295 K): 1.63 (d, 9H, $^2J_{HP}$ = 9.6 Hz, H_{13}), 4.22 (broad, 1H, H_{alkene}), 4.84 (s, 5H, H_1), 5.77 (d, 1H, $^3J_{HH}$ = 8.5 Hz, H_{alkene}), 6.98 (d, $^3J_{HH}$ = 7.9 Hz, H_9), 7.16-7.23 (m, 4H, H_2 + H_4 + H_{11}), 7.26 (m, 2H, H_3), 7.74 (td, 1H, $^3J_{HH}$ = 7.9 Hz, $^4J_{HH}$ = 1.5 Hz, H_{10}), 7.88 (d, 1H, $^3J_{HH}$ = 5.3 Hz, H_{12})

^{31}P{^{1}H} NMR (CD_2Cl_2, 202 MHz, 295 K): -143.0 (sept, $^1J_{PF}$ = 710 Hz, PF_6^-), 11.2(s, PMe_3)

^{13}C{^{1}H} NMR (CD_2Cl_2, 125 MHz, 295 K): 18.2 (d, $^1J_{CP}$ = 32.1 Hz, C_{13}), 44.7 (broad, C_{alkene}), 71.1 (broad, C_{alkene}), 83.91 (s, C_1), 122.0 (s, C_9), 125.1 (s, C_{11}), 126.0 (s, C_4), 127.4 (s, C_2), 129.3 (s, C_3), 138.0 (s, C_{10}), 141.4 (s, C_5), 152.7 (d, $^3J_{CP}$ = 1.3 Hz, C_{12}), 165.0 (s, C_8)

ESI-MS (*m/z*): Observed 424.0765 [M^+], Expected $C_{21}H_{25}NP^{102}Ru$ 424.0768, Error = 0.4 mDa; Observed 325.0417 [M^+ - $C_{14}H_{10}F_3N$], Expected $C_{12}H_{20}N_2P^{102}Ru$ 325.0405, Error = 1.2 mDa.

Elemental Analysis: Anal. $C_{21}H_{25}F_6NP_2Ru$ + 0.15 CH_2Cl_2: Calc. C(43.17) H(4.39) N(2.41), Found C(43.79) H(4.37) N(2.38)

^{1}H NMR (CD_2Cl_2, 500 MHz, 215 K): 1.57 (d, 9H, $^{2}J_{HP}$ = 9.7 Hz, H_{13}), 3.95 (dd, 1H, $^{3}J_{HH}$ = 9.5 Hz, $^{3}J_{HP}$ = 13.0 Hz, H_{alkene}), 4.83 (s, 5H, H_1), 5.73 (d, 1H, $^{3}J_{HH}$ = 9.5 Hz, H_{alkene}), 6.92 (d, 1H, $^{3}J_{HH}$ = 7.8 Hz, H_9), 7.12-7.18 (m, 4H, H_2 + H_4 + H_{11}), 7.22 (m, 2H, H_3), 7.70 (td, 1H, $^{3}J_{HH}$ = 7.9 Hz, $^{4}J_{HH}$ = 1.1 Hz, H_{10}), 7.81 (d, 1H, $^{3}J_{HH}$ = 5.2 Hz, H_{12})

^{31}P{^{1}H} NMR (CD_2Cl_2, 202 MHz, 215 K): -143.2 (sept, $^{1}J_{PF}$ = 710 Hz, PF_6^-), 13.8 (s, PMe_3)

9.5 General experimental procedure for NMR scale reactions

9.5.1 Stoichiometric addition of alkyne to a ruthenium complex

The ruthenium complex (0.027 mmol) was placed in d_2-dichloromethane (0.55 mL). Under a nitrogen atmosphere a stoichiometric quantity of the alkyne (0.027 mmol) was added. The reaction was monitored *via* NMR spectroscopy.

9.5.2 Stoichiometric reaction in the presence of two equivalents of pyridine

The ruthenium complex, **10^{H}** (0.026 mmol) was placed in d_2-dichloromethane (0.55 mL). Pyridine (0.055 mmol) was added to the reaction mixture and allowed to stand for 5 minutes. Under a nitrogen atmosphere a stoichiometric quantity of the alkyne (0.026 mmol) was added. The reaction was monitored *via* NMR spectroscopy.

9.5.3 Stoichiometric reaction in the presence of two equivalents of 4-methyl pyridine

The ruthenium complex, **10^{Me}** (0.026 mmol) was placed in d_2-dichloromethane (0.55 mL). 4-Methylpyridine (0.055 mmol) was added to the reaction mixture and allowed to stand for 5 minutes. Under a nitrogen atmosphere a stoichiometric quantity of the alkyne (0.026 mmol) was added. The reaction was monitored *via* NMR spectroscopy.

9.5.4 Stoichiometric reaction in the presence of two equivalents of 3-methyl pyridine

The ruthenium complex, **11** (0.026 mmol) was placed in d_2-dichloromethane (0.55 mL). 3-Methylpyridine (0.055 mmol) was added to the reaction mixture and allowed to stand for 5 minutes. Under a nitrogen atmosphere a stoichiometric quantity of the alkyne (0.026 mmol) was added. The reaction was monitored *via* NMR spectroscopy.

9.6 Short-Lived Half-Sandwich Ruthenium Vinylidene Intermediate Complexes 19 and 28

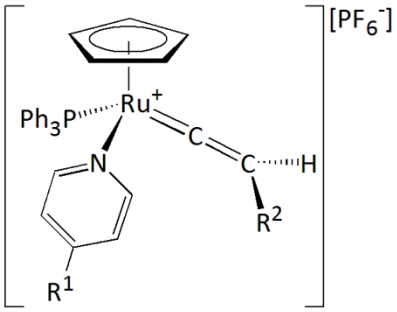

Figure 9.33: Labelled diagram of complexes $\mathbf{19^{R1,R2}}$.

9.6.1 Complex $19^{H,Ph}$.

^{1}H NMR (CD_2Cl_2, 500 MHz, 295 K): 5.14 (broad s, 1H, vinylidene proton), 5.48 (s, 5H, η^5-C_5H_5), 6.97 (m, 2H, *meta* pyridine), 7.55 (t, 1H, $^{3}J_{HH}$ = 7.6 Hz, *para* pyridine), 8.39 (d, 2H, $^{3}J_{HH}$ = 6.5 Hz, *ortho* pyridine)

^{31}P{^{1}H} NMR (CD_2Cl_2, 202 MHz, 295 K): -143.0 (sept, $^{1}J_{PF}$ = 711 Hz, PF_6^-), 51.8 (s, PPh_3)

9.6.2 Complex ^{13}C-$19^{H,Ph}$.

^{1}H NMR (CD_2Cl_2, 500 MHz, 295 K): 5.14 (broad s, 1H, vinylidene proton), 5.49 (s, 5H, η^5-C_5H_5), 6.97 (m, 2H, *meta* pyridine), 7.55 (t, 1H, $^{3}J_{HH}$ = 7.5 Hz, *para* pyridine), 8.38 (d, 2H, $^{3}J_{HH}$ = 6.3 Hz, *ortho* pyridine)

^{31}P{^{1}H} NMR (CD_2Cl_2, 202 MHz, 295 K): -143.0 (sept, $^{1}J_{PF}$ = 711 Hz, PF_6^-), 51.8 (d, $^{2}J_{CP}$ = 16.9 Hz, PPh_3)

^{13}C{^{1}H} NMR (CD_2Cl_2, 125 MHz, 295 K): 355.3 (d, $^{2}J_{CP}$ = 16.9 Hz, α-^{13}C)

9.6.3 Complex $19^{H,C6H4-4-F}$.

^{1}H NMR (CD_2Cl_2, 500 MHz, 295 K): 5.14 (broad singlet, 1H, vinylidene proton), 5.49 (s, 5H, η^5-C_5H_5), 6.96 (lies underneath other peaks), 7.57 (t, 1H, *para* pyridine), 8.35 (d, 2H, *ortho* pyridine)

^{31}P{^{1}H} NMR (CD_2Cl_2, 202 MHz, 295 K): -143.0 (sept, $^{1}J_{PF}$ = 711 Hz, PF_6^-), 51.7 (broad s, PPh_3)

9.6.4 Complex $19^{H, C6H4-4-CF3}$.

^{1}H NMR (CD_2Cl_2, 500 MHz, 295 K): 5.17 (broad singlet, 1H, vinylidene proton), 5.53 (s, 5H, η^5-C_5H_5), 6.99 (t, 2H, *meta* pyridine), 7.57 (lies under other peaks, *para* pyridine), 8.36 (d, 2H, *ortho* pyridine)

^{31}P{^{1}H} NMR (CD_2Cl_2, 202 MHz, 295 K): -143.0 (sept, $^{1}J_{PF}$ = 711 Hz, PF_6^-), 51.0 (broad s, PPh_3)

9.6.5 Complex $19^{H,tBu}$.

^{1}H NMR (CD_2Cl_2, 500 MHz, 295 K): 1.17 (s, 9H, 3x C*H*$_3$), 3.97 (d, 1H, , $^{4}J_{HP}$ = 3.0 Hz, vinylidene proton), 5.31 (s, η^5-C_5H_5), 6.99 (m, 2H, *meta* pyridine), 7.23 (m ,6H, *ortho* phenyl of PPh_3), 7.40 (m ,6H, *meta* phenyl of PPh_3), 7.49 (m, 3H, *para* phenyl of PPh_3), 7.58 (m, 1H, *para* pyridine), 8.45 (m, 2H, *ortho* pyridine)

^{31}P{^{1}H} NMR (CD_2Cl_2, 202 MHz, 295 K): -143.0 (sept, $^{1}J_{PF}$ = 711 Hz, PF_6^-), 53.5 (broad s, PPh_3)

9.6.6 Complex $19^{Me,Ph}$.

^{1}H NMR (CD_2Cl_2, 500 MHz, 295 K): 2.23 (s, 3H, CH_3), 5.13 (broad, vinylidene proton), 5.46 (s, 5H, η^5-C_5H_5), 6.77 (d, 2H, $^{3}J_{HH}$ = 6.2 Hz, *meta* 4-methylpyridine), 7.05 (d, 2H, $^{3}J_{HH}$ = 7.9 Hz, vinylidene ligand phenyl ring), 8.17 (d, 2H, $^{3}J_{HH}$ = 6.2 Hz, *ortho* 4-methylpyridine)

^{31}P{^{1}H} NMR (CD_2Cl_2, 202 MHz, 295 K): -143.0 (sept, $^{1}J_{PF}$ = 711 Hz, PF_6^-), 51.9 (broad s, PPh_3)

9.6.7 Complex $19^{Me,C6H4-4-CF3}$.

^{1}H NMR (CD_2Cl_2, 500 MHz, 295 K): 2.25 (s, 3H, CH_3), 5.14 (broad, 1H, vinylidene proton), 5.51 (s, 5H, η^5-C_5H_5), 6.79 (d, 2H, $^{3}J_{HH}$ = 6.0 Hz, *meta* 4-methylpyridine), 8.14 (d, 2H, $^{3}J_{HH}$ = 6.0 Hz, *ortho* 4-methylpyridine)

^{31}P{^{1}H} NMR (CD_2Cl_2, 202 MHz, 295 K): -143.0 (sept, $^{1}J_{PF}$ = 711 Hz, PF_6^-), 51.1 (broad s, PPh_3)

There is limited evidence for complexes **28**, characterisation data has been obtained from reaction mixture spectra.

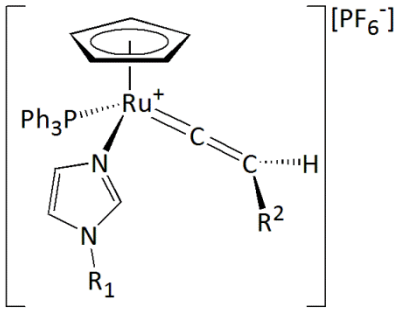

Figure 9.34: Labelled diagram of complexes **28^{R1,R2}**.

9.6.8 Complex 28^{Me,H}.

^{1}H NMR (CD_2Cl_2, 500 MHz, 295 K): 3.39 (s, 3H, CH_3), 5.09 (broad, 1H, vinylidene proton), 5.43 (broad, 5H, η^5-C_5H_5), 6.61 (s, 1H, imidazole), 6.64 (s, 1H, imidazole)

^{31}P{^{1}H} NMR (CD_2Cl_2, 202 MHz, 295 K): -143.0 (sept, $^{1}J_{PF}$ = 711 Hz, PF_6^-), 53.0 (broad s, PPh_3)

9.6.9 Complex 28^{Me,CF3}.

^{1}H NMR (CD_2Cl_2, 500 MHz, 295 K): 3.42 (s, 3H, CH_3), 5.11 (broad, 1H, vinylidene proton), 5.47 (broad, 5H, η^5-C_5H_5), 6.60 (s, 1H, imidazole), 6.63 (s, 1H, imidazole)

^{31}P{^{1}H} NMR (CD_2Cl_2, 202 MHz, 295 K): -143.0 (sept, $^{1}J_{PF}$ = 711 Hz, PF_6^-), 52.1 (broad s, PPh_3)

9.6.10 Complex 28^{tBu,CF3}.

^{1}H NMR (CD_2Cl_2, 500 MHz, 295 K): 1.17 (s, 3H, ^{t}Bu), 5.14 (broad, 1H, vinylidene proton), 5.48 (broad, 5H, η^5-C_5H_5), 6.76 (s, 1H, imidazole), 6.84 (s, 1H, imidazole)

^{31}P{^{1}H} NMR (CD_2Cl_2, 202 MHz, 295 K): -143.0 (sept, $^{1}J_{PF}$ = 711 Hz, PF_6^-), 52.5 (broad s, PPh_3)

9.7 Synthesis of Ruthenium C-H Functionalised Complexes

9.7.1 Reaction of 10^{H} with phenylacetylene.

$[Ru(\eta^5\text{-}C_5H_5)(PPh_3)(NC_5H_5)_2][PF_6]$, **$10^{H}$** (75 mg, 0.1 mmol) was added to an oven-dried Young's ampule. Dichloromethane (3 mL), and pyridine (17 µL, 0.21 mmol) were added and the reaction mixture stirred for 15 minutes. Phenylacetylene (11 µL, 0.1 mmol) was added to the reaction mixture and heated at 50 °C for 15 hours.

The reaction mixture was allowed to cool to room temperature, and the solvent removed under vacuum. The reaction mixture was washed with pentane (10 mL). Slow diffusion of pentane in to dichloromethane containing the reaction mixture afforded a mixture of pale yellow crystals (**$22^{H,H}$**) and orange crystals (**$21^{H,H}$**), where a ratio for **$22^{H,H}$: $21^{H,H}$** of 6:1 was observed. The solvent was removed by filtration and the air-sensitive products dried under vacuum. The relevant crystals of complex **$22^{H,H}$** were picked from the crystallisation. The compound could be purified further *via* further crystallisations.

Alternatively, isolation of complex **$21^{H,H}$** could be achieved *via* the addition of DABCO to the crude reaction mixture containing complexes **$21^{H,H}$** and **$22^{H,H}$**. The reaction mixture was left to stir (16 hours) and then reduced to dryness. Extraction using a mixture of dichloromethane (1 mL) and pentane (10 mL) afforded an orange/ brown precipitate of **$21^{H,H}$**, which could be further purified by slow diffusion of pentane into a dichloromethane solution of the complex **$21^{H,H}$**. The filtrate contained the complex **$23^{H,H}$**, which was reduced in volume (~2 mL) and stored at -20 °C to obtain pure crystals of **$23^{H,H}$**.

Yields for these complexes were not obtained due to purification difficulties.

Characterisation Data of $21^{H,H}$

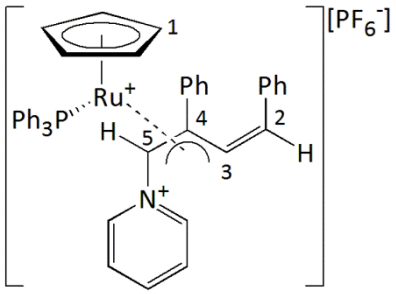

Figure 9.35: Labelled diagram of complex $\mathbf{21^{H,H}}$.

^{1}H NMR (CD_2Cl_2, 500 MHz, 295 K): 4.55 (s, 5H, H_1), 6.51-8.19 (broad peaks in baseline), 7.27-7.35 (m), 7.56 (t, *J* = 7.9Hz), 7.63 (d,*J* = 7.9Hz), 7.82 (s), 7.93-7.98 (m).

^{31}P{^{1}H} NMR (CD_2Cl_2, 202 MHz, 295 K): -143.0 (sept, $^{1}J_{PF}$ = 711 Hz, PF_6^-), 48.1 (s, PPh_3)

^{13}C{^{1}H} NMR (CD_2Cl_2, 125 MHz, 295 K): 47.8 (d, $^{2}J_{CP}$ = 2.1 Hz, C_X),67.1 (d, $^{2}J_{CP}$ = 7.7 Hz, C_5), 89.1 (s, C_1), 126.5, 127.6 (d, J_{CP} = 3.1 Hz, C_4), 128.0-139.5 (br), 128.3 (s), 128.6 (s), 128.6 (s), 128.7 (s), 128.9 (s), 128.9 (s), 129.1 (s), 129.2 (s), 129.2 (s), 129.3 (s), 129.4 (s), 129.8 (s), 130.0 (s), 130.7 (s), 131.2-133.0 (br), 133.2-134.4 (br), 137.0-138.3 (br), 139.8 (d, J_{CP} = 1.9 Hz), 141.0 (s), 142.3 (d, J_{CP} = 1.4 Hz),170.8 (d,$^{2}J_{CP}$ = 12.9 Hz, C_3)

ESI-MS (*m/z*): Observed 712.1714 [M^+], Expected for $C_{44}H_{37}NP^{102}Ru$ 712.1713, Error = 0.0 mDa

Characterisation Data of $22^{H,H}$

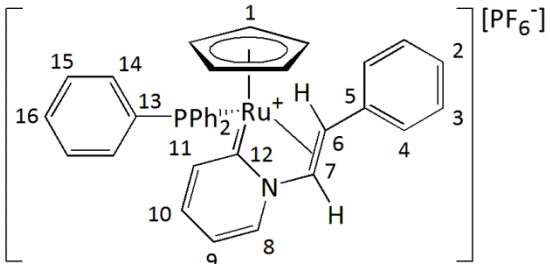

Figure 9.36: Labelled diagram of complex $\mathbf{22^{H,H}}$.

^{1}H NMR (CD_2Cl_2, 500 MHz, 295 K): 3.65 (apparent t, 1H, $^{3}J_{HH}$, $^{3}J_{HP}$ = 9.5 Hz, H_6), 4.95 (s, 5H, H_1), 6.63 (d, 1H, $^{3}J_{HH}$ = 7.8 Hz, H_7), 6.83 (m, 2H, H_3), 7.06 (t, 2H, $^{3}J_{HH}$ = 7.0 Hz, H_9), 7.15 (d, $^{3}J_{HH}$= 8.0 Hz, H_{11}), 7.21 (m, 3H, H_2, H_4), 7.36 (broad, H_{10}, PPh_3), 7.49 (broad, PPh_3), 7.94 (d, 2H, $^{3}J_{HH}$ = 5.7 Hz, H_8)

^{31}P{^{1}H} NMR (CD_2Cl_2, 202 MHz, 295 K): -143.0 (sept, $^{1}J_{PF}$ = 711 Hz, PF_6^-), 53.5 (s, PPh_3)

^{13}C{^{1}H} NMR (CD_2Cl_2, 125 MHz, 295 K): 55.2 (s, C_{alkene}), 69.4 (s, C_{alkene}), 88.5 (s, C_1), 118.5 (C_9), 125.3(s, C_3), 127.3 (s, C_2), 129.2 (s, C_4), 129.1-129.5 (broad, PPh_3), 131.4 (broad, PPh_3), 132.3-134.8 (broad, PPh_3), 136.6 (s, C_{10}), 137.5 (d, $^{3}J_{CP}$ = 2.8 Hz, C_{11}), 140.7 (s, C_5), 143.1 (s, C_8), 180.7 (broad, C_{12})

ESI-MS (*m/z*): Observed: 610.1276 [M^+], Expected $C_{36}H_{31}NP^{102}Ru$ 610.1242, Error = 3.4 mDa; Observed 182.0965, Expected $C_{13}H_{12}N$ 182.0964, Error = 0.0.

Elemental Analysis: Anal. $C_{36}H_{31}F_6NP_2Ru$ + 1 CH_2Cl_2: Calc. C(52.93) H(3.96) N(1.67), Found C(53.05), H(3.94), N(1.76)

^{1}H NMR (CD_2Cl_2, 500 MHz, 225 K): 3.48 (dd, 1H, $^{2}J_{HP}$ = 11.7 Hz, $^{3}J_{HH}$ = 8.0 Hz, H_6), 4.91 (s, 5H, H_1), 6.30 (t, 2H, $^{3}J_{HH}$, $^{3}J_{HP}$ = 9.0 Hz, a-PPh_3 *ortho*), 6.55 (dd, 1H, $^{3}J_{HH}$ = 8.0 Hz, $^{2}J_{HP}$ = 1.2 Hz, H_7), 6.80 (2H, m, H_3), 7.04 (m, 3H, H_9, b-PPh_3 *ortho*), 7.10 (d, 1H, $^{3}J_{HH}$ = 8.3 Hz, H_{11}), 7.17 (m, 3H, H_2, H_4), 7.22 (td, 2H, $^{3}J_{HH}$ = 7.9 Hz, $^{3}J_{HP}$ = 2.6 Hz, a-PPh_3 *meta*), 7.26 (td, 2H, $^{3}J_{HH}$ = 7.8 Hz, $^{3}J_{HP}$ = 1.7 Hz, b-PPh_3 *meta*), 7.35-7.49 (m, *6H-should be 5H*, H_{10}, a-PPh_3 *para*, b-PPh_3 *para*, c-PPh_3 *ortho*), 7.53 (td, 2H, $^{3}J_{HH}$ = 7.4 Hz, $^{3}J_{HP}$ = 1.5 Hz, c-PPh_3 *meta*), 7.59 (t, 1H, $^{3}J_{HH}$ = 7.8 Hz, c-PPh_3 *para*), 7.92 (d, 1H, $^{3}J_{HH}$ = 6.2 Hz, H_8)

^{31}P{^{1}H} NMR (CD_2Cl_2, 202 MHz, 225 K): -143.2 (sept, $^{1}J_{PF}$ = 711 Hz, PF_6^-), 54.1 (s, PPh_3)

Characterisation Data of $23^{H,H}$

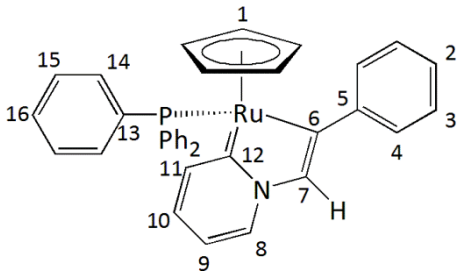

Figure 9.37: Labelled diagram of complex $\mathbf{23^{H,H}}$.

^{1}H NMR (CD_2Cl_2, 500 MHz, 295 K): 4.75 (s, 5H, H_1), 6.51 (td, 1H, $^{3}J_{HH}$ = 6.7 Hz, $^{4}J_{HH}$ = 1.5 Hz, H_9), 6.56 (td, 1H, $^{3}J_{HH}$ = 7.5 Hz, $^{4}J_{HH}$ = 1.1 Hz, H_{10}), 6.99-7.07 (m, 10H, H_2 + H_3 + H_7 + H_{14}), 7.07-7.15 (m, 8H, H_4 + H_{15}), 7.23 (m, 3H, H_{16}), 7.83 (d, 1H, $^{3}J_{HH}$ = 6.2 Hz, H_8), 8.15 (d, $^{3}J_{HH}$ = 7.9 Hz, H_{11})

^{31}P{^{1}H} NMR (CD_2Cl_2, 202 MHz, 295 K): 60.3 (broad s, PPh_3)

^{13}C{^{1}H} NMR (CD_2Cl_2, 125 MHz, 295 K): 83.0 (d, $^{2}J_{CP}$ = 1.8 Hz, C_1), 113.3 (s, C_9), 123.8 (s, C_{10}), 125.0 (s, C_2), 127.3 (d, $^{3}J_{CP}$ = 9.3 Hz, C_{15}), 127.4 (s, $C_{3/4}$), 127.5 (s, $C_{3/4}$), 128.7 (d, $^{4}J_{CP}$ = 2.3 Hz, C_{16}), 132.2 (broad, C_7), 133.5 (d, $^{2}J_{CP}$ = 11.1 Hz, C_{14}), 136.7 (s, C_{11}), 137.4 (broad d, $^{1}J_{CP}$ = 41.3 Hz, C_{13}), 142.8 (s, C_8), 153.0 (broad, C_5), 192.9 (d, $^{2}J_{CP}$ = 12.7 Hz, C_6), 218.3 (d, $^{2}J_{CP}$ = 15.3 Hz, C_{12})

ESI-MS (*m/z*): Observed 610.1228 [M + H^+], Expected $C_{36}H_{31}NP^{102}Ru$ 610.1242, Error = 0.5 mDa.

Elemental Analysis (obtained enough sample for 1 run): Anal. $C_{36}H_{30}NPRu$ + 0.15 CH_2Cl_2: Calc. C(69.87), H(4.91) N(2.25), Found C(69.50) H(5.12) N(2.14)

9.7.2 Reaction of 10^{H} with 4-ethynyl-α,α,α-trifluorobenzene

[Ru(η^5-C_5H_5)(PPh_3)(NC_5H_5)$_2$][PF_6], **10^{H}** (250 mg, 0.34 mmol) was added to a Youngs ampule, and dichloromethane (6.25 mL) added. Pyridine (56 µL, 0.69 mmol) was added, and the reaction mixture stirred for 5 minutes. 4-ethynyl-α,α,α-trifluorobenzene (56 µL, 0.34 mmol) was added to the reaction mixture, and the system sealed. The reaction mixture was heated to 50 °C for 15 hours.

The reaction mixture was allowed to cool, and the solvent removed under vacuum. The brown solid was washed with pentane (2 x10 mL). Slow diffusion of pentane in to the reaction mixture afforded pale yellow crystals. The solvent was removed by filtration and the air-sensitive product dried under vacuum. The compound could be purified further *via* further crystallisations. Yield (135 mg, 48 %)

Characterisation Data

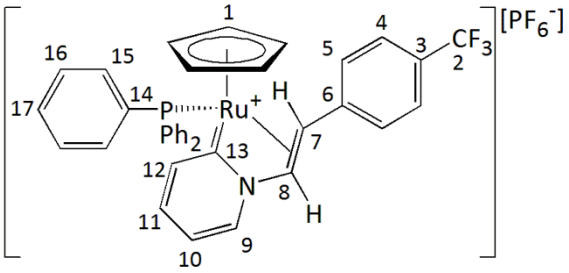

Figure 9.38: Labelled diagram of complex **$22^{H,CF3}$**.

^{1}H NMR (CD_2Cl_2, 500 MHz, 300 K): 3.60 (dd, 1H, $^3J_{HP}$ = 11.4 Hz, $^3J_{HH}$ = 7.9 Hz, H_7), 4.99 (s, 5H, H_1), 6.77 (d, 1H, $^3J_{HH}$ = 7.9 Hz, H_8), 6.92 (d, 2H, $^3J_{HH}$ = 8.2 Hz, H_5), 7.08 (t, $^3J_{HH}$ = 6.8 Hz, H_{10}), 7.12 (d, $^3J_{HH}$ = 7.9 Hz, H_{12}), 7.37 (td, $^3J_{HH}$ = 7.9 Hz, $^4J_{HH}$ = 1.2 Hz, H_{11}), 7.37 (broad, PPh_3), 7.44 (d, $^3J_{HH}$ = 8.2 Hz, H_4), 7.51 (broad, PPh_3), 8.00 (d, 1H, $^3J_{HH}$ = 6.1 Hz, H_9)

^{31}P{^{1}H} NMR (CD_2Cl_2, 202 MHz, 300 K): -143.0 (sept, $^1J_{PF}$ = 711 Hz, PF_6^-), 52.8 (s, PPh_3)

^{13}C{^{1}H} NMR (CD_2Cl_2, 125 MHz, 300 K): 54.8 (s, C_8), 66.6 (d, $^2J_{CP}$ = 3 Hz, C_7), 88.7 (s, C_1), 118.6 (s, C_{10}), 124.5 (q, $^1J_{CF}$ = 272 Hz, C_2), 125.5 (s, C_5), 126.0 (q, $^3J_{CF}$ = 4 Hz, C_4), 128.4 (q, $^2J_{CF}$ = 32 Hz, C_3), 129.3 (broad, PPh_3), 131.5 (broad, PPh_3), 133.6 (broad, PPh_3), 136.8 (s, C_{11}), 137.4 (d, $^3J_{CP}$ = 3 Hz, C_{12}), 143.2 (s, C_9), 145.5 (s, C_6), 179.6 (d, $^2J_{CP}$ = 19 Hz, C_{13})

ESI-MS (*m/z*): Observed 678.1135 [M^+], Expected $C_{37}H_{30}NF_3P^{102}Ru$ 678.1116, Error = 2.0 mDa, Observed 250.0832, Expected $C_{14}H_{11}F_3N$ 250.0838, Error = 0.6 mDa.

Elemental Analysis: Anal. $C_{37}H_{30}F_9NP_2Ru$ + 0.5 CH_2Cl_2: Calc. C(52.06) H(3.61) N(1.62), Found C(52.11) H(3.52) N(1.89)

^{1}H NMR (CD_2Cl_2, 500 MHz, 220 K): 3.43 (dd, 1H, $^3J_{HP}$ = 11.7 Hz, $^3J_{HH}$ = 7.9 Hz, H_7), 4.95 (s, 5H, H_1), 6.31(t, 2H, $^3J_{HH}$, $^3J_{HP}$ = 9.1 Hz, a-PPh_3 *ortho*), 6.68 (d, 1H, $^3J_{HH}$ = 7.9 Hz, H_8), 6.89 (d, 2H, $^3J_{HH}$ = 8.1 Hz, H_5), 6.99 (dd, 2H, $^3J_{HP}$ = 11.0 Hz, $^3J_{HH}$ = 7.9 Hz, b-PPh_3 *ortho*), 7.06 (m, 2H, H_{10}, H_{12}), 7.36 (m, H_{11}), 7.22 (t, 2H, $^3J_{HH}$ = 7.7 Hz, a-PPh_3 *meta*), 7.29 (t, 2H, $^3J_{HH}$ = 7.7 Hz, b-PPh_3 *meta*), 7.37 (m, 3H, a-PPh_3 *para*) & c-PPh_3 *ortho*), 7.42 (d, $^3J_{HH}$ = 8.1 Hz, H_4), 7.46 (t, 1H, $^3J_{HH}$ = 7.3 Hz, b-PPh_3 *para*), 7.54 (t, 2H, $^3J_{HH}$ = 7.2 Hz, c-PPh_3 *meta*), 7.60 (t, 1H, $^3J_{HH}$ = 7.2 Hz, c-PPh_3 *para*), 7.98 (d, 1H, $^3J_{HH}$ = 6.2 Hz, H_9)

^{31}P{^{1}H} NMR (CD_2Cl_2, 202 MHz, 220 K): -143.0 (sept, $^1J_{PF}$ = 711 Hz, PF_6^-), 53.6 (s, PPh_3)

9.7.3 Synthesis of $23^{H,CF3}$.

Complex $\mathbf{22^{H,CF3}}$ (31 mg, 0.037 mmol) and dichloromethane (5 mL) was added. 1,4-Diazabicyclo[2.2.2]octane (8 mg, 0.071 mmol) was added, and stirred at room temperature (15 hours). The reaction mixture solvent was removed under vacuum, and a red solution was extracted with pentane (2 x10 mL), and separated by filtration. The solvent was reduced (approximately 2 mL), and stored at -20 °C, where crystals suitable for X-ray diffraction were grown.

Note: Best to carry out reaction in a Youngs ampule to avoid grease in product, as product is soluble in pentane.

Characterisation Data

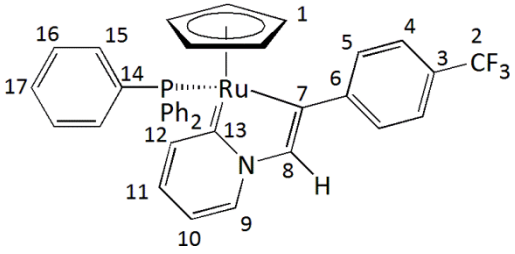

Figure 9.39: Labelled diagram of complex $\mathbf{23^{H,CF3}}$.

^{1}H NMR (700 MHz, 298 K, CD_2Cl_2): 4.73 (s, 5H, H_1), 6.52 (t, 1H, $^{3}J_{HH}$ = 6.7 Hz, H_{10}), 6.58 (t, 1H, $^{3}J_{HH}$ = 7.6 Hz, H_{11}), 6.93 (broad s, 1H, H_8), 7.03 (m, 6H, H_{15}), 7.13 (m, 8H, H_5, H_{16}), 7.24 (t, 3H, $^{3}J_{HH}$ = 7.2 Hz, H_{17}), 7.35 (d, 2H, $^{3}J_{HH}$ = 7.9 Hz, H_4), 7.84 (d, 1H, $^{3}J_{HH}$ = 6.4 Hz, H_{12}), 8.16 (d, 1H, $^{3}J_{HH}$ = 8.3 Hz, H_9)

^{31}P{^{1}H} NMR (202 MHz, 295 K, CD_2Cl_2): 61.2 (s, PPh_3)

^{13}C{^{1}H} NMR (176 MHz, 298 K, CD_2Cl_2): 83.3 (s, C_1), 113.6 (s, C_{10}), 124.2 (q, $^{3}J_{CF}$ = 3.7 Hz, C_4), 124.4 (s, C_{11}), 125.5 (q, $^{1}J_{CF}$ = 271 Hz, C_2), 126.4 (q, $^{2}J_{CF}$ = 31 Hz, C_3), 127.5 (d, $^{3}J_{CP}$ = 8 Hz, C_{16}), 127.6 (s, C_5), 128.9 (s, C_{17}), 133.5 (d, $^{2}J_{CP}$ = 10 Hz, C_{15}), 137.0 (s, C_{12}), 137.3 (broad d, approx 50 Hz, C_{14}), 142.9 (s,C_9), 157.9 (broad s, C_6), 190.2 (broad, C_7), 219.3 (broad, C_{13}) Unfortunately attempts to locate C_8 using a range of 2D-NMR techniques were unsuccessful.

ESI-MS (*m/z*): Observed 677.1035 [M^+], Expected $C_{37}H_{29}NF_3P^{102}Ru$ 677.1038, Error = 0.3 mDa.

Elemental Analysis: Anal. $C_{37}H_{29}F_3NP_2Ru$: Calc. C(65.67) H(4.32) N(2.07), Found C(65.42) H(4.41) N(2.07)

9.7.4 Reaction of 10^{Me} with phenylacetylene.

[Ru(η^5-C_5H_5)(PPh_3)(4-Me-NC_5H_4)$_2$][PF_6], **10^{Me}** (75 mg, 0.099 mmol) was added to a Youngs ampule, and dichloromethane (5 mL) added. 4-Methylpyridine (20 µL, 0.20 mmol, 2 equiv) was added, and the reaction mixture stirred for 5 minutes. Phenylacetylene (13 µL, 0.11 mmol) was added, and the system sealed. The reaction mixture was heated to 50 °C for 15 hours. An aliquot was taken of the reaction mixture in order to determine the % conversion to **$22^{Me,H}$**. A yield of approximately 85 % of **$22^{Me,H}$** was determined.

The reaction mixture was reduced to dryness, and re-dissolved in dichloromethane (5 mL). 1,4-Diazabicyclo[2.2.2]octane (10 mg, 0.08 mmol) was added to the reaction mixture and stirred (16 hours). The solvent was reduced (1 mL) under vacuum. Pentane (10 mL) was added to the reaction flask, and the red filtrate collected *via* filtration. The extraction was repeated twice, and the solvent removed to give **$23^{Me,H}$**.

Pyridinium hexafluorophosphate (20 mg, 0.09 mmol) added to **$23^{Me,H}$** in a dichloromethane solution (5 mL). The reaction solution turned from red to yellow. The filtrate was collected and reduced to give a yellow precipitate. Crystals suitable for X-ray diffraction were grown by slow diffusion of pentane into a dichloromethane solution containing **$22^{Me,H}$**.

Characterisation Data

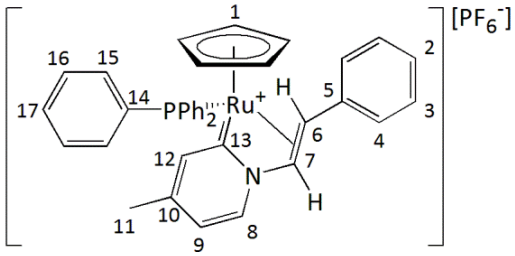

Figure 9.40: Labelled diagram of complex **$22^{Me,H}$**.

Only ^{1}H NMR spectrum and elemental analysis was pure, remaining characterisation was carried out on an impure sample.

^{1}H NMR (CD_2Cl_2, 500 MHz, 295 K): 2.13 (s, 3H, H_{11}), 3.68 (m, 1H, H_{alkene}), 4.92 (s, 5H, H_1), 6.47 (d, $^3J_{HH}$ = 7.8 Hz, H_{alkene}), 6.54-7.85 (broad peak, PPh_3) 6.76 (m, 2H, $H_{3/4}$), 6.84 (m, 2H, H_{12} + H_9), 7.19 (m, 3H, H_2 + $H_{3/4}$), 7.37 (broad, 6H, PPh_3), 7.50 (broad, 4H, PPh_3), 7.72 (d, 1H, $^3J_{HH}$ = 6.4 Hz, H_8)

$^{31}P\{^{1}H\}$ NMR (CD_2Cl_2, 202 MHz, 295 K): -143.0 (sept, $^{1}J_{PF}$ = 711 Hz, PF_6^-), 53.6 (s, PPh_3)

Other $^{31}P\{^{1}H\}$ NMR impurity signals: 29.9 (s, $OPPh_3$), 38.9 (s, impurity), 42.4 (s, impurity)

$^{13}C\{^{1}H\}$ NMR (CD_2Cl_2, 125 MHz, 295 K): 22.2 (s, C_{11}), 54.7 (broad, C_{alkene}), 68.6 (s, C_{alkene}), 88.3 (s, C_1), 120.1 (s, $C_{8/9}$), 125.3 (s, $C_{3/4}$), 127.2 (s, C_2), 129.1 (s, $C_{3/4}$), 129.2 - 129.4 (broad, PPh_3), 131.3 (broad, PPh_3), 133.7 (broad, PPh_3), 137.9 (d, $^{3}J_{CP}$ =3.0 Hz, C_{12}), 140.8 (s, C_5), 141.6 ($C_{8/9}$), 149.7 (s, C_{10}), 178.2 (d, $^{2}J_{CP}$ = 18.4 Hz, C_{13})

Other $^{13}C\{^{1}H\}$ NMR impurity signals: 124.9 (s), 129.0 (s), 131.5, 132.2, 132.3, 133.5 (t), 138.6 (s), 148.4 (s)

ESI-MS (*m/z*): Observed 624.1384 [M^+], Expected $C_{37}H_{33}NPR^{102}Ru$ 624.1389, Error = 0.5 mDa; Observed 196.1114 [$C_{14}H_{14}N^+$], Expected $C_{14}H_{14}N$ 196.1121, Error = 0.7 mDa.

Elemental Analysis (Obtained enough sample for 1 run): Anal. $C_{37}H_{33}F_6NP_2Ru$ + 1 CH_2Cl_2: Calc. C(53.47) H(4.13) N(1.64), Found C(52.95) H(3.97) N(1.84)

9.7.5 Reaction of 10^{Me} with 4-ethynyl-α,α,α-trifluorobenzene.

$[Ru(\eta^5\text{-}C_5H_5)(PPh_3)(4\text{-}Me\text{-}NC_5H_4)_2][PF_6]$, **$10^{Me}$** (76 mg, 0.1 mmol), 4-methylpyridine (19.5 µL, 0.2 mmol) and dichloromethane were added to a Youngs ampule, and the reaction mixture stirred for 15 minutes. 4-ethynyl-α,α,α-trifluorobenzene (24 µL, 0.15 mmol) was added. The reaction mixture was stirred and heated at 50 °C for 24 hours. The reaction mixture was allowed to cool to room temperature and the solvent was removed under vacuum. The reaction mixture was washed with pentane (2 x 10 mL). Slow diffusion of pentane (20 mL) into a dichloromethane solution containing the reaction mixture (2 mL) afforded crystals suitable for X-ray diffraction. The product could be purified further *via* crystallisations. Yield (46 mg, 55 %)

Characterisation Data

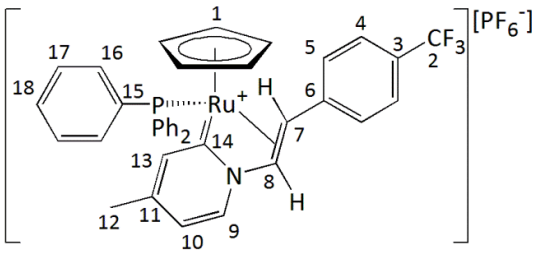

Figure 9.41: Labelled diagram of complex **$22^{Me,CF3}$**.

^{1}H NMR (CD_2Cl_2, 500 MHz, 300 K): 2.13 (s, 3H, H_{12}), 3.62 (dd, 1H, $^3J_{HP}$ = 11.6 Hz, $^3J_{HH}$ = 7.7 Hz, H_7), 4.96 (s, 5H, H_1),6.52-7.77 (broad, PPh_3) 6.68 (d, 1H, $^3J_{HH}$ = 7.7 Hz, H_8), 6.81 (s, 1H, H_{13}), 6.85 (m, 3H, H_5, H_{10}), 7.32-7.42 (broad m, 8H, H_4, PPh_3), 7.51 (broad, 3H, PPh_3), 7.82 (d, 1H, $^3J_{HH}$ = 6.8 Hz, H_9)

$^{31}P\{^1H\}$ NMR (CD_2Cl_2, 202 MHz, 300 K): -143.0 (sept, $^1J_{PF}$ = 711 Hz, PF_6^-), 52.9 (s, PPh_3)

$^{13}C\{^1H\}$ NMR (CD_2Cl_2, 125 MHz, 300 K): 22.3 (s, C_{12}), ~54.1 (lies underneath CD_2Cl_2 peak, alkene), 65.9 (broad, alkene), 88.6 (s, C_1), 120.3 (C_{10}), 124.6 (q, $^1J_{CF}$ = 271 Hz, C_2), 125.5 (s, C_5), 126.0 (q, $^3J_{CF}$ = 4 Hz, C_4), 128.4 (q, $^2J_{CF}$ = 32 Hz, C_3), 129.3 (broad, PPh_3), 131.4 (broad, PPh_3), 133.6 (broad, PPh_3), 137.8 (s, C_{13}), 141.8 (s, C_9), 145.6 (s, C_6), 150.0 (s, C_{11}), 177.1 (d, $^2J_{CP}$ = 18 Hz, C_{14})

ESI-MS (*m/z*): Observed 692.1188 (M^+), Expected $C_{38}H_{31}F_3NP^{102}Ru$ 691.1194, Error = 0.7 mDa

Elemental Analysis: Anal. $C_{38}H_{32}F_9NP_2Ru$: Calc. C(54.55) H(3.86) N(1.67), Found C(54.26) H(3.88) N(1.68)

9.7.6 Synthesis of $23^{Me,CF3}$.

Complex $\mathbf{22}^{Me,CF3}$ (31 mg, 0.037 mmol) in dichloromethane (5 mL) was stirred. 1,4-Diazabicyclo[2.2.2]octane (8 mg, 0.071 mmol) was added, and stirred at room temperature (15 hours). The reaction mixture solvent was removed under vacuum. The red product extracted with pentane (2 x10 mL), and separated by a cannula filtration. The pentane solvent was reduced (approximately 2 mL), and placed in the freezer, where crystals suitable for X-ray diffraction were grown.

Note: Best to carry out reaction in an ampule to avoid grease in product, as product is soluble in pentane.

Characterisation Data

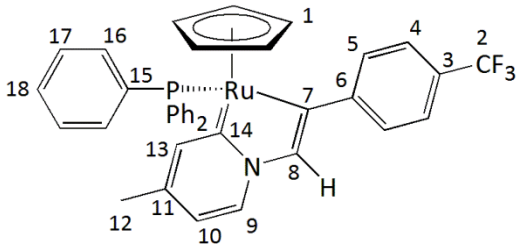

Figure 9.42: Labelled diagram of complex $\mathbf{23}^{Me,CF3}$.

^{1}H NMR (500 MHz, 298 K, CD_2Cl_2): 2.17 (s, 3H, H_{12}), 4.72 (s, 5H, H_1), 6.36 (dd, 1H, $^{3}J_{HH}$ = 6.5 Hz, $^{4}J_{HH}$ = 1.7 Hz, H_{10}), 6.98 (d, 1H, $^{4}J_{HP}$ = 2.4 Hz, H_8), 7.02 (t, 6H, $^{3}J_{HH}$, $^{3}J_{HP}$ = 9.1 Hz, H_{16}), 7.10 (d, 2H, $^{3}J_{HH}$ =8.0 Hz, H_5), 7.14 (td, 6H, $^{3}J_{HH}$ = 7.6 Hz, $^{4}J_{HP}$ = 1.6, H_{17}), 7.24 (t, 3H, $^{3}J_{HH}$ = 7.3 Hz, $^{5}J_{HP}$ = 1.3 Hz, H_{18}), 7.34 (d, 2H, $^{3}J_{HH}$ = 8.0 Hz, H_{17}), 7.72 (d, 1H, $^{3}J_{HH}$ = 6.4 Hz, H_9), 7.96 (s, 1H, H_{13})

^{31}P{^{1}H} NMR (202 MHz, 295 K, CD_2Cl_2): 61.7 (s, PPh_3)

^{13}C{^{1}H}NMR (176 MHz, 298 K, CD_2Cl_2): 20.7 (s, C_{12}), 82.8 (s, C_1), 115.5 (s, C_{10}), 124.2 (q, $^{3}J_{CF}$ = 3.7 Hz, C_4), 125.5 (q, $^{1}J_{CF}$ = 271 Hz, C_2), 126.1 (q, $^{2}J_{CF}$ = 32.0 Hz, C_3), 127.4 (m, C_{17}, C_5), 128.8 (s, C_{18}), 132.4 (s, C_8), 133.4 (d, $^{2}J_{CP}$ = 11 Hz, C_{16}), 135.6 (s, C_{11}), 136.1 (s, C_9), 137.0 (d, $^{1}J_{CP}$ = 41 Hz, C_{15}), 142.9 (s, C_{13}), 157.4 (s, C_6), 187.9 (d, $^{2}J_{CP}$ = 13.2 Hz, C_7), 217.8 (d, $^{2}J_{CP}$ = 15.8 Hz, C_{14})

ESI-MS (*m/z*): Observed 691.1188 [M^+], Expected $C_{38}H_{31}F_3NP^{102}Ru$ 691.1194, Error = 0.7 mDa.

Elemental Analysis: Anal. $C_{38}H_{31}F_3NPRu$: C(66.08) H(4.52) N(2.03), Found C(65.97) H(4.83) N(1.86)

9.7.7 Reaction of 10^{NMe2} with phenylacetylene.

$[Ru(\eta^5\text{-}C_5H_5)(PPh_3)(NC_5H_4\text{-}4\text{-}NMe_2)_2][PF_6]$, **$10^{NMe2}$** (72 mg, 0.08 mmol), and phenylacetylene (10.5 µL, 0.09 mmol) were placed in dichloromethane in a Youngs ampule, and the reaction mixture stirred for 5 days at room temperature (16 hours). To drive the reaction to completion, a further equivalent of phenylacetylene was added and the reaction mixture stirred for 2 days at room temperature. The solvent was removed, and placed in dichloromethane. The slow diffusion of pentane into the dichloromethane layer containing **$22^{NMe2,H}$** afforded crystals suitable for X-ray diffraction. The product could be purified further *via* crystallisations.

Characterisation Data

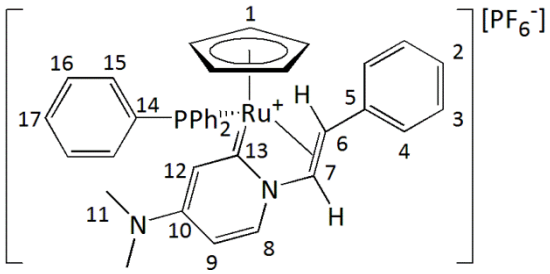

Figure 9.43: Labelled diagram of complex **$22^{NMe2,H}$**.

^{1}H NMR (CD_2Cl_2, 500 MHz, 295 K): 2.82 (broad, 6H, H_{11}), 3.55 (dd, 1H, $^3J_{HP}$ = 11.7 Hz, $^3J_{HH}$ = 7.9 Hz, H_6), 4.86 (s, 5H, H_1), 5.81 (dd, 1H, $^4J_{HH}$ = 2.4 Hz, $^5J_{HH}$ = 1.2 Hz, H_{12}), 6.23 (dd, 1H, $^3J_{HH}$ = 7.3 Hz, $^4J_{HH}$ = 2.8 Hz, H_9), 6.32 (dd, 1H, $^3J_{HH}$ = 7.9 Hz, $^3J_{HP}$ = 1.6 Hz, H_7), 6.79 (m, H_3), 7.14-7.19 (m H2, H_4), 7.29-7.35 (broad m, 9H, H_8, PPh_3), 7.36-7.55 (m ,broad, PPh_3)

Impurity peaks: 6.79 (m), 6.89 (d, 8.8 Hz), 7.06 (m), 7.14-7.19 (m), 7.29-7.35 (broad m), 7.36-7.55 (broad m), 7.79 (d, 1.5 Hz)

$^{31}P\{^1H\}$ NMR (CD_2Cl_2, 202 MHz, 295 K): -143.0 (sept, $^1J_{PF}$ = 711 Hz, PF_6^-), 55.3 (s, PPh_3)

$^{13}C\{^1H\}$ NMR (CD_2Cl_2, 125 MHz, 295 K): 53.1 (s, C_7), 68.4 (d, $^3J_{CP}$ = 2.6 Hz, C_6), 87.8 (d, $^2J_{CP}$ = 1.1 Hz, C_1), 103.1 (s, C_9), 108.3 (s, $C_{3/4}$), 115.7 (d, $^3J_{CP}$ = 2.9 Hz, C_{12}), C_{12}), 125.0 (s, $C_{3/4}$), 126.8 (s, C_2), 128.9-129.4 (broad, PPh_3), 130.7 (broad, PPh_3), 131.1 (broad, PPh_3), 133.0-135.3 (broad, PPh_3), 140.1 (s, C_8), 141.4 (s, C_5), 152.2 (s, C_{10}), 167.2 (d, $^2J_{CP}$ = 20.5 Hz, C_{13})

Broad resonance for C_{11} was not observed, probably is hidden in baseline.

Impurity peaks: 7.13 (s), 33.4 (s), 34.8 (s), 39.4 (s), 40.8 (s), 40.9 (m), 82.6 (s), 108.6 (s), 108.8 (s), 125.6 (s), 127.4 (m), 127.5, 129.0 (d, 1.1 Hz), 129.5(s), 129.7 (s), 129.9 (s), 129.9 (s), 131.4 (s), 139.0 (s), 141.6 (s), 141.7 (s), 142.4 (s), 156.9 (s)

ESI-MS (*m/z*): Observed 653.1655 [M^+], Expected $C_{38}H_{36}N_2P^{102}Ru$ 653.1670, Error = 0.5 mDa.

9.7.8 Reaction of 11 with 4-ethynyl-α,α,α-trifluorobenzene.

[Ru(η^5-C_5H_5)(PPh_3)(3-methylpyridine)$_2$][PF_6], **11** (40 mg, 0.05 mmol) was added to a Youngs ampule, and dichloromethane (3 mL) added. 3-Methylpyridine (10 µL, 0.10 mmol, 2 equiv) was added to the ampule, and the reaction mixture stirred for 5 minutes. 4-Ethynyl-α,α,α-trifluorotoluene (9 µL, 0.05 mmol, 1 equiv) was added to the reaction mixture, and the system sealed. The reaction mixture was heated to 50 °C for 15 hours.

The reaction mixture was allowed to cool, and the solvent removed under vacuum. Slow diffusion of pentane in to the reaction mixture afforded pale yellow crystals. The solvent was removed by filtration and the air-sensitive product dried under vacuum. The compound could be purified further *via* further crystallisations. The ratio of the two isomers changed in different reactions, although care was taken to perform reactions as accurately as possible.

Characterisation Data

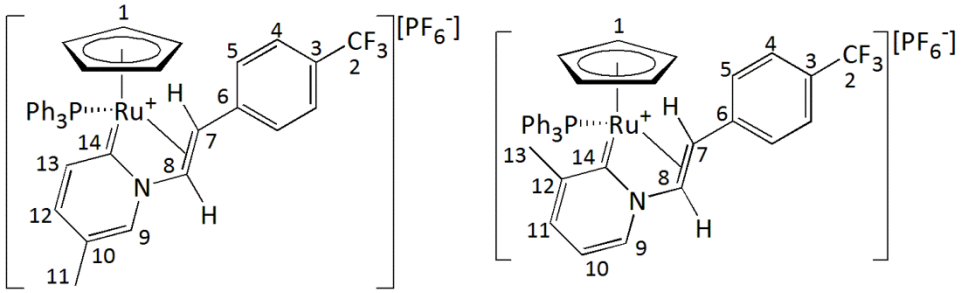

27a^{CF3} **27b^{CF3}**

Figure 9.44: Labelled diagram of complexes **27a^{CF3}** and **27b^{CF3}**.

^{1}H NMR (CD_2Cl_2, 500 MHz, 295 K): 1.64 (s, 2H, a-H_{13}), 2.27 (s, 3H, b-H_{11}), 3.44 (dd, 0.7H, $^3J_{HP}$ = 12.3 Hz, $^3J_{HH}$ = 7.9 Hz, a-H_{alkene}), 3.57 (dd, 1H, $^3J_{HP}$ = 11.4 Hz, $^3J_{HH}$ = 7.9 Hz, b-H_{alkene}), 4.95 (s, 5H, b-H_1), 5.10 (s, 3H, a-H_1), 6.30 (broad, 1H, b-H_{13}), 6.61 (dd, 1H, $^3J_{HP}$ = 1.7 Hz, $^3J_{HH}$ = 7.9 Hz, a-H_{alkene}), 6.71 (dd, 1H, $^3J_{HP}$ = 0.9 Hz, $^3J_{HH}$ = 7.9 Hz, b-H_{alkene}), 6.82 (d, 1.7H, Ar-CF_3), 6.91 (d, 2.4H, Ar-CF_3), 6.93-7.05 (m, 5H, a-H_{10} + other aromatics), 7.12-7.58 (m, 30H, b-H_{12}, a-H_{11}, Ar-CF_3 + other aromatic), 7.82 (d, 0.8H, $^3J_{HH}$ = 6.0 Hz, a-H_9), 7.86 (s, 1H, b-H_9)

^{31}P{^{1}H} NMR (CD_2Cl_2, 202 MHz, 295 K): -143.0 (sept, $^1J_{PF}$ = 711 Hz, PF_6^-), 50.5 (s, a-PPh_3), 53.0 (broad s, b-PPh_3)

^{13}C{^{1}H} NMR (CD_2Cl_2, 125 MHz, 295 K): 17.8 (s), 19.9 (s), 54.5 (s), 54.6 (s), 66.5 (m), 83.6 (s), 86.6 (s), 88.3 (d), 88.6 (d), 118.9 (s), 121.3 (m), 123.5 (d, 4.3 Hz), 124.6

(s), 125.5 (s), 125.7 (d, 4.3 Hz), 125.9 (q), 126.0 (s), 126.1 (q), 127.9 (m), 128.2 (s), 128.4 (s), 128.5 (s), 128.7 (s), 128.8-129.9 (broad m), 129.0 (broad), 129.3-129.5 (m), 131.2-131.7 (broad m) , 132.4-132.6 (broad m), 132.7-133.0 (broad m), 133.1-134.7 (broad), 135.2-135.9 (broad), 136.7 (m), 139.0 (m), 140.9 (s), 142.5 (s), 145.5 (m), 145.7 (m), 147.4 (m), 173.9 (d, $^{2}J_{CP}$ = 18.9 Hz), 179.9 (d, $^{2}J_{CP}$ = 16.6 Hz)

ESI-MS (*m/z*): Observed 692.1229, Expected $C_{38}H_{32}F_{3}NP^{102}Ru$ 692.1273 [M^{+}], Error = 3.4 mDa.

9.7.9 Reaction of 14^{H} with phenylacetylene.

$[Ru(\eta^5\text{-}C_5H_5)(PMe_3)(NC_5H_5)_2][PF_6]$, **$14^{H}$** (40 mg, 0.07 mmol) and pyridine (1.10 mL, 13.6 mmol, 195 equiv) were stirred. Phenylacetylene (16 µL, 0.14 mmol, 2 equiv) was added, and the reaction mixture was heated at 50 °C for 18 hours. The reaction mixture was left to cool to room temperature. The solvent was removed under vacuum. Dichloromethane was added to the brown precipitate (2 mL), followed by the addition of excess pentane (10 mL). The solvent was removed *via* filtration and brown precipitate dried under vacuum. Crystals suitable for X-ray diffraction were grown by slow diffusion of pentane in to a layer of dichloromethane containing the product. The product could be purified further by crystallisations.

Characterisation Data

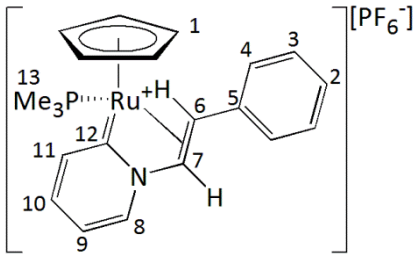

Figure 9.45: Labelled diagram of complex **$30^{H,H}$**.

^{1}H NMR (CD_2Cl_2, 500 MHz, 295 K):1.54 (d, 9H, $^2J_{HP}$ = 9.6 Hz, H_{13}), 3.57 (dd, 1H, $^3J_{HP}$ = 12.9 Hz, $^3J_{HH}$ = 7.0 Hz, H_6), 4.99 (s, 5H, H_1), 6.37 (dd, $^2J_{HP}$ = 7.0 Hz, $^3J_{HP}$ = 1.3 Hz, H_7), 7.04 (m, 1H, H_9), 7.11 (m, 2H, H_4), 7.15 (m, 1H, H_2), 7.24 (m, 2H, H_3), 7.46 (m, 1H, H_{11}), 7.53 (m, 1H, H_{10}), 7.94 (m, 1H, H_8)

$^{31}P\{^1H\}$ NMR (CD_2Cl_2, 202 MHz, 295 K): -143.0 (sept, $^1J_{PF}$ = 710 Hz, PF_6^-), 14.8 (s, PMe_3)

Other $^{31}P\{^1H\}$ NMR peaks: 28.5 ($OPPh_3$)

$^{13}C\{^1H\}$ NMR (CD_2Cl_2, 125 MHz, 295 K): 19.7 (d, $^1J_{CP}$ = 34.2 Hz, C_{13}), 62.1 (d, $^2J_{CP}$ = 4.6 Hz, C_{alkene}), 76.1 (d, $^2J_{CP}$ = 2.4 Hz, C_{alkene}), 87.5 (d, $^2J_{CP}$ = 1.4 Hz, C_1), 118.2 (s, C_9), 125.4 (s, C_4), 126.8 (s, C_2), 129.2 (s, C_3), 136.7 (d, $^3J_{CP}$ = 3.6 Hz, C_{11}), 137.3 (s, C_{10}), 141.9 (s, C_5), 142.7 (s, C_8), 182.3 (d, $^2J_{CP}$ = 19.9 Hz, C_{12})

Other $^{13}C\{^1H\}$ NMR peaks: 52.4 (s), 126.0 (s), 128.0 (s), 128.2 (s), 128.4 (s), 128.8 (s), 156.7 (d, 2.8 Hz)

ESI-MS (*m/z*): Observed 424.0756, Expected $C_{21}H_{25}NP^{102}Ru$ 424.0768, Error = 0.7 mDa.

9.7.10 Reaction of 14^{NMe2} with phenylacetylene.

$[Ru(\eta^5\text{-}C_5H_5)(PMe_3)(DMAP)_2][PF_6]$, **$14^{NMe2}$** (21 mg, 0.03 mmol) and 4-dimethylaminopyridine (9 mg, 0.07 mmol) was added to d_2-dichloromethane. Phenylacetylene (3.4 µL, 0.03 mmol) was added, and the reaction monitored *via* NMR spectroscopy.

Reported data for **$30^{NMe2,H}$** were observed *in situ*, attempts to isolate the product were not successful, therefore only selected data has presented.

Characterisation Data

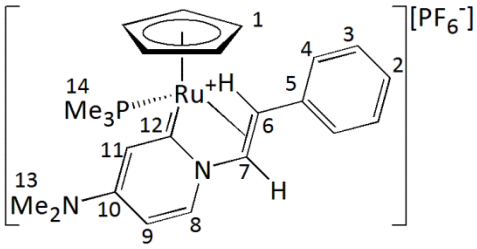

Figure 9.46: Labelled diagram of complex **$30^{NMe2,H}$**.

^{1}H NMR (CD_2Cl_2, 500 MHz, 295 K): 1.55 (d, 9H, $^2J_{HP}$ = 9.5 Hz, H_{14}), 3.04 (s, 6H, H_{13}), 3.47 (dd, 1H, $^3J_{HP}$ = 13.1 Hz, $^3J_{HH}$ = 6.9 Hz, $H_{6/7}$), 4.90 (s, 5H, H_1), 6.10 (dd, 1H, $^3J_{HP}$ = 1.1 Hz, $^3J_{HH}$ = 6.9 Hz, $H_{6/7}$), 6.20 (dd, 1H, $^3J_{HH}$ = 7.3 Hz, $^4J_{HH}$ = 2.7 Hz, H_9), 6.30 (m, 1H, H_{11}), 7.06-7.12 (m, 4H, H_2 + H_4 + Impurity), 7.20 (m, 2.5H, H_3 + Impurity), 7.35 (d, 1.6H, $^3J_{HH}$ = 7.3 Hz, H_8)

$^{31}P\{^1H\}$ NMR (CD_2Cl_2, 202 MHz, 295 K): -143.0 (sept, $^1J_{PF}$ = 711 Hz, PF_6^-), 16.1 (s, PMe_3)

ESI-MS (*m/z*): Observed 467.1195, Expected $C_{23}H_{30}N_2P^{102}Ru$ 467.1191, Error = 0.5 mDa

9.7.11 Reaction of 14^{NMe2} with 4-ethynyl-α,α,α-trifluorobenzene.

$[Ru(\eta^5\text{-}C_5H_5)(PMe_3)(DMAP)_2][PF_6]$, $\mathbf{14^{NMe2}}$ (20 mg, 0.03 mmol) and 4-dimethylaminopyridine (9 mg, 0.07 mmol) was added to d_2-dichloromethane. 4-Ethynyl-α,α,α-trifluorotoluene (5.1 µL, 0.03 mmol) was added, and the reaction monitored *via* NMR spectroscopy.

Reported data for $\mathbf{30^{NMe2,CF3}}$ were observed *in situ*, attempts to isolate the product were not successful, therefore only selected data has presented.

Characterisation Data

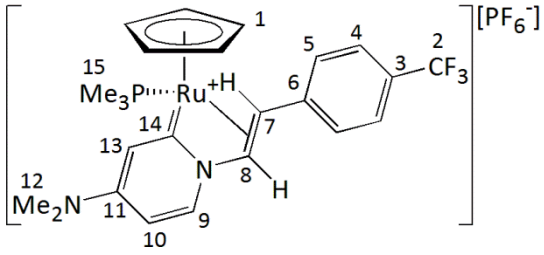

Figure 9.47: Labelled diagram of complex $\mathbf{30^{NMe2,CF3}}$.

^{1}H NMR (CD_2Cl_2, 500 MHz, 295 K): 1.55 (d, 9H, $^2J_{HP}$ = 9.5 Hz, H_{15}), 3.04 (s, 6H, H_{12}), 3.45 (dd, 1H, $^3J_{HP}$ = 13.1 Hz, $^3J_{HH}$ = 6.8 Hz, $H_{7/8}$), 4.92 (s, 5H, H_1), 6.17 (dd, 1H, $^3J_{HH}$ = 6.8 Hz, $H_{7/8}$), 6.21 (dd, 1H, $^3J_{HH}$ = 7.2 Hz, $^4J_{HH}$ = 2.7 Hz, H_{10}), 6.30 (m, 1H, H_{13}), 7.18 (d, 2H, $^3J_{HH}$ = 8.1 Hz, $H_{4/5}$), 7.40 (d, 1H, $^3J_{HH}$ = 7.2 Hz, H_9), 7.45 (d, 2.8H, $^3J_{HH}$ = 8.1 Hz, $H_{4/5}$ + Impurity)

$^{31}P\{^1H\}$ NMR (CD_2Cl_2, 202 MHz, 295 K): -143.0 (sept, $^1J_{PF}$ = 711 Hz, PF_6^-), 15.6 (s, PMe_3)

ESI-MS (*m/z*): Observed 535.1074, Expected $C_{24}H_{29}N_2P^{102}Ru$ 535.1065, Error = 1.0 mDa

9.8 Synthesis of Organic Species and Catalytic Reactions

9.8.1 Synthesis of 2-Styrylpyridine Derivatives.

Literature Preparation

The independent synthesis of the 2-styrylpyridine derivatives was followed as mentioned in the literature.[245]

General methodology for alkenylation reactions of pyridine

The general methodology for the catalytic reactions are mentioned below, however the alkyne and length of heating should be changed accordingly. The reaction scale was generally based on **10^{H}** (40 mg).

Entry	Alkyne	10^{H} (mol %)	Pyridine equivalents	Reaction conditions	Time (hrs)	Percentage Yield / Conversion
1	PhC≡CH	20	20	50 °C	32	14
2	4-CF_3-C_6H_4C≡CH	20	20	50 °C	32	19
3	4-CF_3-C_6H_4C≡CH	100	55	50 °C	72	48[a]
4	5 x 1 equiv PhC≡CH	20	55	50 °C	5 x 24	33[a]
5	5 x 1 equiv 4-CF_3-C_6H_4C≡CH	20	55	50 °C	5 x 24	17[a]
6	4-CF_3-C_6H_4C≡CH	5	20	50 °C	24	2.5[b]
7	4-CF_3-C_6H_4C≡CH	20	55	50 °C	72	49[b]
8	4-CF_3-C_6H_4C≡CH	20	20	50 °C, CH_2Cl_2	48	24[a]
9	4-CF_3-C_6H_4C≡CH	20	20	μwave, 50 °C, CH_2Cl_2	1	7[b]
10	4-CF_3-C_6H_4C≡CH	20	20	μwave, 100 °C	0.5	9[b]

Reaction conditions: Entries 1, 2, 6, 7

To a Young's ampule under nitrogen, [Ru(η^5-C_5H_5)(PPh_3)(NC_5H_5)$_2$][PF_6], pyridine and alkyne were added. The reaction mixture was heated at 50 °C . The reaction mixture was allowed to cool and the product purified either by preparative TLC or column chromatography.

Reaction conditions: Entry 3

To a Young's ampule under nitrogen, $[Ru(\eta^5\text{-}C_5H_5)(PPh_3)(NC_5H_5)_2][PF_6]$ (80 mg, 0.109 mmol, 1 equiv), pyridine (1.2 mL, 14.8 mmol), and 4-ethynyl-α,α,α-trifluorotoluene (18 μL, 0.109 mmol, 1 equiv) were added. The reaction mixture was heated at 50 °C for 72 hours. The reaction mixture was allowed to cool to room temperature. The product was purified using preparative TLC with a solvent eluent of ethyl acetate: hexane (1:3) followed by passage through a silica plug. Conversion was shown to be quantitative by ^{19}F NMR spectroscopy. Isolated yield 13 mg, 48 %.

Reaction conditions: Entries 4, 5

To a Young's ampule under nitrogen, $[Ru(\eta^5\text{-}C_5H_5)(PPh_3)(NC_5H_5)_2][PF_6]$, pyridine and alkyne were added. The reaction mixture was heated at 50 °C . After 24 hours the reaction mixture was removed from the graphite bath and under nitrogen atmosphere a further aliquot of alkyne added and the reaction mixture heated at 50 °C. The final step was repeated four more times. The reaction mixture was allowed to cool and the product purified either by preparative TLC or column chromatography.

Reaction conditions: Entry 8

To a Young's ampule under nitrogen, $[Ru(\eta^5\text{-}C_5H_5)(PPh_3)(NC_5H_5)_2][PF_6]$ (80 mg, 0.109 mmol, 20 mol %), pyridine (880 μL, 10.9 mmol, 20 equiv), dichloromethane (1.50mL, 271 equiv) and 4-ethynyl-α,α,α-trifluorotoluene (90 μL, 0.551 mmol, 1 equiv) were added. The reaction mixture was heated at 50 °C for 48 hours. The product was purified using column chromatography. The reaction mixture was allowed to cool to room temperature. Conversion was shown to be ca. 50 % by ^{19}F NMR spectroscopy, isolated yield 48 mg, 35 %.

Reaction conditions: Entries 9, 10

To a microwave vial under nitrogen, $[Ru(\eta^5\text{-}C_5H_5)(PPh_3)(NC_5H_5)_2][PF_6]$, pyridine (entry 10: dichloromethane) and alkyne were added. The reaction mixture was heated. The reaction mixture was allowed to cool and the reaction mixture analysed by NMR spectroscopy.

Purification

Preparative TLC: The reaction mixture was placed on the preparative TLC plate and a solvent eluent of ethyl acetate: hexane (1:3) was used.

Column chromatography: The product was purified by column chromatography using silica gel with an ethyl acetate: hexane (1:10) eluent to give the product.

Characterisation Data

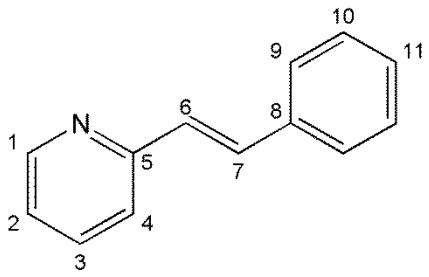

^{1}H NMR (CD_2Cl_2, 500 MHz, 295 K): 7.15 (m, 1H, H_2), 7.18 (d, 1H, $^{3}J_{HH}$ = 16.2 Hz, $H_{6/7}$), 7.30 (t, 1H, 7.4 Hz, H_{11}), 7.38 (m, 3H, H_4 +H_{10}), 7.58 – 7.69 (m, 4H, $H_{6/7}$ + H_3 + H_9), 8.57 (d, 1H, $^{3}J_{HH}$ = 4.5 Hz, H_1)

^{13}C{^{1}H} NMR (CD_2Cl_2, 125 MHz, 295 K): 122.5 (broad s, C_2 + C_4), 127.4 (s, C_9), 128.5 (s, $C_{6/7}$), 128.7 (s, C_{11}), 129.1 (s, C_{10}), 132.8 (s, $C_{6/7}$), 136.9 (s, C_3), 137.1 (s, C_8), 150.4 (s, C_1), 155.9 (s, C_5)

ESI-MS (*m/z*): Observed 182.0960 [M+H^+], Expected $C_{13}H_{12}N$ 182.0964, Error = 0.4 mDa

^{1}H NMR (NC_5D_5, 500 MHz, 295 K): 7.11 (dd, 1H, $^{3}J_{HH}$ = 7.4 Hz, $^{4}J_{HH}$ = 4.7 Hz, H_2), 7.30 (t, 1H, $^{3}J_{HH}$ = 7.4 Hz, H_{11}), 7.38 (t, 2H, $^{3}J_{HH}$ = 7.4 Hz, H_{10}), 7.43-7.47 (m, 2H, H_4 + $H_{6/7}$), 7.61 (td, 1H, $^{3}J_{HH}$ = 7.7 Hz, $^{4}J_{HH}$ = 1.7 Hz, H_3), 7.67 (d, 2H, $^{3}J_{HH}$ = 7.4 Hz, H_9), 8.03 (d, 1H, $^{3}J_{HH}$ = 16.0 Hz, $H_{6/7}$), 8.74 (underneath d_5-pyridine resonance, H_1)

Characterisation Data

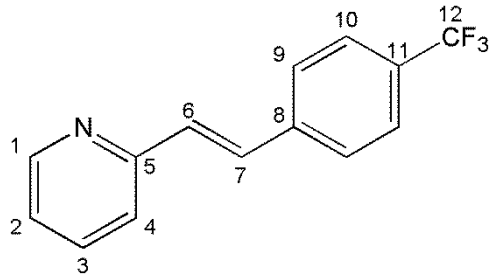

^{1}H NMR (CD_2Cl_2, 500 MHz, 295 K): 7.19 (m, 1H, H_2), 7.27 (d, 1H, $^{3}J_{HH}$ = 16.1 Hz, $H_{6/7}$), 7.41 (d, 1H, 7.8 Hz, H_4), 7.64 (d, 2H, $^{3}J_{HH}$ = 8.4 Hz, H_{10}), 7.67-7.72 (m, 4H, H_3 + H_9 + $H_{6/7}$), 8.59 (d,$^{3}J_{HH}$ = 4.0 Hz, H_1)

^{19}F NMR (CD_2Cl_2, 470MHz, 295 K): -64.09 (s, CF_3)

^{13}C{^{1}H} NMR (CD_2Cl_2, 125 MHz, 295 K): 123.0 (s, C_4), 123.0 (s, C_2), 124.7 (q, $^{1}J_{CF}$ = 272 Hz, C_{12}), 126.0 (q, $^{3}J_{CF}$ = 3.8 Hz, C_{10}), 127.6 (s, C_9), 129.9 (q, $^{2}J_{CF}$ = 32.3 Hz, C_{11}), 130.9 (s, $C_{6/7}$), 131.1 (s, $C_{6/7}$), 137.0 (s, C_3), 140.8 (s, C_8), 150.2 (s, C_1), 155.2 (s, C_5)

ESI-MS (*m/z*): Observed 250.0833 [M+H^+], Expected $C_{14}H_{11}F_3N$ 250.0838, Error = 0.5 mDa.

^{1}H NMR (NC_5D_5, 500 MHz, 295 K): 7.16 (dd, 1H, $^{3}J^{HH}$ = 6.7 Hz, $^{4}J_{HH}$ = 5.1 Hz, H_2), 7.47-7.54 (m, 2H, H_4 + $H_{6/7}$), 7.64-7.68 (m, 3H, H_3 + $H_{9/10}$), 7.74 (d, 2H, $^{3}J_{HH}$ = 7.8 Hz, $H_{9/10}$), 8.00 (d, 1H, $^{3}J_{HH}$ = 15.9 Hz, $H_{6/7}$), 8.76 (d, underneath d_5-pyridine resonance, H_1)

9.8.2 Preparation of Pyridinium Tetrafluoroborate.[339]

A solution of pyridine (1.0 mL, 12.3 mmol) and diethyl ether (5 mL) were stirred a under nitrogen atmosphere and cooled in an ice bath. To this tetrafluoroboric acid diethyl ether complex (2.0 mL, 15 mmol) was added slowly. A white precipitate was collected by filtration and washed with diethyl ether (10 mL). Yield 1.85 g, 90 %.

Characterisation Data

^{1}H NMR (NC_5D_5, 500 MHz, 295 K): 16.99 (broad), pyridine resonances overlap with d_5-pyridine resonances.

9.8.3 Preparation of Pyridinium Hexafluorophosphate.[340]

Using aerobic reaction conditions, a solution of pyridine (1.0 mL, 12.3 mmol) and diethyl ether (25 mL) were stirred in a conical flask in a well ventilated fume-hood. Hexafluorophosphoric acid (60 % solution in water, 2.0 mL, 15 mmol) was added drop-wise to the reaction flask. A white precipitate was collected and dried under vacuum. The product was recrystallised from hot ethanol and washed with diethyl ether (2 x 50 mL). The product was dried under vacuum.

Characterisation Data

^{1}H NMR (d_6-acetone, 500 MHz, 295 K): 8.30 (m, 2H), 8.84 (m, 1H), 9.16 (m,, 2H), 12.68 (broad)

Appendix

Complex 7

Identification code	jml1163
Empirical formula	$C_{15}H_{13}F_6PRu$
Formula weight	439.29
Temperature/K	110.00(10)
Crystal system	monoclinic
Space group	P21/n
a/Å	9.2345(3)
b/Å	21.0319(10)
c/Å	15.3415(8)
α/°	90.00
β/°	93.266(4)
γ/°	90.00
Volume/Å^3	2974.8(2)
Z	8
ρcalc mg/mm^3	1.962
Absorption coefficient /mm^{-1}	1.221
F(000)	1728.0
Crystal size/mm^3	0.3234 × 0.1041 × 0.0726
2Θ range for data collection	5.66 to 64.56°
Index ranges	$-13 \leq h \leq 13$, $-30 \leq k \leq 30$, $-21 \leq l \leq 22$
Reflections collected	28152
Independent reflections	9616[R(int) = 0.0257]
Data/restraints/parameters	9616/0/415
Goodness-of-fit on F2	1.047
Final R indexes [$I \geq 2\sigma$ (I)]	R1 = 0.0285, wR2 = 0.0626
Final R indexes [all data]	R1 = 0.0398, wR2 = 0.0686
Largest diff. peak/hole /e Å^{-3}	0.80/-0.60

Complex 10^{H}

Identification code	jml1002m
Empirical formula	$C_{34}H_{32}Cl_2F_6N_2P_2Ru$
Formula weight	816.53
Temperature/K	110(2)
Crystal system	Triclinic
Space group	P-1
a/Å	9.2639(5)
b/Å	10.8917(5)
c/Å	18.2008(9)
α/°	102.0870(10)
β/°	103.9570(10)
γ/°	101.4050(10)
Volume/Å^3	1682.04(15)
Z	2
ρcalc mg/mm^3	1.612
Absorption coefficient /mm^{-1}	0.782
F(000)	824
Crystal size/mm^3	0.13 x 0.08 x 0.06
2Θ range for data collection	1.98 to 28.32°.
Index ranges	$-12 \leq h \leq 12$, $-14 \leq k \leq 14$, $-24 \leq l \leq 24$
Reflections collected	17464
Independent reflections	8312 [R(int) = 0.0299]
Data/restraints/parameters	8312 / 12 / 488
Goodness-of-fit on F2	1.011
Final R indexes [$I \geq 2\sigma$ (I)]	R1 = 0.0337, wR2 = 0.0729
Final R indexes [all data]	R1 = 0.0503, wR2 = 0.0788
Largest diff. peak/hole / e Å^{-3}	0.581 and -0.717

Complex 10^{Me}

Identification code	jml1110
Empirical formula	$C_{35}H_{34}F_6N_2P_2Ru$
Formula weight	759.65
Temperature/K	110.0
Crystal system	monoclinic
Space group	$P2_1/c$
a/Å	11.5251(3)
b/Å	20.2284(5)
c/Å	13.9040(3)
α/°	90.00
β/°	91.661(3)
γ/°	90.00
Volume/Å^3	3240.14(13)
Z	4
ρcalc mg/mm^3	1.557
Absorption coefficient /mm^{-1}	0.646
F(000)	1544
Crystal size/mm^3	0.1917 × 0.1057 × 0.064
2Θ range for data collection	5.86 to 55.12°
Index ranges	$-12 \leq h \leq 15$, $-19 \leq k \leq 26$, $-18 \leq l \leq 13$
Reflections collected	13662
Independent reflections	7325[R(int) = 0.0232]
Data/restraints/parameters	7325/82/475
Goodness-of-fit on F2	1.045
Final R indexes [$I \geq 2\sigma(I)$]	$R_1 = 0.0535$, $wR_2 = 0.1282$
Final R indexes [all data]	$R_1 = 0.0648$, $wR_2 = 0.1361$
Largest diff. peak/hole / e Å^{-3}	2.586/-1.694

Complex 10^{NMe2}

Identification code	jml1307
Empirical formula	$C_{38}H_{42}Cl_2F_6N_4P_2Ru$
Formula weight	902.67
Temperature/K	110.00(10)
Crystal system	monoclinic
Space group	C2/c
a/Å	27.1714(3)
b/Å	20.9945(2)
c/Å	13.71206(17)
α/°	90.00
β/°	99.4272(12)
γ/°	90.00
Volume/Å^3	7716.42(15)
Z	8
ρcalc mg/mm^3	1.554
Absorption coefficient /mm^{-1}	0.691
F(000)	3680.0
Crystal size/mm^3	0.3313 × 0.2727 × 0.1486
2Θ range for data collection	6.02 to 64.24°
Index ranges	$-40 \leq h \leq 40$, $-30 \leq k \leq 30$, $-20 \leq l \leq 20$
Reflections collected	32900
Independent reflections	12369[R(int) = 0.0245]
Data/restraints/parameters	12369/0/484
Goodness-of-fit on F2	1.029
Final R indexes [$I \geq 2\sigma$ (I)]	R_1 = 0.0335, wR_2 = 0.0787
Final R indexes [all data]	R_1 = 0.0408, wR_2 = 0.0837
Largest diff. peak/hole / e Å^{-3}	1.48/-1.29

Complex 11

Identification code	jml1211
Empirical formula	$C_{36}H_{36}Cl_2F_6N_2P_2Ru$
Formula weight	844.58
Temperature/K	110.00(10)
Crystal system	monoclinic
Space group	$P2_1/c$
a/Å	10.7946(5)
b/Å	15.1082(5)
c/Å	22.6794(10)
α/°	90.00
β/°	103.385(5)
γ/°	90.00
Volume/Å^3	3598.2(3)
Z	4
ρcalc mg/mm^3	1.559
Absorption coefficient /mm^{-1}	0.734
F(000)	1712.0
Crystal size/mm^3	0.28 × 0.08 × 0.03
2Θ range for data collection	5.7 to 64.46°
Index ranges	$-16 \leq h \leq 15$, $-12 \leq k \leq 22$, $-33 \leq l \leq 32$
Reflections collected	27692
Independent reflections	11517[R(int) = 0.0293]
Data/restraints/parameters	11517/36/570
Goodness-of-fit on F2	1.076
Final R indexes [$I \geq 2\sigma$ (I)]	R_1 = 0.0424, wR_2 = 0.1030
Final R indexes [all data]	R_1 = 0.0560, wR_2 = 0.1106
Largest diff. peak/hole / e Å^{-3}	1.08/-0.70

Complex 12

Identification code	jml1238
Empirical formula	$C_{31}H_{30}F_6N_2P_2Ru$
Formula weight	707.58
Temperature/K	110.00(10)
Crystal system	triclinic
Space group	P-1
a/Å	9.4451(4)
b/Å	10.9135(6)
c/Å	16.2138(7)
α/°	102.623(4)
β/°	95.108(3)
γ/°	113.098(5)
Volume/Å^3	1471.46(14)
Z	2
ρcalc mg/mm^3	1.597
Absorption coefficient /mm^{-1}	0.705
F(000)	716.0
Crystal size/mm^3	0.1951 × 0.1794 × 0.1376
2Θ range for data collection	5.76 to 56.64°
Index ranges	$-12 \leq h \leq 12$, $-14 \leq k \leq 7$, $-21 \leq l \leq 21$
Reflections collected	12068
Independent reflections	7007[R(int) = 0.0348]
Data/restraints/parameters	7007/36/432
Goodness-of-fit on F2	1.042
Final R indexes [$I \geq 2\sigma$ (I)]	R_1 = 0.0486, wR_2 = 0.1097
Final R indexes [all data]	R_1 = 0.0816, wR_2 = 0.1258
Largest diff. peak/hole / e Å^{-3}	0.99/-1.06

Complex 13^{Me}

Identification code	jml1162
Empirical formula	$C_{31}H_{32}N_4F_6P_2Ru$
Formula weight	737.62
Temperature/K	110.00(10)
Crystal system	orthorhombic
Space group	$Pna2_1$
a/Å	22.6469(8)
b/Å	13.9495(4)
c/Å	9.7673(4)
α/°	90.00
β/°	90.00
γ/°	90.00
Volume/$Å^3$	3085.60(19)
Z	4
ρcalc mg/mm^3	1.588
Absorption coefficient /mm^{-1}	0.677
F(000)	1496.0
Crystal size/mm^3	0.3916 × 0.0783 × 0.0181
2Θ range for data collection	5.84 to 64.42°
Index ranges	$-32 \leq h \leq 31$, $-20 \leq k \leq 20$, $-11 \leq l \leq 13$
Reflections collected	17379
Independent reflections	8444[R(int) = 0.0297]
Data/restraints/parameters	8444/1/399
Goodness-of-fit on F2	1.069
Final R indexes [$I \geq 2\sigma(I)$]	$R_1 = 0.0315$, $wR_2 = 0.0712$
Final R indexes [all data]	$R_1 = 0.0356$, $wR_2 = 0.0734$
Largest diff. peak/hole / e $Å^{-3}$	0.60/-0.40

Complex 13^{tBu}

Identification code	ml1212
Empirical formula	$C_{37.500015}H_{45.00003}ClF_6N_4P_2Ru$
Formula weight	864.24
Temperature/K	110.00(10)
Crystal system	monoclinic
Space group	$P2_1$
a/Å	15.4108(13)
b/Å	9.5908(4)
c/Å	28.366(2)
α/°	90.00
β/°	104.941(9)
γ/°	90.00
Volume/Å^3	4050.7(5)
Z	4
ρcalc mg/mm^3	1.417
Absorption coefficient /mm^{-1}	0.591
F(000)	1772.0
Crystal size/mm^3	0.2514 × 0.0821 × 0.0322
2Θ range for data collection	5.8 to 57.6°
Index ranges	$-20 \leq h \leq 13$, $-12 \leq k \leq 7$, $-38 \leq l \leq 33$
Reflections collected	17416
Independent reflections	12321[R(int) = 0.0494]
Data/restraints/parameters	12321/545/976
Goodness-of-fit on F2	1.152
Final R indexes [$I \geq 2\sigma$ (I)]	R_1 = 0.0949, wR_2 = 0.2142
Final R indexes [all data]	R_1 = 0.1019, wR_2 = 0.2189
Largest diff. peak/hole / e Å^{-3}	3.55/-1.53

Complex 14^{H}

Identification code	jml1164
Empirical formula	$C_{18}H_{24}N_2F_6P_2Ru$
Formula weight	545.40
Temperature/K	110.00(10)
Crystal system	monoclinic
Space group	C2/c
a/Å	31.046(3)
b/Å	8.5236(7)
c/Å	17.2938(12)
α/°	90.00
β/°	108.356(8)
γ/°	90.00
Volume/$Å^3$	4343.5(6)
Z	8
ρcalc mg/mm^3	1.668
Absorption coefficient /mm^{-1}	0.926
F(000)	2192.0
Crystal size/mm^3	0.2498 × 0.2377 × 0.1032
2Θ range for data collection	6.16 to 64.52°
Index ranges	$-43 \leq h \leq 45$, $-9 \leq k \leq 12$, $-25 \leq l \leq 25$
Reflections collected	22590
Independent reflections	7006[R(int) = 0.0263]
Data/restraints/parameters	7006/0/267
Goodness-of-fit on F2	1.037
Final R indexes [$I \geq 2\sigma(I)$]	$R_1 = 0.0239$, $wR_2 = 0.0529$
Final R indexes [all data]	$R_1 = 0.0280$, $wR_2 = 0.0553$
Largest diff. peak/hole / e $Å^{-3}$	0.50/-0.50

Complex 14^{NMe2}

Identification code	jml1207
Empirical formula	$C_{45.25}H_{71}Cl_{0.5}F_{12}N_8O_{0.25}P_4Ru_2$
Formula weight	1302.85
Temperature/K	110.00(10)
Crystal system	orthorhombic
Space group	Pbcn
a/Å	34.2917(14)
b/Å	18.5242(6)
c/Å	17.6601(7)
α/°	90.00
β/°	90.00
γ/°	90.00
Volume/$Å^3$	11218.1(7)
Z	8
ρcalc mg/mm^3	1.543
Absorption coefficient /mm^{-1}	0.756
F(000)	5320.0
Crystal size/mm^3	0.293 × 0.1553 × 0.044
2Θ range for data collection	5.72 to 54.12°
Index ranges	$-43 \leq h \leq 40$, $-23 \leq k \leq 15$, $-22 \leq l \leq 19$
Reflections collected	32357
Independent reflections	12302[R(int) = 0.0436]
Data/restraints/parameters	12302/71/904
Goodness-of-fit on F2	1.060
Final R indexes [$I \geq 2\sigma$ (I)]	$R_1 = 0.0727$, $wR_2 = 0.1693$
Final R indexes [all data]	$R_1 = 0.0972$, $wR_2 = 0.1849$
Largest diff. peak/hole / e $Å^{-3}$	1.72/-1.50

Complex 15

Identification code	jml1018c
Empirical formula	$C_{136}H_{228}F_{42}N_{12}P_{14}Ru_6$
Formula weight	3869.36
Temperature/K	163.0
Crystal system	rhombohedral
Space group	R-3:r
a/Å	16.9556(10)
b/Å	16.9556(10)
c/Å	16.9556(10)
α/°	105.795
β/°	105.795
γ/°	105.795
Volume/$Å^3$	4185.9(4)
Z	1
ρcalc mg/mm^3	1.5349
Absorption coefficient /mm^{-1}	0.757
F(000)	1975.1
Crystal size/mm^3	0.31 × 0.07 × 0.05
2Θ range for data collection	3.02 to 56.58°
Index ranges	$-22 \leq h \leq 22$, $-22 \leq k \leq 22$, $-22 \leq l \leq 21$
Reflections collected	43426
Independent reflections	6932[R(int) = 0.0808]
Data/restraints/parameters	6932/3/319
Goodness-of-fit on F2	1.041
Final R indexes [$I \geq 2\sigma(I)$]	R_1 = 0.0461, wR_2 = N/A
Final R indexes [all data]	R_1 = 0.0743, wR_2 = 0.1162
Largest diff. peak/hole / e $Å^{-3}$	1.38/-1.47

Complex 16

Identification code	jml1022m
Empirical formula	$C_{33}H_{30}F_6N_2O_3P_2Ru$
Formula weight	779.60
Temperature/K	110(2)
Crystal system	Monoclinic
Space group	P2(1)/c
a/Å	15.795(9)
b/Å	10.873(6)
c/Å	19.527(11)
α/°	90
β/°	103.318(11)
γ/°	90
Volume/$Å^3$	3263(3)
Z	4
ρcalc mg/mm^3	1.587
Absorption coefficient /mm^{-1}	0.650
F(000)	1576
Crystal size/mm^3	0.25 x 0.25 x 0.20
2Θ range for data collection	1.32 to 25.25
Index ranges	-18<=h<=18, -12<=k<=12, -23<=l<=23
Reflections collected	25177
Independent reflections	5771 [R(int) = 0.0600]
Data/restraints/parameters	5771 / 0 / 424
Goodness-of-fit on F2	1.095
Final R indexes [$I \geq 2\sigma$ (I)]	R1 = 0.0653, wR2 = 0.1642
Final R indexes [all data]	R1 = 0.0715, wR2 = 0.1685
Largest diff. peak/hole / e $Å^{-3}$	3.115 and -0.957

Complex 17^{H}

Identification code	jml1107
Empirical formula	$C_{37}H_{33}Cl_2F_6NP_2Ru$
Formula weight	839.55
Temperature/K	110.0
Crystal system	triclinic
Space group	P-1
a/Å	11.4116(7)
b/Å	12.9092(6)
c/Å	13.8078(6)
α/°	85.101(4),
β/°	65.774(5)
γ/°	70.153(5)
Volume/$Å^3$	1741.34(15)
Z	2
ρcalc mg/mm^3	1.601
Absorption coefficient /mm^{-1}	0.757
F(000)	848
Crystal size/mm^3	0.2745 × 0.1787 × 0.1579
2Θ range for data collection	6.12 to 59.14°
Index ranges	$-10 \leq h \leq 15$, $-17 \leq k \leq 17$, $-18 \leq l \leq 19$
Reflections collected	15370
Independent reflections	9706[R(int) = 0.0203]
Data/restraints/parameters	9706/0/450
Goodness-of-fit on F2	1.036
Final R indexes [$I \geq 2\sigma(I)$]	R1 = 0.0270, wR2 = 0.0628
Final R indexes [all data]	R1 = 0.0307, wR2 = 0.0653
Largest diff. peak/hole / e $Å^{-3}$	0.596/-0.495

Complex 17^{CF3}

Identification code	jml1146
Empirical formula	$C_{38}H_{32}Cl_2F_9NP_2Ru$
Formula weight	907.56
Temperature/K	110.00(10)
Crystal system	monoclinic
Space group	$P2_1/n$
a/Å	10.7064(4)
b/Å	18.5122(7)
c/Å	18.6411(7)
α/°	90.00
β/°	90.298(3)
γ/°	90.00
Volume/$Å^3$	3694.6(2)
Z	4
ρcalc mg/mm^3	1.632
Absorption coefficient /mm^{-1}	0.731
F(000)	1824
Crystal size/mm^3	0.2257 × 0.051 × 0.0362
2Θ range for data collection	5.82 to 55.78°
Index ranges	$-8 \leq h \leq 12$, $-14 \leq k \leq 24$, $-23 \leq l \leq 23$
Reflections collected	14218
Independent reflections	7322[R(int) = 0.0334]
Data/restraints/parameters	7322/0/478
Goodness-of-fit on F2	1.048
Final R indexes [$I \geq 2\sigma$ (I)]	$R_1 = 0.0439$, $wR_2 = 0.0751$
Final R indexes [all data]	$R_1 = 0.0602$, $wR_2 = 0.0815$
Largest diff. peak/hole / e $Å^{-3}$	0.742/-0.829

Complex 18

Identification code	jml1228
Empirical formula	$C_{21}H_{25}F_6NP_2Ru$
Formula weight	568.43
Temperature/K	110.00(10)
Crystal system	monoclinic
Space group	$P2_1/n$
a/Å	11.6225(7)
b/Å	12.7440(8)
c/Å	15.3075(10)
α/°	90.00
β/°	91.431(6)
γ/°	90.00
Volume/Å^3	2266.6(2)
Z	4
ρcalc mg/mm^3	1.666
Absorption coefficient /mm^{-1}	0.890
F(000)	1144.0
Crystal size/mm^3	0.3456 × 0.0794 × 0.0554
2Θ range for data collection	6.4 to 57.52°
Index ranges	$-14 \leq h \leq 15$, $-15 \leq k \leq 17$, $-16 \leq l \leq 20$
Reflections collected	10651
Independent reflections	5129[R(int) = 0.0403]
Data/restraints/parameters	5129/46/366
Goodness-of-fit on F2	1.159
Final R indexes [$I \geq 2\sigma$ (I)]	$R_1 = 0.0712$, $wR_2 = 0.1403$
Final R indexes [all data]	$R_1 = 0.0953$, $wR_2 = 0.1533$
Largest diff. peak/hole / e Å^{-3}	1.93/-1.72

Complex $21^{H,H}$

Identification code	2011src0363r1
Empirical formula	$C_{45}H_{39}Cl_2F_6NP_2Ru$
Formula weight	941.68
Temperature/K	120(2)
Crystal system	tetragonal
Space group	$P4_2/n$
a/Å	28.3177(16)
b/Å	28.3177(16)
c/Å	10.7605(6)
α/°	90.00
β/°	90.00
γ/°	90.00
Volume/$Å^3$	8628.8(8)
Z	8
ρcalc mg/mm^3	1.450
Absorption coefficient /mm^{-1}	0.620
F(000)	3824.0
Crystal size/mm^3	0.28 × 0.02 × 0.02
2Θ range for data collection	5.92 to 55.24°
Index ranges	$-36 \leq h \leq 22$, $-36 \leq k \leq 36$, $-12 \leq l \leq 14$
Reflections collected	39939
Independent reflections	9908[R(int) = 0.0830]
Data/restraints/parameters	9908/30/548
Goodness-of-fit on F2	1.047
Final R indexes [$I \geq 2\sigma(I)$]	$R_1 = 0.0981$, $wR_2 = 0.1949$
Final R indexes [all data]	$R_1 = 0.1411$, $wR_2 = 0.2139$
Largest diff. peak/hole / e $Å^{-3}$	2.81/-0.87

Complex $22^{H,H}$

Identification code	jml1112
Empirical formula	$C_{36}H_{31}F_6NP_2Ru$
Formula weight	754.63
Temperature/K	163
Crystal system	monoclinic
Space group	C2/c
a/Å	22.6217(5)
b/Å	20.8294(4)
c/Å	16.0998(3)
α/°	90.00
β/°	102.015(2)
γ/°	90.00
Volume/Å^3	7420.0(3)
Z	8
ρcalc mg/mm^3	1.351
Absorption coefficient /mm^{-1}	0.563
F(000)	3056.0
Crystal size/mm^3	0.2773 × 0.1677 × 0.1
2Θ range for data collection	6.14 to 55.12°
Index ranges	$-29 \leq h \leq 29$, $-27 \leq k \leq 27$, $-20 \leq l \leq 20$
Reflections collected	50183
Independent reflections	8561[R(int) = 0.0291]
Data/restraints/parameters	8561/0/425
Goodness-of-fit on F2	1.113
Final R indexes [$I \geq 2\sigma(I)$]	$R_1 = 0.0262$, $wR_2 = 0.0738$
Final R indexes [all data]	$R_1 = 0.0286$, $wR_2 = 0.0749$
Largest diff. peak/hole / e Å^{-3}	0.41/-0.42

Complex ^{13}C-22^{H,H}

Identification code	jml1009m
Empirical formula	$C_{37}H_{33}Cl_2F_6NP_2Ru$
Formula weight	839.55
Temperature/K	110(2)
Crystal system	Triclinic
Space group	P-1
a/Å	11.3140(6)
b/Å	12.9363(7)
c/Å	13.8288(7)
α/°	78.9050(10)
β/°	66.3940(10)
γ/°	70.5150(10)
Volume/Å^3	1744.35(16)
Z	2
ρcalc mg/mm^3	1.598
Absorption coefficient /mm^{-1}	0.756
F(000)	848
Crystal size/mm^3	0.32 x 0.24 x 0.22
2Θ range for data collection	1.61 to 30.01
Index ranges	-15<=h<=15, -18<=k<=18, -19<=l<=19
Reflections collected	19943
Independent reflections	9826 [R(int) = 0.0225]
Data/restraints/parameters	9826 / 0 / 449
Goodness-of-fit on F2	1.041
Final R indexes [I ≥ 2σ (I)]	R1 = 0.0341, wR2 = 0.0794
Final R indexes [all data]	R1 = 0.0410, wR2 = 0.0835
Largest diff. peak/hole / e Å^{-3}	0.818 and -0.

Complex 22[H,F]

Identification code	jml1114
Empirical formula	$C_{37}H_{32}Cl_2F_7NP_2Ru$
Formula weight	857.55
Temperature/K	110.0
Crystal system	triclinic
Space group	P1
a/Å	8.3978(5)
b/Å	10.6030(5)
c/Å	11.0593(6)
α/°	64.034(5)
β/°	83.156(4)
γ/°	86.664(4)
Volume/Å^3	879.00(8)
Z	1
ρcalc mg/mm^3	1.620
Absorption coefficient /mm^{-1}	0.756
F(000)	432
Crystal size/mm^3	0.187 × 0.138 × 0.119
2Θ range for data collection	6.06 to 64.36°
Index ranges	$-12 \leq h \leq 12$, $-15 \leq k \leq 14$, $-16 \leq l \leq 16$
Reflections collected	21591
Independent reflections	11047[R(int) = 0.0266]
Data/restraints/parameters	11047/3/487
Goodness-of-fit on F2	1.030
Final R indexes [$I \geq 2\sigma(I)$]	$R_1 = 0.0283$, $wR_2 = 0.0653$
Final R indexes [all data]	$R_1 = 0.0292$, $wR_2 = 0.0662$
Largest diff. peak/hole / e Å^{-3}	0.924/-0.505

Complex $22^{H,CF3}$

Identification code	jml1121
Empirical formula	$C_{38}H_{32}Cl_2F_9NP_2Ru$
Formula weight	907.56
Temperature/K	110.0
Crystal system	monoclinic
Space group	$P2_1/n$
a/Å	10.7329(3)
b/Å	18.4072(4)
c/Å	18.7217(5)
α/°	90.00
β/°	91.511(3)
γ/°	90.00
Volume/Å^3	3697.43(15)
Z	4
ρcalc mg/mm^3	1.630
Absorption coefficient /mm^{-1}	0.731
F(000)	1824
Crystal size/mm^3	0.1595 × 0.1051 × 0.0832
2Θ range for data collection	6.12 to 55.9°
Index ranges	$-6 \leq h \leq 14$, $-24 \leq k \leq 22$, $-24 \leq l \leq 22$
Reflections collected	14730
Independent reflections	7417[R(int) = 0.0257]
Data/restraints/parameters	7417/0/478
Goodness-of-fit on F2	1.031
Final R indexes [$I \geq 2\sigma$ (I)]	$R_1 = 0.0374$, $wR_2 = 0.0759$
Final R indexes [all data]	$R_1 = 0.0503$, $wR_2 = 0.0817$
Largest diff. peak/hole / e Å^{-3}	0.916/-1.175

Complex $22^{Me,H}$

Identification code	jml1109
Empirical formula	C38H35Cl2F6NP2Ru
Formula weight	853.58
Temperature/K	110.0
Crystal system	monoclinic
Space group	C2/c
a/Å	33.6565(11)
b/Å	10.6213(2)
c/Å	20.3430(5)
α/°	90.00
β/°	94.793(3)
γ/°	90.00
Volume/Å3	7246.7(3)
Z	8
ρcalc mg/mm3	1.565
Absorption coefficient /mm-1	0.729
F(000)	3456
Crystal size/mm3	0.1972 × 0.0674 × 0.0466
2Θ range for data collection	6.46 to 64.08°
Index ranges	$-49 \leq h \leq 45$, $-15 \leq k \leq 15$, $-16 \leq l \leq 30$
Reflections collected	20757
Independent reflections	11366[R(int) = 0.0255]
Data/restraints/parameters	11366/0/507
Goodness-of-fit on F2	1.046
Final R indexes [$I \geq 2\sigma$ (I)]	R1 = 0.0379, wR2 = 0.0805
Final R indexes [all data]	R1 = 0.0513, wR2 = 0.0867
Largest diff. peak/hole / e Å-3	1.015/-1.016

Complex 22^{Me,CF3}

Identification code	jml1131
Empirical formula	$C_{38}H_{32}F_9NP_2Ru$
Formula weight	836.66
Temperature/K	109.95(10)
Crystal system	triclinic
Space group	P-1
a/Å	10.3542(5)
b/Å	17.2739(9)
c/Å	21.0852(8)
α/°	106.932(4)
β/°	91.081(4)
γ/°	103.714(4)
Volume/Å^3	3489.2(3)
Z	4
ρcalc mg/mm^3	1.593
Absorption coefficient /mm^{-1}	0.619
F(000)	1688.0
Crystal size/mm^3	0.2067 × 0.0925 × 0.0908
2Θ range for data collection	5.94 to 52.04°
Index ranges	$-12 \leq h \leq 12$, $-15 \leq k \leq 21$, $-26 \leq l \leq 25$
Reflections collected	26595
Independent reflections	13557[R(int) = 0.0355]
Data/restraints/parameters	13557/0/937
Goodness-of-fit on F2	1.143
Final R indexes [$I \geq 2\sigma$ (I)]	R_1 = 0.0538, wR_2 = 0.1107
Final R indexes [all data]	R_1 = 0.0681, wR_2 = 0.1175
Largest diff. peak/hole / e Å^{-3}	1.19/-0.90

Complex $22^{NMe2,H}$

Identification code	jml1124
Empirical formula	$C_{39.5}H_{39}Cl_3F_6N_2P_2Ru$
Formula weight	925.09
Temperature/K	110.0
Crystal system	triclinic
Space group	P-1
a/Å	9.8503(5)
b/Å	13.2838(7)
c/Å	14.6501(8)
α/°	90.431(4)
β/°	91.645(4)
γ/°	91.027(4)
Volume/$Å^3$	1915.80(18)
Z	2
ρcalc mg/mm^3	1.604
Absorption coefficient /mm^{-1}	0.764
F(000)	938
Crystal size/mm^3	0.2459 × 0.1692 × 0.1157
2Θ range for data collection	5.76 to 64.3°
Index ranges	$-14 \leq h \leq 14$, $-19 \leq k \leq 18$, $-21 \leq l \leq 21$
Reflections collected	44826
Independent reflections	12496[R(int) = 0.0380]
Data/restraints/parameters	12496/7/507
Goodness-of-fit on F2	1.112
Final R indexes [$I \geq 2\sigma$ (I)]	R1 = 0.0405, wR2 = 0.1089
Final R indexes [all data]	R1 = 0.0465, wR2 = 0.1129
Largest diff. peak/hole / e $Å^{-3}$	1.213/-2.088

Complex 27a^{CF3}

Identification code	jml1217_twin1_hklf4
Empirical formula	$C_{38}H_{32}F_9NP_2Ru$
Formula weight	836.66
Temperature/K	110.00(10)
Crystal system	triclinic
Space group	P-1
a/Å	10.2610(3)
b/Å	17.4414(10)
c/Å	20.2361(11)
α/°	105.462(5)
β/°	90.076(4)
γ/°	101.595(4)
Volume/Å^3	3413.5(3)
Z	4
ρcalc mg/mm^3	1.628
Absorption coefficient /mm^{-1}	0.633
F(000)	1688.0
Crystal size/mm^3	0.337 × 0.0855 × 0.0594
2Θ range for data collection	5.68 to 57.16°
Index ranges	$-13 \leq h \leq 13$, $-22 \leq k \leq 23$, $-26 \leq l \leq 27$
Reflections collected	16509
Independent reflections	16513[R(int) = 0.0000]
Data/restraints/parameters	16513/6/922
Goodness-of-fit on F2	1.026
Final R indexes [$I \geq 2\sigma$ (I)]	R_1 = 0.0608, wR_2 = 0.1575
Final R indexes [all data]	R_1 = 0.0753, wR_2 = 0.1659
Largest diff. peak/hole / e Å^{-3}	1.60/-1.64

Complex $30^{H,H}$

Identification code	jml1233
Empirical formula	$C_{21}H_{25}F_6NP_2Ru$
Formula weight	568.43
Temperature/K	110.00(10)
Crystal system	monoclinic
Space group	$P2_1/c$
a/Å	9.98423(13)
b/Å	12.43212(12)
c/Å	18.40289(18)
α/°	90.00
β/°	104.5013(11)
γ/°	90.00
Volume/Å^3	2211.49(4)
Z	4
ρcalc mg/mm^3	1.707
Absorption coefficient /mm^{-1}	0.913
F(000)	1144.0
Crystal size/mm^3	0.2077 × 0.1435 × 0.12
2Θ range for data collection	6.2 to 64.6°
Index ranges	$-14 \leq h \leq 14$, $-17 \leq k \leq 17$, $-27 \leq l \leq 26$
Reflections collected	20877
Independent reflections	7196[R(int) = 0.0249]
Data/restraints/parameters	7196/0/338
Goodness-of-fit on F2	1.075
Final R indexes [$I \geq 2\sigma$ (I)]	$R_1 = 0.0334$, $wR_2 = 0.0798$
Final R indexes [all data]	$R_1 = 0.0398$, $wR_2 = 0.0838$
Largest diff. peak/hole / e Å^{-3}	2.83/-0.52

Complex $30^{NMe2,H}$

Identification code	jml1208a
Empirical formula	$C_{23}H_{30}F_6N_2P_2Ru$
Formula weight	611.50
Temperature/K	110.00(10)
Crystal system	triclinic
Space group	P-1
a/Å	10.3293(6)
b/Å	11.3493(6)
c/Å	13.1950(9)
α/°	65.248(6)
β/°	86.687(5)
γ/°	63.432(5)
Volume/Å^3	1240.32(16)
Z	2
ρcalc mg/mm^3	1.637
Absorption coefficient /mm^{-1}	0.821
F(000)	620.0
Crystal size/mm^3	0.3231 × 0.2145 × 0.0974
2Θ range for data collection	6.06 to 64.2°
Index ranges	$-13 \leq h \leq 14$, $-16 \leq k \leq 15$, $-18 \leq l \leq 17$
Reflections collected	12816
Independent reflections	7729[R(int) = 0.0197]
Data/restraints/parameters	7729/117/492
Goodness-of-fit on F2	1.124
Final R indexes [$I \geq 2\sigma$ (I)]	$R_1 = 0.0307$, $wR_2 = 0.0736$
Final R indexes [all data]	$R_1 = 0.0354$, $wR_2 = 0.0767$
Largest diff. peak/hole / e Å^{-3}	0.92/-0.87

Complex $30^{H,CF3}$

Identification code	jml1128
Empirical formula	$C_{40}H_{36}F_3NPRu$
Formula weight	719.74
Temperature/K	110.0
Crystal system	monoclinic
Space group	$P2_1/c$
a/Å	12.3602(11)
b/Å	15.4872(11)
c/Å	17.2133(10)
α/°	90.00
β/°	96.724(6)
γ/°	90.00
Volume/$Å^3$	3272.4(4)
Z	4
ρcalc mg/mm^3	1.461
Absorption coefficient /mm^{-1}	0.575
F(000)	1476
Crystal size/mm^3	0.1905 × 0.0984 × 0.0429
2Θ range for data collection	6.52 to 61.18°
Index ranges	$-15 \leq h \leq 16$, $-19 \leq k \leq 20$, $-17 \leq l \leq 24$
Reflections collected	17427
Independent reflections	8791[R(int) = 0.0327]
Data/restraints/parameters	8791/0/436
Goodness-of-fit on F2	1.059
Final R indexes [$I \geq 2\sigma(I)$]	$R_1 = 0.0360$, $wR_2 = 0.0812$
Final R indexes [all data]	$R_1 = 0.0482$, $wR_2 = 0.0879$
Largest diff. peak/hole / e $Å^{-3}$	0.776/-0.869

Complex 30^{NMe2,CF3}

Identification code	jml1138
Empirical formula	$C_{38}H_{31}F_3NPRu$
Formula weight	690.68
Temperature/K	110.00(10)
Crystal system	monoclinic
Space group	P21/c
a/Å	11.6354(2)
b/Å	16.8259(4)
c/Å	17.0044(3)
α/°	90.00
β/°	97.6003(18)
γ/°	90.00
Volume/Å3	3299.82(11)
Z	4
ρcalc mg/mm3	1.390
Absorption coefficient /mm-1	0.567
F(000)	1408
Crystal size/mm3	0.1817 × 0.0935 × 0.0894
2Θ range for data collection	6 to 60.14°
Index ranges	$-15 \leq h \leq 15, 0 \leq k \leq 23, 0 \leq l \leq 23$
Reflections collected	8152
Independent reflections	8152[R(int) = 0.0000]
Data/restraints/parameters	8152/0/402
Goodness-of-fit on F2	1.171
Final R indexes [$I \geq 2\sigma$ (I)]	R1 = 0.0728, wR2 = 0.1799
Final R indexes [all data]	R1 = 0.0932, wR2 = 0.1892
Largest diff. peak/hole / e Å-3	1.308/-1.234

Unexpected structure from 2-methylpyridine ligand

Identification code	jml1324
Empirical formula	$C_{35}H_{40}F_6N_2P_2Ru$
Formula weight	765.70
Temperature/K	110.00(10)
Crystal system	monoclinic
Space group	$P2_1/n$
a/Å	11.0042(2)
b/Å	17.9480(3)
c/Å	17.2178(3)
α/°	90.00
β/°	104.374(2)
γ/°	90.00
Volume/Å^3	3294.13(10)
Z	4
ρcalc mg/mm^3	1.544
Absorption coefficient /mm^{-1}	0.636
F(000)	1568.0
Crystal size/mm^3	0.1138 × 0.1037 × 0.0325
2Θ range for data collection	5.86 to 58.88°
Index ranges	$-10 \leq h \leq 15$, $-23 \leq k \leq 21$, $-23 \leq l \leq 23$
Reflections collected	15635
Independent reflections	7827[R(int) = 0.0299]
Data/restraints/parameters	7827/0/416
Goodness-of-fit on F2	1.028
Final R indexes [$I \geq 2\sigma$ (I)]	$R_1 = 0.0405$, $wR_2 = 0.0896$
Final R indexes [all data]	$R_1 = 0.0516$, $wR_2 = 0.0962$
Largest diff. peak/hole / e Å^{-3}	0.85/-0.76

Definitions

Abbreviations

Å	Angstroms
dppm	Bis(diphenylphosphino)methane
dppe	1,2-Bis(diphenylphosphino)ethane
d	Doublet
δ_c	Carbon Chemical Shift
CO	Carbon Monoxide
PNP	$CH_3CH_2CH_2N(CH_2CH_2PPh_2)_2$
COSY	Correlation Spectroscopy
Cy	Cyclohexane
COD	Cyclooctadiene
η^5-C_5H_5	Cyclopentadienyl
DABCO	1,4-Diazabicyclo[2.2.2]octane
$Tp^{Ms"}$	Dimetallated Hydrotris(3-mesitylpyrazol-1-yl)borate
dd	Doublet of Doublets
DFT	Density Functional Theory
DMSO	Dimethyl Sulphoxide
EI	Electron Impact
equiv.	Equivalents
ESD	Estimated Standard Deviation
ESI	Electrospray Ionisation
FT-IR	Fourier Transform Infra Red
σ_p	Hammett substituent effect
Hz	Hertz
HMBC	Heteronuclear Multiple Bond Correlation
HMQC	Heteronuclear Multiple Quantum Correlation
HOMO	Highest Occupied Molecular Orbital
Tp	Hydridotris(pyrazolyl)borate)
δ_H	Hydrogen Chemical Shift
H	Hydrogen
Tp^{Me2}	Hydrotris(3,5-dimethylpyrazolyl) borate
^{i}Pr	*iso*-Propyl
K	Kelvin

kJ	Kilojoules
L	Ligand
L	Litres
LUMO	Lowest Unoccupied Molecular Orbital
M	Metal
m/z	Mass / Charge
MHz	Megahertz
$Cp^{\wedge}$	η^5-1-Methoxy-2,4-*tert*-butyl-3-neopentyl-cyclopentadienyl
Me	Methyl
μ(prefix)	Micro
min	Minutes
m(prefix)	Milli
mg	Milligram
mol	Moles
m	Multiplet
MS	Mass Spectrometry
NHC	N-Heterocyclic Carbene
NMR	Nuclear Magnetic Resonance
NOESY	Nuclear Overhauser Effect Spectroscopy
ppm	Parts Per Million
η^5-C_5Me_5	Pentamethylcyclopentadienyl
δ_P	Phosphorus Chemical Shift
q	Quartet
s	Singlet
^{t}Bu	*tert*-Butyl
TLC	Thin layer chromatography
TMS	Trimethylsilyl
t	Triplet
VT	Variable Temperature
cm^{-1}	Wavenumber
σ-CAM	Sigma-Complex Assisted Metathesis

Diagram Labels

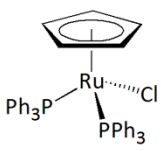

1

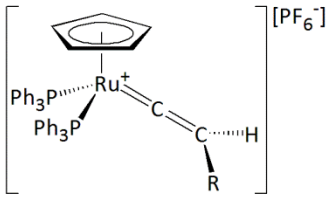

2^{R}

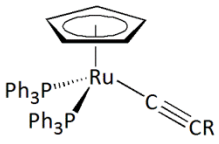

3^{R}

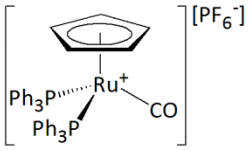

4

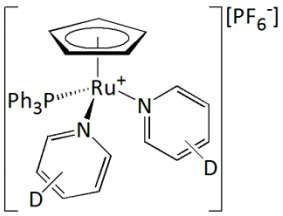

5

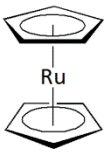

6

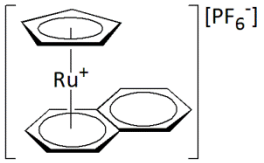

7

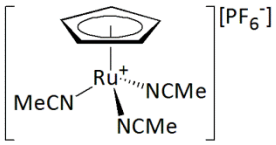

8

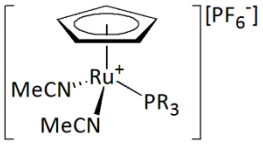

9^{R}

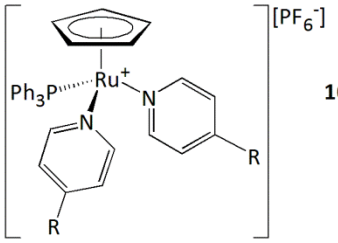

10^{R}

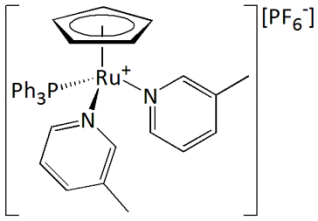

11

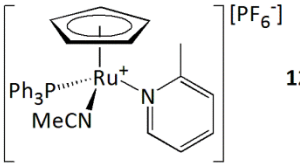

12

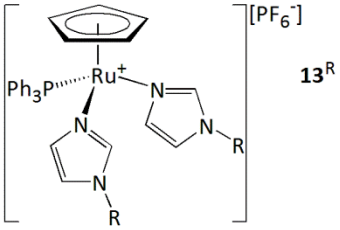

13^{R}

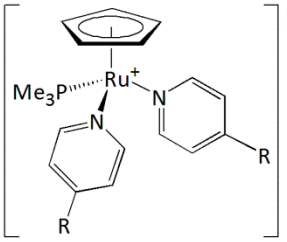

14^{R}

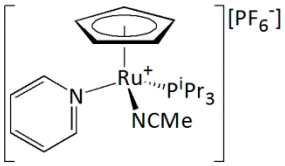

15

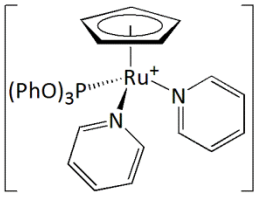

16

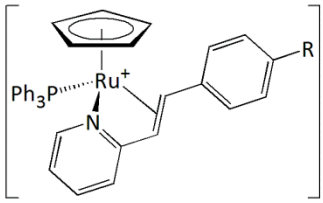

17^{R}

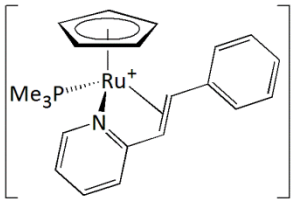

18

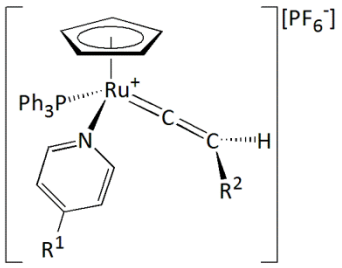

19^{R1,R2}

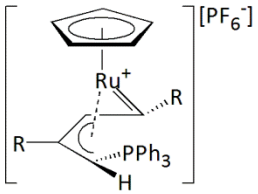

20^{R}

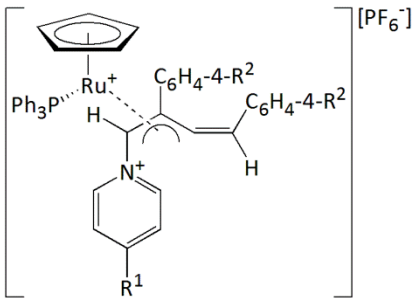

21^{R1,R2}

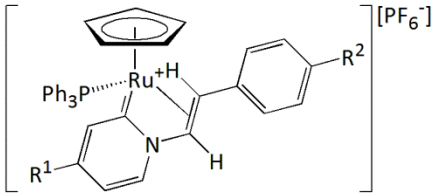

22^{R1,R2}

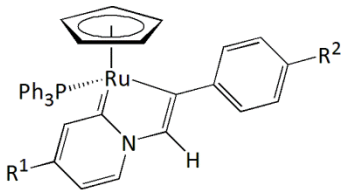

23^{R1,R2}

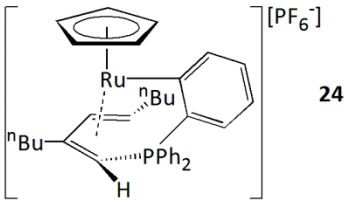

24

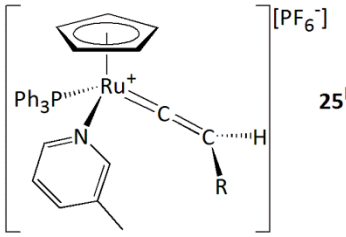

25^{R}

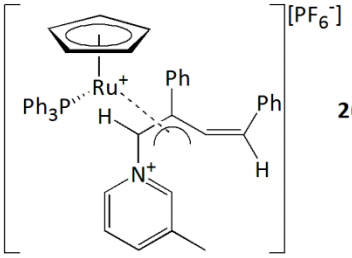

26

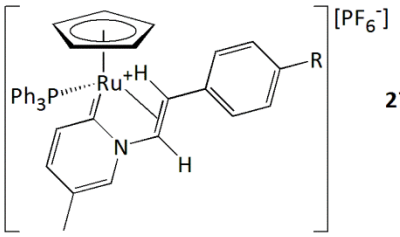

27a^{R}

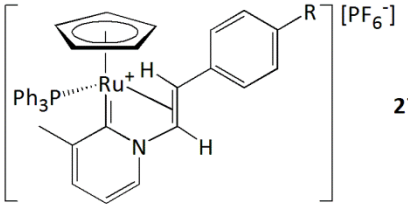

27b^{R}

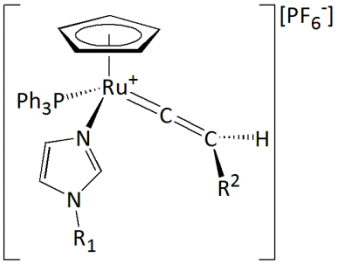

28^{R1,R2}

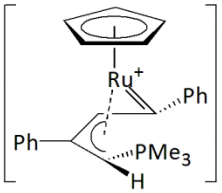

29

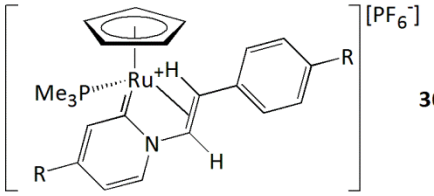

30^{R1,R2}

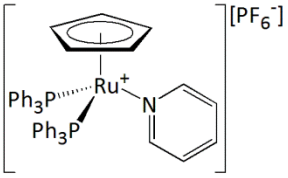

31

References

1. B. M. Trost, *Acc. Chem. Res.*, 2002, **35**, 695.
2. B. M. Trost, *Science*, 1991, **254**, 1471.
3. S. L. Y. Tang, R. L. Smith and M. Poliakoff, *Green Chem.*, 2005, **7**, 761.
4. J. A. Labinger and J. E. Bercaw, *Nature*, 2002, **417**, 507.
5. S. Murai, F. Kakiuchi, S. Sekine, Y. Tanaka, A. Kamatani, M. Sonoda and N. Chatani, *Nature*, 1993, **366**, 529.
6. K. Godula and D. Sames, *Science*, 2006, **312**, 67.
7. F. Kakiuchi and N. Chatani, *Adv. Synth. Catal.*, 2003, **345**, 1077.
8. A. D. Ryabov, *Chem. Rev.*, 1990, **90**, 403.
9. http://www.nobelprize.org/nobel_prizes/lists/all/, on 14/07/2013.
10. T. M. Trnka and R. H. Grubbs, *Acc. Chem. Res.*, 2001, **34**, 18.
11. D. Astruc, *New J. Chem.*, 2005, **29**, 42.
12. P. H. Deshmukh and S. Blechert, *Dalton Trans.*, 2007, 2479.
13. C. C. C. J. Seechurn, M. O. Kitching, T. J. Colacot and V. Snieckus, *Angew. Chem. Int. Ed.*, 2012, **51**, 5062.
14. X.-F. Wu, P. Anbarasan, H. Neumann and M. Beller, *Angew. Chem. Int. Ed.*, 2010, **49**, 9047.
15. L.-C. Campeau and K. Fagnou, *Chem. Soc. Rev.*, 2007, **36**, 1058.
16. A. Togni and L. M. Venanzi, *Angew. Chem. Int. Ed.*, 1994, **33**, 497.
17. P. Atkins, T. Overton, J. Rourke, M. Weller and F. Armstrong, *Inorganic Chemistry*, Fourth Edition edn., 2006.
18. P. B. Dias, M. E. M. Depiedade and J. A. M. Simoes, *Coord. Chem. Rev.*, 1994, **135**, 737.
19. A. G. Orpen and N. G. Connelly, *Organometallics*, 1990, **9**, 1206.
20. C. A. Tolman, *Chem. Rev.*, 1977, **77**, 313.
21. C. A. Tolman, *J. Am. Chem. Soc.*, 1970, **92**, 2953.
22. C. A. Tolman, *J. Am. Chem. Soc.*, 1970, **92**, 2956.
23. T. L. Brown and K. J. Lee, *Coord. Chem. Rev.*, 1993, **128**, 89.
24. D. Gusev, *Organometallics*, 2009, **28**, 763.
25. P. Atkins and J. D. Paula, *Physical Chemistry*, Eight edn., 2006.
26. H. Schumann, M. Speis, W. P. Bosman, J. M. M. Smits and P. T. Beurskens, *J. Organomet. Chem.*, 1991, **403**, 165.
27. M. Berthelot, C. Laurence, M. Safar and F. Besseau, *J. Chem. Soc. Perkin Trans. 2*, 1998, 283.
28. A. Bauza, D. Quinonero, A. Frontera and P. M. Deya, *Phys. Chem. Chem. Phys.*, 2011, **13**, 20371.
29. J. Clayden, N. Greeves, S. Warren and P. Wothers, *Organic Chemistry*, 2001.
30. B. C. and D. P., *Metal Vinylidenes and Allenylidenes in Catalysis*, First edn., 2008.
31. M. I. Bruce, *Chem. Rev.*, 1991, **91**, 197.
32. K. M. Ervin, S. Gronert, S. E. Barlow, M. K. Gilles, A. G. Harrison, V. M. Bierbaum, C. H. Depuy, W. C. Lineberger and G. B. Ellison, *J. Am. Chem. Soc.*, 1990, **112**, 5750.
33. R. P. Duran, V. T. Amorebieta and A. J. Colussi, *J. Am. Chem. Soc.*, 1987, **109**, 3154.
34. M. M. Gallo, T. P. Hamilton and H. F. Schaefer, *J. Am. Chem. Soc.*, 1990, **112**, 8714.
35. J. Silvestre and R. Hoffmann, *Helv. Chim. Acta*, 1985, **68**, 1461.

36. P. J. Stang, *Acc. Chem. Res.*, 1982, **15**, 348.
37. P. J. Stang, *Chem. Rev.*, 1978, **78**, 383.
38. B. Solaja, J. Huguet, M. Karpf and A. S. Dreiding, *Tetrahedron*, 1987, **43**, 4875.
39. J. Ackroyd, M. Karpf and A. S. Dreiding, *Helv. Chim. Acta*, 1984, **67**, 1963.
40. B. M. Trost, M. U. Frederiksen and M. T. Rudd, *Angew. Chem. Int. Ed.*, 2005, **44**, 6630.
41. K. H. Dotz, *Angew. Chem. Int. Ed. Eng.*, 1984, **23**, 587.
42. A. B. Antonova, N. E. Kolobova, P. V. Petrovsky, B. V. Lokshin and N. S. Obezyuk, *J. Organomet. Chem.*, 1977, **137**, 55.
43. C. Bruneau and P. H. Dixneuf, *Acc. Chem. Res*, 1999, **32**, 311.
44. H. Katayama and F. Ozawa, *Coord. Chem. Rev.*, 2004, **248**, 1703.
45. J. M. Lynam, *Chem. Eur. J.*, 2010, **16**, 8238.
46. B. M. Trost, *Angew. Chem. Int. Ed. Engl.*, 1995, **34**, 259.
47. V. Cadierno, M. P. Gamasa and J. Gimeno, *Coord. Chem. Rev.*, 2004, **248**, 1627.
48. R. R. Schrock, *Acc. Chem. Res.*, 1979, **12**, 98.
49. E. O. Fischer and A. Maasbol, *Angew. Chem. Int. Ed.*, 1964, **3**, 580.
50. Y. Wakatsuki, *J. Organomet. Chem.*, 2004, **689**, 4092.
51. F. Delbecq, *J. Organomet. Chem.*, 1991, **406**, 171.
52. N. M. Kostic and R. F. Fenske, *Organometallics*, 1982, **1**, 974.
53. H. Werner, *Angew. Chem. Int. Ed. Engl*, 1990, **29**, 1077.
54. M. I. Bruce and R. C. Wallis, *Aust. J. Chem.*, 1979, **32**, 1471.
55. P. T. Czech, X. Q. Ye and R. F. Fenske, *Organometallics*, 1990, **9**, 2016.
56. O. M. Abusalah and M. I. Bruce, *J. Chem. Soc. Dalton Trans.*, 1975, 2311.
57. C. W. Chang, Y. C. Lin, G. H. Lee, S. L. Huang and Y. Wang, *Organometallics*, 1998, **17**, 2534.
58. K. H. Chen, Y. J. Feng, H. W. Ma, Y. C. Lin, Y. H. Liu and T. S. Kuo, *Organometallics*, 2010, **29**, 6829.
59. P. C. Ting, Y. C. Lin, G. H. Lee, M. C. Cheng and Y. Wang, *J. Am. Chem. Soc.*, 1996, **118**, 6433.
60. M. Bassetti, V. Cadierno, J. Gimeno and C. Pasquini, *Organometallics*, 2008, **27**, 5009.
61. V. Cadierno, M. P. Gamasa, J. Gimeno, E. Perez-Carreno and S. Garcia-Granda, *J. Organomet. Chem.*, 2003, **670**, 75.
62. V. Cadierno, M. P. Gamasa and J. Gimeno, *J. Organomet. Chem.*, 2001, **621**, 39.
63. V. Cadierno, M. P. Gamasa, J. Gimeno, E. Perez-Carreno and S. Garcia-Granda, *Organometallics*, 1999, **18**, 2821.
64. Y. Wakatsuki, N. Koga, H. Yamazaki and K. Morokuma, *J. Am. Chem. Soc.*, 1994, **116**, 8105.
65. F. De Angelis, A. Sgamellotti and N. Re, *Organometallics*, 2002, **21**, 2715.
66. F. De Angelis, A. Sgamellotti and N. Re, *Organometallics*, 2002, **21**, 5944.
67. F. De Angelis, A. Sgamellotti and N. Re, *Dalton Trans.*, 2004, 3225.
68. I. D. I. Rios, M. J. Tenorio, M. C. Puerta and P. Valerga, *J. Chem. Soc. Chem. Commun.*, 1995, 1757.
69. I. deLosRios, M. J. Tenorio, M. C. Puerta and P. Valerga, *Journal of the American Chemical Society*, 1997, **119**, 6529-6538.
70. E. Bustelo, I. de los Rios, M. J. Tenorio, M. C. Puerta and P. Valerga, *Monatsh. Chem.*, 2000, **131**, 1311.
71. H. Aneetha, M. Jimenez-Tenorio, M. C. Puerta, P. Valerga and K. Mereiter, *Organometallics*, 2003, **22**, 2001.

72. E. Bustelo, J. J. Carbo, A. Lledos, K. Mereiter, M. C. Puerta and P. Valerga, *J. Am. Chem. Soc.*, 2003, **125**, 3311.
73. M. Jimenez-Tenorio, M. D. Palacios, M. C. Puerta and P. Valerga, *J. Organomet. Chem.*, 2004, **689**, 2853.
74. M. Olivan, E. Clot, O. Eisenstein and K. G. Caulton, *Organometallics*, 1998, **17**, 3091.
75. M. Arndt, K. S. M. Salih, A. Fromm, L. J. Goossen, F. Menges and G. Niedner-Schatteburg, *J. Am. Chem. Soc.*, 2011, **133**, 7428.
76. M. Tokunaga, T. Suzuki, N. Koga, T. Fukushima, A. Horiuchi and Y. Wakatsuki, *J. Am. Chem. Soc.*, 2001, **123**, 11917.
77. H. Katayama, C. Wada, K. Taniguchi and F. Ozawa, *Organometallics*, 2002, **21**, 3285.
78. I. de los Rios, E. Bustelo, M. Carmen Puerta and P. Valerga, *Organometallics*, 2010, **29**, 1740.
79. V. K. Singh, E. Bustelo, I. de los Rios, I. Macias-Arce, M. Carmen Puerta, P. Valerga, M. Angel Ortuno, G. Ujaque and A. Lledos, *Organometallics*, 2011, **30**, 4014.
80. C. Bruneau and P. H. Dixneuf, *Angew. Chem. Int. Ed.*, 2006, **45**, 2176.
81. M. C. Puerta and P. Valerga, *Coord. Chem. Rev.*, 1999, **193**, 977.
82. T. Naota, H. Takaya and S. I. Murahashi, *Chem. Rev.*, 1998, **98**, 2599.
83. Y. Wakatsuki, Z. M. Hou and M. Tokunaga, *Chem. Rec.*, 2003, **3**, 144.
84. C. Bianchini, M. Peruzzini, F. Zanobini, P. Frediani and A. Albinati, *J. Am. Chem. Soc.*, 1991, **113**, 5453.
85. C. S. Yi and N. H. Liu, *Organometallics*, 1996, **15**, 3968.
86. J.-H. Lee and K. G. Caulton, *J. Organomet. Chem.*, 2008, **693**, 1664.
87. M. Bassetti, C. Pasquini, A. Raneri and D. Rosato, *J. Org. Chem.*, 2007, **72**, 4558.
88. H. Katayama, M. Nakayama, T. Nakano, C. Wada, K. Akamatsu and F. Ozawa, *Macromolecules*, 2004, **37**, 13.
89. C. Bianchini, P. Innocenti, M. Peruzzini, A. Romerosa and F. Zanobini, *Organometallics*, 1996, **15**, 272.
90. C. Slugovc, D. Doberer, C. Gemel, R. Schmid, K. Kirchner, B. Winkler and F. Stelzer, *Monatsh. Chem.*, 1998, **129**, 221.
91. X. G. Chen, P. Xue, H. H. Y. Sung, I. D. Williams, M. Peruzzini, C. Bianchini and G. C. Jia, *Organometallics*, 2005, **24**, 4330.
92. J. Tripathy and M. Bhattacharjee, *Tetrahedron Lett.*, 2009, **50**, 4863.
93. B. O. Ozturk, S. Karabulut and Y. Imamoglu, *Appl. Catal., A*, 2012, **433**, 214.
94. C. Bianchini, P. Frediani, D. Masi, M. Peruzzini and F. Zanobini, *Organometallics*, 1994, **13**, 4616.
95. G. C. Jia, A. L. Rheingold and D. W. Meek, *Organometallics*, 1989, **8**, 1378.
96. J. M. Lynam, T. D. Nixon and A. C. Whitwood, *J. Organomet. Chem.*, 2008, **693**, 3103.
97. G. Dominguez and J. Perez-Castells, *Chem. Soc. Rev.*, 2011, **40**, 3430.
98. S. Medina, G. Dominguez and J. Perez-Castells, *Org. Lett.*, 2012, **14**, 4982.
99. Y. Yamamoto, H. Kitahara, R. Ogawa, H. Kawaguchi, K. Tatsumi and K. Itoh, *J. Am. Chem. Soc.*, 2000, **122**, 4310.
100. B. Dutta, B. F. E. Curchod, P. Campomanes, E. Solari, R. Scopelliti, U. Rothlisberger and K. Severin, *Chem. Eur. J.*, 2010, **16**, 8400.
101. D. S. Perekalin, E. A. Trifonova, P. V. Petrovskii and A. R. Kudinov, *Russ. Chem. Bull.*, 2012, **60**, 2110.
102. J. A. Varela and C. Saa, *J. Organomet. Chem.*, 2009, **694**, 143.

103. K. Kirchner, M. J. Calhorda, R. Schmid and L. F. Veiros, *J. Am. Chem. Soc.*, 2003, **125**, 11721.
104. Y. Yamamoto, T. Arakawa, R. Ogawa and K. Itoh, *J. Am. Chem. Soc.*, 2003, **125**, 12143.
105. S. Sanz, L. A. Jones, F. Mohr and M. Laguna, *Organometallics*, 2007, **26**, 952.
106. R. Casado, M. Contel, M. Laguna, P. Romero and S. Sanz, *J. Am. Chem. Soc.*, 2003, **125**, 11925.
107. G. Dong, P. Teo, Z. K. Wickens and R. H. Grubbs, *Science*, 2011, **333**, 1609.
108. M. Tokunaga and Y. Wakatsuki, *Angew. Chem. Int. Ed. Engl.*, 1998, **37**, 2867.
109. T. Suzuki, M. Tokunaga and Y. Wakatsuki, *Org. Lett.*, 2001, **3**, 735.
110. D. B. Grotjahn, *Dalton Trans.*, 2008, 6497.
111. D. B. Grotjahn and D. A. Lev, *J. Am. Chem. Soc*, 2004, **126**, 12232.
112. F. Chevallier and B. Breit, *Angew. Chem. Int. Ed. Engl.*, 2006, **45**, 1599.
113. A. Labonne, T. Kribber and L. Hintermann, *Org. Lett.*, 2006, **8**, 5853.
114. www.sigmaaldrich.com/catalog/product/aldrich/673307?lang=en& `region =GB, on 26/04/2013.
115. D. B. Grotjahn, C. D. Incarvito and A. L. Rheingold, *Angew. Chem. Int. Ed. Engl.*, 2001, **40**, 3884.
116. D. B. Grotjahn, V. Miranda-Soto, E. J. Kragulj, D. A. Lev, G. Erdogan, X. Zeng and A. L. Cooksy, *J. Am. Chem. Soc.*, 2008, **130**, 20.
117. D. B. Grotjahn, *Chem. Eur. J.*, 2005, **11**, 7146.
118. D. B. Grotjahn, *Top. Catal.*, 2010, **53**, 1009.
119. J. M. Oconnor and L. Pu, *J. Am. Chem. Soc.*, 1990, **112**, 9013.
120. C. Bianchini, J. A. Casares, M. Peruzzini, A. Romerosa and F. Zanobini, *J. Am. Chem. Soc.*, 1996, **118**, 4585.
121. Y. Fukumoto, T. Dohi, H. Masaoka, N. Chatani and S. Murai, *Organometallics*, 2002, **21**, 3845.
122. F. E. McDonald and A. K. Chatterjee, *Tetrahedron Lett.*, 1997, **38**, 7687.
123. L. J. Goossen, J. E. Rauhaus and G. J. Deng, *Angew. Chem. Int. Ed.*, 2005, **44**, 4042.
124. P.-Y. Chiang, Y.-C. Lin, Y. Wang and Y.-H. Liu, *Organometallics*, 2010, **29**, 5776.
125. D. R. Carbery, *Org. Biomol. Chem.*, 2008, **6**, 3455.
126. C. Gemel, V. N. Sapunov, K. Mereiter, M. Ferencic, R. Schmid and K. Kirchner, *Inorg. Chim. Act.*, 1999, **286**, 114.
127. W. W. Seidel, W. Dachtler and T. Pape, *Z. Anorg. Allg. Chem.*, 2012, **638**, 116.
128. A. L. Osipov, D. V. Gutsulyak, L. G. Kuzmina, J. A. K. Howard, D. A. Lemenovskii, G. Suess-Fink and G. I. Nikonov, *J. Organomet. Chem.*, 2007, **692**, 5081.
129. D. V. Gutsulyak, A. van der Est and G. I. Nikonov, *Angew. Chem. Int. Ed. Engl.*, 2011, **50**, 1384.
130. C. M. Standfest-Hauser, K. Mereiter, R. Schmid and K. Kirchner, *Dalton Trans.*, 2003, 2329.
131. E. Ruba, W. Simanko, K. Mauthner, K. M. Soldouzi, C. Slugovc, K. Mereiter, R. Schmid and K. Kirchner, *Organometallics*, 1999, **18**, 3843.
132. E. Ruba, K. Mereiter, R. Schmid, V. N. Sapunov, K. Kirchner, H. Schottenberger, M. J. Calhorda and L. F. Veiros, *Chem. Eur. J.*, 2002, **8**, 3948.
133. E. Becker, C. Slugovc, E. Ruba, C. Standfest-Hauser, K. Mereiter, R. Schmid and K. Kirchner, *J. Organomet. Chem.*, 2002, **649**, 55.
134. C. Slugovc, E. Ruba, R. Schmid, K. Kirchner and K. Mereiter, *Monatsh. Chem.*, 2000, **131**, 1241.

135. W. Luginbuhl, P. Zbinden, P. A. Pittet, T. Armbruster, H. B. Burgi, A. E. Merbach and A. Ludi, *Inorg. Chem.*, 1991, **30**, 2350.
136. K. Mauthner, K. M. Soldouzi, K. Mereiter, R. Schmid and K. Kirchner, *Organometallics*, 1999, **18**, 4681.
137. B. M. Trost and C. M. Older, *Organometallics*, 2002, **21**, 2544.
138. R. Schmid and K. Kirchner, *Eur. J. Inorg. Chem.*, 2004, 2609.
139. E. Ruba, K. Mereiter, R. Schmid, K. Kirchner, E. Bustelo, M. C. Puerta and P. Valerga, *Organometallics*, 2002, **21**, 2912.
140. M. A. Esteruelas, I. Fernandez, A. Herrera, M. Martin-Ortiz, R. Martinez-Alvarez, M. Olivan, E. Onate, M. A. Sierra and M. Valencia, *Organometallics*, 2010, **29**, 976.
141. T. Bolano, M. A. Esteruelas and E. Onate, *J. Organomet. Chem.*, 2011, **696**, 3911.
142. R. Castro-Rodrigo, M. A. Esteruelas, S. Fuertes, A. M. Lopez, S. Mozo and E. Onate, *Organometallics*, 2009, **28**, 5941.
143. M. A. Esteruelas, I. Fernandez, S. Fuertes, A. M. Lopez, E. Onate and M. A. Sierra, *Organometallics*, 2009, **28**, 4876.
144. M. Baya, M. A. Esteruelas, A. I. Gonzalez, A. M. Lopez and E. Onate, *Organometallics*, 2005, **24**, 1225.
145. T. Bolano, R. Castarlenas, M. A. Esteruelas and E. Onate, *J. Am. Chem. Soc.*, 2006, **128**, 3965.
146. Y. Alvarado, P. J. Daff, P. J. Perez, M. L. Poveda, R. SanchezDelgado and E. Carmona, *Organometallics*, 1996, **15**, 2192.
147. F. M. Alias, M. L. Poveda, M. Sellin, E. Carmona, E. Gutierrez-Puebla and A. Monge, *Organometallics*, 1998, **17**, 4124.
148. F. M. Alias, P. J. Daff, M. Paneque, M. L. Poveda, E. Carmona, P. J. Perez, V. Salazar, Y. Alvarado, R. Atencio and R. Sanchez-Delgado, *Chem. Eur. J.*, 2002, **8**, 5132.
149. M. L. Buil, M. A. Esteruelas, A. M. Lopez and E. Onate, *Organometallics*, 2003, **22**, 5274.
150. L. Busetto, C. Camiletti, V. Zanotti, V. G. Alvano and P. Sabatino, *J. Organomet. Chem.*, 2000, **593**, 335.
151. C. M. Crudden and D. P. Allen, *Coord. Chem. Rev.*, 2004, **248**, 2247.
152. A. Furstner, *Angew. Chem. Int. Ed. Engl.*, 2000, **39**, 3012.
153. R. H. Grubbs, *Tetrahedron*, 2004, **60**, 7117.
154. N. M. Scott and S. P. Nolan, *Eur. J. Inorg. Chem.*, 2005, 1815.
155. W. A. Herrmann, *Angew. Chem. Int. Ed. Engl.*, 2002, **41**, 1290.
156. A. J. Arduengo, R. L. Harlow and M. Kline, *J. Am. Chem. Soc.*, 1991, **113**, 361.
157. S. Díez-González, *N-Heterocyclic Carbenes*, Royal Society of Chemistry, 2011.
158. D. Bourissou, O. Guerret, F. P. Gabbai and G. Bertrand, *Chem. Rev.*, 2000, **100**, 39.
159. C. Heinemann, T. Muller, Y. Apeloig and H. Schwarz, *J. Am. Chem. Soc.*, 1996, **118**, 2023.
160. C. Boehme and G. Frenking, *J. Am. Chem. Soc.*, 1996, **118**, 2039.
161. R. Tonner, G. Heydenrych and G. Frenking, *Chem. Asian J.*, 2007, **2**, 1555.
162. L. Cavallo, A. Correa, C. Costabile and H. Jacobsen, *J. Organomet. Chem.*, 2005, **690**, 5407.
163. R. H. Crabtree, *J. Organomet. Chem.*, 2005, **690**, 5451.
164. H. Jacobsen, A. Correa, A. Poater, C. Costabile and L. Cavallo, *Coord. Chem. Rev.*, 2009, **253**, 687.
165. H. Jacobsen, A. Correa, C. Costabile and L. Cavallo, *J. Organomet. Chem.*, 2006, **691**, 4350.

166. R. G. Bergman, *Nature*, 2007, **446**, 391.
167. D. A. Colby, A. S. Tsai, R. G. Bergman and J. A. Ellman, *Acc. Chem. Res.*, 2012, **45**, 814.
168. J. C. Lewis, R. G. Bergman and J. A. Ellman, *Acc. Chem. Res.*, 2008, **41**, 1013.
169. J. C. Lewis, R. G. Bergman and J. A. Ellman, *J. Am. Chem. Soc.*, 2007, **129**, 5332.
170. K. L. Tan, S. Park, J. A. Ellman and R. G. Bergman, *J. Org. Chem.*, 2004, **69**, 7329.
171. J. C. Lewis, A. M. Berman, R. G. Bergman and J. A. Ellman, *J. Am. Chem. Soc.*, 2008, **130**, 2493.
172. D. A. Colby, R. G. Bergman and J. A. Ellman, *J. Am. Chem. Soc.*, 2008, **130**, 3645.
173. R. M. Martin, R. G. Bergman and J. A. Ellman, *J. Org. Chem.*, 2012, **77**, 2501.
174. M. A. Ischay, M. K. Takase, R. G. Bergman and J. A. Ellman, *J. Am. Chem. Soc.*, 2013, **135**, 2478.
175. S. Duttwyler, S. Chen, M. K. Takase, K. B. Wiberg, R. G. Bergman and J. A. Ellman, *Science*, 2013, **339**, 678.
176. M. Brasse, J. Campora, J. A. Ellman and R. G. Bergman, *J. Am. Chem. Soc.*, 2013, **135**, 6427.
177. Y. Lian, T. Huber, K. D. Hesp, R. G. Bergman and J. A. Ellman, *Angew. Chem. Int. Ed. Engl.*, 2013, **52**, 629.
178. S. H. Wiedemann, J. C. Lewis, J. A. Ellman and R. G. Bergman, *J. Am. Chem. Soc.*, 2006, **128**, 2452.
179. C. Samojlowicz, M. Bieniek and K. Grela, *Chem. Rev.*, 2009, **109**, 3708.
180. O. Schuster, L. Yang, H. G. Raubenheimer and M. Albrecht, *Chem. Rev.*, 2009, **109**, 3445.
181. A. A. Tukov, A. T. Normand and M. S. Nechaev, *Dalton Trans.*, 2009, 7015.
182. M. R. F. Ashworth, R. P. Daffern and D. L. Hammick, *J. Chem. Soc.*, 1939, 809.
183. P. Dyson and D. L. Hammick, *J. Chem. Soc.*, 1937, 1724.
184. H. G. Raubenheimer, J. G. Toerien, G. J. Kruger, R. Otte, W. E. Van Zyl and P. Olivier, *J. Organomet. Chem.*, 1994, **466**, 291.
185. E. Stander-Grobler, C. E. Strasser, O. Schuster, S. Cronje and H. Raubenheimer, *Inorg. Chim. Acta*, 2011, **376**, 87.
186. P. J. Fraser, W. R. Roper and F. G. A. Stone, *J. Chem. Soc., Dalton Trans.*, 1974, 760.
187. K. Hata, Y. Segawa and K. Itami, *Chem. Comm.*, 2012, **48**, 6642.
188. J. S. Owen, J. A. Labinger and J. E. Bercaw, *J. Am. Chem. Soc.*, 2004, **126**, 8247.
189. J. A. Cabeza, I. del Rio, E. Perez-Carreno, M. G. Sanchez-Vega and D. Vazquez-Garcia, *Angew. Chem. Int. Ed.*, 2009, **48**, 555.
190. J. A. Cabeza, I. del Rio, E. Perez-Carreno and V. Pruneda, *Organometallics*, 2011, **30**, 1148.
191. D. Lavorato, J. K. Terlouw, T. K. Dargel, W. Koch, G. A. McGibbon and H. Schwarz, *J. Am. Chem. Soc.*, 1996, **118**, 11898.
192. D. J. Lavorato, J. K. Terlouw, G. A. McGibbon, T. K. Dargel, W. Koch and H. Schwarz, *Int. J. Mass Spectrom.*, 1998, **180**, 7.
193. C. J. Emanuel and P. B. Shevlin, *J. Am. Chem. Soc.*, 1994, **116**, 5991.
194. C. Segarra, E. Mas-Marza, J. A. Mata and E. Peris, *Organometallics*, 2012, **31**, 5169.
195. A. McSkimming, M. Bhadbhade and S. B. Colbran, *Dalton Trans.*, 2010, **39**, 10581.

196. A. McSkimming, G. E. Ball, M. M. Bhadbhade and S. B. Colbran, *Inorg. Chem.*, 2012, **51**, 2191.
197. R. Lalrempuia, N. D. McDaniel, H. Mueller-Bunz, S. Bernhard and M. Albrecht, *Angew. Chem. Int. Ed.*, 2010, **49**, 9765.
198. M. Rosello-Merino, J. Diez and S. Conejero, *Chem. Comm.*, 2010, **46**, 9247.
199. H. G. Raubenheimer, M. Desmet, P. Olivier and G. J. Kruger, *J. Chem. Soc., Dalton Trans.*, 1996, 4431.
200. E. Stander-Grobler, O. Schuster, G. Heydenrych, S. Cronje, E. Tosh, M. Albrecht, G. Frenking and H. G. Raubenheimer, *Organometallics*, 2010, **29**, 5821.
201. R. H. Crabtree, *Coord. Chem. Rev.*, 2013, **257**, 755.
202. G. Heydenrych, M. von Hopffgarten, E. Stander, O. Schuster, H. G. Raubenheimer and G. Frenking, *Eur. J. Inorg. Chem.*, 2009, 1892.
203. G. Frenking, K. Wichmann, N. Frohlich, J. Grobe, W. Golla, D. Le Van, B. Krebs and M. Lage, *Organometallics*, 2002, **21**, 2921.
204. H. G. Raubenheimer and S. Cronje, *Dalton Trans.*, 2008, 1265.
205. D. Kunz, *Angew. Chem. Int. Ed.*, 2007, **46**, 3405.
206. E. Alvarez, S. Conejero, M. Paneque, A. Petronilho, M. L. Poveda, O. Serrano and E. Carmona, *J. Am. Chem. Soc.*, 2006, **128**, 13060.
207. E. Alvarez, S. Conejero, P. Lara, J. A. Lopez, M. Paneque, A. Petronilho, M. L. Poveda, D. del Rio, O. Serrano and E. Carmona, *J. Am. Chem. Soc.*, 2007, **129**, 14130.
208. S. Conejero, J. Lopez-Serrano, M. Paneque, A. Petronilho, M. L. Poveda, F. Vattier, E. Alvarez and E. Carmona, *Chem. Eur. J.*, 2012, **18**, 4644.
209. S. Conejero, P. Lara, M. Paneque, A. Petronilho, M. L. Poveda, O. Serrano, F. Vattier, E. Alvarez, C. Maya, V. Salazar and E. Carmona, *Angew. Chem. Int. Ed.*, 2008, **47**, 4380.
210. M. Paneque, M. L. Poveda, F. Vattier, E. Alvarez and E. Carmona, *Chem. Comm.*, 2009, 5561.
211. S. Conejero, C. Maya, M. Paneque, A. Petronilho, M. L. Poveda, F. Vattier, E. Alvarez, E. Carmona, A. Laguna and O. Crespo, *Dalton Trans.*, 2012, **41**, 14126.
212. H. C. Brown, *J. Chem. Soc. (Res.)*, 1956, 1248.
213. C. Cristobal, Y. A. Hernandez, J. Lopez-Serrano, M. Paneque, A. Petronilho, M. L. Poveda, V. Salazar, F. Vattier, E. Alvarez, C. Maya and E. Carmona, *Chem. Eur. J.*, 2013, **19**, 4003.
214. M. A. Esteruelas, F. J. Fernandez-Alvarez, M. Olivan and E. Onate, *Organometallics*, 2009, **28**, 2276.
215. G. Song, Y. Li, S. Chen and X. Li, *Chem. Comm.*, 2008, 3558.
216. Y. Su, G. Y. Song, K. L. Han and X. W. Li, *J. Organomet. Chem.*, 2011, **696**, 1640.
217. E. Alvarez, Y. A. Hernandez, J. Lopez-Serrano, C. Maya, M. Paneque, A. Petronilho, M. L. Poveda, V. Salazar, F. Vattier and E. Carmona, *Angew. Chem. Int. Ed.*, 2010, **49**, 3496.
218. Y. A. Hernandez, J. Lopez-Serrano, M. Paneque, M. L. Poveda, F. Vattier, V. Salazar, E. Alvarez and E. Carmona, *Chem. Eur. J.*, 2011, **17**, 9302.
219. D. G. Johnson, J. M. Lynam, J. M. Slattery and C. E. Welby, *Dalton Trans.*, 2010, **39**, 10432.
220. C. E. Welby, T. O. Eschemann, C. A. Unsworth, E. J. Smith, R. J. Thatcher, A. C. Whitwood and J. M. Lynam, *Eur. J. Inorg. Chem.*, 2012, 1493.
221. M. A. Esteruelas, F. J. Fernandez-Alvarez and E. Onate, *J. Am. Chem. Soc.*, 2006, **128**, 13044.

222. M. A. Esteruelas, F. J. Fernandez-Alvarez and E. Onate, *Organometallics*, 2007, **26**, 5239.
223. M. A. Esteruelas, F. J. Fernandez-Alvarez and E. Onate, *Organometallics*, 2008, **27**, 6236.
224. M. L. Buil, M. A. Esteruelas, K. Garces, M. Olivan and E. Onate, *J. Am. Chem. Soc.*, 2007, **129**, 10998.
225. M. A. Esteruelas, E. Forcen, M. Olivan and E. Onate, *Organometallics*, 2008, **27**, 6188.
226. B. Eguillor, M. A. Esteruelas, J. Garcia-Raboso, M. Olivan and E. Onate, *Organometallics*, 2009, **28**, 3700.
227. S. Bajo, M. A. Esteruelas, A. M. Lopez and E. Onate, *Organometallics*, 2012, **31**, 8618.
228. J. A. Bull, J. J. Mousseau, G. Pelletier and A. B. Charette, *Chem. Rev.*, 2012, **112**, 2642.
229. L. McMurray, F. O'Hara and M. J. Gaunt, *Chem. Soc. Rev.*, 2011, **40**, 1885.
230. T. Laird, *Org. Process Res. Dev.*, 2006, **10**, 851.
231. J. S. Carey, D. Laffan, C. Thomson and M. T. Williams, *Org. Biomol. Chem.*, 2006, **4**, 2337.
232. Y. Nakao, *Synthesis-Stuttgart*, 2011, 3209.
233. J. J. Mousseau, J. A. Bull and A. B. Charette, *Angew. Chem. Int. Ed.*, 2010, **49**, 1115.
234. K. Shen, Y. Fu, J.-N. Li, L. Liu and Q.-X. Guo, *Tetrahedron*, 2007, **63**, 1568.
235. M. Schlosser and F. Mongin, *Chem. Soc. Rev.*, 2007, **36**, 1161.
236. I. J. S. Fairlamb, *Chem. Soc. Rev.*, 2007, **36**, 1036.
237. Y. Nakao, K. S. Kanyiva and T. Hiyama, *J. Am. Chem. Soc.*, 2008, **130**, 2448.
238. K. S. Kanyiva, Y. Nakao and T. Hiyama, *Angew. Chem. Int. Ed.*, 2007, **46**, 8872.
239. Y. Nakao, Y. Yamada, N. Kashihara and T. Hiyama, *J. Am. Chem. Soc.*, 2010, **132**, 13666.
240. Scifinder search in July 2013.
241. K. Karami, M. Ghasemi and N. H. Naeini, *Tetrahedron Lett.*, 2013, **54**, 1352.
242. S. M. Islam, N. Salam, P. Mondal and A. S. Roy, *J. Mol. Catal. A: Chem.*, 2013, **366**, 321.
243. E. Shirakawa, X. Zhang and T. Hayashi, *Angew. Chem. Int. Ed.*, 2011, **50**, 4671.
244. M. L. Kantam, P. V. Reddy, P. Srinivas and S. Bhargava, *Tetrahedron Lett.*, 2011, **52**, 4490.
245. Z. Ye, F. Chen, F. Luo, W. Wang, B. Lin, X. Jia and J. Cheng, *Synlett*, 2009, 2198.
246. W. C. Frank, Y. C. Kim and R. F. Heck, *J. Org. Chem.*, 1978, **43**, 2947.
247. O. Navarro, N. Marion, J. Mei and S. P. Nolan, *Chem. Eur. J.*, 2006, **12**, 5142.
248. G. A. Molander and M. R. Rivero, *Org. Lett.*, 2002, **4**, 107.
249. P. Wen, Y. Li, K. Zhou, C. Ma, X. Lan, C. Ma and G. Huang, *Adv. Synth. Catal.*, 2012, **354**, 2135.
250. M. Kim, J. Kwak and S. Chang, *Angew. Chem. Int. Ed.*, 2009, **48**, 8935.
251. L. Ilies, S. Asako and E. Nakamura, *J. Am. Chem. Soc.*, 2011, **133**, 7672.
252. S. C. Soederman and A. L. Schwan, *J. Org. Chem.*, 2012, **77**, 10978.
253. M. Murakami and S. Hori, *J. Am. Chem. Soc.*, 2003, **125**, 4720.
254. V. Ritleng, C. Sirlin and M. Pfeffer, *Chem. Rev.*, 2002, **102**, 1731.
255. N. T. S. Phan, M. Van Der Sluys and C. W. Jones, *Adv. Synth. Catal.*, 2006, **348**, 609.
256. C. B. Ziegler and R. F. Heck, *J. Org. Chem.*, 1978, **43**, 2941.
257. D. Mc Cartney and P. J. Guiry, *Chem. Soc. Rev.*, 2011, **40**, 5122-5150.

258. J. Le Bras and J. Muzart, *Chem. Rev.*, 2011, **111**, 1170.
259. J. P. Knowles and A. Whiting, *Org. Biomol. Chem.*, 2007, **5**, 31.
260. R. F. Heck, *Org. React.*, 1982, **27**, 345.
261. T. Mizoroki, K. Mori and A. Ozaki, *Bull. Chem. Soc. Jpn.*, 1971, **44**, 581.
262. C. G. Jia, D. G. Piao, J. Z. Oyamada, W. J. Lu, T. Kitamura and Y. Fujiwara, *Science*, 2000, **287**, 1992.
263. Y. Fujiwara, I. Moritani, S. Danno, R. Asano and Teranish.S, *J. Am. Chem. Soc.*, 1969, **91**, 7166.
264. C. G. Jia, T. Kitamura and Y. Fujiwara, *Acc. Chem. Res.*, 2001, **34**, 633.
265. M. I. Bruce, C. Hameister, A. G. Swincer and R. C. Wallis, *Inorg. Synth.*, 1982, **21**, 78.
266. D. B. Grotjahn, *Chem.- Eur. J.*, 2005, **11**, 7146.
267. F. M. Conroy-Lewis and S. J. Simpson, *J. Organomet. Chem.*, 1987, **322**, 221.
268. E. Ruba, K. Mereiter, R. Schmid and K. Kirchner, *Chem. Comm.*, 2001, 1996.
269. A. Nakamura, A. Hamasaki, S. Goto, M. Utsunomiya and M. Tokunaga, *Adv. Synth. Catal.*, 2011, **353**, 973.
270. D. V. Gutsulyak, S. F. Vyboishchikov and G. I. Nikonov, *J. Am. Chem. Soc.*, 2010, **132**, 5950.
271. N. Kumagai, S. Matsunaga and M. Shibasaki, *Tetrahedron*, 2007, **63**, 8598.
272. N. Kumagai, S. Matsunaga and M. Shibasaki, *J. Am. Chem. Soc.* , 2004, **126**, 13632.
273. B. M. Trost and R. J. Kulawiec, *J. Am. Chem. Soc.*, 1993, **115**, 2027.
274. C. Slugovc, E. Ruba, R. Schmid and K. Kirchner, *Organometallics*, 1999, **18**, 4230.
275. www.sigmaaldrich.com/catalog/product/aldrich/673307?lang=en&region=GB, on 26/04/2013.
276. T. P. Gill and K. R. Mann, *Organometallics*, 1982, **1**, 485.
277. R. A. Zelonka and M. C. Baird, *J. Can. Chem.*, 1972, **50**, 3063.
278. R. A. Zelonka and M. C. Baird, *J. Organomet. Chem.*, 1972, **44**, 383.
279. M. A. Bennett, T. N. Huang and T. W. Turney, *J. Chem. Soc. Chem. Comm.*, 1979, 312.
280. M. A. Bennett and T. W. Matheson, *J. Organomet. Chem.*, 1978, **153**, C25.
281. A. Mercier, W. C. Yeo, J. Y. Chou, P. D. Chaudhuri, G. Bernardinelli and E. P. Kundig, *Chem. Comm.*, 2009, 5227.
282. E. P. Kundig and F. R. Monnier, *Adv. Synth. Catal.*, 2004, **346**, 901.
283. A. N. Nesmeyanov, N. A. Volkenau, I. N. Bolesova and L. S. Shulpina, *J. Organomet. Chem.*, 1979, **182**, C36.
284. E. Roman and D. Astruc, *Inorg. Chim. Acta*, 1979, **37**, L465.
285. M. J. Mayor-Lopez and J. Weber, *Chem. Phys. Lett.*, 1997, **281**, 226.
286. E. J. P. Malar, *Eur. J. Inorg. Chem.*, 2004, 2723.
287. T. S. Morais, M. Helena Garcia, M. Paula Robalo, M. F. M. Piedade, M. Teresa Duarte, M. Jose Villa de Brito and P. J. Amorim Madeira, *J. Organomet. Chem.*, 2012, **713**, 112.
288. V. Moreno, M. Font-Bardia, T. Calvet, J. Lorenzo, F. X. Aviles, M. H. Garcia, T. S. Morais, A. Valente and M. P. Robalo, *J. Inorg. Biochem.*, 2011, **105**, 241.
289. L. Hintermann, L. Xiao, A. Labonne and U. Englert, *Organometallics*, 2009, **28**, 5739.
290. E. E. Karslyan, D. S. Perekalin, P. V. Petrovskii, A. O. Borisova and A. R. Kudinov, *Russ. Chem. Bull.*, 2009, **58**, 585.
291. D. S. Perekalin, E. E. Karslyan, P. V. Petrovskii, A. O. Borissova, K. A. Lyssenko and A. R. Kudinov, *Eur. J. Inorg. Chem.*, 2012, 1485.
292. L. P. Hammett, *J. Am. Chem. Soc.*, 1937, **59**, 96.

293. H. H. Jaffe, *Chem. Rev.*, 1953, **53**, 191.
294. D. H. McDaniel and H. C. Brown, *J. Org. Chem.*, 1958, **23**, 420.
295. C. Hansch, A. Leo and R. W. Taft, *Chem. Rev.*, 1991, **91**, 165.
296. R. H. Fish, H. S. Kim and R. H. Fong, *Organometallics*, 1991, **10**, 770.
297. M. H. Garcia, T. S. Morais, P. Florindo, M. F. M. Piedade, V. Moreno, C. Ciudad and V. Noe, *J. Inorg. Biochem*, 2009, **103**, 354.
298. A. G. Orpen, L. Brammer, F. H. Allen, O. Kennard, D. G. Watson and R. Taylor, *J. Chem. Soc., Dalton Trans.*, 1989, S1.
299. P. E. Garrou, *Chem. Rev.*, 1985, **85**, 171.
300. P. van Leeuwen, *Appl. Catal., A*, 2001, **212**, 61.
301. S. I. Kozhushkov and L. Ackermann, *Chem. Sci.*, 2013, **4**, 886.
302. M. J. Percino, V. M. Chapela, M. Salmon, G. EspinosaPerez, A. M. Herrera and A. Flores, *J. Chem. Crystallogr.*, 1997, **27**, 549.
303. P. Barrio, M. A. Esteruelas and E. Onate, *Organometallics*, 2004, **23**, 3627.
304. M. A. Esteruelas, F. J. Fernandez-Alvarez, M. Olivan and E. Onate, *J. Am. Chem. Soc.*, 2006, **128**, 4596.
305. M. L. Buil, M. A. Esteruelas, E. Goni, M. Olivan and E. Onate, *Organometallics*, 2006, **25**, 3076.
306. J. Yamaguchi, A. D. Yamaguchi and K. Itami, *Angew. Chem. Int. Ed.*, 2012, **51**, 8960.
307. D. A. Colby, R. G. Bergman and J. A. Ellman, *Chem. Rev.*, 2010, **110**, 624.
308. A. M. Berman, J. C. Lewis, R. G. Bergman and J. A. Ellman, *J. Am. Chem. Soc.*, 2008, **130**, 14926.
309. A. S. Tsai, R. G. Bergman and J. A. Ellman, *J. Am. Chem. Soc.*, 2008, **130**, 6316.
310. J. W. Faller, D. F. Chodosh and D. Katahira, *J. Organomet. Chem.*, 1980, **187**, 227.
311. J. W. Faller and A. M. Rosan, *J. Am. Chem. Soc.*, 1976, **98**, 3388.
312. J. W. Faller, C. C. Chen, M. J. Mattina and Jakubows.A, *J. Organomet. Chem.*, 1973, **52**, 361.
313. S. A. Benyunes, R. J. Deeth, A. Fries, M. Green, M. McPartlin and C. B. M. Nation, *J. Chem. Soc., Dalton Trans.*, 1992, 3453.
314. M. I. Bruce, M. A. Fox, P. J. Low, B. W. Skelton and N. N. Zaitseva, *Dalton Trans.*, 2010, **39**, 3759.
315. C. S. Yi, N. H. Liu, A. L. Rheingold and L. M. LiableSands, *Organometallics*, 1997, **16**, 3910.
316. B. J. Brisdon, R. J. Deeth, A. G. W. Hodson, C. M. Kemp, M. F. Mahon and K. C. Molloy, *Organometallics*, 1991, **10**, 1107.
317. B. J. Brisdon and R. A. Walton, *Polyhedron*, 1995, **14**, 1259.
318. O. Eisenstein and R. Hoffmann, *J. Am. Chem. Soc.*, 1981, **103**, 4308.
319. O. Eisenstein and R. Hoffmann, *J. Am. Chem. Soc.*, 1980, **102**, 6148.
320. Y. Takahata and D. P. Chong, *Int. J. Quantum Chem.*, 2005, **103**, 509.
321. G. K. S. Prakash and A. K. Yudin, *Chem. Rev.*, 1997, **97**, 757.
322. R. R. Holmes, *Chem. Rev.*, 1996, **96**, 927.
323. Sheldric.Ws, *J. Chem. Soc., Dalton Trans.*, 1974, 1402.
324. Y. Wakatsuki, *J. Organomet. Chem.*, 2004, **689**, 4092.
325. B. Deklerkengels, J. G. P. Delis, K. Vrieze, K. Goubitz and J. Fraanje, *Organometallics*, 1994, **13**, 3269.
326. S. A. Matchett, B. R. Schmiege-Boyle, J. Cooper, D. Fratterelli, K. Olson, J. Roberts, J. Thommen, D. Tigelaar and F. Winkler, *Organometallics*, 2003, **22**, 5047.

327. A. F. Borowski, S. SaboEtienne, M. L. Christ, B. Donnadieu and B. Chaudret, *Organometallics*, 1996, **15**, 1427.
328. J. B. Aberg, M. C. Warner and J.-E. Backvall, *J. Am. Chem. Soc.*, 2009, **131**, 13622.
329. E. O. Changamu, H. B. Friedrich and M. Rademeyer, *J. Organomet. Chem.*, 2008, **693**, 164.
330. M. L. Buil, M. A. Esteruelas, K. Garces, M. Olivan and E. Onate, *Organometallics*, 2008, **27**, 4680.
331. A. Furstner, L. Ackermann, B. Gabor, R. Goddard, C. W. Lehmann, R. Mynott, F. Stelzer and O. R. Thiel, *Chem. Eur. J.*, 2001, **7**, 3236.
332. A. C. Hillier, W. J. Sommer, B. S. Yong, J. L. Petersen, L. Cavallo and S. P. Nolan, *Organometallics*, 2003, **22**, 4322.
333. S. Burling, M. F. Mahon, R. E. Powell, M. K. Whittlesey and J. M. J. Williams, *J. Am. Chem. Soc.*, 2006, **128**, 13702.
334. K. Abdur-Rashid, T. Fedorkiw, A. J. Lough and R. H. Morris, *Organometallics*, 2004, **23**, 86.
335. D. S. Frohnapfel and J. L. Templeton, *Coord. Chem. Rev.*, 2000, **206**, 199.
336. S. H. Choi and Z. Y. Lin, *Organometallics*, 1999, **18**, 2473.
337. D. G. Johnson, J. M. Lynam, N. S. Mistry, J. M. Slattery, R. J. Thatcher and A. C. Whitwood, *J. Am. Chem. Soc.*, 2013, **135**, 2222.
338. D. S. Perekalin, E. E. Karslyan, E. A. Trifonova, A. I. Konovalov, N. L. Loskutova, Y. V. Nelyubina and A. R. Kudinov, *Eur. J. Inorg. Chem.*, 2013, 481.
339. F. Santoro, M. Althaus, C. Bonaccorsi, S. Gischig and A. Mezzetti, *Organometallics*, 2008, **27**, 3866.
340. K. S. Mohamed and D. K. Padma, *Spectrochim. Acta, Part A*, 1985, **41**, 725.